Applications of Layered Double Hydroxides as Inorganic Adjuvants

Hannah Buckley

A thesis submitted in part fulfilment of the requirements for the degree of Doctor of Philosophy at the University of Oxford

New College

Oxford

October 2014

The work described in this thesis was carried out in the Chemistry Research Laboratory, Mansfield Road, Oxford and at the Nuffield Department of Surgical Sciences, John Radcliffe Hospital, Oxford from October 2011 to October 2014 under the supervision of Professor Dermot O'Hare. All the work described is my own unless stated to the contrary, and has not been submitted for any degree at this or any other university.

Hannah Buckley

October 2014

Abstract

Applications of Layered Double Hydroxides as Inorganic Adjuvants

Hannah Buckley New College
DPhil Thesis Michaelmas Term 2014

The primary aim of this thesis is to explore the immunostimulatory properties of a family of layered, crystalline, inorganic materials known as layered double hydroxides (LDHs).

Chapter One provides an introduction to relevant aspects of the immune system, and the context for investigating the immunostimulatory properties of inorganic materials in terms of vaccine/adjuvant formulations. The possible mechanisms of action of commercial adjuvant materials are also reviewed, and the structure, synthesis methods and applications of LDHs are discussed.

Chapter Two details the controlled synthesis and characterisation of LDHs in specific particle sizes. A series of MgAl-CO_3 LDHs with precisely controlled particle sizes ranging from 20 to 10000 nm were successfully synthesised, then the techniques used were extended to other compositions to create a panel of LDHs for use in subsequent Chapters.

In **Chapter Three**, the responses of monocyte-derived dendritic cells (Mo-DC) to the LDH particle sizes discussed in Chapter Two are assessed in terms of viability, surface molecule expression, and cytokine secretion. A statistical modelling approach using the physicochemical properties of the LDHs as explanatory variables for immune responses was employed to evaluate the validity of the model formulated in the previous work, and to establish if particle size could be used to improve its predictive ability. It was found that strong relationships between LDH particle size and certain Mo-DC responses exist, and that these responses could be predicted with a high degree of accuracy.

Chapter Four is concerned with the investigation of T cell responses to LDH-stimulated allogeneic Mo-DC. Various methods were used for assessing T cell division and proliferation, and a protocol for intracellular cytokine staining was developed to probe T cell polarisation. Five LDHs, which have elicited potentially interesting T cell responses in previous work, were selected for investigation. However, using the assays described, no discernible improvement in proliferation or polarisation was observed with any of the LDHs tested.

Chapter Five presents an initial exploration of the interactions between LDH particles and cells. Experiments have shown that LDH particles both adhere to and are internalised by Mo-DC. Variations in the extent of internalisation with both particle size and composition were highlighted by confocal microscopy studies. Through investigations into interactions between LDH particles and the plasma membrane using protease enzymes, it was revealed that adhesion of LDH particles is partly protein-dependent. Further studies have also demonstrated a pH-dependent element to particle association with Mo-DC.

Details of the experimental procedures employed are included in **Chapter Six**. Supplementary information referred to in the main thesis may be found in the **Appendices**.

Acknowledgements

Firstly, I would like to thank Professor Dermot O'Hare for his guidance throughout the last three years. Also, huge thanks to Professor Jon Austyn, for effectively acting as my second supervisor at the JR, and initiating me into the big, bad world of immunobiology. I am hugely grateful to Dr Stephen Preston for all the help throughout my DPhil and for being a genuinely great person to work with. Thanks also to Dr Gareth Williams for always being just an email away.

Chapter Three contains a lot of complicated statistics, none of which could have happened without the help of Dr George Nicholson for which I am hugely grateful, and best of luck with fatherhood. Thanks also to Professor Daniel Lunn for his help with the stats early on, and for the referral to George. Sincere thanks to all who have helped with the many instruments and techniques detailed within: Dr Rob Jacobs for the AFM, and general SAF assistance; Dr Jamie Warner for help with TEM in the Materials department; Andrew Allan and Jennifer Holter for assistance with TEM and SEM at Harwell campus; Dr Richard Cooper for the TGA training; Dr Kerstin Jurkschat for help with the zetasizer; Dr Janet Digby for giving up most of a day to help with the Luminex experiments; Dr Joanna Hester for the radiation training and always being happy to answer a question or two; Amy Hong and Professor Adrian Smith for use of various bits of kit in Zoology; and Dr Chris Lagerholm at the WIMM for all the training, assistance and advice relating to confocal microscopy.

I have been fortunate to work with a multitude of colourful characters in both the NDS and the chemistry department. At the NDS: firstly, Lena – whenever I find myself listening to Big fm's party beats on a weekday morning I will think of you. Secondly, Gareth Plant – you have kept me entertained through some of my darkest hours in tissue culture. Thanks also to Oliwia for helpful confocal advice and the odd Maxwells encounter. Thanks to all in the Wood group for advice, entertaining conversation and providing sympathetic ears to my moaning: Jess, Kate, Renee, Ivana, Stephen, Andrew, Suhma, Matt, Rebecca, Steffi and Masaaki. Also, a special mention to the NDS admin staff, in particular Val, for putting up with all my last-minute blood orders. In the CRL, thanks to all of the O'Hareem, past and present: Henery, Yue, Coops, party Dave, Golf, Michelle, Andrew, Anchalee, Mark and Saul (who could forget that game of Kerplunk?), Charles, Hasna, Team Part 2 throughout the years (Emily, Jamie, Dan, Ali, George, Ella, Chloe, Jack, Jack, Ryan, Olivia) and our many interesting visitors (Shuangde, Yufei, Mingfei, Kentaro, Nidwaree, Stone, Irvin...). You are a weird and wonderful bunch, and memories of gin-rums, council notices and short suits will stay with me forever. In particular thanks to JC, Zoe, Chris and Chunping for their proof reading; to Joyce for the wedding invite, it was a long way to travel but it was worth it; and to Sam for being a great friend and travelling companion on our Italian adventures. Also, special thanks to the ICL office staff, Hazel, Pam, Trish, and Hilary. Thanks also to Prof Peter Battle for allowing me to teach at St Catherine's, and all your support over my years at Oxford, and also to Phil Wiseman for the junior demonstrator job.

Huge thanks to my DPhil housemates, Aileen (you're SO hot!), Alice, and Tom, for the fish finger sandwiches, the New college gossip, the laughs and the terrible TV. Also to Hilary, Naomi, Charlotte and Caroline – Dragonquest adventure golf was a lifesaver; Claire, Katie, Rachel, Lindsay, Sophie, Sarah, Kate, Rob, Hannah, Zara and Helena. Stewart – thanks for putting up with me, you kept me going through some very stressful times! Finally, special thanks to my family, Mum, Dad, Rachel, and Uncle Caroline for all of your love and support.

Abbreviations

2,2-ABS	2,2'-Azino-bis(3-ethylbenzothiazoline-6-sulfonic acid)
7-AAD	7-aminoactinomycin D
Ab	Antibody
AFM	Atomic force microscopy
allo	Allogeneic
APC	Allophycocyanin (fluorophore) or antigen presenting cell depending on context
ARR	Ammonia releasing reagent
ASC	Apoptosis associated speck-like protein containing a CARD
ATP	Adenosine triphosphate
BIC	Bayesian information criterion
BSA	Bovine serum albumin
BV	Brilliant violet™
CARD	Caspase recruitment domain
CCR	C-C chemokine receptor
CD	Cluster of differentiation
CDS	Crystallite domain size
CFSE	Carboxyfluoroscein succinimidyl ester
CTL	Cytotoxic lymphocyte
CTLA-4	Cytotoxic T lymphocyte antigen 4
Cy	Cyanine
DAMP	Damage associated molecular pattern
DAPI	4',6-diamidino-2-phenylindole
DC	Dendritic cell
DDS	Dodecyl sulphate
DI	De-ionised
DLS	Dynamic light scattering
DMSO	Dimethyl sulfoxide
DNA	Deoxyribonucleic acid
DOF	Degrees of freedom
EA	Elemental analysis
EDTA	Ethylenediaminetetraacetic acid
EDX	Energy dispersive x-ray specstroscopy
ELISA	Enzyme linked immunosorbent assay
FCS	Fetal calf serum
FITC	Fluoroscein isothiocyanate
FSC	Forward scatter
FTIR	Fourier transform infrared
FWHM	Full-width at half-maximum height
GMCSF	Granulocyte macrophage colony stimulating factor
GMFI	Geometric mean fluorescence intensity
HBS	Hank’s balanced salt
HEPES	4-(2-Hydroxyethyl)piperazine-1-ethanesulfonic acid, N-(2-Hydroxyethyl)piperazine-N'-(2-ethanesulfonic acid)
HLA	Human leukocyte antigen
HMT	Hexamethylenetetramine
HOPG	Highly ordered pyrolytic graphite
HOS	Human osteosarcoma
HT	Hydrothermal

IEP	Isoelectric point
IFN	Interferon
IL	Interleukin
ITAMs	Immunoreceptor tyrosine based activation motifs
KO	Knockout
LC	Langerhans cell
LDH	Layered double hydroxide
LDO	Layered double oxide
LPS	Lipopolysaccharide
LRR	Leucine rich repeat
LS	Logarithmic score
LY	Lucifer yellow
MHC	Major histocompatability complex
MLR	Mixed leukocyte reaction
Mo	Monocyte
Mo-DC	Monocyte-derived dendritic cell
MSU	Monosodium urate
NBS	Nucleotide binding site
NK cell	Natural killer cell
NKT cell	Natural killer T cell
NLR	NOD-like receptor
NOD	Nucleotide-binding oligomerisation domain
O/N	Overnight
OVA	Ovalbumin
PAMP	Pathogen associated molecular pattern
PBS	Phosphate buffered saline
PE	Phycoerythrin
PFA	Paraformaldehyde
PI3K	Phosphoinositide 3-kinase
PMA	Phorbol 12-myristate 13 acetate
PRR	Pattern recognition receptor
PYD	Pyrin domain
RER	Rough endoplasmic reticulum
RMSE	Root mean squared error
RNA	Ribonucleic acid
RPM	Revolutions per minute
RPMI	Roswell Park Memorial Institute
RT	Room temperature
SEM	Scanning electron microscopy
SNAS	Separate nucleation and aging steps
SSC	Side scatter
Syk	Spleen tyrosine kinase
TAP	Transporter associated with antigen processing
TCR	T cell receptor
TEM	Transmission electron microscopy
TGA	Thermogravimetric analysis
TLR	Toll-like receptor
TNF	Tumour necrosis factor
XRD	X-ray diffraction

Table of contents

Chapter One: Introduction

1.1 Overview

Inorganic materials have been used to stimulate the immune system as adjuvants in vaccines since the early twentieth century.[1] The main material used commercially is a heterogeneous mixture of inorganic compounds referred to as 'alum' by immunologists, comprising materials such as aluminium oxyhydroxide, aluminium hydroxyphosphate and magnesium hydroxide.[2,3] Despite being a poorly characterised mixture, until recently alum-based adjuvants were the only adjuvants licensed for use in humans in the USA.[4] Investigations into new inorganic adjuvants are few, and even the mechanism of action of established adjuvants is not well understood.[5]

Inorganic chemistry offers a plethora of materials with enormous variety in composition, structure and morphology for immunologists to utilise. In contrast to alums, layered double hydroxides (LDHs) are a family of homogeneous, crystalline materials with highly tuneable properties such as composition, particle size, and morphology.[6,7] Previous work by Williams *et al*. has confirmed their ability to stimulate immune responses, both *in vitro* and *in vivo*.[8] Moreover, they demonstrated for the first time that a subset of the physical and chemical properties of the LDH material can be employed to predict the immune response highlighting "*the possibility of rational manipulation of immunity for therapeutic purposes*".[8]

1.2 Immunological Background

The immune system may be considered as having two parts: innate and adaptive. The innate immune system is able to rapidly recognise and defend against a multitude of common pathogens. The adaptive immune system takes longer to take full effect, but is subsequently able to 'remember' an infection and provide a rapid response should that infection be encountered again. Generating immunological memory of a specific disease without the danger of genuine infection is the goal of vaccination. '*Exploring immunology: Concepts and evidence*' provides general background information on immunology.[9] Some specific topics of particular relevance are briefly reviewed in the following pages.

1.2.1 Recognition of danger

Activation of the innate immune system occurs upon recognition of 'danger signals' by certain cells. These signals may be pathogen related [pathogen associated molecular patterns

(PAMPs)] or damage related [damage associated molecular patterns (DAMPs)].[10] These are typically recognised by cells such as by macrophages and dendritic cells, both of which are found near any surface in the body exposed to the outside environment, such as in the lungs, under the skin and the lining of the gut.[11–13]

The recognition of danger signals is performed by sets of plasma membrane, endosomal and cytoplasmic receptors known as pattern recognition receptors (PRRs). Toll-like receptors (TLRs) detect conserved components of pathogens such as lipopolysaccharide,[14] lipoteichoic acid, single-stranded RNA, flagellin, and CpG DNA[15] at the plasma membrane, or in endosomes (reviewed here).[16] Upon binding of the appropriate ligand, a TLR will initiate signalling cascades *via* adaptor molecules such as MyD88 or TRIF. This results in gene expression, commonly controlled by primary transcription factor NF-κB,[17] with ensuing secretion of pro-inflammatory cytokines and/or increased expression of certain plasma membrane molecules, for example, cluster of differentiation 86 (CD86) in DC. Other PRRs include C-type lectin receptors that bind to carbohydrates, such as the macrophage mannose receptor or dectin 1,[18,19] and scavenger receptors, all of which may initiate pathogen internalisation.[20] NOD (nucleotide-binding oligomerisation domain)-like receptors (NLRs) function within the cytoplasm and are capable of detecting intracellular pathogen components (e.g. peptidoglycan)[21] as well as DAMPs such as adenosine triphosphate (ATP) or uric acid crystals.[22,23]

1.2.2 Dendritic cells

Dendritic cells (DCs) are defined by their unique ability to activate naïve T cells.[24,25] Several subsets of DC have been characterised, with their identities distinguished by their roles, phenotype and location in the body. Langerhans cells (LC) are a self-renewing population in the epidermis capable of migrating to lymph nodes upon contact with inflammatory mediators.[26] They express langerin (CD207, a lectin receptor), and contain Birbeck granules, the role of which is unclear.[13,27] LC are considered a specialised subset of myeloid DC, as they share a common bone marrow generated precursor. Myeloid DC, characterised by high expression of CD11c, are present in low numbers throughout the epidermis and mucosal tissues.[28] They follow a migration pattern from the blood to the peripheral tissues, then onwards to the lymphoid tissues.[29] Unlike myeloid DC, plasmacytoid DC (pDC) do not express high levels of CD11c.[29,30] They are primarily located in the blood and lymphoid tissues, producing strong anti-viral immune responses through secretion of type 1 interferons. However, their role in antigen presentation is unclear.[30] It has been shown that mDC and pDC

possess complementary sets of TLRs.[31] Depending on conditions, circulating inflammatory monocytes may also develop into DC (Mo-DC) upon recruitment to sites of inflammation.[32]

1.2.3 Antigen presentation and dendritic cell maturation

T cells are only able to recognise components of pathogens (e.g. proteins) when they are presented on major histocompatability complex (MHC) class I or II surface molecules on another cell.[33] All cells have MHC class I molecules, which inform cytotoxic lymphocytes (CTLs) whether a cell is infected and needs destroying. Only certain cells, often referred to as antigen presenting cells (APCs) have MHC class II molecules. These are primarily macrophages, DCs and B cells.[34] Before presentation, a protein must be processed into peptides suitable for mounting in the peptide-binding groove of the MHC class I or II molecules.

In the absence of infection, cytosolic proteins are tagged for degradation and recycling by ubiquitin. This directs them to the proteasome, a cylindrical multi-protein complex with multiple catalytic sites, which breaks up them into smaller peptides for recycling.[35] When cytokines such as interferon-γ (IFN-γ) are produced in response to infection, changes to the sub-unit proteins of the proteasome occur, creating the immunoproteasome.[36] The peptides produced by the immunoproteasome are generally better-suited for mounting on MHC class I molecules.[37] When the cell is infected, some of these peptides will be derived from the pathogen. These peptides are then transported by TAP (transporter associated with antigen processing) to the rough endoplasmic reticulum (RER) where newly synthesised MHC class I molecules reside.[38,39] TAP forms part of a peptide loading complex which places the peptide in the groove, and the entire peptide-MHC class I complex is transported to the cell surface. The structure of MHC class I molecules consists of one heavy chain protein which contains the entire peptide binding groove associated with a β_2 microglobulin molecule.[40]

Following uptake of extracellular proteins, processing into shorter peptide sequences is achieved in the hydrolytic environment upon endolysosome formation. A brief discussion of the various mechanisms of cellular uptake is provided at the start of Chapter Five. MHC class II has a different structure to MHC class I in that a complex of two transmembrane protein chains (α and β) forms the peptide-binding groove. MHC class II is synthesised in the RER complexed to an invariant chain molecule which chaperones it to the endosomes using a targeting sequence.[41] To prevent binding of non-endosomal peptides, the peptide-binding groove is blocked by part of the invariant chain until delivery of the complex

to an endosome, whereupon the invariant chain is cleaved until only one part remains blocking the groove (class II-associated invariant chain peptides or 'CLIP').[42] This remaining fragment may spontaneously release, or its release may be mediated by other molecules present, for example HLA-DM (human leukocyte antigen DM).[43] The empty groove may now be filled with a high-affinity peptide from the contents of the endosome,[44] after which the peptide-MHC class II complex is transported to the cell surface.[41]

Crucially, MHC class I molecules typically present peptides from proteins found in the cytoplasm whilst MHC class II molecules present peptides derived from extracellular proteins. In the absence of an infection, both processes still occur continuously, but only self-antigen is presented. If a virus infects a cell, fragments of virus-associated protein will be presented on the MHC class I molecules; alternatively if a phagocytic cell engulfs a bacteria, for example, bacterial peptides will be presented on the MHC class II molecules.

Peptides loaded onto MHC Class I molecules are intracellular in origin; logically, DC infection by an intracellular pathogen should be a prerequisite for DC MHC Class I antigen presentation. However, DCs are able to present extracellular material on MHC Class I molecules through the poorly understood phenomenon of cross-presentation, thereby circumventing the requirement for infection.[28]

'Immature' DCs, which have not yet been exposed to activation signals (PAMPs, DAMPs), continuously sample the surrounding environment through various endocytic pathways.[45] However, antigen presentation is inefficient because the self peptide-MHC complexes on the surface of the DC are constantly recycled, and are therefore transient in nature.[40] Upon maturation in response to danger signals DCs lose their ability to internalise antigen,[46] and the turnover of MHC class II molecules on the plasma membrane decreases.[47,48] This allows them to accumulate greater numbers of pathogen specific MHC class II-peptide complexes, creating a 'snapshot' of the environment at the time of infection. Mature DCs also increase their expression of surface molecules required for T cell activation (costimulatory molecules) such as CD86, and secrete pro-inflammatory cytokines.

Maturation signals may come directly from the pathogen e.g. *via* ligation of TLRs.[15] Alternatively, other innate lymphocytes [natural killer (NK) cells, natural killer T cells (NKT) and γδ T cells] are able to induce DC maturation in a non-TLR dependent manner, for instance through the release of cytokines such as tumour necrosis factor α (TNF-α).[49] A full

discussion of DC maturation and costimulatory molecule expression may be found in the introduction to Chapter Three.

1.2.4 T cell activation

DCs continuously migrate from the tissues to the secondary lymphoid organs (steady-state migration); this process is enhanced during infection.[50] Immature DC transport fragments of self antigen (e.g. from apoptotic cells) on their MHC molecules, possibly promoting T cell tolerance whereas mature DC transport pathogen-derived antigen peptides from sites of infection to induce the adaptive immune response.[46,51,52]

Once in the secondary lymphoid organs, DCs encounter large numbers of CD4 expressing ($CD4^+$) naïve T cells which are not usually found in the peripheral tissue.[53] Here they undergo multiple encounters with naïve $CD4^+$ T cells, until a one recognises its cognate peptide (epitope) presented in the peptide-binding groove of the MHC Class II molecules on the surface of the DC (Figure 1.1).[54,55]

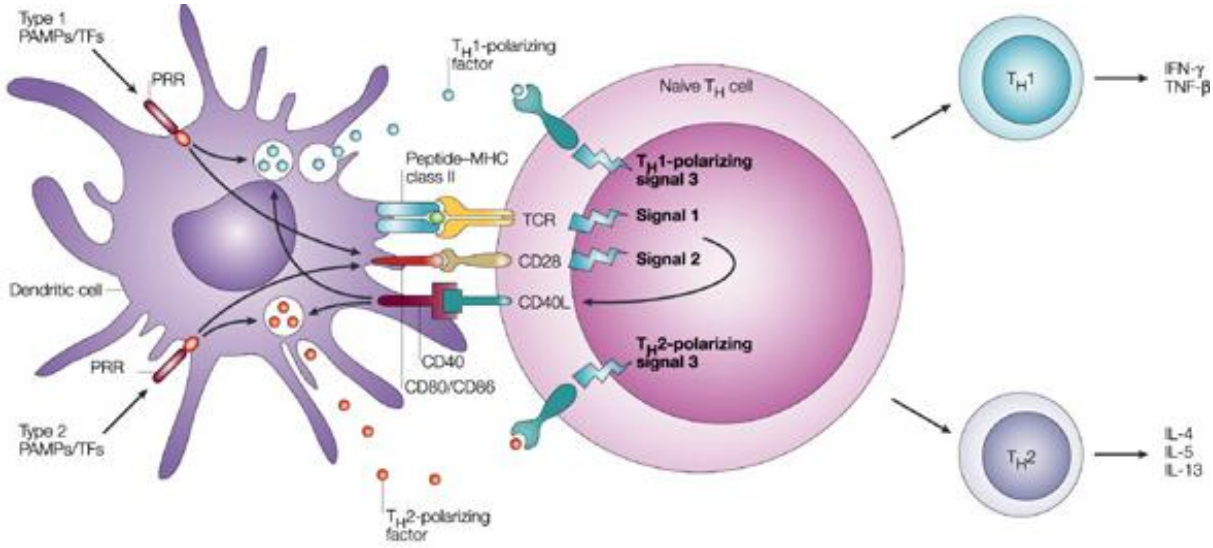

Figure 1.1: Schematic of $CD4^+$ T cell activation by dendritic cells.[29] DCs are activated by recognition of danger signals through their pattern recognition receptors (PRRs), inducing increased expression of surface molecules such as MHC class II and CD86, and increased cytokine secretion. Upon contact with naïve T cells in the lymph nodes, T cells recognise their epitope through the T cell receptor (signal one) and receive costimulation through binding of other surface molecules (signal two). The cytokines secreted by the DC, and other surrounding cells convey information to the T cell causing it to tailor its response to type of pathogen involved (T cell polarisation).

Subsequent activation of the naïve T cell requires at least two sets of signals: firstly, the T cell receptor (TCR) and the surface molecule CD4 must engage with the peptide-MHC class II complex on the DC; secondly, costimulatory molecules on the DC must bind to their corresponding molecules on the T cell, (e.g. CD80/CD86-CD28). Together, these signals

induce interleukin-2 (IL-2) gene transcription, secretion and increased expression of the IL-2 receptor (CD25).[56,57] IL-2 is a T cell growth factor, promoting survival and proliferation of the original antigen-specific T cell *via* clonal expansion.[58]

Polarising cytokines provide the third signal for full activation and differentiation of naïve T cells.[59] Crucially, DCs are able to convey information from the site of infection to naïve $CD4^+$ T cells, directing development into helper T cells (T_h cells) optimised to deal with the specific pathogen involved.[47] Briefly, T_h1 cells are best suited to combating intracellular pathogens such as viruses whilst T_h2 are more effective against extracellular pathogens such as parasites.[60] A more detailed discussion of T_h subsets and their functions can be found in the introduction to Chapter Four.

Furthermore, signals supplied by the T cell to the DC, e.g. through binding of CD40 with CD40 ligand, stimulate greater expression of additional costimulatory molecules on the DC itself.[61,62] This enhancement in DC costimulatory ability by $CD4^+$ T cells is referred to as 'DC licensing' and is covered in more detail in the introduction to Chapter Four. Consequently, the DC is able to activate $CD8^+$ naïve T cells which recognise their epitope in MHC class I molecules. Activated $CD8^+$ T cells can develop into cytotoxic lymphocytes (CTLs), which are essential in combating intracellular pathogens, such as viruses, as they are capable of recognising infected cells by scanning their MHC Class I molecules and triggering apoptosis (controlled cell death).

1.2.5 Immunological memory

Effector T cells (T_h cells and CTLs) migrate to the site of infection to contribute to the overall immune response. Once an infection has been cleared it is no longer essential to maintain elevated numbers of these cells. However, retaining a pool of antigen specific memory T cells is advantageous should the infection ever be encountered again. It is proposed that this pool of memory T cells consists of sub-populations: effector memory (T_{EM}) cells, which migrate to the infected tissue and central memory (T_{CM}) cells which reside in the secondary lymphoid organs.[63] T_{CM} cells act as a reservoir and will rapidly proliferate and differentiate into effector T cells upon reinfection. More detailed discussion of effector and memory T cells may be found in the introduction to Chapter Four.

1.3 Vaccines and adjuvants

Vaccines usually comprise two active components: the antigen and the adjuvant. The antigen represents the biological 'target' of the vaccine. This must be in a form that provides sufficient information for the body to recognise the actual pathogen, but is safe enough to be administered without great risk to the patient. It has been found that immunisation is greatly enhanced when the antigen is used in conjunction with an adjuvant. This is a material that provides 'danger signals' thereby triggering immune responses, but does not directly confer immunity.

Vaccination dates back to sixteenth century China, where immunity to smallpox was induced in children by variolation, or even by wearing the unwashed clothes of a smallpox sufferer.[64] Modern vaccination originates in the pioneering work of Edward Jenner in the eighteenth century. Since then control of diseases including smallpox, poliomyelitis, mumps, measles, rubella, pertussis and tetanus has been achieved.[65] However, many challenges in vaccine development still exist; for example, the appearance of human immunodeficiency virus (HIV) several decades ago has yet to see an effective vaccine developed. Specific features of this virus, such as its rapid mutation rate, complement inhibition, effect on MHC class I complexes, and CD4-binding ability make it particularly difficult to develop a vaccination strategy against.[66–68] However, work done identifying common HIV envelope proteins and the antibodies that recognise them may be paving the way for future innovation in this field.[69]

With the prolonged lifetimes in the developed world afforded by improvements in medicine, hygiene and nutrition new problems emerge: increased occurrences of certain cancer types[70] and diseases associated with aging populations, for instance dementia. Vaccinations against viruses associated against some varieties of cancer, for example hepatitis B and liver cancer have proved effective,[71] and it is hoped that the recent vaccination campaign against human papilloma virus (HPV) will result in a decline in cervical cancer instances too.[72] However, developing vaccines against tumour cells is difficult, as all targets involved are made by the host, so subtle differences between healthy and cancerous cells must be utilised and the issue of tumour tolerance overcome.[73] Currently, only one licensed anti-cancer vaccine is approved for use in the USA.[74] One critical problem that needs to be addressed is the inability of current vaccines to induce a strong cytotoxic lymphocyte (CTL) response.[75] This is crucial for adequate defence to be conferred against intracellular pathogens, such as viruses, and for destruction of cancerous cells.

At present, only diseases affecting large markets in wealthy countries tend to merit vaccine development, due to the need for companies to recoup the high costs of research and clinical trials through sales. Consequently, research into vaccination against diseases affecting the developing world is often underfunded.[76] Recently, this has become particularly evident in the Ebola outbreak in West Africa; the rarity or Ebola and lack of commercial opportunities in vaccination have meant that any candidate vaccines are only in the early stages of development.[77,78]

1.3.1 Types of vaccine

The earliest vaccines, such as the use of the cowpox virus to immunise against related smallpox virus, employed whole organisms.[79] Inactivating entire pathogens using chemicals has proved effective, for example, the poliovirus in the Salk poliovaccine is inactivated by cross-linking the proteins with formaldehyde.[80] Another approach to using the entire pathogen is to weaken it to produce an attenuated vaccine. This method was employed in the live-attenuated oral polio vaccine developed by Sabin, where the virus was grown in non-human tissue to promote weakening mutations.[81,82] Other viral diseases that have been successfully prevented with live-attenuated vaccines include influenza and mumps.[76,84] Live-attenuated vaccines have the advantage that, unlike other vaccines, the virus is still able to infect APCs. Virus-derived peptides can be presented on MHC class I molecules thus stimulating the production of CTLs. On the other hand, safety concerns around *in vivo* mutations leading to more virulent strains developing, alongside the risks posed to immunosuppressed individuals mean this strategy cannot be used universally.[85]

A different method of vaccination is to use an acellular vaccine; instead of a whole organism, a characteristic part of the pathogen, for example a protein, is used to 'educate' the recipient's immune system. One example of this is the hepatitis B sub-unit vaccine which uses small particles of the envelope protein hepatitis B surface antigen. Initially this was isolated from the blood of carriers and inactivated with formalin but subsequently methods were developed allowing it to be grown in yeast cells.[86,87] Inactivated bacterial toxins ('toxoids') may also be used, for example in combined vaccines against diphtheria and tetanus.[88] If a vaccinated individual contracts the disease, they are then able to make antibodies that can neutralise the harmful toxins secreted by the pathogen. While these vaccines are very safe, the lack of an actively infectious agent means resulting CTL responses are poor. Often, this is not an issue, as the pathogen itself is not reliant on infecting host cells, and generation of memory B cell and helper T cell responses alone are sufficient to confer long-term immunity. However, it

means great thought must be put in to using similar tactics to combat organisms that do infect host cells.

In the 1990s, gene-based techniques have been developed in which plasmid DNA encoding the vaccine antigen is used to confer immunity.[89] Following transfection of the DNA, the cellular machinery synthesises the antigen, resulting in presentation on both MHC class I and II surface molecules.[65] This approach has promise not just for vaccination against infectious agents, but also for cancer and autoimmune diseases,[90] since the antigen encoded in the DNA may also be a self-antigen. However, limitations have been discovered: uptake of the DNA into APCs is often inefficient, although techniques employing microparticles are being investigated to combat this,[91] and stimulation of the innate immune system is poor. Nevertheless, there are signs that this approach may be effective for combating genetically diverse viruses such as HIV.[92]

1.3.2 Adjuvant materials

Whilst 'old-fashioned' live vaccines, such as that against yellow fever, are extremely valuable, most modern vaccines are acellular and often struggle to elicit strong immune responses in isolation, requiring an adjuvant to work effectively.[79,93] Adjuvants provide additional 'danger' signals to the recipient, triggering a strong response from the innate immune system leading to a more robust adaptive immune response as well. A large number of materials, both biological and synthetic, have been tested but only a few have been licensed for use in humans (Table 1.1).[94] As the primary cell linking the innate and adaptive immune systems, DC activation is crucial for an adjuvant to be effective.[95] Therefore studying the responses of DCs *in vitro* to adjuvant materials is a useful starting point for establishing their potential utility.

Table 1.1: Details of commercial vaccine adjuvants, both licensed and unlicensed.[94]

Adjuvant name (year licensed)	Adjuvant class	Components	Vaccines (disease)
Adjuvants licensed for use in human vaccines			
Alum* (1924)	Mineral salts	Aluminium phosphate or aluminium hydroxide	Various
MF59 (Novartis; 1997)	Oil-in-water emulsion	Squalene, polysorbate 80 (Tween 80; ICI Americas), sorbitan trioleate (Span 85; Croda International)	Fluad (seasonal influenza), Focetria (pandemic influenza), Aflunov (pre-pandemic influenza)
AS03 (GlaxoSmithKline; 2009)	Oil-in-water emulsion	Squalene, Tween 80, α-tocopherol	Pandremix (pandemic influenza), Prepandrix (pre-pandemic influenza)
Virosomes (Berna Biotech; 2000)	Liposomes	Lipids, hemagglutinin	Inflexal (seasonal influenza), Epaxal (hepatitis A)
AS04* (GlaxoSmithKline; 2005)	Alum-absorbed TLR4 agonist	Aluminium hydroxide, MPL	Fendrix (hepatitis B), Cervarix (human papilloma virus)
Vaccine adjuvants tested in humans but not licensed for use			
CpG 7909, CpG 1018	TLR9 agonist	CpG oligonucleotides alone or combined with alum/emulsions	–
Imidazoquinolines	TLR7 and TLR8 agonists	Small molecules	–
Poly I:C	TLR3 agonist	Double-stranded RNA analogues	–
Pam3Cys	TLR2 agonist	Lipopeptide	–
Flagellin	TLR5 agonist	Bacterial protein linked to antigen	–
Iscomatrix	Combination	Saponin, cholesterol, dipalmitoylphosphatidylcholine	–
AS01	Combination	Liposome, MPL, saponin (QS21)	–
AS02	Combination	Oil-in-water emulsion, MPL, saponin (QS21)	–
AF03	Oil-in-water emulsion	Squalene, Montane 80, Eumulgin B1 PH	–
CAF01	Combination	Liposome, DDA, TDB	–
IC31	Combination	Oligonucleotide, cationic peptides	–

AF03, adjuvant formulation 03; CAF01, cationic adjuvant formulation 01; DDA, dimethyldioctadecylammonium; MPL, monophosphoryl lipid A; Pam3Cys, tripalmitoyl-S-glyceryl cysteine; Poly I:C, polyinosinic–polycytidylic acid; TDB, trehalose dibehenate; TLR, Toll-like receptor. *Adjuvants licensed in the United States.

1.3.2.1 Biological and molecular adjuvants

A number of biological and molecular adjuvants have been investigated, and are discussed in detail in the review by Petrovsky and Aguilar.[96] TLR agonists naturally promote strong immune responses therefore are obvious adjuvant candidates. However, only one, a monophosphoryl lipid A derivative, in combination with alum (AS04 from GlaxoSmithKline, Table 1.1) is licensed for use in humans.[97,98] The potency of TLR ligand based adjuvants can lead to excessive inflammatory responses and development of autoimmune disease, raising serious safety concerns. For instance, adverse reactions to the unmethylated CpG adjuvant (a TLR9 agonist) halted the Heplisav hepatitis B vaccine trial.[99] Other TLR agonists studied include Imiquimod, Resiquimod (both TLR7 agonists);[100,101] lipopolysaccharide (a TLR4 agonist);[102] and poly I:C (a TLR3 agonist).[103] It may also be argued that widely-used whole organism live/attenuated vaccines harness the immunostimulatory properties of the TLR agonists they contain, e.g. in the yellow fever vaccine.[104]

Activation of the immune system may also be achieved by administering cytokines as an adjuvant, either directly in the formulation,[105] or encoded in plasmid DNA.[106,107] Plant based materials such as polysaccharides,[108,109] and saponins have also received attention.[110] Liposomes, artificial vesicles comprising a lipid bilayer, may also be used as both an adjuvant

and as a delivery vector for the antigen.[111] They have been used in combination with other adjuvants to modify their activity, for example, cholesterol containing liposomes mediate the cellular damage caused by the cholesterol binding saponin QS21,[112] or liposomes complexed to TLR agonists.[113]

1.3.2.2 Alum adjuvants

The word 'alum', as used by immunologists, refers to a broad class of aluminium containing materials. Originally, vaccine formulations were created by precipitation of a bacterial toxin with a metal salt, then re-dissolving in a suitable solvent to purify. However, when immunising guinea-pigs against diphtheria in the 1920s, Glenny *et al*. discovered that using the insoluble precipitate directly was more successful than using the purified toxoid.[114] Nearly one hundred years later alum is still the most widely used adjuvant in humans.[115] Examples of vaccines containing alum adjuvants include the diphtheria-tetanus-pertussis combination vaccine, and the Hepatitis A, HPV and pneumococcal vaccines.[116]

An assortment of commercial alums exist, containing a number of inorganic materials (Figure 1.2): aluminium hydroxide [$Al(OH)_3$, which is able to activate complement],[117] aluminium oxyhydroxide [boehmite – AlO(OH)], amorphous aluminium phosphate [$Al(PO_4).x(H_2O)$], magnesium hydroxide [$Mg(OH)_2$] and aluminium potassium sulphate ($AlK(SO_4)_2$], alongside buffers and stabilisers.[2,115,118] Originally, the term 'alum' referred to aluminium potassium sulphate, [$AlK(SO_4)_2$] as used by Glenny *et al*.[114] but is now used more generally to refer to any aluminium-containing inorganic adjuvant.

Batch-to-batch variability has been noted in alum adjuvants in the past, suggesting that the physicochemical properties of the material, such as pH, particle size and electrical charge, can affect the immunological response.[119] Hogenesch and Hem draw further attention to the variations in structure, isoelectric points, pH, morphology, electrostatics, adsorption and ligand exchange properties found in commercial alums in their review.[118]

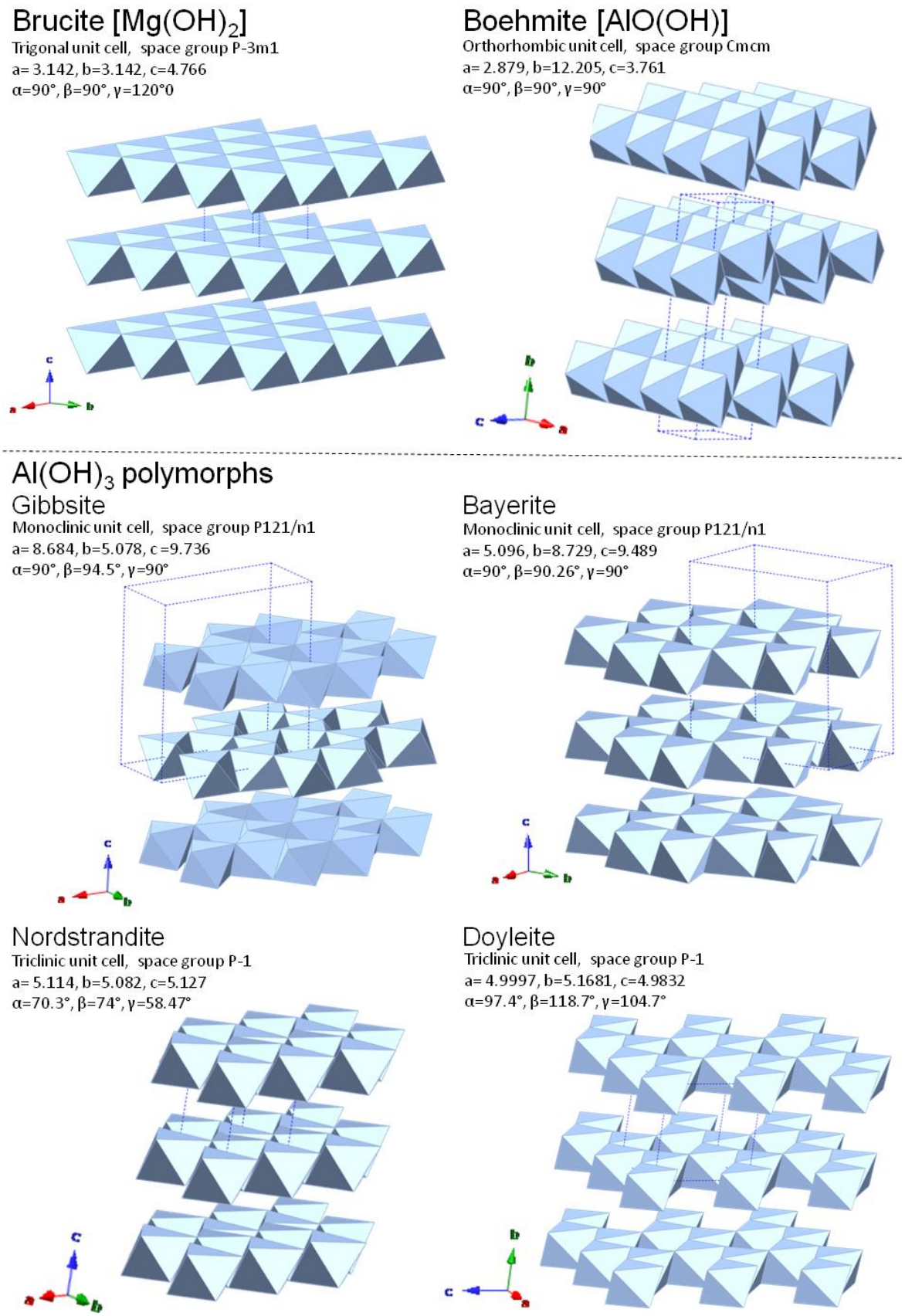

Figure 1.2: Crystal structures for crystalline inorganic materials commonly found in alum adjuvants. $Mg(OH)_2$ (Brucite);[120] Aluminium oxhyhydroxide [AlO(OH) – boehmite];[121] and four polymorphs of $Al(OH)_3$: gibbsite,[122] bayerite,[123] nordstrandite,[124] and doyleite.[125] All structures are based around layers of edge-sharing $M(OH)_6$ octahedra.

1.3.2.3 Alternative inorganic adjuvants

Another commonly used adjuvant formulation is oil-in-water emulsions. These may take the form of mineral oils, such as paraffin oil, with a surfactant (mannide mono-oleate), known incomplete Freund's adjuvant.[126] Complete Freund's adjuvant also contains mycobacteria.[127] It has not been used in humans due to its toxicity, but has been used extensively in animal studies.[126] In humans, the related squalene-in-water emulsion adjuvant, MF59, has been licensed for use in influenza vaccines (Table 1.1).[128,129] As with alum adjuvants, their mechanism of action has not been clearly defined, but is thought to involve enhanced antigen uptake and induction of a local inflammatory response, leading to recruitment of other cells of the innate immune system.[129]

Due to the success of alum adjuvants, adjuvant properties of other crystalline inorganic materials have been investigated. Aluminium oxyhydroxide [AlO(OH)], a component of some alum adjuvants, is readily synthesised in a variety of shapes and morphologies.[130] In combination with PAMPs (extracts from *tubercle bacillus*) Wang *et al*. reported enhanced uptake by macrophage-like cells, and increased GM-CSF and IL-4 concentrations relative to commercial alum in mice.[131] Other simple inorganic materials such as calcium phosphate are also effective: He and co-workers detail improvements in immunisation of mice against herpes simplex virus and Epstein Barr virus with calcium phosphate nanoparticles over commercial alums.[132] Calcium phosphate has also been utilised as a biodegradable platform for CpG DNA (a TLR 9 agonist) to create a combined particulate-molecular adjuvant.[133] Other metal-based materials that have also been tested for immunostimulatory ability include gold nanorods, spheres and cubes;[134,135] and silver,[136] cobalt oxide[137] and zinc oxide nanoparticles.[138]

The ability of silica to activate the Nalp3 inflammasome and trigger similar immune responses to alum is already known as a result of silicosis (fibrotic pulmonary disease).[139] Research into bovine serum albumin (BSA) loaded silica microspheres and silica particles illustrated that these immunostimulatory effects could be harnessed in a controlled manner.[140,141]

1.3.3 Mechanism of action of alum adjuvants

1.3.3.1 The depot effect

The mechanism of action of alum adjuvants is still subject to debate and as yet there is no definitive explanation of how they work. Over the years various hypotheses have been put

forward but early ideas considered their effectiveness was due to a 'depot effect'. It was envisaged that the particulate matter present in the adjuvant adsorbs the antigen onto its surface, providing slow release and also maximising interaction time between the antigen and the APC.[142] However, studies have shown that removal of the injection site after vaccination does not affect the development of the humoral immune response.[143] Furthermore, experiments conducted by Gupta *et al*. with ^{14}C labelled tetanus toxoid adsorbed on $Al(PO_4)$ showed that, after four weeks, only two to three percent of the radioactivity received remained at the injection site.[144] Although doubt has been cast over the prolonged release effects of antigen adsorbed on alum, it is possible that it remains adsorbed for sufficient time to facilitate uptake by APCs.[97]

1.3.3.2 Inflammasomes

The influx of cells to the injection site, observed in *in vivo* responses to alum, requires an induction of inflammation by the local cells that come into contact with the vaccine mixture.[145] Crucially, it has been shown that activation of the innate immune system by alum does not involve toll-like-receptor (TLR) activation but is nevertheless able to induce pro-inflammatory cytokine secretion.[118] This has been corroborated in the findings of Gavin *et al*. that MyD88 and TRIF deficient mice still develop antibody responses to antigen co-administered with common adjuvants.[146] Intuitively this makes sense: TLRs are designed to detect complex molecular pathogen components as opposed to crystalline materials. Experiments using gene knock-out mice have implicated the Nalp3 inflammasome in the immune response to alum.[147,148]

Inflammasomes are cytosolic multi-protein complexes assembled when NLRs recognise their molecular trigger. Similar to TLRs, these receptors feature leucine rich repeats (LRRs), but are only found in the cytoplasm.[149] Inflammasomes may assemble in response to both microbial stimuli and DAMPs, for example adenosine triphosphate (ATP) and uric acid crystals.[149,150] The NLR Nalp3 (Figure 1.3)[150] comprises an LRR, a nucleotide binding site (NBS) and a pyrin domain (PYD). This interacts with the PYD of the adaptor protein ASC (apoptosis-associated speck-like protein containing a CARD) upon Nalp3 oligomerisation in response to danger signals.[151] In turn, the caspase recruitment domain (CARD) on ASC interacts with the enzyme pro-caspase-1,[152] autocatalytically cleaving it into its two active subunits. These are then able to proteolytically cleave pro-IL-1β into its active form and release of pro-inflammatory cytokines such as IL-1β, IL-18 and IL-33 ensues.[153,154] The identity of the cytokines released has been linked to biasing towards a T_h2 response

overall.[148,154] The combination of the three components, Nalp3, ASC and caspase-1 is referred to as the Nalp3 inflammasome. Specifically Nalp3 is thought to be activated by stress signals, and signs of membrane damage, such as K^+ efflux, have also been implicated.[155]

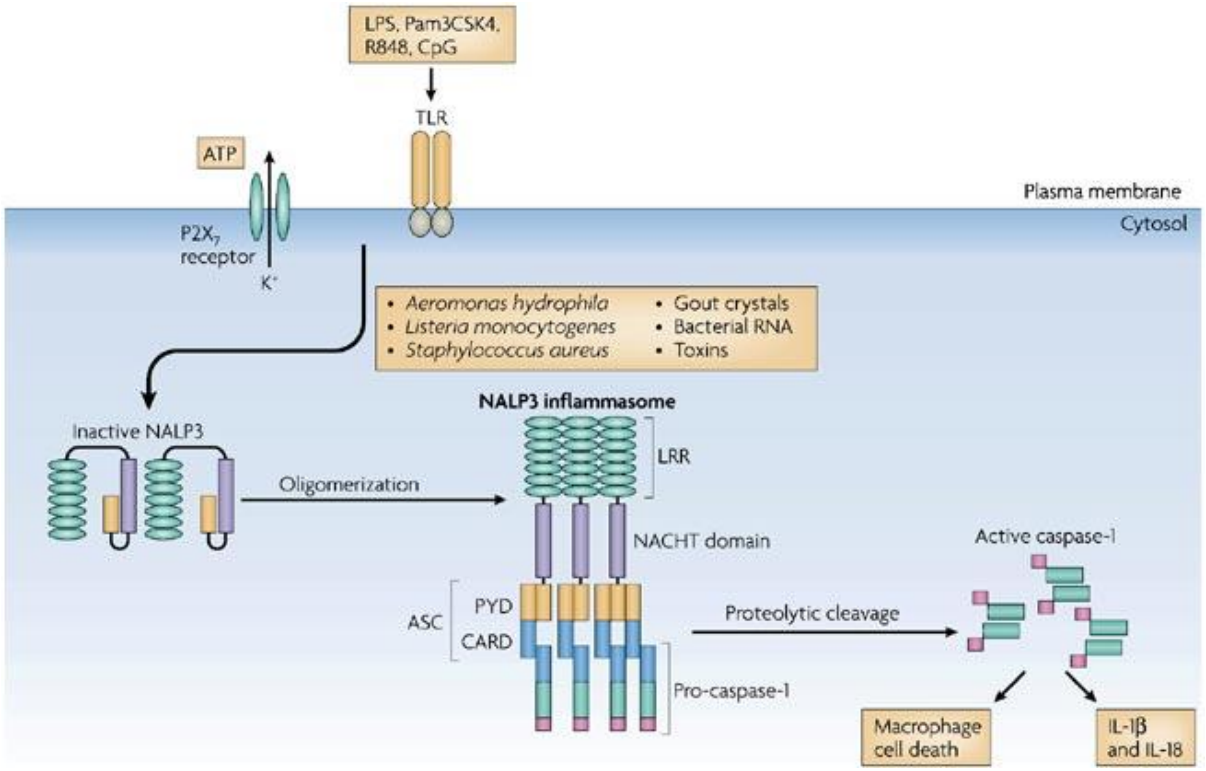

Figure 1.3: Schematic of the activation and assembly of the Nalp3 inflammasome.[150] Nalp3 oligomerises in response to danger signals, interacting with ASC, which is then able to cleave pro-caspase 1 to its active form. The active forms of pro-inflammatory cytokines such as IL-1β, are then produced from their precursors.

1.3.3.3 Nalp3 inflammasome activation

It is possible that alum adjuvants trigger Nalp3 inflammasome activation through analogous mechanisms to other documented crystalline materials, for example silica, asbestos and monosodium urate (MSU). Many reports suggest that uptake of the alum adjuvant *via* phagocytosis is needed for activation of the innate immune system.[5,139,156,157] Indeed, use of uptake inhibitors such as cytochalasin D (an actin polymerisation inhibitor) reveal that uptake is essential for crystalline materials such as silica and MSU to initiate IL-1β production, but not for non-crystalline stimuli such as ATP and the imidazo-quinoline derivative R-848.[139] Frustrated phagocytosis (a process where a phagocyte fails to engulf an object, often because it is too large)[158] produces reactive oxygen species, *via* NADPH oxidase, that have also been implicated in inflammation through the Nalp3 inflammasome in response to asbestos and silica particles.[156]

Upon internalisation, endosomal acidification may cause alum particles to dissolve, resulting in an imbalance in osmotic pressure, lysosomal destabilisation and rupture.[135,139,142,159] The resulting increase in ion concentration within the cell causes aquaporins to open, allowing water into the cell and causing the overall intracellular K^+ concentration to drop. Potassium efflux can act as a danger signal; indeed, some bacteria (e.g. *Aeromonas hydrophila*, *Staphylococcus aureus*) release pore-forming toxins which permeabilise the plasma membrane, causing a decrease in intracellular $[K^+]$.[160] Pétrilli *et al*. demonstrated that Nalp3 inflammasome activation can occur in response to K^+ efflux from cells.[161] Morevoer, K^+ efflux has been implicated in the activation of the Nalp3 inflammasome in *in vitro* studies studies on MSU crystals using lysosomal acidification inhibitors (chloroquine, NH_4Cl), and aquaporin inhibitors (HgCl, phloretin).[162] Furthermore, studies show that placing murine bone marrow-derived DCs in a solution with increased extracellular K^+ concentration can inhibit Nalp3 activation in response to uric acid crystals and other particulate adjuvants.[159]

In addition, alum has been linked to formation of uric acid in *in vivo* studies employing the uricase enzyme, which catalyzes the oxidation of uric acid to 5-hydroxyisourate. Reduced numbers of antigen positive inflammatory monocytes were found when the enzyme was administered to mice alongside alum and OVA antigen.[163] Uric acid is a by-product of necrosis, which also causes cells to secrete pro-inflammatory molecules which could further enhance adjuvant effects.[164] Other molecules linked to necrotic cell death, such as extracellular DNA and ATP have also been proposed as agents involved in the immune response to alum.[165–167] Double-stranded DNA is capable of acting as a DAMP, causing increased expression of MHC class I, II and other co-stimulatory molecules.[168] It has been observed that damage to the surrounding tissue may indirectly activate APCs *via* endogenous stress signals,[143] and these have been shown to act as 'natural adjuvants'.[169]

In conclusion, the possible ways alum triggers Nalp3 activation include direct action of alum particles on the cells, for example, *via* internalisation and membrane rupture, leading to pro-inflammatory cytokine secretion (IL-1β etc); or damage inflicted to one cell resulting in release of DAMPs (DNA, ATP, uric acid) that trigger responses in the surrounding cells; or perhaps most likely, a combination of the two. Secretion of pro-inflammatory cytokines and other chemokines at the local level subsequently leads to recruitment of other cells of the immune system[145] and encourages migration of antigen-loaded DCs to the secondary lymphoid tissues to start the adaptive immune response.[163]

1.3.3.4 Interaction with the cell membrane

Another possible mechanism of activation of cells in response to alum adjuvants involves the interactions between the surface of the crystal and the plasma membrane of the cell. Flach and co-workers highlight the strong affinity of alum crystals for membrane lipids on DCs,[170] leading to a 'lipid sorting' process possibly mediated by hydrogen bonding between the two. The same research group also found a similar process may be involved in interactions between DCs and MSU crystals.[171] They suggest that lipid sorting results in phosphorylation of ITAMs (immunoreceptor tyrosine-based activation motif), Syk (spleen tyrosine kinase) recruitment and activation of the PI3K (phosphoinositide 3-kinase) inflammatory pathway. Their investigations also revealed this process was Nalp3-independent, highlighting another potential pathway for immune responses to alum adjuvants.

1.3.3.5 Cell recruitment

Following injection of alum, the inflammatory response triggered leads to an influx of cells to the injection site. Calabro *et al*. confirmed that, in reactions to both alum and MF59, chemokine concentrations increased and local recruitment of neutrophils, monocytes, eosinophils, macrophages and DCs ensued.[145] Investigations into the initiation of the cellular influx have been conducted. Seubert *et al*.[172] have shown human monocyte-derived DCs (Mo-DCs) and macrophages increase cytokine and chemokine secretion in response to alum (and MF59) adjuvants *in vitro*. Other studies also confirm that exposure to alum is sufficient to induce significant increases in MHC, cell adhesion and costimulatory molecules on human monocytes.[173] Work by Kool *et al*. also shows that alum promotes maturation of monocytes to Mo-DCs *in vivo*.[163] Again, this highlights the utility in studying DC responses to adjuvant materials in order to establish their efficacy.

1.4 Layered Double Hydroxides

Layered double hydroxides (LDHs) are a large family of layered inorganic materials. They exist in both naturally occurring forms, for example as the mineral hydrotalcite discovered in Sweden in the 19th century, and synthetic variants. They have been the subject of sustained interest over the past few decades due to their highly tuneable properties and applications in a diverse array of fields.

LDHs are often discussed alongside other clay-like materials such as montmorillonite, as they have layered structures with readily exchangeable intercalated anions and high internal surface areas.[174] LDHs are sometimes referred to as 'anionic clays' since the interlayer

species are anionic as opposed to cationic. Clay minerals have been used extensively for therapeutic purposes throughout human history, for example as mineral supplements for pregnant women, as preventatives against contact dermatitis, and more recently as adsorption agents for fungal toxins.[175–177]

1.4.1 Structure of layered double hydroxides

The composition of the naturally occurring mineral LDH, hydrotalcite, was elucidated by Manasse as $[Mg_6Al_2(OH)_{16}](CO_3)\cdot 4H_2O$.[178] Subsequently, synthetic versions of hydrotalcite were synthesised and characterised in the 1940s. Feitknecht proposed that their structure consisted of alternating layers of $Mg(OH)_6$ octahedra and $Al(OH)_6$ octahedra, referred to as 'doppelschichtstrukturen" (double sheet structures).[179,180] X-ray crystallographic analysis by Allman disproved this hypothesis, confirming that both cations were present in the same layer.[181]

Overall, the structure is closely related to that of brucite $[Mg(OH)_2]$, which is based on the CdI_2 structure and consists of layers of edge-sharing $Mg(OH)_6$ octahedra held together by hydrogen bonding between the hydroxyl groups (Figure 1.2).[182] In the LDH structure, a portion of the M^{2+} cations are replaced with M^{3+} cations to impart a net positive charge to the layers. This is balanced by the intercalation of charge-compensating anions, the identity of which influences the interlayer spacing [Figure 1.4(a)]. Water molecules are often co-intercalated alongside the anions during synthesis to give the general formula of an LDH as $[M^{z+}_{1-x}M^{3+}_{x}(OH)_2]^{a+}(X^{n-})_{a/n}\cdot mH_2O$.[183] These water molecules are fluxional, forming hydrogen bonds to the metal hydroxide layers, and the quantity present depends on the synthesis parameters such as anion identity and reaction temperature.[184] In the stoichiometric formula, generally $z = 2$ (therefore $a = x$), although exceptions are known. For a pure phase to be obtained, x typically lies in the region 0.2-0.4.[185] Throughout this thesis, LDHs are identified by abbreviated formulae for brevity ($M^{z+}M^{3+}$-X^{n-} LDH, e.g. MgAl-CO_3 LDH), rather than the full stoichiometric formula.

The identities of M^{2+} and M^{3+} are readily altered: commonly reported divalent cations include Mg^{2+}, Ca^{2+}, Fe^{2+}, Mn^{2+}, Co^{2+}, Ni^{2+} and Zn^{2+} whilst known trivalent cations include Al^{3+}, Fe^{3+}, Ga^{3+}, Co^{3+}, V^{3+} and Sc^{3+}.[186] Furthermore, there are reports of 'ternary' and even 'quaternary' LDHs in which more than one type of M^{2+} or M^{3+} cation is integrated into the layers.[187,188] Some flexibility in the charge of the metal cations may be afforded: Li^+ is the only example of a singly charged cation in an LDH, with extra positive charge provided by an

increased proportion of Al^{3+}, for instance in $[LiAl_2(OH)_7]\cdot 2H_2O$.[189] Conversely, it is also possible to synthesise LDHs with cations of a higher charge, such as Sn^{4+}.[190] The inclusion of paramagnetic transition metal ions such as Co^{2+} has led to investigations into their magnetic properties, as the readily tuneable particle size of LDHs permits synthesis of single magnetic domains.[191]

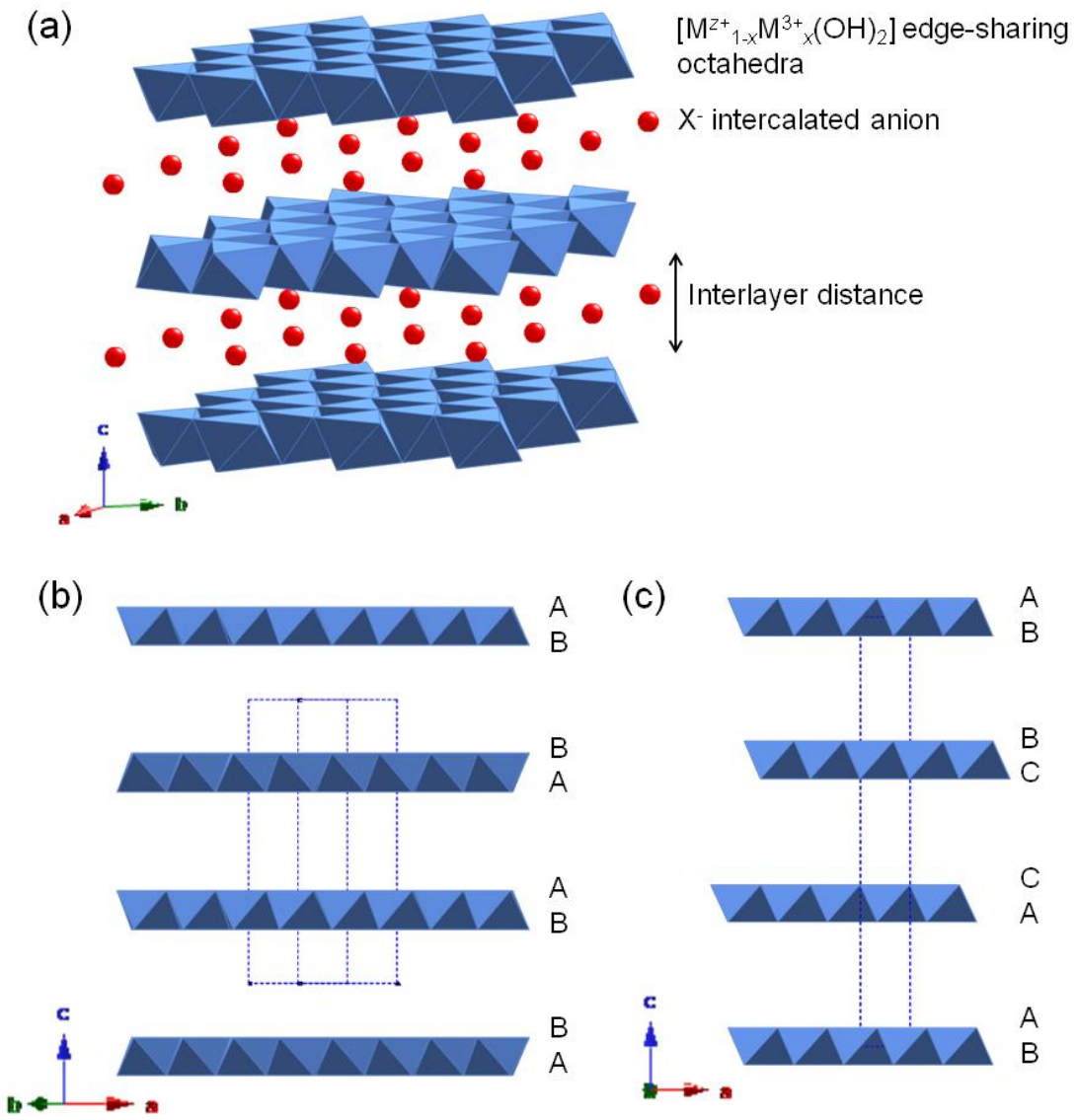

Figure 1.4: (a) General schematic of an LDH structure showing layers of edge-sharing $[M(OH)_6]$ octahedra and intercalated anions; (b) hexagonal (2H) packing sequence;[192] and (c) rhombohedral (3R) packing sequence.[193] Dotted lines indicate the unit cell; A, B and C denote the hydroxide packing sequence relative to the *c*-axis, interlayer anions are omitted for clarity.

Due to their excellent ion exchange capabilities, a vast array of anions have been intercalated into LDHs. These include simple inorganic anions (Cl^-, NO_3^-, OH^-, CO_3^{2-}, F^-, Br^-) and also more complex ions such as organic species (for example, carboxylates such as tartrate and succinate),[194,195] polyoxometalates,[196] C_{60} molecules[197] and coordination complexes.[198] Larger

biologically relevant molecules such as polysaccharides,[199] amino acids,[200] nucleosides, and DNA have also been successfully intercalated into LDHs.[201,202]

LDHs exhibit polymorphism with both rhombohedral (denoted as 3R) and hexagonal (2H) stacking sequences observed, for example in sjorgrenite (hexagonal) and pyroaurite (rhombohedral), both mineral forms of $[Mg_6Fe_2(OH)_{16}](CO_3)\cdot 4H_2O$.[181] The polymorphs are best considered in terms of the position of the hydroxide ions in the layers: if A, B and C indicate hydroxide ion positions whilst *m* and *x* indicating the metal and anion positions, the hexagonal stacking sequence is {A*m*B *x* B*m*A *x* A*m*B *x*...} whereas the rhombohedral sequence is {A*m*B *x* B*m*C *x* C*m*A *x*...} [Figure 1.4(b)/(c)]. Synthetic routes to the different polymorphs have been described, notably for the Li^+ containing LDHs. Selection of the appropriate $Al(OH)_3$ precursor material from gibbsite or bayerite followed by reaction with a lithium salt solution will yield the hexagonal or rhombohedral variant respectively.[203]

1.4.2 Synthesis methods

The most widely used method of LDH synthesis is coprecipitation. A solution of the metal cations is added to a basic solution of the desired anion, and the reaction mixture aged at a specific temperature for a given time. This may be performed under 'high supersaturation' conditions using more concentrated metal solutions and higher pHs, characterised by high rates of nucleation and large numbers of smaller particles.[204,205] 'Low supersaturation' conditions use low reagent concentrations, slow addition times and a pH range typically from 7 to 10.[187] Often, low supersaturation conditions lead to more crystalline materials than high supersaturation conditions, as the rate of crystal growth is greater than that of nucleation.[187] The effects of changing the parameters involved in the coprecipitation method, for example solution concentration, reaction time, aging temperature and pH control, have been extensively investigated.[206,207] Common precursor materials include metal nitrates, chlorides and oxides. Aging methods such as hydrothermal treatment, sonication and microwave irradiation of the reaction mixture have also been explored.[208–210]

Owing to their facile intercalation chemistry, exchange of the interlayer anion for another species is readily achieved by immersing an LDH in a solution of the target anion. This method may be used as an alternative to direct coprecipitation with the target anion, for instance when testing LDHs as a method to remove undesirable anionic species from solution for environmental applications.[211] *In situ* studies have revealed the complexity of this

apparently straight-forward process: anion exchange may proceed directly from reactants to products, or occur in two stages *via* an identifiable intermediate.[212]

Another approach to intercalation utilises the 'memory effect': calcining an LDH at elevated temperature (~600 °C) removes the adsorbed and interlayer water and the anions to afford a layered double oxide (LDO).[213,214] Treatment of the LDO with a solution of the target anion 'reconstructs' the original LDH, but with the target anion incorporated. This approach has had success in intercalation of zwitterionic amino acids, although carbonate ions were also included.[200] Other ways of accomplishing intercalation of uncharged species involve using anionic molecules such as cyclodextrins to create hydrophobic pockets within the LDH into which neutral species (e.g. ferrocene) may reside.[215]

More complex LDH synthesis methods have also been developed, often producing novel morphologies. Gunawan *et al*. used a non-aqueous solvent/surfactant approach (ethylene glycol/methanol/sodium dodecyl sulphate) to produce coral-like porous microspheres.[216] Surfactant molecules have also found use in the 'reverse micelle' method, where they form water droplet micro-reactors in oil-in-water emulsions, thus allowing careful tailoring of LDH particle size.[217] Composite materials, comprising a 'core-shell' structure have recently been gaining interest: growth of LDH particles on Fe_3O_4 microspheres produces particles that are not only magnetic, but incorporate the ion-exchange/release characteristics of an LDH.[218,219] Additionally, it is possible to remove the core template providing a route to hollow LDH spheres.[220] Cation-exchanged polymer resin beads may also be used as both the metal ion source and the scaffold on which highly orientated LDH crystals form.[221]

1.4.3 Post-synthesis modifications

Occasionally, it is desirable to modify the properties of an LDH after synthesis, for example to increase the surface area or to functionalise the surface. One way of achieving the former objective is to use the aqueous miscible organic solvent treatment (AMOST): newly-synthesised LDH particles are dispersed in a solvent such as methanol or acetone before drying.[222] This replaces the water adsorbed on the surface with more hydrophobic solvent molecules, leading to exfoliation of the LDH layers, minimal aggregation and very high surface areas (> 200 m^2g^{-1}). Delamination to single layers may also be achieved in formamide using sonication or agitation, or by using high shear conditions.[223–225] Post-synthesis mechanical treatment of LDHs can be used to increase surface area and reduce crystallite size, although extensive milling times do result in agglomeration and breakdown of

the crystal structure.[226] Exfoliation/delamination to yield an LDH with greater surface area is useful in catalyst supports, as higher numbers of active sites per unit mass may be achieved.[222]

Functionalisation of an LDH surface may be attempted for a number of reasons. Binding of certain biological ligands could target the LDH particles to specific cell types/cellular uptake pathways which has applications in gene therapy and drug delivery.[227] For instance, Tyner and co-workers managed to intercalate the non-ionic cytotoxic drug camptothecin in anionic surfactant micelles into MgAl LDHs.[228] It was found that modifying the LDH surface with various succinimidyl molecules, then conjugating proteins and biopolymers could improve targeting, notably for the human A33 membrane antigen, a biomarker for colon cancer.[229] Grafting silyl groups onto LDH surfaces increases their hydrophobicity which may be useful for improving the dispersal characteristics in organic solvents and polymers, and provides a means of cross-linking LDH particles.[230,231] Wang *et al*. probed the use of amino silanes to improve CO_2 absorption characteristics[232] and they have also been investigated as additives to improve the flame retardant properties of polymers.[233] Grafting of fluorescent molecules onto LDHs has also found use in imaging cell-particle interactions.[234]

1.4.4 General applications of LDHs

Several uses for LDHs have already been mentioned, however, a significant number of other applications exist. The LDHs themselves may be used as precursors in the synthesis of other inorganic compounds, such as spinels and LDOs.[235,236] Moreover, LDHs have generated interest as basic catalysts for a number of reactions including oxidation of phenol,[237] methanol,[238] and methane;[239] oxidative bromination;[240] conversion of acrylonitrile to acrylamide;[241] and in preparation of propylene glycol monomethyl ether.[242] Detailed microscopy studies of LDH-catalysed esterification/ester hydrolysis reactions have shown that the reaction catalysed may depend onto which crystal face of the LDH the substrates attach.[243] By incorporating transition metal ions into the LDH structure it is possible to create semiconductors in which defects in the structure serve to prevent electron-hole recombination, leading to their investigation as candidate materials for water splitting photocatalysts.[244]

LDHs have also found use as a support materials for other catalytic species for example, supporting gold nanoparticles for CO oxidation,[245] palladium complexes for coupling reactions,[246] and iron porphyrins for oxidation reactions.[247] A thorough review of LDH uses in

catalysis may be found here,[248] highlighting the wider aims of using LDHs in catalysis such as greenhouse gas storage/decomposition, or removal of volatile organic compounds from waste.

The adsorption and anion exchange characteristics of LDHs have been exploited in a number of different fields. They may be used to capture undesirable anionic waste products from water streams by intercalation or adsorption, releasing harmless anions instead. Removal of pollutants such as reactive dyes,[249] 2-chlorophenol (a carcinogen)[250] and other chlorinated organic molecules with LDHs has been probed.[251] Alternatively, LDHs may be employed as a means of storing and releasing molecules in a controlled fashion. This is desirable for stable retention of food additives e.g. vitamins and flavouring compounds.[252,253] Intercalation of dye molecules (fluorescein, methyl orange, ammonium 1-anilinonaphthalene-8-sulfonate)[254–256] into LDHs may prove useful in optical devices, photoluminescent materials or in water hardness monitoring *via* replacement of intercalated dye molecules with carbonate, yielding an monitorable colour change.[195]

1.4.5 Biological applications of LDHs

LDHs have found use in an enormous number of biological applications due to their low toxicity.[6] One major use of LDHs in biology is as drug deliver vectors, reviewed here by Yang and Sheldon.[257] Intercalation of drug molecules yields a number of advantages in their stability,[257] slow release within the therapeutic window and in the appropriate area of the body, taste masking[258] and targeting to specific cells.[228] Examples of successfully intercalated drugs include anti-inflammatory agents ibuprofen[259] and fenbufen;[260] the anti-cancer drug methotrexate;[261] leishmaniasis treatments;[262] antibiotics;[263] levadopa (a treatment for Parkinson's disease)[264] and angiotensin-converting enzyme inhibitors such as captopril.[265] The anti-coagulant heparin has also been intercalated in the hope that this will increase its half-life *in vivo*.[266]

Other biological applications of LDHs utilise their adsorption characteristics, e.g. in protein purification,[218] or as anti-microbial materials. This is either by virtue of intercalating antimicrobial anions such as ortho-hydroxybenzoate or as biogranulation reagents which aggregate bacteria to facilitate their removal from waste water.[267,268] Their potential use as bone tissue engineering scaffolds has also been documented, as they may be synthesised to contain the same elements as those found in bone (Ca, Mg) and have demonstrated good compatability with osteosarcoma cells.[269]

1.4.6 LDHs as adjuvants

Due to their similar structure and chemical make-up to materials commonly found in alums (Figure 1.2), it was hypothesised by Williams *et al*. that layered double hydroxides (LDHs) would also be effective as adjuvants.[8] Subsequent experiments proved they could promote DC maturation *in vitro*, and antigen-specific antibody responses in mice.[8] The magnitude and nature of these responses could be statistically modelled using a subset of the physicochemical properties of the LDH material. As a result of this, the response to different LDH compositions could be accurately predicted, indicating a relationship between the chemistry of a material and its immunostimulatory properties. Li *et al*. have also demonstrated the ability of LDHs to promote DC maturation,[270] leading to exploration of their use as a combined delivery vectors and adjuvant in plasmid DNA vaccines.[271] Recent work in rabbits has highlighted enhanced antibody production in response to LDHs and mineral oils over mineral oil adjuvants alone.[272]

1.5 Aims of this thesis

The principal aim of this thesis is to explore immune responses to LDHs with a view to their use as adjuvants. Specifically, three areas were identified for investigation. Firstly, determining the effect of altering LDH particle size on immune responses, as only a limited number of other studies have focussed on the particle size of materials in the context of immunology or adjuvant design. Moreover, by introducing particle size as an additional variable, the validity of using the physicochemical properties of LDHs as predictors of immune responses will be corroborated.

Secondly, probing the responses of human T cells to LDH-stimulated Mo-DCs. These responses could affect the possible applications of vaccines containing LDH adjuvants, as these materials may alter the extent and kinetics of T cell proliferation, or elicit a specific pattern of T cell polarisation.

Thirdly, starting to explore the processes through which LDH particles interact with DCs to induce immune responses. Overall, it was hoped the research conducted would bring to light relationships between immune response and the chemical properties of LDHs, and highlight factors to consider when investigating and developing inorganic materials as adjuvants.

1.6 References

(1) Lindblad, E. B. *Vaccine* **2004**, *22*, 3658.
(2) Marrack, P.; McKee, A. S.; Munks, M. W. *Nat. Rev. Immunol.* **2009**, *9*, 287.
(3) Fisher, H. *Part II Thesis: Biomedical Applications of Layered Metal Hydroxides*; University of Oxford, 2010; pp. 16–29.
(4) Vaccine Safety & Availability, U.S. Food and Drug Administration http://www.fda.gov/BiologicsBloodVaccines/SafetyAvailability/VaccineSafety/ucm187810.htm.
(5) Brewer, J. M. *Immunol. Lett.* **2006**, *102*, 10.
(6) Delhoyo, C. *Appl. Clay Sci.* **2007**, *36*, 103.
(7) Kuang, Y.; Zhao, L.; Zhang, S.; Zhang, F.; Dong, M.; Xu, S. *Materials (Basel)*. **2010**, *3*, 5220.
(8) Williams, G. R.; Fierens, K.; Preston, S. G.; Rysnik, O.; Lunn, D.; De Prijck, S.; Kool, M.; Buckley, H.; Austyn, J. M.; O'Hare, D.; Lambrecht, B. N. *J. Exp. Med.* **2014**, *211*, 1019.
(9) MacPherson, G.; Austyn, J. *Exploring Immunology: Concepts and Evidence*; 1st ed.; Wiley-Blackwell, 2012.
(10) Muñoz-Planillo, R.; Kuffa, P.; Martínez-Colón, G.; Smith, B. L.; Rajendiran, T. M.; Núñez, G. *Immunity* **2013**, *38*, 1142.
(11) Kirby, A. C.; Raynes, J. G.; Kaye, P. M. *J. Infect. Dis.* **2006**, *193*, 205.
(12) Mann, E. R.; Landy, J. D.; Bernardo, D.; Peake, S. T. C.; Hart, A. L.; Al-Hassi, H. O.; Knight, S. C. *Immunol. Lett.* **2013**, *150*, 30.
(13) Merad, M.; Ginhoux, F.; Collin, M. *Nat. Rev. Immunol.* **2008**, *8*, 935.
(14) Jones, B. W.; Means, T. K.; Heldwein, K. A.; Keen, M. A.; Hill, P. J.; Belisle, J. T.; Fenton, M. J. *J. Leukoc. Biol.* **2001**, *69*, 1036.
(15) Beutler, B. *Nature* **2004**, *430*, 257.
(16) Akira, S.; Takeda, K. *Nat. Rev. Immunol.* **2004**, *4*, 499.
(17) Baeuerle, P. A.; Henkel, T. *Annu. Rev. Immunol.* **1994**, *12*, 141.
(18) Stahl, P. D.; Ezekowitzt, R. A. B. *Curr. Opin. Immunol.* **1998**, *10*, 50.
(19) Stuart, L. M.; Ezekowitz, R. A. B. *Immunity* **2005**, *22*, 539.
(20) Peiser, L.; Mukhopadhyay, S.; Gordon, S. *Curr. Opin. Immunol.* **2002**, *14*, 123.
(21) Inohara, N.; Nuñez, G. *Nat. Rev. Immunol.* **2003**, *3*, 371.
(22) Kummer, J. A.; Broekhuizen, R.; Everett, H.; Agostini, L.; Kuijk, L.; Martinon, F.; van Bruggen, R.; Tschopp, J. *J. Histochem. Cytochem.* **2007**, *55*, 443.
(23) Shi, Y.; Evans, J. E.; Rock, K. L. *Nature* **2003**, *425*, 516.
(24) Lanzavecchia, A.; Sallusto, F. *Cell* **2001**, *106*, 263.
(25) Chapuis, F.; Rosenzwajg, M.; Yagello, M.; Ekman, M.; Biberfeld, P.; Gluckman, J. C. *Eur. J. Immunol.* **1997**, *27*, 431.
(26) Austyn, J. M. *J. Exp. Med.* **1996**, *183*, 1287.
(27) Romani, N.; Brunner, P. M.; Stingl, G. *J. Invest. Dermatol.* **2012**, *132*, 872.
(28) Banchereau, J.; Steinman, R. M. *Nature* **1998**, *392*, 245.
(29) Kapsenberg, M. L. *Nat. Rev. Immunol.* **2003**, *3*, 984.
(30) Mckenna, K.; Beignon, A.; Bhardwaj, N. *J. Virol.* **2005**, *79*, 17.
(31) Jarrossay, D.; Napolitani, G.; Colonna, M.; Sallusto, F.; Lanzavecchia, A. *Eur. J. Immunol.* **2001**, *31*, 3388.
(32) Zhou, L.; Tedder, T. F. *Proc. Natl. Acad. Sci. U.S.A.* **1996**, *93*, 2588.
(33) Braciale, T. J.; Braciale, V. L. *Immunol. Today* **1991**, *12*, 124.
(34) Ting, J. P.-Y.; Trowsdale, J. *Cell* **2002**, *109*, S21.
(35) Hasselgren, P. O.; Fischer, J. E. *Ann. Surg.* **1997**, *225*, 307.
(36) Khan, S.; van den Broek, M.; Schwarz, K.; de Giuli, R.; Diener, P.-A.; Groettrup, M. *J. Immunol.* **2001**, *167*, 6859.
(37) Van den Eynde, B. J.; Morel, S. *Curr. Opin. Immunol.* **2001**, *13*, 147.
(38) Rock, K. L.; Gramm, C.; Rothstein, L.; Clark, K.; Stein, R.; Dick, L.; Hwang, D.; Goldberg, A. L. *Cell* **1994**, *78*, 761.
(39) Ortmann, B.; Androlewicz, M. J.; Cresswell, P. *Nature* **1994**, *368*, 864.

(40) Fremont, D. H.; Matsumura, M.; Stura, E. A.; Peterson, P. A.; Wilson, I. A. *Science* **1992**, *257*, 919.
(41) Berger, A. C.; Roche, P. A. *J. Cell Sci.* **2009**, *122*, 1.
(42) Wolf, P. R.; Ploegh, H. L. *Annu. Rev. Cell Dev. Biol.* **1995**, *11*, 267.
(43) Denzin, L. K.; Cresswell, P. *Cell* **1995**, *82*, 155.
(44) Fremont, D. H.; Hendrickson, W. A.; Marrack, P.; Kappler, J. *Science* **1996**, *272*, 1001.
(45) Théry, C.; Amigorena, S. *Curr. Opin. Immunol.* **2001**, *13*, 45.
(46) Reis e Sousa, C. *Nat. Rev. Immunol.* **2006**, *6*, 476.
(47) Guermonprez, P.; Valladeau, J.; Zitvogel, L.; Théry, C.; Amigorena, S. *Annu. Rev. Immunol.* **2002**, *20*, 621.
(48) Wilson, N. S.; El-Sukkari, D.; Villadangos, J. A. *Immunobiology* **2004**, *103*, 2187.
(49) Münz, C.; Steinman, R. M.; Fujii, S. *J. Exp. Med.* **2005**, *202*, 203.
(50) Martín-Fontecha, A.; Lanzavecchia, A.; Sallusto, F. *Handb. Exp. Pharmacol.* **2009**, *188*, 31.
(51) Huang, F. P.; Platt, N.; Wykes, M.; Major, J. R.; Powell, T. J.; Jenkins, C. D.; MacPherson, G. G. *J. Exp. Med.* **2000**, *191*, 435.
(52) Moll, H.; Fuchs, H.; Blank, C.; Röllinghoff, M. *Eur. J. Immunol.* **1993**, *23*, 1595.
(53) Cose, S. *Immunology* **2007**, *120*, 1.
(54) Reinherz, E. L.; Tan, K.; Tang, L.; Kern, P.; Liu, J.; Xiong, Y.; Hussey, R. E.; Smolyar, A.; Hare, B.; Zhang, R.; Joachimiak, A.; Chang, H.-C.; Wagner, G.; Wang, J. *Science* **1999**, *286*, 1913.
(55) Ingulli, E.; Mondino, A.; Khoruts, A.; Jenkins, M. K. *J. Exp. Med.* **1997**, *185*, 2133.
(56) Keir, M. E.; Sharpe, A. H. *Immunol. Rev.* **2005**, *204*, 128.
(57) Umlauf, S. W.; Beverly, B.; Lantz, O.; Schwartz, R. H. *Mol. Cell. Biol.* **1995**, *15*, 3197.
(58) Malek, T. R. *Annu. Rev. Immunol.* **2008**, *26*, 453.
(59) Curtsinger, J. M.; Schmidt, C. S.; Mondino, A.; Lins, D. C.; Kedl, R. M.; Jenkins, M. K.; Mescher, M. F. *J. Immunol.* **1999**, *162*, 3256.
(60) Zhu, J.; Paul, W. E. *Blood* **2008**, *112*, 1557.
(61) Cella, M.; Scheidegger, D.; Palmer-Lehmann, K.; Lane, P.; Lanzavecchia, A.; Alber, G. *J. Exp. Med.* **1996**, *184*, 747.
(62) Libby, P. *Cell. Mol. life Sci.* **2001**, *58*, 4.
(63) Sallusto, F.; Geginat, J.; Lanzavecchia, A. *Annu. Rev. Immunol.* **2004**, *22*, 745.
(64) Plotkin, S. *History of vaccine development*; Springer: New York, 2011.
(65) Nabel, G. J. *N. Engl. J. Med.* **2013**, *368*, 551.
(66) Finlay, B. B.; McFadden, G. *Cell* **2006**, *124*, 767.
(67) Alcami, A.; Koszinowski, U. H. *Trends Microbiol.* **2000**, *8*, 410.
(68) Ryu, S.-E.; Kwong, P. D.; Truneh, A.; Porter, T. G.; Arthos, J.; Rosenberg, M.; Dai, X.; Xuong, N.; Axel, R.; Sweet, R. W.; Hendrickson, W. A. *Nature* **1990**, *348*, 419.
(69) Forsell, M. N. E.; Soldemo, M.; Dosenovic, P.; Wyatt, R. T.; Karlsson, M. C. I.; Karlsson Hedestam, G. B. *J. Immunol.* **2013**, *191*, 44.
(70) Parkin, D. M.; Bray, F.; Ferlay, J.; Pisani, P. *CA. Cancer J. Clin.* **2002**, *55*, 74.
(71) World Health Organisation. Hepatitis B (Fact Sheet No.204).
(72) Markwoitz, L. E.; Dunne, E. F.; Araiya, M.; Lawson, H. W.; Chesson, H.; Unger, E. R. *Centers for Disease Control and Prevention: Morbidity and Mortality Weekly Report* **2007**, *56*.
(73) Rivoltini, L.; Canese, P.; Huber, V.; Iero, M.; Pilla, L.; Valenti, R.; Fais, S.; Lozupone, F.; Casati, C.; Castelli, C.; Parmiani, G. *Expert Opin. Biol. Ther.* **2005**, *5*, 463.
(74) Vonderheide, R. H.; Nathanson, K. L. *Nat. Med.* **2013**, *19*, 1098.
(75) Dubensky, T. W.; Liu, M. A.; Ulmer, J. B. *Mol. Med.* **2000**, *6*, 723.
(76) Hotez, P. J.; Molyneux, D. H.; Fenwick, A.; Kumaresan, J.; Sachs, S. E.; Sachs, J. D.; Savioli, L. *N. Engl. J. Med.* **2007**, *357*, 1018.
(77) BBC News. Ebola: Experimental drugs and vaccines http://www.bbc.co.uk/news/health-28663217.
(78) World Health Organisation. Ebola Virus Disease (Fact Sheet No.103) http://www.who.int/mediacentre/factsheets/fs103/en/.
(79) Ulmer, J. B.; Valley, U.; Rappuoli, R. *Nat. Biotechnol.* **2006**, *24*, 1377.

(80) Salk, J. *JAMA J. Am. Med. Assoc.* **1959**, *169*, 1829.
(81) Sabin, A. B.; Ramos-Alvarez, M.; Alvarez-Amezquita, J.; Pelon, W.; Michaels, R. H.; Spigland, I.; Koch, M. A.; Barnes, J. M.; Rhim, J. S. *JAMA J. Am. Med. Assoc.* **1960**, *173*, 79.
(82) Sabin, A. B. *J. Infect. Dis.* **1985**, *151*, 420.
(83) Belshe, R. B.; Mendelman, P. M.; Treanor, J.; King, J.; Gruber, W. C.; Piedra, P.; Bernstein, D. I.; Hayden, F. G.; Kotloff, K.; Zangwill, K.; Iacuzio, D.; Wolff, M. *N. Engl. J. Med.* **1998**, *338*, 1405.
(84) Hilleman, M. R. In *History of Vaccine Development*; Plotkin, S. A., Ed.; Springer: New York, NY, 2011; pp. 207–218.
(85) Gregory, A. E.; Titball, R.; Williamson, D. *Front. Cell. Infect. Microbiol.* **2013**, *3*, 13.
(86) McAuliffe, V. J.; Purcell, R. H.; Gerin, J. L. *Rev. Infect. Dis.* **1980**, *2*, 470.
(87) Merck & Co. *Recombivax hb® Hepatitis B Vaccine (Recombinant) Prescribing information*.
(88) Robbins, J. B.; Schneerson, R.; Trollfors, B.; Sato, H.; Sato, Y.; Rappuoli, R.; Keith, J. M. *J. Infect. Dis.* **2005**, *191*, 81.
(89) Leitner, W. W.; Ying, H.; Restifo, N. P. *Vaccine* **1999**, *18*, 765.
(90) Liu, M.; Acres, B.; Balloul, J.-M.; Bizouarne, N.; Paul, S.; Slos, P.; Squiban, P. *Proc. Natl. Acad. Sci. U.S.A.* **2004**, *101 Suppl.*, 14567.
(91) Ulmer, J. B.; Wahren, B.; Liu, M. A. *Trends Mol. Med.* **2006**, *12*, 216.
(92) Santra, S.; Korber, B. T.; Muldoon, M.; Barouch, D. H.; Nabel, G. J.; Gao, F.; Hahn, B. H.; Haynes, B. F.; Letvin, N. L. *Proc. Natl. Acad. Sci. U.S.A.* **2008**, *105*, 10489.
(93) Schubert, C. *Nat. Med.* **2009**, *15*, 984.
(94) Rappuoli, R.; Mandl, C. W.; Black, S.; De Gregorio, E. *Nat. Rev. Immunol.* **2011**, *11*, 865.
(95) Sun, H.; Pollock, K. G. J.; Brewer, J. M. *Vaccine* **2003**, *21*, 849.
(96) Petrovsky, N.; Aguilar, J. C. *Immunol. Cell Biol.* **2004**, *82*, 488.
(97) Reed, S. G.; Bertholet, S.; Coler, R. N.; Friede, M. *Trends Immunol.* **2009**, *30*, 23.
(98) Garçon, N.; Chomez, P.; Mechelen, M. Van. *Expert Rev. Vaccines* **2007**, *6*, 723.
(99) DeFrancesco, L. *Nat. Biotechnol.* **2008**, *26*, 484.
(100) Adams, S.; O'Neill, D. W.; Nonaka, D.; Hardin, E.; Chiriboga, L.; Siu, K.; Cruz, C. M.; Angiulli, A.; Angiulli, F.; Ritter, E.; Holman, R. M.; Shapiro, R. L.; Berman, R. S.; Berner, N.; Shao, Y.; Manches, O.; Pan, L.; Venhaus, R. R.; Hoffman, E. W.; Jungbluth, A.; Gnjatic, S.; Old, L.; Pavlick, A. C.; Bhardwaj, N. *J. Immunol.* **2008**, *181*, 776.
(101) Weeratna, R. D.; Makinen, S. R.; McCluskie, M. J.; Davis, H. L. *Vaccine* **2005**, *23*, 5263.
(102) A. Johnson, S. Gaines, M. L. *J. Exp. Med.* **1956**, *103*, 225.
(103) Xiao, H.; Peng, Y.; Hong, Y.; Huang, L.; Guo, Z. S.; Bartlett, D. L.; Fu, N.; Munn, D. H.; Mellor, A.; He, Y. *J. Immunol.* **2013**, *190*, 5866.
(104) Duthie, M. S.; Windish, H. P.; Fox, C. B.; Reed, S. G. *Immunol. Rev.* **2011**, *239*, 178.
(105) Kayamuro, H.; Yoshioka, Y.; Abe, Y.; Arita, S.; Katayama, K.; Nomura, T.; Yoshikawa, T.; Kubota-Koketsu, R.; Ikuta, K.; Okamoto, S.; Mori, Y.; Kunisawa, J.; Kiyono, H.; Itoh, N.; Nagano, K.; Kamada, H.; Tsutsumi, Y.; Tsunoda, S. *J. Virol.* **2010**, *84*, 12703.
(106) Min, W.; Lillehoj, H. S.; Burnside, J.; Weining, K. C.; Staeheli, P.; Zhu, J. J. *Vaccine* **2002**, *20*, 267.
(107) Sin, J.-I.; Kim, J. J.; Arnold, R. L.; Khushroo, E.; Mccallus, D.; Pachuk, C.; Mcelhiney, S. P.; Wolf, M. W.; Bruin, S. J. P.; Higgins, T. J.; Ciccarelli, R. B.; Weiner, D. B. *J. Immunol.* **1999**, *162*, 2912.
(108) Petrovsky, N. *Vaccine* **2006**, *24*, S2.
(109) Nicklin, S.; Atkinson, H. A. C.; Miller, K. *Food Addit. Contam.* **1988**, *5*, 573.
(110) Schijns, V. E. J. C.; Lavelle, E. C. *Expert Rev. Vaccines* **2011**, *10*, 539.
(111) Gregoriadis, G.; Gursel, I.; Gursel, M.; McCormack, B. *J. Control. Release* **1996**, *41*, 49.
(112) Alving, C. R.; Peachman, K. K.; Rao, M.; Reed, S. G. *Curr. Opin. Immunol.* **2012**, *24*, 310.
(113) Zaks, K.; Jordan, M.; Guth, A.; Sellins, K.; Kedl, R.; Izzo, A.; Bosio, C.; Dow, S. *J. Immunol.* **2006**, *176*, 7335.
(114) Glenny, A. T.; Pope, C. G. *J. Pathol. Bacteriol.* **1926**, *29*, 31.
(115) Baylor, N. W.; Egan, W.; Richman, P. *Vaccine* **2002**, *20 Suppl 3*, S18.
(116) Kool, M.; Fierens, K.; Lambrecht, B. N. *J. Med. Microbiol.* **2012**, *61*, 927.
(117) Ramanathan, V. D.; Badenoch-Jones, P.; Turk, J. L. *Immunology* **1979**, *37*, 881.

(118) Hem, S. L.; Hogenesch, H. *Expert Rev. Vaccines* **2007**, *6*, 685.
(119) Li, H.; Nookala, S.; Re, F. *J. Immunol.* **2007**, *178*, 5271.
(120) Zigan, F.; Rothbauer, R. *Neues Jahrb. fuer Mineral.* **1967**, *4*, 137.
(121) Bokhimi, X.; Toledo-Antonio, J. A.; Guzmán-Castillo, M. L.; Hernández-Beltrán, F. *J. Solid State Chem.* **2001**, *159*, 32.
(122) Saalfeld, B. H. *Zeitschrift für Krist.* **1974**, *139*, 129.
(123) Balan, E.; Blanchard, M.; Hochepied, J.-F.; Lazzeri, M. *Phys. Chem. Miner.* **2008**, *35*, 279.
(124) Bosmans, H. J. *Acta Crystallogr. Sect. B: Struct. Crystallogr. Cryst. Chem.* **1970**, *26*, 649.
(125) Clark, G. R.; Rodgers, K. A.; Henderson, G. S. *Zeitschrift für Krist.* **2010**, *213*, 96.
(126) Billiau, A.; Matthys, P. *J. Leukoc. Biol.* **2001**, *70*, 849.
(127) Dvorak, A. M.; Dvorak, H. F. *Immunology* **1974**, *27*, 99.
(128) Podda, A. *Vaccine* **2001**, *19*, 2673.
(129) O'Hagan, D. T.; Rappuoli, R.; De Gregorio, E.; Tsai, T.; Del Giudice, G. *Expert Rev. Vaccines* **2011**, *10*, 447.
(130) Sun, B.; Ji, Z.; Liao, Y.; Wang, M.; Wang, X.; Dong, J. *ACS Nano* **2013**, *7*, 10834.
(131) Wang, X.; Li, X.; Sogo, Y.; Ito, A. *RSC Adv.* **2013**, *3*, 8164.
(132) He, Q.; Mitchell, A. R.; Johnson, S. L.; Wagner-Bartak, C.; Morcol, T.; Bell, S. J. D. *Clin. Vaccine Immunol.* **2000**, *7*, 899.
(133) Knuschke, T.; Sokolova, V.; Rotan, O.; Wadwa, M.; Tenbusch, M.; Hansen, W.; Staeheli, P.; Epple, M.; Buer, J.; Westendorf, A. M. *J. Immunol.* **2013**.
(134) Xu, L.; Liu, Y.; Chen, Z.; Li, W.; Liu, Y.; Wang, L.; Liu, Y.; Wu, X.; Ji, Y.; Zhao, Y.; Ma, L.; Shao, Y.; Chen, C. *Nano Lett.* **2012**, *12*, 2003.
(135) Niikura, K.; Matsunaga, T.; Suzuki, T.; Kobayashi, S.; Yamaguchi, H.; Orba, Y.; Kawaguchi, A.; Hasegawa, H.; Kajino, K.; Ninomiya, T.; Ijiro, K.; Sawa, H. *ACS Nano* **2013**, *7*, 3926.
(136) Xu, Y.; Tang, H.; Liu, J.-H.; Wang, H.; Liu, Y. *Toxicol. Lett.* **2013**, *219*, 42.
(137) Cho, W.-S.; Dart, K.; Nowakowska, D. J.; Zheng, X.; Donaldson, K.; Howie, S. E. M. *Nanomedicine* **2012**, *7*, 1495.
(138) Roy, R.; Kumar, S.; Verma, A. K.; Sharma, A.; Chaudhari, B. P.; Tripathi, A.; Das, M.; Dwivedi, P. D. *Int. Immunol.* **2014**, *26*, 159.
(139) Hornung, V.; Bauernfeind, F.; Halle, A.; Samstad, E. O.; Kono, H.; Rock, K. L.; Fitzgerald, K. A.; Latz, E. *Nat. Immunol.* **2008**, *9*, 847.
(140) Wang, T.; Jiang, H.; Zhao, Q.; Wang, S.; Zou, M.; Cheng, G. *Int. J. Pharm.* **2012**, *436*, 351.
(141) Vallhov, H.; Kupferschmidt, N.; Gabrielsson, S.; Paulie, S.; Strømme, M.; Garcia-Bennett, A. E.; Scheynius, A. *Small* **2012**, *8*, 2116.
(142) Aimanianda, V.; Haensler, J.; Lacroix-Desmazes, S.; Kaveri, S. V; Bayry, J. *Trends Pharmacol. Sci.* **2009**, *30*, 287.
(143) HogenEsch, H. *Vaccine* **2002**, *20 Suppl 3*, S34.
(144) Gupta, R. K.; Chang, A. C.; Griffin, P.; Rivera, R.; Siber, G. R. *Vaccine* **1996**, *14*, 1412.
(145) Calabro, S.; Tortoli, M.; Baudner, B. C.; Pacitto, A.; Cortese, M.; O'Hagan, D. T.; De Gregorio, E.; Seubert, A.; Wack, A. *Vaccine* **2011**, *29*, 1812.
(146) Gavin, A. L.; Hoebe, K.; Duong, B.; Ota, T.; Martin, C.; Beutler, B.; Nemazee, D. *Science* **2006**, *314*, 1936.
(147) Eisenbarth, S. C.; Colegio, O. R.; O'Connor, W.; Sutterwala, F. S.; Flavell, R. A. *Nature* **2008**, *453*, 1122.
(148) Li, H.; Willingham, S. B.; Ting, J. P.-Y.; Re, F. *J. Immunol.* **2008**, *181*, 17.
(149) Sutterwala, F. S.; Ogura, Y.; Flavell, R. a. *J. Leukoc. Biol.* **2007**, *82*, 259.
(150) Mariathasan, S.; Monack, D. M. *Nat. Rev. Immunol.* **2007**, *7*, 31.
(151) Dowds, T. A.; Masumoto, J.; Zhu, L.; Inohara, N.; Núñez, G. *J. Biol. Chem.* **2004**, *279*, 21924.
(152) Srinivasula, S. M.; Poyet, J.-L.; Razmara, M.; Datta, P.; Zhang, Z.; Alnemri, E. S. *J. Biol. Chem.* **2002**, *277*, 21119.
(153) Martinon, F.; Burns, K.; Tschopp, J. *Mol. Cell* **2002**, *10*, 417.
(154) Schmitz, J.; Owyang, A.; Oldham, E.; Song, Y.; Murphy, E.; McClanahan, T. K.; Zurawski, G.; Moshrefi, M.; Qin, J.; Li, X.; Gorman, D. M.; Bazan, J. F.; Kastelein, R. A. *Immunity* **2005**, *23*, 479.

(155) Mariathasan, S.; Weiss, D. S.; Newton, K.; McBride, J.; O'Rourke, K.; Roose-Girma, M.; Lee, W. P.; Weinrauch, Y.; Monack, D. M.; Dixit, V. M. *Nature* **2006**, *440*, 228.
(156) Dostert, C.; Pétrilli, V.; Bruggen, R. Van; Steele, C.; Mossman, B. T.; Tschopp, J. *Science* **2008**, *320*, 674.
(157) Morefield, G. L.; Sokolovska, A.; Jiang, D.; HogenEsch, H.; Robinson, J. P.; Hem, S. L. *Vaccine* **2005**, *23*, 1588.
(158) Cannon, G. J.; Swanson, J. A. *J. Cell Sci.* **1992**, *101*, 907.
(159) Sharp, F. A.; Ruane, D.; Claass, B.; Creagh, E.; Harris, J.; Malyala, P.; Singh, M.; O'Hagan, D. T.; Pétrilli, V.; Tschopp, J.; O'Neill, L. A. J.; Lavelle, E. C. *Proc. Natl. Acad. Sci. U.S.A.* **2009**, *106*, 870.
(160) Gurcel, L.; Abrami, L.; Girardin, S.; Tschopp, J.; van der Goot, F. G. *Cell* **2006**, *126*, 1135.
(161) Pétrilli, V.; Papin, S.; Dostert, C.; Mayor, a; Martinon, F.; Tschopp, J. *Cell Death Differ.* **2007**, *14*, 1583.
(162) Schorn, C.; Frey, B.; Lauber, K.; Janko, C.; Strysio, M.; Keppeler, H.; Gaipl, U. S.; Voll, R. E.; Springer, E.; Munoz, L. E.; Schett, G.; Herrmann, M. *J. Biol. Chem.* **2011**, *286*, 35.
(163) Kool, M.; Soullié, T.; van Nimwegen, M.; Willart, M. A. M.; Muskens, F.; Jung, S.; Hoogsteden, H. C.; Hammad, H.; Lambrecht, B. N. *J. Exp. Med.* **2008**, *205*, 869.
(164) Kono, H.; Chen, C.; Ontiveros, F.; Rock, K. L. *J. Clin. Invest.* **2010**, *120*, 1939.
(165) Schnurr, M.; Then, F.; Galambos, P.; Scholz, C.; Siegmund, B.; Endres, S.; Eigler, A. *J. Immunol.* **2000**, *165*, 4704.
(166) Wilkin, F.; Duhant, X.; Bruyns, C.; Suarez-Huerta, N.; Boeynaems, J.-M.; Robaye, B. *J. Immunol.* **2001**, *166*, 7172.
(167) Marichal, T.; Ohata, K.; Bedoret, D.; Mesnil, C.; Sabatel, C.; Kobiyama, K.; Lekeux, P.; Coban, C.; Akira, S.; Ishii, K. J.; Bureau, F.; Desmet, C. J. *Nat. Med.* **2011**, *17*, 996.
(168) Ishii, K. J.; Suzuki, K.; Coban, C.; Takeshita, F.; Itoh, Y.; Matoba, H.; Kohn, L. D.; Klinman, D. M. *J. Immunol.* **2001**, *167*, 2602.
(169) Gallucci, S.; Lolkema, M.; Matzinger, P. *Nat. Med.* **1999**, *5*, 1249.
(170) Flach, T. L.; Ng, G.; Hari, A.; Desrosiers, M. D.; Zhang, P.; Ward, S. M.; Seamone, M. E.; Vilaysane, A.; Mucsi, A. D.; Fong, Y.; Prenner, E.; Ling, C. C.; Tschopp, J.; Muruve, D. A.; Amrein, M. W.; Shi, Y. *Nat. Med.* **2011**, *17*, 479.
(171) Ng, G.; Sharma, K.; Ward, S. M.; Desrosiers, M. D.; Leslie, A.; Schoel, W. M.; Li, T.; Lowell, C. A.; Ling, C.; Amrein, W.; Shi, Y. *Immunity* **2009**, *29*, 807.
(172) Seubert, A.; Monaci, E.; Pizza, M.; O'Hagan, D. T.; Wack, A. *J. Immunol.* **2008**, *180*, 5402.
(173) Ulanova, M.; Tarkowski, A.; Hahn-Zoric, M.; Hanson, L. Å. *Infect. Immun.* **2001**, *69*, 1151.
(174) Choy, J.; Choi, S.; Oh, J.; Park, T. *Appl. Clay Sci.* **2007**, *36*, 122.
(175) Diamond, J. M. *Nature* **1999**, *400*, 120.
(176) Saary, J.; Qureshi, R.; Palda, V.; DeKoven, J.; Pratt, M.; Skotnicki-Grant, S.; Holness, L. *J. Am. Acad. Dermatol.* **2005**, *53*, 845.
(177) Zeng, L.; Wang, S.; Peng, X.; Geng, J.; Chen, C.; Li, M. *Appl. Clay Sci.* **2013**, *83-84*, 231.
(178) Manasse, E. *Nat. Proc. Verb* **1915**, *24*, 92.
(179) Feitknecht, W. *Helv. Chim. Acta* **1942**, *27*, 131.
(180) Cavani, F.; Trifiro, F.; Vaccari, A. *Catal. Today* **1991**, *11*, 173.
(181) Allmann, R. *Acta Crystallogr. Sect. B: Struct. Crystallogr. Cryst. Chem.* **1968**, *B24*, 972.
(182) Duffy, T.; Shu, J.; Mao, H.; Hemley, R. *Phys. Chem. Miner.* **1995**, *22*, 277.
(183) Nalawade, P.; Aware, B.; Kadam, V. J.; Hirlekar, R. S. *J. Sci. Ind. Res.* **2009**, *68*, 267.
(184) Khan, A. I.; O'Hare, D. *J. Mater. Chem.* **2002**, *12*, 3191.
(185) Wang, Q.; O'Hare, D. *Chem. Rev.* **2012**, *112*, 4124.
(186) Kuang, Y.; Zhao, L.; Zhang, S.; Zhang, F.; Dong, M.; Xu, S. *Materials (Basel).* **2010**, *3*, 5220.
(187) Cavani, F.; Trifiro, F.; Vaccari, A. *Catal. Today* **1991**, *11*, 173.
(188) Marchi, A. J.; Apesteguıa, C. R. *Appl. Clay Sci.* **1998**, *13*, 35.
(189) Poeppelmeier, K. R.; Hwu, S. J. *Inorg. Chem.* **1987**, *5*, 3297.
(190) Velu, S.; Suzuki, K.; Osaki, T.; Ohashi, F.; Tomura, S. *Mater. Res. Bull.* **2000**, *34*, 1707.
(191) Wang, C. J.; Wu, Y. A.; Jacobs, R. M. J.; Warner, J. H.; Williams, G. R.; O'Hare, D. *Chem. Mater.* **2011**, *23*, 171.

(192) Arakcheeva, A. V.; Pushcharovsky, D. Y.; Rastsvetaeva, R. K.; Atencio, D.; Lubman, G. U. . *Crystallogr. Reports* **1996**, *41*, 972.
(193) Allmann, R.; Jepsen, H. P. . *Neues Jahrb. fur Mineral.* **1969**, 544.
(194) Prevot, V.; Forano, C.; Besse, J. P.; Abraham, F. *Inorg. Chem.* **1998**, *1669*, 4293.
(195) Khan, A. I.; Ragavan, A.; Fong, B.; Markland, C.; Brien, M. O.; Dunbar, T. G.; Williams, G. R.; O'Hare, D. *Ind. Eng. Chem. Res.* **2009**, *48*, 10196.
(196) Kwon, T.; Pinnavaia, T. *Chem. Mater.* **1989**, *1*, 381.
(197) Tseng, W.; Lin, J.; Mou, C.; Cheng, S.; Liu, S.; Chu, P. P.; Liu, H. *J. Am. Chem. Soc.* **1996**, *118*, 4411.
(198) Rives, V.; Ulibarri, M. A. *Coord. Chem. Rev.* **1999**, *181*, 61.
(199) Darder, M.; Lopez-Blanco, M.; Aranda, P.; Leroux, F.; Ruiz-Hitzky, E. *Chem. Mater.* **2005**, *17*, 1969.
(200) Nakayama, H.; Wada, N.; Tsuhako, M. *Int. J. Pharm.* **2004**, *269*, 469.
(201) Choy, J.-H.; Kwak, S.-Y.; Park, J.-S.; Jeong, Y.-J.; Portier, J. *J. Am. Chem. Soc.* **1999**, *121*, 1399.
(202) Desigaux, L.; Belkacem, M. Ben; Richard, P.; Cellier, J.; Léone, P.; Cario, L.; Leroux, F.; Taviot-Guého, C.; Pitard, B. *Nano Lett.* **2006**, *6*, 199.
(203) Williams, G. R.; Fogg, A. M.; Sloan, J.; Taviot-Guého, C.; O'Hare, D. *Dalton Trans.* **2007**, *2*, 3499.
(204) Zhang, W. H.; Guo, X. D.; He, J.; Qian, Z. Y. *J. Eur. Ceram. Soc.* **2008**, *28*, 1623.
(205) Sparks, D. E.; Morgan, T.; Patterson, P. M.; Tackett, S. A.; Morris, E.; Crocker, M. *Appl. Catal. B Environ.* **2008**, *82*, 190.
(206) Yun, S. K.; Pinnavaia, T. J. *Chem. Mater.* **1995**, *7*, 348.
(207) Chang, Z.; Evans, D. G.; Duan, X.; Vial, C.; Ghanbaja, J.; Prevot, V.; de Roy, M.; Forano, C. *J. Solid State Chem.* **2005**, *178*, 2766.
(208) Xu, Z. P.; Stevenson, G.; Lu, C.-Q.; Lu, G. Q. M. *J. Phys. Chem. B* **2006**, *110*, 16923.
(209) Climent, M. J.; Corma, A.; Iborra, S.; Epping, K.; Velty, A. *J. Catal.* **2004**, *225*, 316.
(210) Komarneni, S.; Li, Q. H.; Roy, R. *J. Mater. Res.* **2011**, *11*, 1866.
(211) Goh, K.-H.; Lim, T.-T.; Dong, Z. *Water Res.* **2008**, *42*, 1343.
(212) Fogg, A. M.; Dunn, J. S.; O'Hare, D. *Chem. Mater.* **1998**, *2*, 356.
(213) Ogawa, M.; Inomata, K. *Chem. Lett.* **2005**, *34*, 810.
(214) Rocha, J.; Rives, V.; Ulibarri, M. A. **1999**, *3*, 2499.
(215) Mohanambe, L.; Vasudevan, S. *Inorg. Chem.* **2005**, *44*, 2128.
(216) Gunawan, P.; Xu, R. *J. Mater. Chem.* **2008**, *18*, 2112.
(217) Wongariyakawee, A.; Schäeffel, F.; Warner, J. H.; O'Hare, D. *J. Mater. Chem.* **2012**, *22*, 7751.
(218) Shao, M.; Ning, F.; Zhao, J.; Wei, M.; Evans, D. G.; Duan, X. *J. Am. Chem. Soc.* **2012**, *134*, 1071.
(219) Li, L.; Feng, Y.; Li, Y.; Zhao, W.; Shi, J. *Angew. Chem. Int. Ed. Engl.* **2009**, *48*, 5888.
(220) Shao, M.; Ning, F.; Zhao, Y.; Zhao, J.; Wei, M.; Evans, D. G.; Duan, X. *Chem. Mater.* **2012**, *24*, 1192.
(221) Du, Y.; Hu, G.; O'Hare, D. *J. Mater. Chem.* **2009**, *19*, 1160.
(222) Wang, Q.; O'Hare, D. *Chem. Commun.* **2013**, *49*, 6301.
(223) Wu, Q.; Olafsen, A.; Vistad, Ø. B.; Roots, J.; Norby, P. *J. Mater. Chem.* **2005**, *15*, 4695.
(224) Liu, Z.; Ma, R.; Ebina, Y.; Iyi, N.; Takada, K.; Sasaki, T. *Langmuir* **2007**, *23*, 861.
(225) O'Leary, S.; O'Hare, D.; Seeley, G. *Chem. Commun. (Camb).* **2002**, 1506.
(226) Wang, Y.; Luo, S.; Wang, Z.; Fu, Y. *Appl. Clay Sci.* **2013**.
(227) Dey, S. K.; Sistiabudi, R. *Mater. Res. Innov.* **2007**, *11*, 108.
(228) Tyner, K. M.; Schiffman, S. R.; Giannelis, E. P. *J. Control. Release* **2004**, *95*, 501.
(229) Heath, J. K.; White, S. J.; Johnstone, C. N.; Catimel, B.; Simpson, R. J.; Moritz, R. L.; Tu, G. F.; Ji, H.; Whitehead, R. H.; Groenen, L. C.; Scott, A. M.; Ritter, G.; Cohen, L.; Welt, S.; Old, L. J.; Nice, E. C.; Burgess, A. W. *Proc. Natl. Acad. Sci. U.S.A.* **1997**, *94*, 469.
(230) Tao, Q.; He, H.; Frost, R. L.; Yuan, P.; Zhu, J. *Appl. Surf. Sci.* **2009**, *255*, 4334.
(231) Tao, Q.; He, H.; Li, T.; Frost, R. L.; Zhang, D.; He, Z. *J. Solid State Chem.* **2014**, *213*, 176.
(232) Wang, J.; Stevens, L. A.; Drage, T. C.; Wood, J. *Chem. Eng. Sci.* **2012**, *68*, 424.

(233) Tao, Q.; He, H.; Frost, R. L.; Yuan, P.; Zhu, J. *J. Therm. Anal. Calorim.* **2009**, *101*, 153.
(234) Xu, Z. P.; Zeng, Q. H.; Lu, G. Q.; Yu, A. B. *Chem. Eng. Sci.* **2006**, *61*, 1027.
(235) Li, F.; Liu, J.; Evans, D. G.; Duan, X. *Chem. Mater.* **2004**, *16*, 1597.
(236) Carlino, S.; Hudson, M. J.; Husain, S. W.; Knowles, J. A. *Solid State Ionics* **1996**, *84*, 117.
(237) Alejandre, A.; Medina, F.; Rodriguez, X.; Salagre, P.; Cesteros, Y.; Sueiras, J. E. *Appl. Catal. B Environ.* **2001**, *30*, 195.
(238) Velu, S.; Suzuki, K.; Osaki, T. *Catal. Letters* **1999**, *62*, 159.
(239) Morioka, H.; Shimizu, Y.; Sukenobu, M.; Ito, K.; Tanabe, E.; Shishido, T.; Takehira, K. *Appl. Catal. A Gen.* **2001**, *215*, 11.
(240) Sels, B.; De Vos, D.; Buntinx, M.; Pierard, F.; Kirsch-De Mesmaeker, A.; Jacobs, P. *Nature* **1999**, *400*, 855.
(241) Ichikawa, S.; Miyazoe, S.; Matsuoka, O. *Chem. Lett.* **2011**, *40*, 512.
(242) Zeng, H.; Wang, Y.; Feng, Z.; You, K.; Zhao, C.; Sun, J.; Liu, P. *Catal. Letters* **2010**, *137*, 94.
(243) Roeffaers, M. B. J.; Sels, B. F.; Uji-I, H.; De Schryver, F. C.; Jacobs, P. A.; De Vos, D. E.; Hofkens, J. *Nature* **2006**, *439*, 572.
(244) Zhao, Y.; Li, B.; Wang, Q.; Gao, W.; Wang, C. J.; Wei, M.; Evans, D. G.; Duan, X.; O'Hare, D. *Chem. Sci.* **2014**, *5*, 951.
(245) Chang, C.-T.; Liaw, B.-J.; Huang, C.-T.; Chen, Y.-Z. *Appl. Catal. A Gen.* **2007**, *332*, 216.
(246) Choudary, B. M.; Madhi, S.; Chowdari, N. S.; Kantam, M. L.; Sreedhar, B. *J. Am. Chem. Soc.* **2002**, *124*, 14127.
(247) Nakagaki, S.; Halma, M.; Bail, A.; Arízaga, G. G. C.; Wypych, F. *J. Colloid Interface Sci.* **2005**, *281*, 417.
(248) Xu, Z. P.; Zhang, J.; Adebajo, M. O.; Zhang, H.; Zhou, C. *Appl. Clay Sci.* **2011**, *53*, 139.
(249) Asouhidou, D. D.; Triantafyllidis, K. S.; Lazaridis, N. K.; Matis, K. A. *J. Chem. Technol. Biotechnol.* **2012**, *87*, 575.
(250) Chuang, Y. H.; Tzou, Y. M.; Wang, M. K.; Liu, C. H.; Chiang, P. N. *Ind. Eng. Chem. Res.* **2008**, *47*, 3813.
(251) Zhao, H.; Nagy, K. L. *J. Colloid Interface Sci.* **2004**, *274*, 613.
(252) Aisawa, S.; Higashiyama, N.; Takahashi, S.; Hirahara, H.; Ikematsu, D.; Kondo, H.; Nakayama, H.; Narita, E. *Appl. Clay Sci.* **2007**, *35*, 146.
(253) Markland, C.; Williams, G. R.; O'Hare, D. *J. Mater. Chem.* **2011**, *21*, 17896.
(254) Costantino, U.; Coletti, N.; Nocchetti, M.; Aloisi, G. G.; Elisei, F.; Latterini, L. *Langmuir* **2000**, *16*, 10351.
(255) Costantino, U.; Coletti, N.; Nocchetti, M.; Aloisi, G. G.; Elisei, F. *Langmuir* **1999**, *15*, 4454.
(256) Sun, Z.; Jin, L.; Shi, W.; Wei, M.; Duan, X. *Chem. Eng. J.* **2010**, *161*, 293.
(257) Yang, L.; Sheldon, B. W.; Webster, T. J. *Am. Ceram. Soc. Bull. 89*.
(258) Lee, J.-H.; Choi, G.; Oh, Y.-J.; Park, J. W.; Choy, Y. Bin; Park, M. C.; Yoon, Y. J.; Lee, H. J.; Chang, H. C.; Choy, J.-H. *Int. J. Nanomedicine* **2012**, *7*, 1635.
(259) Ambrogi, V.; Fardella, G.; Grandolini, G.; Perioli, L. *Int. J. Pharm.* **2001**, *220*, 23.
(260) Li, B.; He, J.; Gevans, D.; Duan, X. *Appl. Clay Sci.* **2004**, *27*, 199.
(261) Oh, J.-M.; Park, C.-B.; Choy, J.-H. *J. Nanosci. Nanotechnol.* **2011**, *11*, 1632.
(262) Menezes, J.; da Silva, T.; dos Santos, J.; Catari, E.; Meneghetti, M.; da Matta, C.; Alexandre-Moreira, M.; Santos-Magalhães, N.; Grillo, L.; Dornelas, C. *Appl. Clay Sci.* **2014**, *91-92*, 127.
(263) Trikeriotis, M.; Ghanotakis, D. F. *Int. J. Pharm.* **2007**, *332*, 176.
(264) Wei, M.; Pu, M.; Guo, J.; Han, J.; Li, F.; He, J.; Evans, D. G. *Chem. Mater.* **2008**, *20*, 5169.
(265) Zhang, H.; Zou, K.; Guo, S.; Duan, X. *J. Solid State Chem.* **2006**, *179*, 1792.
(266) Gu, Z.; Thomas, A. C.; Xu, Z. P.; Campbell, J. H.; Qing, G.; Lu, M. *Chem. Mater.* **2008**, *20*, 3715.
(267) Bugatti, V.; Esposito, L.; Franzetti, L.; Tammaro, L.; Vittoria, V. *Appl. Clay Sci.* **2013**, *75-76*, 46.
(268) Liu, J.; Duan, C.; Zhou, J.; Li, X.; Qian, G.; Xu, Z. P. *Appl. Clay Sci.* **2013**, *75-76*, 39.
(269) Fayyazbakhsh, F.; Solati-Hashjin, M.; Shokrgozar, M. A.; Bonakdar, S.; Ganji, Y.; Mirjordavi, N.; Ghavimi, S. A.; Khashayar, P. *Key Eng. Mater.* **2011**, *493-494*, 902.
(270) Li, A.; Qin, L.; Zhu, D.; Zhu, R.; Sun, J.; Wang, S. *Biomaterials* **2010**, *31*, 748.
(271) Li, A.; Qin, L.; Wang, W.; Zhu, R.; Yu, Y.; Liu, H.; Wang, S. *Biomaterials* **2011**, *32*, 469.

(272) Shafik, H. M.; Ayoub, S. M.; Ebeid, N. H.; Someda, H. H. *J. Radioanal. Nucl. Chem.* **2014**, *301*, 81.

Chapter Two: Synthesis and Characterisation of Layered Double Hydroxides with Narrow Particle Size Distributions for Use in Immunological Experiments

2.1 Introduction

A limited number of studies detail the effects of particle size on the immune response; these mainly evaluate a small number and range of sizes, generally on the tens to hundreds of nanometres scale.[1–3] Accordingly, there is a requirement to establish the effects of particle size on immunogenicity systematically over a size range from nanometres to micrometres, as this could have implications for the rational design of adjuvant materials. Layered double hydroxides (LDHs) are a class of inorganic materials with highly tuneable properties including particle size. Control of this attribute has particular industrial relevance, for example in anti-reflective coatings, CO_2 capture materials and capacitors.[4–6] Consequently, a wide variety of techniques have been developed to tailor particle size in these materials, some of which are reviewed below. Details of their biocompatibility, such as low cytotoxicity, also make them excellent candidate materials for adjuvants.[7,8]

2.1.1 Methods for controlling particle size

2.1.1.1 Hydrothermal treatment

LDHs form through a nucleation-crystal growth pathway:[9] crystallites are formed during nucleation, then either dissolve again or undergo a process of crystal growth and Ostwald ripening, a dissolution-crystalisation process noted in LDH formation.[10] Methods attempting to control specific steps in this process have been developed, such as the SNAS approach (separate nucleation and aging steps). Simultaneous nucleation of all LDH particles is achieved by rapidly mixing reagents to obtain a slurry which is then aged hyrothermally.[11] Consequently, all particles experience the same length of nucleation and aging time. By ensuring equal aging time, the SNAS approach affords particles with a more uniform size. In conventional coprecipitation, nucleation occurs over an extended period as the solutions are combined, thus particles formed earlier are aged for longer, and a broad distribution of particle sizes may result.

Moreover, controlling the reaction length and temperature of the hydrothermal aging step directly influences the average size of the particles formed. Reactions carried out by Xu and co-workers involved rapid pre-mixing of reagents, isolation and washing of the MgAl-Cl LDH slurry using centrifugation, then hydrothermal aging from 80 to 150 °C for 2 to 144 hours.[12] Both aging temperature and time influenced the product particle size. A trend of increasing particle size (from 70 to 300 nm) was noted with increasing time and temperature, with the authors specifically stating that "*an increase in temperature by 10 °C can lead to an increase in the hydrodynamic diameter by 10-15 nm on average*".[12] The shortest and longest aging times (2/144 hours) were not sufficient to create a uniform dispersion of individual LDH crystallites. It was hypothesised that during the first few hours of hydrothermal aging the aggregates in the slurry disperse, then undergo Ostwald ripening and growth and may re-aggregate at later aging times.

Subsequently this approach has been extended to other LDH compositions (MgAl-CO_3, LiAl-CO_3)[7,13,14] and the effects of eliminating the pre-aging washing step have been explored.[15] Indeed, hydrothermal aging is compatible with the 'salt-oxide' method described by Albiston and co-workers, in which magnesium oxide is used as the source of Mg^{2+}, affording particles with diameters up to 770 nm.[16]

2.1.1.2 pH control

In conventional coprecipitation reactions, control of pH may be used to attain certain particle sizes and morphologies. A systematic study of this effect was conducted by Wang *et al*. demonstrating that the isolectric point (IEP, the pH at which the surface carries no charge) of the LDH plays a critical role.[5] Typically, for a MgAl-CO_3 LDH this is at approximately pH 10.[17] Coprecipitation at the IEP produces 'rosette' or 'flower-like' LDHs, whereas coprecipitation at pH 11 or above yields uniformly sized nanoparticles around 30 nm in diameter. Particles form rapidly at high pH, but grow slowly, as the negative surface charge and the charges on the ions in solution [$Al(OH)_4^-$ and CO_3^{2-}] repel each other resulting in small particle sizes.

2.1.1.3 Homogeneous coprecipitation methods

One method of achieving the 'low supersaturation' conditions required for large, highly crystalline particles is by using an amine releasing reagent (ARR) such as urea or hexamethylenetetramine (HMT).[18] Upon heating, these reagents break down to release ammonia and carbonate, gradually raising the pH. The example of urea is shown in

Equation 2.1.[19] The initial breakdown of urea to ammonium cyanate is rate-determining, with ensuing fast hydrolysis.[20]

$$H_2NCONH_2 \xrightarrow{Rate\ determining\ step} NH_4^+ + NCO^-$$

$$NCO^- + 2H_2O \xrightarrow{Fast} NH_4^+ + CO_3^{2-}$$

Equation 2.1: Breakdown of urea upon heating in aqueous solution.[19]

The slow increase in pH results in less frequent nucleation events than when 'high supersaturation' techniques are employed. The overall pH never rises as high as the IEP, hence crystal growth is encouraged, and large hexagonal platelets form. The effects of altering the concentration of both HMT and urea were probed by Okamoto and co-workers, who determined that lower ARR concentrations yield larger platelets with diameters of 10 μm.[21] Since carbonate forms as a breakdown product of the ARR, this method is only suitable for synthesis of carbonate intercalated LDHs. Carbonate preferentially intercalates into LDHs over other anions present in the reaction mixture due to its high charge density.[22] Successful synthesis of MgAl-CO_3, LiAl-CO_3 and NiAl-CO_3 LDHs have all been reported using urea.[6,23,24]

2.1.1.4 Other methods of controlling particle size

The technique of using reverse micelles for synthesis of LDHs was documented by Hu *et al*. in 2005.[25] In this method, water pockets were formed in a non-miscible solvent (isooctane) by surfactant molecules, e.g. sodium dodecyl sulphate (NaDDS), with 1-butanol as a co-surfactant. These water pockets act as 'micro-reactors', the size of which may be tailored by altering the water/surfactant/solvent ratios.[9] In light of this, it is possible to control LDH particle size by tuning the water to surfactant ratio since the dimensions of the micelle limit the LDH particle size. CaAl-, CoAl- and MgAl-DDS LDHs have all been prepared in this fashion, with precisely controlled mean particle sizes from 10 to 50 nm for CaAl-DDS LDHs and 60 to 160 nm for CoAl-DDS LDHs.[26,27] Unusual belt-like and rod-like morphologies have been achieved by adding copolymers to alter the LDH aspect ratio.[25]

Altering the solvent used for synthesis may also affect the particle size of the products. Chang and co-workers investigated the effects of varying the ratios of water to ethanol and water to ethylene glycol in ZnAl-CO_3 LDH synthesis *via* continuous coprecipitation, determining that the addition of an organic solvent reduced particle size.[28] High-energy ball milling may also be used to reduce the powder dimensions of an LDH.[29]

2.1.2 Scope of this Chapter

The primary aim of this chapter is to synthesise and characterise a library of LDH particles with narrow size distributions for use in subsequent *in vitro* testing. Due to the quantity of research into MgAl-CO_3 particle size control, this was the initial focus of the work. Subsequently, successful approaches were extended to synthesise LDHs with controlled particle sizes in other compositions (LiAl-CO_3, MgFe-CO_3). The commercial adjuvants (Imject and Alhydrogel) included in the biological assays were also characterised.

2.2 Results and discussion

2.2.1 Synthesis of MgAl-CO_3 LDHs

Synthesis at high pH, hydrothermal aging, and use of ARRs were selected as the best methods to synthesise a broad range of MgAl-CO_3 LDH particle sizes. Reverse micelle methods were not employed as they yield DDS intercalated products which would require further processing to convert to the carbonate. Detailed synthesis procedures may be found in Chapter Six. The compositions of the resulting LDHs were assessed using elemental analysis (EA, for C, H and N), energy-dispersive X-ray spectroscopy (EDX) and thermogravimetric analysis (TGA). Chemical formulae obtained from combining the results of all three techniques are provided in Table 2.1.

Table 2.1: Approximate chemical formulae and synthesis outlines of MgAl-CO_3 LDHs. RT = room temperature, O/N = overnight. Approximate LDH sizes were obtained from transmission electron microscopy (TEM) images (Section 2.2.1.3).

Approx LDH size (nm)	Chemical formula (from EDX, EA and TGA)	Synthesis method
20	$[Mg_{3.1}Al(OH)_{8.3}](CO_3)_{0.5}\cdot 2.6H_2O$	Coprecipitation pH 12 RT O/N
40	$[Mg_{2.6}Al(OH)_{7.1}](CO_3)_{0.5}\cdot 2H_2O$	Hydrothermal 100 °C 24 hrs
60	$[Mg_{1.7}Al(OH)_{5.5}](CO_3)_{0.5}\cdot 1.4H_2O$	Coprecipitation 90 °C 72 hrs
70	$[Mg_{2.8}Al(OH)_{7.7}](CO_3)_{0.5}\cdot 2H_2O$	Hydrothermal 120 °C 24 hrs
190	$[Mg_{3.0}Al(OH)_{8}](CO_3)_{0.5}\cdot 1.9H_2O$	Hydrothermal 150 °C 24 hrs
210	$[Mg_{2.9}Al(OH)_{7.8}](CO_3)_{0.5}\cdot 1.7H_2O$	Hydrothermal 150 °C 48 hrs
400	$[Mg_{2.9}Al(OH)_{7.7}](CO_3)_{0.5}\cdot 1.5H_2O$	Hydrothermal 180 °C 48 hrs
1070	$[Mg_{2.1}Al(OH)_{6.3}](CO_3)_{0.5}\cdot 1.3H_2O$	0.24 M HMT 140 °C 24 hrs
2160	$[Mg_{2.2}Al(OH)_{6.3}](CO_3)_{0.5}\cdot 1.4H_2O$	0.19 M HMT 140 °C 24 hrs
2560	$[Mg_{2.1}Al(OH)_{6.3}](CO_3)_{0.5}\cdot 1.3H_2O$	0.8 M Urea 100 °C 24 hrs
9900	$[Mg_{2.2}Al(OH)_{6.4}](CO_3)_{0.5}\cdot 1.3H_2O$	0.13 M HMT 140 °C 24 hrs

Small variations in composition with synthesis method are present: typically the Mg:Al ratio varies between 3 and 1.7. Variations of the Mg:Al ratio from four to two are possible ($x = 0.2$ to $x = 0.33$ in $[M^{z+}_{1-x}M^{3+}_{x}(OH)_2]^{a+}(X^{n-})_{a/n}\cdot mH_2O$) whilst still maintaining a phase-pure sample.[30] The above data for the 20 nm MgAl-CO_3 LDH are consistent with that obtained by

Wang *et al.* using the high pH method yielding a Mg:Al ratio of three.[5] The water content is generally higher for coprecipitation/hydrothermally synthesised LDHs.

2.2.1.1 Powder X-ray diffraction

All MgAl-CO_3 LDHs were synthesised as phase pure products. Powder X-ray diffraction (XRD) data is shown in Figure 2.1. Patterns were indexed to a hexagonal unit cell for hydrotalcite ($a = b$ = ~3 Å, c = 22.7 Å) space group $R\bar{3}m$.[31] Celref software was employed to obtain refined estimates of the lattice parameters, provided in Table 2.2.[32] A list of indexed reflections for each MgAl-CO_3 LDH is supplied in Appendix A.2.1.

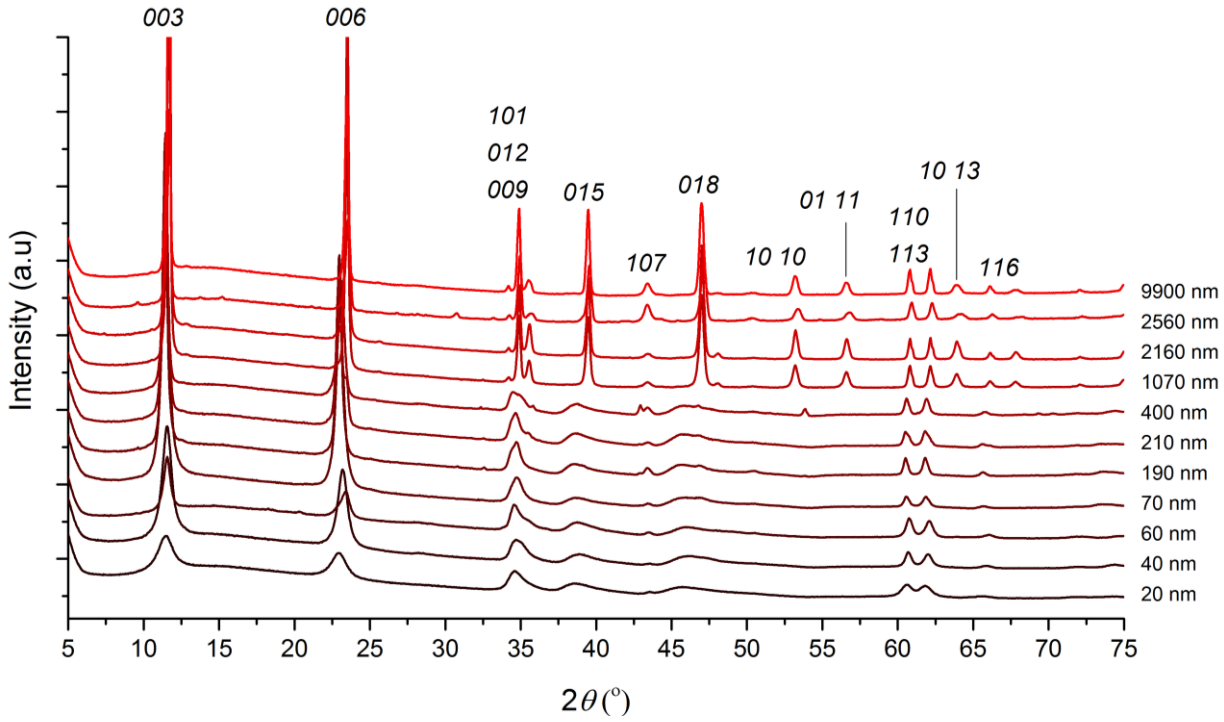

Figure 2.1: Indexed powder X-ray diffraction data for MgAl-CO_3 LDHs.

Table 2.2: Refined unit cell parameters for MgAl-CO_3 LDHs, indexed to a hexagonal unit cell, space group $R\bar{3}m$.

Approx LDH size (nm)	$a(=b)$ parameter (Å)	c-parameter (Å)	Volume (Å^3)
20	3.058(2)	23.31(4)	188.8
40	3.054(3)	23.21(8)	187.6
60	3.048(7)	22.78(1)	183.4
70	3.056(8)	23.50(0)	190.2
190	3.059(0)	23.51(3)	190.6
210	3.195(4)	22.56(5)	199.5
400	3.039(7)	22.51(4)	180.2
1070	3.047(6)	22.72(1)	182.8
2160	3.047(2)	22.72(0)	182.7
2560	3.042(3)	22.62(7)	181.4
9900	3.046(1)	22.71(5)	182.5

The *a*- and *b*-parameters change little with synthesis method. A small decrease in the *c*-parameter is noted, correlating with a decrease in the inter-layer distance due to fewer co-intercalated water molecules. Sharper reflections indicating increased crystallinity are observed with greater particle size. This is confirmed by calculation of the full-width at half-maximum height (FWHM) (Table 2.3), which decreases for reflections from the larger particles. A decrease in FWHM is particularly apparent when moving from coprecipitation/hydrothermally aged LDHs to ARR synthesised LDHs.

Table 2.3: Positions and line widths of selected Bragg reflections, with estimates of the crystallite domain size obtained from the Scherrer equation for MgAl-CO_3 LDHs. FWHM = full width at half maximum, CDS = crystallite domain size, Scherer equation: $CDS(\tau) = K\lambda(\beta\cos\Theta)^{-1}$, K = 0.89.[33]

	Bragg reflection							
	003				***110***			
Approx LDH size (nm)	***d*-spacing (Å)**	**2Θ (°)**	**FWHM (°)**	**CDS (nm)**	***d*-spacing (Å)**	**2Θ (°)**	**FWHM (°)**	**CDS (nm)**
20	7.68	11.5	0.84	21.5	1.53	60.6	0.59	59.8
40	7.65	11.6	0.59	30.6	1.53	60.7	0.39	84.4
60	7.65	11.6	0.39	45.9	1.52	60.8	0.39	79.3
70	7.71	11.5	0.39	47.2	1.53	60.6	0.33	114
190	7.75	11.4	0.32	57.6	1.53	60.5	0.33	121
210	7.76	11.4	0.39	48.2	1.53	60.5	0.45	88.8
400	7.72	11.5	0.26	71.0	1.53	60.6	0.33	112
1070	7.58	11.7	0.26	67.0	1.52	60.8	0.26	116
2160	7.60	11.7	0.26	67.5	1.52	60.8	0.26	114
2560	7.56	11.7	0.26	66.5	1.52	60.9	0.33	84.6
9900	7.59	11.7	0.26	67.1	1.52	60.8	0.26	117

One way to quantify crystallinity is by estimating the crystallite domain size (CDS) using the Scherrer equation. The CDS corresponds to the average size of a coherent, uninterrupted crystalline domain within a particle and may correlate with (though not necessarily equal) the particle size. FWHM values were obtained for the *003* and *110* reflections and used to compute the CDS in the *ab* plane (*110*) and along the *c*-axis (*003*). All LDH samples were shown to be hexagonal platelets (Section 2.2.1.3) with the *c*-axis perpendicular to the plane of the plate. Consequently, the CDS corresponding to the *c*-axis is smaller than that corresponding to the *ab*-plane. The Scherrer equation may only be effectively applied to particle sizes below ~100 nm, because above this size the contribution to peak broadening is difficult to ascertain given the resolution of the instrument.[34] Taking this into consideration, increases in CDS for both reflections are still noted with increasing particle size for particles smaller than 100 nm.

2.2.1.2 Fourier transform infrared spectroscopy

Fourier transform infrared (FTIR) spectra were recorded for all MgAl-CO_3 LDHs between 700 and 4000 cm^{-1} and are collated in Figure 2.2.

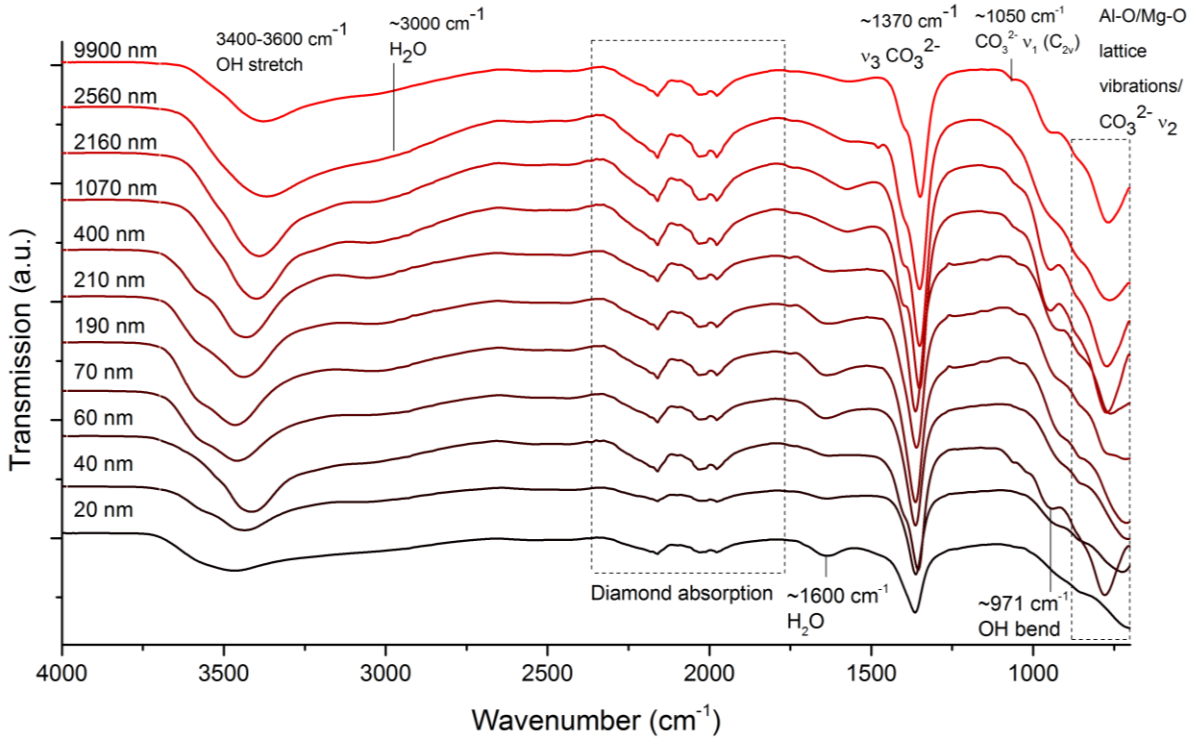

Figure 2.2: FTIR spectroscopy data for MgAl-CO_3 LDHs.

The spectra appear very similar for all MgAl-CO_3 LDHs. The strong absorption at 1370 cm^{-1} corresponds to the ν_3 carbonate stretching mode (in D_{3h} symmetry) with weak absorptions around 850 cm^{-1} due to the ν_2 mode, partially obscured by M-O vibration bands.[35] The carbonate absorption at 1370 cm^{-1} occasionally exhibits a shoulder closer to 1400 cm^{-1} due to lowering of the symmetry of the carbonate ion to C_{2v} in the interlayer space, which may also yield a band at ~1050 cm^{-1} (ν_1 mode).[36] The shoulder at approximately 971 cm^{-1} results from hydroxide bending modes and overlaps with absorptions at lower wavenumber (200-800 cm^{-1}) due to metal-oxygen vibrations within the layers.[37] The broad absorbance at 3400-3600 cm^{-1} corresponds to the OH stretching modes. Absorptions due to co-intercalated water molecules may be found at ~3000 cm^{-1} (broadened from hydrogen bonding between the interlayer anions and H_2O)[38] and ~1600 cm^{-1} (H_2O bending).[39]

2.2.1.3 Transmission electron microscopy

In order to characterise the size, size distribution and morphology of the MgAl-CO_3 LDH particles, transmission electron microscopy (TEM) studies were conducted. Representative TEM images and size distribution histograms are shown in Figure 2.3. Several images of each sample were taken in different areas of the grid. Mean particle sizes with standard deviations were calculated from measuring the diameter of at least 100 different particles. Standard deviations (σ) and variances (σ^2) were calculated (Table 2.4).

Table 2.4: MgAl-CO_3 LDH particle diameters from TEM images, means obtained from measurement of > 100 particles. 'σ' = standard deviation, 'σ^2' = variance. '*' indicates that the particle diameter was calculated from SEM images (Section 2.2.1.4) as the largest LDH particles were typically too large for the field of view on the TEM.

MgAl-CO_3 LDH (approx size/nm)	Mean particle diameter (nm)	σ	σ^2
20	19.6	5.2	27
40	42.4	13	169
60	64	14	196
70	71.56	21	449
190	187.7	70	4960
210	205.1	75	5580
400	400.2	142	20100
1070	1071	300	90000
2160	2158	790	624
2560	2560	485	235000
9900	9897*	1379	1900000

The standard deviation and variance of the particle size increase with the diameter, revealing broader distributions at larger particle sizes. However, the ratio of the standard deviation to the diameter remains fairly constant. Overall, a high degree of size control is achieved using the selected synthesis methods. All particles exhibit hexagonal platelet morphology, most clearly distinguishable for particles larger than 100 nm. For the largest size (9900 nm), most particles were too large to fit in the field of view of the instrument, therefore particle size measurements were performed on SEM images instead (Section 2.2.1.4).

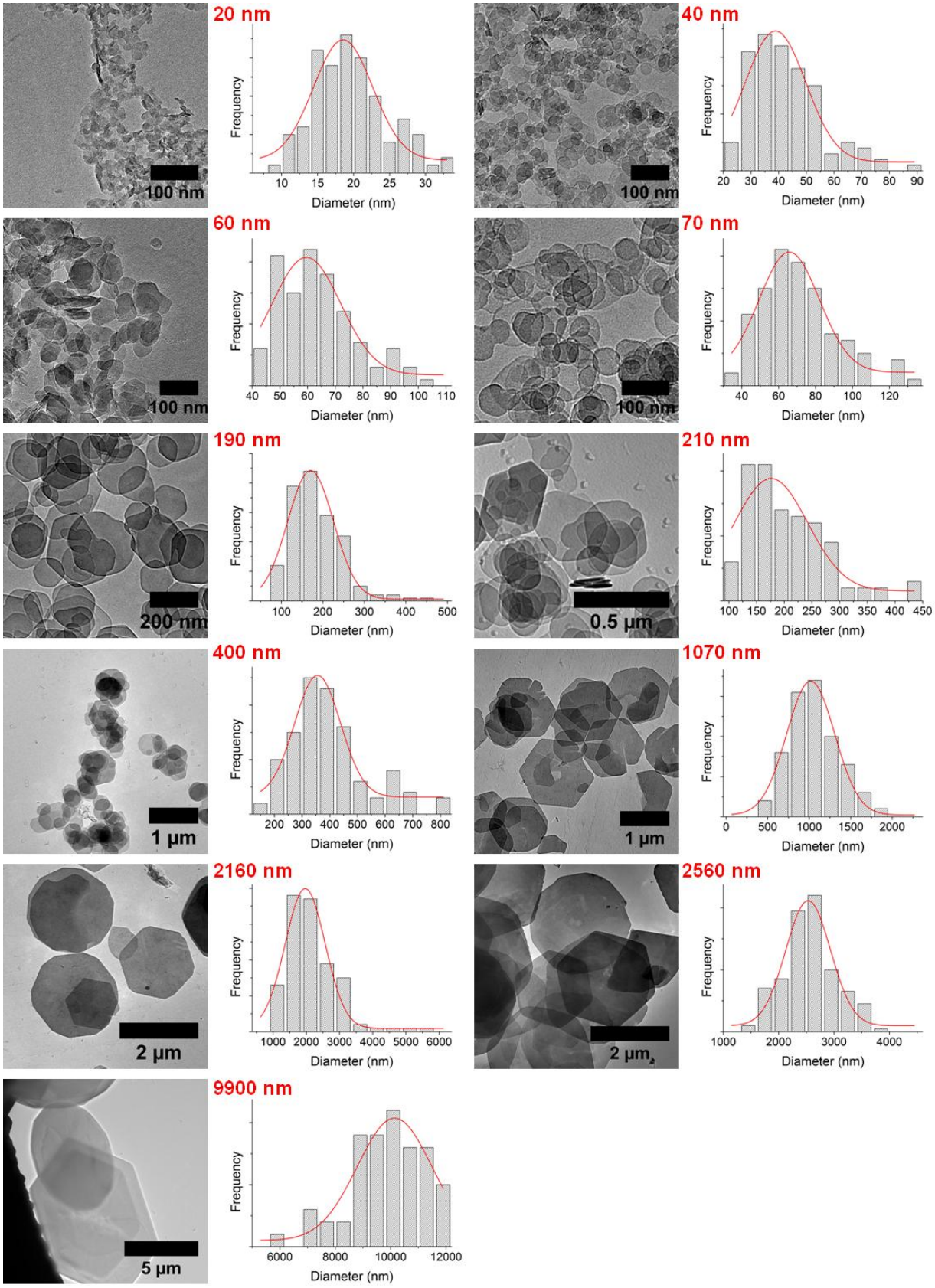

Figure 2.3: Representative TEM images with particle size distributions. Red lines indicate the best fit of a Gaussian curve, showing approximately normal distribution. The size distribution plot for 9900 nm MgAl-CO_3 LDH is from measurements obtained from SEM images.

2.2.1.4 Scanning electron microscopy

Scanning electron microscopy (SEM) was employed to determine the particle size distribution for the largest particle size (9900 nm) (Figure 2.4). Some particles exhibit a rosette type morphology (also documented by Okamoto *et al*.) which may be a consequence of fewer nucleation events occurring at low HMT concentration leading to two (or more) crystals growing from a single aluminium hydroxide nucleus.[21] Due to their close proximity, they interfere with each other to give an altered morphology. An alternative reason for this morphology is the formation of intergrowth phases in the *00l* direction, which grow at an angle to the original crystal.[40] Many plate like particles were also observed, and the mean particle size was calculated from the diameter of the platelet/rosette.

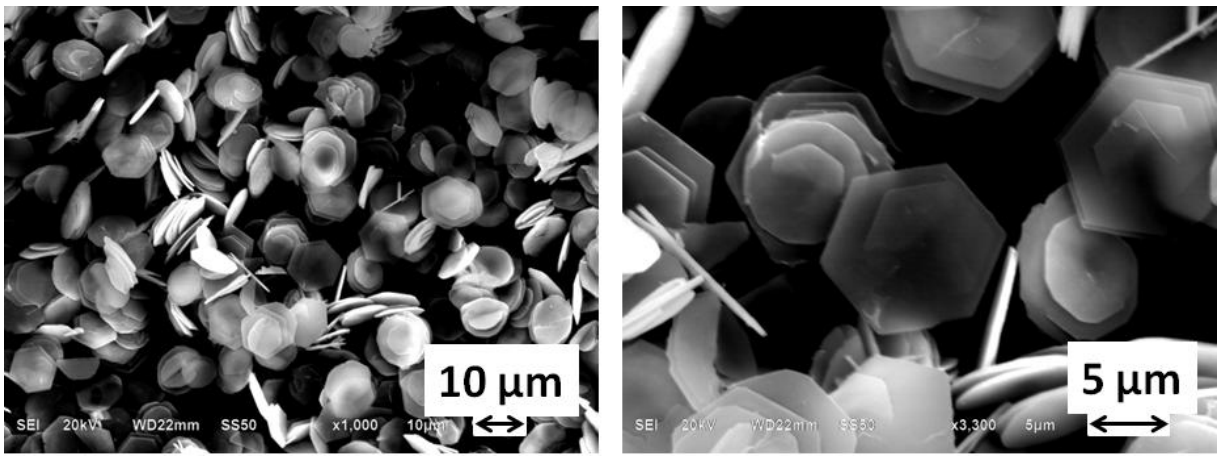

Figure 2.4: Representative SEM images of the 9900 nm MgAl-CO_3 LDH. Left hand side 1000x magnification, right hand side 3300x magnification.

For the other LDHs synthesised *via* homogeneous coprecipitation, distinct particles could be distinguished at higher magnifications, corresponding to similar sizes as those noted in the TEM images. Large aggregates, with dimensions of several tens of microns, were revealed under SEM analysis for the smaller particle sizes, alongside more disperse areas of sample corresponding to smaller aggregates or individual particles. Generally, the resolution of the instrument was not sufficient to image individual particles for these samples.

2.2.1.5 Atomic force microscopy

Atomic force microscopy (AFM) studies were carried out to further validate the particle diameters obtained from TEM, and to establish the particle thickness. A selection of MgAl-CO_3 LDHs was analysed, with a view to establishing how the particle thickness changes with increasing diameter, i.e. the aspect ratio. A few milligrams of LDH were dispersed in ethanol using sonication, then spin coated onto a highly ordered pyrolytic

graphite (HOPG) substrate. Images of the MgAl-CO_3 LDHs analysed are supplied in Figures 2.5 and 2.6.

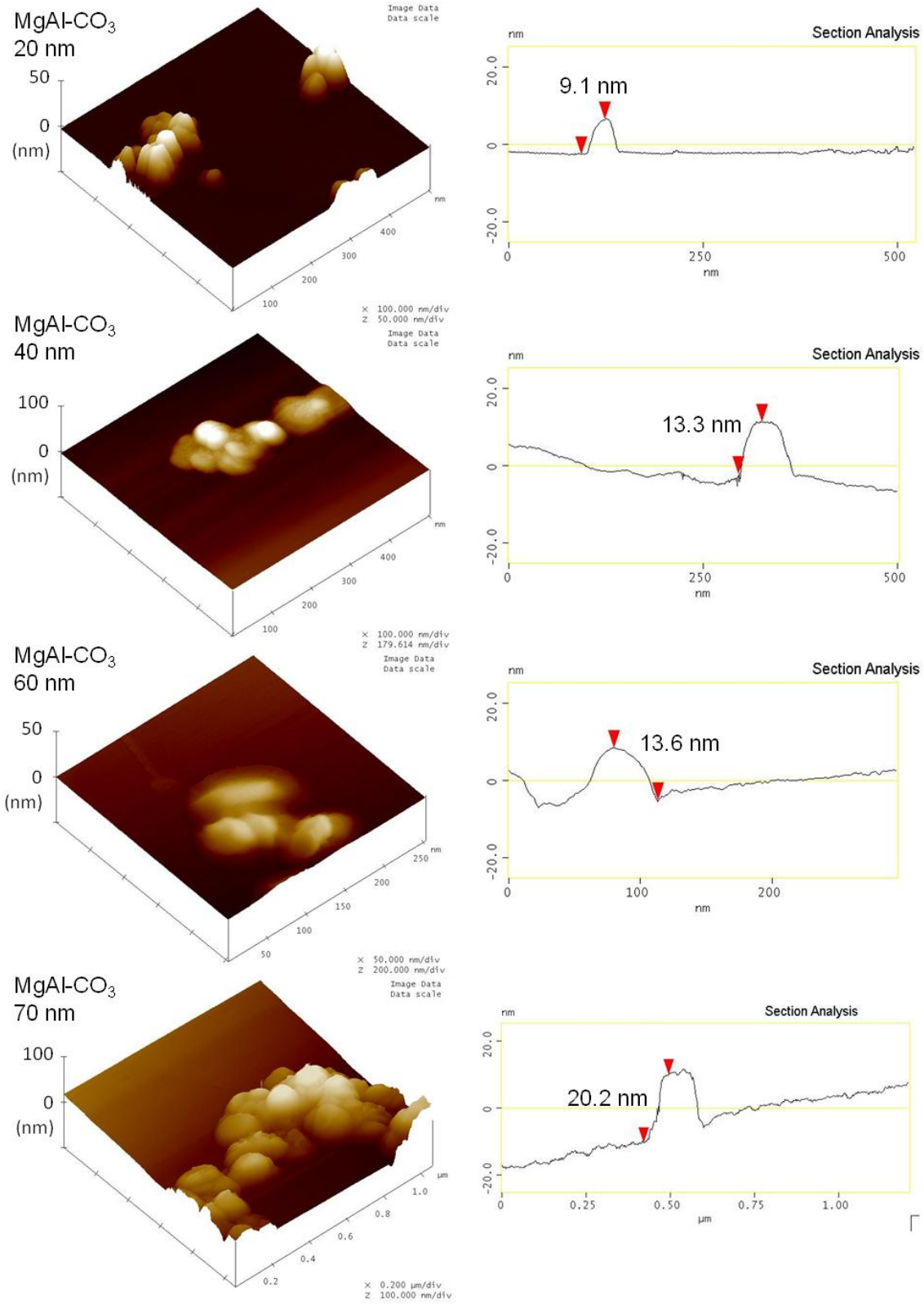

Figure 2.5: Three dimensional AFM images and representative cross sections of MgAl-CO_3 LDHs (20, 40, 60, 70 nm).

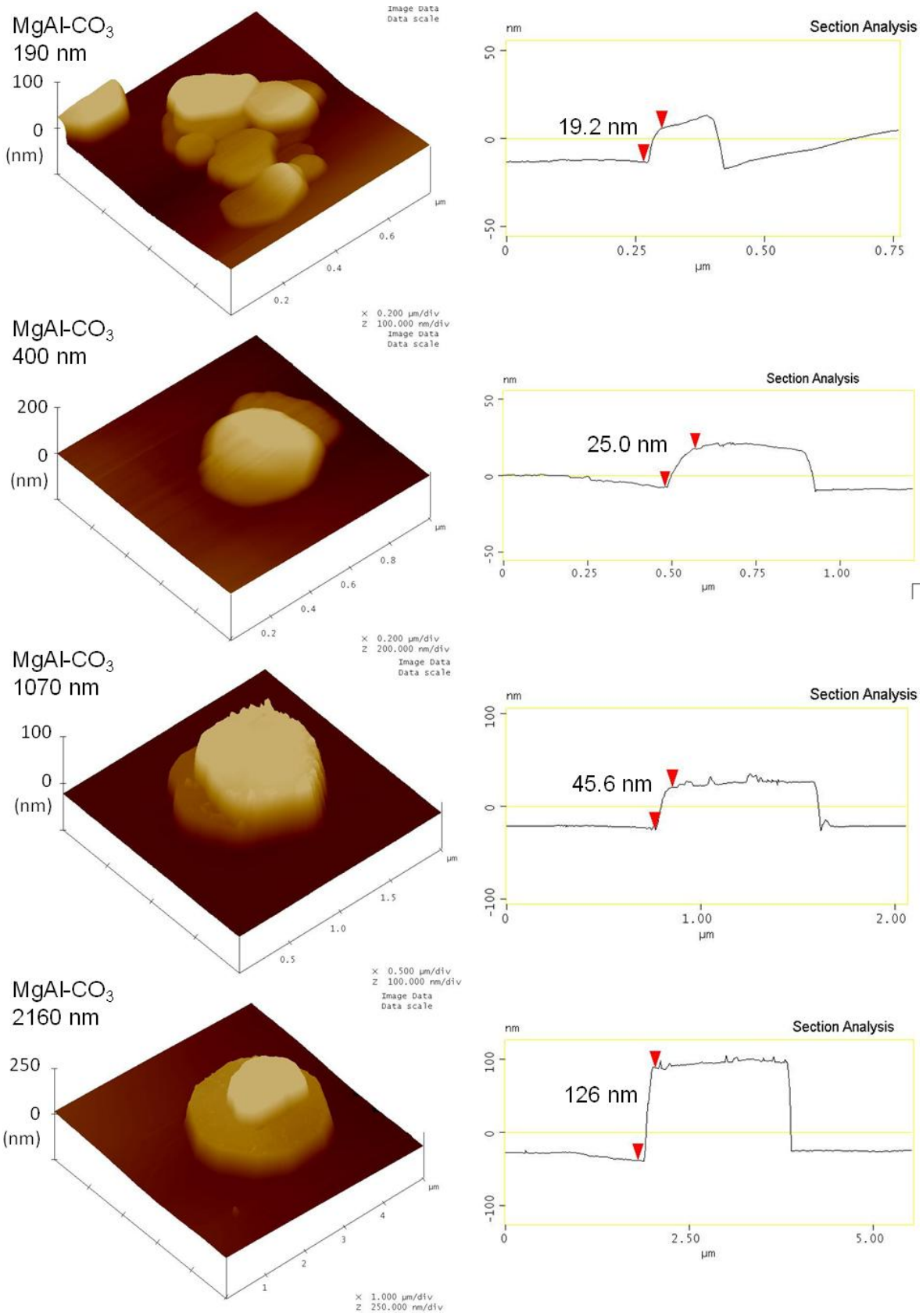

Figure 2.6: Three dimensional AFM images and representative cross sections of MgAl-CO_3 LDHs (190, 400, 1070, 2160 nm).

Difficulties arose in analysing particle sizes above 1 μm as stacked or edge-on particles exceeded the operational height of the AFM probe. Consequently, data for a limited number of particles were collected. Particle diameters and morphologies observed using AFM are consistent with those from TEM images. Table 2.5 displays the mean particle thickness and aspect ratio of the LDHs analysed.

Table 2.5: Diameter (from TEM measurements), approximate area of face (assuming circular disc-like morphology), particle thickness and aspect ratios for MgAl-CO_3 LDHs analysed by AFM. 'σ' = standard deviation. * only two measurements made due to difficulty in finding particles on the HOPG substrate and the number of particles that would fit in the field of view.

Mean diameter from TEM (nm)	Area (approx circle) (nm^2)	Particle thickness from AFM (nm)	σ	Aspect Ratio (nm)
19.6	61.6	7.7	0.4	8.0
42.4	133	14	1.9	9.8
64	201	11	1.5	18
71.56	225	13	4.0	17
187.7	590	17	9.5	34
400.2	1260	28	10	46
1071	3360	31	6.2	110
2158	6780	120*	0.9	56

Particle thickness increases with particle diameter, but not at the same rate. This is evidenced by the increasing aspect ratio, taken as the ratio between the top surface area and the thickness.[26] This reflects the tendency for larger particles to grow in the direction of the *ab*-plane, perpendicular to the direction of the layer stacking. During formation, LDHs preferentially grow in the direction of the *ab*-plane, possibly because it is entropically (and/or electrostatically) favourable to add ions onto existing layers in a crystal than to add a completely new layer.[41]

Moreover, some of the aspect ratios for the larger LDH particles are very high; aspect ratios from small values (5-10) up to 100 have been reported for LDHs in the literature.[42,43] The interlayer distance in MgAl-CO_3 LDHs is approximately 0.75 nm.[44] AFM measurements reveal the MgAl-CO_3 particles comprise of around ten to at least forty layers. Time constraints on the instrument prohibited full investigation of all LDH compositions. These observations are assumed to be illustrative of the behaviour of all of the LDHs in this chapter, as the range of the particle sizes of the MgAl-CO_3 LDHs investigated encompasses the size ranges of the other two LDH compositions (LiAl-CO_3 and MgFe-CO_3).

2.2.1.6 Zeta potential measurements

Prior work by Williams *et al*. implicates zeta potential as a key factor in modelling and predicting immune responses.[45] Particles in solution carry an overall charge at their surface,

resulting in association of oppositely charged ions from the solution with the surface. When a particle moves through the solution, a layer of closely associated ions move with it, whilst the more diffuse outer layer ions do not. These layers together comprise the electrical double layer. Zeta potential is the potential difference at the surface of hydrodynamic shear, or the boundary between the closely bound ions and diffuse outer layer. It is stated that for a suspension to be stable with respect to flocculation, its zeta potential must be below -30 mV or above +30 mV.[46] Zeta potential and pH measurements were performed on LDHs dispersed in phosphate buffered saline (PBS) at 10 mg/mL (Table 2.6).

Table 2.6: Zeta potential and pH measurements for MgAl-CO_3 LDHs at 10 mg/mL in PBS. 'σ' = standard deviation, all measurements were conducted at 25 °C.

MgAl-CO_3 LDH (approx size/nm)	Zeta potential (mV)	σ	pH (meter)	pH (paper)
20	-12.6	1.46	9.2	~9.25
40	-15.2	3.55	8.97	8.5
60	-26.7	4.9	9.16	9
70	-23.1	5.16	8.35	8
190	-18.6	6.68	8.17	8
210	-11.5	7.86	8.16	8
400	-15.7	10.78	7.4	8
1070	24.5	8.68	7.48	8
2160	2.7	5.95	7.94	8
2560	1.7	2.55	8.7	~8.25
9900	-0.6	0.96	7.86	8

Overall, all LDHs give alkaline suspensions, due to the presence of the hydroxide groups in the layers. The variation in pH may be a result of the synthesis method used: LDHs synthesised using coprecipitation/hydrothermal methods use higher pHs and stronger bases (usually NaOH). Despite the washing steps, traces of the bases remain yielding higher pHs when the particles are resuspended in PBS. Generally, with increasing pH, zeta potentials become more negative, as particle surfaces acquire more negative charge from the solution. Zeta potential values were negative for the smaller-sized particles, indicating a negatively charged surface, and become more positive for the larger particles. This approximately follows the pH of the suspensions, with the suspensions of smaller particles commonly having higher pHs. Documented zeta potentials for LDHs are typically positive, although many of these measurements were made in deionised water.[2] PBS contains a number of ions (Na^+, Cl^-, K^+, $H_2PO_4^-$, HPO_4^{2-}) that increase its ionic strength compared to water, and may alter the surface charge of the LDH.[47] Changes in ionic strength may have a profound effect on the size of the electrical double layer and the charges at the surface of the material.[46]

The smaller zeta potential values for the large MgAl-CO_3 LDHs synthesised using ARRs (2160, 2560 and 9900 nm) indicate the pH is close to the IEP. The IEP of MgAl-CO_3 LDH has been reported as pH 10,[17] although many factors, such as the ionic strength of the medium can affect this. For larger particles the proportion of the surface area of the LDH comprising the metal hydroxide sheets compared to the interlayer galleries is greater, as evidenced by the aspect ratios obtained from AFM studies in Section 2.2.1.5. Overall, the surface charge on the metal hydroxide sheets is more positive compared to the exposed interlayer galleries which contain the charge-compensating anions. Consequently, it may be hypothesised that a larger LDH particle at identical pH to a smaller particle will possess a more positive zeta potential, and at alkaline pHs this may take a value closer to zero.

2.2.1.7 Dynamic light scattering measurements

To determine the hydrodynamic size of the LDHs, as they are used in *in vitro* assays in Chapter Three, 50 µL of a 10 mg/mL LDH suspension in PBS was diluted to 500 µg/mL in 1 mL complete culture medium (RPMI medium supplemented with 10% fetal calf serum, penicillin/streptomycin and L-glutamine).

Table 2.7: Data for the most intense peak from DLS studies of MgAl-CO_3 LDHs. 'σ' = standard deviation. Approximate LDH size in left hand column is from TEM images.

Approx LDH size (nm)	Diameter (nm)	σ	Peak area (%)	σ
20	302	17.7	81.6	2.69
40	840	266	58.9	5.45
60	565	192	94.7	2.90
70	724	91.3	68.0	6.11
190	1530	1020	97.5	3.29
210	767	105	97.5	2.97
400	577	129	97.0	3.16
1070	872	178	100	0
2160	1100	73.5	100	0
2560	2270	992	90.6	16.3
9900	8744	1290	54.7	45.6

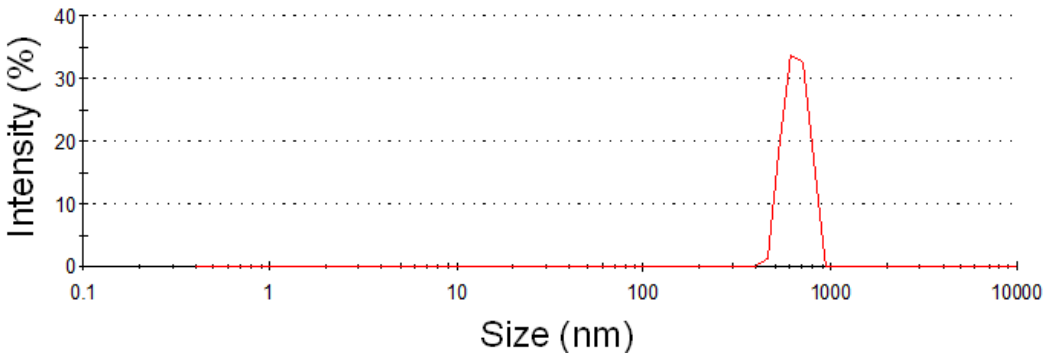

Figure 2.7: Illustrative DLS plot for 210 nm MgAl-CO_3 LDH. For plots with more than one peak, the most intense peak was selected for analysis.

Mean dynamic light scattering (DLS) measurements for the most intense peak were calculated to investigate overall trends in the hydrodynamic size of the particles (Table 2.7). An illustrative DLS distribution plot is provided in Figure 2.7. All hydrodynamic diameters are much larger than the particle diameters recorded using TEM, indicating a degree of aggregation in suspension. This is consistent with the zeta potential results discussed in Section 2.2.1.6, which reveal all zeta potentials for MgAl-CO_3 LDHs were within the range for flocculation/aggregation. It is possible that the behaviour of the particles is affected by the proteins, ions and various supplements in the medium as they may be adsorbed on the surface, yielding greater hydrodynamic diameters and influencing particle-particle interactions. Furthermore, anisotropic disc or plate-like particles may show complex stacking or ordering affects as well.[48]

2.2.2 Synthesis of LiAl-CO_3 LDHs

The methods applied previously to MgAl-CO_3 LDHs were extended to synthesise LiAl-CO_3 LDHs. Synthesis at high pH (> pH12) yielded products with broad reflections in the XRD spectra equivalent to the desired LDH structure. However, TEM images revealed them to be very fragmented particles with a broad size distribution, thus unsuitable for the purposes of this work. Conventional coprecipitation with aging at room temperature produced very small LiAl-CO_3 LDH particles (10-20 nm) which have a narrow size distribution (Table 2.8); adjusting the aging temperature to 75 °C yields larger particles. Hydrothermal treatment was successful at tailoring the LiAl-CO_3 particle size (for 350 and 810 nm particles) although aging temperatures of 150 °C and above resulted in the formation of impurities, identifiable as lithium aluminium oxide ($LiAlO_2$).

Table 2.8: Chemical formulae and synthesis outlines of LiAl-CO_3 LDHs. RT = room temperature, O/N = overnight. Approximate LDH sizes obtained from TEM images (Section 2.2.2.3).

Approx LDH size (nm)	Chemical formula (from EDX, EA and TGA)	Synthesis method
10	$[LiAl_2(OH)_6](CO_3)_{0.5}\cdot 0.8H_2O$	Coprecipitation RT O/N
30	$[LiAl_2(OH)_6](CO_3)_{0.5}\cdot 0.8H_2O$	Coprecipitation RT O/N using LiOH
100	$[LiAl_2(OH)_6](CO_3)_{0.5}\cdot 1.7H_2O$	Coprecipitation 75 °C O/N
350	$[LiAl_2(OH)_6](CO_3)_{0.5}\cdot 0.7H_2O$	Hydrothermal 100 °C 24 hrs
810	$[LiAl_2(OH)_6](CO_3)_{0.5}\cdot 0.8H_2O$	Hydrothermal 120 °C 24 hrs
1240	$[LiAl_2(OH)_6](CO_3)_{0.5}\cdot 0.9H_2O$	1 M Urea 120 °C O/N

Attempts were made to use HMT as an ammonia releasing reagent in order to tune LiAl-CO_3 LDH particle size above 1 μm. Unlike the MgAl-CO_3 LDHs synthesised using HMT, the products of these reactions exhibited broad reflections in their powder XRD data, resembling those of LDHs but at lower *d*-spacing. Sharp impurity reflections corresponding to bayerite

($Al(OH)_3$) were also observed. Use of 1 M urea as the ARR did yield a highly crystalline phase-pure LDH product. Decreasing the urea concentration to 0.33 M did not dramatically affect LDH particle size, whereas increasing it to 3 M resulted in fragmented particles with a broad size distribution. Table 2.8 details the compositions (as calculated from EA, EDX and TGA data) and mean sizes of the LiAl-CO_3 compounds chosen for further investigation. Full details of the synthesis methods may be found in Section 6.3.3. Composition remained approximately constant between LDHs, with an increase in co-intercalated water noted for 100 nm LiAl-CO_3 LDH.

2.2.2.1 Powder X-ray diffraction

Powder XRD data for LiAl-CO_3 LDHs are shown in Figure 2.8. LiAl LDHs exhibit polymorphism with both hexagonal and rhombohedral forms documented.[49,50,51] Britto and Kamath demonstrated that LiAl-CO_3 LDH products from lithium salt intercalation into bayerite may be indexed to a monoclinic unit cell and that LiAl-CO_3 attained *via* coprecipitation/urea hydrolysis exhibited comparable XRD patterns.[52] Other reports on urea synthesised LiAl-CO_3 LDH also specify a similar monoclinic unit cell, space group C2/m, a = 5.0901(8) Å, b = 8.801(1) Å, c = 7.730(1) Å, β = 103.08(1)°.[24] Therefore this unit cell was chosen for indexing the LiAl-CO_3 LDH products.

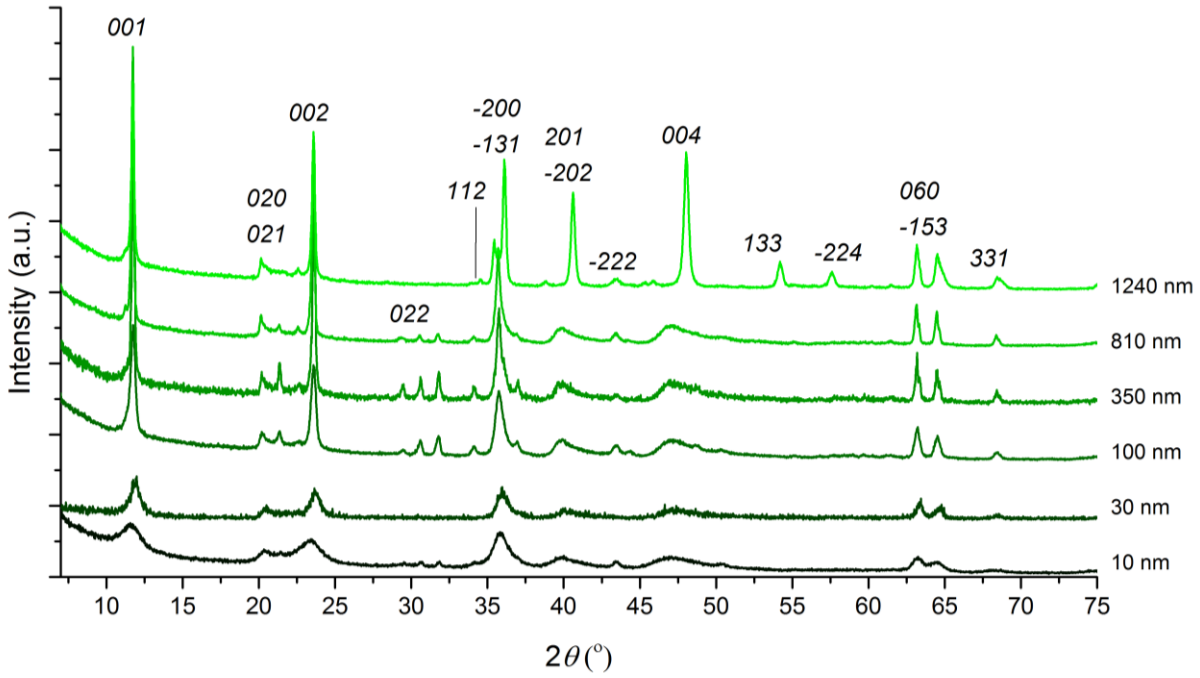

Figure 2.8: Indexed powder X-ray diffraction data for LiAl-CO_3 LDHs.

Table 2.9: Refined unit cell parameters for LiAl-CO_3 LDHs, indexed to a monoclinic unit cell, space group C2/m.

Approx LDH size (nm)	*a*-parameter (Å)	*b*-parameter (Å)	*c*-parameter (Å)	*β* (°)	Volume (Å^3)
10	5.082(2)	8.910(9)	7.824(2)	100.3(7)	348.5
30	5.078(7)	8.781(7)	7.588(9)	100.5(5)	332.7
100	5.123(9)	8.671(6)	7.701(8)	101.0(7)	335.8
350	4.998(2)	9.012(3)	7.740(0)	102.1(6)	340.8
810	5.137(0)	8.992(0)	7.724(1)	101.5(7)	349.6
1240	5.129(9)	8.845(5)	7.790(0)	103.6(9)	343.4

A full list of indexed reflections for each LiAl-CO_3 LDH may be found in Appendix A.2.2. Variations in lattice parameters and unit cell volumes between samples are small (Table 2.9). No clear trend can be ascertained in these variations, and it may be assumed that the lattice parameters are not affected by the preparation method. In an analogous fashion to the MgAl-CO_3 LDHs, greater crystallinity is observed with increasing particle size, indicated by a decrease in the full width at half maximum height (FWHM) of the reflections (Table 2.10). Analysis of the *001* and *060* reflections using the Scherrer equation confirms that CDS is increasing both within the layers (*060*) and perpendicular to the layers (*001*).

Table 2.10: Positions and line widths of selected Bragg reflections, with estimates of the crystallite domain size obtained from the Scherrer equation for LiAl-CO_3 LDHs. FWHM = full width at half maximum, CDS = crystallite domain size, Scherrer equation: $CDS = K\lambda(\beta\cos\Theta)^{-1}$, K = 0.89 [33]

	Bragg reflection							
	001				*060*			
Approx LDH size (nm)	*d*-spacing (Å)	2Θ (°)	FWHM (°)	CDS (nm)	*d*-spacing (Å)	2Θ (°)	FWHM (°)	CDS (nm)
10	7.70	11.5	0.40	45.6	1.47	63.1	0.74	21.5
30	7.41	11.9	0.65	25.3	1.47	63.4	0.65	24.9
100	7.52	11.8	0.27	63.8	1.47	63.2	0.23	68.3
350	7.52	11.8	0.20	84.9	1.47	63.2	0.34	47.7
810	7.55	11.7	0.20	85.9	1.47	63.1	0.34	47.5
1240	7.55	11.7	0.27	64.3	1.47	63.2	0.27	59.5

2.2.2.2 Fourier transform infrared spectroscopy

FTIR spectroscopy was used to confirm the presence of the interlayer carbonate anion and other characteristic LDH absorptions (Figure 2.9). All LDHs exhibit similar IR spectra with comparable features to those observed for MgAl-CO_3 LDHs.

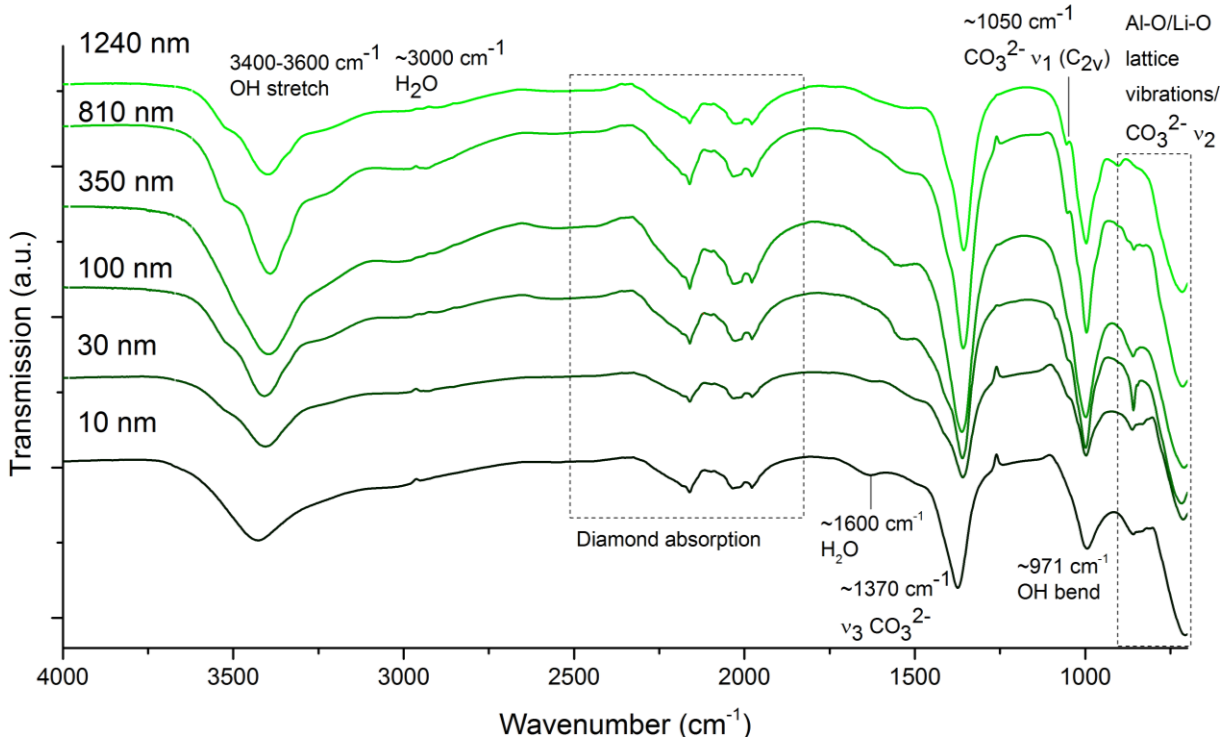

Figure 2.9: FTIR data for LiAl-CO_3 LDHs.

2.2.2.3 Transmission electron microscopy

TEM was used to determine particle sizes and size distributions (Figure 2.10). Particle size distributions for all LiAl-CO_3 LDHs are narrow, and display little overlap, indicating successful control of particle size (Table 2.11).

Table 2.11: LiAl-CO_3 LDH particle diameter from TEM images, means obtained from measurement of >100 particles. 'σ' = standard deviation, 'σ^2' = variance.

Approx LDH size (nm)	Mean particle diameter (nm)	σ	σ^2
10	10.1	2.3	5.3
30	29.2	7.7	58.8
100	98.5	34	1140
350	350.6	153	23500
810	810	231	53300
1240	1236	450	203000

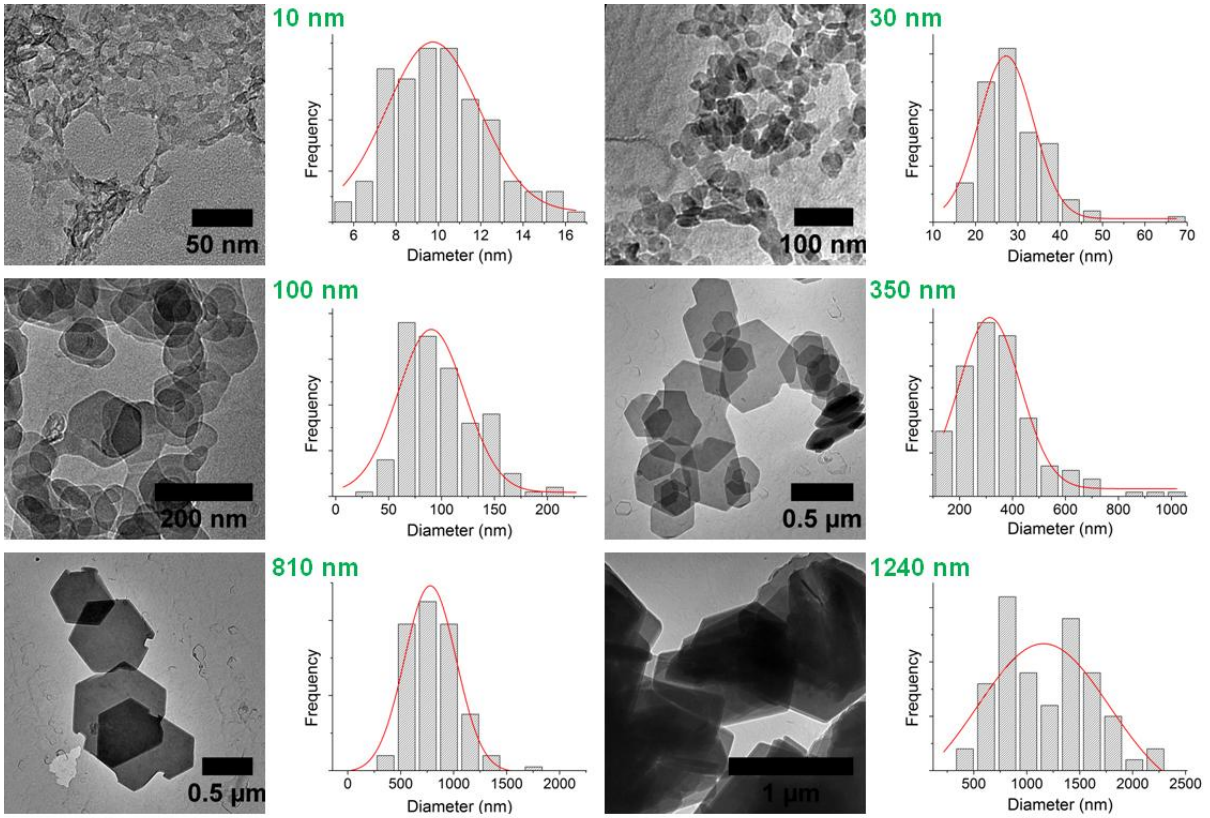

Figure 2.10: Representative TEM images with particle size distributions for LiAl-CO_3 LDHs. Red lines indicate the best fit of a Gaussian curve, showing approximately normal distribution.

All particles exhibit platelet morphology, with the hexagonal shape most evident for larger particles over 100 nm in diameter. The 1240 nm LiAl-CO_3 LDH particles appear to comprise of several layers, and the overall morphology is difficult to resolve from TEM images. Further investigation into this using SEM is described in Section 2.2.2.4.

2.2.2.4 Scanning electron microscopy

SEM images reveal that for smaller particle sizes, large irregularly shaped aggregates are present. For the hydrothermally synthesised samples (350 and 810 nm LiAl-CO_3) individual particles, consistent in size with those observed in TEM images could be discerned at high magnification (Figure 2.11). The LiAl-CO_3 LDH synthesised using homogeneous coprecipitation with urea displays a crumpled, almost ruffled morphology. This is similar to the 'rosette' type morphology, observed for the 9900 nm MgAl-CO_3 LDH sample, and is consistent with the overlapping layers observed in the TEM images. Again this could be a consequence of intergrowth phases, or multiple crystallites growing from a single nucleus, as described in Section 2.2.1.4.[21]

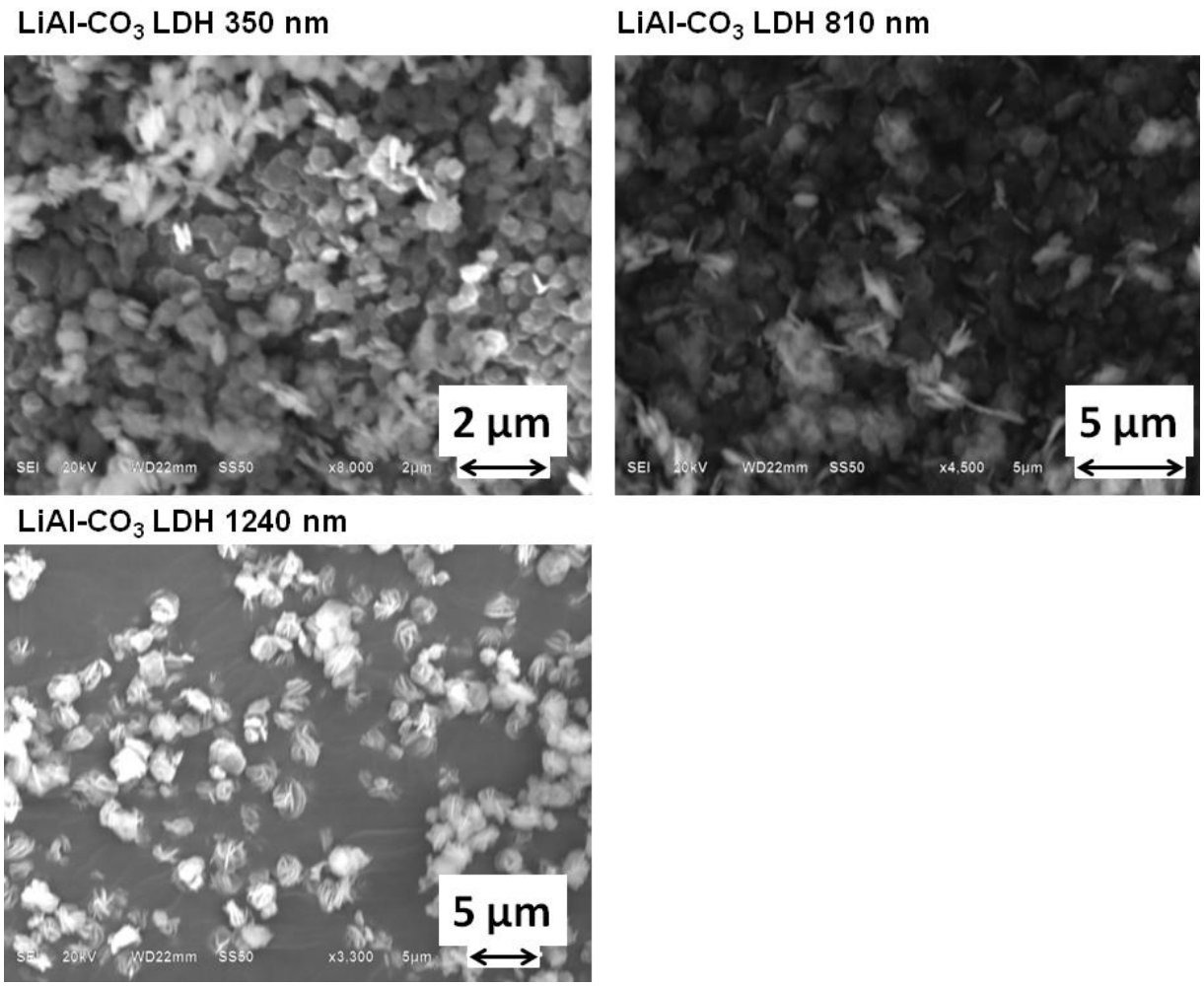

Figure 2.11: Representative SEM images of 350 nm LiAl-CO_3 (8000x magnification), 810 nm LiAl-CO_3 (4500x magnification) and 1240 nm LiAl-CO_3 LDH (3300x magnification).

2.2.2.5 Zeta potential measurements

Zeta potential measurements were undertaken for LiAl-CO_3 LDHs in PBS (Table 2.12). All LDHs raised the pH of the PBS significantly above the starting value of ~pH 7.4.

Table 2.12: Zeta potential and pH measurement data for LiAl-CO_3 LDHs at 10 mg/mL in PBS. 'σ' = standard deviation, all measurements were conducted at 25 °C.

Approx LDH size (nm)	Zeta potential (mV)	σ	pH (meter)	pH (paper)
10	-35.9	5.74	9.56	10
30	-40.6	9.59	9.12	8.5
100	-41.5	6.58	10.1	10
350	20.0	8.82	9.57	10
810	2.7	0.97	9.52	9
1240	3.1	1.51	7.88	8

Smaller particles display zeta potentials below -30 mV, indicating that they form stable suspensions without flocculation. Larger particle sizes produce more positive zeta potentials within the range of flocculation. The pH of the suspension of the 1240 nm LiAl-CO_3 LDH

particles synthesised using the urea method is lower than that of the other LDHs synthesised under more basic conditions. In conclusion, similar trends to those for the MgAl-CO_3 LDHs are observed and the reasons outlined in Section 2.2.1.6 may also be proposed for the observed increase in zeta potential with particle size for the LiAl-CO_3 LDHs.

2.2.2.6 Dynamic light scattering measurements

DLS measurements to obtain the hydrodynamic diameter of the particles were performed on LiAl-CO_3 LDHs in complete culture medium, as outlined in Section 2.2.1.7. Mean diameter values for the most intense peak were calculated (Table 2.13). All LDHs exist as aggregates around 1 μm in diameter: some show lower intensity peaks at smaller diameter, corresponding to smaller aggregates or non-aggregated particles. The mean diameter of the aggregates is larger for LDH particles with diameters over 100 nm (from TEM data), although anomalously small for 1240 nm LiAl-CO_3 LDH, possibly due to aggregation/sedimentation of the particles affecting the measurement.

Table 2.13: Data for the most intense peak from DLS studies of LiAl-CO_3 LDHs. 'σ' = standard deviation.

Approx LDH size (nm)	Diameter (nm)	σ	Peak area (%)	σ
10	867	154	97.9	3.5
30	851	317	55.0	6.0
100	1960	975	91.5	13.2
350	1220	231	96.6	5.6
810	1370	110	100.0	0.0
1240	782	86.3	100.0	0.0

2.2.3 Synthesis of MgFe-CO_3 LDHs

The synthesis methods outlined for LiAl-CO_3 and MgAl-CO_3 LDHs were also applied to MgFe-CO_3 LDHs. In this instance, the high pH coprecipitation method which yielded ~20 nm particles for MgAl-CO_3 LDH was successful, producing similarly sized particles (Table 2.14).

Table 2.14: Chemical formulae and synthesis outlines of MgFe-CO_3 LDHs. RT = room temperature, O/N = overnight. Approximate LDH sizes obtained from TEM images (Section 2.2.3.3).

Approx LDH size (nm)	Chemical formula (from EDX, EA and TGA)	Synthesis method
20	$[Mg_{3.1}Fe(OH)_{8.2}](CO_3)_{0.5}\cdot 1.8H_2O$	pH 12.5 RT 24 hrs
60	$[Mg_{3.3}Fe(OH)_{8.5}](CO_3)_{0.5}\cdot 1.7H_2O$	Hydrothermal 70 °C 24 hrs
70	$[Mg_{3.9}Fe(OH)_{9.8}](CO_3)_{0.5}\cdot 1.9H_2O$	Coprecipitation 80 °C O/N
100	$[Mg_{4.2}Fe(OH)_{10.3}](CO_3)_{0.5}\cdot 1.9H_2O$	Hydrothermal 90 °C 24 hrs
180	$[Mg_{3.9}Fe(OH)_{9.8}](CO_3)_{0.5}\cdot 1.8H_2O$	Hydrothermal 120 °C 24 hrs

Hydrothermal treatment with increasing aging temperature also produced particles with larger diameters. However, at aging temperatures above 120 °C impurity phases identified as $MgCO_3$ (magnesite) were observed in the powder X-ray diffraction data. Mg:Fe ratios are

generally around three to four, consistent with the literature; Mg:Fe ratios of four have been documented for MgFe-CO_3 LDHs synthesised *via* treatment of brucite with a solution of $Fe(NO_3)_3$ and Na_2CO_3.[53] Hydrothermal synthesis with urea and HMT as the ARRs did not yield LDH products. With urea, hydrated $MgCO_3$ formed whilst with HMT, Fe_2O_3 was produced. Han *et al*. have attempted synthesis of MgFe-LDHs with urea, and also failed, attributing this to the formation of an "$Fe(OH)_3$" gel instead.[54]

2.2.3.1 Powder X-ray diffraction

MgFe-CO_3 LDHs were indexed to a hexagonal unit cell, space group $R\bar{3}m$ as detailed by Manohara *et al* (Figure 2.12).[53] Full tables of indexed reflections may be found in Appendix A.2.3. Lattice parameters are approximately constant for all samples (Table 2.15). The *c*-parameter does correlate with the number of co-intercalated water moledules, as the LDH with the smallest number (60 nm MgFe-CO_3 LDH) also has the smallest *c*-parameter.

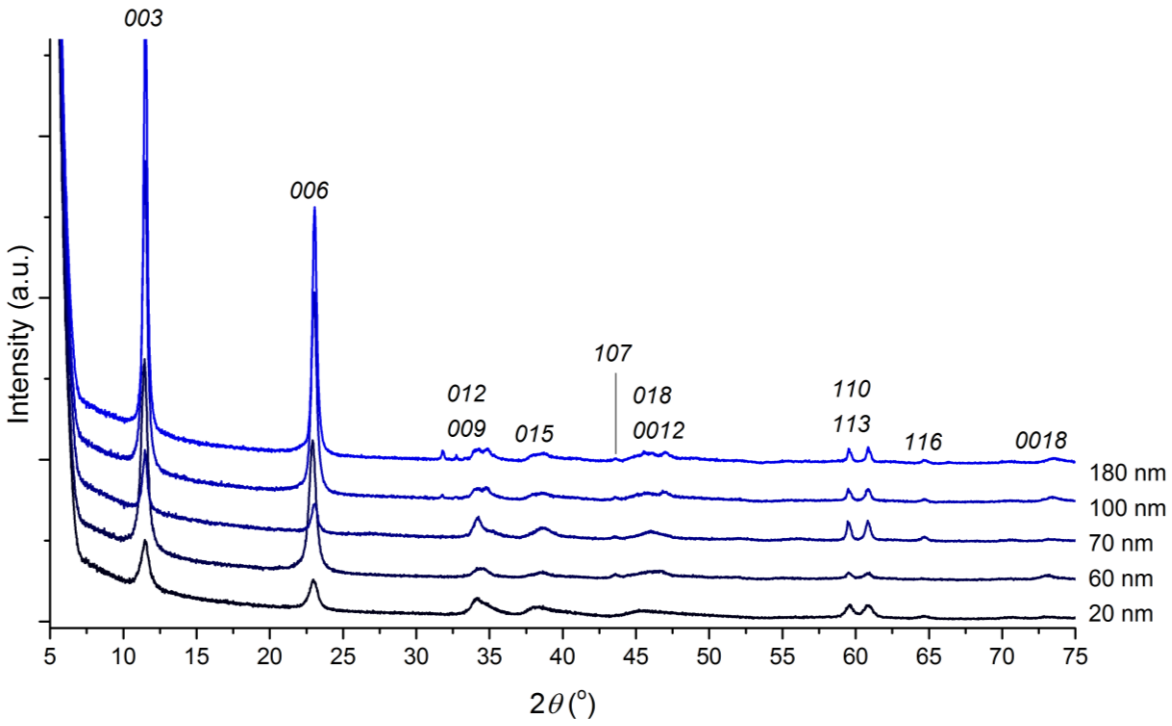

Figure 2.12: Indexed powder X-ray diffraction data for MgFe-CO_3 LDHs.

Table 2.15: Refined unit cell parameters for MgFe-CO_3 LDHs, indexed to a hexagonal unit cell, space group $R\bar{3}m$.

Approx LDH size (nm)	*a*(=*b*)parameter (Å)	*c*-parameter (Å)	Volume (Å^3)
20	3.102(9)	23.54(2)	196.3
60	3.108(0)	23.07(9)	193.1
70	3.101(7)	23.15(7)	192.9
100	3.102(7)	23.24(2)	193.8
180	3.102(9)	23.20(9)	193.5

Analysis of the *003* reflection using the Scherrer equation showed increasing crystallite domain size, in line with increasing particle size (Table 2.16). Due to the low intensity and the broadness of the reflections in the powder XRD patterns, analysis of a *0kl* reflection was not possible.

Table 2.16: Positions and line widths of the *003* Bragg reflection with estimates of the crystallite domain size obtained from the Scherrer equation for MgFe-CO_3 LDHs. FWHM = full width at half maximum, CDS = crystallite domain size, Scherrer equation: $CDS = K\lambda(\beta\cos\Theta)^{-1}$, K = 0.89 [33]

Approx LDH size (nm)	*d*-spacing (Å)	2Θ (°)	FWHM (°)	CDS (nm)
20	7.67	11.5	0.54	33.7
60	7.73	11.4	0.43	42.7
70	7.69	11.5	0.37	49.5
100	7.71	11.5	0.33	55.0
180	7.68	11.5	0.23	77.5

2.2.3.2 Fourier transform infrared spectroscopy

FTIR spectroscopy was employed to establish the presence of inter-layer carbonate, and the characteristic LDH absorptions (Figure 2.13). IR data are similar to those observed for the other two LDH compositions.

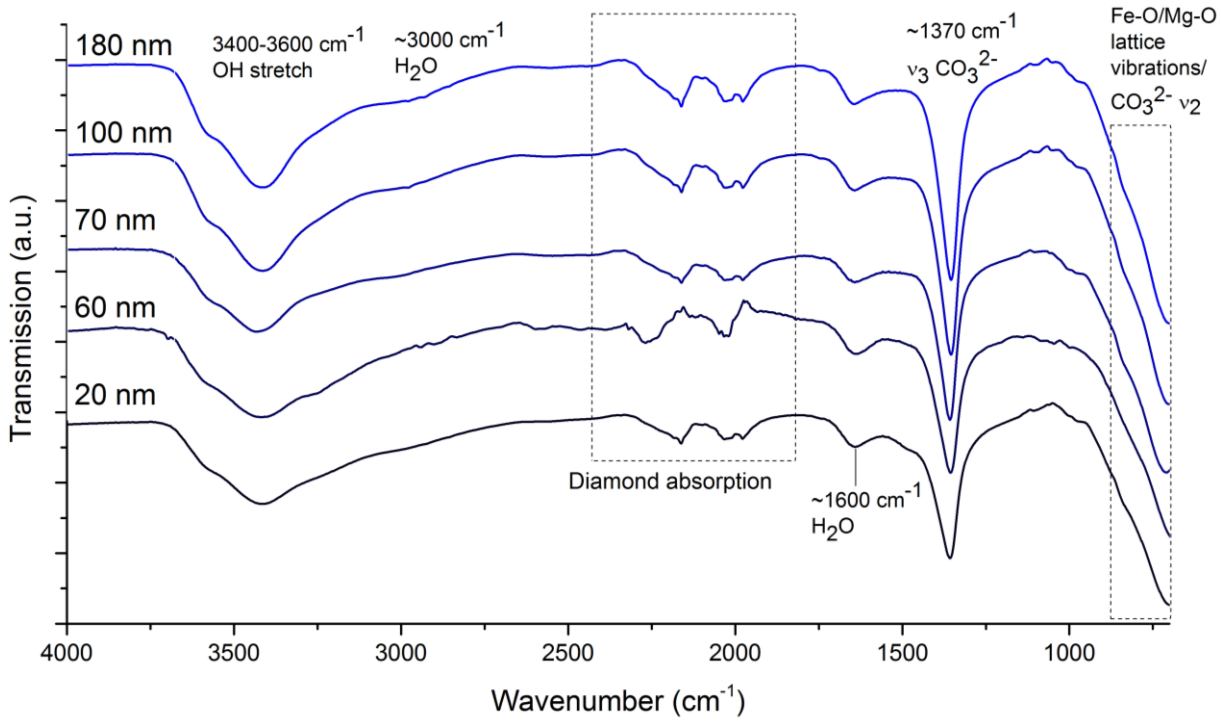

Figure 2.13: FTIR data for MgFe-CO_3 LDHs

2.2.3.3 Transmission electron microscopy

Particle sizes and particle size distributions from TEM images are supplied in Table 2.17 and Figure 2.14. The standard deviation increases with the particle diameter and some distributions do overlap. All MgFe-CO_3 LDHs exhibit platelet morphology. The size of MgFe-CO_3 particles was limited to a maximum of 180 nm by the availability of suitable synthesis methods.

Table 2.17: MgFe-CO_3 LDH particle diameter from TEM images, means obtained from measurement of >100 particles. 'σ' = standard deviation, 'σ^2' = variance.

Approx LDH size (nm)	Mean particle diameter (nm)	σ	σ^2
20	19.7	4.3	18.49
60	57.1	18.8	353.44
70	66.66	19.7	388.09
100	97.1	36.6	1339.56
180	183.7	58.9	3469.21

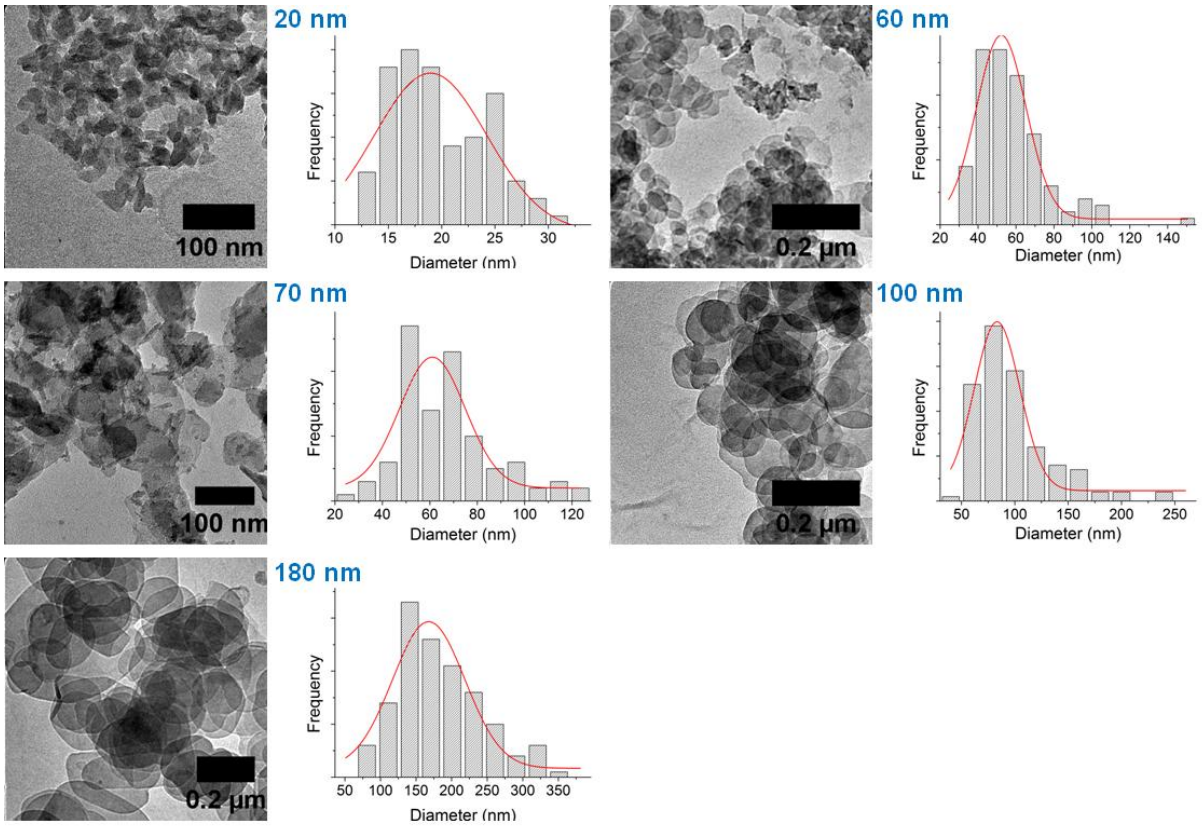

Figure 2.14: Representative TEM images with particle size distributions for MgFe-CO_3 LDHs. Red lines indicate the best fit of a Gaussian curve, showing approximately normal distribution.

2.2.3.4 Zeta potential measurements

Table 2.18 displays the results of zeta potential measurements made on 10 mg/mL suspensions of MgFe-CO_3 LDHs in PBS. All LDHs exhibit negative zeta potentials within the -30 mV to +30 mV range for particle flocculation, consistent with the propensity for aggregation observed in the DLS data. For the other LDH compositions, which were synthesised in larger particle sizes, a trend towards more positive zeta potentials was observed around 1 μm (for MgAl-CO_3) and 350 nm (for LiAl-CO_3). However, the maximum size of the MgFe-CO_3 LDH is below these values, consequently this trend could not be confirmed for this LDH composition.

Table 2.18: Zeta potential and pH measurements for MgFe-CO_3 LDHs at 10 mg/mL in PBS. 'σ' = standard deviation, all measurements performed at 25 °C.

Approx LDH size (nm)	Zeta potential (mV)	σ	pH (meter)	pH (paper)
20	-23.0	3.71	9.34	9
60	-14.1	3.51	9.15	8.5-9
70	-22.8	7.38	9.06	8.5
100	-19.0	3.82	8.7	8
180	-25.5	6.39	8.32	8

2.2.3.5 Dynamic light scattering measurements

Table 2.19 shows DLS data collected in complete culture medium as outlined previously. All MgFe-CO_3 LDHs display aggregation, which is more pronounced for the smaller particles, consistent with the zeta potentials described in the preceding section. Some sizes of MgFe-CO_3 LDH exhibit other, less intense, peaks at higher diameter, corresponding to larger aggregates.

Table 2.19: Data for the most intense peak from DLS studies of MgFe-CO_3 LDHs. 'σ' = standard deviation.

Approx LDH size (nm)	Diameter (nm)	σ	Peak area (%)	σ
20	1770	989	68.2	10.3
60	888	635	52.1	12.7
70	1300	170	85.7	11.3
100	443	36.3	97.9	1.9
180	755	90.6	88.1	5.8

2.2.4 Synthesis of other LDH compositions

Attempts were made to extend the successful synthesis methods to other LDHs containing anions apart from carbonate. Homogeneous coprecipitation methods using urea/HMT were not suitable because these invariably yield the carbonate containing product. Efforts were made to substitute the carbonate for an alternative species by using a slightly acidic solution of the desired anion.[55–57] However, this method generally yielded a mixture of both the carbonated and decarbonated products, rather than a pure phase.

The utility of reconstruction reactions was also explored. In these, the selected LDH is heated, thereby removing adsorbed and co-intercalated water molecules and interlayer anions, to produce a layered double oxide (LDO) and then 'reconstructed' in a solution of the replacement anion. The products of this were significantly less crystalline than the starting materials. Powder XRD reflections did indicate LDH formation, but due to the broadness of the peaks it was difficult to discern whether a change in the interlayer distance consistent with anion exchange had actually occurred, particularly as the size of both anions was similar.

Details of the successfully synthesised LDHs are supplied in Table 2.20. Other chemically pure LDHs were synthesised but displayed broad particle size distributions when analysed using TEM. Consequently, they were rejected for use in immunological assays investigating particle size effects. Generally, coprecipitation reactions did yield single phases with fairly narrow particle size distributions. Attempts to use hydrothermal methods to tune the size of CaAl LDHs resulted in both the LDH and impurity $CaCO_3$ phases forming. Increasing the reaction temperature during the CaAl-NO_3 LDH synthesis also resulted in impurities forming.

Table 2.20: Chemical formulae and synthesis outlines of the other LDHs. RT = room temperature, O/N = overnight. Approximate LDH sizes obtained from TEM images.

LDH composition	Approx LDH size (nm)	Chemical formula (from EDX, EA and TGA)	Synthesis method
MgAl-NO_3	70	$[Mg_{1.6}Al(OH)_{5.3}](NO_3)\cdot 0.4H_2O$	Coprecipitation 90 °C 72 hrs
MgAl-NO_3	160	$[Mg_{1.6}Al(OH)_{5.3}](NO_3)\cdot 0.5H_2O$	Hydrothermal 150 °C 24 hrs
MgFe-NO_3	50	$[Mg_{1.8}Fe(OH)_{5.5}](NO_3)\cdot 0.9H_2O$	Coprecipitation 80 °C 72 hrs
CaAl-NO_3	540	$[Ca_{1.7}Al(OH)_{5.3}](NO_3)\cdot 0.5H_2O$	Coprecipitation pH 11.5 RT O/N
CaAl-Cl	550	$[Ca_{1.7}Al(OH)_{5.4}]Cl\cdot 0.7H_2O$	Coprecipitation pH 11.5 65 °C O/N
MgAl-Cl	50	$[Mg_{2.4}Al(OH)_{6.7}]Cl\cdot H_2O$	Coprecipitation 80 °C 72 hrs

Full characterising data, including indexed powder XRD patterns and indexing, lattice parameters, FTIR spectra, TEM images, DLS and zeta potential analysis may be found in Appendix A.3.

2.2.5 Endotoxin testing

Four MgAl-CO_3 LDHs (20, 60, 1070 and 2160 nm) were tested for the presence of endotoxin. Samples were analysed by Lonza, (Rapid-Endotest service) using the Kinetic QCL™ limulus amebocyte assay. LDH samples were shaken for two hours in sterile PBS and an aliquot of the PBS sent for testing. The endotoxin content of all supernatants fell below the detectable range of the assay, less than 0.005 EU (endotoxin units)/mL. Due to the high cost of testing, not all LDH samples were tested; however, from these results it was assumed that generally the preparation and handling of the materials had not introduced any detectable contamination.

2.2.6 Commercial adjuvant characterisation

Powder X-ray diffraction analyses were conducted on dried samples of the commercial adjuvants, Imject and Alhydrogel. Imject consists primarily of brucite [$Mg(OH)_2$] with some reflections attributable to an aluminium phosphate containing phase (Figure 2.15). Alhydrogel reflections could be indexed to boehmite [AlO(OH)]. Both were consistent with observations made in complete characterisation studies of adjuvant materials conducted previously in the O'Hare group.[58]

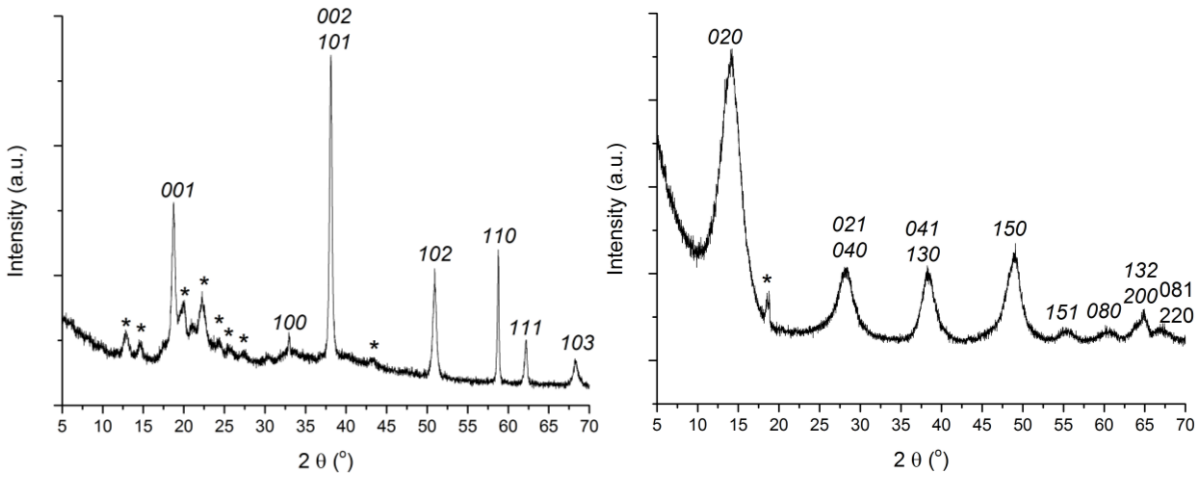

Figure 2.15: Indexed powder XRD patterns for Imject (left) and Alhydrogel (right). Indexed reflections for Imject indexed to brucite [$Mg(OH)_2$], trigonal unit cell, a = 3.14 Å, c = 4.77 Å, space group $P\bar{3}m1$, reflections marked '*' correspond to $AlPO_4$ and $AlPO_4{\cdot}xH_2O$. Indexed reflections for Alhydrogel correspond to boehmite [AlO(OH)], orthorhombic unit cell, a = 2.87 Å, b = 12.23 Å, c = 3.70 Å space group Cmcm, unindexed reflection marked '*' may correspond to bayerite [$Al(OH)_3$].

While the commercial adjuvants are not directly comparable to the LDHs as they comprise different materials and structures, TEM images were obtained to give an impression of the particle size distribution in these materials (Figure 2.16). Imject exists as both plate-like and rod-like particles with dimensions of around 100 to 200 nm. Some areas of the TEM grid were covered with a material with a gelatinous appearance, possibly caused by the stabiliser used to maintain an even suspension. Alhydrogel comprises particles with a flake-like morphology, less than 100 nm in length.

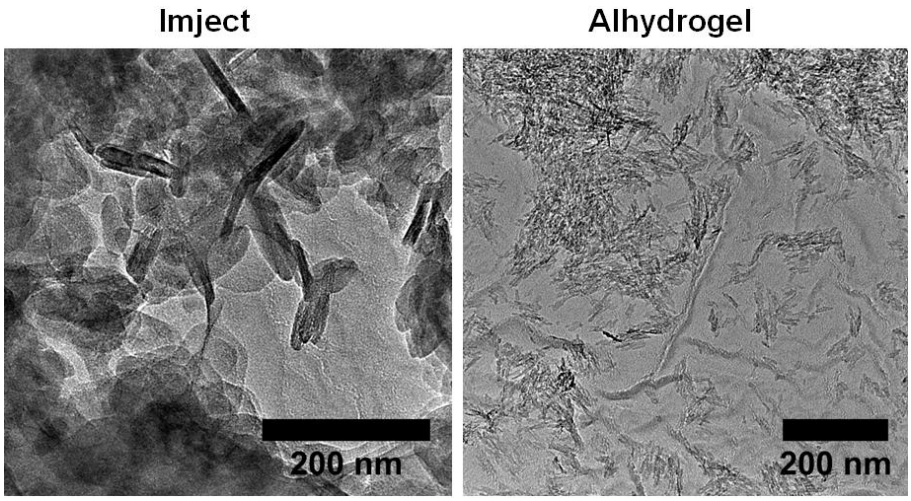

Figure 2.16: TEM images of commercial adjuvants Imject and Alhydrogel.

2.3 Conclusion

A panel of MgAl-CO_3 LDHs with precisely controlled particle sizes ranging from 20 to approximately 10000 nm were successfully synthesised using three main techniques: coprecipitation, hydrothermal treatment of the mixture resulting from rapid coprecipitation and homogeneous coprecipitation using amine releasing reagents. These methods were subsequently extended to LiAl-CO_3 and MgFe-CO_3 LDHs, to produce a library of fully-characterised LDHs with different chemical compositions and particle sizes. The crystalline phases comprising the two commercial adjuvants, Imject and Alhydrogel, were also confirmed.

All of the LDHs detailed in this chapter (MgAl-CO_3, LiAl-CO_3, MgFe-CO_3 and the other compositions) are employed in the *in vitro* dendritic cell assays and statistical modelling described in Chapter Three. Four of the LDHs synthesised *via* general coprecipitation methods (60 nm MgAl-CO_3, 70 nm MgFe-CO_3, 70 nm MgAl-NO_3 and the CaAl-NO_3 LDH) were also used in T cell response experiments in Chapter Four.

2.4 References

(1) Jiang, W.; Kim, B. Y. S.; Rutka, J. T.; Chan, W. C. W. *Nat. Nanotechnol.* **2008**, *3*, 145.
(2) Li, X.; Sloat, B. R.; Yanasarn, N.; Cui, Z. *Eur. J. Pharm. Biopharm.* **2011**, *78*, 107.
(3) Sun, B.; Ji, Z.; Liao, Y.; Wang, M.; Wang, X.; Dong, J. *ACS Nano* **2013**, *7*, 10834.
(4) Han, J.; Dou, Y.; Wei, M.; Evans, D. G.; Duan, X. *Chem. Eng. J.* **2011**, *169*, 371.
(5) Wang, Q.; Tay, H. H.; Guo, Z.; Chen, L.; Liu, Y.; Chang, J.; Zhong, Z.; Luo, J.; Borgna, A. *Appl. Clay Sci.* **2012**, *55*, 18.
(6) Song, Y.; Wang, J.; Li, Z.; Guan, D.; Mann, T.; Liu, Q.; Zhang, M.; Liu, L. *Microporous Mesoporous Mater.* **2012**, *148*, 159.
(7) Choi, S.-J.; Oh, J.-M.; Choy, J.-H. *J. Nanosci. Nanotechnol.* **2008**, *8*, 5297.
(8) Delhoyo, C. *Appl. Clay Sci.* **2007**, *36*, 103.
(9) Hu, G.; Wang, N.; O'Hare, D.; Davis, J. *J. Mater. Chem.* **2007**, *17*, 2257.
(10) Xu, Z. P.; Qing, G.; Lu, M. *Chem. Mater.* **2005**, *17*, 1055.
(11) Zhao, Y.; Li, F.; Zhang, R.; Evans, D. G.; Duan, X. *Chem. Mater.* **2002**, *14*, 4286.
(12) Xu, Z. P.; Stevenson, G.; Lu, C.-Q.; Lu, G. Q. M. *J. Phys. Chem. B* **2006**, *110*, 16923.
(13) Oh, J.-M.; Choi, S.-J.; Lee, G.-E.; Kim, J.-E.; Choy, J.-H. *Chem. Asian J.* **2009**, *4*, 67.
(14) Wang, J.; Lei, Z.; Qin, H.; Zhang, L.; Li, F. *Ind. Eng. Chem. Res.* **2011**, 7120.
(15) Oh, J.; Hwang, S.; Choy, J. *Solid State Ionics* **2002**, *151*, 285.
(16) Albiston, L.; Franklin, K. R.; Lee, E.; Smeuldersb, J. B. A. F. *J. Mater. Chem.* **1996**, *6*, 871.
(17) Chang, C.-T.; Liaw, B.-J.; Huang, C.-T.; Chen, Y.-Z. *Appl. Catal. A Gen.* **2007**, *332*, 216.
(18) Rao, M. M.; Reddy, B. R.; Jayalakshmi, M.; Jaya, V. S.; Sridhar, B. *Mater. Res. Bull.* **2005**, *40*, 347.
(19) Shaw, W. H. R.; Walker, D. G. *J. Am. Chem. Soc.* **1958**, *80*, 5337.
(20) Adachi-Pagano, M.; Forano, C.; Besse, J.-P. *J. Mater. Chem.* **2003**, *13*, 1988.
(21) Okamoto, K.; Iyi, N.; Sasaki, T. *Appl. Clay Sci.* **2007**, *37*, 23.
(22) Miyata, S. *Clays Clay Miner.* **1975**, *23*, 369.
(23) Ogawa, M.; Kaiho, H. *Langmuir* **2002**, *18*, 4240.
(24) Kang, H.; Leoni, M.; He, H.; Huang, G.; Yang, X. *Eur. J. Inorg. Chem.* **2012**, *2012*, 3859.
(25) Hu, G.; O'Hare, D. *J. Am. Chem. Soc.* **2005**, *127*, 17808.
(26) Wongariyakawee, A.; Schäeffel, F.; Warner, J. H.; O'Hare, D. *J. Mater. Chem.* **2012**, *22*, 7751.
(27) Wang, C. J.; Wu, Y. A.; Jacobs, R. M. J.; Warner, J. H.; Williams, G. R.; O'Hare, D. *Chem. Mater.* **2011**, *23*, 171.
(28) Chang, Z.; Evans, D. G.; Duan, X.; Vial, C.; Ghanbaja, J.; Prevot, V.; de Roy, M.; Forano, C. *J. Solid State Chem.* **2005**, *178*, 2766.
(29) Bugatti, V.; Esposito, L.; Franzetti, L.; Tammaro, L.; Vittoria, V. *Appl. Clay Sci.* **2013**, *75-76*, 46.
(30) Williams, G. R.; Fogg, A. M.; Sloan, J.; Taviot-Guého, C.; O'Hare, D. *Dalton Trans.* **2007**, *2*, 3499.
(31) Bellotto, M.; Rebours, B.; Clause, O.; Lynch, J.; Cedex, R. M.; Bazin, D.; Elkaı, E. *J. Phys. Chem.* **1996**, *100*, 8527.
(32) Laugier, J.; Bochu, B. CELREF, 2003, http://www.inpg.fr/LMGP.
(33) Drits, V. A.; Srodon, J.; Eberl, D. D. *Clays Clay Miner.* **1997**, *45* , 461.
(34) Scardi, P.; Leoni, M.; Delhez, R. *J. Appl. Crystallogr.* **2004**, *37*, 381.
(35) Prevot, V.; Forano, C.; Besse, J. P.; Abraham, F. *Inorg. Chem.* **1998**, *1669*, 4293.
(36) Hernandez-Moreno, M. J.; Ulibarri, M. A.; Rendon, J. L.; Serna, C. J. *Phys. Chem. Miner.* **1985**, *12*, 34.
(37) Cavani, F.; Trifiro, F.; Vaccari, A. *Catal. Today* **1991**, *11*, 173.
(38) White, W. B. *Am. Mineral.* **1971**, *56*, 46.
(39) Bish, D. L.; Brindley, G. W. *Am. Mineral.* **1977**, *62*, 458.
(40) Roeffaers, M. B. J.; Sels, B. F.; Uji-I, H.; De Schryver, F. C.; Jacobs, P. A.; De Vos, D. E.; Hofkens, J. *Nature* **2006**, *439*, 572.
(41) Kuang, Y.; Zhao, L.; Zhang, S.; Zhang, F.; Dong, M.; Xu, S. *Materials (Basel).* **2010**, *3*, 5220.

(42) Xu, Z. P.; Stevenson, G. S.; Lu, C.-Q.; Lu, G. Q. M.; Bartlett, P. F.; Gray, P. P. *J. Am. Chem. Soc.* **2006**, *128*, 36.
(43) Liu, Z.; Ma, R.; Ebina, Y.; Iyi, N.; Takada, K.; Sasaki, T. *Langmuir* **2007**, 861.
(44) Kanezaki, E. *Solid State Ionics* **1998**, *106*, 279.
(45) Williams, G. R.; Fierens, K.; Preston, S. G.; Rysnik, O.; Lunn, D.; De Prijck, S.; Kool, M.; Buckley, H.; Austyn, J. M.; O'Hare, D.; Lambrecht, B. N. *J. Exp. Med.* **2014**, *211*, 1019.
(46) Malvern Instruments. *Zeta Potential: An Introduction in 30 Minutes (Zetasizer Nano series technical note)*; Vol. 2, pp. 1–6.
(47) Sigma-Aldrich. *Product Information: Dulbecco's Phosphate Buffered Saline*; 2014; Vol. 182.
(48) Qazi, S. J. S.; Karlsson, G.; Rennie, A. R. *J. Colloid Interface Sci.* **2010**, *348*, 80.
(49) Poeppelmeier, K. R.; Hwu, S. J. *Inorg. Chem.* **1987**, *5*, 3297.
(50) Khan, A. I.; Williams, G. R.; Hu, G.; Rees, N. H.; O'Hare, D. *J. Solid State Chem.* **2010**, *183*, 2877.
(51) Markland, C.; Williams, G. R.; O'Hare, D. *J. Mater. Chem.* **2011**, *21*, 17896.
(52) Britto, S.; Kamath, P. V. *Inorg. Chem.* **2011**, *50*, 5619.
(53) Manohara, G. V; Prasanna, S. V; Kamath, P. V. *Eur. J. Inorg. Chem.* **2011**, 2624.
(54) Han, Y.; Liu, Z.; Yang, Z.; Wang, Z.; Tang, X.; Wang, T.; Fan, L.; Ooi, K. *Chem. Mater.* **2008**, *20*, 360.
(55) Iyi, N.; Matsumoto, T.; Kaneko, Y.; Kitamura, K. *Chem. Mater.* **2004**, 2926.
(56) Iyi, N.; Yamada, H.; Sasaki, T. *Appl. Clay Sci.* **2011**, *54*, 132.
(57) Xu, K. L.; Chen, G. M.; Shen, J. Q. *Chinese Chem. Lett.* **2012**, *23*, 805.
(58) Fisher, H. *Part II Thesis: Biomedical Applications of Layered Metal Hydroxides*; University of Oxford, 2010; pp. 16–29.

Chapter Three: Impact of Particle Size on Human Monocyte-Derived Dendritic Cells *In Vitro*

3.1 Introduction

Dendritic cells (DCs) are generally thought to be unique in their capacity to activate naïve T cells, and act as the bridge between the innate and adaptive immune responses.[1] Effective T cell activation requires at least two sets of signals; firstly, T cell receptor (TCR) recognition of the T cell epitope in the major histocompatability complex (MHC) molecules on the surface of the DC must occur; secondly, costimulatory molecules on the DC must engage with their counterparts on the surface of the T cell (e.g. CD80/CD86-CD28 interactions). This costimulation provides crucial activation signals to the T cell, initially triggering interlueukin-2 (IL-2) secretion, as well as supplying additional activation signals to the DC itself. Critically, in the absence of the second signal, T cells may become anergic and resistant to future attempts to induce proliferation.[2,3] Immature DCs do not express sufficient levels of the costimulatory molecules required to provide the second signal. Instead, expression of these molecules occurs in response to maturation signals received by the DC. DCs have been implicated as a target cell in the mechanism of action of alum adjuvants,[4] although the exact mechanism is still subject to speculation. Moreover, alum adjuvants induce increased expression of the costimulatory molecules required for T cell activation, the first step in achieving the objective of long-term immunity through vaccination.[5] Therefore studying the *in vitro* DC responses to materials is a useful starting point for establishing their potential as adjuvants.

3.1.1 DC maturation and costimulatory molecule expression

DCs have been shown to mature *in vitro* in response to a wide number of stimuli. These may be divided into three groups: firstly pathogen-associated molecular patterns (PAMPs), for example toll-like receptor (TLR) agonists such as lipopolysaccharide (LPS);[6] secondly damage-associated molecular patterns (DAMPs) associated with tissue damage and necrotic cell death (e.g. uric acid and ATP); and thirdly pro-inflammatory cytokines (e.g. TNF-α, IL-6 etc).[7–9] Upon receiving maturation signals, DCs typically up-regulate expression of surface molecules associated with T cell costimulation, and secrete pro-inflammatory cytokines. Expression of these costimulatory molecules is used to assess whether a stimulus is able to induce DC maturation or not. Mature DCs lose their capacity for phagocytosis, but greatly

increase their expression of MHC class I and II molecules, making them more efficient at antigen presentation.[10]

Two of the primary molecules expressed early on in DC maturation are CD80 (B7-1) and CD86 (B7-2). During costimulation these molecules bind to the T cell surface molecule CD28.[11] CD28 binding provides the second signal, contributing to T cell activation by promoting IL-2 gene transcription and regulating entry to the cell cycle.[12,13] At later stages, T cells express cytotoxic T-lymphocyte antigen-4 (CTLA-4), which may also bind to CD80/CD86 and has a role in regulation and tolerance induction.[14] Another member of the B7 family expressed on mature DCs is CD274 (also known as B7-H1 or programmed death ligand-1, PD-L1). This binds to CD279 (or programmed death-1, PD-1) and is structurally similar to CD80 and CD86. CD279 may have a regulatory role, since CD279 gene knock-out mice develop autoimmune disorders.[15] Further studies have confirmed this, demonstrating that CD274-CD279 interactions have a role in limiting immune responses and controlling self-tolerance.[16] CD275 [B7-H2 or inducible costimulator (ICOS) ligand] is a member of the B7 family expressed on immature DCs which binds to ICOS, a molecule only present on activated T cells.[17,18] While its function is unclear, it may nevertheless be a marker of immature DCs as it is down-regulated upon stimulation with LPS.[17] CD83 is a further surface molecule traditionally used as a marker for mature DCs,[19] although its overall role in the immune system is unclear, its presence does correlate with improved DC function.[20]

Signals are not only transferred from the DC to the T cell but also *vice versa*: CD40 is increased on DC maturation,[10] binding to CD40 ligand (CD40L/CD154) on activated $CD4^+$ T cells. This interaction stimulates increased adhesion and costimulatory molecule expression on the DC as well as promoting IL-12 secretion, a cytokine crucial for T_h1 differentiation.[21] Further DC maturation as a result of CD40L-CD40 interactions is referred to as 'DC licensing' and is often essential for the ability of the DC to facilitate $CD8^+$ T cell priming in T cell dependent responses.[22] A typical timeline of DC maturation may be considered as: immature ($CD275^+$), then mature and capable of $CD4^+$ T cell activation ($CD80^+$, $CD86^+$, $CD274^+$, $CD83^+$) then mature and licensed for $CD8^+$ T cell priming.[23]

3.1.2 Monocyte differentiation to dendritic cells *in vitro*

DCs are present in the blood at very low frequencies (0.25 - 0.884% peripheral blood leukocytes);[24] therefore methods of producing larger numbers of DC for use in experiments *in vitro* are required. Monocytes, a DC precursor *in vivo*, are present in much greater

concentrations (2-10% of leukocytes). Consequently, methods have been developed for differentiating monocytes isolated from human blood into DCs (Mo-DCs). Incubation with granulocyte macrophage colony stimulating factor (GM-CSF) and IL-4 for five or more days causes monocytes to develop into DCs.[25] The addition of IL-4 induces loss of the M-CSF receptor, discouraging differentiation into macrophages.[26]

Monocyte differentiation occurs without proliferation (as determined by tritiated thymidine incorporation assays) and is characterised by acquisition of DC morphology, increased CD1a expression, and decreased CD14 and CD64 expression.[27] Following incubation with GM-CSF and IL-4, Mo-DCs exhibit an immature phenotype. At this stage, the differentiation is not irreversible, since transferring the immature Mo-DC to medium without cytokines, or medium containing macrophage colony stimulating factor (M-CSF), causes the $CD1a^+$ DCs to convert to $CD1a^-CD14^+$ macrophages.[25] Methods of inducing rapid differentiation (within 48 hours) from monocytes to mature DCs have been reported, by employing pro-inflammatory cytokines (TNF-α , IL-1 , IL-6, PGE_2) in addition to GM-CSF and IL-4 for the final 24 hours of the culture.[7,28] However, *in vivo*, direct activation of DCs with PAMPs is required for effective $CD4^+$ and $CD8^+$ T cell priming, as demonstrated by Kratky *et al*.[29]

All Mo-DCs used in this Chapter were differentiated from enriched human monocytes over six days using GM-CSF and IL-4, and the terms Mo-DC and DC are used interchangeably in the discussion of these experiments.

3.1.3 Immunogenic synthetic materials

Various synthetic materials have been shown to trigger DC maturation *in vitro*. Vallhov *et al*. demonstrated that mesoporous silica particles could increase CD86 expression on human Mo-DC.[30] Metal-based inorganic materials, such as TiO_2 nanoparticles, NiTi rapidly solidified shape-memory alloy ribbons, and alum adjuvants themselves have been shown to induce classic maturation markers on human Mo-DCs.[31–33] Furthermore, titanium particles promote strong Nalp3-mediated immune responses *in vivo*,[34] consistent with mechanisms proposed for the action of alum adjuvants. This implies a common pathway for the immune system to both recognise and respond to inorganic materials.

The properties of nanoparticles may be tailored by functionalisation with biological species to create hybrid materials. Roles for hybridised nanoparticles in subunit vaccines are receiving a great deal of interest, since antigen can be incorporated into their formulation providing an all-in-one antigen and adjuvant.[35] By way of illustration, gold nanoparticles have been

conjugated to tumour-related glycan antigen polymers[36] or coated in West Nile virus envelope protein E as potential vaccines.[37] The latter study also implicated the size and shape of the nanoparticles as factors determining their activity both *in vitro* and *in vivo*.

A limited number of investigations into the immunogenic properties of layered double hydroxides (LDHs) exist. Li and co-workers investigated MgAl-NO_3 LDHs with varying ratios of Mg to Al revealing some capacity to induce up-regulation of CD86 and CD40 in murine bone marrow-derived DCs.[38] Follow-up studies utilised these LDHs as delivery vectors for DNA vaccines.[39] Williams *et al*. confirmed the ability of LDHs to stimulate human Mo-DCs in more extensive studies using a range of nine LDH compositions.[40]

3.1.4 Impact of particle size on immune responses

Research has revealed that cells of various types are sensitive to the size of the object they encounter. For instance, *in vivo*, the distribution of uncoated spherical silica beads injected intravenously into mice was found to be dependent on their size.[41] The effect of object size on uptake and localisation within the cell has also been probed: *in vitro* studies reveal stark differences in macrophage uptake of silica beads in different sizes.[42] The morphology of layered double hydroxide (LDH) particles may also determine their location within the cell.[43] Given the sensitivity of some biological responses to particle size, it is logical that immune responses may also be receptive to altering this parameter.

Some studies into dependence of immune responses (for example, costimulatory molecule expression, cytokine and antibody production) on the particle size of various inorganic materials have been performed. For instance, the aforementioned work into human DC responses to TiO_2 nanoparticles carried out by Schanen *et al*. illuminated non-uniform responses to different polymorphs (rutile 7-10 nm particles, anatase 15-20 nm particles) and morphologies (nanotubes, 70-150 nm length).[31] Other work highlights the use of silica (SiO_2) particles: Wang and co-workers report on the use of particles in oral vaccine adjuvants with mean sizes of 130 nm, 430 nm and 1-2 μm but with differing pore size.[44] They noted significant differences in antibody secretion in mice in response to the particles, indicating the potential for particle size to influence immune responses *in vivo*. Sun *et al*. investigated cellular responses to AlO(OH) nanorods in five sizes (from approximately 100 nm to 1 μm). Smaller nanorods induced greater IL-1β secretion in THP-1 cells and increased CD86 and CD80 expression in murine bone marrow-derived DCs.[45]

Differences in intracellular targeting of LDH nanoparticles with specific sizes has been noted by Chung (50 and 100 nm particles) and Oh (50, 100, 200 and 350 nm particles), demonstrating enhanced rates of uptake by human osteosarcoma cells (MNNG/HOS cell line) for the smaller 50 nm particles.[46,47] An investigation into cytotoxicity of 50, 100, 200 and 350 nm LDH particles by Choi noted variations in the viability and IL-8 production by human lung epithelial carcinoma cells (A549) *in vitro,* in particular that smaller particles were more cytotoxic.[48] However, none of these studies on LDHs utilised the full range of potential LDH particle sizes, or focused specifically on maturation of DCs in relation to adjuvanticity.

Synthetic organic materials have also been the subject of investigation: Li and co-workers concluded that 230 nm particles were most effective at producing OVA specific antibody responses in mice when testing the adjuvanticity of 230 nm and 708 nm ovalbumin (OVA) conjugated to particles synthesised from lecithin/glycerol monostearate.[49] They noted that "*future studies attempting to correlate the size of nanoparticles and their adjuvant activities need to consider formulation parameters to ensure that the particles are different only in size"*.

Critically, many studies suggest that altering particle size *does* have an effect on cell response, despite the different identities of materials investigated. However, these studies are disparate in nature, varying in terms of materials studied, morphology and size of particles, and immune responses recorded. Many focus on only a small number of sizes within a fairly narrow range; some simultaneously alter other parameters such as pore size and particle morphology making the effect of size itself difficult to determine. Accordingly, there is a requirement for a systematic investigation of particle size effects on immunogenicity across as wide a range of sizes as possible. As demonstrated in Chapter Two, synthesis of LDHs with near-identical compositions and particle sizes spanning several orders of magnitude is possible. In conjunction with their proven ability to elicit Mo-DC responses, this makes them excellent candidates for more thorough investigation into this area.

3.1.5 Statistical modelling of immune responses

In the prior work by Williams *et al*.[40] a novel statistical approach linking the physicochemical properties of a material and the immune response induced was developed. Nine LDHs with different compositions (LiAl-CO_3, LiAl-Cl, CaAl-NO_3, CaAl-Cl, MgAl-NO_3, MgAl-CO_3, MgFe-CO_3, MgFe-NO_3, MgFe-Cl LDH) were synthesised and their properties fully characterised. All possible combinations of either three or four properties of the LDH were

assessed to establish which subset had the highest correlation with the mean responses. This yielded a model of the form shown in Equation 3.1.

$$\ln response = A + B\sum_{i=1}^{i=3} C_i P_i$$

Equation 3.1: Model developed by Williams *et al*. for predicting immunological responses.[40] *A*, *B* and *C* are coefficients dependent on the response, and P_i is a physicochemical property of the LDH.

The subset of properties found to have the highest correlation was the radius of M^+/M^{2+} in the LDH, the *c*-parameter and the zeta potential. Two further LDHs (LiAl-NO_3 and MgAl-Cl LDH) were synthesised and characterised, and their properties used to predict the immune responses they would elicit. Subsequent testing proved these predictions were highly accurate and for the first time it was demonstrated that it is possible to model and predict immunogenicity based on chemistry.

3.1.6 Scope of this Chapter

Several references are made in the literature to the effects of changing particle size on immune responses; however, this has not been probed systematically over a wide range of sizes. The LDHs described in Chapter Two have mean sizes covering several orders of magnitude (from 10 nm up to 10 μm) with relatively uniform compositions for a given LDH (e.g. MgAl-CO_3). Consequently, they represent a library of particles covering a far larger size range than any previously described. Given the precedent of sensitivity in cell behaviour to particle size set in the literature, it was hypothesised that the responses of DCs would differ depending on the particle size of the LDH they were exposed to.

To test this hypothesis, *in vitro* tests on human Mo-DCs from multiple donors were conducted. Firstly, an optimum concentration of LDH particles was established through preliminary experiments. Secondly, DC viability was assessed in response to the full panel of LDHs described in Chapter Two. Thirdly, in combination with viability assessment, expression of surface molecules and cytokine secretion were also evaluated to determine whether DC response varies with particle size. Fourthly, statistical analysis was performed to extend the approach used by Williams *et al*.,[40] with the aim of determining the validity of their model with the new data collected, and whether it could be improved or refined by incorporating size as a further physicochemical property.

3.2 Results

3.2.1 Overview of experimental set-up and analysis

Mo-DCs were isolated and cultured according to the protocol described in Section 6.2.1. Prior to addition to the cells, all LDHs were dispersed in sterile phosphate-buffered saline (PBS) using sonication. Mo-DCs were incubated with the LDH particles overnight to allow sufficient time for the DC response to develop. Indeed, most *in vitro* Mo-DC experiments outlined in the literature have similar incubation times, for instance 16 or 24 hours.[31,45] Negative control wells of unstimulated cells, positive controls of cells stimulated with LPS (10 ng/mL), and the commercial alum adjuvants Imject and Alhydrogel (both at 500 µg/mL) were included for comparison. After overnight incubation cells were stained for viability with 7-aminoactinomycin D (7-AAD) and Annexin V, and fluorophore-conjugated antibodies against the surface molecules specified, then analysed by flow cytometry. The general gating strategy in the flow cytometry data employed throughout this chapter is supplied in Figure 3.1.

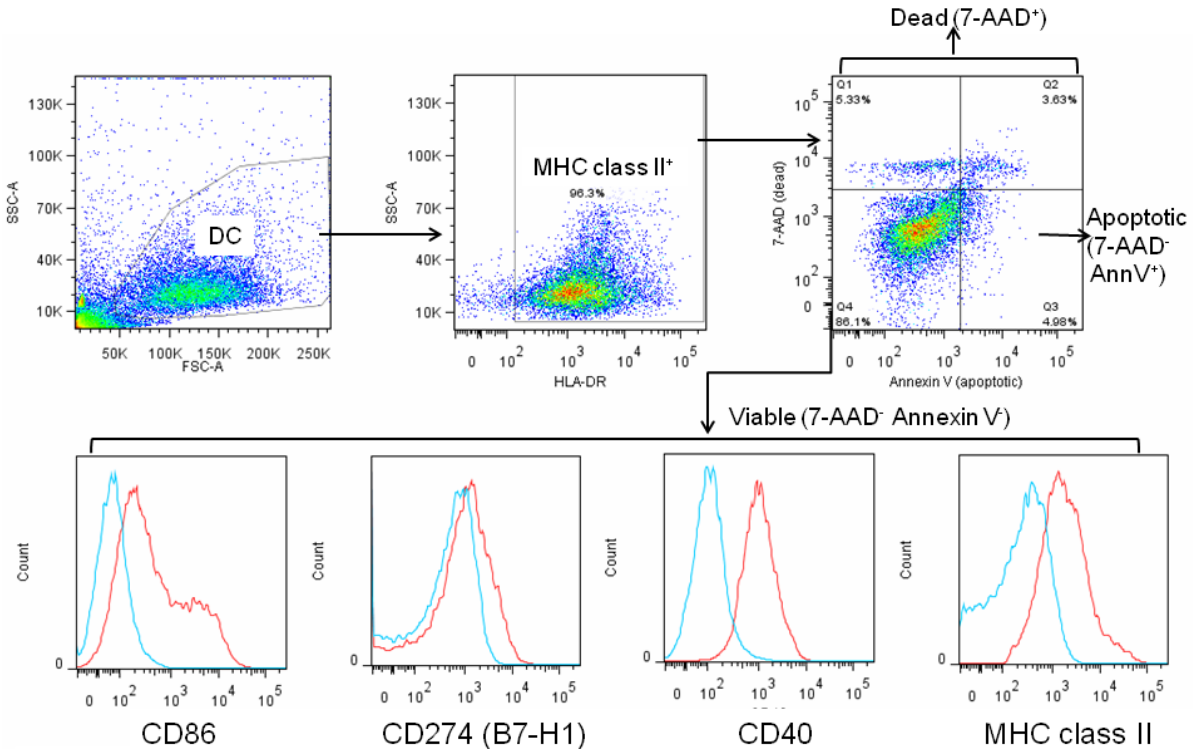

Figure 3.1: Gating strategy used for analysis of *in vitro* Mo-DC assay data to determine viability and costimulatory molecule expression. Firstly, the DC gate was set in the FSC/SSC, then MHC class II positive events selected. Finally, viable cells were designated as 7-AAD$^-$Annexin V$^-$, apoptotic cells as 7-AAD$^-$Annexin V$^+$ and dead cells as 7-AAD$^+$. Surface molecule expression was established by analysing the GMFI of the appropriate fluorophore for cells in the viable gate. The example above shows the fluorescence histograms of the isotype control (blue line) and stained LPS treated Mo-DC positive control (red line) for four surface molecules [CD86, CD274 (B7-H1), CD40 and MHC class II].

MHC class II positive cells were selected from the cells gate set in the forward scatter/side scatter (FSC/SSC). This minimised the amount of unstained debris in the analysis. Dead cells were defined as 7-AAD$^+$, apoptotic cells as 7-AAD$^-$Annexin V$^+$, and viable cells as 7-AAD$^-$Annexin V$^-$. In experiments where only 7-AAD staining was performed, cell death was recorded as the percentage cells 7-AAD$^+$. In subsequent analysis of cell forward scatter, side scatter and surface molecule expression (Sections 3.2.4 and 3.2.5), only cells in the 'viable' gate were assessed. Responses were recorded as geometric mean fluorescence intensity (GMFI) to account for the log-normal appearance of the response data observed in the histograms for each fluorescence channel. Appropriate single-well isotype controls were included for each condition in all experiments, and the background GMFI values from these were subtracted from the data for the experimental wells.

Unless otherwise stated, for every condition tested, three technical replicates were set up. It was confirmed by flow cytometry that LDH particles were not autofluorescent in the channels used, hence did not influence the results of any assays relying on fluorescence (e.g. flow cytometry, resazurin assays). Normalisation of the data, taking inter-donor variability into account, was performed on results from experiments on multiple donors to produce estimates and 95% confidence intervals. Additionally, significance data (p-values) compared to a reference level fixed effect (untreated cells, LPS, commercial adjuvants, etc) were calculated.

3.2.2 Preliminary LDH concentration studies

The concentration of the particles used can affect both cell viability and cellular response. Therefore it is crucial to select a concentration that is appropriate for the cell/particle combination under investigation. Titrations of LDH concentration for two differently-sized MgAl-CO_3 LDHs (as synthesised and characterised in Chapter Two) were performed to establish the effect of LDH dose on viability and surface molecule expression by human Mo-DCs. A smaller particle size (60 nm MgAl-CO_3 LDH) and a larger particle size (2560 nm MgAl-CO_3 LDH) were selected. Mo-DCs were incubated overnight with each LDH at concentrations from 50 μg/mL to 5000 μg/mL and assessed for necrotic cell death and costimulatory molecule expression using flow cytometry. Full tables of significance data for both responses are supplied in Appendix B.1. A balance between high viability and strong cellular response was sought after. This was with a view to enable larger assays involving many more LDHs to be performed using high-throughput techniques such as flow cytometry and enzyme-linked immunosorbent assays (ELISA).

3.2.2.1 LDH concentration effects on cell viability

Initial experiments were performed on Mo-DC from two donors. Viability data, as determined by 7-AAD staining, are shown below in Figure 3.2.

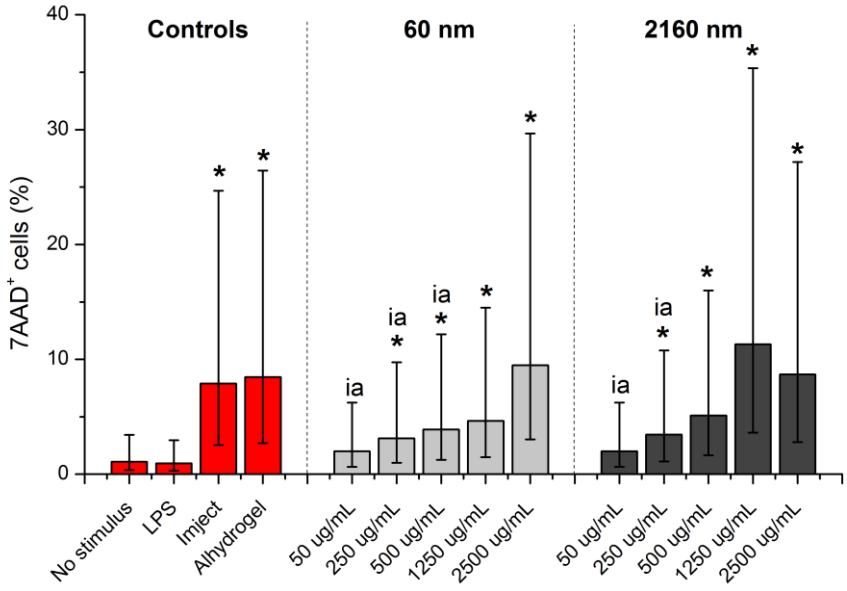

Figure 3.2: Percentages of dead Mo-DC (7-AAD$^+$) in response to a titration of LDH particles, to determine the LDH concentration for use in subsequent assays. Mo-DC were incubated overnight with varying LDH concentrations of small (60 nm diameter) and large (2160 nm diameter) MgAl-CO_3 LDH particles, stained for viability and surface molecule expression, then analysed using flow cytomtery. Unstimulated cells were included as a negative control, and Imject and Alhydrogel (both at 500 μg/mL) were included for comparison. Dead cells were determined as the percentage 7-AAD$^+$. Plotted values are normalised means from two donors. Error bars indicate 95% confidence intervals, '*', 'i' and 'a' indicate significant differences ($p<0.05$) relative to unstimulated cells, Imject and Alhydrogel treatments respectively.

Generally, cell death is greater at higher LDH concentrations. At all except the lowest concentration (50 μg/mL) of both sizes of MgAl-CO_3 LDH, statistically significant increases in the percentage of dead cells are observed relative to unstimulated cells. Lower concentrations of both particle sizes (<1250 μg/mL for 60 nm particles and <500 μg/mL for 2160 nm particles) also demonstrate diminished cell death compared to the commercial adjuvants Imject and Alhydrogel. No LDH concentration produces significantly greater cell death than the two commercial adjuvants. Forward scatter/side scatter plots for the higher concentrations of LDH were more difficult to analyse due to the greater quantity of particles present.

3.2.2.2 LDH concentration effects on surface molecule expression

In conjunction with viability assessments, cells were stained for CD86, CD274 (B7-H1), CD40, and MHC class II (HLA-DR) and analysed by flow cytometry (Figure 3.3).

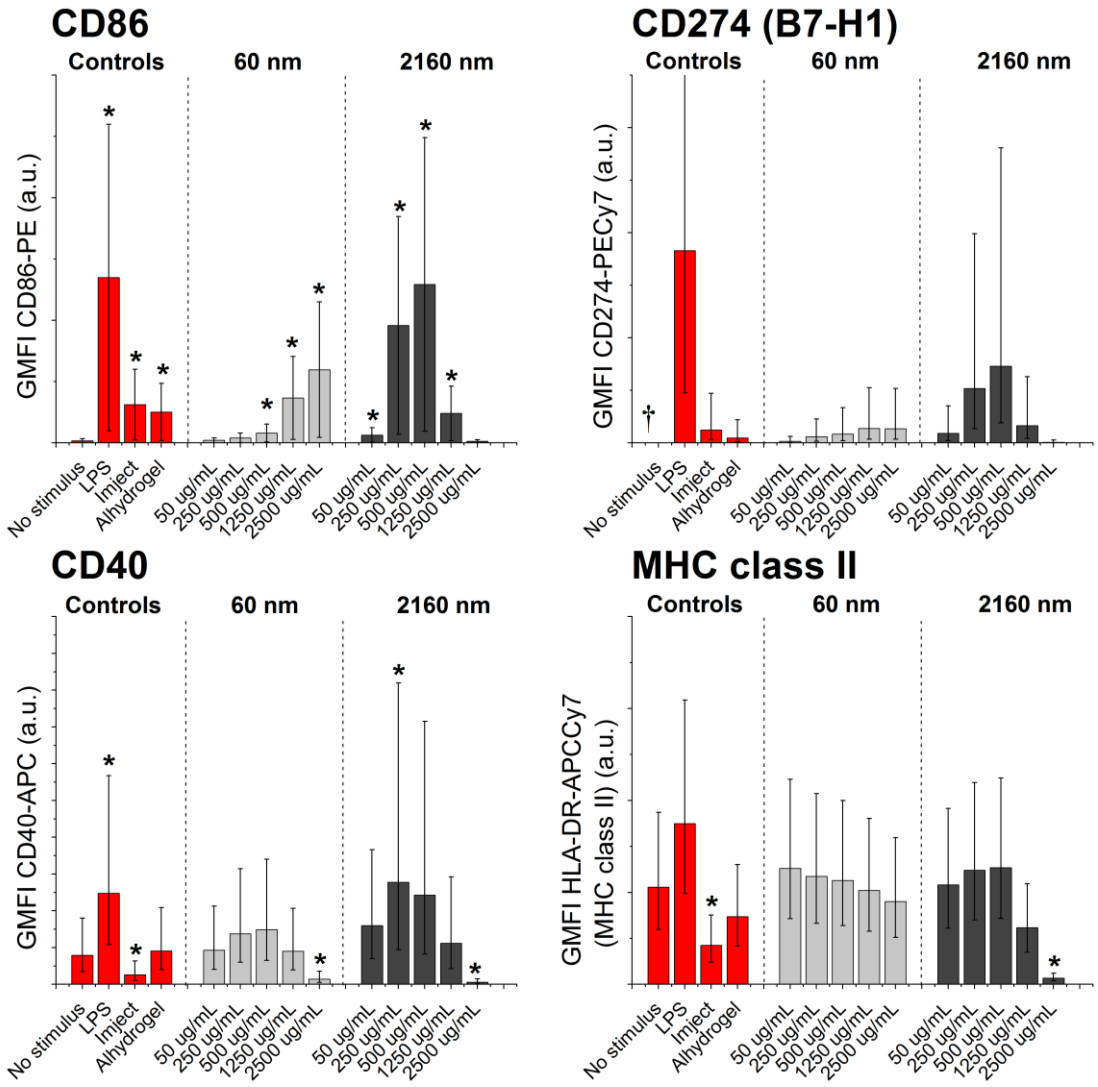

Figure 3.3: Mo-DC surface molecule expression in response to a titration of LDH particles, to determine the LDH concentration for use in subsequent assays. Mo-DCs were incubated overnight with varying LDH concentrations of small (60 nm diameter) and large (2160 nm diameter) MgAl-CO_3 LDH particles, stained for CD86, CD274 (B7-H1), CD40 and MHC class II then analysed using flow cytomtery. GMFI of cells in the viable (7-AAD$^-$) gate were used for analysis. † - no CD274 (B7-H1) data is shown for the untreated cells as subtracting the PE-cyanine 7 isotype control values gave negative results, consequently, statistical comparisons between the untreated cells and the LDH-treated cells could not be made. Plotted values are normalised means from two donors. Error bars indicate 95% confidence intervals, '*' indicates a significant difference ($p<0.05$) relative to the unstimulated cells control.

LDH dose dependence is apparent for CD86, where higher concentrations generally induce greater expression. However, for the larger MgAl-CO_3 LDH particles, this decreases again at the two highest concentrations. CD274 (B7-H1) also shows some evidence of concentration dependence, although the significance of this could not be determined due to the difficulty in

obtaining a background reading for untreated cells. Both CD40 and MHC class II show little concentration dependence, although it may be noted that for all four molecules, a decrease is observed at the highest LDH concentration. At the highest concentrations (1000 and 5000 μg/mL) analysis was hindered by the large number of events in the forward scatter/side scatter. Consequently, these concentrations were rejected for use in future experiments.

A concentration of 500 μg/mL was selected for use in subsequent experiments; at this concentration viability was not adversely affected but cellular response could still be determined. This is consistent with studies into ZnAl-LDH and MgAl-LDH toxicity performed by Choi *et al*. on various cell lines, where concentrations up to 500 μg/mL were found to have no significant effect on cytotoxicity in incubations up to 48 hours.[50]

3.2.3 DC viability studies

Further experiments were conducted at the chosen LDH concentration of 500 μg/mL to determine the effects of altering the LDH particle size on Mo-DC viability, using the full panel of LDHs synthesised in Chapter Two. Imject and Alhydrogel were included for comparison purposes in all experiments. Insights into the nature of cell death were provided by Annexin V/7-AAD staining. The results of these were then confirmed using resazurin assays.

3.2.3.1 7-AAD/Annexin V staining results

In conjunction with staining for costimulatory molecules (Section 3.2.5), Mo-DCs were simultaneously stained for cell death with the non-vital DNA dye 7-AAD,[51] and apoptosis with Annexin V-FITC, then analysed using flow cytometry. Figure 3.4 displays plots of particle size (mean values from TEM measurements) *versus* percentage dead or apoptotic cells for each of the LDH compositions. Significance testing was also performed to give the significance data supplied in Appendix B.2.

Incubation with every LDH size produces significantly higher percentages of dead cells compared to the unstimulated control. However, overall the estimated mean values for the percentages of both dead and apoptotic cells are generally quite low; no LDH particle size induces significantly higher cell death or apoptosis than the commercial adjuvants. All three LDH compositions with multiple particle sizes (MgAl-CO_3, LiAl-CO_3 and MgFe-CO_3) show greater cell death for LDH particle sizes above approximately 100 nm, although for MgAl-CO_3 and LiAl-CO_3 LDH this decreases for the largest particles.

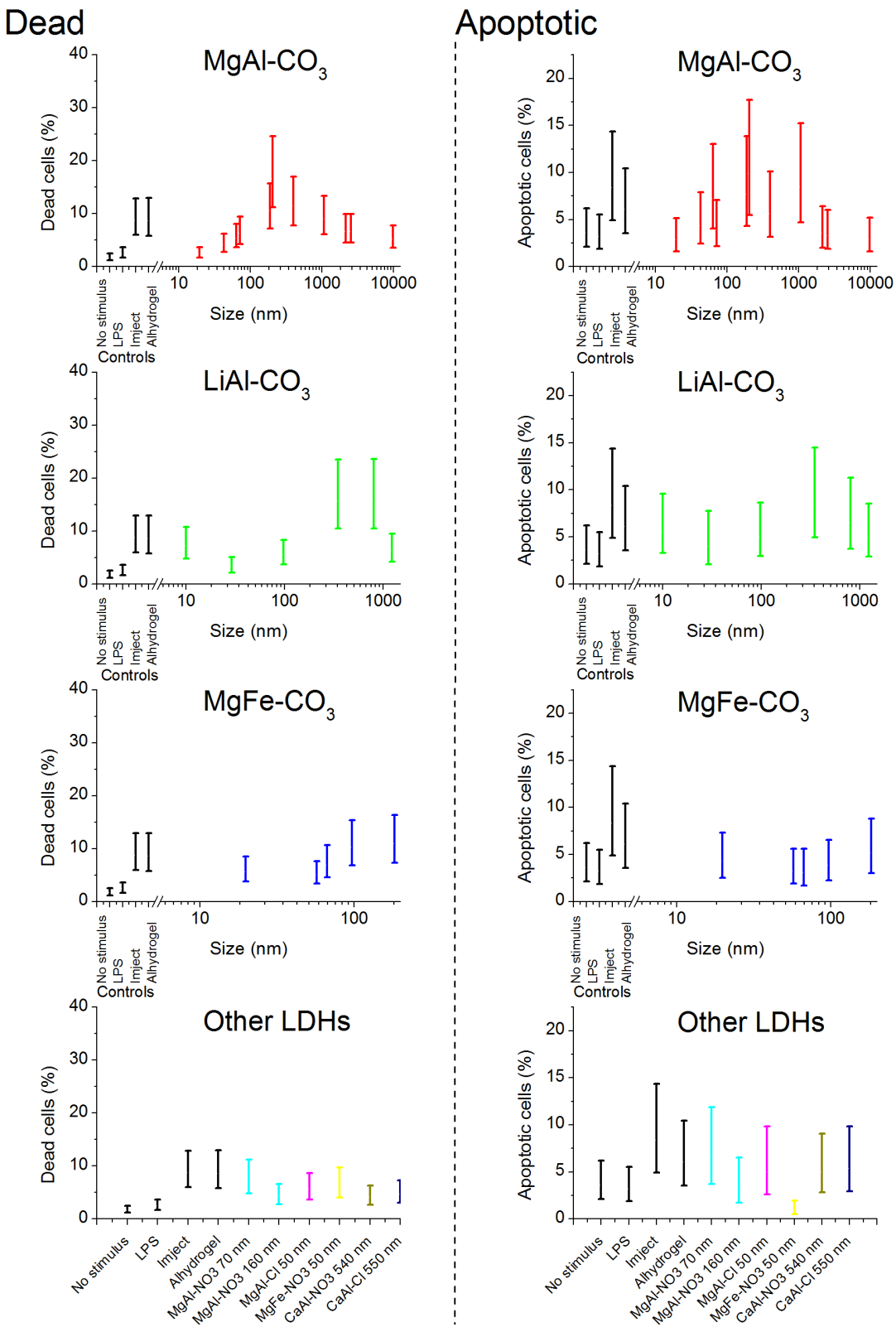

Figure 3.4: Estimated means of percentages of Mo-DCs dead or apoptotic, measured in response to each LDH described in Chapter Two, as a function of particle size. Scatter plots of percentage cells dead (left hand side, 7-AAD$^+$) and apoptotic (right hand side, 7-AAD$^-$Annexin V$^+$) *versus* particle size, grouped by LDH composition (MgAl-CO_3, LiAl-CO_3, MgFe-CO_3, and other LDH compositions). Mo-DCs were incubated overnight with the LDHs detailed in Chapter Two at 500 μg/mL, then stained (7-AAD/Annexin V) and analysed by flow cytometry. Data were normalised across multiple donors for each response, n = 15 for dead, n = 3 for apoptotic. Error bars indicate 95% confidence intervals.

The percentage of apoptotic cells displays no clear change with increasing particle size. Overall, induction of apoptosis is low, which is to be expected, as generally apoptosis is mediated by receptors such as the Fas and TNF receptors or an absence of growth/survival factors.[52] Possibly, some stress-induced apoptosis may be occurring, as the presence of LDH particles inside the cell may perturb the endoplasmic reticulum or cause DNA damage.[53,54] Further investigations into LDH internalisation may be found in Chapter Five.

3.2.3.2 Resazurin assays

The resazurin assay monitors reduction of resazurin by the metabolic activity of viable cells to the highly fluorescent resorufin.[55] Normalised data collected from two donors are shown in Figure 3.5. Full tables of significance data for each LDH compared to the unstimulated, Imject and Alhydrogel controls may be found in Appendix B.2.

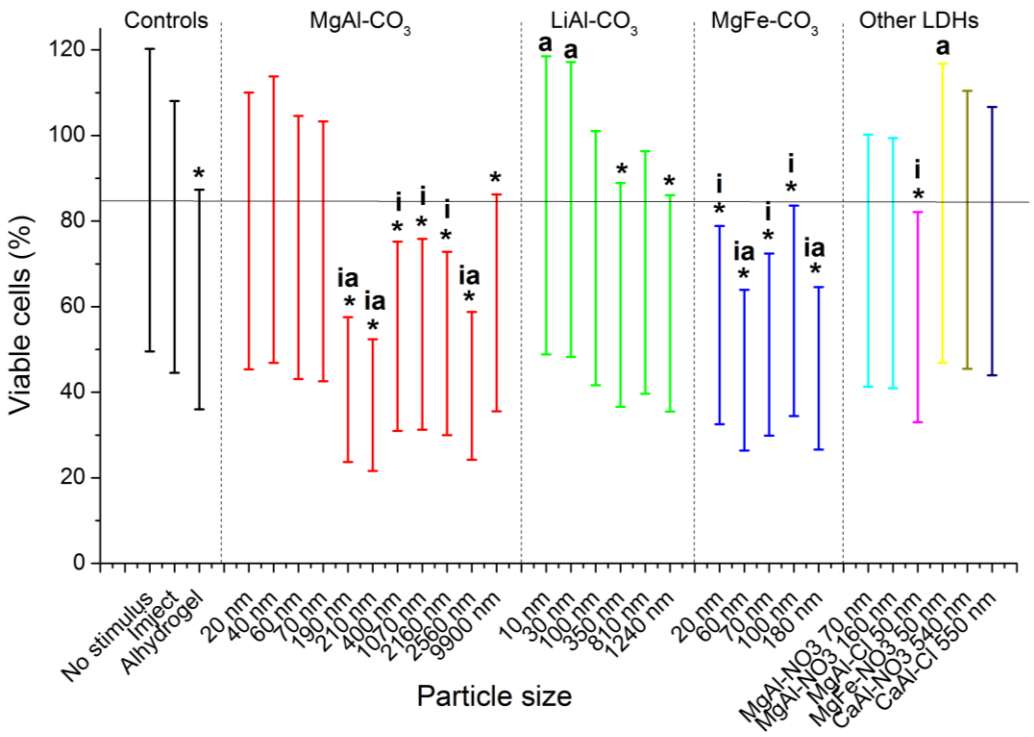

Figure 3.5: Percentages of viable Mo-DC determined by resazurin assays, measured in response to each LDH described in Chapter Two. Mo-DCs from two donors were incubated overnight with LDHs at 500 μg/mL, then incubated for two hours with resazurin after which resorufin fluorescence was measured on a fluorometer. A titration of Mo-DC was used to create a calibration curve. Percentage viable cells were calculated and normalised across the two donors. Error bars denote 95% confidence intervals, '*' denotes values significantly different ($p<0.05$) from unstimulated cells, 'i' from Imject and 'a' from Alhydrogel. The horizontal line represents the mean value for untreated cells.

Generally, the percentage of viable cells decreases with LDH treatment. Moreover, the larger particle sizes within the MgAl-CO_3 and LiAl-CO_3 LDH compositions instigate lower viability than the smaller particle sizes, specifically, those particle sizes above 100 nm give

significantly lower percentages of viable cells than the untreated cells negative control. This corroborates the findings from the viability staining assays. As a group, the MgFe-CO_3 LDHs typically impair viability more than the other compounds, even in smaller particle sizes.

3.2.4 Studies of cell forward scatter and side scatter

In flow cytometry, the forward scatter (FSC) of light reflected from a cell correlates with its size whilst the side scatter (SSC) of the reflected light is related to its granularity or complexity.[56] Changes in the FSC and SSC positions of DCs were observed following incubation with the LDHs of different particle sizes (Figure 3.6). Further investigation into these effects was carried out by calculating the mean FSC and SSC values for the viable cells (Figure 3.7) across all the donors assessed. Full tables of significance data relative to the unstimulated, LPS stimulated, and commercial adjuvant-treated Mo-DC controls may be found in Appendix B.3.

Generally, the FSC values of the cells incubated with LDHs are higher than those of the untreated control cells. Additionally, all LDHs cause the cells to move to significantly higher SSC than the untreated cells control. For particles above approximately 70 to 100 nm in size, a marked increase in SSC is noted compared to the smaller particles, particularly for the LiAl-CO_3 and MgFe-CO_3 LDHs. The SSC positions of the LDH-treated cells are higher than those of the commercial adjuvants for most LDHs in the larger particle sizes. This may signify greater association of LDH particles with Mo-DCs compared to the commercial adjuvants.

The most likely explanation is that changes in FSC and SSC reflect association between Mo-DCs and particles. Adhesion of particles to the cells, or uptake of particles by the cells, would increase both their size and complexity, resulting in altered FSC/SSC positions compared to untreated cells. Larger particle sizes could exacerbate this, as adhesion or uptake of these may yield a more pronounced change to the complexity of the cell compared to the smaller particle sizes. From this data, it cannot be discerned whether particles are entering the cells or adhering to the surface; further investigations into these interactions may be found in Chapter Five. Another contributing factor could be the altered size and complexity resulting from changes in morphology in cells undergoing necrosis. In the early stages of necrosis, cell mitochondria swell up, and in later stages the plasma membrane starts to rupture, both of which may increase the complexity of the cell and move it to higher SSC.[57]

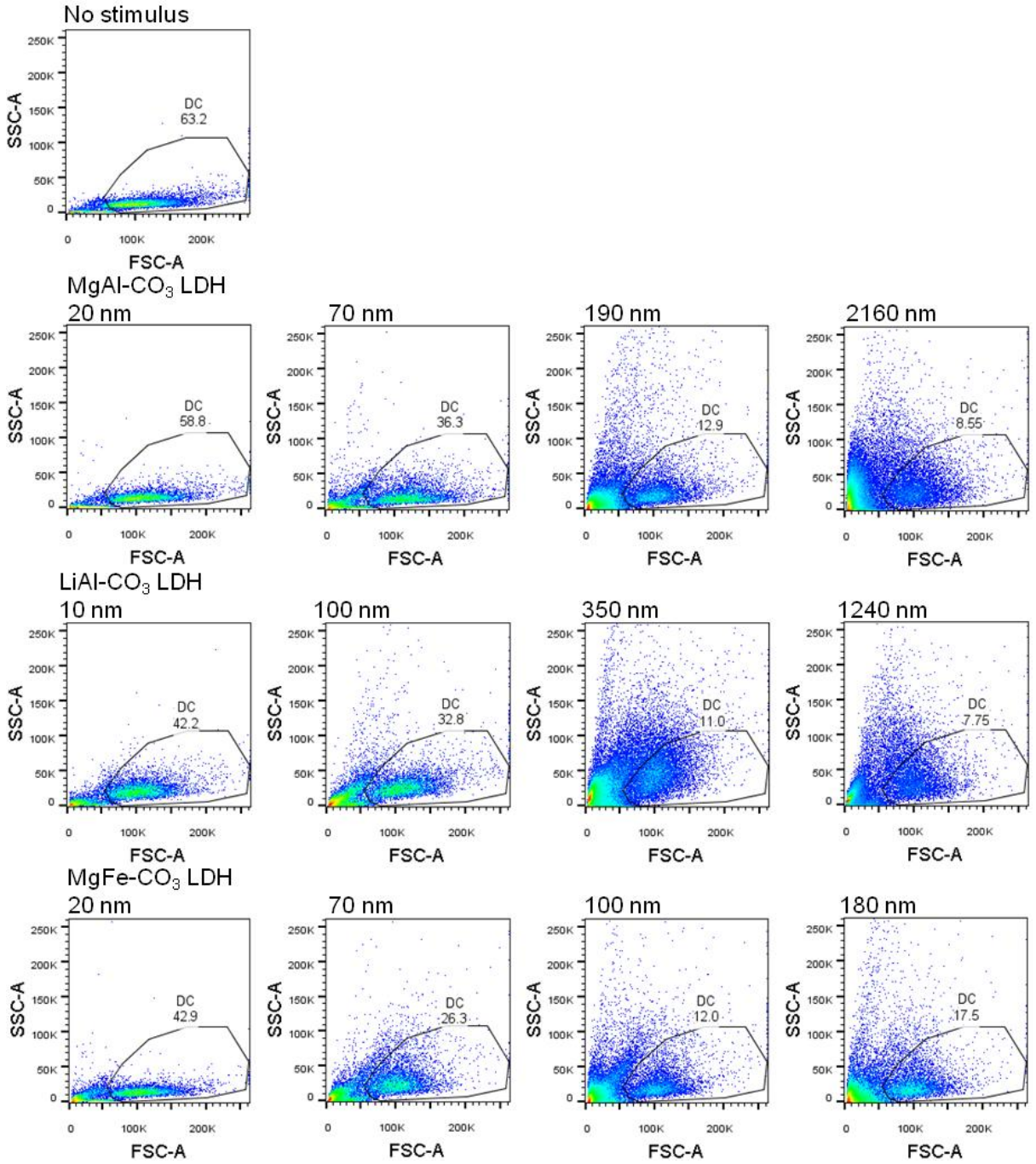

Figure 3.6: Illustrative FSC/SSC plots for Mo-DCs treated with different LDH particle sizes. Mo-DCs were incubated overnight with selection of different sized LDHs at 500 μg/mL, or without LDH (as a control), then analysed by flow cytometry. Plots show the raw data (ungated) to give an impression of the changes observed in the FSC/SSC in response to the different particle sizes during analysis.

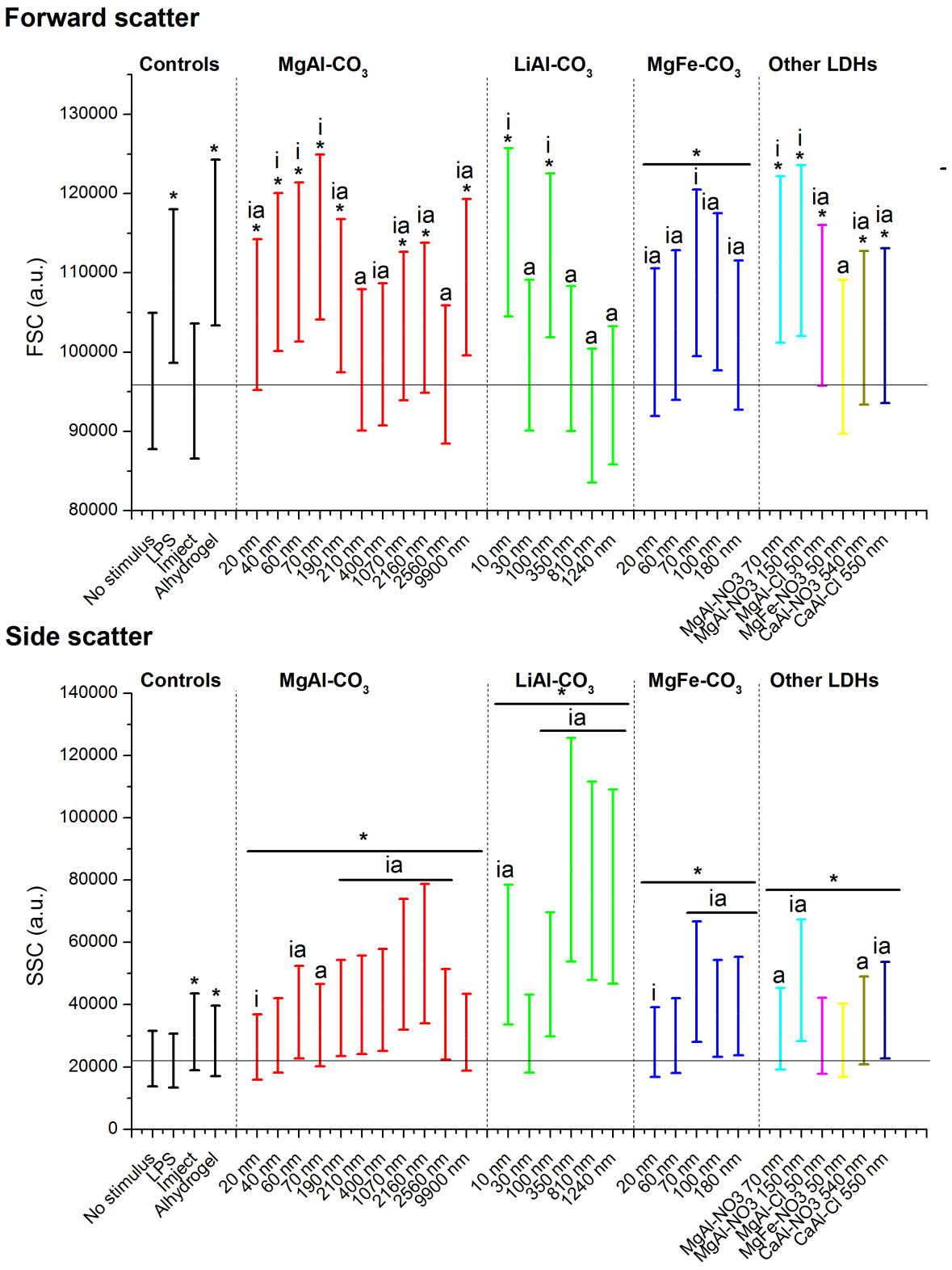

Figure 3.7: FSC and SSC of viable Mo-DCs, measured in response to each LDH detailed in Chapter Two. Mo-DCs were incubated overnight with LDHs at 500 µg/mL, then assessed using flow cytometry, gating on the viable cells (7-AAD$^-$ or 7-AAD$^-$/Annexin V$^-$). Mo-DCs from 14 donors were analysed, in parallel with other experiments investigating viability and surface molecule expression. Data shown is normalised across all donors. Error bars indicate 95% confidence intervals. '*' denotes values significantly different ($p<0.05$) from unstimulated cells, 'i' from Imject and 'a' from Alhydrogel. The horizontal line marks the mean of the unstimulated cells control for visual comparison.

3.2.5 Surface molecule expression

In order to establish the effects of particle size on DC maturation, Mo-DCs were stained for the surface molecules CD86, CD274 (B7-H1), CD83, CD40, CD275 (B7-H2), MHC class I (HLA-A, B, and C), and MHC class II (HLA-DR) after overnight incubation with the LDHs, then analysed by flow cytometry. Full details of the antibodies used are supplied in Section 6.4.2. Figures 3.8 to 3.11 display scatter plots for expression of each surface molecule investigated for each LDH composition (MgAl-CO_3, LiAl-CO_3, MgFe-CO_3) *versus* particle size, with separate plots for the miscellaneous LDH compositions in single particle sizes. Controls (untreated cells, LPS, Imject and Alhydrogel) are included on all individual plots for comparison purposes. Significance data from comparison to the control conditions are provided in Appendix B.4.

Within a given group of chemically homogenous LDHs, marked differences in expression of some surface molecules are observed when particle size is altered. These responses may be divided into three categories: those that generally increase with increasing particle size, those that generally decrease with increasing particle size and those that change little with increasing particle size.

Across all surface molecules analysed, those clearly showing greater expression with increasing particle size were CD86 and CD83 (Figure 3.8). For CD86 and CD83 expression, a slight decrease is noted for the largest particle sizes in the MgAl-CO_3 and LiAl-CO_3 LDH compositions. There is also some evidence for greater CD274 expression with increasing particle size for the MgAl-CO_3 and MgFe-CO_3 LDHs (Figure 3.9). Mo-DC expression of CD275 noticeably decreases with increasing particle size (Figure 3.9). If, as suggested in the literature, this is a marker for immature DC, this observation is consistent with the increased expression of maturation markers (CD86, CD83 etc).

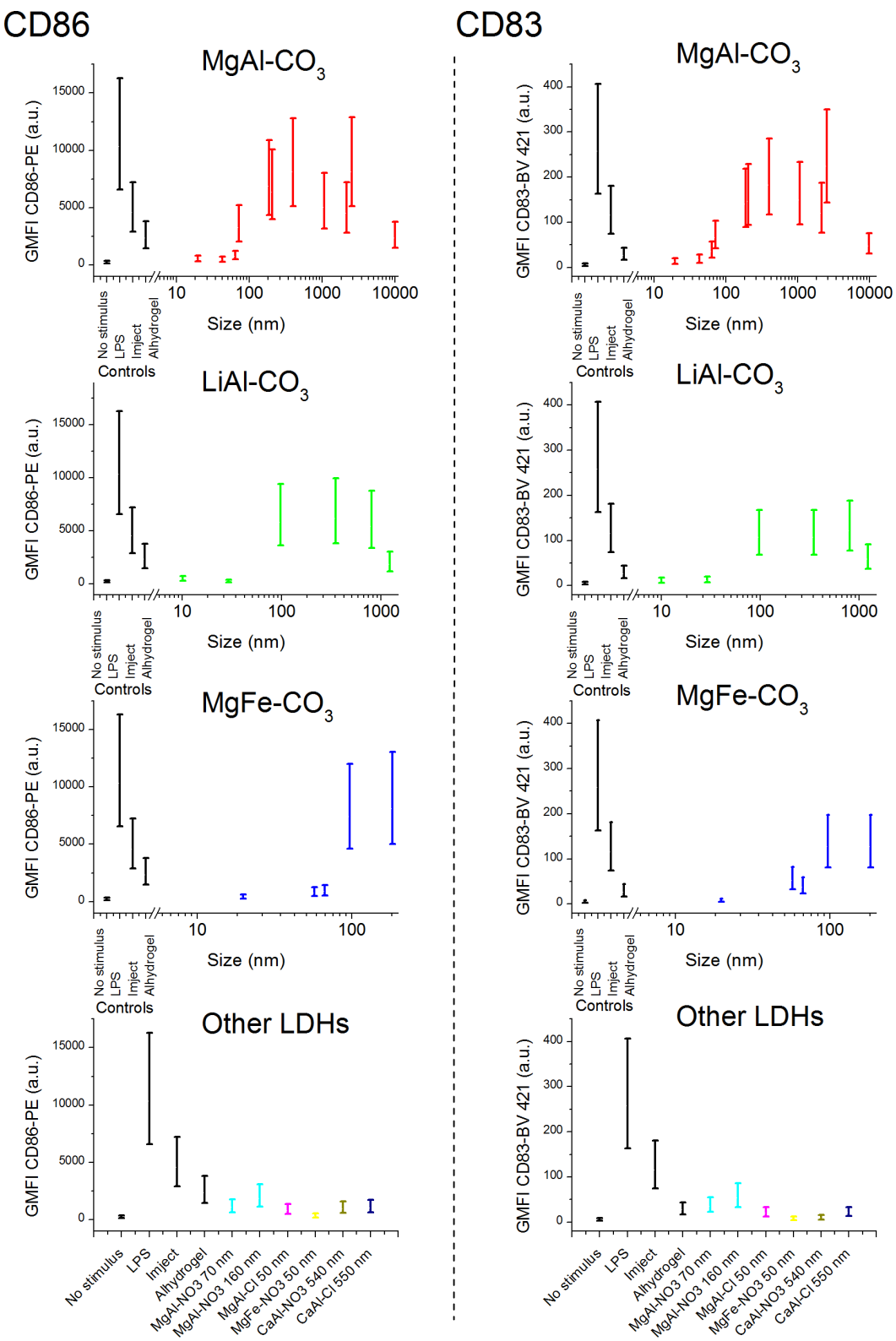

Figure 3.8: Mo-DC expression of CD86 and CD83, measured in response to each LDH described in Chapter Two, plotted as a function of particle size. Scatter plots of CD86 expression (left hand side) and CD83 expression (right hand side) *versus* particle size, grouped by LDH composition (MgAl-CO_3, LiAl-CO_3, MgFe-CO_3, and other LDH compositions). Mo-DCs were incubated overnight with the LDHs detailed in Chapter Two at 500 µg/mL, stained for viability and surface molecules then analysed using flow cytometry. GMFI of viable cells (7-AAD$^-$/7-AAD$^-$Annexin V$^-$) were used in the analysis. Data from multiple donors were normalised across to account for inter-donor variability (CD86, n = 15; CD83, n = 4). Error bars indicate 95% confidence intervals.

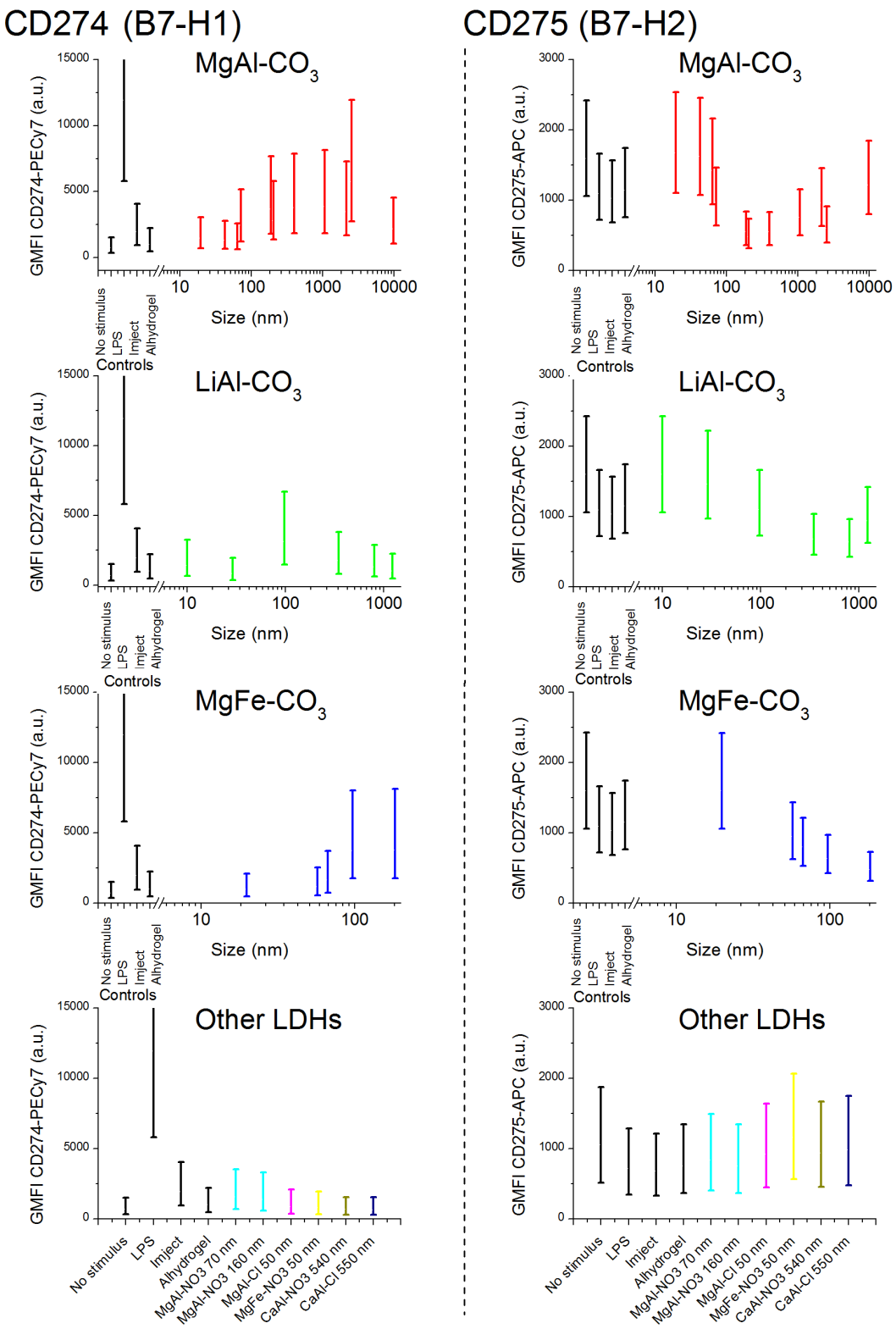

Figure 3.9 : Mo-DC expression of CD274 (B7-H1) and CD275 (B7-H2), measured in response to each LDH described in Chapter Two, plotted as a function of particle size. Scatter plots of B7-H1 expression (left hand side) and B7-H2 expression (right hand side) *versus* particle size, grouped by LDH composition (MgAl-CO_3, LiAl-CO_3, MgFe-CO_3, and other LDH compositions). Mo-DCs were incubated overnight with the LDHs detailed in Chapter Two at 500 µg/mL, stained for viability and surface molecules then analysed using flow cytometry. GMFI of viable cells (7-AAD$^-$/7-AAD$^-$Annexin V$^-$) were used for analysis. Data from multiple donors were normalised across to account for inter-donor variability (CD274, n = 11; CD275, n = 4). Error bars indicate 95% confidence intervals.

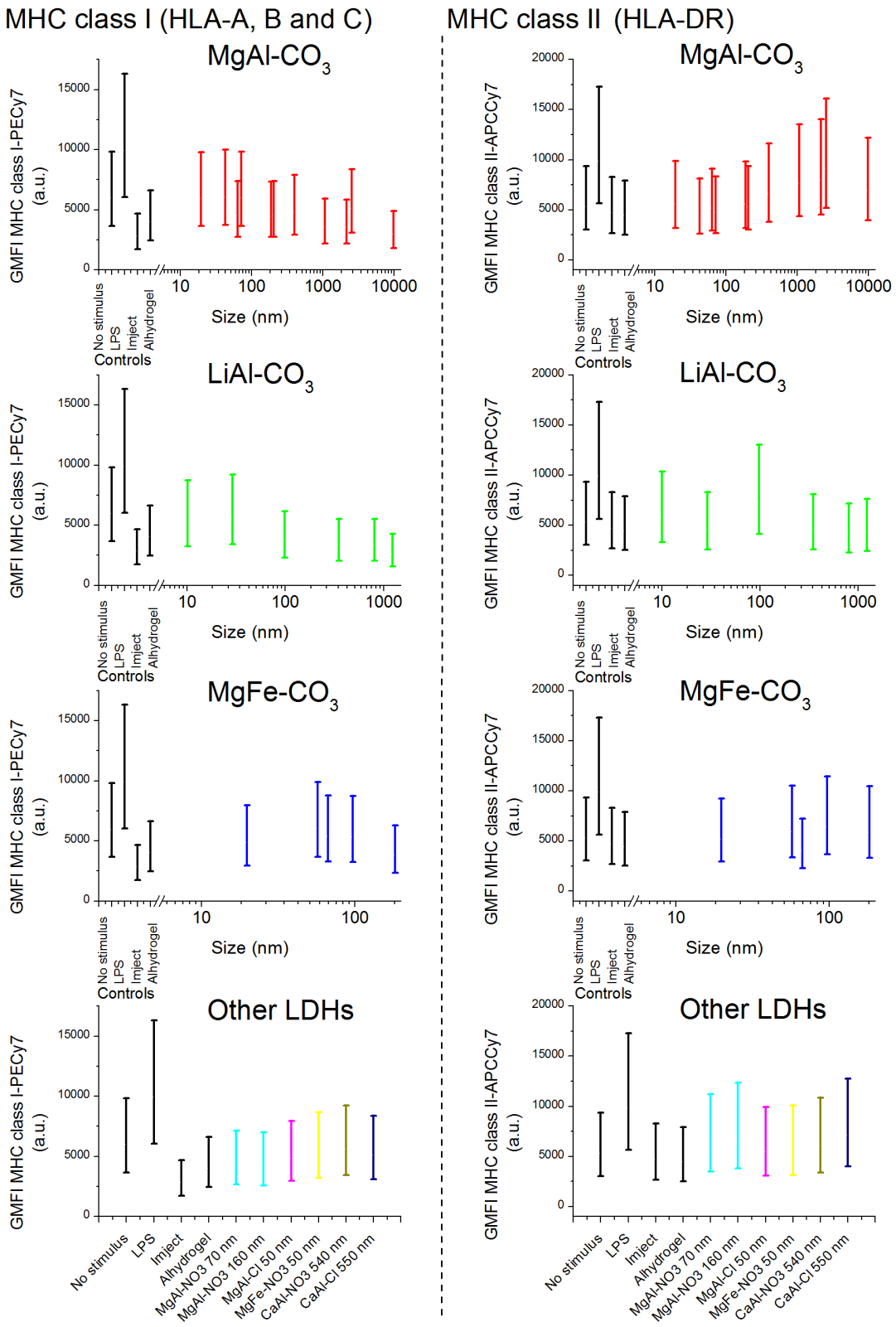

Figure 3.10: Mo-DC expression of MHC class I (HLA-A,B,C) and MHC class II (HLA-DR), measured in response to each LDH described in Chapter Two, plotted as a function of particle size. Scatter plots of MHC class I expression (left hand side) and MHC class II expression (right hand side) *versus* particle size, grouped by LDH composition ($MgAl\text{-}CO_3$, $LiAl\text{-}CO_3$, $MgFe\text{-}CO_3$, and other LDH compositions). Mo-DCs were incubated overnight with the LDHs detailed in Chapter Two at 500 µg/mL, stained for viability and surface molecules then analysed using flow cytometry. GMFIs of viable cells ($7\text{-}AAD^-/7\text{-}AAD^-Annexin\ V^-$) were used for analysis. Data from multiple donors were normalised across to account for inter-donor variability (MHC class I, $n = 4$; MHC class II, $n = 15$). Error bars indicate 95% confidence intervals.

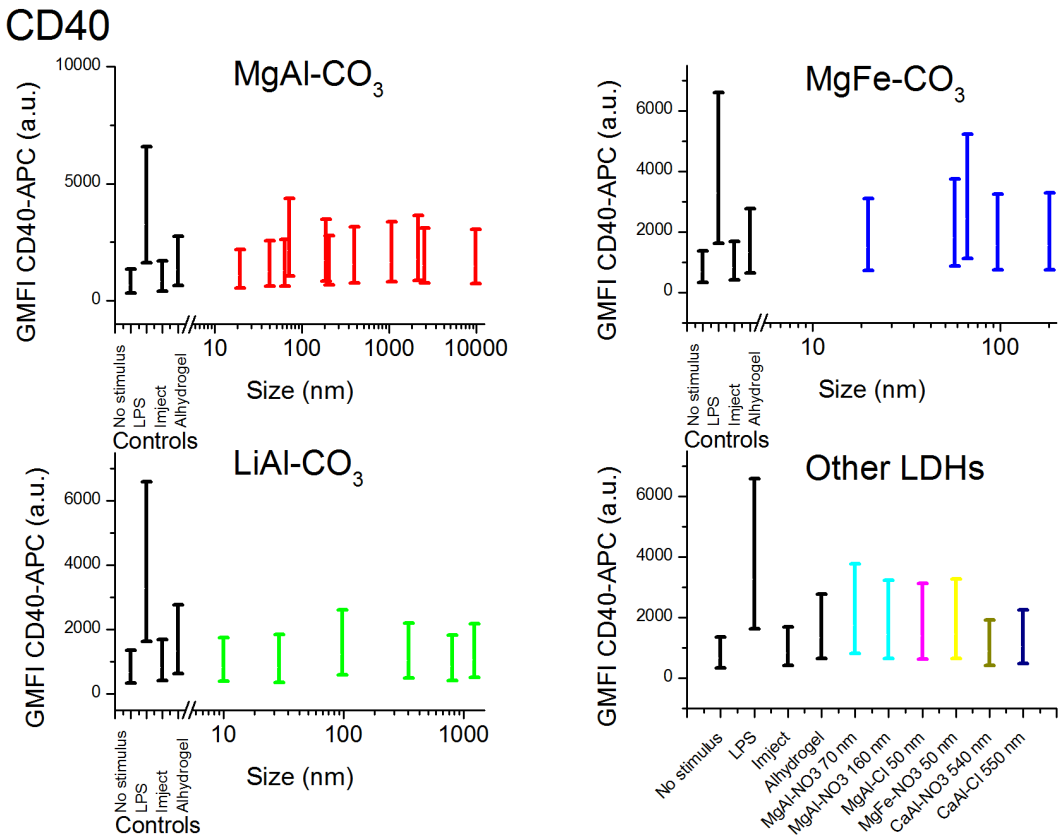

Figure 3.11: Mo-DC expression of CD40, measured in response to each LDH described in Chapter Two, plotted as a function of particle size. Scatter plots of CD40 expression *versus* particle size, grouped by LDH composition (MgAl-CO_3, LiAl-CO_3, MgFe-CO_3, and other LDH compositions). Mo-DCs were incubated overnight with the LDHs detailed in Chapter Two at 500 μg/mL, stained for viability and surface molecules then analysed using flow cytometry. GMFIs of viable cells (7-AAD$^-$/7-AAD$^-$Annexin V$^-$) were used for analysis. Data from multiple donors were normalised across to account for inter-donor variability (CD40, n = 11). Error bars indicate 95% confidence intervals.

Expression of MHC class I changes little with increasing particle size (Figure 3.10), and remains similar to that of the negative control; for the MgAl-CO_3 and LiAl-CO_3 LDH compositions, a slight decrease is noted but this effect is small when compared to the more dramatic changes noted in CD86, CD83 or CD275 expression. Expression of MHC class II also stays fairly static with increasing particle size, comparable to the negative control (Figure 3.10). A marginal increase in MHC class II expression is noted for DC treated with the MgAl-CO_3 LDH. CD40 expression does not appear to change with increasing particle size, and is similar to that of the negative control (Figure 3.11). More detailed modelling, taking into account variations in other LDH physicochemical properties and correlations with particle size across all LDH compositions may be found in Section 3.3.

Moreover, the patterns observed in responses that vary strongly with particle size (CD86, CD83, CD274 and CD275) are consistent across the three main LDH compositions (MgAl-CO_3, LiAl-CO_3 and MgFe-CO_3 LDH). In other words, changing the LDH composition

does not alter the overall behaviour of these responses to increasing particle size. This could indicate the presence of a common mechanism for DC response to LDH particles, regardless of the chemical composition.

When compared to the commercial adjuvants, some responses are enhanced by LDHs. For example, Mo-DC expression of CD86 and CD83 is higher in response to the larger LDH particle sizes than the commercial adjuvants, whilst the smaller particle sizes (10 - 70 nm) are significantly *less* effective (Figure 3.8). Several of the larger MgAl-CO_3 LDHs (> 400 nm) enhance MHC class II expression relative to Imject and Alhydrogel (Figure 3.10).

3.2.6 Cytokine secretion

To further assess the effect of LDH size on DC immune responses, supernatants from the assays detailed in Section 3.2.5 were analysed for the pro-inflammatory cytokines TNF-α, IL-6 and IL-1β (Figures 3.12 and 3.13) using ELISAs. Significance data comparing cytokine secretion in the response to LDHs to the controls and commercial adjuvants may be found in Appendix B.5. Without a stimulus present, the amounts produced were often too low to quantify using the standard curves. LPS stimulation produced readings above the range of the standard curves used and was therefore often too high to quantify.

For both TNF-α and IL-6 (Figure 3.12), greater cytokine secretion by Mo-DCs is observed in response to larger particle sizes for the MgAl-CO_3 and LiAl-CO_3 LDHs, mirroring the patterns noted for certain costimulatory molecules (CD86, CD83). By visual inspection, no change in secretion of these two cytokines appears in response to the different sized MgFe-CO_3 LDH particles. A decrease in concentration of both cytokines in response to the largest MgAl-CO_3 and LiAl-CO_3 LDH particle sizes is also observed, analogous to the patterns seen for some of the costimulatory molecules (CD86, CD83, CD274).

In comparison to Imject, treatment of Mo-DC with some of the larger LDH particles (MgAl-CO_3: > 1070 nm; LiAl-CO_3: 350 nm; MgFe-CO_3: 60 and 100 nm) induces higher concentrations of TNF-α and IL-6. Little difference in TNF-α secretion is noted relative to Alhydrogel, but for IL-6 the larger MgAl-CO_3 LDH particle sizes do induce significantly higher secretion.

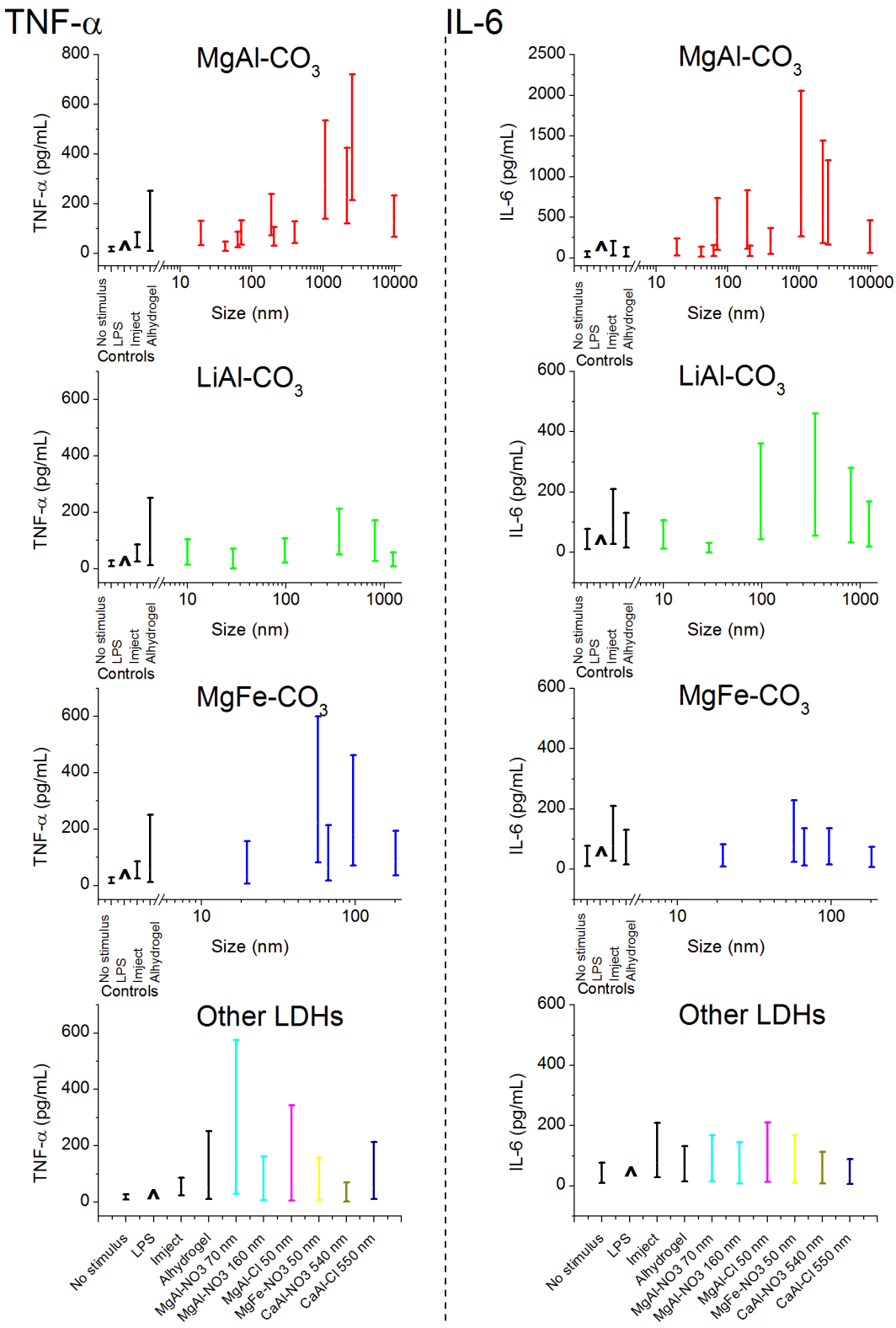

Figure 3.12: Mo-DC secretion of the cytokines TNF-α and IL-6 in response to each LDH described in Chapter Two, plotted as a function of particle size. Scatter plots of TNF-α concentration (left hand side) and IL-6 concentration (right hand side) *versus* particle size, grouped by LDH composition ($MgAl\text{-}CO_3$, $LiAl\text{-}CO_3$, $MgFe\text{-}CO_3$, and other LDH compositions). Mo-DCs were incubated overnight with the LDHs detailed in Chapter Two at 500 μg/mL, and the supernatants retained for cytokine analysis using ELISA. Data from multiple donors were normalised across to account for inter-donor variability (TNF-α, $n = 11$; IL-6, $n = 11$). Error bars indicate 95% confidence intervals. '^' indicates values above the range of the standard curve, 'v' indicates values below the range of the standard curve.

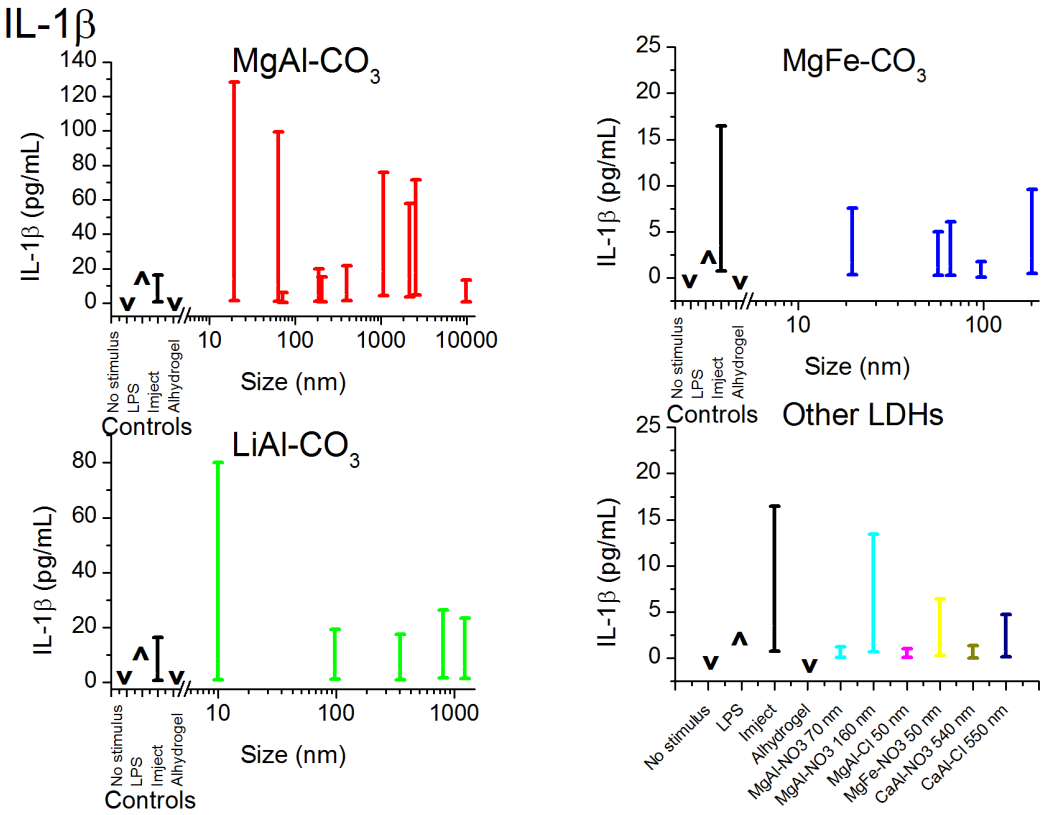

Figure 3.13: Mo-DC secretion of the cytokine IL-1β in response to each LDH described in Chapter Two, plotted as a function of particle size. Scatter plots of IL-1β concentration *versus* particle size, grouped by LDH composition (MgAl-CO_3, LiAl-CO_3, MgFe-CO_3, and other LDH compositions). Mo-DCs were incubated overnight with the LDHs detailed in Chapter Two at 500 μg/mL, and the supernatants retained for cytokine analysis using ELISA. Data from multiple donors were normalised across to account for inter-donor variability (IL-1β, n = 4). Error bars indicate 95% confidence intervals. '^' indicates values above the range of the standard curve, 'v' indicates values below the range of the standard curve.

Secretion of IL-1β by DCs in response to all stimuli except LPS is generally very low (Figure 3.13), and exhibits no discernible pattern with increasing particle size; some of the errors on these measurements are large, and it is possible that collecting more data from further donors could clarify any underlying effects. Further statistical analysis of the data for all three cytokines is described in Section 3.3.

3.2.7 Cytokine and chemokine analysis using the Luminex system

Further tests of the ability of LDHs of discrete sizes to promote Mo-DC responses of differing magnitude were implemented. Assay supernatants from overnight incubation of Mo-DCs from three donors with two or three particle sizes for each of the three main LDH compositions (MgAl-CO_3: 40, 190 and 2560 nm; LiAl-CO_3: 10 and 810 nm; MgFe-CO_3: 20 and 100 nm) were analysed using a Luminex system for other cytokines and chemokines. Unstimulated cells and LPS treated cells were included as a positive and a negative control respectively.

Luminex assays work in a similar way to ELISAs but mount the capture antibodies on fluorescently coded magnetic beads. These beads incorporate two different fluorescent dyes in varying concentrations, allowing a two dimensional 'map' to be plotted with different bead sets in different regions. Each bead set is conjugated to a capture antibody for a specific molecule. The beads are incubated with the supernatant, then a biotinylated detection antibody, and finally a streptavadin-PE conjugate. Cytokine/chemokine concentration may be determined from the PE fluorescence of the corresponding bead set, distinguishable from other cytokines/chemokine bead sets by its fluorescence in the channels of the two fluorescent coding dyes. Data is collected on a specialised flow cytometer. This technique allows large numbers of responses to be assessed in a single assay. Standard curves are used to calibrate cytokine/chemokine concentrations.

A broad range of cytokines were tested: pro-inflammatory cytokines (TNF-α, IL-1β), cytokines associated with T_h1 polarisation (IL-12p70),[58] antiviral responses (IFN-α), macrophage activation (IFN-γ), granulocyte proliferation (G-CSF),[59] anti-inflammatory cytokines (IL-10),[60] and memory T cell generation (IL-15).[61] Chemokines, molecules associated with cell migration, include IL-8 and MIP-1β (neutrophil recruitment),[62,63] IP10 (or CXCL10 – pro-inflammatory chemokine associated with general leukocyte recruitment)[64] and MCP-1 (monocyte chemoattractant protein 1 associated with monocyte/macrophage migration).[65] Figure 3.14 shows normalised Mo-DC responses for each cytokine/chemokine assessed. Full significance data may be found in Appendix B.6. The lower limit for reliable detection in the assay was 3.2 pg/mL.

G-CSF, IL-10, IL-8, IP10, MCP-1, MIP-1β and TNF-α are all produced at detectable concentrations. Greater concentrations of G-CSF, IL-8, IP10, MIP1β and TNF-α were secreted by Mo-DCs treated with the larger LDH particle sizes in each composition. The reverse of this is observed for the cytokine IL-10, with larger particles inhibiting secretion. IL-10 has an anti-inflammatory role, and secretion of IL-10 is shown to correlate inversely with secretion of pro-inflammatory cytokines such as TNF-α.[66]

Concentrations at or below the baseline for detection were recorded for IFN-γ, IL-1β IL-12p70, IL-15, IFN α, and IL-5, except for the LPS positive controls. Overall these results agree with those from surface molecule analysis and cytokine secretion results from ELISAs: specifically that the magnitudes of some Mo-DC responses vary depending on the particle size of the LDH they are treated with.

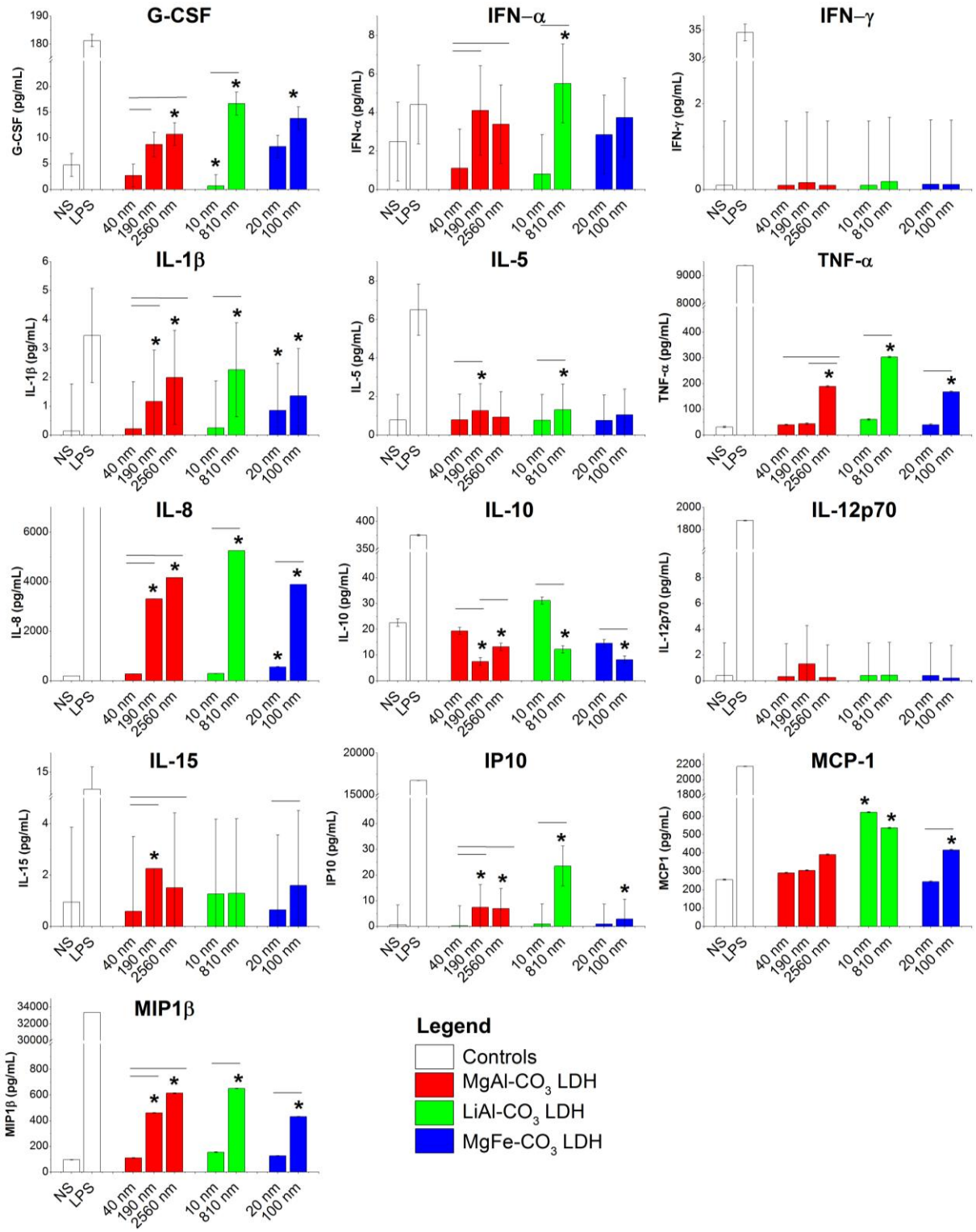

Figure 3.14: Further cytokine/chemokine secretion data from Luminex analysis of supernatants from Mo-DCs treated with selected LDH particle sizes. Mo-DCs from three donors were incubated overnight with a small and a large LDH from each of the three main compositions under investigation ($MgAl\text{-}CO_3$: 40, 190 and 2560 nm; $LiAl\text{-}CO_3$: 10 and 810 nm; $MgFe\text{-}CO_3$: 20 and 100 nm), then supernatants analysed for cytokines (G-CSF, IFN-α, IFN-γ, IL-1β, IL-5, TNF-α, IL-10, IL-12p70 and IL-15) and chemokines (IL-8, IP10, MCP-1 and MIP1β) using the Luminex system. Data plotted are normalised to account for inter-donor variation. Error bars indicate 95% confidence intervals. Values statistically significant ($p<0.05$) relative to unstimulated cells are indicated by '*', significant differences between sizes of a given LDH composition are indicated by a bar over the two columns.

3.3 Statistical analysis

Prior work by Williams *et al*. on adjuvant effects of LDHs showed that a subset of the physicochemical properties of the LDH material could accurately model and predict immune responses.[40] The overall set of physicochemical properties from which this subset was derived included intrinsic properties of the elements that compose each LDH ($M^{1+/2+}$ and M^{3+} radii;[67] $M^{1+/2+}$ and M^{3+} Pauling electronegativities; $M^{1+/2+}$ and M^{3+} standard reduction potentials) and properties measured during the characterisation of the LDH (*a*- and *c*-parameters; zeta potential; pH). Particle size was not included in this analysis, although supplementary data to their work does supply some details of particle size measurements. Generally, these indicate individual particle sizes to be in the range of 30 to 200 nm, often less than 100 nm, yielding a relatively limited size range across the LDH compositions. A statistical approach was adopted where every combination of three or four physicochemical properties were analysed for their ability to model the responses. The subset demonstrating highest correlation with the mean observed responses was used to accurately predict the responses to two new, untested LDHs.

Initial inspection of the DC response data strongly suggests that size is a parameter affecting the magnitude of response. Therefore, for the data described in this Chapter, additional LDH properties were included: mean particle size (the diameter measured using TEM), the molar ratio of $M^{1+/2+}$:M^{3+} and the mass percentage carbon (in the form of carbonate) in the LDH. A table of all the LDH properties used in the analysis may be found in Appendix B.7.1.

Statistical modelling was performed with several intentions: firstly, to determine the capacity of the original subset of physicochemical properties used by Williams *et al*.[40] to model the new data collected; secondly, whether including size improves the fit of the original model; thirdly, to establish whether a better model can be derived from all of the physicochemical properties measured for the group of LDHs tested in this Chapter. Together, these would confirm whether the original set of properties used are optimal for modelling immune responses to LDHs, or whether the other properties included (e.g. particle size) exhibit stronger relationships with immune responses. Moreover, by conducting these analyses, the general validity of the approach of linking chemical properties and immune responses will be assessed.

Statistical modelling was performed by Dr. George Nicholson (Department of Statistics, University of Oxford) to whom sincere thanks are given. Full details of data processing, model selection, size functions and model evaluation are supplied in Section 6.4.7.

3.3.1 Model fitting

After data processing and normalisation, linear models were fitted to the estimates of DC response for each of the various combinations of three or four LDH physicochemical properties. In linear regression, one or more explanatory variables (also known as regressors, in this case the LDH properties, x_i in Equation 3.2) are used to model the dependent variable (Y_i, the estimated mean of a given Mo-DC response to a given LDH, e.g. CD86 expression).[68]

$$Y_i = \beta_0 + \beta_j x_i + \cdots + \varepsilon_i$$

Equation 3.2: General equation for linear regression. β_0 and β_j are the regression parameters: β_0 gives the intercept of the model when all x_is are zero, whilst β_j are the coefficients for each explanatory variable (LDH property) where $j > 0$. ε_j is the error term or residual, a measure of the deviation of the dependent variable from that explained by the explanatory variables. Subscript '*i*' denotes the individual response to a given LDH (for example, the CD86 response to 20 nm MgAl-CO_3 LDH particles).

The coefficients are optimised, using the ordinary least squares approach, to give the minimum value for the sum of the squares of the error terms for each response. Models consisted of combinations of up to four LDH properties, plus a function of particle size (*f*(size)) which together provide the explanatory variables (x_is) in the above equation. The Bayesian information criterion (BIC) was used to select models.[69]

Two types of model were fitted: models using the same subset of properties for all DC responses, 'shared' models, and 'non-shared' individual models where each response is modelled by its own optimum subset of properties. In the shared models, the number of degrees of freedom (DOF) of *f*(size) was allowed to vary between zero and four for *each* response; individual responses had their own functions of size but shared the same subset of other LDH properties between them.

Four shared models were fitted: (1) the original model using the subset of LDH properties specified by Williams and co-workers ("original"), (2) the original model with a function of size added ("original with size"), (3) the best new model using any subset of LDH properties not including particle size as a parameter ("new without size"), and (4) the best new model using any subset of LDH properties including a function of particle size as a parameter ("new with size"). In addition, two non-shared models were fitted which, respectively, were either forced to include a function of size ("non-shared with size"), or allowed to use any of the properties except particle size ("non-shared without size"). Details of the subsets of LDH physicochemical properties used in each model may be found in Table 3.1, and coefficients (β_j in Equation 3.2) for each LDH response in Appendix B.7.2. When considering the

properties in the optimum models it is worth considering that, for every model, alternative subsets of LDH properties exist that can perform almost or equally as well.

Table 3.1: Subsets of LDH physicochemical property used in each of the four models. Zeta = zeta potential, *c*-para = *c* parameter, SRP $M^{1+/2}$= standard reduction potential of $M^{1+/2+}$, pHa = pH of 10 mg/mL LDH suspension in PBS determined by pH meter, pHb= pH of 10 mg/mL LDH suspension in PBS determined by pH paper, %C is percentage carbon by mass (as carbonate), *f*(size, DOF 0-4) indicates a function of size with up to four degrees of freedom.

Model	Response	LDH property subset	*f*(size) DOF
Shared models			
Original	All	Zeta, radius of $M^{1+/2+}$, *c*-para	
Original with size	All	Zeta, radius of $M^{1+/2+}$, *c*-para	0-4
New without size	All	Zeta, pHb, %C	
New with size	All	radius of $M^{1+/2+}$, c-para, M2:M3 ratio	0-4
Non-shared models			
Non-shared without size	CD86	radius of $M^{1+/2+}$, pHb, %C	
	CD83	radius of $M^{1+/2+}$, pHa, %C	
	CD274	radius of $M^{1+/2+}$, *c*-para, pHb, %C	
	CD275	Zeta, *c*-para, pHb, M2:M3 ratio	
	MHC1	Zeta, *c*-para, pHb	
	MHC2	*c*-para	
	CD40	pHa, M2:M3 ratio	
	TNF-α	Zeta, pHb, M2:M3 ratio, %C	
	IL-6	Zeta, radius of M^{3+}, SRP $M^{1+/2}$, %C	
	IL-1β	Zeta, %C	
Non-shared with size	CD86	radius of $M^{1+/2+}$, %C	4
	CD83	radius of $M^{1+/2+}$, %C	4
	CD274	SRP $M^{1+/2}$, %C	2
	CD275	radius of $M^{1+/2+}$, *c*-para, M2:M3 ratio	4
	MHC1	radius of M^{3+}, pHa, pHb, M2:M3 ratio	1
	MHC2	*c*-para	1
	CD40	pHa, M2:M3 ratio	0
	TNF-α	radius of $M^{1+/2+}$, M3, SRP $M^{1+/2}$, pHa	3
	IL-6	radius of M^{3+}, SRP $M^{1+/2}$, %C	1
	IL-1β	radius of $M^{1+/2+}$, pHb	4

3.3.2 Model evaluation

Testing the predictive ability of a model was performed by cross validation. In this instance, all sizes of a given composition (e.g. all LiAl-CO_3 LDHs) are excluded from the data set. The remaining data are used as a training set, in conjunction with the subset of properties selected, to predict the responses to the excluded composition (a form of 'leave-many-out' cross validation, referred to as 'leave-one-compostion-out' cross validation).[70]

Comparisons of predicted *versus* actual response were conducted, and four measures of predictive accuracy calculated for each model. These include the root mean squared error (RMSE) between the predicted values and the observed values; the logarithmic score (LS),[71] which takes into account the standard errors of the predictive values, and returns higher values for more accurate predictions; Pearson's correlation coefficient, 'r', which may take

values between -1 (perfect negative correlation) and +1 (perfect positive correlation); and Q^2, an estimate of the proportion of variance in the observed values that is explained in the predicted values. Further details of all these statistics may be found in Section 6.4.7.3.

Crucially, Veerasamy *et al*. detail the use of Q^2 as a test of predictive accuracy for analogous problems: predicting changes in biological activity from altering molecular structure (quantitative structure-activity relationship (QSAR)).[72] Generally it is agreed that a model has a useful degree of predictive ability if $Q^2 > 0.5$, with perfect prediction being $Q^2 = 1$.

3.3.3 Comparisons between models

The values for the various measures of predictive ability detailed in the preceding section from leave-one-composition out cross-validation are shown in Table 3.2. By inspection of the best statistic for each response, highlighted in yellow, the original model consistently fails to produce the best prediction. Adding size onto the original model as an extra variable marginally improves the RMSE between predicted and observed data. Between the pair of models ("original" and "original with size") the model including size yields the lowest RMSE for seven out of ten responses. Some improvement in the correlation coefficient ('r') is also noted when size is incorporated, with $r > 0.5$ for CD86, CD83 and CD40. However, overall neither variant of the original model exhibits strong correlation between predicted and observed responses (r), or predictive accuracy as judged by Q^2 for any Mo-DC response.

Although the original model was developed on datasets of immunological responses to LDHs, it demonstrates poor fit and predictive power for this dataset. The set of LDHs investigated by Williams *et al*. consisted of different compositions (LiAl-CO_3, MgAl-Cl, etc.) but contained no 'within-composition' variation, as only single samples of each composition were used, and size was not included as a physicochemical property. Even if it had been, the data indicates most samples were of similar size and so this parameter might not have been useful in modelling the observed responses. The predictive ability of the model from Williams *et al*. is more likely to be based on 'between-composition' variation rather than 'within-composition' variation. Consequently, it is poor at predicting the large changes in magnitude of response observed when the composition of the material remains approximately constant but other 'within-composition' factors such as particle size are altered. This may explain the improvements noted, for instance in r for CD86, CD83 and CD40, when a function of particle size is added to the original model.

Table 3.2: Testing of predictive accuracy using leave-one-composition out cross validation for each model, for every DC response. All four statistics (RMSE, LS, r and Q^2) are displayed, with optimum values for each response highlighted. MHC1 = MHC class I, MHC2 = MHC class II.

	Model	Response									
		CD86	CD83	CD274	CD275	MHC1	MHC2	CD40	TNF-α	IL-6	IL-1β
		RMSE - lowest value for each response highlighted									
RMSE	original	2.12	2.14	1.57	0.96	0.28	0.24	0.23	3.86	2.82	1.72
	original with size	1.42	1.23	1.38	1.00	0.43	0.24	0.20	2.66	2.01	1.00
	new without size	1.09	0.78	0.50	0.38	0.25	0.28	0.24	1.14	1.04	0.84
	new with size	0.76	0.84	1.16	0.28	0.28	0.20	0.32	1.85	0.91	2.29
	non-shared without size	0.97	0.82	0.44	0.46	0.21	0.25	0.18	1.14	0.87	0.83
	non-shared with size	0.58	0.45	0.67	0.19	0.16	0.21	0.18	1.36	0.85	0.64
		Logarithmic score - maximum value for each response highlighted									
LS	original	-28.8	-26.0	-17.3	-2.1	22.3	25.3	26.7	-62.2	-59.2	-29.8
	original with size	-16.4	-11.5	-27.3	-14.2	20.7	25.3	26.4	-72.7	-37.7	-6.9
	new without size	-18.0	-8.6	4.4	11.7	23.9	20.7	21.5	-23.3	-23.2	-11.2
	new with size	-8.1	-2.2	-13.2	26.5	24.0	27.0	22.3	-38.3	-22.6	-33.6
	non-shared without size	-17.8	-17.7	3.2	11.6	32.3	28.8	32.0	-23.3	-11.5	-13.7
	non-shared with size	2.4	9.0	-2.5	29.6	38.2	31.6	32.0	-33.1	-9.3	0.4
		Correlation coefficient - values >0.5 highlighted in grey, strongest correlation for each response highlighted in yellow									
Correlation coefficient (r)	original	0.03	-0.02	-0.09	0.01	0.10	-0.44	0.43	-0.09	-0.09	0.22
	original with size	0.55	0.52	-0.01	0.28	0.09	-0.44	0.63	-0.16	0.02	0.44
	new without size	0.42	0.59	0.57	0.45	0.24	-0.65	0.38	0.36	0.35	0.45
	new with size	0.82	0.77	0.30	0.84	0.40	0.47	0.62	-0.08	0.50	0.20
	non-shared without size	0.57	0.57	0.68	0.42	0.58	-0.42	0.69	0.36	0.57	0.43
	non-shared with size	0.87	0.89	0.53	0.90	0.77	-0.08	0.69	0.19	0.60	0.74
		Q^2 - values greater than 0.5 highlighted									
Q^2	original	0.00	0.00	0.00	0.00	0.00	0.00	0.14	0.00	0.00	0.00
	original with size	0.00	0.00	0.00	0.00	0.00	0.00	0.35	0.00	0.00	0.00
	new without size	0.11	0.33	0.26	0.15	0.00	0.00	0.11	0.00	0.00	0.10
	new with size	0.57	0.22	0.00	0.54	0.00	0.01	0.00	0.00	0.19	0.00
	non-shared without size	0.31	0.26	0.43	0.00	0.02	0.00	0.47	0.00	0.27	0.12
	non-shared with size	0.75	0.78	0.00	0.78	0.49	0.00	0.47	0.00	0.30	0.48

New shared models, formed from the subset of LDH properties which produced the lowest aggregate BIC across all responses (Table 3.1), were developed. Generally, these perform better than the "original model" and the "original model with size" (lower RMSEs, higher LSs, and higher degrees of correlation between predicted and observed data for most responses). Critically, it appears that including a function of particle size in the new models has some effect on the predictive ability. Q^2 is the most relevant measure of predictive ability, as it is commonly used for similar datasets.[72] In the "new model with size" CD86 has $Q^2 = 0.57$, and CD275 (B7-H2) has $Q^2 = 0.54$, an improvement on the equivalent Q^2 values for the "new model without size". For other measures, including particle size as a variable has little effect and results in no clear improvement other than for the aforementioned Q^2 values.

A more flexible approach, in which each response is modelled individually from its own subset of LDH properties, yields improved measures of fit and predictive accuracy. Both non-shared models demonstrate improved results over the four shared models; for RMSE and r, both non-shared models account for eight out of ten best values. In particular, forcing all the individual models to include some function of particle size yields the best outcome in terms of RMSE (seven out of ten responses with lowest values across all models), LS (maximum value

across all models for seven out of ten responses) and r (strongest correlation across all models for six out of ten responses). Furthermore, for the "non-shared with size" model, three responses (CD86, CD83 and CD275 (B7-H2)) have Q^2 values greater than 0.5 showing good predictive ability. Indeed, for most estimates of predictive accuracy the non-shared models including size out-perform those that exclude it.

3.3.4 Effects of particle size in the 'optimum' model

Closer inspection of the optimum individual models for each response ("non-shared with size") illuminates changes in DC behaviour with increasing particle size. As the model is built from data for every LDH, it takes into account all of the sizes and compositions to give an overall description of the Mo-DC response behaviour. Plots of the size functions, with inflection points, used in the optimum non-shared models are provided in Figure 3.15.

The size functions display three types of DC response: increasing with particle size, little change and decreasing with particle size. This corroborates the observations made on the raw data in Section 3.2.5. CD86, CD83, CD274 (B7-H1), MHC class II and all cytokines display a general increase in response with particle size. For CD86, CD83, CD274 (B7-H1) and the cytokines, these functions cover several orders of magnitude in response, indicating large changes with increasing particle size. However, the functions for MHC class I and II span a smaller response range (less than one order of magnitude) on the log scale *y*-axis, whilst the function for CD40 has zero degrees of freedom, effectively excluding particle size as an explanatory variable for this response. Consequently, MHC class I, MHC class II and CD40 may be considered as largely unaffected by changing particle size, confirming observations made on the results described in Section 3.2.5. The function for CD275 (B7-H2) expression shows decreasing response with increasing particle size.

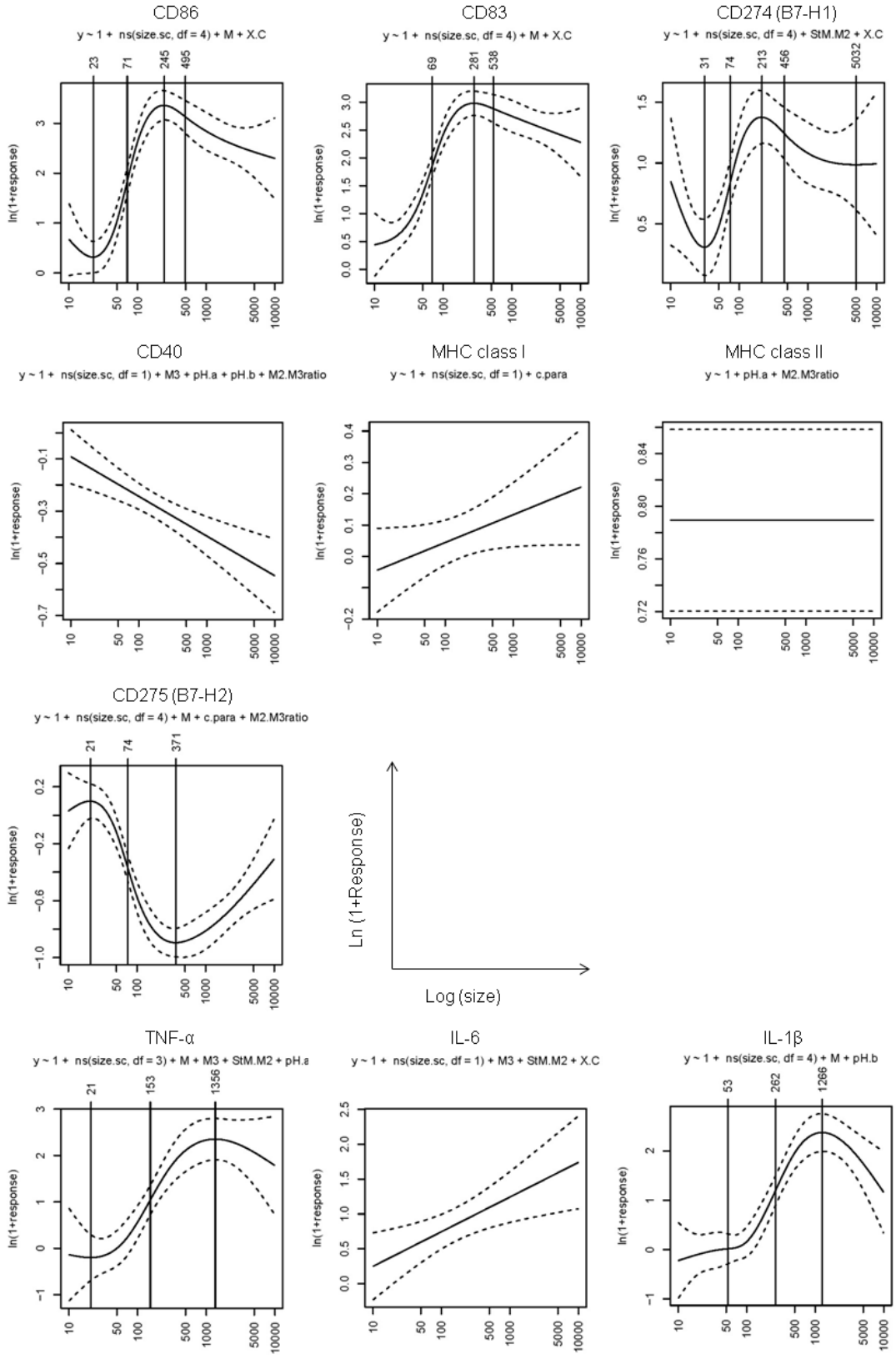

Figure 3.15: Functions of particle size used to model each each response in the "non-shared models with size". Functions take the form of natural cubic spline with up to three knots. The number of degrees of freedom ['ns(size.sc df = *x*'), where the number of degrees of freedom corresponds to the number of basis functions in the spline] are also supplied as well as the other physicochemical properties included in the model for each response (also listed in Table 3.1). Turning points and points of inflection are indicated on the plots. Dotted lines indicate 95% confidence intervals.

Overall, insights provided by modelling techniques into the behaviour of Mo-DC response under changing particle size are in agreement with those observed in the raw data in Figures 3.8 to 3.11, Section 3.2.5. Crucially, for some responses there is evidence of a relationship between particle size and cell response, particularly the models for the three responses with the best degree of predictive ability, as determined by Q^2 (CD86, CD83 and CD275 (B7-H2)). The strong increase in predictive ability for these three response models when *f*(size) is included suggests particle size is a factor that determines Mo-DC responses.

However, to describe each response as 'increasing' or 'decreasing' with particle size oversimplifies the shapes of the functions. For both CD86 and CD83 (two of the three responses with a good degree of predictability, as determined from Q^2) the shape of the function reveals a threshold between lower and higher response. Analogously, for CD275 (also with a $Q^2 > 0.5$), a cut-off point exists between increased and decreased expression, but with a function that is almost a mirror image of those for CD86 and CD83. Analysis of the inflection points of the functions for these three responses gives values of 71, 69 and 74 nm for CD86, CD83 and CD275 respectively. Given that the size range extends from approximately 10 to 10000 nm, these values are in remarkably close agreement with each other. The maxima (or minimum in the case of CD275) of the functions for these responses all fall in the 200-400 nm region. The function of size for CD274 (B7-H1) also gives a threshold at 74 nm and a maximum at 213 nm, a similar order of magnitude to the more accurately predicted responses. The consistency in the size values for the threshold and maximum costimulatory molecule expression suggest an optimum size for promoting the strongest responses.

For the cytokine responses, maxima at 1356 and 1266 nm in the functions are noted for TNF-α and IL-1β respectively. Given the similarity in these values, it may tentatively be suggested that an optimum particle size yielding greatest cytokine secretion also exists.

3.4 Discussion

The results of *in vitro* Mo-DC assays and subsequent statistical analyses connect particle size with the magnitude of DC response. Modelling each response individually results in the best predictive ability overall, as determined through cross-validation. The models for the three responses with the best degree of predictive ability ($Q^2 > 0.5$; CD86, CD83 and CD275) all incorporate particle size as an explanatory variable. In QSAR models, the 'gold standard' in predictive ability is external validation, i.e. predicting then testing a completely new set of

compounds not included in the original model. Ideally, for further validation, responses to a new LDH composition in various particle sizes would be predicted then tested.

Certain Mo-DC responses are more sensitive than others to stimulation by LDHs. In particular, increased expression of CD86, CD83, CD274 (B7-H1), CD275 (B7-H2), CD40, and the cytokines (TNF-α, IL-6, IL-1β) occurs with LDH treatment compared to the untreated control. On the other hand, MHC class I and MHC class II molecules remain largely unaffected. Moreover, Ulanova *et al*. demonstrated that HLA-DQ and MHC class I expression were unaffected by $Al(OH)_3$ alum, hinting that some cellular responses are more sensitive to crystalline inorganic materials than others.[33] It is also possible that production of some surface molecules may require longer incubation times than those used in this Chapter (overnight, approximately 16 hours). The time-dependence of chemokine production and surface molecule expression by maturing human Mo-DCs over 60 hours was recorded by Sallusto *et al*. revealing different kinetics exist for different responses.[73] In particular, high expression of the chemokine receptor CCR7 was not reached until 40 to 50 hours after stimulation. Future studies could investigate the kinetics of Mo-DC responses to LDHs in a time-course experiment, including shorter and longer incubation times than those probed in this Chapter.

It is possible that LDHs may act through perturbations to the extracellular environment. Cellular immune responses can be sensitive to hyper- and hypotonic conditions and changes in extracellular pH.[74–76] The pHs of the 10 mg/mL LDH suspensions detailed in Chapter Two are alkaline (typically pH 8-10), and it is certainly possible that ions from the LDH leach into the medium. Shapiro and Dinarello demonstrated that treating human peripheral blood mononuclear cells (PBMCs) with high concentrations of KI and NaCl induces IL-8 production, although little research into the effects of non-biological ions on DCs has been conducted. Studies into treatment of Jurkat T cells with metal ions by Caicedo *et al*.[77] established that extracellular Al^{3+} and Fe^{3+} (both of which are present in some of the LDHs tested in this Chapter) do not significantly decrease viability. However, the LDHs used here include many other ions, and have the additional complication of existing as solid particles.

Internalisation of FITC-labelled MgAl-Cl LDH particles *via* endocytosis has been demonstrated in work by Xu and co-workers.[43] Furthermore, studies into the mechanism of alum adjuvants demonstrate that particle uptake is also essential to elicit an immune response.[78] Xu proposes that following endocytosis, the decreasing pH in the endosomal

compartment initiates solvation of the LDH particles. The ensuing release of anions and cations produces a buffering effect, and an osmotic pressure imbalance between the endosome and the surrounding cytoplasm leading to endosomal destabilistaion. Influx of water molecules occurs to address this imbalance, causing swelling and possible rupture of the endosome. This resulting increase in ion concentration in the cytoplasm may lead to an osmotic imbalance between the cytoplasm and the extracellular environment. This can be reduced by a mechanism termed regulatory volume decrease (RVD), in which K^+ and Cl^- exit the cell *via* ion channels.[79] Lower levels of intracellular K^+ may be indicative of the presence of pore-forming bacterial toxins (nigericin for example) and can initiate immune responses through the Nalp3 inflammasome.[80] This pathway has been implicated in reactions to a diverse array of materials, both molecular and particulate.[81] For instance, Munoz-Planillo *et al*. observed K^+ efflux and Nalp3 activation in response to particulate matter ($Al(OH)_3$, silica) as downstream effects relative to increased membrane permeability, suggesting membrane disruption is a component of the mechanism by which particulate matter induces inflammatory responses. Membrane damage caused by endosomal rupture could in some cases, lead to necrotic cell death, releasing DAMPs into the surrounding medium.

Analysis of the correlation between the percentage of dead cells and the DC responses (Appendix B.7.3) does show moderate, significant positive correlation between CD86, CD83 and IL-1β expression and cell death. All other responses showed lower values. Qualitatively, the 70 nm threshold for increased CD86 and CD83 expression (and decreased CD275 expression) corresponds to the observed increase the percentage of dead cells noted in Section 3.2.3. There is a precedent for the products of dead or dying cells initiating DC responses, suggesting this as one possible mechanism by which particles are promoting maturation. For example, proteins usually found inside the cell, such as high-mobility group box 1 protein (HMGB1), may bind to receptors on the DC's surface and initiate gene transcription *via* NF-κB.[82] This results in increased expression of maturity markers such as CD80, CD83 and CD86, and increased pro-inflammatory cytokine secretion.[83] Other examples of materials released from dying cells that induce inflammation include local increases in ATP concentration,[84,85] uric acid,[86] heat shock proteins,[87] nucleotides,[88] and DNA.[89] Instances exist of inorganic materials, including alum adjuvants, promoting cell death and activation of inflammatory responses, are detailed in the review by Gallo and Gallucci.[90]

For the three responses that could be accurately predicted (CD86, CD83 and CD275) a sharp increase (or decrease for CD275) in the function of particle size modelling the response

occurs at approximately 70 nm. All three functions also have maxima (or minima for CD275) in a similar region (200-500 nm). The size dependence of cellular responses may originate from the nature of the uptake mechanism into the DC. Oh *et al*. established that clathrin-mediated endocytosis, in which clathrin-coated pits on the surface of a cell invaginate to form endosomes, is the primary mechanism through which 50-200 nm MgAl-CO_3 LDH particles are internalised. However, 350 nm particles were thought to enter the cell non-specifically.[47,91] Uptake was fastest for 50 nm particles and it was proposed that particles less than 100 nm behave differently, due to their higher surface area which leads to faster solvation. This could cause the cut-off in cellular response at approximately 70 nm; larger particles are less readily dissolved, hence persist in the cell and exhibit a greater capacity to inflict damage and provoke inflammatory responses. For larger LDH particles, it is possible that they may be undergoing frustrated phagocytosis, which has also been linked to development of inflammatory responses.[92,93]

Additionally, lipid rafts on the surface of cells are also involved in internalisation of non-biological materials such as silica and polystyrene microparticles.[94,95] Moreover, alum adjuvants themselves have been shown to bind to lipids with high affinity, triggering DC responses by altering their structures and initiating receptor independent cell activation.[96,97] Lipid rafts may range in size from a few tens of nanometres to nearly a micron.[98,99] It is possible that only particles of a sufficient size (and correct orientation) are capable of triggering signalling pathways through this mechanism: smaller particles are unable to bind to a large enough area of the plasma membrane to alter the lipid structure sufficiently.

3.5 Conclusion

High-throughput testing of the LDHs described in Chapter Two with Mo-DCs *in vitro* was conducted at an optimised LDH concentration (500 μg/mL). This represents the first time, for any material, that immune responses have been assessed over a particle size range of this magnitude (10-10000 nm). Cell viability, expression of seven different surface molecules [CD86, CD83, CD274 (B7-H1), CD275 (B7-H2), MHC class I, MHC class II, CD40] and secretion of three cytokines (TNF-α, IL-6, IL-1β) were assessed. Several of these responses (CD83, CD275, MHC class I) were not investigated in the previous work by William *et al*.[40] Moreover, initial visual inspection of the data indicated large differences in the magnitude of certain Mo-DC responses to varying particle size within a given LDH composition. Further

exploration using Luminex analysis highlighted other Mo-DC cytokine/chemokine responses that may be sensitive to changes in particle size.

Statistical modelling techniques were employed to investigate the relationship between the physicochemical properties of the LDH and the DC response elicited. Analysis of the various measures of predictive accuracy, as assessed using cross-validation, revealed that the original model was poor at predicting DC responses for this dataset, but its predictive ability could be marginally improved by including a function of particle size. Response-specific subsets of LDH properties, including a function of particle size, provided the best predictive ability: three surface molecules (CD86, CD83 and CD275) could be predicted with a high degree of accuracy ($Q^2 > 0.5$), proving that the approach developed previously can be extended to include new physicochemical properties and immune responses. The functions modelling the relationship between particle size and Mo-DC response suggest a size threshold at approximately 70 nm, above which greater CD86, CD83 and diminished CD275 (B7-H2) expression were observed. The optimum particle size for DC costimulatory molecule expression is in the region 200-500 nm, with suggestion of a higher maximum for optimum cytokine secretion.

Overall, these results suggest that a relationship between the particle size of the LDH and specific Mo-DC responses measured *in vitro* exists. Statistical modelling of these responses can, in some instances, offer accurate predictions of DC response when particle size is used as an explanatory variable. In conclusion, particle size is an important factor to consider when exploring the immunogenicity of LDHs for use in adjuvants.

3.6 References

(1) Lanzavecchia, A.; Sallusto, F. *Cell* **2001**, *106*, 263.
(2) DeSilva, D. R.; Urdahl, K. B.; Jenkins, M. K. *J. Immunol.* **1991**, *147*, 3261.
(3) Schwartz, R. H. *J. Exp. Med.* **1996**, *184*, 1.
(4) Aimanianda, V.; Haensler, J.; Lacroix-Desmazes, S.; Kaveri, S. V; Bayry, J. *Trends Pharmacol. Sci.* **2009**, *30*, 287.
(5) Kool, M.; Soullié, T.; van Nimwegen, M.; Willart, M. A. M.; Muskens, F.; Jung, S.; Hoogsteden, H. C.; Hammad, H.; Lambrecht, B. N. *J. Exp. Med.* **2008**, *205*, 869.
(6) Akira, S.; Takeda, K. *Nat. Rev. Immunol.* **2004**, *4*, 499.
(7) Dauer, M.; Obermaier, B.; Herten, J.; Haerle, C.; Pohl, K.; Rothenfusser, S.; Schnurr, M.; Endres, S.; Eigler, A. *J. Immunol.* **2003**, *170*, 4069.
(8) Shi, Y.; Evans, J. E.; Rock, K. L. *Nature* **2003**, *425*, 516.
(9) Schnurr, M.; Then, F.; Galambos, P.; Scholz, C.; Siegmund, B.; Endres, S.; Eigler, A. *J. Immunol.* **2000**, *165*, 4704.
(10) Banchereau, J.; Steinman, R. M. *Nature* **1998**, *392*, 245.
(11) Keir, M. E.; Sharpe, A. H. *Immunol. Rev.* **2005**, *204*, 128.
(12) Fraser, J. D.; Irving, B. A.; Crabtree, G. R.; Weiss, A. *Science* **1991**, *251*, 313.
(13) Appleman, L. J.; Berezovskaya, A.; Grass, I.; Boussiotis, V. A. *J. Immunol.* **2000**, *164*, 144.
(14) Tivol, E. A.; Borriello, F.; Schweitzer, A. N.; Lynch, W. P.; Bluestone, J. A.; Sharpe, A. H. *Immunity* **1995**, *3*, 541.
(15) Nishimura, H.; Nose, M.; Hiai, H.; Minato, N.; Honjo, T. *Immunity* **1999**, *11*, 141.
(16) Keir, M. E.; Francisco, L. M.; Sharpe, A. H. *Curr. Opin. Immunol.* **2007**, *19*, 309.
(17) Wang, S.; Zhu, G.; Chapoval, A. I.; Dong, H.; Tamada, K.; Ni, J.; Chen, L. *Blood* **2000**, *96*, 2808.
(18) Hutloff, A.; Dittrich, A. M.; Beier, K. C.; Eljaschewitsch, B.; Kraft, R.; Anagnostopoulos, I.; Kroczek, R. A. *Nature* **1999**, *397*, 263.
(19) Munster, D. J.; MacDonald, K. P. A.; Kato, M.; Hart, D. J. N. *Int. Immunol.* **2004**, *16*, 33.
(20) Aerts-Toegaert, C.; Heirman, C.; Tuyaerts, S.; Corthals, J.; Aerts, J. L.; Bonehill, A.; Thielemans, K.; Breckpot, K. *Eur. J. Immunol.* **2007**, *37*, 686.
(21) Cella, M.; Scheidegger, D.; Palmer-Lehmann, K.; Lane, P.; Lanzavecchia, A.; Alber, G. *J. Exp. Med.* **1996**, *184*, 747.
(22) Guermonprez, P.; Valladeau, J.; Zitvogel, L.; Théry, C.; Amigorena, S. *Annu. Rev. Immunol.* **2002**, *20*, 621.
(23) Reis e Sousa, C. *Nat. Rev. Immunol.* **2006**, *6*, 476.
(24) Haller Hasskamp, J.; Zapas, J. L.; Elias, E. G. *Am. J. Hematol.* **2005**, *78*, 314.
(25) Palucka, K. A.; Taquet, N.; Sanchez-Chapuis, F.; Gluckman, J. C. *J. Immunol.* **1998**, *160*, 4587.
(26) Hiasa, M.; Abe, M.; Nakano, A.; Oda, A.; Amou, H.; Kido, S.; Takeuchi, K.; Kagawa, K.; Yata, K.; Hashimoto, T.; Ozaki, S.; Asaoka, K.; Tanaka, E.; Moriyama, K. *Blood* **2009**, *114*, 1.
(27) Chapuis, F.; Rosenzwajg, M.; Yagello, M.; Ekman, M.; Biberfeld, P.; Gluckman, J. C. *Eur. J. Immunol.* **1997**, *27*, 431.
(28) Zhou, L.; Tedder, T. F. *Proc. Natl. Acad. Sci. U.S.A.* **1996**, *93*, 2588.
(29) Kratky, W.; Reis e Sousa, C.; Oxenius, A.; Spörri, R. *Proc. Natl. Acad. Sci. U.S.A.* **2011**, *108*, 17414.
(30) Vallhov, H.; Kupferschmidt, N.; Gabrielsson, S.; Paulie, S.; Strømme, M.; Garcia-Bennett, A. E.; Scheynius, A. *Small* **2012**, *8*, 2116.
(31) Schanen, B. C.; Karakoti, A. S.; Seal, S.; Drake III, D. R.; Warren, W. L.; Self, W. T. *ACS Nano* **2009**, *3*, 2523.
(32) Tomić, S.; Rudolf, R.; Brunčko, M.; Anžel, I.; Savić, V.; Colić, M. *Eur. Cell. Mater.* **2012**, *23*, 58.
(33) Ulanova, M.; Tarkowski, A.; Hahn-Zoric, M.; Hanson, L. Å. *Infect. Immun.* **2001**, *69*, 1151.
(34) St Pierre, C. A.; Chan, M.; Iwakura, Y.; Ayers, D. C.; Kurt-Jones, E. A.; Finberg, R. W. *J. Orthop. Res.* **2010**, *28*, 1418.

(35) Gregory, A. E.; Titball, R.; Williamson, D. *Front. Cell. Infect. Microbiol.* **2013**, *3*, 13.
(36) Parry, A. L.; Clemson, N. A.; Ellis, J.; Bernhard, S. S. R.; Davis, B. G.; Cameron, N. R. *J. Am. Chem. Soc.* **2013**, *135*, 9362.
(37) Niikura, K.; Matsunaga, T.; Suzuki, T.; Kobayashi, S.; Yamaguchi, H.; Orba, Y.; Kawaguchi, A.; Hasegawa, H.; Kajino, K.; Ninomiya, T.; Ijiro, K.; Sawa, H. *ACS Nano* **2013**, *7*, 3926.
(38) Li, A.; Qin, L.; Zhu, D.; Zhu, R.; Sun, J.; Wang, S. *Biomaterials* **2010**, *31*, 748.
(39) Li, A.; Qin, L.; Wang, W.; Zhu, R.; Yu, Y.; Liu, H.; Wang, S. *Biomaterials* **2011**, *32*, 469.
(40) Williams, G. R.; Fierens, K.; Preston, S. G.; Rysnik, O.; Lunn, D.; De Prijck, S.; Kool, M.; Buckley, H.; Austyn, J. M.; O'Hare, D.; Lambrecht, B. N. *J. Exp. Med.* **2014**, *211*, 1019.
(41) Decuzzi, P.; Godin, B.; Tanaka, T.; Lee, S.-Y.; Chiappini, C.; Liu, X.; Ferrari, M. *J. Control. Release* **2010**, *141*, 320.
(42) Leclerc, L.; Rima, W.; Boudard, D.; Pourchez, J.; Forest, V.; Bin, V.; Mowat, P.; Perriat, P.; Tillement, O.; Grosseau, P.; Bernache-Assollant, D.; Cottier, M. *Inhal. Toxicol.* **2012**, *24*, 580.
(43) Xu, Z. P.; Niebert, M.; Porazik, K.; Walker, T. L.; Cooper, H. M.; Middelberg, A. P. J.; Gray, P. P.; Bartlett, P. F.; Lu, G. Q. M. *J. Control. Release* **2008**, *130*, 86.
(44) Wang, T.; Jiang, H.; Zhao, Q.; Wang, S.; Zou, M.; Cheng, G. *Int. J. Pharm.* **2012**, *436*, 351.
(45) Sun, B.; Ji, Z.; Liao, Y.; Wang, M.; Wang, X.; Dong, J. *ACS Nano* **2013**, *7*, 10834.
(46) Chung, H.-E.; Park, D.-H.; Choy, J.-H.; Choi, S.-J. *Appl. Clay Sci.* **2012**, *65-66*, 24.
(47) Oh, J.-M.; Choi, S.-J.; Lee, G.-E.; Kim, J.-E.; Choy, J.-H. *Chem. Asian J.* **2009**, *4*, 67.
(48) Choi, S.-J.; Oh, J.-M.; Choy, J.-H. *J. Nanosci. Nanotechnol.* **2008**, *8*, 5297.
(49) Li, X.; Sloat, B. R.; Yanasarn, N.; Cui, Z. *Eur. J. Pharm. Biopharm.* **2011**, *78*, 107.
(50) Choi, S. J.; Oh, J. M.; Park, T.; Choy, J. H. *J. Nanosci. Nanotechnol.* **2007**, *7*, 4017.
(51) Schmid, I.; Krall, W. J.; Uittenbogaart, C. H.; Braun, J.; Giorgi, J. V. *Cytometry* **1992**, *13*, 204.
(52) Elmore, S. *Toxicol. Pathol.* **2007**, *35*, 495.
(53) Szegezdi, E.; Logue, S. E.; Gorman, A. M.; Samali, A. *EMBO Rep.* **2006**, *7*, 880.
(54) Lassus, P.; Opitz-Araya, X.; Lazebnik, Y. *Science* **2002**, *297*, 1352.
(55) O'Brien, J.; Wilson, I.; Orton, T.; Pognan, F. *Eur. J. Biochem.* **2000**, *267*, 5421.
(56) Loken, M. R.; Herzenber, L. a. *Ann. N. Y. Acad. Sci.* **1975**, *254*, 163.
(57) Darzynkiewicz, Z.; Juan, G.; Li, X.; Gorczyca, W.; Murakami, T.; Traganos, F. *Cytometry* **1997**, *27*, 1.
(58) Zhu, J.; Yamane, H.; Paul, W. E. *Annu. Rev. Immunol.* **2010**, *28*, 445.
(59) Metcalf, D. *Science* **1985**, *229*, 16.
(60) Saraiva, M.; O'Garra, A. *Nat. Rev. Immunol.* **2010**, *10*, 170.
(61) Di Sabatino, A.; Calarota, S. A.; Vidali, F.; Macdonald, T. T.; Corazza, G. R. *Cytokine Growth Factor Rev.* **2011**, *22*, 19.
(62) Harada, A.; Sekido, N.; Akahoshi, T.; Wada, T.; Mukaida, N.; Matsushima, K. *J. Leukoc. Biol.* **1994**, *56*, 559.
(63) Sherry, B.; Tekamp-Olson, P.; Gallegos, C.; Bauer, D.; Davatelis, G.; Wolpe, S. D.; Masiarz, F.; Coit, D.; Cerami, A. *J. Exp. Med.* **1988**, *168*, 2251.
(64) Lee, E. Y.; Lee, Z.-H.; Song, Y. W. *Autoimmun. Rev.* **2009**, *8*, 379.
(65) Deshmane, S. L.; Kremlev, S.; Amini, S.; Sawaya, B. E. *J. Interf. Cytokine Res.* **2009**, *29*, 313.
(66) Voll, R. E.; Herrmann, M.; Roth, E. A.; Stach, C.; Kalden, J. R.; Girkontaite, I. *Nature* **1997**, *390*, 350.
(67) Shannon, R. D.; Prewitt, C. T. *Acta Crystallogr. Sect. B: Struct. Crystallogr. Cryst. Chem.* **1969**, *25*, 925.
(68) Snijders, T. A. B.; Bosker, R. J. *Multilevel Analysis: An Introduction to Basic and Advanced Multilevel Modelling*; 2nd ed.; 2012.
(69) Schwarz, G. *Ann. Stat.* **1978**, *6*, 461.
(70) Leach, A. R. *Molecular Modelling: Principles and Applications*; 2nd ed.; Pearson Education Limited, 2001; pp. 695–702.
(71) Gneiting, T.; Katzfuss, M. *Annu. Rev. Stat. its Appl.* **2014**, *1*, 125.
(72) Veerasamy, R.; Rajak, H.; Jain, A.; Sivadasan, S.; Varghese, C. P.; Agrawal, R. K. *Int. J. Drug Des. Disocovery* **2011**, *2*, 511.

(73) Sallusto, F.; Palermo, B.; Lenig, D.; Miettinen, M.; Matikainen, S.; Julkunen, I.; Forster, R.; Burgstahler, R.; Lipp, M.; Lanzavecchia, A. *Eur. J. Immunol.* **1999**, *29*, 1617.
(74) Compan, V.; Baroja-Mazo, A.; López-Castejón, G.; Gomez, A. I.; Martínez, C. M.; Angosto, D.; Montero, M. T.; Herranz, A. S.; Bazán, E.; Reimers, D.; Mulero, V.; Pelegrín, P. *Immunity* **2012**, *37*, 487.
(75) Shapiro, L.; Dinarello, C. A. *Proc. Natl. Acad. Sci. U.S.A.* **1995**, *92*, 12230.
(76) Jancic, C. C.; Cabrini, M.; Gabelloni, M. L.; Rodríguez Rodrigues, C.; Salamone, G.; Trevani, A. S.; Geffner, J. *Cytokine* **2012**, *57*, 258.
(77) Caicedo, M.; Jacobs, J. J.; Reddy, A.; Hallab, N. J. *J. Biomed. Mater. Res. A* **2008**, *86*, 905.
(78) Hornung, V.; Bauernfeind, F.; Halle, A.; Samstad, E. O.; Kono, H.; Rock, K. L.; Fitzgerald, K. A.; Latz, E. *Nat. Immunol.* **2008**, *9*, 847.
(79) Garber, S. S.; Cahalan, M. D. *Cell. Physiol. Biochem.* **1997**, *7*, 229.
(80) Gurcel, L.; Abrami, L.; Girardin, S.; Tschopp, J.; van der Goot, F. G. *Cell* **2006**, *126*, 1135.
(81) Muñoz-Planillo, R.; Kuffa, P.; Martínez-Colón, G.; Smith, B. L.; Rajendiran, T. M.; Núñez, G. *Immunity* **2013**, *38*, 1142.
(82) Rosin, D. L.; Okusa, M. D. *J. Am. Soc. Nephrol.* **2011**, *22*, 416.
(83) Yang, D.; Chen, Q.; Yang, H.; Tracey, K. J.; Bustin, M.; Oppenheim, J. J. *J. Leukoc. Biol.* **2007**, *81*, 59.
(84) Zeiser, R.; Penack, O.; Holler, E.; Idzko, M. *J. Mol. Med. (Berl).* **2011**, *89*, 833.
(85) Wilkin, F.; Duhant, X.; Bruyns, C.; Suarez-Huerta, N.; Boeynaems, J.-M.; Robaye, B. *J. Immunol.* **2001**, *166*, 7172.
(86) Shi, Y.; Evans, J. E.; Rock, K. L. *Nature* **2003**, *425*, 516.
(87) Basu, S.; Binder, R. J.; Suto, R.; Anderson, K. M.; Srivastava, P. K. *Int. Immunol.* **2000**, *12*, 1539.
(88) Marriott, I.; Inscho, E. W.; Bost, K. L. *Cell. Immunol.* **1999**, *195*, 147.
(89) Marichal, T.; Ohata, K.; Bedoret, D.; Mesnil, C.; Sabatel, C.; Kobiyama, K.; Lekeux, P.; Coban, C.; Akira, S.; Ishii, K. J.; Bureau, F.; Desmet, C. J. *Nat. Med.* **2011**, *17*, 996.
(90) Gallo, P. M.; Gallucci, S. *Front. Immunol.* **2013**, *4*, 1.
(91) Oh, J.-M.; Choi, S.-J.; Kim, S.-T.; Choy, J.-H. *Bioconjug. Chem.* **2006**, *17*, 1411.
(92) Schinwald, A.; Donaldson, K. *Part. Fibre Toxicol.* **2012**, *9*, 34.
(93) Vaine, C. A.; Patel, M. K.; Zhu, J.; Lee, E.; Finberg, R. W.; Hayward, R. C.; Kurt-Jones, E. A. *J. Immunol.* **2013**, *190*, 3525.
(94) Hamilton, R. F.; Thakur, S. A.; Mayfair, J. K.; Holian, A. *J. Biol. Chem.* **2006**, *281*, 34218.
(95) Nagao, G.; Ishii, K.; Hirota, K.; Makino, K.; Terada, H. *Anticancer Res.* **2010**, *30*, 3167.
(96) Flach, T. L.; Ng, G.; Hari, A.; Desrosiers, M. D.; Zhang, P.; Ward, S. M.; Seamone, M. E.; Vilaysane, A.; Mucsi, A. D.; Fong, Y.; Prenner, E.; Ling, C. C.; Tschopp, J.; Muruve, D. A.; Amrein, M. W.; Shi, Y. *Nat. Med.* **2011**, *17*, 479.
(97) Ng, G.; Sharma, K.; Ward, S. M.; Desrosiers, M. D.; Stephens, L. A.; Schoel, W. M.; Li, T.; Lowell, C. A.; Ling, C.-C.; Amrein, M. W.; Shi, Y. *Immunity* **2008**, *29*, 807.
(98) Yuan, C.; Furlong, J.; Burgos, P.; Johnston, L. J. *Biophys. J.* **2002**, *82*, 2526.
(99) Edidin, M. *Trends Cell Biol.* **2001**, *11*, 492.

Chapter Four: Assessing Human T Cell Responses to Layered Double Hydroxide-Stimulated Dendritic Cells

4.1 Introduction

Dendritic cells (DCs) activate naïve T cells through cognate antigen recognition (signal one) and costimulatory molecule binding (signal two) (Figure 4.1).[1,2] Further cues from the activating DCs, alongside other cells in the environment, provide a third signal which conveys information to the T cells allowing them to optimise their response to the pathogen present, known as T cell polarisation.

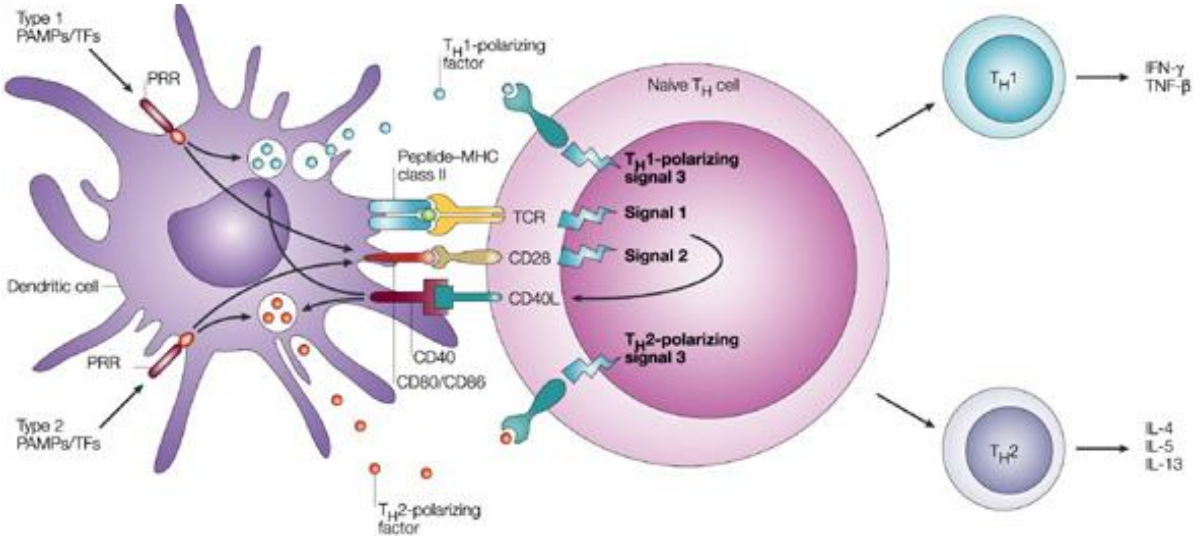

Figure 4.1: Review of activation of CD4$^+$ T cells by DCs.[2] DCs are activated by recognition of danger signals through their pattern recognition receptors (PRRs), inducing increased expression of surface molecules, such as MHC class II and CD86, and increased cytokine secretion. Upon contact with naïve T cells in the lymph nodes, T cells recognise their epitope through T cell receptors (signal one) and receive costimulation through binding of other surface molecules (signal two). The cytokines secreted by the DCs and other surrounding cells convey information to the T cell tailoring its response to type of pathogen involved (T cell polarisation).

4.1.1 CD4$^+$ T cell polarisation and function

After activation, naïve CD4$^+$ T cells undergo clonal expansion to a population of 'T_h0' T cells. These cells secrete a non-specific panel of cytokines, although it has also been proposed that they may actually comprise a pool of mixed T cell subsets.[3] Continued exposure to certain stimuli, such as specific combinations of cytokines, can differentiate the T_h0 cells into polarised T cell subsets.[4] Other factors, such as the antigen dose, the nature of the peptide being presented to the T cell receptor (TCR) and the form of the costimulatory signals also affect T cell polarisation.[3,5] A number of T cell subsets have been described (e.g.

T_h1, T_h2, T_h17, T_{fh}), characterised by their cytokine secretion, transcription factors involved in differentiation, and responses induced in other cells of the immune system.[6] More thorough discussion of various T_h subsets, their differentiation and roles may be found in the reviews by Zhu and co-workers[6,7] or Moser and co-workers.[8]

Briefly, the T_h1 subset T cells are characterised by IFN-γ secretion; this cytokine potently activates macrophages, increasing their microbicidal ability and encourages opsonising antibody production (for instance IgG2a in mice).[9,10] The combination of these effects makes T_h1 T cells best suited to responding to intracellular pathogens including viruses. T_h2 cells typically secrete IL-3, IL-4, IL-5 and IL-13, cytokines which act to increase IgE antibody production and encourage eosinophil and basophil recruitment.[6] These cells are primarily concerned with combating extracellular bacteria and parasites, as they are able to release cytoplasmic granules;[11,12] the granules contain a number of enzymes that are antibacterial and/or toxic to parasites.[13] T_h17 cells characteristically produce IL-17 and IL-22.[7] They have a role in protecting against certain extracellular bacteria and fungi, and have also been implicated in some autoimmune conditions.[14,15]

4.1.2 $CD8^+$ T cell activation

Activation of $CD8^+$ T cells is usually preceded by DC contact with $CD4^+$ T cells, a concept referred to as 'DC licensing'. It is possible that this acts as a control mechanism, to limit potentially damaging $CD8^+$ T cell responses and to distinguish between immunity and tolerance.[16] Activated $CD4^+$ T cells can provide additional activation signals to DCs, *via* CD40-CD40 ligand interactions.[17] Experiments in gene knockout mice (MHC class II KO or $CD4^+$ T cell depleted) by Smith *et al.* proved that $CD4^+$ T cell assistance was required for a $CD8^+$ T cell response.[18] It is also possible that ligation of other molecules on the surface of DCs such as TNF receptors or pattern recognition receptors (for example by lipopolysaccharide, LPS) can have similar effects to contact with activated $CD4^+$ T cells.[19,20] These 'licensing' signals cause DCs to express new costimulatory molecules (including 4-1BB ligand and CD70),[21] increase expression of pre-existing ones, and increase cytokine secretion.

The activation of $CD8^+$ T cells proceeds in a similar manner as that for $CD4^+$ T cells: the TCR recognises the cognate peptide in the MHC class I molecules on the surface of the DC (signal one) and various pairs of molecules [for instance CD80/CD86-CD28, CD70-CD27

and 4-1BB-ligand-4-1BB (CD37)] bind to transmit the second signal.[21,22] IL-2 secreted by activated $CD4^+$ T cells may also assist in inducing $CD8^+$ T cell proliferation.

4.1.3 $CD8^+$ T cell function

The main function of effector $CD8^+$ T cells is to recognise and destroy infected cells by screening MHC class I molecules for their cognate peptide. When a $CD8^+$ T cell recognises its cognate peptide, it is able to promote apoptosis through two main mechanisms: delivering cytoplasmic granules containing enzymes (granzyme A and B) to the target cell *via* secretion of pore-forming perforin molecules, or through binding Fas ligand (CD95L) to Fas receptor (CD95) on target cells. Effector $CD8^+$ T cells also secrete cytokines which mediate the immune response such as IFN-γ and TNF-α, the latter of which may also contribute to induction of apoptosis. A detailed discussion of $CD8^+$ T cell functions may be found in the review by Harty *et al*.[23]

4.1.4 Memory T cells

After an infection has cleared, the quantity of antigen-specific effector T cells declines because maintenance of a large population is no longer required for defence, and also because retaining every effector T cell produced during an individual's lifetime would be physically impossible.[24] Several mechanisms of effector T cell reduction have been proposed including apoptosis induced by lower levels of IL-2 (and other growth factors), regulatory effects of perforin and IFN-γ and an absence of CD40-CD40 ligand interactions.[25] It is likely that $CD4^+$ and $CD8^+$ effector T cell populations are reduced by different mechanisms; studies in gene KO mice implicate a number of molecules in $CD4^+$ depletion (CTLA4, PD-1, Fas, etc.) whereas reduction of $CD8^+$ T cells may be regulated by IFN-γ.[26,27]

Following contraction of the effector T cell pool, a small population of memory T cells remains, generally distinguished from naïve T cells by a $CD45RA^-CD45RO^+$ phenotype (in humans), and migration patterns through the peripheral tissues as opposed to the lymphatic system.[28] How these cells are derived from the large numbers of effector T cells present during the infection is still unclear: various hypotheses are discussed in the review by Kaech and co-workers,[25] and Ahmed and Grey.[29]

The processes through which the resulting memory population is maintained are subject to debate. TCR ligation may not be necessary to maintain a $CD8^+$ T cell memory population,[24] but this is not clear for $CD4^+$ memory T cells.[30] The cytokine IL-15 has a crucial role in $CD8^+$ memory T cell proliferation and survival.[31] In some specific instances, for example in

individuals with latent tuberculosis infections, continued exposure to the bacteria and its secretions also helps to maintain a memory T cell population.[32] Follicular DCs (FDCs – not DCs in the conventional sense as they do not originate from bone marrow and do not present antigen in the usual way *via* MHC molecules) are found in the B cell follicles of secondary lymphoid tissue. They have a role in forming antigen-specific memory B cell populations by assisting in affinity maturation through antigen presentation on iccosomes.[33,34] It is possible that these memory B cells can then present this antigen to memory T cells, thereby maintaining a low level of background stimulation.[29,35]

The threshold for activation of memory T cells is lower than that of naïve T cells; this minimises the damage to the host by halting pathogen replication as soon as possible.[36] The activating cells for memory T cells are not limited to DCs; B cells and other MHC class II expressing cells, e.g. macrophages, can also perform this task.[37] Memory $CD8^+$ T cells do not require licensing from $CD4^+$ T cells to reactivate. Indeed, in some cases exposure to antigen-MHC complex alone provides sufficient stimulation although, contrary to what might be expected, recent work has shown that smaller antigen doses activate naïve but not memory $CD8^+$ T cells.[38,39] Another contributing factor to the rapid response from memory T cells is that the frequency of antigen specific cells is 5-100 times higher in individuals who have experienced an infection compared to naïve individuals, even after the contraction of the effector T cell pool.[29]

The location of memory T cells also enables improved responsiveness to re-infection. Effector memory T cells (T_{EM}) are found in mucosal tissues, at the frontline of the body's defences.[40] They are able to rapidly produce effector cytokines upon restimulation, and appear to maintain their original subset identity (T_h1, T_h2, etc.) unless subjected to sufficiently polarising conditions.[41] Central memory T cells (T_{CM}) circulate through the secondary lymphoid tissue and, having little to no effector function themselves, are able to proliferate rapidly to produce an effector T cell population.[42] In contrast, T_{EM} cells have lower expansion potential.[43] Typically, T_{EM} cells do not express C-C chemokine receptor type 7 (CCR7), a chemokine receptor that guides homing to the lymph nodes, whereas T_{CM} cells are CCR7 positive.[44,42]

Vaccines aim to produce a sufficient number of memory T cells to provide long-lived immunity. As a result, good adjuvants should enhance naïve T cell proliferation and memory T cell responses. Many vaccinations require boosters to ensure a sufficient long-term

memory: these enhance antigen affinity and promote proliferation of the memory population.[25]

4.1.5 Mixed leukocyte reactions

Mixed leukocyte reactions (MLRs) are an *in vitro* method for assessing T cell proliferation. Generally, these assays consist of isolating then mixing stimulator cells and responder cells, usually T cells, in a set ratio, then analysing proliferation at various time points, traditionally by tritiated thymidine incorporation. The two cell sets may be allogeneic (different individual) or occasionally xenogeneic (different species).[45,46] Often, to focus solely on the proliferation of the responder cell, the stimulator cell will be inactivated by irradiation.[47]

DCs are the most potent stimulator of T cell proliferation in allogeneic MLRs (allo-MLRs), over macrophages and B cells.[48,49] Monocyte-derived DCs (Mo-DCs) developed from treatment of monocytes with GM-CSF and IL-4, also demonstrate good allostimulatory properties in the MLR.[50,51] The stimulus in the allo-MLRs is the recognition of 'foreign' MHC molecules on the stimulator cells by the responder cells.[52–54] As such allo-MLRs have been used as an *in vitro* technique for investigating the mechanisms of graft or transplant rejection.[55] Altering the conditions in MLRs can provide information about immune function. For example, Godfrey *et al*. demonstrated the suppressor function of $CD4^+CD25^+$ regulatory T cells by adding them to an allogeneic DC-$CD4^+$ T cell MLR, noting blocked proliferation.[56] On the other hand, introducing additional stimuli, such as LPS or IL-12, or pre-treatment of the stimulator cells (for instance, in investigations by Yang *et al*. into the effects of extracellular high mobility group box-1 protein) may enhance proliferation in allogeneic MLRs.[57–59]

The ratios of responder to stimulator cells have been scrutinised in various studies. Crow *et al*. used equal parts stimulator:responder cells in their studies into the allostimulatory properties of different cell types.[48] However, numerous examples in the literature show that DCs are capable of stimulating strong T cell responses at much lower ratios: 1:10,[56] 1:(30-100),[60] and even as low as 1:(250-6250).[59] For the work described in this Chapter, a DC:T cell ratio of 1:10 has been used.

4.1.6 Layered double hydroxides used in this Chapter

In this chapter, five LDHs are chosen for investigation: MgAl-CO_3, MgAl-NO_3, LiAl-CO_3, CaAl-NO_3 and MgFe-CO_3 LDH. This selection was made based on earlier *in vivo* studies in mice and prelimary T cell expansion data collected by Williams and co-workers.[61] CaAl-NO_3

LDH induced the highest IgE and IgG1 ovalbumin (OVA) specific antibody responses in mice (indicative of a T_h2 type response), whereas MgFe-CO_3 induced the highest IgG2c OVA specific antibody response (indicative of a T_h1 type response). LiAl-CO_3 LDH was the most effective promoter of DC maturation as assessed by pro-inflammatory cytokine secretion (IL-1β, IL-6, TNF-α, IL-12p70, etc.), and CD40, CD86, and CD274 expression. Expansion of OVA specific $CD8^+$ T cells was noted for MgAl-CO_3 and MgAl-NO_3 LDHs, implying these LDHs might induce robust $CD8^+$ T cell responses.

These five LDHs were prepared by methods analogous to those used by Williams and co-workers.[61] The MgAl-CO_3, MgAl-NO_3, CaAl-NO_3 and MgFe-CO_3 LDHs were all prepared by coprecipitation. Detailed synthesis methods are supplied in Chapter Six, characterising data may be found in Chapter Two. LiAl-CO_3 LDH was synthesised from gibbsite for consistency with the earlier work (characterising data supplied in Appendix C.1).[61]

4.1.7 Scope of this Chapter

The work by Williams *et al*. and the particle size investigations described in Chapter Three confirm that LDHs have a profound effect on specific Mo-DC responses over a short time period (< 24 hours). Therefore, it was hypothesised that LDH-stimulated Mo-DCs would alter subsequent T cell responses compared to non-LDH treated Mo-DC. This could have implications for the suitability of vaccines containing LDH adjuvants, as these materials may alter the amount and kinetics of T cell proliferation, or elicit a specific pattern of T cell polarisation.

This Chapter investigates human T cell responses to allogeneic Mo-DCs in the presence of the five different LDH compositions described in Section 4.1.6. An initial time course experiment comprising a co-culture of whole T cells and allogeneic Mo-DC was performed to establish the time points to assess T cell responses in subsequent experiments. Following on from this, the effects of the five LDHs on responses of naïve or memory T cells co-cultured with allogeneic Mo-DC were probed.

T cell division was assessed by staining T cells with carboxyfluoruoscein succinimidyl ester (CFSE). Tritiated thymidine incorporation assays were utilised for further assessment of proliferation. IL-2 secretion was evaluated by enzyme-linked immunosorbent assays (ELISA). An intracellular cytokine staining protocol was developed and used to determine whether any significant T cell polarisation had occurred.

4.2 Experimental set-up

All results described in this Chapter are from MLR experiments where human T cells (whole/naïve/memory, as specified in individual sections) were co-cultured with allogeneic Mo-DC. To assess cell division in the MLRs, T cells were stained with CFSE prior to mixing with Mo-DCs. CFSE covalently binds to amines inside the cell; as the cell divides, the CFSE is partitioned, halving the per-cell fluorescence. Measurement of the CFSE fluorescence provides a measure of cell division; cells which are undivided will be strongly CFSE fluorescent ($CFSE^{high}$) whereas those that have divided will exhibit lower fluorescence ($CFSE^{low}$). T cells were then mixed in a 10:1 ratio with allogeneic Mo-DC (except for the T cell only control conditions). Stimuli (LDHs, LPS, commercial adjuvants) were added directly to the wells containing the cell mix, as opposed to pre-treatment of the Mo-DC. This was because it was very difficult to separate DC and LDH; indeed, Chapter Five demonstrates that LDHs adhere to the surface of DCs, and both are pelleted in the wells upon centrifugation. Tritiated thymidine incorporation experiments were set up in an analogous manner, but without CFSE staining.

For intracellular cytokine staining, at the timepoint of choice cells were stimulated with phorbol 12-myristate 13-acetate (PMA) and ionomycin (to stimulate cytokine production) in conjunction with the protein transport inhibitor brefeldin A for five hours. After this, cells were stained for the surface markers CD4, CD8 and CD209 (DC sign - to exclude Mo-DC from the analysis) and for viability. Supernatants were harvested and frozen for subsequent analysis of IL-2 secretion. Cells were then fixed and permeabilised in order that staining for the three signature cytokines IFN-γ (T_h1), IL-4 (T_h2) and IL-17 (T_h17) could be performed. Pooled isotype control wells were incorporated, and used to set the gates in the strategy outlined in the next section. Cells were then analysed using flow cytometry. The full methods for all procedures used are supplied in Section 6.5.

4.2.1 Gating strategy

For analysis of the flow cytometry data for all the CFSE dilution/intracellular cytokine staining experiments the gating strategy shown in Figure 4.2 was employed. Firstly, lymphocytes were selected in the forward scatter/side scatter (FSC/SSC). Secondly, dead cells and Mo-DC were excluded using the same fluorescence channel. Then, $CD4^+$ and $CD8^+$ T cells were gated independently, and the division of each assessed by calculating the percentages of $CFSE^{high}$ (undivided) and $CFSE^{low}$ (divided) cells. The individual

sub-populations of $CD4^+/CD8^+$ undivided/divided cells were then assessed for percentages of cytokine positive cells (IFN-γ^+, IL-4^+, IL-17^+ and the double-positive populations IFN-γ^+IL-4^+ and IFN-γ^+IL-17^+). The double-positive IL-4^+IL-17^+ population was excluded from the analysis, as the percentages of cells IL-4^+IL-17^+ was negligible.

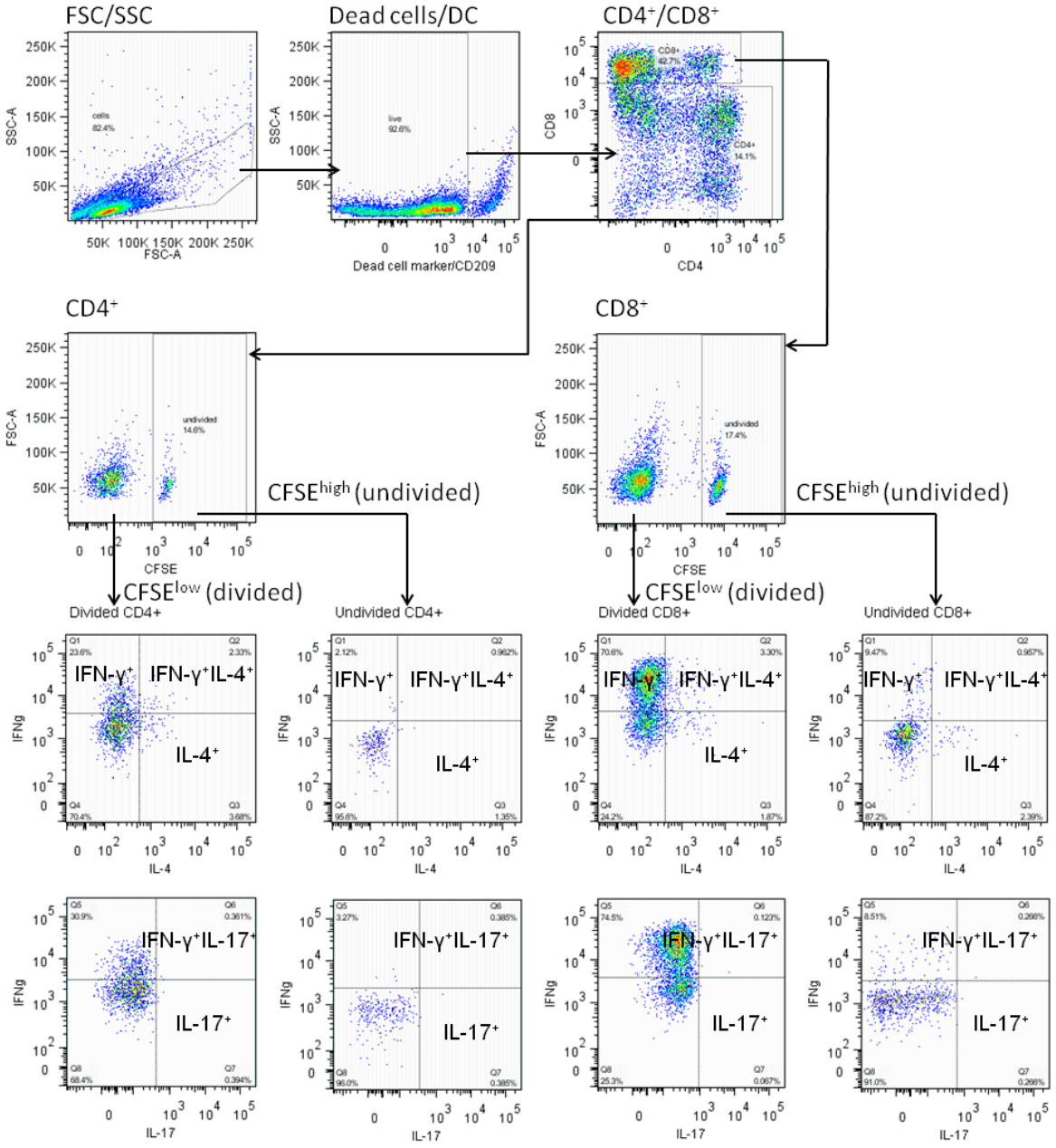

Figure 4.2: Gating strategy for determining cell division and cytokine positive populations in MLR experiments. (1) Set lymphocyte gate in FSC/SSC; (2) gate out dead cells (viability dye) and Mo-DC (CD209 - both APC^+); (3) gate on $CD4^+$ ($APC\text{-}Cy7^+$) or $CD8^+$ ($PE\text{-}Cy7^+$) T cells; (4) set undivided/divided cell gates ($CFSE^{high}/CFSE^{low}$), (5) set gates for IFN-γ^+, IL-4^+, IL-17^+, IFN-γ^+IL-4^+ and IFN-γ^+IL-17^+ within each sub-population ($CD4^+$ undivided, $CD4^+$ divided, $CD8^+$ undivided, $CD8^+$ divided) by comparing to isotype controls.

To calculate the total percentage of T cells that express a given cytokine, the proportions of cytokine positive cells in each of the sub-populations ($CD4^+$ undivided, $CD4^+$ divided, $CD8^+$

undivided and $CD8^+$ divided) were multiplied by the proportion of the total T cells in that sub-population. The individual contributions from the four sub-populations were then summed to give the total percentage of positive T cells for each cytokine.

4.2.2 Generation of positive controls for intracellular cytokine staining

Positive control cells with detectable populations of IFN-γ, IL-4 and IL-17 positive cells were generated and frozen. These were then thawed and stimulated/stained in tandem with the experimental wells to confirm intracellular cytokine staining had been carried out correctly. The protocols used for generating these controls are supplied in Section 6.5.4.

4.3 Results

4.3.1 Preliminary time course experiment

An initial time course experiment on whole T cells co-cultured with allogeneic Mo-DCs (allo-DCs) was carried out as a means to establish what time points would merit further investigation. Cells from one pair of donors (one donor for Mo-DC, one for T cells) were assessed. The control conditions were: T cells only (without allo-DCs); T cells with allo-DC without any extra stimulus as a negative control (background allo-response); and T cells with allo-DCs and LPS as a positive control. In order that comparisons with a commercial adjuvant could be made, T cells and allo-DCs with Imject were also included for comparison. To establish whether and at what point in time LDHs affect the MLR response, T cells with allo-DCs were also incubated with LiAl-CO_3 LDH. Cells were analysed at days three, five, seven and ten for proliferation and cytokine production. Each condition was tested in duplicate. Significance data between all conditions and days is supplied in Appendix C.2.

4.3.1.1 T cell division from CFSE dilution data

Figure 4.3 displays proliferation data for the preliminary time course experiment expressed as the percentage of divided $CD4^+$ or $CD8^+$ T cells. Overall, addition of the LiAl-CO_3 LDH to the T cell/allo-DC mix does not enhance or diminish cell division above the baseline from the background allo-response for either the $CD4^+$ or $CD8^+$ T cell population. There is some suggestion that, at day five, LDH treatment does give a small increase in $CD4^+$ T cell proliferation over the background and LPS-stimulated controls.

Imject noticeably hinders proliferation of both $CD4^+$ and $CD8^+$ T cells at the later time points (days seven and ten), compared to all other conditions imposed on the cells (unstimulated, LPS- and LDH-stimulated). Due to the large number of FSC/SSC events noted when Imject

was added to the co-culture, some difficulties occurred when attempting to gate on the cells for Imject treated wells.

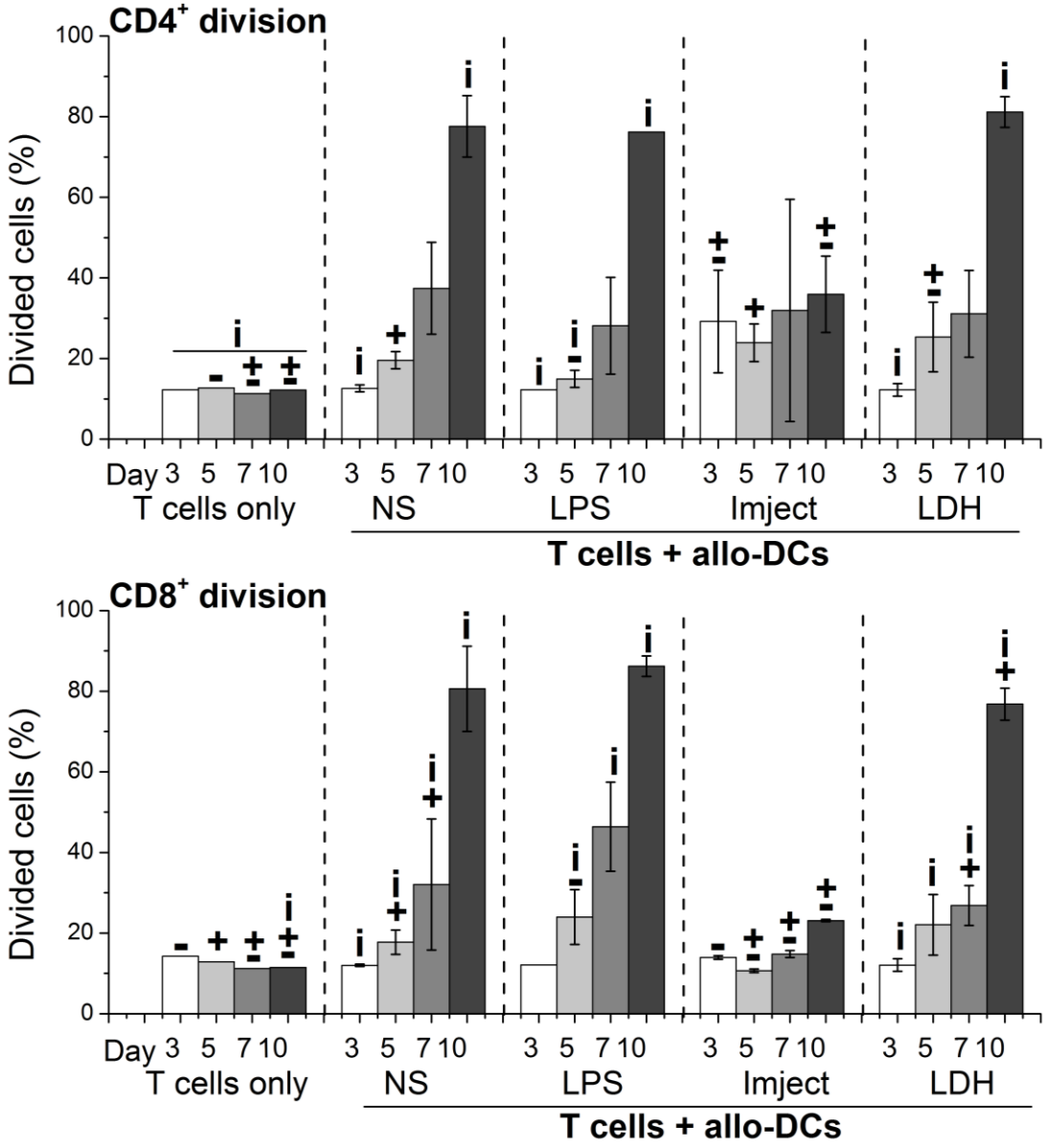

Figure 4.3: T cell division data for the preliminary time course experiment in which whole T cells were co-cultured with allogeneic Mo-DCs, with/without LDH and other control conditions. Whole T cells were isolated from PBMCs, stained with CFSE, then co-cultured with allogeneic Mo-DCs, with LiAl-CO_3 LDH and other control conditions for three, five, seven and ten days. On the day of analysis, cells were stained for surface molecules, viability and intracellular cytokines and analysed by flow cytometry. Divided cells were taken as the percent of $CD4^+$ or $CD8^+$ T cells in the $CFSE^{low}$ population. NS = no stimulus, LDH = LiAl-CO_3 LDH synthesised from gibbsite. Error bars indicate two standard deviations. '-' indicates results significantly different ($p<0.05$) to the negative control (T cells/allo-DCs with no extra stimulus – background allo-response), '+' relative to the positive control (T cells/allo-DCs + LPS), and 'i' relative to the Imject treated T cells/allo-DCs, for the day specified.

4.3.1.2 Cytokine production

Figure 4.4 displays the percentage of T cells in each cytokine positive (IFN-γ^+, IL-4^+, IL-17^+) or double positive (IFN-γ^+IL-4^+ and IFN-γ^+IL-17^+) population for every day analysed in the preliminary time course experiment. The total height of the bars indicates the total percentage of all T cells positive, or double positive, for a given cytokine/pair of cytokines. The different coloured regions of the bars correspond to the contributions from the four sub-populations of T cells ($CD4^+$/$CD8^+$ divided/undivided).

Addition of LiAl-CO_3 LDH does not enhance production of any of the cytokines, and indeed may suppress the final proportion of T cells expressing IFN-γ at day ten compared to the negative (T cells/allo-DC without stimulus) and positive (LPS-treated T cells/allo-DC) controls. Treatment with LiAl-CO_3 LDH yields comparable IL-4^+ T cell proportions to the negative and positive controls. Overall, Imject treated cells give very low percentages of cytokine positive T cells, below those of both the controls and the LDH.

In conclusion, the LiAl-CO_3 LDH does not appear to induce either significantly higher proportions of cytokine secreting T cells, or alter polarisation compared to the background allo-response. Neither does it enhance T cell division, as assessed by CFSE dilution. However, only one LDH was investigated in these early experiments, and previous work has shown that immune responses are sensitive to the physicochemical properties of the LDHs used. Given that little response to any of the treatments was observed at day three, day five was chosen as a point that captures the early stages in the MLR response. Observations made at day ten provide insights into the later stages of the response. Consequently, these two timepoints were used in experiments on naïve T cells in Section 4.3.2.

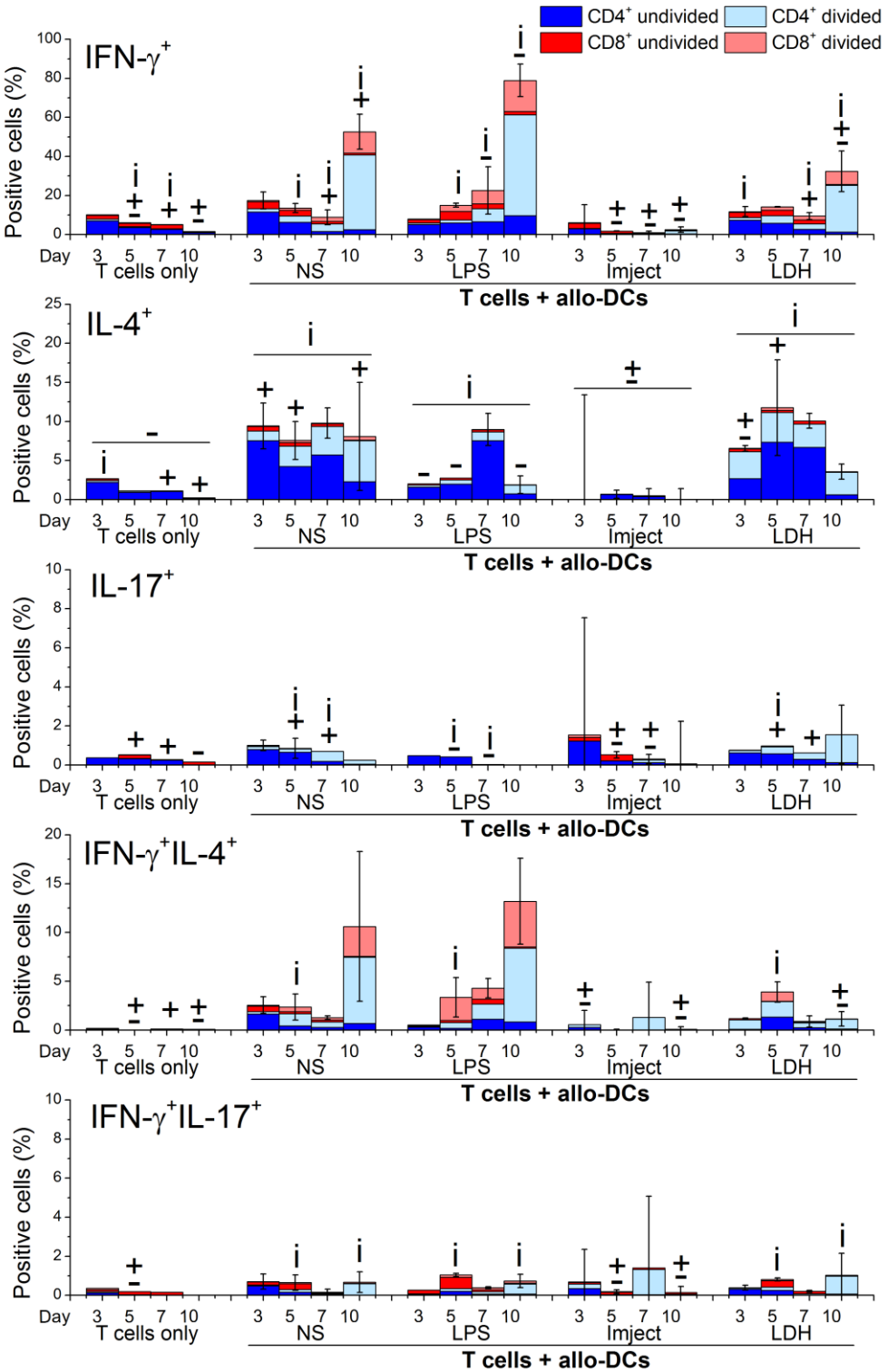

Figure 4.4: Percentages of all T cells in cytokine single (IFN-γ^+, IL-4^+, IL-17^+) and double positive (IFN-γ^+IL-4^+ and IFN-γ^+IL-17^+) populations in the preliminary time course experiment. Whole T cells were stained with CFSE, then incubated with allogeneic Mo-DCs, with/without LiAl-CO_3 LDH and other control conditions for three, five, seven and ten days. On the day of analysis, cells were stained for surface molecules, viability and intracellular cytokines and analysed by flow cytometry. The total height of the bars indicates the total percentage of all T cells positive, or double positive, for a given cytokine/pair of cytokines. Different colours indicate the proportion of the T cells contributing from each sub-population ($CD4^+$ undivided, $CD4^+$ divided, $CD8^+$ undivided, $CD8^+$ divided). NS = no stimulus, LDH = LiAl-CO_3 LDH synthesised from gibbsite. Error bars indicate two standard deviations. '-' indicates results significantly different ($p<0.05$) to the negative control (T cells/allo-DCs with no extra stimulus – background allo-response), '+' relative to the positive control (T cells/allo-DCs + LPS), and 'i' relative to the Imject treated T cells/allo-DCs, for the day specified.

4.3.2 Naïve T cell experiments

The two timepoints determined in the preceding section, days five and ten, were further explored by co-culturing purified naïve T cells with allogeneic Mo-DC. This was with a view to establish the effects of LDH-stimulated Mo-DCs on the initial activation of naïve T cells.

4.3.2.1 Experimental set-up

Detailed descriptions of the protocol for setting up these experiments may be found in Sections 6.5.2 and 6.5.3. Briefly, naïve T cells were obtained in >90% purity ($CD4^+$ - defined as $CD3^+CD4^+CD45RA^+$) and >95% purity ($CD8^+$ - defined as $CD3^+CD8^+CD45RA^+$). Allogeneic Mo-DCs were added to the T cells at a ratio of 1:10, except for the T cells only control wells. The control conditions included were: T cells only (without allo-DCs); T cells with allo-DCs without any extra stimulus as a negative control (background allo-response); and T cells with allo-DCs and LPS as a positive control. Due to the difficulties encountered gating on cells incubated with Imject during the time course, Alhydrogel was used as the comparison adjuvant instead. Five LDH compositions were added to the cells: MgAl-CO_3, MgAl-NO_3, LiAl-CO_3, CaAl-NO_3 and MgFe-CO_3. This selection was based on earlier *in vivo* studies in mice and preliminary T cell expansion data collected by Williams and co-workers described in Section 4.1.6.[61]

Three pairs of donors (one donor for Mo-DC, one for T cells) were investigated in CFSE dilution/intracellular cytokine staining experiments. Tritiated thymidine incorporation data was collected for two pairs of donors to further explore the effect of LDHs on the early stages of proliferation. Data processing similar to that in Chapter Three was carried out; normalisation, taking into account variability between donor pairs was performed to produce estimates and confidence intervals. Full tables of significance data for CFSE dilution, IL-2 secretion, tritiated thmidine incorporation and cytokine expression were calculated and may be found in Appendix C.3.

4.3.2.2 T cell division from CFSE dilution data

Figure 4.5 displays proliferation data from CFSE dilution expressed as the percentage of divided $CD4^+$ or $CD8^+$ T cells for naïve T cells co-cultured with allogeneic Mo-DCs treated with the various stimuli and controls.

At day five, treatment with the five LDHs yields greater percentages of divided $CD4^+$ T cells than the background allo-response. At this point, three of the five LDHs (MgAl-NO_3,

LiAl-CO_3 and CaAl-NO_3 LDH) also give enhanced $CD8^+$ division relative to the background. This could indicate LDHs have a slight accelerating effect on the early stages of proliferation.

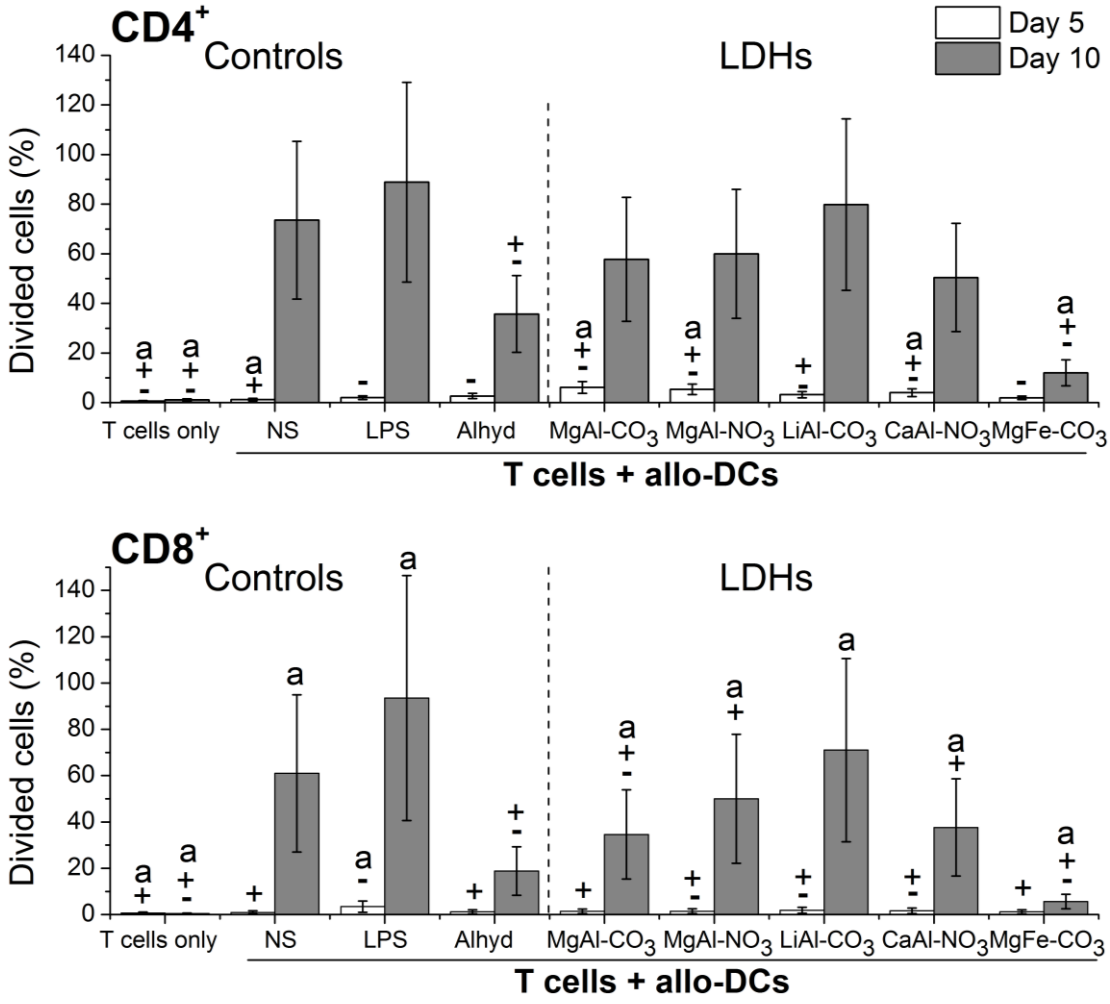

Figure 4.5: T cell division data from experiments in which naïve T cells were co-cultured with allogeneic Mo-DCs, with/without LDHs and other control conditions. Naïve T cells were isolated, stained with CFSE, then incubated with allogeneic Mo-DCs, with/without LDHs and other control conditions for five and ten days. On the day of analysis, cells were stained for surface molecules, viability and intracellular cytokines and analysed by flow cytometry. Divided cells were taken as the percent of $CD4^+$ or $CD8^+$ T cells in the $CFSE^{low}$ population. Normalised data from three donors (day five) and two donors (day ten) are shown. NS = no stimulus, Alhyd = Alhydrogel. Error bars indicate 95% confidence intervals. '-' indicates results significantly different ($p<0.05$) to the negative control (T cells/allo-DCs with no extra stimulus – background allo-response), '+' relative to the positive control (T cells/allo-DCs + LPS), and 'a' relative to the Alhydrogel treated T cells/allo-DCs, for the day specified.

However, addition of LDHs to the allo-MLR does not enhance proliferation in the long-term. By day ten there is no enhancement in $CD4^+$ or $CD8^+$ T cell division in the presence of LDHs relative to the negative or positive controls. Indeed the MgFe-CO_3 LDH induces significantly lower percentages of divided T cells than all three control conditions (background allo-response, LPS treated cells and Alhydrogel treated cells). Alhydrogel treatment generally induces similar levels of cell division to the LDHs. Some LDHs do induce greater percentages

of divided $CD4^+$ T cells at day five, and also $CD8^+$ T cells at day ten, but taken as a whole this is a small difference.

4.3.2.3 IL-2 secretion

Supernatants from the CFSE/intracellular cytokine staining assays were analysed for production of the cytokine IL-2 using ELISAs (Figure 4.6). IL-2 has a crucial role promoting the initial clonal expansion of antigen specific T cells, and is produced during the early stages of proliferation.[62]

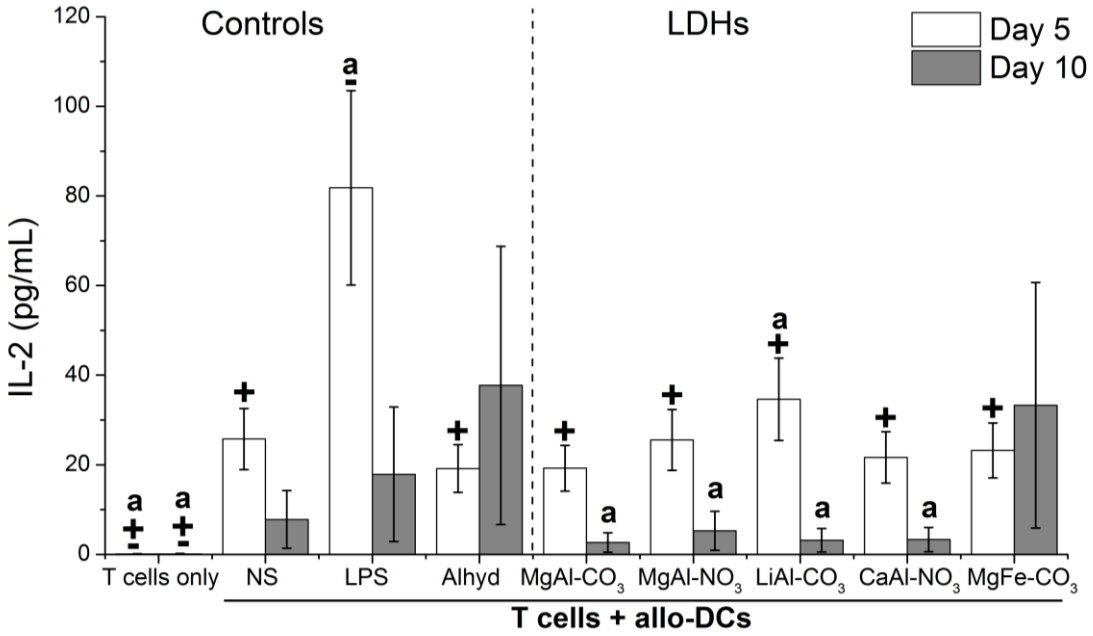

Figure 4.6: IL-2 secretion by naïve T cells co-cultured with allogeneic Mo-DCs, with/without LDHs and other control conditions. Naïve T cells were isolated, stained with CFSE, then incubated with allogeneic Mo-DC, with/without LDHs and other control conditions. When cells were stained at days five and ten, supernatants were harvested, frozen, and later analysed for IL-2 using ELISAs. Normalised data from three donors (day five) and two donors (day ten) are shown. NS = no stimulus, Alhyd = Alhydrogel. Error bars indicate 95% confidence intervals. '-' indicates results significantly different ($p<0.05$) to the negative control (T cells/allo-DCs with no extra stimulus – background allo-response), '+' relative to the positive control (T cells/allo-DCs + LPS), and 'a' relative to the Alhydrogel treated T cells/allo-DCs, for the day specified.

In contrast to the proliferation data obtained through CFSE staining, the highest IL-2 concentrations are observed at day five. At this point, none of the LDHs significantly increase or decrease IL-2 production relative to the background allo-response (negative control). By day ten, IL-2 concentrations are lower for all conditions. Again, no major differences between the LDHs and the background allo-reponse or the commercial adjuvant Alhydrogel are present.

4.3.2.4 Tritiated thymidine incorporation assays

Thymidine is one of the four deoxyribonucleosides in DNA. When a small amount of tritiated thymidine is added to the cell culture medium it is incorporated by dividing cells during DNA synthesis. The radioactivity attributable to the cells can then be measured, and used to compare the amount of cell division that has occurred. Unlike in flow cytometry, analysis of the data is simpler as there is no requirement for gating strategies, thus a more accurate idea of T cell proliferation may be obtained.

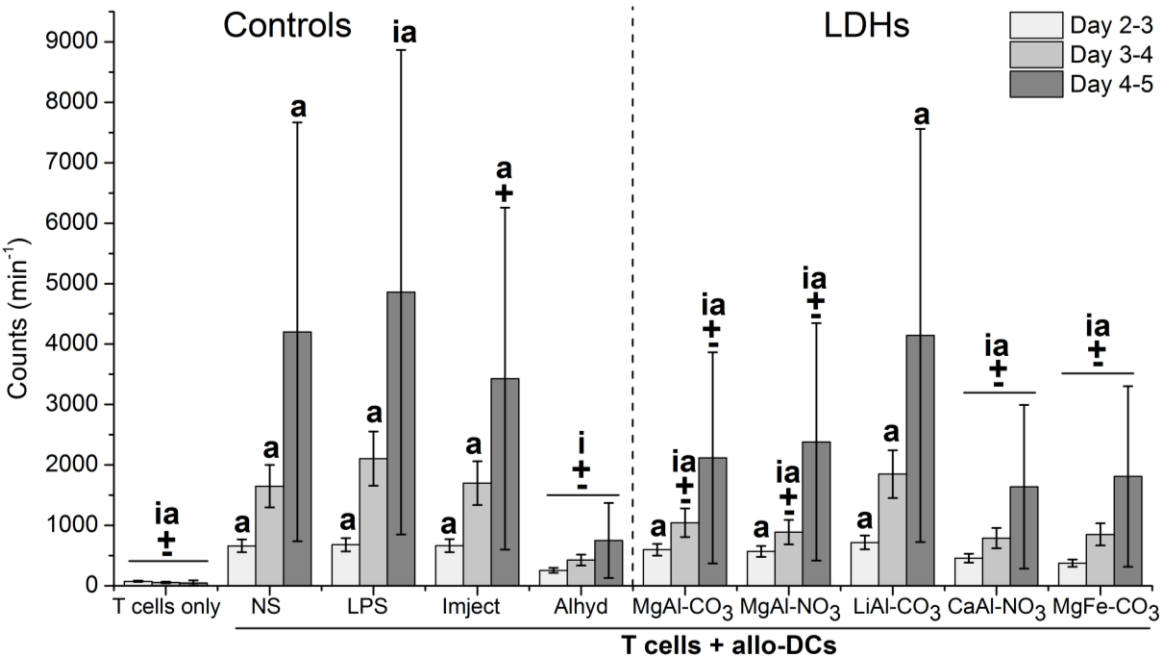

Figure 4.7: Tritiated thymidine incorporation data for days two to five from experiments in which naïve T cells were co-cultured with allogeneic Mo-DCs, with/without LDHs and other control conditions. Naïve T cells were isolated and co-cultured with allogeneic Mo-DC, with/without LDHs and other control conditions. At days two, three and four the cells were pulsed overnight with tritiated thymidine, then dried onto filter papers and radioactivity corresponding to tritiated thymidine incorporation during DNA synthesis assessed using a liquid scintillation counter. Normalised data from two donors are displayed. Error bars indicate 95% confidence intervals. NS = no stimulus, Alhyd = Alhydrogel. '-' indicates results significantly different ($p<0.05$) to the negative control (T cells/allo-DCs with no extra stimulus – background allo-response), '+' relative to the positive control (T cells/allo-DCs + LPS), and 'i' or 'a' relative to the Imject or Alhydrogel treated T cells/allo-DCs, for the day specified.

Tritiated thymidine incorporation assays focusing on the first few days of T cell proliferation were conducted (Figure 4.7). This was done to confirm the enhancement in cell division with LDHs observed at day five in the CFSE dilution experiments. T cell-DC clusters and T cell blasting were observable under the microscope on day two, consequently this was chosen as the starting point for the time course. All pulses with tritiated thymidine were performed overnight (18 hours). Imject was included as an extra control condition in these assays.

From these assays, no LDH enhances proliferation relative to the baseline of the allo-response. Indeed, four of the LDHs (all except LiAl-CO_3) display significantly reduced incorporation compared to the unstimulated and LPS stimulated control wells for days 3-4 and 4-5. These assays also confirm that LDHs generally suppress T cell responses less than the commercial adjuvant Alhydrogel.

4.3.2.5 Cytokine production

Figure 4.8 displays the percentage T cells in each cytokine positive (IFN-γ^+, IL-4^+, IL-17^+) or double positive (IFN-γ^+IL-4^+ and IFN-γ^+IL-17^+) population for days five and ten in the naïve T cell-allogeneic Mo-DC MLR. The total height of the bars indicates the total percentage of all T cells positive, or double positive, for a given cytokine/pair of cytokines. The different coloured regions of the bars reflect the contributions from the four sub-populations of T cells ($CD4^+$/$CD8^+$ divided/undivided).

None of the cytokine responses to LDHs are greater those of the background allo-response. Only two of the LDHs (LiAl-CO_3 and CaAl-NO_3) consistently give comparable proportions of T cells IFN-γ^+ and IL-4^+ to the background allo-response. The other three frequently produce significantly smaller positive fractions (for example, the percentages of IFN-γ^+ T cells with MgAl-NO_3 and MgFe-CO_3 LDH are significantly lower than the background at day ten). The MgFe-CO_3 LDH generally elicits the lowest cytokine responses. This approximately correlates with the division data; the LiAl-CO_3 and CaAl-NO_3 LDHs tend to hinder T cell proliferation the least, whilst MgFe-CO_3 LDH exhibits the strongest reduction in the fraction of divided T cells. Little difference can be discerned between the T cell responses to LDHs and Alhydrogel; typically, the proportions of cytokine expressing T cells they induce are comparable. However, LiAl-CO_3 and CaAl-NO_3 LDH do induce marginally higher percentages of IFN-γ^+ T cells at day five. In summary, LDHs do not appear to enhance the capacity of Mo-DC to stimulate allogeneic naïve T cell proliferative responses or improve cytokine secretion relative to the background allo-response.

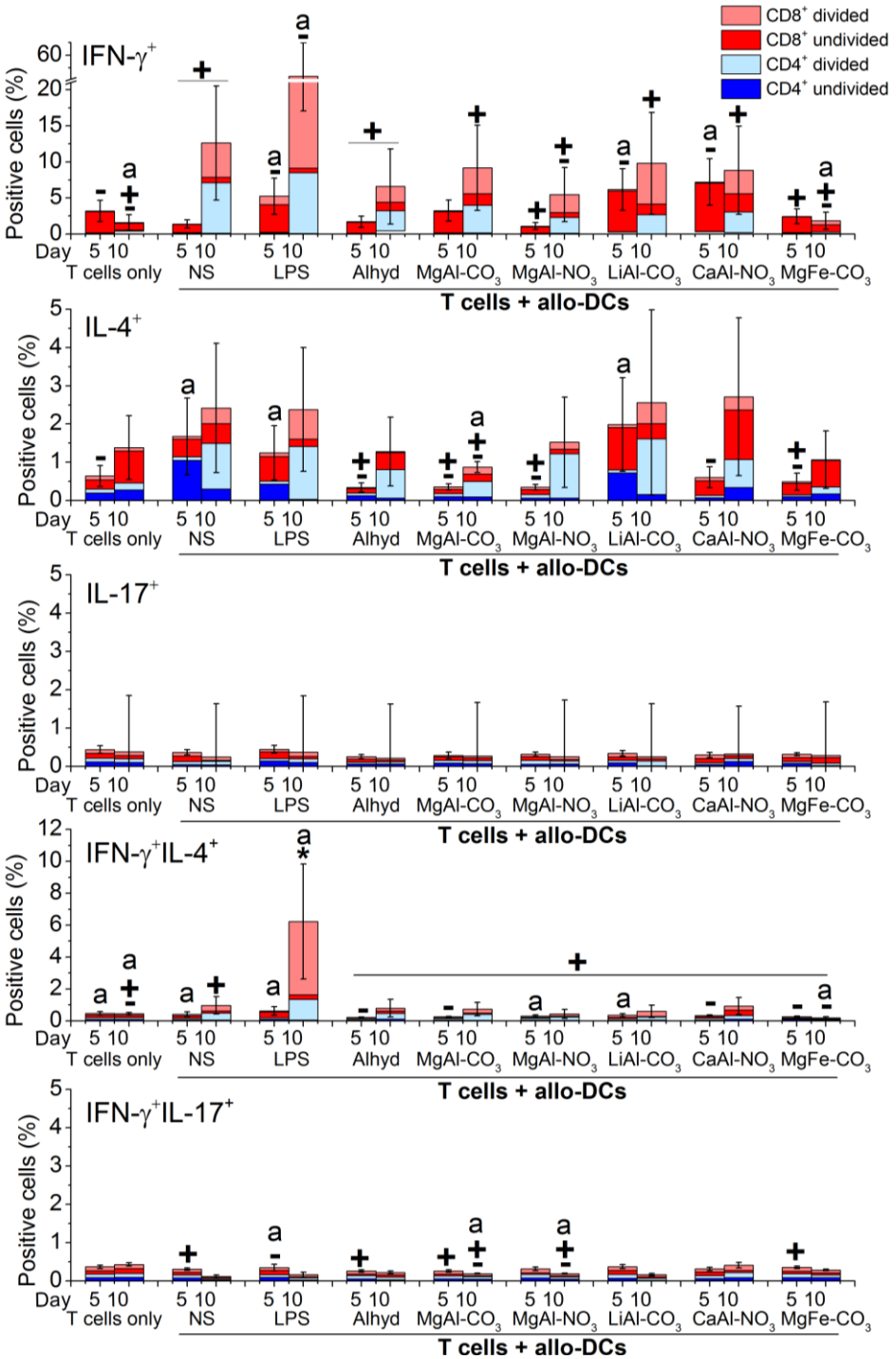

Figure 4.8: Percentages of T cells in single (IFN-γ$^+$, IL-4$^+$, IL-17$^+$) and double positive (IFN-γ$^+$IL-4$^+$ and IFN-γ$^+$IL-17$^+$) cytokine populations in the MLRs in which naïve T cells were co-cultured with allogeneic Mo-DC, with/without LDHs and other control conditions. Naïve T cells were isolated, stained with CFSE, then incubated with allogeneic Mo-DC, with/without LDHs and other control conditions for five and ten days. On the day of analysis, cells were stained for surface molecules, viability and intracellular cytokines and analysed by flow cytometry. Normalised data from three donors (day five) and two donors (day ten) are shown. The total height of the bars indicates the total percentage of all T cells positive, or double positive, for a given cytokine/pair of cytokines. Different colours indicate the proportion of the T cells contributing from each sub-population (CD4$^+$ undivided, CD4$^+$ divided, CD8$^+$ undivided, CD8$^+$ divided). NS = no stimulus, Alhyd = Alhydrogel. Error bars indicate 95% confidence intervals. '-' indicates results significantly different ($p<0.05$) to the negative control (T cells/allo-DCs with no extra stimulus – background allo-response), '+' relative to the positive control (T cells/allo-DCs + LPS), and 'a' relative to the Alhydrogel treated T cells/allo-DCs, for the day specified.

4.3.3 Memory T cell Responses

When a vaccine is administered, the vaccine mixture comes into contact with cells in the tissue, including memory T cells. Their response to the antigen/adjuvant combination could affect maturation of local DCs and the signals they later convey to naïve T cells. Moreover, if it is being administered as a booster to a previous vaccination, promoting memory T cell expansion is important to ensure sufficient vaccine efficacy.

4.3.3.1 Experimental set-up

Memory T cell experiments were set up in an analogous fashion to the naïve T cell experiments detailed in Section 4.3.2. Human $CD4^+$ and $CD8^+$ memory T cells were isolated at >90% $CD3^+CD4^+CD45RO^+$ or $CD3^+CD8^+CD45RO^+$ purity respectively. Positive (T cells with allo-DC and LPS), negative (T cells plus allo-DC with no extra stimulus) and T cell only controls were included, alongside Imject, Alhydrogel and the five LDHs specified in Section 4.1.6.

Responses were assessed at days two, five and seven. Experiments with cells from three pairs of donors were conducted, of which one pair only yielded sufficient T cells for analysis at days two and five. Analysis at day two was incorporated because the memory response develops more rapidly than the naïve responses, and is more sensitive to stimulation. Significance data for all responses analysed may be found in Appendix C.4.

4.3.3.2 T cell division from CFSE dilution data

Figure 4.9 displays $CD4^+$ and $CD8^+$ division data from CFSE dilution for memory T cells co-cultured with allogeneic Mo-DC with the various stimuli and controls.

At day two, virtually no division (<3%) is noted for any of the conditions. By day five, modest proliferation (~10%) of both $CD4^+$ and $CD8^+$ memory T cells has occurred. At this point, for both $CD4^+$ and $CD8^+$ T cells, all LDHs except LiAl-CO_3 and CaAl-NO_3 yield significantly lower divided populations than the background allo-response. At day seven, no significant enhancement in $CD4^+$ division is noted in response to LDH treatment. However, distinctions between the effects of the different treatments on $CD8^+$ memory T cell proliferation can be made: all LDHs except MgFe-CO_3 induce higher proportions of divided cells than the negative control (background allo-response).

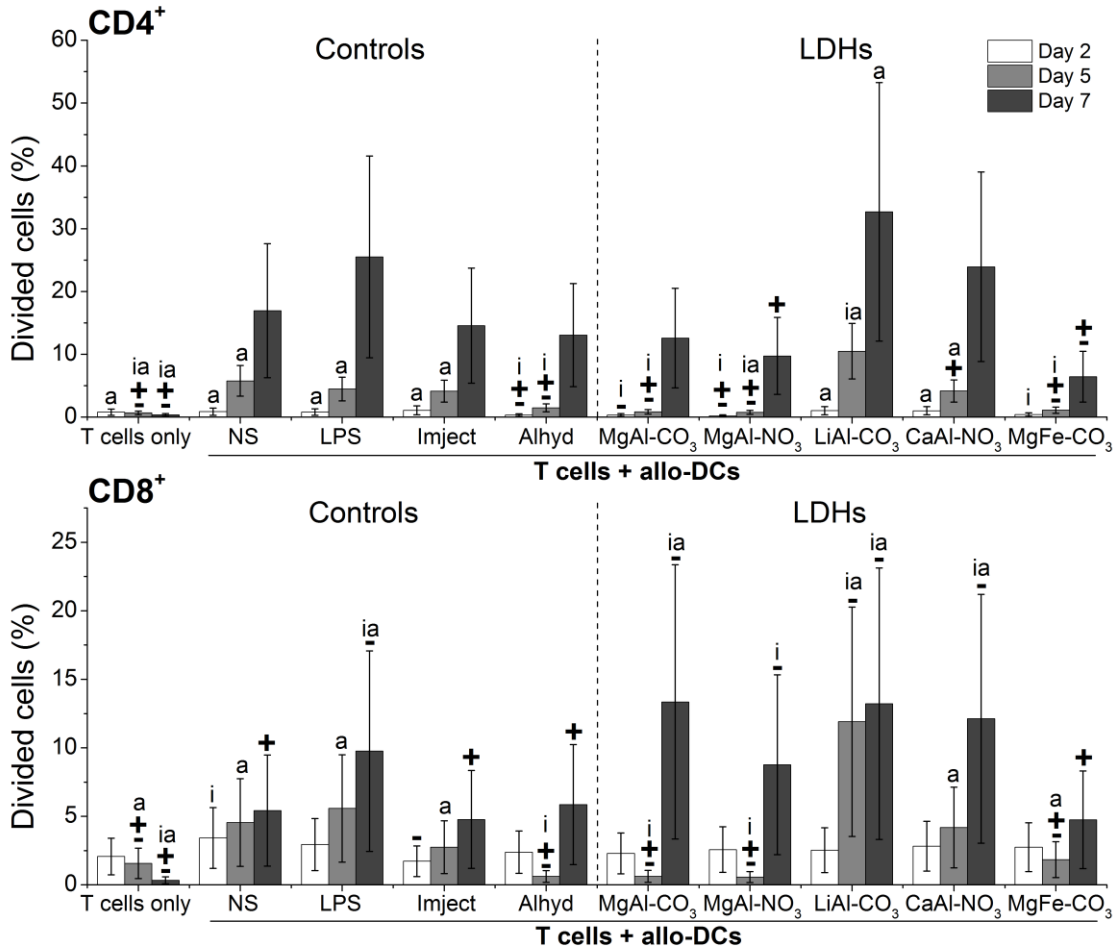

Figure 4.9: Cell division from CFSE dilution data from experiments in which memory T cells were co-cultured with allogeneic Mo-DCs, with/without LDHs and other control conditions. Memory T cells were isolated, stained with CFSE, then co-cultured with allogeneic Mo-DCs, with/without LDHs and other control conditions for two, five and seven days. On the day of analysis, cells were stained for surface molecules, viability and intracellular cytokines and analysed by flow cytometry. Divided cells were taken as the percent of $CD4^+$ or $CD8^+$ T cells in the $CFSE^{low}$ population. Normalised data from three donors (days two and five) and two donors (day seven) are shown. NS = no stimulus, Alhyd = Alhydrogel. Error bars indicate 95% confidence intervals. '-' indicates results significantly different ($p<0.05$) to the negative control (T cells/allo-DCs with no extra stimulus – background allo-response), '+' relative to the positive control (T cells/allo-DCs + LPS), and 'i' or 'a' relative to the Imject or Alhydrogel treated T cells/allo-DCs, for the day specified.

In comparison to the commercial adjuvants, only LiAl-CO_3 LDH yields increased both $CD4^+$ and $CD8^+$ cell division relative to Imject at day five. Alhydrogel stimulates cell proliferation poorly: two LDHs (LiAl-CO_3 and CaAl-NO_3) proffer improved $CD4^+$ division and three LDHs (LiAl-CO_3, CaAl-NO_3 and MgFe-CO_3) improved $CD8^+$ division at day five. At day seven, three LDHs (MgAl-CO_3, LiAl-CO_3 and CaAl-NO_3) display enhanced $CD8^+$ division compared to the Alhydrogel control.

In summary, addition of either LDHs or commercial adjuvants to the MLR does not induce a great increase in memory T cell division. Some marginal improvements in response to LDHs over the commercial adjuvants are observed, particularly for $CD8^+$ T cell division.

4.3.3.3 IL-2 secretion

All assay supernatants from the memory T cell CFSE/intracellular cytokine staining assays were analysed for secretion of IL-2 using ELISAs. Normalised data for all days are displayed in Figure 4.10.

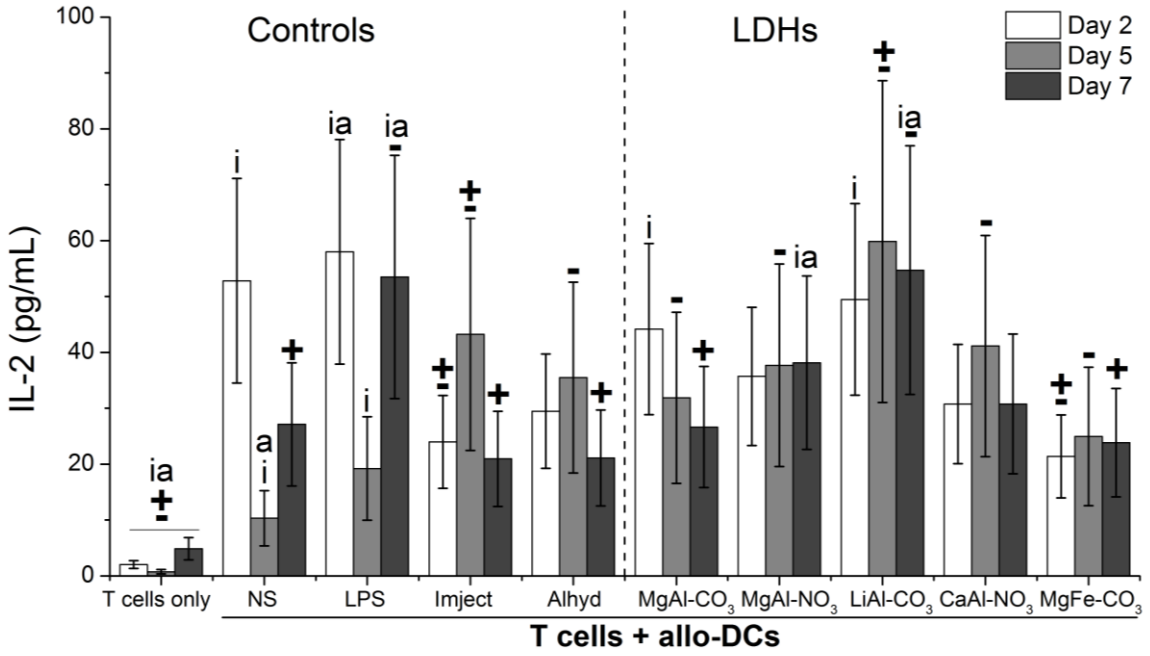

Figure 4.10: IL-2 secretion by memory T cells co-cultured with allogeneic Mo-DCs, with/without LDHs and other control conditions. Memory T cells were isolated, stained with CFSE, then co-cultured with allogeneic Mo-DC, with/without LDHs and other control conditions for two, five and seven days. When cells were stained, supernatants were harvested, frozen, then later analysed for IL-2 using ELISAs. Normalised data from three donors (days two and five) and two donors (day seven) are shown. NS = no stimulus, Alhyd = Alhydrogel. Error bars indicate 95% confidence intervals. '-' indicates results significantly different ($p<0.05$) to the negative control (T cells/allo-DCs with no extra stimulus – background allo-response), '+' relative to the positive control (T cells/allo-DCs + LPS), and 'i' or 'a' relative to the Imject or Alhydrogel treated T cells/allo-DCs, for the day specified.

At day two, little difference in IL-2 concentration between the LDHs and the background allo-response is present. However, at day five, all LDHs display enhanced IL-2 secretion relative to the background; indeed, LiAl-CO_3 LDH treatment gives a marginal increase in concentration. MgFe-CO_3 LDH consistently gives lower concentrations of IL-2, corroborating the CFSE dilution data which revealed low proliferation for this LDH.

Compared to the commercial adjuvants at day five, no LDH exhibits a significant difference in IL-2 concentration. However, at day seven, both MgAl-NO_3 and LiAl-CO_3 LDHs afford greater IL-2 concentrations than the two commercial adjuvants. In a similar fashion to the CFSE data, some small enhancements compared to the background allo-response in IL-2 secretion are noted for certain LDHs, but other LDHs appear to decrease responses instead.

4.3.3.4 Cytokine production

Data collected from intracellular cytokine staining for all memory T cells is supplied in Figure 4.11, showing the percentages of memory T cells that account for cytokine positive (IFN-γ^+, IL-4^+, IL-17^+) and double positive (IFN-γ^+IL-4^+ and IFN-γ^+IL-17^+) populations at days two, five and seven in the memory T cell-allogeneic Mo-DC MLRs. The total height of the bars indicates the total percentage of all T cells positive, or double positive, for a given cytokine/pair of cytokines. The different coloured regions of the bars reflect the contributions from the four sub-populations of T cells ($CD4^+$/$CD8^+$ divided/undivided).

Addition of LDHs to the cells does not lead to any enhancement in cytokine production compared to the background allo-response at any of the timepoints investigated. Indeed for IL-4, all LDHs except LiAl-CO_3 LDH typically give decreased proportions of cytokine positive T cells. No LDH gives an appreciable increase in the proportion of IFN-γ^+ T cells compared to the background at any of the days assessed. The proportion of IL-17 expressing cells remains approximately constant across all conditions. Generally, the LiAl-CO_3 LDH displays greater fractions of cytokine positive memory T cells compared to the other four LDHs.

The Imject treated cells exhibit very low levels of cytokine production; the five LDHs typically induce higher percentages of cytokine positive T cells for all cytokines and at all days. Even at day seven, the percentages of Imject treated cytokine producing cells are very low, implying this adjuvant may be having a suppressive effect *in vitro*. Alhydrogel is also a poor inducer of cytokine response: all LDHs yield larger IFN-γ^+ percentages at day two, all except MgFe-CO_3 at day five and two (LiAl-CO_3 and CaAl-NO_3) at day seven.

In summary, treatment of a memory T cell/allogeneic Mo-DC co-culture with the five LDHs or the commercial adjuvants does not induce any significant improvements in either cell division or cytokine production. Differences between the responses to the five LDHs are noticeable: LiAl-CO_3 consistently exhibits the greatest T cell responses of the five compounds. There is some suggestion that addition of the LiAl-CO_3 LDH slightly enhances proliferation, for instance in the $CD8^+$ T cell division data and IL-2 secretion at day five. To fully confirm this, tritiated thymidine incorporation assays would be performed, however time and expense constraints have prohibited this.

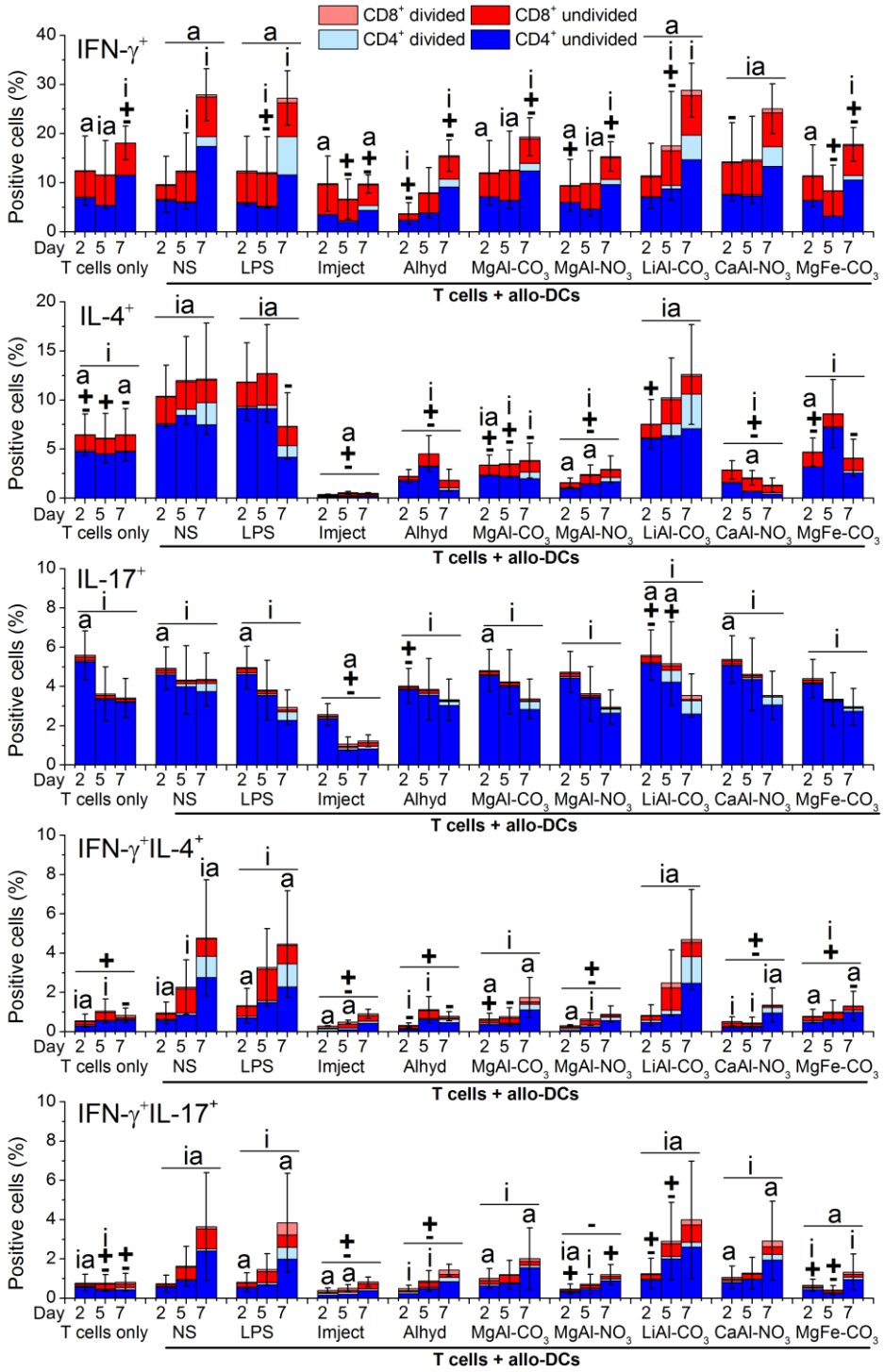

Figure 4.11: Percentages of T cells in single (IFN-γ^+, IL-4^+, IL-17^+) and double positive (IFN-γ^+IL-4^+ and IFN-γ^+IL-17^+) cytokine populations in the MLRs in which memory T cells were co-cultured with allogeneic Mo-DCs, with/without LDHs and other control conditions. Memory T cells were isolated, stained with CFSE, then co-cultured with allogeneic Mo-DC, with/without LDHs and other control conditions for two, five and seven days. On the day of analysis, cells were stained for surface molecules, viability and intracellular cytokines and analysed by flow cytometry. Normalised data from three donors (days two and five) and two donors (day seven) are shown. The total height of the bars indicates the total percentage of all T cells positive, or double positive, for a given cytokine/pair of cytokines. Different colours indicate the proportion of the T cells contributing from each sub-population ($CD4^+$ undivided, $CD4^+$ divided, $CD8^+$ undivided, $CD8^+$ divided). NS = no stimulus, Alhyd = Alhydrogel. Error bars indicate 95% confidence intervals. '-' indicates results significantly different ($p<0.05$) to the negative control (T cells/allo-DCs with no extra stimulus – background allo-response), '+' relative to the positive control (T cells/allo-DCs + LPS), and 'i' or 'a' relative to the Imject or Alhydrogel treated T cells/allo-DCs, for the day specified.

4.4 Discussion

The results in this Chapter provide new information about the effect of LDHs on the allogeneic MLR; it appears that there is a general inability for LDHs to enhance the T cell response in the allogeneic MLRs assessed. One reason for the reduced responses (both proliferation and cytokine production) to the LDHs compared to the background allo-response may be their impact on cell viability. Studies into DC response, both in Chapter Three and the prior work,[61] look at shorter overnight incubations, whereas the assays described in this Chapter were performed over much longer time periods. It is likely that over longer periods of time the LDHs are toxic to both the Mo-DC and the T cells at the concentration used, which may explain the low responses. In conjunction with the experiments detailed in Section 3.2, the viability of Mo-DCs after overnight treatment with the five LDHs tested in this chapter were measured by 7AAD staining. Some variations in the viability were noted (Figure 4.12).

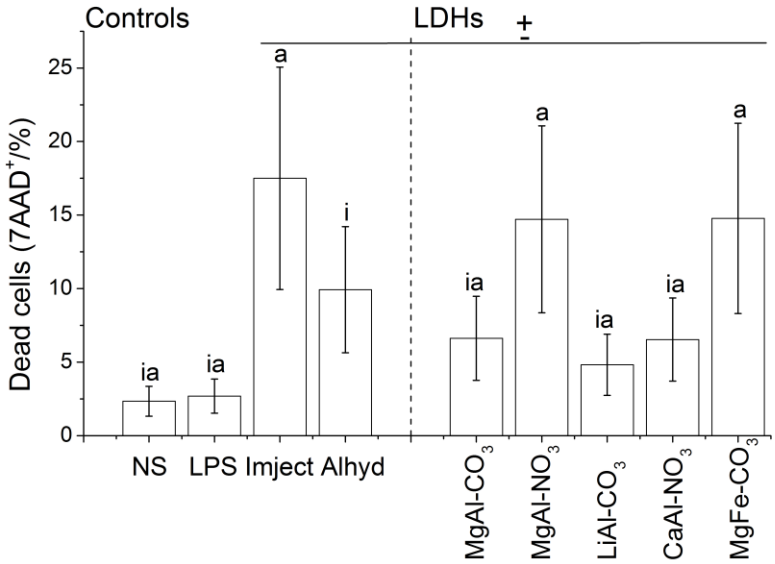

Figure 4.12: Mo-DC viability following treatment with the five LDHs used in the MLR experiments. Mo-DC from two donors were incubated overnight with the five LDHs used in the MLRs (at 500 μg/mL) and other controls, then stained with 7AAD and analysed by flow cytometry. Cells in the lymphocyte gate were used for analysis and data were normalised to account for inter donor variability. 'NS' = no stimulus, Alhyd = Alhydrogel. Error bars indicate 95% confidence intervals. '-' indicates results significantly different ($p<0.05$) to the unstimulated cells control, '+' to the LPS-stimulated control, 'i' and 'a' to the Imject and Alhydrogel controls, respectively.

LiAl-CO_3, CaAl-NO_3 and MgAl-CO_3 all display significantly lower percentages of dead cells ($7AAD^+$) in comparison to the other two LDHS (MgAl-NO_3 and MgFe-CO_3), Imject, and Alhydrogel. Crucially, all LDHs and commercial adjuvants induce significantly greater amounts of cell death compared to the untreated Mo-DC and the LPS-treated Mo-DC. This mirrors the observations made on the MLR assays: it is likely that decreased DC viability leads to lower T cell responses in the MLR, as fewer centres for focal stimulation are present.

In addition, fewer viable DC could lead to lower concentrations of cytokines needed for T cell activation. Furthermore, the LDHs could be directly impacting the viability of the T cells.

The intracellular cytokine staining results show no clear polarisation towards a specific 'T_h' response when LDHs are included in the assays. Generally, IFN-γ is the primary cytokine secreted for all conditions, including the controls, for both naïve and memory T cells. This is consistent with reports of intracellular cytokine staining on PBMC, in which the proportion of cells IFN-γ^+ was around 30% whereas the proportion IL-4^+ was much lower, approximately 1-3%.[63] IL-4 can have an effect on T cell proliferation: cultures of murine T cells without IL-4 exhibit a later onset of division than those that include it.[62] Generally, those LDHs which demonstrate the lowest reduction of proliferation (LiAl-CO_3) do give greater proportions of T cells IL-4^+, both in the naïve and memory T cell MLRs.

A further general conclusion is that the LDHs invariably elicited slightly higher responses than the commercial adjuvants. In particular, Imject elicits poor T cell responses, and presents some difficulties in accurately gating on the cells. Taking this into consideration, it can be proposed that the most accurate techniques for analysing T cell responses in experiments where large amounts of particulate material may confound analysis of flow cytometry data are those that do not involve extensive gating strategies in the analysis. For example, tritiated thymidine incorporation assays to establish proliferation, and ELISAs to establish cytokine secretion. However, these techniques result in a loss of detail when it comes to analysing T cell sub-populations ($CD4^+$/$CD8^+$, undivided/divided or even naïve/memory), which is a great benefit of using flow cytometry.

It is important to consider that these are *in vitro* observations. The implications for *in vivo* testing are potentially quite different. Cell death has been linked to immune responses,[64–66] therefore it may be hypothesised that those LDHs which induce lower viability may actually trigger more robust responses *in vivo*. On the other hand, this could have important consequences for adjuvant safety, as extensive cell death at the site of injection may cause tissue damage. Moreover, severe inflammatory responses in response to potent immunostimulant adjuvants have halted vaccine trials in the past.[67] Another crucial difference *in vivo* is the spatial separation between the injection site and the naïve T cells. DC could internalise antigen and LDH particles, then travel to the lymph nodes. Consequently, the amount of LDH a naïve T cell is exposed to in reality would be much less than what is present

at the injection site; the close proximity between the two in the MLR experiments outlined in this Chapter is not representative or appropriate.

Furthermore, the overall immune response is not just reliant on T cells; a multitude of other cell types (B cells, NK cells, neutrophils, macrophages, etc.) also contribute. In the future, *in vivo* experiments would be the best way of assessing the full immune response to LDHs. For instance, immunisation studies in mice could be conducted using a model antigen (for example, OVA) with the different LDHs as adjuvants alongside appropriate controls. B cell antibody responses could be measured by ELISA assessment of the serum.[68] Also, T cell isolation and intracellular cytokine staining, similar to that detailed in this Chapter, may be employed to probe T cell polarisation effects. This would provide a more realistic impression of how these adjuvants might work in a clinical setting, providing information on differences in both humoral and cellular reactions.

4.5 Conclusion

For the first time, experiments probing human T cell responses to LDH-stimulated Mo-DCs have been conducted, with a view to assess their adjuvant potential in a more complex setting than the DC maturation assays detailed in Chapter Three. Five LDHs with different compositions were tested ($MgAl\text{-}CO_3$, $MgAl\text{-}NO_3$, $LiAl\text{-}CO_3$, $CaAl\text{-}NO_3$ and $MgFe\text{-}CO_3$) in co-cultures of naïve/memory T cells with allogeneic Mo-DCs.

On the whole, addition of LDHs to the cells depresses the proliferation and cytokine production relative to the background allo-response. The commercial adjuvants Imject and Alhydrogel also reduce T cell responses, often to a greater extent than the LDHs. The results in this Chapter also highlight differences in proliferative and cytokine responses to the five LDHs tested: for example, $LiAl\text{-}CO_3$ does not reduce these responses to the same extent as $MgFe\text{-}CO_3$ LDH. However, it is likely that at the concentrations and time periods employed, the toxicity effects of LDHs do not make these assays ideal for establishing T cell responses. A more appropriate method for investigating the wider immune response to LDHs would be to conduct *in vivo* experiments.

4.6 References

(1) Curtsinger, J. M.; Schmidt, C. S.; Mondino, A.; Lins, D. C.; Kedl, R. M.; Jenkins, M. K.; Mescher, M. F. *J. Immunol.* **1999**, *162*, 3256.
(2) Kapsenberg, M. L. *Nat. Rev. Immunol.* **2003**, *3*, 984.
(3) Constant, S. L.; Bottomly, K. *Annu. Rev. Immunol.* **1997**, *15*, 297.
(4) Seder, R. A.; Paul, W. E. *Annu. Rev. Immunol.* **1994**, *12*, 635.
(5) Sloan-Lancaster, J.; Allen, P. M. *Annu. Rev. Immunol.* **1996**, *14*, 1.
(6) Zhu, J.; Paul, W. E. *Blood* **2008**, *112*, 1557.
(7) Zhu, J.; Yamane, H.; Paul, W. E. *Annu. Rev. Immunol.* **2010**, *28*, 445.
(8) Moser, M.; Murphy, K. M. *Nat. Immunol.* **2000**, *1*, 199.
(9) Boehm, U.; Klamp, T.; Groot, M.; Howard, J. C. *Annu. Rev. Immunol.* **1997**, *15*, 749.
(10) Collins, J. T.; Dunnick, W. A. *Int. Immunol.* **1993**, *5*, 885.
(11) Sanderson, C. J. *Blood* **1992**, *79*, 3101.
(12) Muniz, V. S.; Weller, P. F.; Neves, J. S. *J. Leukoc. Biol.* **2012**, *92*, 281.
(13) Green, A. R. *Postgraduate Haematology*; Hoffbrand, A. V.; Catovsky, D.; Tuddenham, E. G. D.; Green, A. R., Eds.; 6th ed.; Wiley-Blackwell, 2011; p. 319.
(14) Korn, T.; Bettelli, E.; Oukka, M.; Kuchroo, V. K. *Annu. Rev. Immunol.* **2009**, *27*, 485.
(15) McGeachy, M. J.; McSorley, S. J. *J. Immunol.* **2012**, *189*, 3285.
(16) Belz, G. T.; Heath, W. R.; Carbone, F. R. *Immunol. Cell Biol.* **2002**, *80*, 463.
(17) Caux, B. C.; Massacrier, C.; Vanbervliet, B.; Dubois, B.; Van Kooten, C.; Durand, I.; Banchereau, J. *J. Exp. Med.* **1994**, *180*, 1263.
(18) Smith, C. M.; Wilson, N. S.; Waithman, J.; Villadangos, J. A.; Carbone, F. R.; Heath, W. R.; Belz, G. T. *Nat. Immunol.* **2004**, *5*, 1143.
(19) Guermonprez, P.; Valladeau, J.; Zitvogel, L.; Théry, C.; Amigorena, S. *Annu. Rev. Immunol.* **2002**, *20*, 621.
(20) Schuurhuis, D. H.; Laban, S.; Toes, R. E.; Ricciardi-Castagnoli, P.; Kleijmeer, M. J.; van der Voort, E. I.; Rea, D.; Offringa, R.; Geuze, H. J.; Melief, C. J.; Ossendorp, F. *J. Exp. Med.* **2000**, *192*, 145.
(21) Keller, A. M.; Xiao, Y.; Peperzak, V.; Naik, S. H.; Borst, J. *Blood* **2009**, *113*, 5167.
(22) Tan, J. T.; Whitmire, J. K.; Ahmed, R.; Pearson, T. C.; Larsen, C. P. *J. Immunol.* **1999**, *163*, 4859.
(23) Harty, J. T.; Tvinnereim, A. R.; White, D. W. *Annu. Rev. Immunol.* **2000**, *18*, 275.
(24) Sprent, J.; Surh, C. D. *Curr. Opin. Immunol.* **2001**, *13*, 248.
(25) Kaech, S. M.; Wherry, E. J.; Ahmed, R. *Nat. Rev. Immunol.* **2002**, *2*, 251.
(26) Sprent, J.; Surh, C. D. *Annu. Rev. Immunol.* **2002**, *20*, 551.
(27) Badovinac, V. P. *Science* **2000**, *290*, 1354.
(28) Mackay, C. R. *Nature* **1999**, *7*, 659.
(29) Ahmed, R.; Gray, D. *Science* **1996**, *272*, 54.
(30) Van Essen, D.; Dullforce, P.; Brocker, T.; Gray, D. *J. Immunol.* **2000**, *165*, 3640.
(31) Di Sabatino, A.; Calarota, S. A.; Vidali, F.; Macdonald, T. T.; Corazza, G. R. *Cytokine Growth Factor Rev.* **2011**, *22*, 19.
(32) Lindestam Arlehamn, C. S.; Gerasimova, A.; Mele, F.; Henderson, R.; Swann, J.; Greenbaum, J. A.; Kim, Y.; Sidney, J.; James, E. A.; Taplitz, R.; McKinney, D. M.; Kwok, W. W.; Grey, H.; Sallusto, F.; Peters, B.; Sette, A. *PLoS Pathog.* **2013**, *9*, 1.
(33) Heesters, B. A.; Myers, R. C.; Carroll, M. C. *Nat. Rev. Immunol.* **2014**, *14*, 495.
(34) Tew, J. G.; Wu, J.; Qin, D.; Helm, S.; Burton, G. F.; Szakal, A. K. *Immunol. Rev.* **1997**, *156*, 39.
(35) Kosco, M. H.; Szakal, A. K.; Tew, J. G. *J. Immunol.* **1988**, *140*, 354.
(36) MacLeod, M. K. L.; Kappler, J. W.; Marrack, P. *Immunology* **2010**, *130*, 10.
(37) Croft, M.; Bradley, L. M.; Swain, S. L. *J. Immunol.* **1994**, *152*, 2675.
(38) Lalvani, A.; Brookes, R.; Hambleton, S.; Britton, W. J.; Hill, A. V. S.; McMichael, A. J. *J. Exp. Med.* **1997**, *186*, 859.
(39) Mehlhop-Williams, E. R.; Bevan, M. J. *J. Exp. Med.* **2014**, *211*, 345.
(40) Moser, B.; Loetscher, P. *Nat. Immunol.* **2001**, *2*, 123.

(41) Messi, M.; Giacchetto, I.; Nagata, K.; Lanzavecchia, A.; Natoli, G.; Sallusto, F. *Nat. Immunol.* **2003**, *4*, 78.
(42) Sallusto, F.; Geginat, J.; Lanzavecchia, A. *Annu. Rev. Immunol.* **2004**, *22*, 745.
(43) Geginat, J.; Lanzavecchia, A.; Sallusto, F. *Blood* **2003**, *101*, 4260.
(44) Förster, R.; Davalos-Misslitz, A. C.; Rot, A. *Nat. Rev. Immunol.* **2008**, *8*, 362.
(45) Weksler, M. E.; Kozak, R. *J. Exp. Med.* **1977**, *146*, 1833.
(46) Lafferty, K. J.; Cunningham, A. J. *Aust. J. Exp. Biol. Med. Sci.* **1975**, *53*, 27.
(47) Kuntz, M. M.; Innes, J. B.; Weksler, M. E. *J. Exp. Med.* **1976**, *143*, 1042.
(48) Crow, M. K.; Kunkel, H. G. *Clin. Exp. Immunol.* **1982**, *49*, 338.
(49) Steinman, R. M.; Witmer, M. D. *Proc. Natl. Acad. Sci. U.S.A.* **1978**, *75*, 5132.
(50) Chapuis, F.; Rosenzwajg, M.; Yagello, M.; Ekman, M.; Biberfeld, P.; Gluckman, J. C. *Eur. J. Immunol.* **1997**, *27*, 431.
(51) Palucka, K. A.; Taquet, N.; Sanchez-Chapuis, F.; Gluckman, J. C. *J. Immunol.* **1998**, *160*, 4587.
(52) Banchereau, J.; Steinman, R. M. *Nature* **1998**, *392*, 245.
(53) Gould, D. S.; Auchincloss, H. *Immunol. Today* **1999**, *20*, 77.
(54) Tapirdamaz, O.; Mancham, S.; van der Laan, L. J. W.; Kazemier, G.; Thielemans, K.; Metselaar, H. J.; Kwekkeboom, J. *PLoS One* **2010**, *5*, 1.
(55) Widmer, M. B.; Bach, F. H. *J. Exp. Med.* **1972**, *135*, 1204.
(56) Godfrey, W. R.; Ge, Y. G.; Spoden, D. J.; Levine, B. L.; June, C. H.; Blazar, B. R.; Porter, S. B. *Immunobiology* **2004**, *104*, 453.
(57) Lindén, O.; Dohlsten, M.; Boketoft, A.; Hedlund, G.; Sjögren, H. O. *Scand. J. Immunol.* **1987**, *26*, 223.
(58) Nishioka, Y.; Wen, H.; Mitani, K.; Robbins, P. D.; Lotze, M. T. *J. Leukoc. Biol.* **2003**, *73*, 621.
(59) Yang, D.; Chen, Q.; Yang, H.; Tracey, K. J.; Bustin, M.; Oppenheim, J. J. *J. Leukoc. Biol.* **2007**, *81*, 59.
(60) Austyn, J.; Steinman, R.; Weinstein, D. *J. Exp. Med.* **1983**, *157*.
(61) Williams, G. R.; Fierens, K.; Preston, S. G.; Rysnik, O.; Lunn, D.; De Prijck, S.; Kool, M.; Buckley, H.; Austyn, J. M.; O'Hare, D.; Lambrecht, B. N. *J. Exp. Med.* **2014**, *211*, 1019.
(62) Gett, A. V; Hodgkin, P. D. *Proc. Natl. Acad. Sci. U.S.A.* **1998**, *95*, 9488.
(63) Jung, T.; Schauer, U.; Heusser, C.; Neumann, C.; Rieger, C. *J. Immunol. Methods* **1993**, *159*, 197.
(64) Basu, S.; Binder, R. J.; Suto, R.; Anderson, K. M.; Srivastava, P. K. *Int. Immunol.* **2000**, *12*, 1539.
(65) Shi, Y.; Evans, J. E.; Rock, K. L. *Nature* **2003**, *425*, 516.
(66) Rosin, D. L.; Okusa, M. D. *J. Am. Soc. Nephrol.* **2011**, *22*, 416.
(67) DeFrancesco, L. *Nat. Biotechnol.* **2008**, *26*, 484.
(68) Sun, H.-X.; Wang, H.; Xu, H.; Ni, Y. *Vaccine* **2009**, *27*, 3984.

Chapter Five: An Investigation into Layered Double Hydroxide-Dendritic Cell Interactions

5.1 Introduction

In Chapter Three, the ability of layered double hydroxide (LDH) particles to elicit immune responses was demonstrated *in vitro*. In the literature, reports describe interactions between alum adjuvants and cells that could be linked to induction of inflammation. Some focus on direct contact with the plasma membrane,[1] whilst others implicate internalisation.[2] Given the similarity with these materials, study of these two types of interactions represents a logical starting point for investigating the mechanism of action of LDH particles.

5.1.1 Mechanisms of cellular uptake

Cells may achieve internalisation of extracellular material through a variety of mechanisms, which are specific for different size ranges of material. Several reviews provide detailed coverage of these topics, for instance Connor and Schmid,[3] Marsh,[4] and Stuart and Ezekowitz.[5] A general schematic of the mechanisms discussed is provided in Figure 5.1.[6]

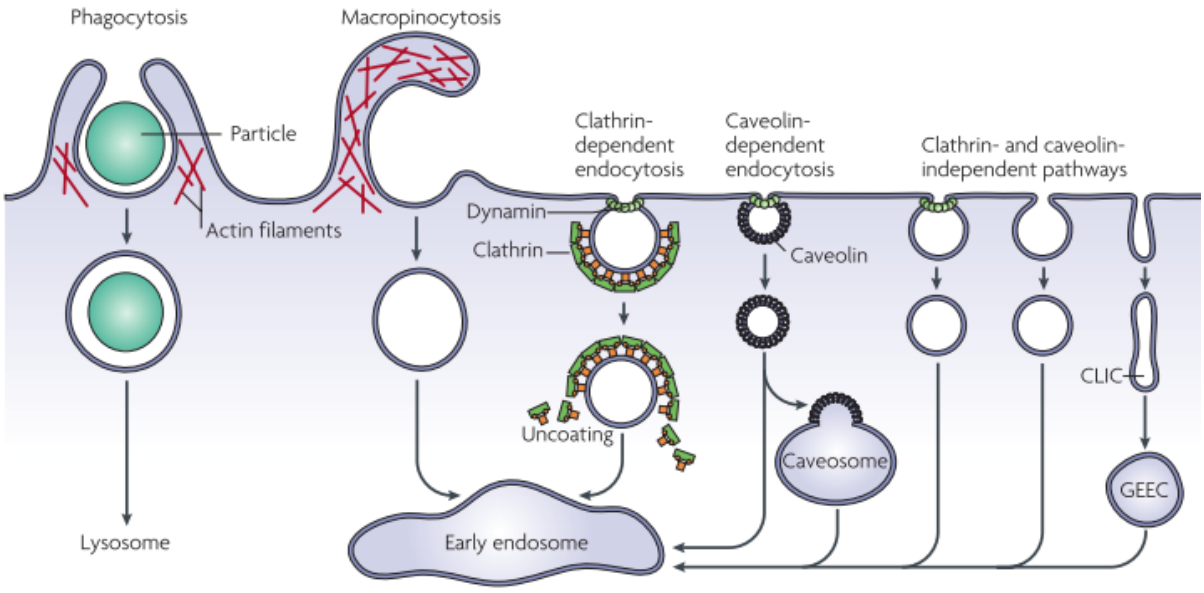

Figure 5.1: Mechanisms of cellular uptake: phagocytosis, macropinocytosis, clathrin mediated endoctyosis, caveolae dependent endocytosis and clathrin/caveolae independent endocytosis.[6]

5.1.1.1 Phagocytosis

Phagocytosis is a receptor mediated process which certain cells, or 'professional phagocytes', are capable of performing (e.g. macrophages, monocytes, neutrophils).[5,7,3] Its main purpose is

to remove infectious agents and to clear apoptotic cells and other debris, typically 0.5 μm or larger.[7] The phagocytic ability of Langerhans cells (a subset of dendritic cell) was confirmed by Reis e Sousa *et al.*, using a number of fluorescently labelled targets including zymosan, intact bacteria, and 0.5-3.5 μm latex spheres.[8]

In the initial stages of phagocytosis, a cell must recognise the infectious agent or alternatively, the altered self, to be internalised through various receptors. For example, mannose receptors bind to the carbohydrates that are a conserved structural feature of bacteria. Scavenger receptors recognise lipopolysaccharide (LPS), lipoteichoic acid, and CpG DNA as well as features of apoptotic cells. [9,10] Targets opsonised with antibodies, lectins or complement are also detected by various receptors, such as Fcγ receptors, which bind the constant Fc region of the opsonising antibody.[11]

Upon receptor binding, signalling cascades are initiated which lead to actin-dependent rearrangement of the cytoskeleton (reviewed here).[12] This forms an enveloping phagocytic cup around the target, which eventually invaginates to form a phagosome. Disruptors of actin microfilament polymerisation, for example cytochalasins and latruculin A, have been shown to inhibit this process.[12,13] Once inside the phagosome, the internalised pathogen is destroyed in the hydrolytic environment produced upon fusion with lysosomes.[5] Fragments may then be processed for antigen presentation.

5.1.1.2 Macropinocytosis

Macropinocytosis provides a non-selective uptake route for bulk extracellular fluid in large vesicles (0.2 to 5 μm).[14,15] The mechanism is linked to membrane ruffling, which may be triggered by growth factors, or particle-membrane interactions.[16,17] It is an actin-dependent process in which the membrane ruffles close around the object and pinch off to form the macropinosome. Unlike in phagocytosis, the area of the plasma membrane which becomes the macropinosome does not concentrate receptors or display any specific coat molecules.[14] The contents of macropinsosomes may be degraded following fusion with lysosomes, or recycled back to the cell surface.

5.1.1.3 Clathrin-mediated endocytosis

Clathrin-mediated endocytosis occurs in all cell types, and provides a means of concentrating and internalising trans-membrane receptor complexes (e.g. transferrin receptors, low-density lipoprotein receptors). Clathrin is a three-legged protein that forms cage-like structures under physiological conditions when controlled by an assembly protein or adaptor protein complex.[3]

This deforms the membrane into a curved, clathrin-coated pit that invaginates with the help of the enzyme dyanmin to form a clathrin-coated vesicle inside the cell.[4] Typically, these pits are around 85-110 nm in diameter.[15]

5.1.1.4 Caveolae-mediated endocytosis

Caveolae are pits on the cell surface rich in cholesterol, sphingolipids and various trans-membrane proteins, and may be disrupted by cholesterol depletion.[18] They are thought to have roles in the transport of various species across the plasma membrane, including cholesterol, Ca^{2+}, albumin, insulin and opportunistic viruses.[18,19] Their structure originates from the action of caveolin, a protein which binds cholesterol in the inner leaflet of the plasma membrane.[3] These pits are small (50-80 nm in diameter),[6] although they have been implicated in uptake of objects up to 1 μm in size.[20] Uptake of caveolae is initiated by ligation and cross linking of their receptors, and is also a dynamin dependent process.[21]

5.1.1.5 Clathrin- and caveolae-independent endocytosis

Mobile lipid rafts, typically 40-50 nm in diameter, that are rich in cholesterol and associated with elevated concentrations of receptors and signalling molecules are also thought to play a role in endoctyosis.[3,22] Overall the mechanism is poorly understood, but may be exploited by viruses, such as simian virus 40, to enter cells.[23]

5.1.2 Mechanisms of uptake of inorganic materials

Several of the mechanisms outlined have been implicated in the internalisation of inorganic materials. For instance, phagocytosis of asbestos and silica particles was shown to be crucial for an inflammatory response to occur.[24] Inflammatory responses in alveolar macrophages were attributed to frustrated phagocytosis of silver nanowires above a certain length.[25]

Macropinocytosis, with its lack of requirement for specific receptor signalling, might be predicted as a common mechanism for non-opsonised particulate matter to enter the cell. This was shown to be the case for DNA coated single-walled carbon nanotubes (SWCNTs)[26] and polystyrene microspheres.[17] Indeed, it was through experiments conducted by Champion *et al*. into phagocytosis/macropinocytosis of polystyrene microparticles that a dependence on the geometry of the target was discovered; the initial contact angle between the cell surface and the particle determines whether macrophages 'spread' over the target or actually internalise it.[27] Many other studies also use polystyrene microspheres as probes of uptake mechanism. For instance, Rejman *et al*. employed them to look at uptake processes in non-phagocytic B16 cells.[20] They discovered that microspheres with diameters less than 200 nm were internalised

through a clathrin-dependent pathway, whereas larger particles utilised a caveolae-dependent route. LDH internalisation has also been linked to clathrin-mediated endoctyosis by two separate research groups.[28,29]

5.1.3 Particle-plasma membrane interactions

The dependence of internalisation of 3 μm fluorescent polystyrene latex microspheres on lipid rafts was demonstrated by Nagao *et al*.[30] by depleting plasma membrane cholesterol with chemicals such as methyl-β-cyclodextrin. Ng and co-workers analysed the strength of binding of monosodium urate (MSU) crystals with the cell membrane using a modified atomic force microscope (AFM). MSU was found to preferentially bind to cholesterol rich areas of cell membranes, triggering Syk kinase-dependent signalling pathways.[31] Later studies by the same research group into alum adjuvant interactions with dendritic cell (DC) plasma membranes showed a bias towards sphingomyelin binding, with induction of similar downstream signalling.[1]

5.1.4 THP-1 cells

The THP-1 cell line was used for some of the experiments detailed in this chapter as it provides a reliable supply of large numbers of monocytic cells. This cell line was isolated from a patient with monocytic leukemia over 30 years ago.[32] THP-1 cells are capable of phagoctyosis, express HLA molecules and secrete cytokines such as TNF-α, IL-1α and IL-1β.[33] Adoption of macrophage characteristics may be induced in THP-1 cells by incubating with phorbol 12-myristate 13-acetate (PMA).[34]

5.1.5 Scope of this Chapter

This chapter sets out to explore the possible interactions between LDH particles and DCs: Firstly, as suggested by the literature, to establish whether DCs can internalise LDH particles and what impact particle size and composition have on this process; secondly, to investigate what mechanisms of uptake might be involved in particle internalisation; thirdly, to probe plasma membrane-LDH particle interactions.

5.2 Investigations into uptake of LDH particles

5.2.1 Synthesis of FITC-labelled LDHs

In order to readily visualise LDH particles using fluorescence-based microscopy techniques, a range of fluoroscein isothiocyanate (FITC) labelled LDH particles were synthesised. FITC can be deprotonated to its anionic form as it contains a carboxylic acid group, therefore may be intercalated into LDHs or covalently grafted onto the surface using an amino silane.[29,35] However, this is not always necessary, and facile labelling of LDHs may be achieved by stirring the LDH in a dilute solution of FITC for one hour to permit adsorption.[29]

Firstly, six differently-sized MgAl-CO_3 LDHs were synthesised, then labelled with FITC. Secondly, to probe the effects of changing LDH composition, seven more LDHs with different compositions were also synthesised through general coprecipitation methods and labelled with FITC. Selected composition and synthesis data for the various sizes and compositions of FITC-labelled LDH are supplied in Table 5.1. Full characterising data for all LDHs are supplied in Appendix D.1.

Table 5.1: Selected details of FITC-labelled LDHs employed in this Chapter. Approximate chemical formulae obtained from thermogravimetric analysis (TGA), energy dispersive X-ray spectorscopy (EDX) and elemental analysis (C, H, N) for FITC-labelled LDHs. Mean particles sizes were obtained from transmission electron microscopy (TEM) images. Zeta potentials were measured at 10 mg/mL in phosphate buffered saline (PBS). RT = room temperature, O/N = overnight. '**' for CaAl-LDHs indicates observation of significant numbers of particles both 100s of nm in diameter and also <200 nm.

FITC labelled LDH	Approx LDH size (nm)	Zeta potential (mV)	Chemical formula (from EDX, CHN and TGA)	Synthesis method
MgAl-CO_3	14	-21.5	$[Mg_{3.2}Al(OH)_{8.4}](CO_3)_{0.5}\cdot 3.2H_2O$	Coprecipitation pH 12 RT
MgAl-CO_3	60	-33.0	$[Mg_{1.8}Al(OH)_{5.6}](CO_3)_{0.5}\cdot 1.2H_2O$	Coprecipitation 90 °C 72 hrs
MgAl-CO_3	140	-36.8	$[Mg_{2.7}Al(OH)_{7.3}](CO_3)_{0.5}\cdot 2.1H_2O$	Hydrothermal 160 °C O/N
MgAl-CO_3	300	8.9	$[Mg_{2.8}Al(OH)_{7.7}](CO_3)_{0.5}\cdot 2.4H_2O$	Hydrothermal 180 °C O/N
MgAl-CO_3	920	18.9	$[Mg_{2.1}Al(OH)_{6.1}](CO_3)_{0.5}\cdot 1.7H_2O$	0.24 M HMT 140 °C O/N
MgAl-CO_3	1610	1.5	$[Mg_2Al(OH)_{6.1}](CO_3)_{0.5}\cdot 1.7H_2O$	0.22 M HMT 140 °C O/N
MgAl-NO_3	50	-18.7	$[Mg_{1.6}Al(OH)_{5.3}](NO_3)\cdot 0.8H_2O$	Coprecipitation 90 °C 72 hrs
MgAl-Cl	40	-31.6	$[Mg_{1.7}Al(OH)_{5.4}]Cl\cdot 0.7H_2O$	Coprecipitation 80 °C 72 hrs
LiAl-CO_3	80	-49.7	$[LiAl_2(OH)_6](CO_3)_{0.5}\cdot 2.8H_2O$	Coprecipitation 75 °C O/N
MgFe-CO_3	60	-33.3	$[Mg_{2.8}Fe(OH)_{7.7}](CO_3)_{0.5}\cdot 2H_2O$	Coprecipitation 80 °C O/N
MgFe-NO_3	30	-25.1	$[Mg_{2.2}Fe(OH)_{6.4}](NO_3)\cdot 0.9H_2O$	Coprecipitation 80 °C 72 hrs
CaAl-NO_3	**	39.4	$[Ca_{2.7}Al(OH)_{7.4}](NO_3)\cdot 1.3H_2O$	Coprecipitation pH 11.5 RT O/N
CaAl-Cl	**	1.7	$[Ca_{1.1}Al(OH)_{4.2}]Cl\cdot 0.5H_2O$	Coprecipitation pH 11.5 65 °C O/N

The FITC contribution to the chemical formula was excluded as no change in the interlayer spacing compared to the LDH starting materials was observable using powder X-ray diffraction. Also, Fourier transform infrared (FTIR) analyses display no strong

FITC-associated absorptions. Therefore it was assumed that only very small quantities of FITC were adsorbed onto the surface and little, if any, was intercalated. However, a marked colour change, from white to yellow/orange was noted after FITC labelling. Accordingly, comparisons of the LDH particle FITC fluorescence measured using flow cytometry showed a marked increase in FITC fluorescence for the labelled particles (Figure 5.2). The zeta potentials for FITC-labelled LDHs are generally negative, similar to those for the unlabelled LDHs discussed in Chapter Two. The larger FITC labelled MgAl-CO_3 LDHs have more positive zeta potentials, which is also consistent with the patterns previously observed. Illustrative transmission electron microscope (TEM) images of the different particle sizes of FITC labelled MgAl-CO_3 LDH are supplied in Figure 5.2. Images were obtained after FITC labelling, and show no differences in morphology compared to non-labelled MgAl-CO_3 LDHs.

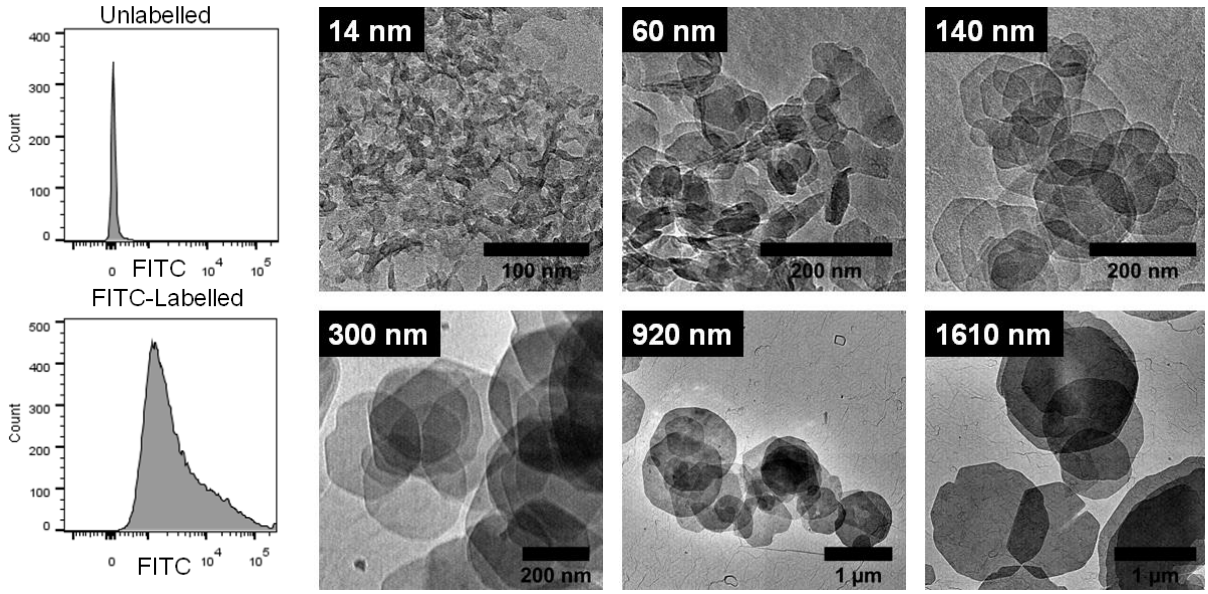

Figure 5.2: Left hand side: fluorescence histograms of unlabelled and FITC-labelled MgAl-CO_3 LDHs from flow cytometry; right hand side: TEM images of FITC-labelled MgAl-CO_3 LDHs synthesised in different particle sizes.

To establish the optimum LDH concentration for use in microscopy studies, a titration of LDH with peripheral blood mononuclear cells (PBMC) was performed. Difficulties were encountered discerning the cells under fluorescence microscopy, due to the high numbers of LDH particles present when LDHs were used at 500 µg/mL. Therefore a lower concentration of 100 µg/mL was used for all microscopy experiments detailed in this Chapter. Flow cytometry experiments use the same LDH concentration (500 µg/mL) as experiments detailed in Chapter Three.

5.2.2 Preliminary experiments investigating the effect of temperature on cell-particle interactions

Generally, cellular uptake processes are temperature dependent.[36] Consequently, it was hypothesised that if LDHs were primarily being internalised by Mo-DC, cells incubated with FITC-labelled LDH particles on ice would exhibit lower FITC fluorescence than if they were incubated with FITC-labelled LDH particles at 37 °C. Alternatively, if LDH particles were adhering to the cell surface, high fluorescence would be expected at both temperatures. Conversely, if LDH FITC fluorescence associated cells was low at both temperatures, this might be indicative of very little cell-particle association.

As a starting point for investigating LDH particle-cell interactions, FITC-labelled MgAl-CO_3 LDHs were incubated for 15 minutes or two hours with Mo-DC either on ice or at 37 °C. After incubation, cells were stained for CD209 then analysed using flow cytometry, gating on CD209 positive events (Mo-DCs) and recording FITC fluorescence associated with the cells. To further validate the flow cytometry results similar experiments using fluorescence microscopy were also conducted.

5.2.2.1 Flow cytometry results

FITC fluorescence data for Mo-DC treated with each size of FITC-labelled MgAl-CO_3 LDH are supplied in Figure 5.3. Cells treated with 3 μm FITC-labelled polystyrene beads were used as a positive control for internalisation. Direct comparisons of the fluorescence between the particles in different sizes cannot be made because the extent of FITC labelling for each particle size varies. However, comparisons can be made between the treatment temperatures for a given MgAl-CO_3 LDH particle size.

DCs treated with both the fluorescent bead control and the FITC-labelled LDHs display much higher FITC fluorescence than the background autofluorescence from the untreated cells, indicating some degree of cell-particle association. The cells treated with FITC-labelled beads display much higher FITC fluorescence after two hours, indicating a time-dependent association. At this point, the cells incubated at 4 °C have significantly less FITC fluorescence associated with them, implying beads interact less with cells at low temperature, most likely due to reduced internalisation.

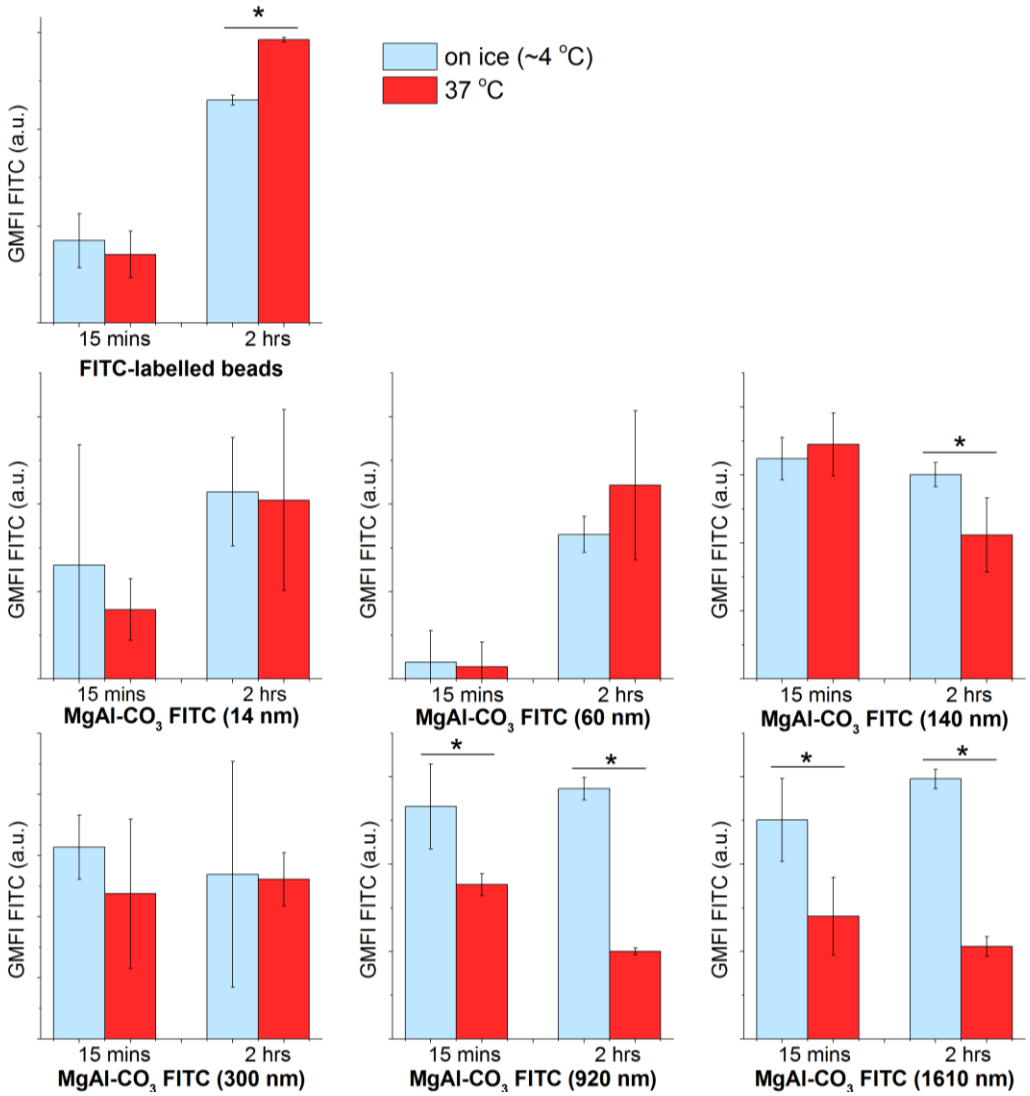

Figure 5.3: Cell-associated FITC fluorescence data from incubation of Mo-DC with FITC-labelled MgAl-CO_3 LDHs on ice (at ~4 °C) or at 37 °C. Mo-DC were incubated with FITC-labelled MgAl-CO_3 LDH particles (at 500 µg/mL) for either 15 minutes or two hours on ice or at 37 °C. Cells were stained for CD209 (DC sign) then analysed by flow cytometry. The geometric mean FITC fluorescence (GMFI FITC) of the $CD209^+$ cells in the cells gate (FSC/SSC) is displayed. Error bars indicate two standard deviations, '*' denotes a significant difference ($p<0.05$) between the means of the two treatments**.**

Generally, there is no decrease in FITC fluorescence associated with DCs between the two treatment temperatures, for all LDH sizes, at both times. To account for the observed behaviour, it may be hypothesised that LDH particles adhere to the cell plasma membrane regardless of temperature.

After 15 minutes on ice, the larger (920 nm and 1610 nm) FITC labelled MgAl-CO_3 particles show significantly higher cell-associated FITC fluorescence than at 37 °C. This is also evident after two hours, at which point the cells treated with 140 nm FITC labelled MgAl-CO_3 LDH display similar results. Increases in association after incubation on ice compared to 37 °C may be due to a decrease in viability when cells are kept at low temperature for prolonged periods;

cells undergoing necrosis experience rupture of the plasma membrane which may expose components of the cell which are 'stickier' to LDHs.[37] However, after 15 minutes it is unlikely that much cell death has occurred. Temperature can affect the mobility of the components of the plasma membrane, which may influence association.[38,39] Less mobile plasma membrane components may provide a more static, stable platform for LDHs to bind to at low temperature. This may be of particular importance for larger particles which could require binding to multiple regions of the membrane simultaneously due to their greater size.

For most LDHs (140, 300, 920 and 1610 nm) there is no discernible difference between cell-associated FITC fluorescence at the two time points, implying rapid association between cells and LDH particles. However, the smaller LDH sizes (14 and 60 nm) do show an increase in association with time. The association between LDH particles and DC, regardless of temperature and length of incubation, implies an inherent attraction between the surfaces of the two species. Internalisation of LDH particles may also be occurring, but is neither proved nor disproved by these initial results.

5.2.2.2 Fluorescence microscopy study

Representative fluorescence microscopy images for Mo-DCs treated either on ice or at 37 °C for two hours with 300 and 920 nm FITC-labelled MgAl-CO_3 LDH are shown in Figure 5.4. Fluorescence microscopy images show cell-LDH association after treatment at both temperatures, in agreement with the flow cytometry data in the preceding section. In particular bright-field images show close association between cells and particles (darker areas) regardless of incubation temperature. After treatment on ice, the LDH particles appear slightly distanced from the nuclei, implying internalisation has not occurred. This is particularly noticeable for in the bright-field images for both particle sizes. However, association with the cell surface is still noticeable. After treatment at 37 °C, particles of both sizes appear close to the cell nuclei, suggesting some internalisation has occurred.

Overall these preliminary experiments suggest that LDH particles attach to cells regardless of temperature, implying an inherent attraction between the surfaces of the two, and suggest that particles may be internalised at 37 °C. Further work confirming particle uptake is detailed in the following sections.

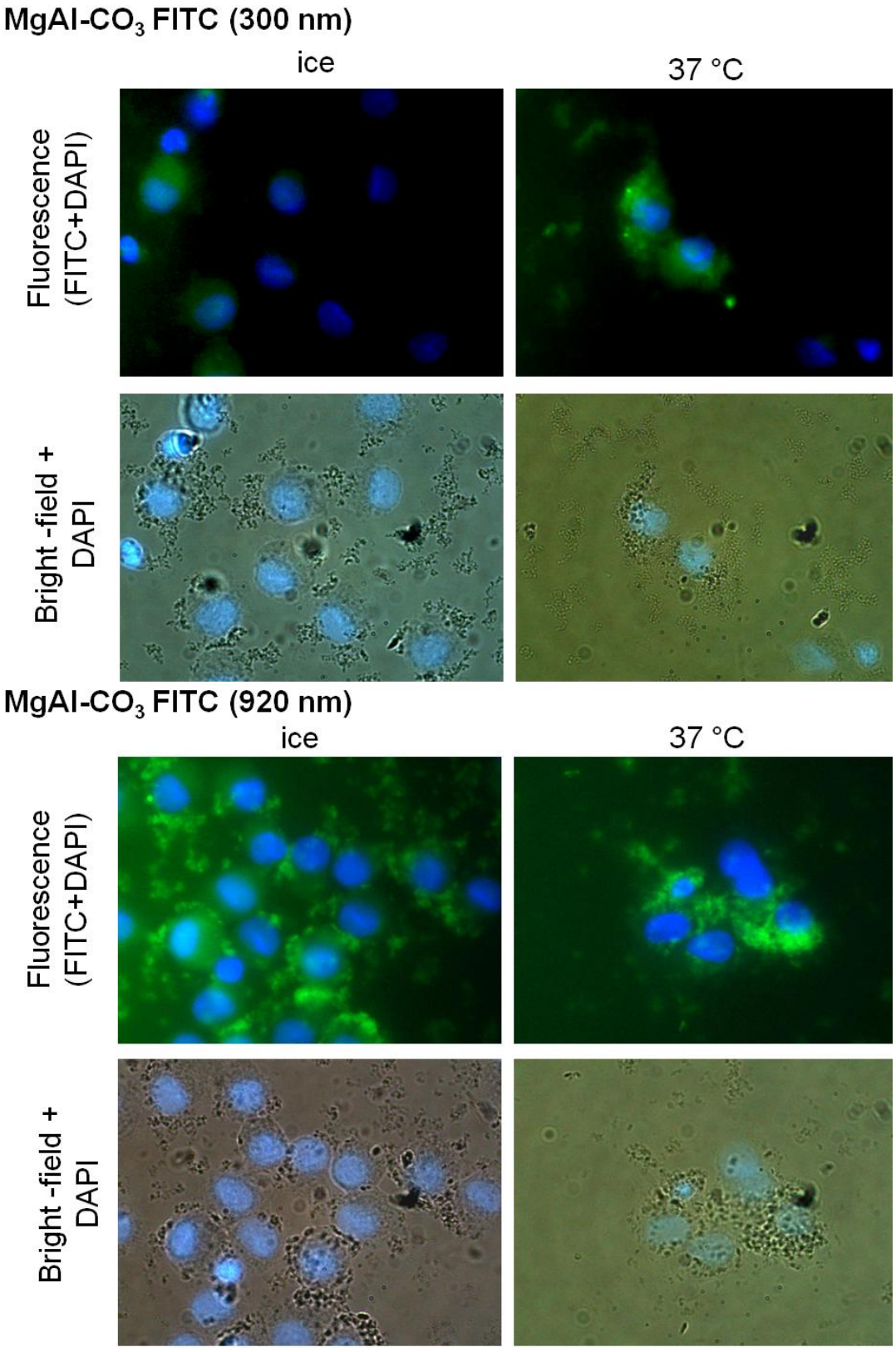

Figure 5.4: Fluorescence microscopy images of Mo-DC incubated with either 300 or 920 nm FITC-labelled MgAl-CO_3 LDHs on ice (at ~4 °C) or at 37 °C for two hours. Mo-DC and LDH (100 µg/mL) were incubated for two hours on ice (at ~4 °C) or at 37 °C. After incubation, all cells were transferred onto ice, fixed with paraformaldehyde (PFA) and cell nuclei stained with 4',6-diamidino-2-phenylindole (DAPI, blue fluorescence). Green fluorescence indicates FITC labelled LDH particles. Both merged FITC/DAPI fluorescence and merged DAPI/bright-field images are displayed.

5.2.3 Examination of LDH uptake using Lucifer yellow

Lucifer yellow (LY) is a membrane-impermeable fluorescent dye, only capable of entering cells when they internalise other target material. Flow cytometry studies by Schorn and co-workers into uptake of monosodium urate (MSU) crystals revealed increased LY fluorescence with MSU treatment compared to the untreated cells control.[40] Reis e Sousa *et al*. and Seubert *et al*. also report using LY to probe the kinetics of particle uptake.[8,41]

THP-1 cells were incubated with LY and unlabelled MgAl-CO_3 and LiAl-CO_3 LDHs (described in Chapter Two), then LY fluorescence was assessed using flow cytometry and confocal microscopy. Cells treated with LY, but no extra stimulus, were used as a negative control; cells treated with LY and unlabelled polystyrene beads (3 μm diameter) were used as a positive control. To check LY exclusion from intact cells in the absence of particulate material, a control experiment was carried out: unpermeabilised and permeabilised cells were incubated with LY and analysed on a flow cytometer. As expected, permeabilised cells had much higher LY fluorescence.

The top half of Figure 5.5 displays LY fluorescence associated with the cells, measured by flow cytometry. Incubation with every LDH tested significantly enhances LY fluorescence compared to the background from the negative control. For the MgAl-CO_3 LDHs, maximum LY incorporation was achieved for the 40 and 70 nm LDHs. These results were further validated using confocal microscopy on cells with LY alone, and cells with LY and the 70 nm MgAl-CO_3 particles (bottom of Figure 5.5). Cells incubated without LDH particles show very low levels of background LY fluorescence, whereas those treated with LY in the presence of LDH particles are much brighter. In conclusion, these results strongly suggest that LDHs are internalised by cells, or at least disrupt the cell membrane in such a way as to allow LY into the cytoplasm. To fully confirm the location of the particles, further confocal microscopy experiments were performed, detailed in the following section.

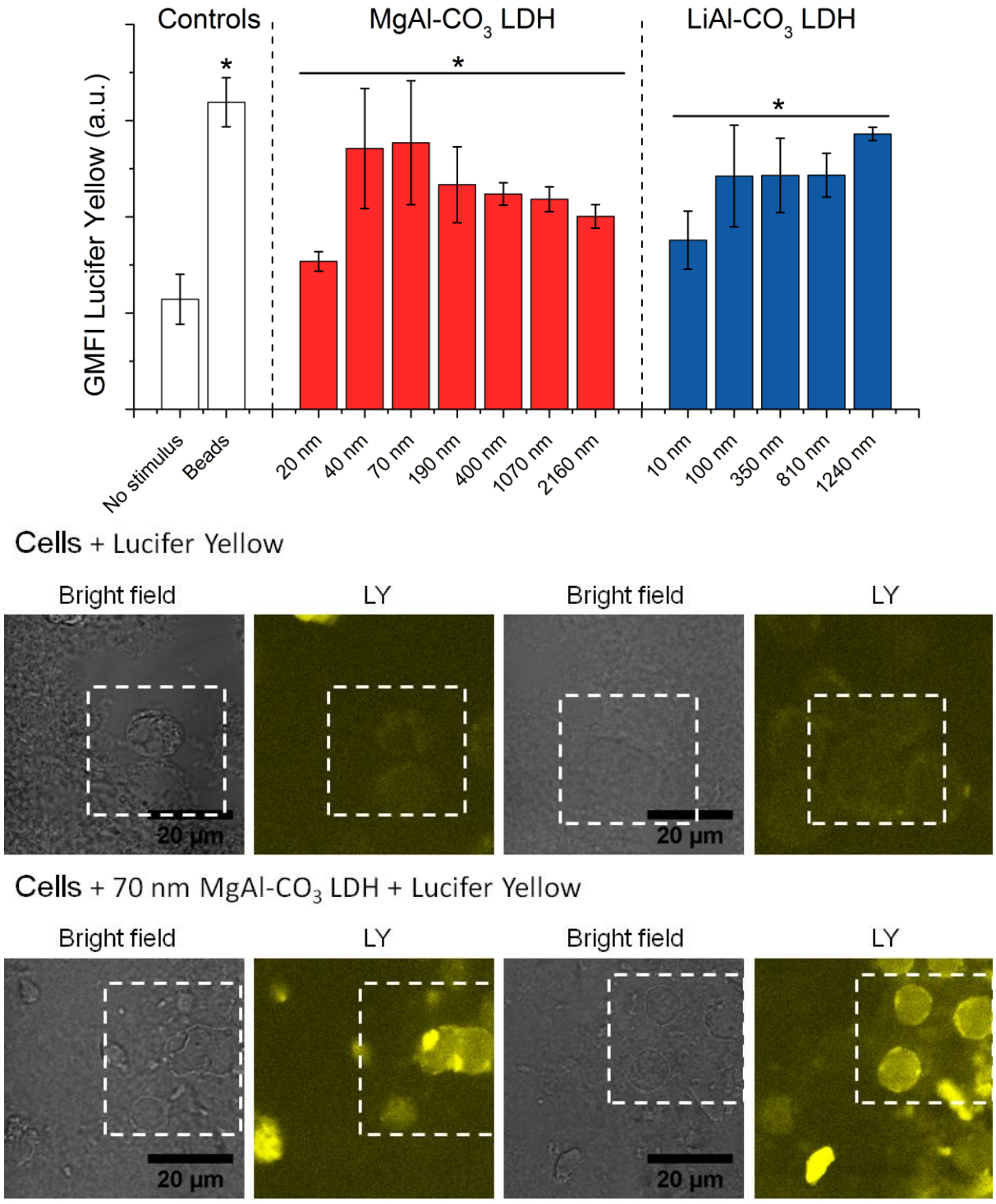

Figure 5.5: Lucifer yellow incorporation into THP-1 cells in the presence or absence of LDH particles, as assessed by flow cytometry and confocal microscopy. Top: membrane impermeable dye Lucifer yellow (20 µg/mL) and LDH particles (500 µg/mL, a selection of sizes of both MgAl-CO_3 and LiAl-CO_3 LDH compositions) were added to THP-1 cells, incubated for two hours then analysed using flow cytometry. Geometric mean fluorescence intensities (GMFI) of events in the cells gate were recorded. Error bars indicate two standard deviations, '*' denotes values significantly different to the negative control (cells/Lucifer yellow without LDH or beads). Bottom: Confocal microscopy images of cells treated with Lucifer yellow with/without 70 nm MgAl-CO_3 LDH. THP-1 cells were treated with Lucifer yellow with/without LDH for two hours. After incubation cells were washed, fixed with PFA and mounted on slides for imaging. Bright-field and fluorescence images are displayed, with cells highlighted. Microscope settings were kept identical for both samples.

5.2.4 Confocal microscopy studies

The chief advantage of using confocal microscopy as opposed to conventional fluorescence microscopy is being able to image in one focal plane of the sample. During conventional microscopy, light from both the focal plane and other out-of-focus planes is collected. This results in a high background component from the out of focus planes contributing to the image and poor resolution in the *z*-direction (sample depth). Consequently, it can be difficult to discern where objects in the image are relative to each other in three dimensions. Confocal microscopy overcomes this by including a pinhole at a position which selects only the light reflected from the focal point of the light source on the sample, blocking the majority of the out of focus light. This provides improved resolution in the *z*-direction. By altering the focal point, 'slices' may be taken through an object to build up a three dimensional representation.

5.2.4.1 Confocal microscopy study of FITC-labelled MgAl-CO_3 LDHs

Mo-DC were incubated with FITC-labelled MgAl-CO_3 LDH particles for two hours at 37 °C. Cell nuclei were stained with DAPI (blue) and lysosomes stained with Lysotracker Red. Confocal images of Mo-DC with the different sizes of FITC-labelled MgAl-CO_3 LDH, as well as untreated Mo-DC are supplied in Figure 5.6. Untreated Mo-DC show very low autofluorescence in the FITC detection channel, hence background autofluorescence from the cells did not interfere with locating the FITC labelled LDH particles.

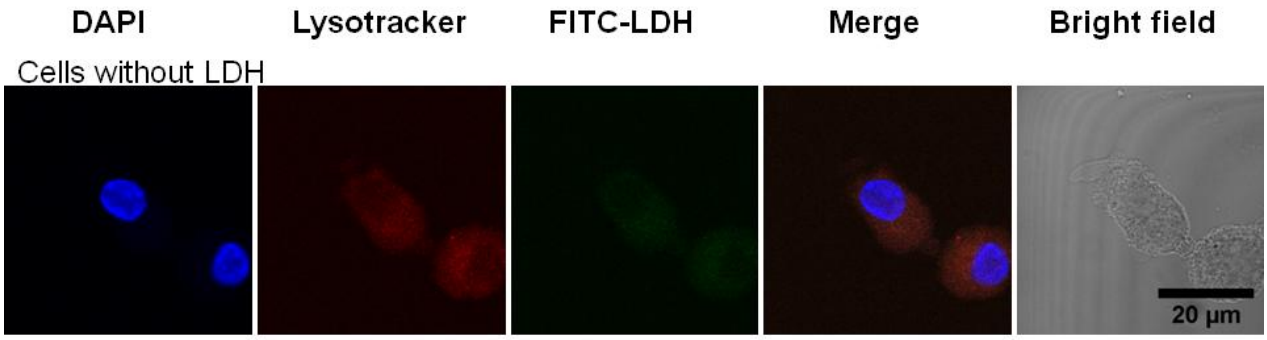

Figure 5.6 (continued on next page): Confocal images of Mo-DC incubated with different sizes of FITC-labelled MgAl-CO_3 LDH. Mo-DC were incubated for two hours with LDH particles (at 100 µg/mL) and the lysosomal dye Lysotracker Red. Cells were then fixed with paraformaldehyde (PFA), the nuclei stained with DAPI and mounted onto slides for imaging using laser scanning confocal microscopy. Separate fluorescence, bright-field and merged images are displayed. DAPI (blue) = nucleus, Lysotracker Red = lysosomes, FITC (green) = LDH particles.

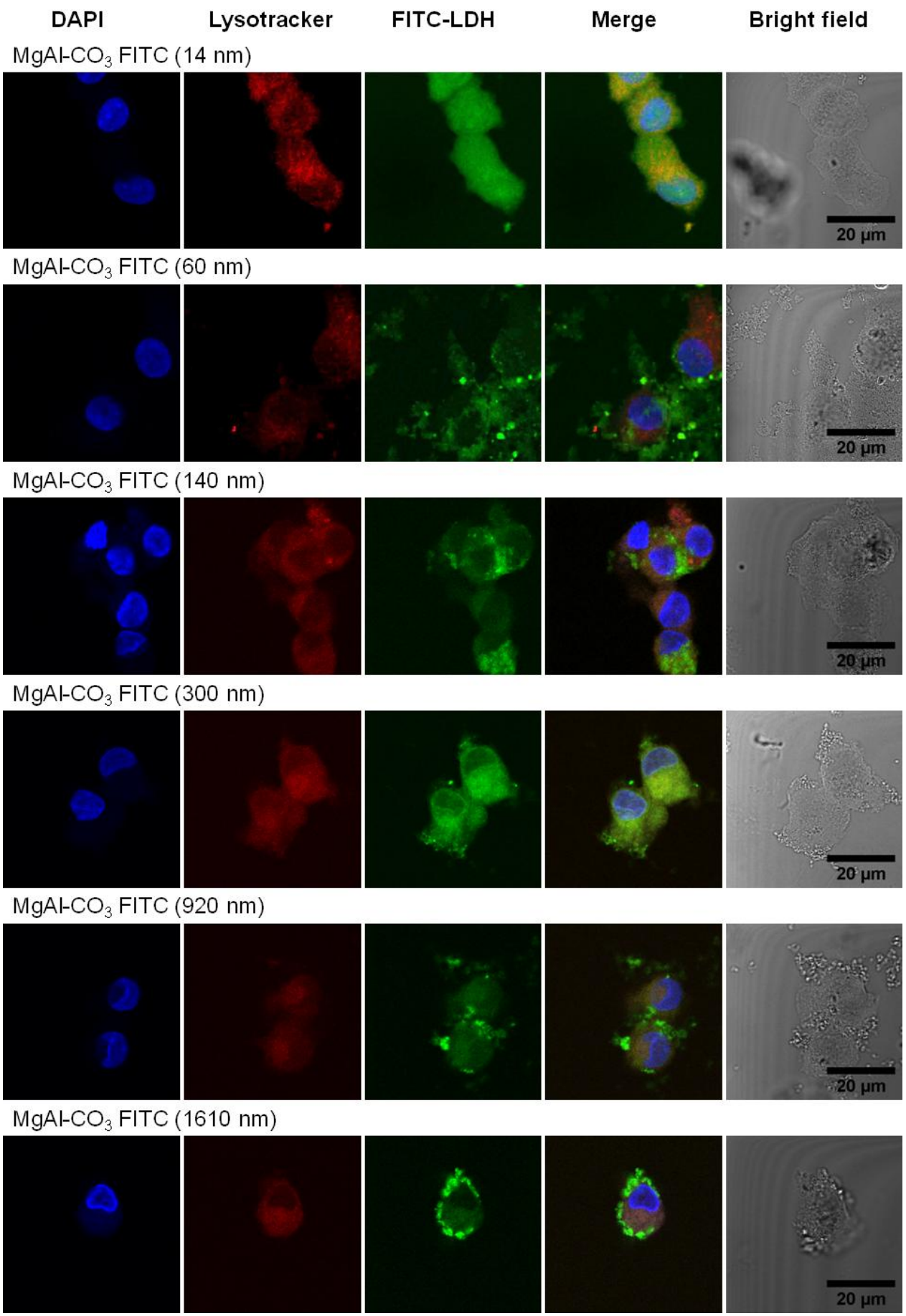
DAPI
Lysotracker
FITC-LDH
Merge
Bright field
MgAl-CO3 FITC (14 nm)
MgAl-CO3 FITC (60 nm)
MgAl-CO3 FITC (140 nm)
MgAl-CO3 FITC (300 nm)
MgAl-CO3 FITC (920 nm)
MgAl-CO3 FITC (1610 nm)
20 µm

All of the smaller LDH sizes (14 to 300 nm) appear inside the cells, as indicated by the close proximity of FITC fluorescence to the nucleus, and also in bright-field images where granular areas within the cells suggest the presence of LDH particles in the cytoplasm. Additionally, both fluorescence and bright-field images show LDH particles closely associated with the outside of the cells for all particle sizes. Some co-localisation of particles with lysosomes was observed, although the lysosomal staining was not as effective as was desired. Generally, no co-localisation of LDH particles with cell nuclei is observed, except for the smallest 14 nm particles. In some cases, for example the 300 nm LDH particles, FITC fluorescence is observed throughout the cytoplasm of the cell. It is possible that a very large number of particles have been internalised. Alternatively, LDH particles may have escaped the endosomal pathway and become evenly distributed throughout the cytoplasm, perhaps as a result of endosomal destabilisation, releasing both FITC-labelled LDH debris and free FITC.

For smaller particles, the resolution of the microscope is not sufficient to observe individual particles. However for the largest LDH particles (1610 nm) individual particles may be discerned. Larger particles (923 nm and 1607 nm) show a tendency to adhere to the surface of the cells, with fewer internalised particles noted. The lower degree of internalisation observed with larger particles may point towards an internalisation pathway that is most efficient for smaller objects. More detailed investigation into the possible mechanisms of uptake may be found in Section 5.2.5, and a summary table of all the observations made on LDHs incubated with cells is provided in Section 5.2.6.

5.2.4.2 *Z*-stack images

In *z*-stacked images the microscope is configured to record 0.5 μm-spaced slices through the sample, to give a three dimensional picture and further validate LDH internalisation. Figure 5.7 displays sections through a single Mo-DC treated with the 140 nm FITC labelled MgAl-CO_3 LDH. Images for the other five LDH sizes are supplied in Appendix D.2.

At the start of the sequence of *z*-stacked images (images 0-4) no LDH particles are observed. By the fifth image, the cell nucleus comes into focus, indicating the microscope is scanning directly through the cell. At this point, areas of FITC fluorescence appear (green colour) adjacent to the nucleus, suggesting the presence of LDH particles inside the cell. The presence of particles close to the nucleus continues throughout the ensuing images (6-18) as the cell remains in the focal plane. The proximity of the FITC-labelled LDHs to the nucleus strongly implies internalisation. Also, the observation of particles in the same focal plane as the

nucleus rules out the possibility that LDH particles are attached to the top and bottom surfaces of the cell. *Z*-stacked images for the other sizes of FITC-labelled MgAl-CO_3 LDH also show similar behaviour.

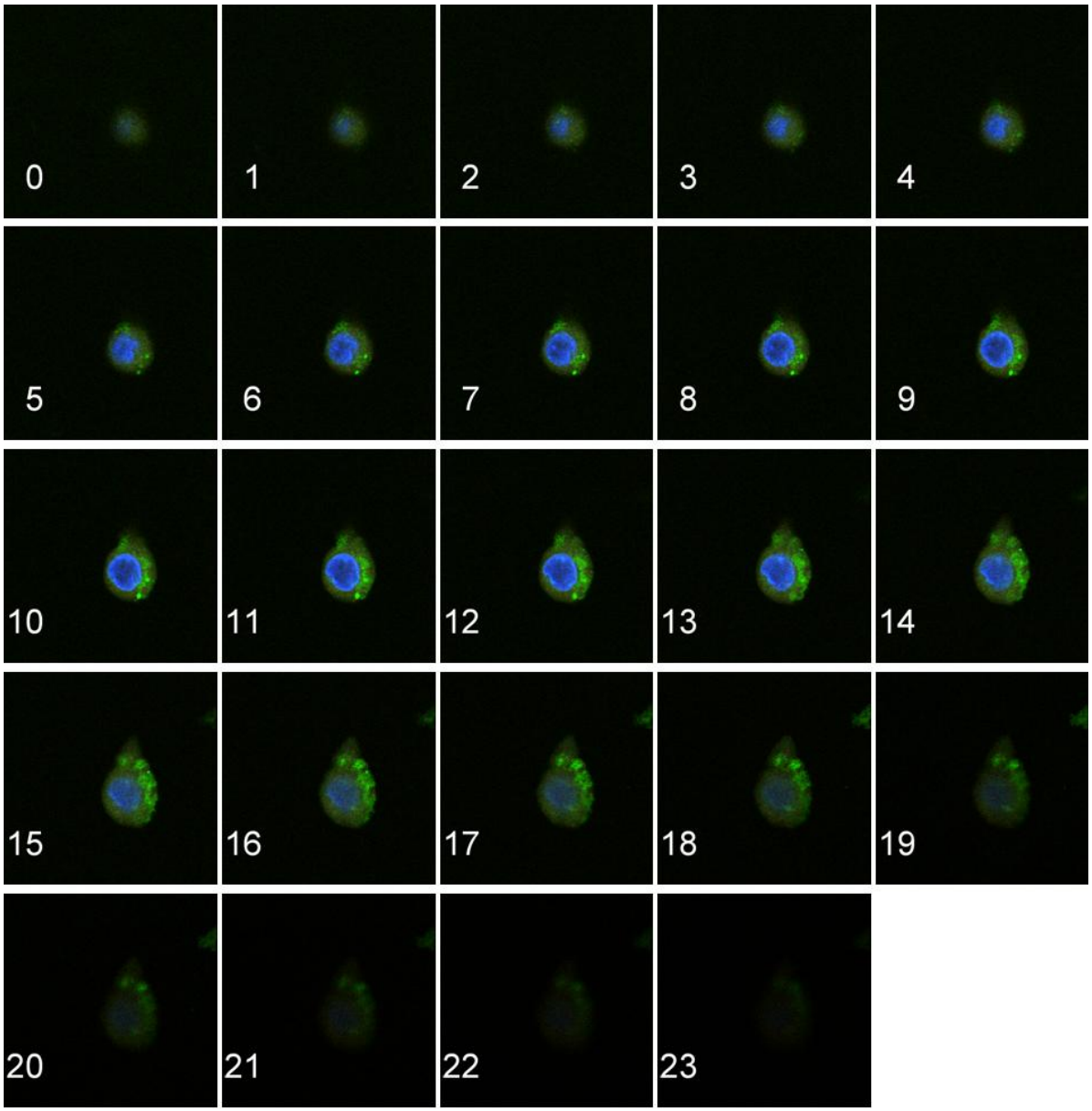

Figure 5.7: *Z*-stacked images of Mo-DC incubated with 140 nm FITC-labelled MgAl-CO_3 LDH particles. *Z*-stacked images for Mo-DC treated with 140 nm FITC labelled MgAl-CO_3 LDH. Mo-DC were incubated for two hours with LDH particles. Cells were then fixed with PFA, the nuclei stained with DAPI and cells mounted onto slides for analysis using laser scanning confocal microscopy. Images display merged fluorescence for two channels [DAPI (blue) = nucleus, FITC (green) = LDH particles] taken at 0.5 μm intervals through the depth of the sample.

In summary, confocal microscopy studies confirm that LDHs are both adhering to and being internalised by DCs. This sheds light on two interactions that could potentially cause the DC responses observed following treatment with LDHs in Chapter Three. Separate investigations

into both the mechanism of uptake, and particle-cell surface interactions may be found in later sections of this chapter.

5.2.4.3 Confocal microscopy study of other FITC-labelled LDH compositions

In order to probe the effect of LDH composition on particle-DC interactions, further confocal microscopy studies were conducted on the other FITC-labelled LDHs. The MgAl-NO_3, MgAl-Cl, MgFe-CO_3, MgFe-NO_3, and LiAl-CO_3 LDH compositions have similar mean particle sizes (30 to 80 nm). The FITC-labelled CaAl-NO_3 and CaAl-Cl LDHs were fragmented, consisting of both larger (hundreds of nanometres) and smaller particles.

Images reveal that some compositions are more readily internalised than others (Figure 5.8). The LiAl-CO_3 and MgAl-Cl LDH particles both appear in moderate amounts within the cells. In contrast, the cytoplasm of the cells treated with the MgFe-CO_3 and MgFe-NO_3 LDH particles exhibit extensive FITC fluorescence, implying facile internalisation of these compounds. In previous chapters, it was noted that MgFe-CO_3 LDHs gave decreased cell viability (Chapter Three) and lower T cell responses (Chapter Four). It is possible that the greater concentrations of these particles inside the cell hinder cell function and rupture cell membranes, leading to the observed effects. FITC-labelled MgAl-NO_3, CaAl-NO_3 and CaAl-Cl LDHs primarily adhere to the outside of the cells, with a few particles noted within the cytoplasm. A summary table of all the observations made on LDHs incubated with cells is provided in Section 5.2.6.

It is possible that subtle differences in the surface chemistry of the LDH compositions are responsible for the patterns in DC behaviour observed. Whilst some LDH association may occur regardless of the LDH composition, only particles with certain surface characteristics interact with the membrane in a way that promotes uptake. Hydrogen bonding almost certainly affects the interactions between components of the plasma membrane and LDHs. This depends on the acidity of the hydroxide groups on the LDH surface, which in turn would be influenced by the composition of the LDH. Ideally, further LDH compositions would be synthesised and tested, with thorough analysis of their surface properties, e.g. surface acidity assessed using Hammet indicators,[42,43] and surface area assessments using Brunauer, Emmett and Teller (BET) surface analysis.

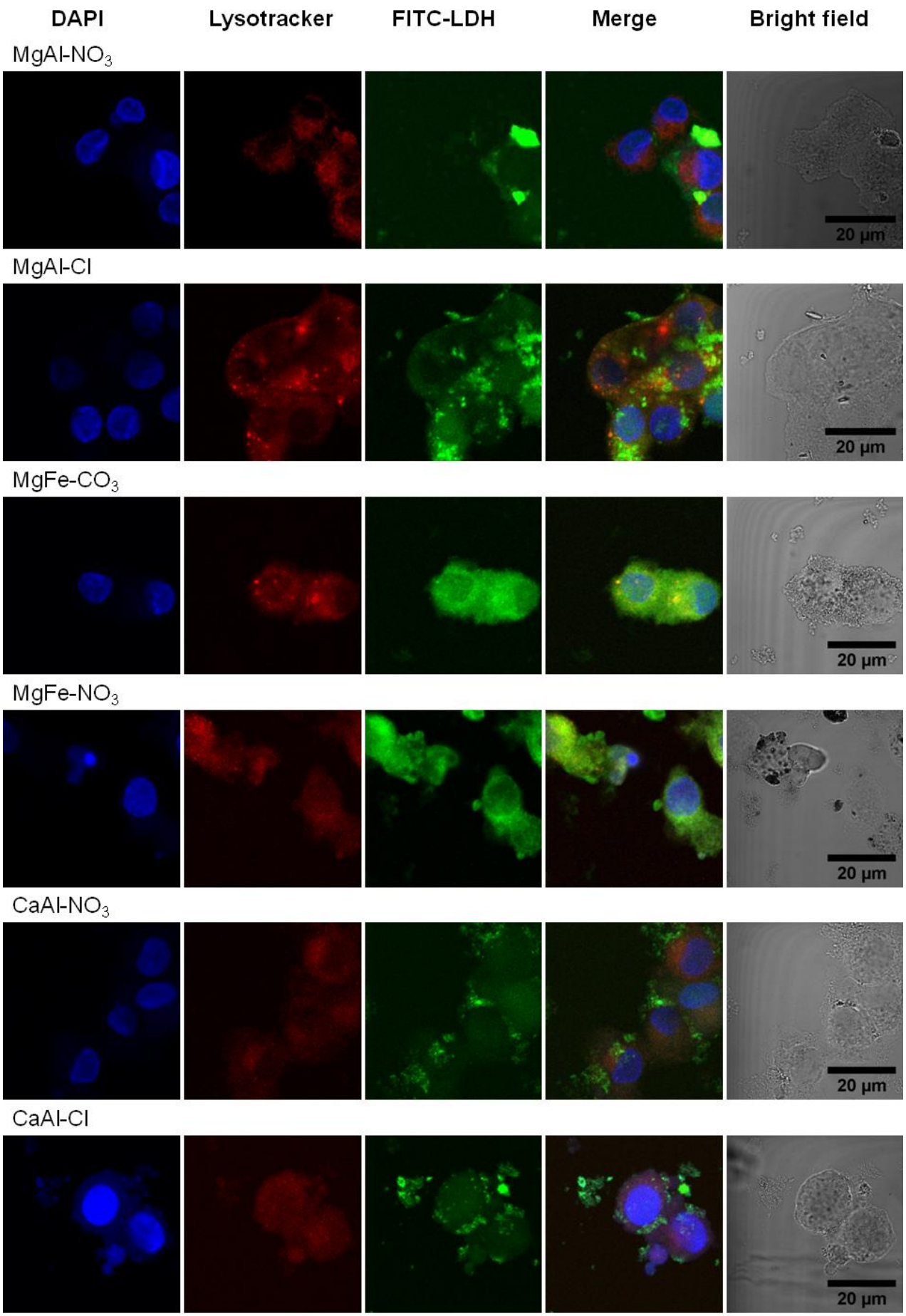
DAPI
Lysotracker
FITC-LDH
Merge
Bright field
MgAl-NO3
MgAl-Cl
MgFe-CO3
MgFe-NO3
CaAl-NO3
CaAl-Cl
20 µm

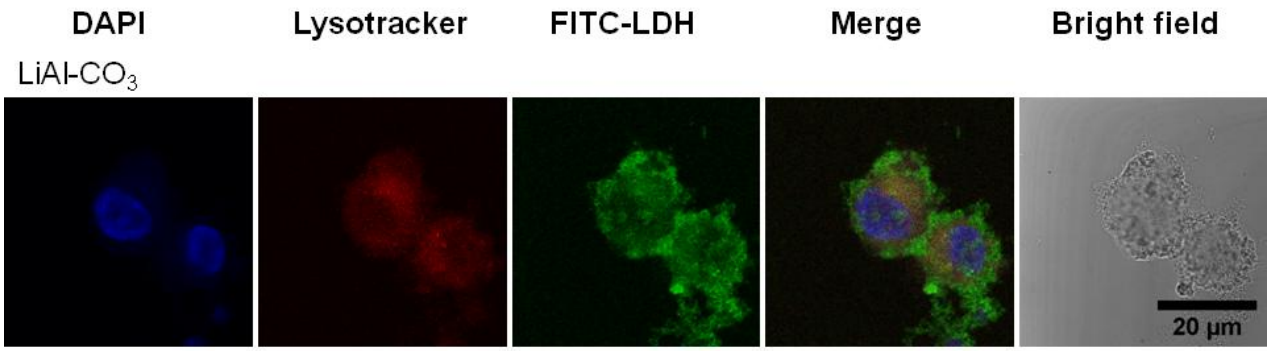

Figure 5.8 (also on preceding page): Confocal images of Mo-DC incubated with FITC-labelled LDHs in various compositions. Mo-DC were incubated for two hours with LDH particles and the lysosomal dye Lysotracker Red. Cells were then fixed with PFA, the nuclei stained with DAPI and mounted onto slides for analysis using laser scanning confocal microscopy. Separate fluorescence, bright-field and merged images are displayed. DAPI (blue) = nucleus, Lysotracker Red = lysosomes, FITC (green) = LDH particles.

5.2.5 Uptake inhibition experiments

To probe the mechanism of LDH particle uptake, further experiments using the FITC-labelled MgAl-CO_3 LDHs in conjunction with various inhibitors were conducted. The inhibitors chosen were: latrunculin A, an actin polymerisation inhibitor derived from the Red Sea sponge, which binds to actin monomers;[13,44] chlorpromazine, a clathrin-mediated endocytosis inhibitor, which inhibits the formation of clathrin-coated pits on the surface membrane by disrupting the recycling of adaptor protein-2 (AP-2) from endosomes - AP-2 plays a role in assembling membrane bound proteins with clathrin prior to internalisation;[44,45] amiloride, a macropinocytosis inhibitor that blocks Na^+/H^+ exchange, altering sub-membranous pH;[46] chloroquine, an endosomal acidification inhibitor;[47] and filipin III, which disrupts cholesterol based membrane rafts, impairing caveolae internalisation.[19,48] This panel of inhibitors covers a broad range of uptake mechanisms that have previously been implicated in the internalisation of particulate matter, for instance: actin dependent phagocytosis of asbestos and silica particles,[24] macropinocytosis of single-walled carbon nanotubes,[26] clathrin mediated endocytosis and lysosomal acidification in LDH particle uptake,[29,28] and lipid raft binding to alum adjuvants.[49] All inhibitors were first titrated for cytotoxicity on THP-1 cells. Full details of the concentrations used may be found in Chapter Six.

5.2.5.1 Flow cytometry results

THP-1 cells were pre-treated overnight with the various inhibitors, then FITC-labelled MgAl-CO_3 LDHs (60, 300, and 920 nm) were added to the wells addition for a further two hours. FITC-labelled beads were included as a positive control. Cells were washed then analysed by flow cytometry. The FITC fluorescence of events in the cells gate was recorded as a measure of cell-particle association. To check that the presence of the inhibitors in the

medium did not fundamentally alter the fluorescence intensity of the particles, FITC-labelled LDHs were also added to wells that contained the inhibitor in culture medium without cells as a background check. Fluorescence data for cells treated with the three LDH particle sizes and the FITC-labelled beads control are supplied in Figure 5.9.

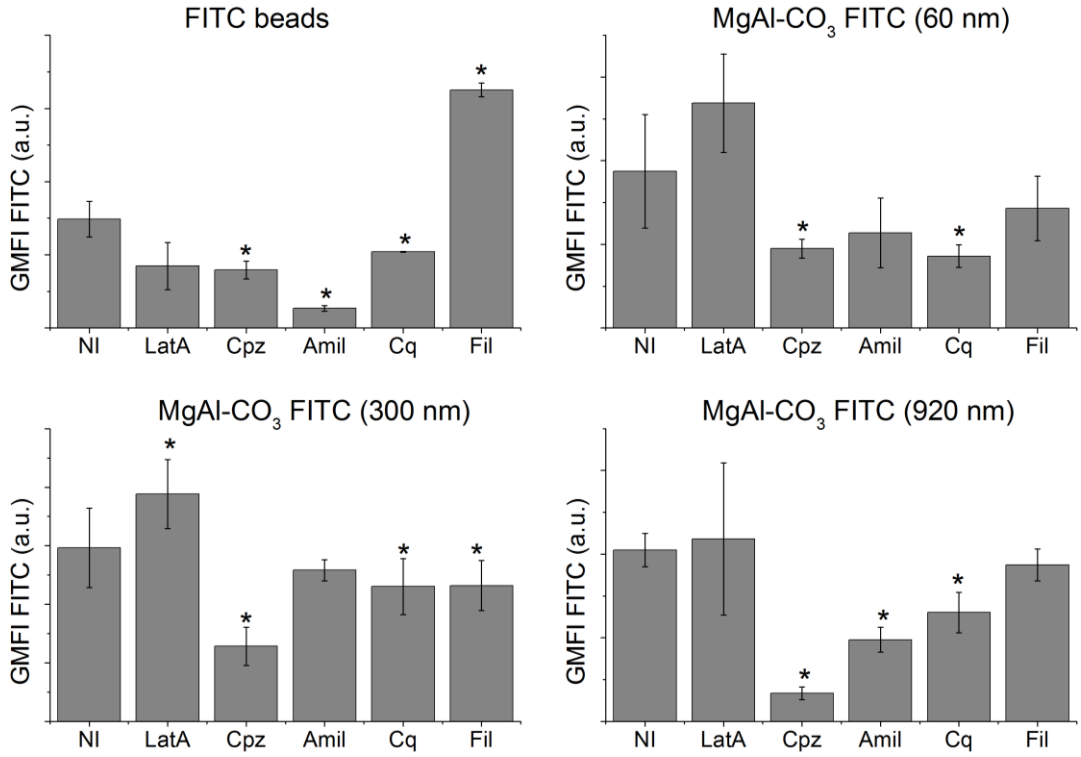

Figure 5.9: Investigation into the effect of uptake inhibitors on fluorescence from FITC-labelled MgAl-CO_3 LDHs associated with THP-1 cells. THP-1 cells were incubated overnight with five inhibitors (no inhibitor – "NI", latrunculin A – "LatA", chlorpromazine – "Cpz", amiloride – "Amil", chloroquine –" Cq" and filipin III – "Fil"), treated with FITC-labelled beads/LDH for two hours, then analysed by flow cytometry. Barcharts show the GMFI FITC fluorescence associated with cells after treatment with different uptake inhibitors. Error bars indicate two standard deviations, '*' indicates values significantly different ($p<0.05$) from the no inhibitor (NI) control.

Latrunculin A generally does not yield decreased FITC fluorescence for the FITC-labelled LDH particles. This implies that phagocytosis, or at least actin polymerisation, is not involved in LDH particle internalisation. Generally, phagocytosis requires ligation of specific receptors on the surface of the cell;[5] as inorganic materials, LDH particles lack the biological markers needed to bind these receptors.

Amiloride is an inhibitor of macropinocytosis, a non-receptor-mediated process for uptake of large volumes of the surrounding medium, and has a marked effect on fluorescence from FITC-labelled beads. However, amiloride only induces a significant decrease in cell-associated FITC fluorescence for the 920 nm LDH particles. Possibly, due to their greater size, the larger particles are more reliant on this mechanism for cellular uptake. This

contradicts the finding from latrunculin A treatment that actin polymerisation is not involved; clarification could be sought by testing other actin polymerisation inhibitors.

Filipin III marginally decreases LDH particle association with the cells although this is only significant for the 300 nm particles. This hints that disruption of cholesterol on the plasma membrane does have a small effect on LDH adhesion to cells, but given the nature of this experiment, it is impossible to determine whether changes to the fluorescence are due to particle internalisation or binding to the surface. Chloroquine treatment does slightly decrease cell-associated FITC fluorescence. Chloroquine hinders fusion of endosomes with acidic lysosomes,[50] thereby potentially disrupting an intracellular trafficking pathway of LDHs through the cells, making internalisation less likely.

Treatment with chlorpromazine consistently decreases cell-associated FITC fluorescence for all three LDHs.[51] Clathrin-mediated endoctyosis has been previously implicated in the internalisation of LDH particles in work by Oh *et al*. and Xu *et al*.[28,29,35] Disruption of the clathrin lattices on the cell membrane could have two effects on cell-particle interactions: firstly, it would prohibit internalisation *via* this mechanism, and secondly, it could be that LDH particles have a greater affinity for clathrin-rich areas. Depletion of these areas results in reduced LDH adhesion to the cell surface. Further investigation of the protein dependence of LDH binding to the cell surface is described in Section 5.3.1.

5.2.5.2 Confocal microscopy study

Confocal microscopy studies were conducted to confirm the results in the preceding section. Figure 5.10 shows images obtained of THP-1 cells treated with each of the inhibitors, then incubated with the 300 nm FITC-labelled MgAl-CO_3 LDH particles.

For the untreated THP-1cells and cells treated with the inhibitors that did not greatly decrease FITC fluorescence in the flow cytometry studies (latrunculin A, amiloride, chloroquine, filipin III), LDH particles appear closely associated with the cells. However, the THP-1 cells treated with chlorpromazine display lower FITC fluorescence in the fluorescence images and fewer particles associated with cells in the bright-field images compared to the other treatments, corroborating the results obtained from flow cytometry experiments.

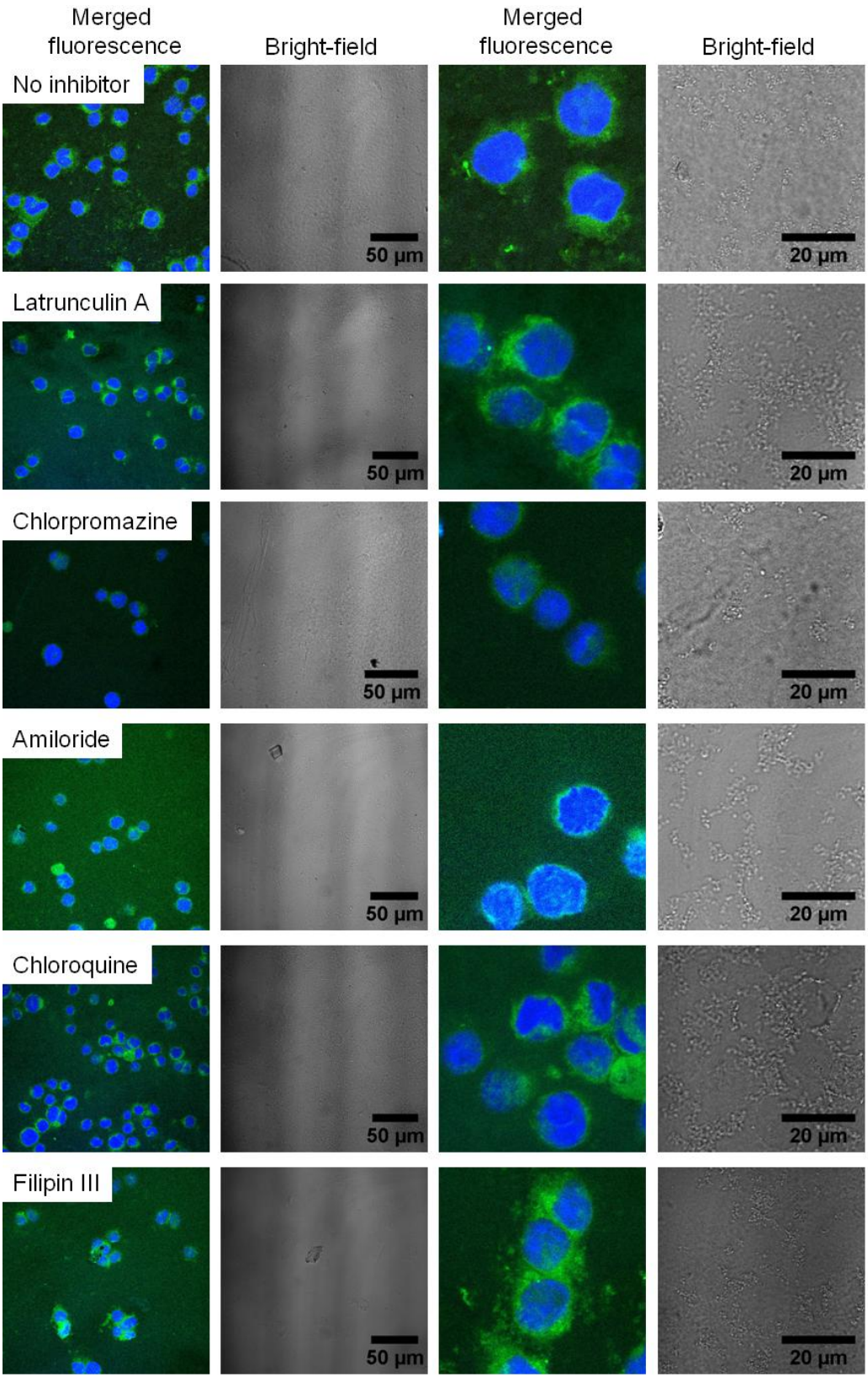

Figure 5.10: Confocal microscopy study into the effect of inhibitors on association of 300 nm FITC-labelled MgAl-CO_3 LDH particles with THP-1 cells. THP-1 were incubated overnight with the inhibitors, then for two hours with LDH particles (100 µg/mL). Cells were then fixed with PFA, the nuclei stained with DAPI and mounted onto slides for analysis using laser scanning confocal microscopy. Separate fluorescence, bright-field and merged images are displayed. DAPI (blue) = nucleus, FITC (green) = LDH particles.

5.2.6 Summary of uptake studies and particle localisation

Table 5.2 provides a summary of the results of particle localisation investigations under confocal microscopy, and uptake mechanism studies, for every LDH investigated.

Table 5.2: Summary of observations made from confocal microscopy and uptake studies. '**' indicates no assessment of uptake mechanisms with the inhibitors was performed.

LDH composition/size	Position in cell (confocal)	Possible uptake mechanisms
MgAl-CO_3 (14 nm)	Cytoplasm, possibly in nucleus	**
MgAl-CO_3 (60 nm)	Cytoplasm, surface of cells	Clathrin-mediated endocytosis, lysosomal acidification
MgAl-CO_3 (140 nm)	Cytoplasm, surface of cells	**
MgAl-CO_3 (300 nm)	Extensive fluorescence in cytoplasm, some associated with cell surface	Clathrin-mediated endocytosis, lysosomal acidification, lipid rafts
MgAl-CO_3 (920 nm)	Primarily stuck to surface, a few internalised	Clathrin-mediated endocytosis, macropinocytosis, lysosomal acidification
MgAl-CO_3 (1610 nm)	Primarily stuck to surface, a few internalised	**
MgAl-NO_3	Primarily stuck to surface, a few internalised	**
MgAl-Cl	Cytoplasm, surface of cells	**
LiAl-CO_3	Cytoplasm, surface of cells	**
MgFe-CO_3	Extensive fluorescence in cytoplasm, some associated with cell surface	**
MgFe-NO_3	Extensive fluorescence in cytoplasm, some associated with cell surface	**
CaAl-NO_3	Primarily stuck to surface, a few internalised	**
CaAl-Cl	Primarily stuck to surface, a few internalised	**

5.3 Investigations into LDH-plasma membrane interactions

Experiments indicate that LDH particles are both internalised by cells and adhere to the plasma membrane. Treatment with chlorpromazine, a disruptor of clathrin-coated pits on the plasma membrane, reduces association between cells and particles, and could block uptake, implying a degree of protein dependence in the cell-particle interactions. In this section, the protein dependence of cell-particle adhesion is probed by pre-treating cells with three protease enzymes, then assessing the degree of cell-particle association using flow cytometry. It is also possible that there is an electrostatic component to the adhesion. Since surface charge is dependent on the surrounding pH, cells were treated with LDH particles at various pHs to ascertain the effect on binding.

5.3.1 Protein dependence

To disrupt proteins on the cell surface, cells were treated with trypsin, pepsin or papain. Trypsin is a serine protease found in the digestive system, that cleaves proteins at the C-terminal end of lysine or arginine residues. It is most active at pH 7-8,[52] and dilute solutions

are commonly used to disengage adherent cells from surfaces. Trypsin has also been used to cleave glycoproteins from the surface of erythrocytes.[53] Pepsin is another digestive enzyme, but has optimal activity in more acidic environments (pH 1.5-3).[54] Pepsin is commonly used to separate the antigen-binding fragments from the rest of the antibody, and preferentially cleaves peptides at hydrophobic, aromatic amino acid residues (e.g. phenylalanine, tryptophan, tyrosine).[55] Papain is a cysteine protease isolated from papaya, with a broad specificity for cleaving peptides and proteins.[56] It is most efficient at pH 6 to 7, in the presence of the amino acid L-cysteine.[57]

5.3.1.1 Trypsin dependence

In initial experiments, live Mo-DC were treated with the FITC-labelled MgAl-CO_3 LDH particles for two hours at 37 °C, then trypsinised using a 1 x concentration (0.25%) of trypsin in PBS/EDTA and analysed by flow cytometry for FITC fluorescence associated with the cells [Figure 5.11 (a)]. For the majority of the LDH sizes, a significant decrease in cell-associated FITC fluorescence is observed with trypsin compared to treatment with control solutions of trypsin-free PBS and PBS/EDTA. However, this experiment was conducted on live cells at physiological temperature, so interference from internalisation of LDH particles could not be excluded.

To focus solely on surface interactions, experiments were modified to reduce uptake by either keeping the cells on ice [Figure 5.11 (b)] or by pre-fixing the cells with paraformaldehyde [Figure 5.11 (c)]. The results of both of these experiments are consistent with those from the initial experiment at 37 °C. A decrease in binding upon trypsinisation is common to all six sizes of FITC-labelled MgAl-CO_3 LDH. This suggests that regardless of particle size, LDH adhesion to cell surfaces is partly protein dependent. Treating cells with trypsin-free PBS/EDTA consistently has little effect on LDH binding compared to the PBS control. Therefore in subsequent trypsin experiments, only PBS was used as the control solution. This also illustrates that there is no dependence on extracellular calcium concentration for LDH association, as EDTA is a Ca^{2+} chelating agent.

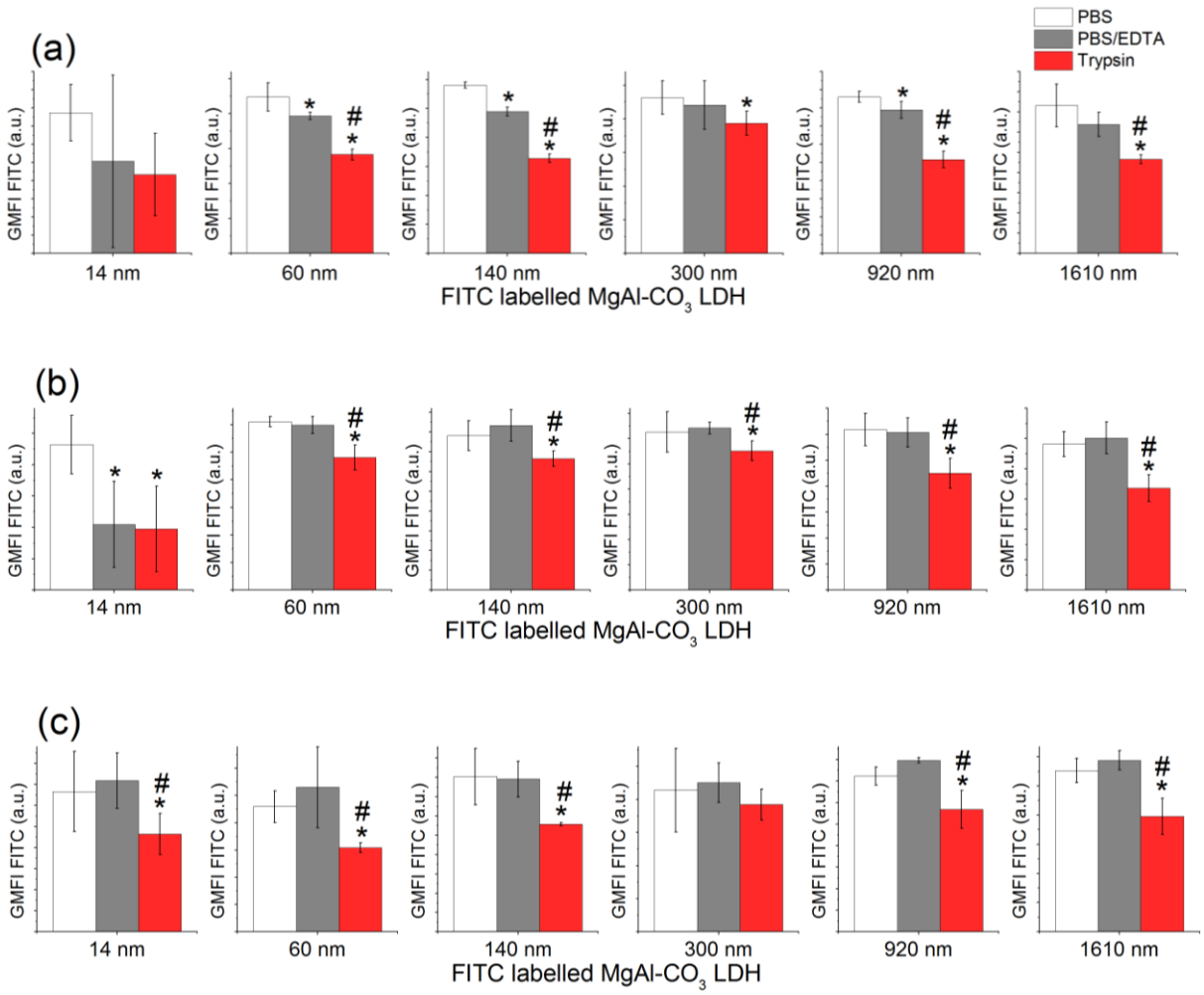

Figure 5.11: Investigations into the effect of trypsin treatment on FITC-labelled LDH particle association with Mo-DC. (a) Mo-DC incubated with LDH for two hours at 37 °C, (b) Mo-DC incubated with LDH for two hours on ice (~4 °C) to minimise uptake and (c) pre-fixed Mo-DC incubated with LDHs for two hours at 37 °C. Following incubation, Mo-DC were treated with either trypsin, or the control buffers (PBS or PBS/EDTA) and analysed using flow cytometry. GMFI values for FITC fluorescence in the cells gate were recorded. '*' and '#' indicate significant differences ($p<0.05$) relative to the PBS and PBS/EDTA controls respectively. Error bars indicate two standard deviations.

The sensitivity of Mo-DC-particle interactions to trypsin concentration was probed by comparing the effects of trypsin at either 1 x (0.25%) or 10 x (2.5%) concentrations [Figure 5.12 (a)]. To determine the specificity of this phenomenon, analogous experiments using 1 x and 10 x trypsin concentrations were performed on THP-1 cells and PBMC [Figure 5.12 (b) and (c)].

For Mo-DC, treatment with the 10 x trypsin concentration inhibits cell-particle adhesion significantly more than the 1 x trypsin concentration for five of the six LDH sizes. As expected in light of earlier results, increased protein removal from the cell surface decreases LDH adhesion. However, even when using more concentrated trypsin solutions, some FITC

fluorescence is still present, indicating that LDHs not only binding to trypsin sensitive proteins, but to other components of the cell membrane as well.

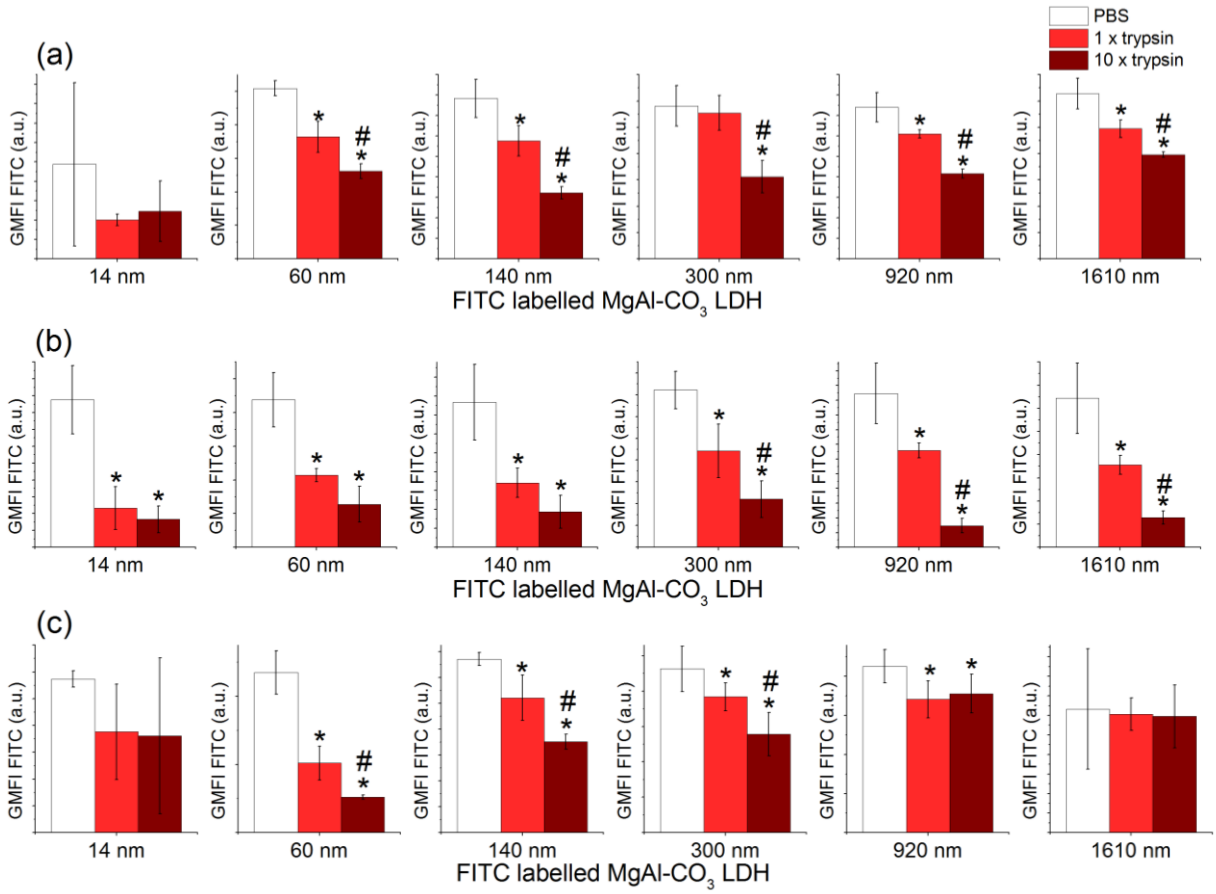

Figure 5.12: Investigations into the effect of trypsin concentration on FITC-labelled LDH particle association with Mo-DC, THP-1 cells and PBMC. Testing the trypsin sensitivity of cell-particle interactions for pre-fixed (a) Mo-DC, (b) THP-1 and (c) PBMC. Cells were fixed with PFA, then incubated for one hour with FITC-labelled MgAl-CO_3 LDH particles. Following incubation, cells were treated with either a 1 x or 10 x working concentration of trypsin, or PBS as a control, and analysed using flow cytometry. GMFI values for FITC fluorescence in the cells gate were recorded. '*' and '#' indicate significant differences ($p<0.05$) relative to the PBS and 1 x trypsin concentration conditions respectively. Error bars indicate two standard deviations.

Trypsinised THP-1 cells consistently bind LDH less compared to untrypsinised cells [Figure 5.12 (b)]; three particle sizes also show sensitivity to the concentration of trypsin used. For PBMC, four of the six sizes of the FITC-labelled MgAl-CO_3 LDH exhibit trypsin sensitive binding, with concentration dependence noted for three of these. The fact that both THP-1 cells and PBMC show some degree of sensitivity to trypsin confirms that this is not a Mo-DC specific effect, and may reflect a general interaction between cells and LDHs.

Furthermore, reversing the order of cell treatment, i.e. trypsinising before incubation with FITC-labelled LDH particles also decreases LDH binding (Figure 5.13). When performed in this order, the 1 x and 10 x trypsin concentrations give similar levels of LDH adhesion.

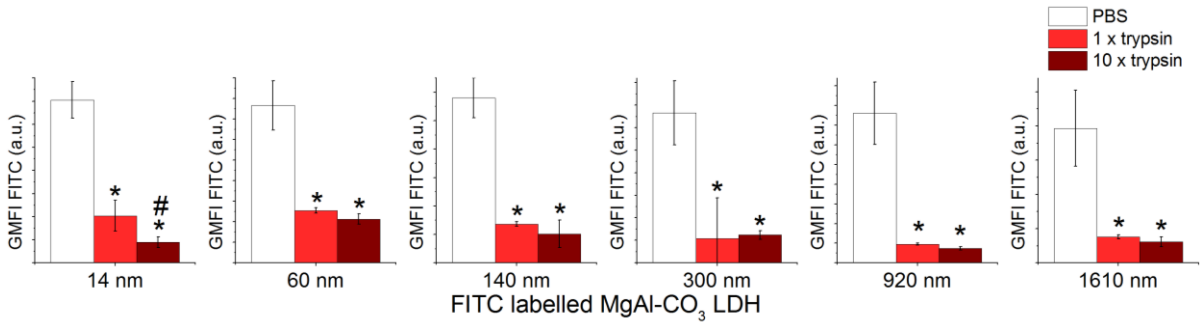

Figure 5.13: Investigation into the effect of pre-treating THP-1 cells with trypsin before incubation with FITC-labelled LDH particles. Cells were fixed with PFA, then treated with either the 1 x or 10 x trypsin concentrations or PBS control. Subsequently they were incubated for 30 minutes with FITC-labelled MgAl-CO_3 LDH particles and analysed using flow cytometry. GMFI values for FITC fluorescence in the cells gate were recorded. '*' and '#' indicate significant differences ($p<0.05$) relative to the PBS and 1 x trypsin concentration conditions respectively. Error bars indicate two standard deviations.

To confirm protein removal/disruption, Mo-DC were stimulated overnight with lipopolysaccharide (LPS) to promote surface molecule expression, treated with PBS/EDTA as a negative control, or 1 x and 10 x trypsin working concentrations, then stained for a panel of surface molecules (CD14, CD209, CD274, MHC class II, CD40, CD86, CD275, CD283 and CD1a) and analysed using flow cytometry. Results, provided in Appendix D.3, show reduced antibody binding, and some dependence on trypsin concentration, for most molecules. Not all molecules are affected; binding of antibodies for CD274 and MHC class II remains approximately constant regardless of trypsinisation. This confirms that the effect observed is not a down-regulation event of all molecules in response to trypsin, but genuine perturbation to the existing surface molecules, some of which are more sensitive to trypsinisation than others.

5.3.1.2 Pepsin dependence

Further validation of the protein dependence of LDH binding to the cell surface membrane was achieved using the enzyme pepsin. THP-1 cells were fixed, then pre-treated with the buffer (10mM HCl in PBS) either with or without pepsin before addition of LDH particles (Figure 5.14).

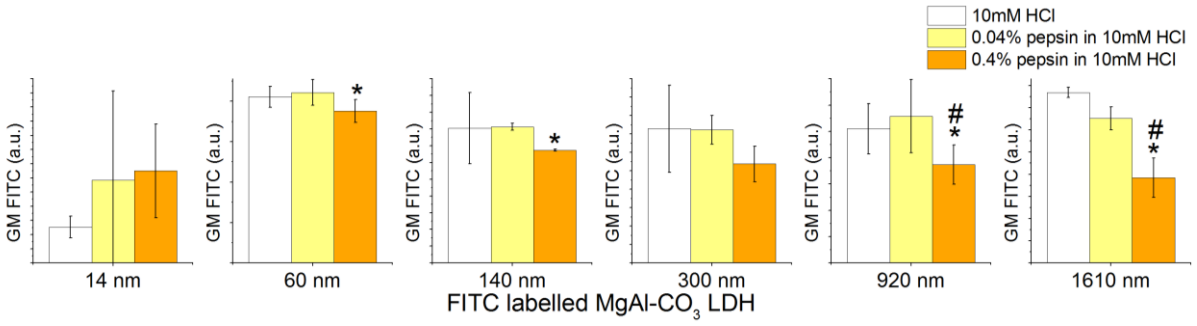

Figure 5.14: Investigation into the effect of pepsin treatment on FITC-labelled LDH particle association with THP-1 cells. Cells were fixed with PFA, then treated with either the pepsin buffer alone (10 mM HCl), or 0.04% and 0.4% pepsin in the pepsin buffer. Subsequently they were incubated for 30 minutes with FITC-labelled MgAl-CO_3 LDH particles and analysed using flow cytometry. GMFI values for FITC fluorescence in the cells gate were recorded. '*' and '#' indicate significant differences ($p<0.05$) relative to the pepsin buffer only and 0.04% pepsin treatments respectively. Error bars indicate two standard deviations.

Pre-treatment of THP-1 cells with 0.4% pepsin decreases LDH adhesion compared to buffer without pepsin for four of the six LDHs. Use of higher concentrations of pepsin could not be attempted, as it is only slightly soluble. However, use of a lower concentration of pepsin (0.04%) revealed no significant difference to cells treated with the buffer alone.

5.3.1.3 Papain dependence

One further protease enzyme was tested to validate the protein-dependence of LDH binding highlighted in trypsin and pepsin studies. Two experiments were conducted on THP-1 cells: firstly, cells were fixed and pre-treated with papain, then incubated with FITC-labelled MgAl-CO_3 LDH particles [Figure 5.15 (a)]; secondly, cells were fixed, incubated with LDH particles, then treated with papain [Figure 5.15 (b)]. Two concentrations were tested, 0.05 and 0.5 mg/mL.

Results for both experiments corroborate the results from trypsin and pepsin studies in the preceding sections. When cells are treated with papain before incubation with LDH [Figure 5.15 (a)], significantly less LDH particle binding for both 0.05 and 0.5 mg/mL concentrations is noted for the majority of LDH particle sizes. For half of the LDHs, some concentration dependence is also noted. When THP-1 cells are incubated with FITC-labelled

MgAl-CO_3 LDH particles, then treated with papain [Figure 5.15 (b)], all LDH sizes bind less to papain-treated cells than those treated with the buffer.

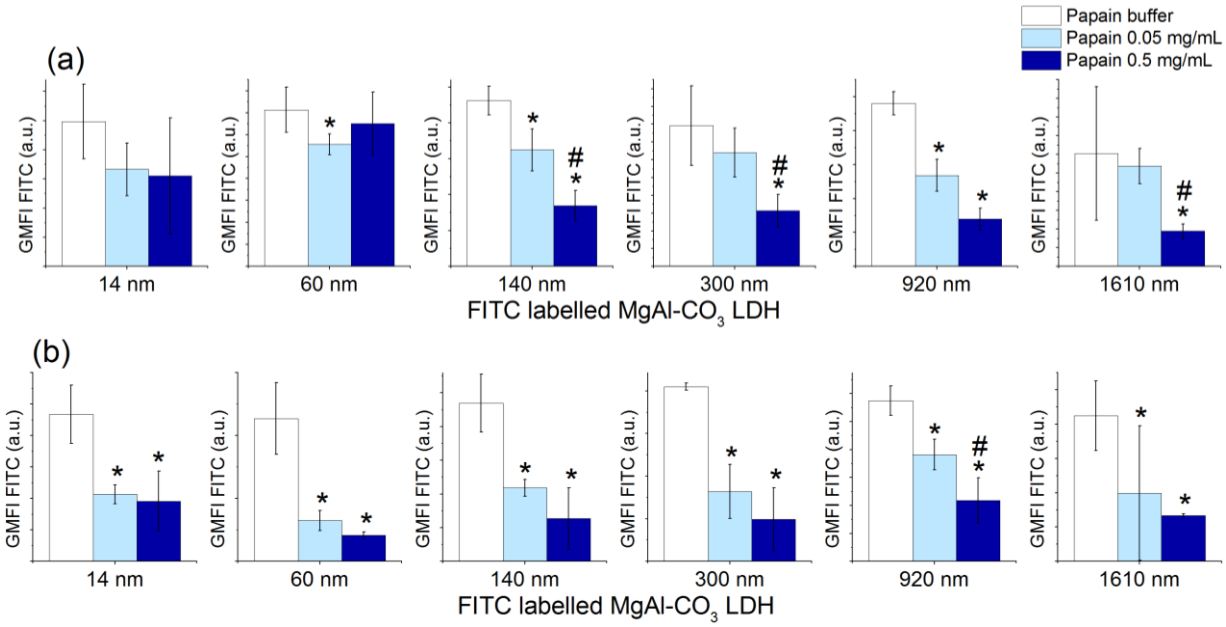

Figure 5.15: Investigation into the effects of papain treatment on LDH binding to THP-1 cells either before (a) or after (b) incubation with FITC-labelled LDH particles. Cells were fixed with PFA, then (a) pre-treated with papain, then incubated with FITC-labelled MgAl-CO_3 LDH particles for one hour, or (b) treated with papain after incubation with LDH for one hour. Subsequently cells were analysed using flow cytometry. GMFI values for FITC fluorescence in the cells gate were recorded. '*' and '#' indicate significant differences ($p<0.05$) relative to the papain buffer only and 0.05 mg/mL papain treatments respectively. Error bars indicate two standard deviations.

A control experiment was also conducted in an analogous fashion to the trypsin experiment, looking at antibody binding to surface molecules (Appendix D.4). THP-1 cells were stimulated overnight with LPS to promote greater surface molecule expression, then treated with 0.05 or 0.5 mg/mL papain solutions or papain-free buffer. Cells were then stained for a panel of surface molecules (CD1a, CD14, CD86, CD283, CD274, MHC class I, CD209, CD40, CD275) and analysed using flow cytometry. Results show depleted antibody binding to certain molecules, notably CD40, CD209, CD275 and CD14. This confirms that disruption to specific membrane bound proteins is occurring, rather than general papain-induced down-regulation of all surface molecules. In conclusion, treatment with the three protease enzymes typically decreases LDH binding to the cell types studied, indicating a protein-dependent component to cell-particle association.

5.3.2 pH dependence

It is also possible that electrostatics contribute to the binding of LDH particles to the plasma membrane of DCs. The surface charge of the objects within a solution may be changed by

altering the pH, providing a mechanism for probing electrostatic cell-particle interactions. In more acidic environments, surfaces tend to be positively charged as exposed functional groups become protonated, whereas at higher pHs de-protonation leads to an accumulation of negative charge. The pH at which the surface charge is zero is the isoelectric point (IEP).

A series of buffers from pH 3 to 10 were prepared. All buffers contained NaCl and KCl at equivalent concentrations to those found in PBS to prevent osmotic lysis of the cells. Interactions between pre-fixed Mo-DC and the 300 nm FITC-labelled MgAl-CO_3 LDH were investigated by analysing the cell-associated FITC fluorescence at different pHs using flow cytometry [Figure 5.16 (a)]. FITC is a pH sensitive dye,[58] therefore calibration measurements for the FITC-labelled LDH at each pH were obtained on a fluorometer and used to scale the flow cytometry results appropriately. Zeta potential measurements were measured separately for cells and particles at each pH under investigation to ascertain the effect of pH on their surface charges [Figure 5.16 (b)]. In an attempt to minimise LDH solvation at low pH, short incubation times were employed for both the flow cytometry experiments and zeta potential measurements.

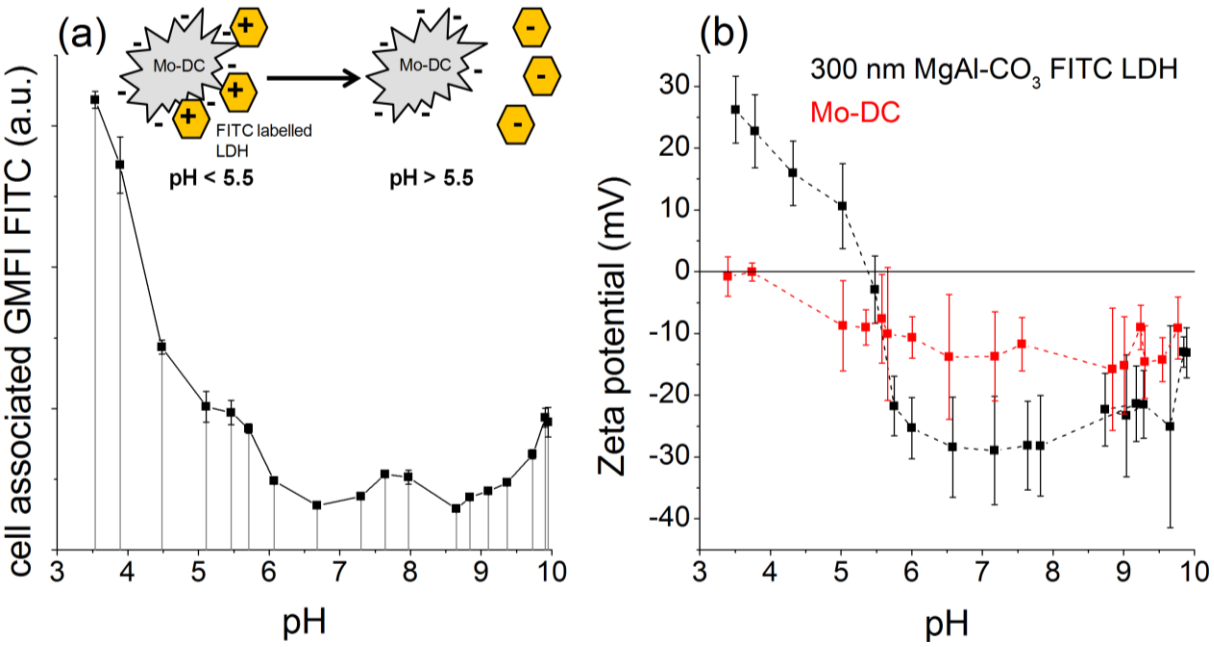

Figure 5.16: Investigation into the effect of pH on LDH particle binding to Mo-DC. (a) 300 nm FITC-labelled MgAl-CO_3 LDH (500 µg/mL) binding to Mo-DC as a function of pH, assessed using flow cytometry in buffers from pH 3 to 10. Data were corrected for the pH dependence of FITC fluorescence. Schematic above the graph suggests potential Mo-DC-particle interactions at different pHs. (b) Plot of pH *versus* zeta potential for 300 nm FITC-labelled MgAl-CO_3 LDH and Mo-DC. Zeta potentials of suspensions of either fixed Mo-DC or 300 nm FITC-labelled MgAl-CO_3 were recorded separately at analogous concentrations to those used in flow cytometry.

Analysis of the zeta potential data reveals that the 300 nm FITC-labelled MgAl-CO_3 LDH exhibits a positive zeta potential, corresponding to a net positive charge on its surface, at low pH [Figure 5.16 (b)]. The IEP is approximately pH 5.5; typically, LDHs exhibit much higher IEPs,[59] although many of the measurements described in the literature were made in deionised water whereas these measurements were conducted in buffers supplemented with large numbers of additional ions. The ionic strength of the medium can have a profound effect on the size of the electrical double layer, the charges at the surface of the material, and consequently also on the IEP.[60] Mo-DCs display slightly negative zeta potentials at low pH, which become more negative at higher pH. This is similar to the zeta potentials recorded for bacteria by Wilson *et al.*[61] Cell membranes generally have a negative charge, as a large proportion of their area is comprised of phospholipid head groups.[62]

Below pH 5.5 there is a notable increase in LDH binding to the cell surface [Figure 5.16 (a)], corresponding to the pH range where the zeta potentials of the two species (LDH and Mo-DC) indicate they are oppositely charged. This explains the increased attraction between the two species at low pH, and implies that electrostatics play a role in LDH adhesion to cells. Between pH 6 to 9 less association is observed, with a slight increase noted at pH 10. In this pH range, both the LDH particles and cells exhibit like charges. However, some adhesion is observed at all pHs, possibly as a result of local effects where specific areas of the plasma membrane remain attractive to LDH particles, despite the overall analysis of the two species predicting they should repel on electrostatic grounds.

5.4 Discussion

The results described in this chapter highlight various aspects of the interactions between cells (primarily Mo-DC) and LDH particles. Firstly, a combination of LDH internalisation and LDH adsorption onto the cell surface occurs. Indeed, both of these interactions have been implicated in alum adjuvant activity in the literature. For instance, Flach and co-workers found that alum binds to lipid rafts on the DC surface with high affinity, whilst various reports detail a requirement for actual internalisation of alum particles.[24,2] It is possible that these interactions represent different points on a continuum, i.e. LDH particles attach to the plasma membrane and are subsequently internalised. One method for detailed assessment of this would be time-lapse microscopy, which would provide an insight into the various stages as DCs encounter LDH particles. Scanning electron microscopy (SEM) analysis could be used to image LDH particles that are attached to the cell surface or partially internalised.

Elemental mapping using EDX can accurately distinguish between the cell surface and the LDH from the differences in their surface chemistry.

Studies using confocal microscopy and Lucifer yellow confirm that LDHs undergo uptake into Mo-DC, consistent with observations on other cell types in the literature.[28,29,63,64] Uptake inhibitor experiments suggest clathrin-mediated endocytosis as the primary mechanism through which LDH particles are internalised. It may be hypothesised that LDH binding to membrane proteins such as clathrin marks the start of the internalisation process, which is corroborated by the protein dependence in cell-particle associations detailed in this Chapter. In the future, this could be explored by looking for co-localistion of LDH particles with clathrin-coated pits using confocal microscopy, or by testing other clathrin-mediated endocytosis inhibitors such as amantadine-HCl.[65] No decrease in particle uptake is noted with the actin polymerisation inhibitor, latrunculin A, although in some cases amiloride does have an effect. To further clarify whether LDH uptake is actin dependent, confocal studies using a stain for actin filaments such as fluorescently-labelled phalloidin could be conducted in the presence or absence of actin polymerisation inhibitors (latrunculin A, cytochalasins etc).

Confocal microscopy studies show that the larger LDH particles have a tendency to adhere to the cell membrane, and are internalised less than smaller particles. It may be that both smaller and larger particles are adsorbed by protein rich areas of the cell surface, but the larger particles are less readily internalised. Typically, the size of the clathrin-coated pits is around 85 to 110 nm.[15] Consequently they are too small to internalise the larger particles, which may be a micron and above in size. They may act as a means of attaching particles to the cell surface for a sufficient period of time for other internalisation pathways to occur (e.g. macropinocytosis).

Studies reveal both protein-based and electrostatic components to cell surface-LDH interactions. The affinity of LDH surfaces for proteins has been documented for example in creating haemoglobin-LDH nano-hybrid materials for catalysis.[66,67] Furthermore, efforts have been made to utilise this attraction for applications in protein sorting/purification, which implies a degree of selectivity in protein binding to LDHs. For instance, Shao *et al*. suggest that the Ni^{2+} sites in Fe_3O_4@SiO_2@NiAl-LDH core-shell microspheres act as a binding site for histidine.[68] Possibly, similar local interactions are responsible for the LDH-plasma membrane attraction, and these are disrupted by treatment with protease enzymes.

A greater association between cells and particles is noted when the two are oppositely charged at low pH. Zeta potentials generally increase with LDH particle size (Section 2.2.1.6), i.e. larger particles tend to have more positive charge. However, confocal microscopy reveals LDHs of all sizes associate with cells at physiological pHs even though their zeta potentials indicate both are negatively charged. Perhaps, some association between LDH particles and cell surfaces is always present purely because both are highly hydrophilic. For cells, both the phospholipid head groups and the side chains of the various polypeptides that make up the proteins on the plasma membrane are able to hydrogen bond to nearby water molecules. The surface of the LDH is covered with hydroxyl groups also capable of hydrogen bonding. Regardless of the pH or the nature of the proteins exposed on the cell surface, some degree of hydrogen bonding between the two is always possible. Were further studies into this phenomenon carried out, it may be helpful to assess acidity of the LDH surfaces using Hammet indicators.[69] Additionally, the effects of altered acidity and surface charge could be probed by LDH surface modification. For example, increased hydrophobicity may be attained by grafting silyl groups onto the surface.[70,71]

The experiments detailed in this Chapter explore initial cell-particle interactions, but do not address what the downstream effects of these might be, for example, the signalling pathways activated that lead to the responses observed in Chapter Three. Nalp3 inflammasome activation has been widely linked to inflammatory responses to alum adjuvants and other particulate materials.[72] This may be tested by looking at the effect of Nalp3 inhibitors such as glyburide[73] or the pan-caspase inhibitor zVAD[24] on cellular responses. Further detail could be provided by looking for proteins associated with the Nalp3 inflammasome pathway in Western blots, for example Nalp3 protein, ASC, CARD and the activated forms of caspase 1.[74,75] Flach *et al*. implicate receptor aggregation and signalling *via* the protein tyrosine kinase Syk in their studies into alum binding to lipid rich areas of the plasma membrane.[1] Western blots could also be used to test for the active phosphorylated version of Syk, or other signalling components or transcription factors of interest e.g. NF-κB, interferon regulatory factors.

5.5 Conclusion

Two interactions were highlighted for investigation at the start of this Chapter: internalisation of LDH particles and adhesion of LDH particles to the plasma membrane. Lucifer yellow and confocal microscopy studies confirm that LDH particles are internalised by cells. Furthermore, variations in uptake patterns between the different particle sizes of FITC-labelled MgAl-CO_3 and the different LDH compositions are highlighted. Previous confocal microscopy studies looking at uptake of LDH particles have only focused on the smaller particle sizes, for instance Chung *et al*. studied localisation of 50 and 100 nm particles,[63] whilst Xu and co-workers investigated cellular uptake of plate-like (50-150 nm) and rod-like (100-200 nm) LDH particles.[29] Consequently, these results represent the first time DC-LDH interactions have been imaged for a range of LDH sizes of this magnitude. Uptake inhibitor studies reveal that treatment with chlorpromazine, a disruptor of clathrin-coated pits on the plasma membrane, diminishes LDH association with THP-1 cells for all three sizes of LDH tested.

Initial experiments looking at the temperature dependence of cell-particle interactions show that association between cells and particles does not decrease at low temperature, implying an inherent attraction between the two surfaces. Experiments assessing the protein dependence of LDH adhesion to cells establish that disrupting the surface proteins with protease enzymes has a negative effect on LDH binding. Additionally, LDH adhesion exhibits a pH dependence that correlates with the changes in the overall surface charges on the cells and particles. Overall, these results show that LDH particles are internalised to varying extents depending on particle size and composition, and that LDH adhesion to the plasma membrane displays both protein and pH dependence.

5.6 References

(1) Flach, T. L.; Ng, G.; Hari, A.; Desrosiers, M. D.; Zhang, P.; Ward, S. M.; Seamone, M. E.; Vilaysane, A.; Mucsi, A. D.; Fong, Y.; Prenner, E.; Ling, C. C.; Tschopp, J.; Muruve, D. A.; Amrein, M. W.; Shi, Y. *Nat. Med.* **2011**, *17*, 479.
(2) Hornung, V.; Bauernfeind, F.; Halle, A.; Samstad, E. O.; Kono, H.; Rock, K. L.; Fitzgerald, K. A.; Latz, E. *Nat. Immunol.* **2008**, *9*, 847.
(3) Conner, S. D.; Schmid, S. L. *Nature* **2003**, *422*, 37.
(4) Marsh, M. *Science* **1999**, *285*, 215.
(5) Stuart, L. M.; Ezekowitz, R. A. B. *Immunity* **2005**, *22*, 539.
(6) Mayor, S.; Pagano, R. E. *Nat. Rev. Mol. Cell Biol.* **2007**, *8*, 603.
(7) Aderem, A.; Underhill, D. M. *Annu. Rev. Immunol.* **1999**, *17*, 593.
(8) Reis e Sousa, C.; Stahl, P. D.; Austyn, J. M. *J. Exp. Med.* **1993**, *178*, 509.
(9) Stahl, P. D.; Ezekowitzt, R. A. B. *Curr. Opin. Immunol.* **1998**, *10*, 50.
(10) Peiser, L.; Mukhopadhyay, S.; Gordon, S. *Curr. Opin. Immunol.* **2002**, *14*, 123.
(11) Cannon, G. J.; Swanson, J. A. *J. Cell Sci.* **1992**, *101*, 907.
(12) May, R. C.; Machesky, L. M. *J. Cell Sci.* **2000**, *114*, 1061.
(13) De Oliveira, C. A.; Mantovani, B. *Life Sci.* **1988**, *43*, 1825.
(14) Lim, J. P.; Gleeson, P. A. *Immunol. Cell Biol.* **2011**, *89*, 836.
(15) Swanson, J.; Watts, C. *Trends Cell Biol.* **1995**, *5*, 424.
(16) Racoosin, E. L.; Swanson, J. A. *J. Cell Sci.* **1992**, *102*, 867.
(17) Champion, J. A.; Walker, A.; Mitragotri, S. *Pharm. Res.* **2009**, *25*, 1815.
(18) Anderson, R. G. W. *Biochemistry* **1998**, *67*, 199.
(19) Schnitzer, J. E.; Oh, P.; Pinney, E.; Allard, J. *J. Cell Biol.* **1994**, *127*, 1217.
(20) Rejman, J.; Oberle, V.; Zuhorn, I. S.; Hoekstra, D. *Biochem. J.* **2004**, *377*, 159.
(21) Henley, J. R.; Krueger, E. W. A.; Oswald, B. J.; Mcniven, M. A. *J. Cell Biol.* **1998**, *141*, 85.
(22) Edidin, M. *Trends Cell Biol.* **2001**, *11*, 492.
(23) Damm, E.-M.; Pelkmans, L.; Kartenbeck, J.; Mezzacasa, A.; Kurzchalia, T.; Helenius, A. *J. Cell Biol.* **2005**, *168*, 477.
(24) Dostert, C.; Pétrilli, V.; Bruggen, R. Van; Steele, C.; Mossman, B. T.; Tschopp, J. *Science* **2008**, *320*, 674.
(25) Schinwald, A.; Donaldson, K. *Part. Fibre Toxicol.* **2012**, *9*, 34.
(26) Bhattacharya, S.; Roxbury, D.; Gong, X.; Mukhopadhyay, D.; Jagota, A. *Nano Lett.* **2012**, *12*, 1826.
(27) Champion, J. A.; Mitragotri, S. *Proc. Natl. Acad. Sci. U.S.A.* **2006**, *103*, 4930.
(28) Oh, J.-M.; Choi, S.-J.; Kim, S.-T.; Choy, J.-H. *Bioconjug. Chem.* **2006**, *17*, 1411.
(29) Xu, Z. P.; Niebert, M.; Porazik, K.; Walker, T. L.; Cooper, H. M.; Middelberg, A. P. J.; Gray, P. P.; Bartlett, P. F.; Lu, G. Q. M. *J. Control. Release* **2008**, *130*, 86.
(30) Nagao, G.; Ishii, K.; Hirota, K.; Makino, K.; Terada, H. *Anticancer Res.* **2010**, *30*, 3167.
(31) Ng, G.; Sharma, K.; Ward, S. M.; Desrosiers, M. D.; Leslie, A.; Schoel, W. M.; Li, T.; Lowell, C. A.; Ling, C.; Amrein, W.; Shi, Y. *Immunity* **2009**, *29*, 807.
(32) Tsuchiya, S.; Yamabe, M.; Yamaguchi, Y.; Kobayashi, Y.; Konno, T.; Tada, K. *Int. J. Cancer* **1980**, *26*, 171.
(33) Sato, Y.; Yokoyama, A.; Shibata, K.; Akimoto, Y.; Ogino, S.; Nodasaka, Y.; Kohgo, T.; Tamura, K.; Akasaka, T.; Uo, M.; Motomiya, K.; Jeyadevan, B.; Ishiguro, M.; Hatakeyama, R.; Watari, F.; Tohji, K. *Mol. Biosyst.* **2005**, *1*, 176.
(34) Auwerx, J. *Cell. Mol. Life Sci.* **1991**, *47*, 22.
(35) Oh, J.-M.; Choi, S.-J.; Lee, G.-E.; Kim, J.-E.; Choy, J.-H. *Chem. Asian J.* **2009**, *4*, 67.
(36) Ledingham, J. C. G. *Proc. R. Soc. London. Ser. B. Contain. Pap. a Biol. Character* **1908**, *80*, 188.
(37) Darzynkiewicz, Z.; Juan, G.; Li, X.; Gorczyca, W.; Murakami, T.; Traganos, F. *Cytometry* **1997**, *27*, 1.
(38) Singer, S. J.; Nicolson, G. L. *Science* **1972**, *175*, 720.
(39) Frye, L. D.; Edidin, M. *J. Cell Sci.* **1970**, *7*, 319.

(40) Schorn, C.; Frey, B.; Lauber, K.; Janko, C.; Strysio, M.; Keppeler, H.; Gaipl, U. S.; Voll, R. E.; Springer, E.; Munoz, L. E.; Schett, G.; Herrmann, M. *J. Biol. Chem.* **2011**, *286*, 35.
(41) Seubert, A.; Monaci, E.; Pizza, M.; O'Hagan, D. T.; Wack, A. *J. Immunol.* **2008**, *180*, 5402.
(42) Chisem, I. C.; Jones, W.; Martın, I.; Martin, C.; Rives, V. *J. Mater. Chem.* **1998**, *8*, 1917.
(43) Frenkel, M. *Anal. Chem.* **1975**, *47*, 598.
(44) Boisvert, M.; Fernandes, S.; Tijssen, P. *J. Virol.* **2010**, *84*, 7782.
(45) Pearse, B. M.; Smith, C. J.; Owen, D. J. *Curr. Opin. Struct. Biol.* **2000**, *10*, 220.
(46) Koivusalo, M.; Welch, C.; Hayashi, H.; Scott, C. C.; Kim, M.; Alexander, T.; Touret, N.; Hahn, K. M.; Grinstein, S. *J. Cell Biol.* **2010**, *188*, 547.
(47) Erbacher, P.; Roche, A. C.; Monsigny, M.; Midoux, P. *Exp. Cell Res.* **1996**, *225*, 186.
(48) Hasebe, R.; Suzuki, T.; Makino, Y.; Igarashi, M.; Yamanouchi, S.; Maeda, A.; Horiuchi, M.; Sawa, H.; Kimura, T. *BMC Microbiol.* **2010**, *10*, 165.
(49) Kool, M.; Fierens, K.; Lambrecht, B. N. *J. Med. Microbiol.* **2012**, *61*, 927.
(50) Schaer, C. A.; Laczko, E.; Schoedon, G.; Schaer, D. J.; Vallelian, F. *Oxid. Med. Cell. Longev.* **2013**, *2013*, 1.
(51) Wang, L.; Rothberg, K. G.; Anderson, R. G. W. *J. Cell Biol.* **1993**, *123*, 1107.
(52) Sipos, T.; Merkel, J. R. *Biochemistry* **1970**, *9*, 2766.
(53) Phillips, D. R. *Biochemistry* **1972**, *11*, 4582.
(54) Bathoorn, E.; Daly, P.; Gaiser, B.; Sternad, K.; Poland, C.; Macnee, W.; Drost, E. M. *Int. J. Inflam.* **2011**, *2011*, 1.
(55) Tang, J. *Nature* **1963**, *199*, 1094.
(56) Amri, E.; Mamboya, F. *Am. J. Biochem. Biotechnol.* **2012**, *8*, 99.
(57) Sigma-Aldrich. Analytical Enzymes: Papain http://www.sigmaaldrich.com/life-science/metabolomics/enzyme-explorer/analytical-enzymes/papain.html.
(58) Martin, M. M.; Lindqvist, L. *J. Lumin.* **1975**, *10*, 381.
(59) Li, X.; Sloat, B. R.; Yanasarn, N.; Cui, Z. *Eur. J. Pharm. Biopharm.* **2011**, *78*, 107.
(60) Malvern Instruments. *Zeta Potential: An Introduction in 30 Minutes (Zetasizer Nano series technical note)*; Vol. 2, pp. 1–6.
(61) Wilson, W. W.; Wade, M. M.; Holman, S. C.; Champlin, F. R. *J. Microbiol. Methods* **2001**, *43*, 153.
(62) Cooper, G. M. *The Cell: A Molecular Approach.*; 2nd ed.; Sinauer Associates: Sunderland (MA), 2000.
(63) Chung, H.-E.; Park, D.-H.; Choy, J.-H.; Choi, S.-J. *Appl. Clay Sci.* **2012**, *65-66*, 24.
(64) Xu, Z. P.; Zeng, Q. H.; Lu, G. Q.; Yu, A. B. *Chem. Eng. Sci.* **2006**, *61*, 1027.
(65) Perry, D. G.; Daugherty, G. L.; Martin, W. J. *J. Immunol.* **1999**, *162*, 380.
(66) Kong, X.; Rao, X.; Han, J.; Wei, M.; Duan, X. *Biosens. Bioelectron.* **2010**, *26*, 549.
(67) Charradi, K.; Forano, C.; Prevot, V.; Madern, D.; Ben Haj Amara, A.; Mousty, C. *Langmuir* **2010**, *26*, 9997.
(68) Shao, M.; Ning, F.; Zhao, J.; Wei, M.; Evans, D. G.; Duan, X. *J. Am. Chem. Soc.* **2012**, *134*, 1071.
(69) Zeng, H.; Wang, Y.; Feng, Z.; You, K.; Zhao, C.; Sun, J.; Liu, P. *Catal. Letters* **2010**, *137*, 94.
(70) Tao, Q.; He, H.; Frost, R. L.; Yuan, P.; Zhu, J. *Appl. Surf. Sci.* **2009**, *255*, 4334.
(71) Tao, Q.; He, H.; Li, T.; Frost, R. L.; Zhang, D.; He, Z. *J. Solid State Chem.* **2014**, *213*, 176.
(72) Eisenbarth, S. C.; Colegio, O. R.; O'Connor, W.; Sutterwala, F. S.; Flavell, R. A. *Nature* **2008**, *453*, 1122.
(73) Lamkanfi, M.; Mueller, J. L.; Vitari, A. C.; Misaghi, S.; Fedorova, A.; Deshayes, K.; Lee, W. P.; Hoffman, H. M.; Dixit, V. M. *J. Cell Biol.* **2009**, *187*, 61.
(74) Kolly, L.; Busso, N.; Palmer, G.; Talabot-Ayer, D.; Chobaz, V.; So, A. *Immunology* **2010**, *129*, 178.
(75) Kummer, J. A.; Broekhuizen, R.; Everett, H.; Agostini, L.; Kuijk, L.; Martinon, F.; van Bruggen, R.; Tschopp, J. *J. Histochem. Cytochem.* **2007**, *55*, 443.

Chapter Six: Experimental Methods

6.1 Analytical techniques for LDH characterisation

6.1.1 Powder X-ray diffraction

Powder X-ray diffraction (XRD) data were recorded on a PANalytical X'pert Pro diffractometer operating at 40 kV/40 mA. Samples were placed into steel sample holders, which were spun at 15 RPM during recording, and analysed from 2° to 75° using Cu kα radiation (λ = 1.54178 Å) and a slit size of 2°.

6.1.2 Fourier transform infrared spectroscopy

Fourier transform infrared (FTIR) spectra were recorded on a Bio-Rad FTS-6000 instrument. Samples were mounted on a DuraSamplIR Diamond ATR stage, and absorbance recorded between 700-6000 cm^{-1}, 128 scans with 4 cm^{-1} resolution. A background absorbance from the diamond surface is observed in the 1900-2350 cm^{-1} region of the spectrum

6.1.3 Elemental analysis

Elemental analyses for carbon, hydrogen and nitrogen were performed by Stephen Boyer at the School of Human Sciences, London Metropolitan University, using the quantitative combustion technique.

6.1.4 Thermogravimetric analysis

Thermogravimetric analysis (TGA) was carried out on a Perkin Elmer TGA7 with a TAC7/DX thermal analysis controller. A few milligrams of sample were placed in a platinum crucible suspended from a platinum wire, which was weighed empty first. Sample mass was recorded under a continuous flow of N_2 from room temperature to 600 °C at 10 °C/minute. At the start of the program several minutes at room temperature were included to allow the sample mass to settle, and at the final temperature to ensure mass loss was complete.

6.1.5 Scanning electron microscopy and energy dispersive X-ray spectroscopy

Scanning electron microscopy (SEM) and energy dispersive X-ray (EDX) spectroscopy were conducted at the Research Complex at Harwell on a JSM-6610LV low vacuum SEM fitted with an EDX spectrometer at an accelerating voltage of 20 kV. Prior to analysis, samples were mounted on adhesive carbon tape attached to metal stubs, and sputter-coated with a

10 nm layer of platinum using a Quorum Q150T ES Sputter Coater/Carbon Coater to facilitate imaging. Signals from the platinum were excluded when analysing the EDX results.

6.1.6 Transmission electron microscopy

Transmission electron microscopy (TEM) was carried out at the Research Complex at Harwell on a Jeol JEM-2100 TEM at an accelerating voltage of 200 kV fitted with a LaB_6 filament. Some samples were analysed at the Department of Materials, University of Oxford, on a JEOL 4000EX microscope at either 80 kV (low magnification) or 400 kV (high magnification). Samples were prepared by dispersing a few milligrams of material in ethanol with sonication for 20 minutes, then drying onto carbon films on copper grids (300 mesh, Agar scientific) and allowing to dry. Image analysis was undertaken using Image J software.[1]

6.1.7 Atomic force microscopy

Atomic force microscopy (AFM) studies were conducted at the Surface Analysis Facility, Department of Chemistry, University of Oxford, on a Multimode Nanoscope (Digital Instruments) by Dr Robert Jacobs. Samples were prepared for AFM by dispersing a few milligrams in ethanol, then spin coating at 3000 RPM for 30 seconds onto a highly ordered pyrolytic graphite (HOPG) substrate. Measurements were conducted at room temperature in tapping mode with a 4909E piezoelectric scanner and a μmasch NSC15/Al BS tip (resonance frequency of 325 kHz).

6.1.8 Dynamic light scattering and zeta potential measurements

Zeta potentials and dynamic light scattering (DLS) measurements were performed at the Department of Materials (University of Oxford) at Begbroke Science Park. In preparation for zeta potential/DLS measurements, LDHs were dispersed in phosphate buffered saline (PBS, #D8537, Sigma-Aldrich) at a concentration of 10 mg/mL by sonication for approximately 30 minutes. Zeta potential measurements were made directly on the resulting suspension, using a Malvern Zetasizer (Nano series) with a folded capillary cell. The pH of the suspensions was measured using a Hanna instruments 8424 microcomputer pH meter.

For DLS measurements, 50 μL of the LDH suspension in PBS was added to 1 mL of RPMI-1640 (#R0883, Sigma-Aldrich) supplemented with 10% fetal calf serum (FCS, #10270-098, Gibco Life Technologies), 2 mM L-glutamine (#G7513, Sigma-Aldrich), 50 U/mL penicillin and 50 μg/mL streptomycin (#P4333, Sigma-Aldrich), to give a final concentration of 500 μg/mL, identical to that used in the majority of biological assays. Samples were placed in folded capillary cells, and measured at the default angle of 173° using

non-invasive backscatter technology. For both techniques, samples were allowed to equilibrate to 25 °C for two minutes prior to measurement and multiple readings were taken to produce an average.

6.1.9 Endotoxin testing

LDH samples were dispersed at 10 mg/mL in sterile PBS and shaken for two hours. Aliquots of the PBS were sent for testing at Lonza, *via* the Rapid-Endotest service where they were analysed using the Kinetic QCL™ limulus amebocyte assay.

6.2 General biological techniques

Unless specified otherwise, all biological assays and cell culture were conducted at the Nuffield Department of Surgical Sciences, Level 6, John Radcliffe Hospital.

6.2.1 Generation of monocyte-derived dendritic cells

Human monocyte-derived dendritic cells (Mo-DC) were isolated from leukocyte cones (National Blood Service) taken from healthy donors. Cones were drained into 50 mL centrifuge tubes under aseptic conditions, and the volume made up to approximately 35 mL using sterile PBS. Samples were underlaid with around 12 mL of density gradient medium (Lymphoprep, #07811, Stemcell Technologies), then centrifuged at 2000 RPM with slow acceleration and the brake switched off. The white interface layer was extracted, and washed twice with PBS supplemented with 2% FCS (first wash at 1400 RPM, second wash at 1200 RPM, both for ten minutes). The third wash was with PBS/EDTA (#BE02-017F, BioWhittaker) supplemented with 2% FCS at 1000 RPM for ten minutes. At this point, the resulting peripheral blood monocytic cells (PBMC) were enriched for monocytes using Stemcell Easysep™ human monocyte enrichment kits (#19059, Stemcell Technologies), following the manufacturer's instructions. Isolated monocytes were washed twice with Hank's balanced salt solution (HBS, #H8264, Sigma-Aldrich) with 2% FCS then re-suspended at 5 x 10^5 cell/mL in RPMI with 10% FCS, 2 mM L-glutamine, 50 U/mL penicillin and 50 µg/mL streptomycin (referred to as complete RPMI from this point forwards) supplemented with 1000 U/mL granulocyte macrophage colony-stimulating factor (GM-CSF, #300-03, PeproTech; or #04-rHuGM-CSF, Gentaur) and 500 U/mL interleukin-4 (IL-4, #200-04, PeproTech) and kept in 75 cm^2 tissue culture flasks (Corning) at a maximum of 60 mL cells/flask at 37 °C in a humidified 5% CO_2 atmosphere. Mo-DC were cultured for six days from isolation before use. On day three, one third of the volume of cells was removed, centrifuged at 1200 RPM for seven minutes, the supernatant decanted and the cells re-

suspended in an equivalent volume of fresh medium with cytokines, and returned to the original flask.

6.2.2 THP-1 cell line culture

Cells of the human monocytic cell line THP-1 were obtained from the Department of Medicine, University College London. Cells were maintained using aseptic techniques in complete RPMI, supplemented with 2-mercaptoethanol (#M7522, Sigma-Aldrich) at a working concentration of 50 μM in incubators at 37 °C, in a 5% CO_2 humidified atmosphere. Cells were placed in a 75 cm^2 tissue culture flask at a starting concentration of 2 x 10^5 cells/mL, 20 mL per flask, and sub-cultivated approximately every six to eight days to the starting concentration in fresh medium.

6.2.3 Freezing and thawing cell samples

Cells were frozen in cryovials at >1 x 10^6 cells/vial in Voluven® (6% hydroxyethyl starch in 0.9% sodium chloride), supplemented with 5% dimethyl sulfoxide (DMSO, #D2650, Sigma-Aldrich) and 7% FCS. Cells were cooled to -80 °C in freezing containers which limit the cooling rate to approximately 1 °C/minute. Vials were then transferred to liquid nitrogen storage. Samples were thawed by placing the cryovials in a 37 °C water bath until contents had defrosted, then immediately diluted in chilled PBS supplemented with 2% FCS (PBS/FCS), centrifuged for 5 minutes at 1200 RPM/4 °C then re-suspended in fresh medium.

6.2.4 Flow cytometry

Flow cytometry was performed on a BD FACS CANTO II instrument, with the BD FACSDiva™ Software package. Subsequent data analysis was performed using FlowJo software. Unless specified, samples were analysed as soon as staining was complete.

6.3 Experimental procedures for Chapter Two

6.3.1 Starting materials

$Mg(NO_3)_2 \cdot 6H_2O$, Na_2CO_3, $MgCl_2 \cdot 6H_2O$, urea, $LiOH \cdot H_2O$ and $Ca(NO_3)_2 \cdot 4H_2O$ were all obtained from Sigma-Aldrich. $Al(NO_3)_3 \cdot 9H_2O$, $AlCl_3 \cdot 6H_2O$, $NaNO_3$ and $CaCl_2$ were purchased from Fluka Analytical. $FeCl_3$ (anhydrous) and $Fe(NO_3)_3 \cdot 9H_2O$ were from BDH chemicals. Hexamethylenetetramine (HMT) was from Riedel de Haën. NaOH pellets were from Fisher Scientific.

6.3.2 Synthesis of MgAl-CO_3 LDHs

20 nm MgAl-CO_3 LDH particles: 150 mL of a solution of $Mg(NO_3)_2$ (75 mM) and $Al(NO_3)_3$ (25 mM) was added dropwise at room temperature with stirring to 150 mL of a 0.5 M Na_2CO_3 solution. A constant pH of 12 was maintained by appropriate addition of 3 M NaOH to the reaction mixture using an auto-titrator (Syrris, Atlas Syringe Pump). Products were washed two or three times with deionised (DI) H_2O using centrifugation (five minutes at 4000 RPM), followed by one final wash in acetone, re-suspension in acetone and drying in air at room temperature. Unless stated otherwise, all LDH products were isolated and washed in this fashion.

60 nm MgAl-CO_3 LDH particles: 100 mL of a solution of $Mg(NO_3)_2$ (0.8 M) and $Al(NO_3)_3$ (0.3 M) was added dropwise to 100 mL of a solution of Na_2CO_3 (0.4 M) and NaOH (1.5 M) at 90 °C with stirring. The reaction mixture was aged for 72 hours at 90 °C.

40, 70, 190, 200 and 400 nm MgAl-CO_3 LDH particles: 20 mL of a solution of $MgCl_2$ (3 mM) and $AlCl_3$ (1 mM) was added quickly to 80 mL of a solution of NaOH (0.15 M) and Na_2CO_3 (0.036 M). The mixture was stirred vigorously for ten minutes then transferred to Teflon lined autoclaves and placed in a pre-heated oven for the temperature and reaction times specified in Chapter Two. After removal from the oven, autoclaves were left to cool to room temperature and the products washed as outlined above.

1070, 2160, 2560 and 9900 nm MgAl-CO_3 LDH particles: A solution of $Mg(NO_3)_2$ (0.1 M) and $Al(NO_3)_3$ (0.05 M) was prepared, then HMT added so that the concentration of HMT varied between 0.24 M and 0.13 M. After ten minutes vigorous stirring, the mixture was transferred to autoclaves and heated at 140 °C for 24 hours. Synthesis using urea as the ARR was performed as follows: 0.1 M $MgCl_2$ and $AlCl_3$ solutions and a 1 M urea solution were prepared. These were mixed in the volume ratio 4:1:10 (Mg:Al:Urea), stirred vigorously for ten minutes then transferred to autoclaves and heated at 100 °C for 24 hours.

6.3.3 Synthesis of LiAl-CO_3 LDHs

10, 30 and 100 nm LiAl-CO_3 LDH particles: 250 mL of a 0.4 M solution of $Al(NO_3)_3$ was added dropwise with continuous stirring to 600 mL of a solution of LiOH (1.86 M) and Na_2CO_3 (0.17 M). Solutions were aged overnight at either room temperature (10 nm LiAl-CO_3 LDH) or 75 °C (100 nm LiAl-CO_3 LDH). The resulting precipitate was isolated using vaccum filtration and washed repeatedly with DI H_2O, with a final acetone wash. For

the 30 nm LiAl-CO_3, 125 mL of a 0.4 M $Al(NO_3)_3$ solution was added dropwise to 300 mL of a LiOH (1.5 M) $NaNO_3$ (0.67 M) solution and aged overnight at room temperature.

350 and 810 nm LiAl-CO_3 LDH particles: 42 mL of a 0.4 M $Al(NO_3)_3$ solution was added rapidly to 100 mL of a solution of LiOH (0.24 M) and Na_2CO_3 (0.17 M). The mixture was stirred vigorously for 10 minutes then transferred to Teflon lined autoclaves and placed in a pre-heated oven at either 100 °C (350 nm particles) or 120 °C (810 nm particles) for 24 hours.

1240 nm LiAl-CO_3 LDH particles: 15 mL of a 0.1 M $AlCl_3$ solution and 15 mL of a 0.1 M LiCl solution were mixed vigorously with 100 mL of a 1 M solution of urea for 10 minutes. The reaction mixture was transferred to Teflon lined autoclaves and placed in a pre-heated oven at 100 °C for 24 hours.

6.3.4 Synthesis of MgFe-CO_3 LDHs

20 nm MgFe-CO_3 LDH particles: 150 mL of a solution of $Mg(NO_3)_2$ (0.75 M) and $Fe(NO_3)_3$ (0.25 M) was added dropwise to 150 mL 0.5 M Na_2CO_3, with the pH maintained at 12.5 by addition of 3 M NaOH using an auto-titrator. The reaction mixture was aged at room temperature for 24 hours.

70 nm MgFe-CO_3 LDH particles: 150 mL of a solution of $FeCl_3$ (0.17 M) and $MgCl_2$ (0.33 M) was heated to 80 °C then the pH raised to 10 by dropwise addition of a solution of NaOH (1.5 M) and Na_2CO_3 (0.7 M). The resulting precipitate was aged at 80 °C overnight.

60, 100 and 180 nm MgFe-CO_3 LDH particles: 100 mL of a solution of $MgCl_2$ (3 mM) and $FeCl_3$ (1 mM) was mixed with 200 mL of a solution of NaOH (0.15 M) and Na_2CO_3 (0.28 M) and stirred vigorously for 10 minutes. The reaction mixture was then transferred to Teflon lined autoclaves and moved to a preheated oven at either 70 (60 nm), 90 (100 nm) or 120 °C (180 nm) for 24 hours.

6.3.5 Synthesis of other LDHs

All solutions used for synthesising LDHs containing anions other than carbonate were degassed by bubbling N_2 through them for at least 10 minutes prior to use.

6.3.5.1 MgAl-NO_3 LDHs

70 nm MgAl-NO_3 LDH particles: 80 mL of a solution of $Mg(NO_3)_2$ (1 M) and $Al(NO_3)_3$ (0.35 M) was added dropwise to 100 mL of a solution of NaOH (1.5 M) and $NaNO_3$ (1.12 M) at 90 °C with stirring, under flowing N_2. The reaction mixture was sealed from air and aged

for approximately 72 hours at 90 °C and the product isolated using vacuum filtration, washed repeatedly with DI H_2O, dispersed in acetone and dried at room temperature.

160 nm MgAl-NO_3 LDH particles: 100 mL of a solution of $Mg(NO_3)_2$ (3 mM) and $Al(NO_3)_3$ (1 mM) was added quickly to 400 mL of a solution of NaOH (0.14 M) and $NaNO_3$ (0.3 M) and stirred vigorously for ten minutes under flowing N_2. The reaction mixture was transferred to autoclaves and heated at 150 °C for 24 hours.

6.3.5.2 MgAl-Cl LDH

100 mL of a solution of $MgCl_2$ (0.55 M) and $AlCl_3$ (0.28 M) was added dropwise to 100 mL of a solution of NaCl (1 M) and NaOH (1.75 M) at 80 °C under flowing N_2. The reaction mixture was sealed under N_2 and aged for approximately 72 hours at 80 °C. The product was isolated using vacuum filtration and washed repeatedly with DI H_2O, with a final acetone wash and dried at room temperature.

6.3.5.3 MgFe-NO_3 LDH

100 mL of a solution of $Mg(NO_3)_2$ (0.55 M) and $Fe(NO_3)_3$ (0.28 M) was added dropwise to 100 mL of a solution of NaOH (1.75 M) and $NaNO_3$ (1 M) at 80 °C under flowing N_2, with the pH kept above 8. The reaction mixture was sealed under N_2 and aged for 3 days at 80 °C. The product was isolated using vacuum filtration and washed repeatedly with DI H_2O, with a final wash using acetone and dried at room temperature.

6.3.5.4 CaAl-NO_3 LDH:

40 mL of a degassed solution of $Ca(NO_3)_2$ (0.9 M), $Al(NO_3)_3$ (0.39 M) and $NaNO_3$ (1.32 M) was adjusted to pH 11.5 by addition of 4 M NaOH using an auto-titrator. The reaction mixture was sealed under N_2 and aged overnight at room temperature.

6.3.5.5 CaAl-Cl LDH

250 mL of a degassed 3:2 ethanol:water mix was adjusted to pH 4 using HCl, followed by adjustment to pH 11.5 using 2 M NaOH with an autotitrator. 10 mL of a solution of $CaCl_2$ (0.89 M) and $Al(NO_3)_3$ (0.33 M) was then added dropwise, with pH maintained at 11.5. The reaction mixture was sealed under N_2 and aged at 65 °C for 24 hours.

6.4 Experimental procedures for Chapter Three

6.4.1 Set-up of Mo-DC assays

LDHs were weighed and dispersed in sterile PBS by sonicating for approximately 30 minutes to give 10 mg/mL suspensions. Imject (#77161, Thermoscientific) and Alhydrogel (#vac-alu-50, InvivoGen) were also diluted to 10 mg/mL in PBS.

Mo-DCs isolated as described in Section 6.2.1 were harvested on day six under aseptic conditions, counted, and re-suspended in fresh medium (complete RPMI with GM-CSF and IL-4) at 5×10^5 cells/mL, then 200 μL/well of cells were seeded in flat-bottomed 96-well tissue culture plates and 10 μL of the 10 mg/mL LDH or commercial adjuvant suspension was added to the wells. LPS (Lipopolysaccharides from *Eescherichia coli* 055:B5, #L4005, Sigma-Aldrich) was added to positive control wells at 10 ng/mL. 10 μL of sterile PBS was added to negative control wells. Three technical replicates were used for each condition. Plates were incubated overnight (approximately 16-18 hours) at 37 °C in a humidified 5% CO_2 atmosphere.

6.4.2 Surface molecule and viability staining

After overnight incubation, plate contents were transferred to round-bottomed 96-well plates and kept on ice. Well contents were pelleted (1500 RPM, 2 minutes, 4 °C), then 150 μL supernatant decanted into separate 96-well plates and frozen for later cytokine analysis using ELISAs. The pellets were re-suspended in 150 μL PBS/EDTA, supplemented with 2% FCS, and aliquots from wells subjected to the same treatment pooled for isotype controls. Cells were then pelleted and re-suspended in 50 μL surface molecule antibody staining mix (in HBS supplemented with 2% FCS – HBS/FCS) and incubated for 30 minutes on ice in the dark. Details of the antibodies and isotypes used may be found in Table 6.1.

Table 6.1: Antibodies and isotype controls used for anlaysis of surface molecule expression by Mo-DC.

Surface molecule	Antibody and fluorophore	Manufacturer	Catalogue number	Isotype control	Catalogue number
CD86	anti-CD86 PE	eBioscience	#12-0869	mouse IgG2bκ	#12-4732
CD274 (B7-H1)	anti-B7-H1 PE-Cy7	eBioscience	#25-5983	mouse IgG1κ	#25-2714
CD40	anti-CD40 APC	eBioscience	#17-0409	mouse IgG1κ	#17-4714
MHC class II (HLA-DR)	anti-HLA-DR APCefluor®780	eBioscience	#47-9956	mouse IgG2bκ	#47-4732
CD83	anti-CD83 Brilliant Violet™ 421	Biolegend	#305324	mouse IgG1κ	#400157
CD275 (B7-H2)	anti-B7-H2 APC	eBioscience	#17-5889	mouse IgG1κ	#17-4714
MHC class I (HLA-A,B,C)	anti-HLA-ABC PE-Cy7	eBioscience	#25-9983	mouse IgG2aκ	#25-4724

After this cells were washed once with HBS/FCS, then re-suspended in 100 µL/well HBS/FCS with 2 µg/mL 7-AAD (#A9400, Sigma-Aldrich). For some experiments, Annexin V staining was also performed. Following incubation with the surface staining mix, cells were washed once with PBS, then re-suspended in 20 µL of a 0.5 µg/mL Annexin V-FITC solution (#A9210, Sigma-Aldrich) in binding buffer [100 mM HEPES (#H3375), 1.4 M NaCl, 25 mM $CaCl_2$ (all from Sigma-Aldrich)]. After incubation for 10 minutes at room temperature, 180 µL of binding buffer was added, cells washed once with 200 µL of binding buffer, then re-suspended in a 2 µg/mL 7-AAD solution. Cells were analysed by flow cytometry immediately after staining was complete.

6.4.3 Resazurin assays

Resazurin assays were conducted in the Deparment of Zoology, University of Oxford. Mo-DC assays were set up as described in Section 6.4.1 in flexible flat-bottom plates (BD Falcon) suitable for reading on a plate reader. After overnight incubation, 20 µL of a 0.5 mM stock solution of resazurin (#R7017, Sigma-Aldrich) was added directly to the wells, and the plates incubated at 37 °C in a humidified 5% CO_2 atmosphere. After two hours, the absorption of the wells was recorded at 600 nm on a Fluostar Omega microplate reader (BMG Labtech). Titrations of cells at known concentrations were used as standard curves to quantify overall cell number, and were analysed using a linear regression fit on Omega software (BMG Labtech).

6.4.4 TNF-α, IL-6 and IL-1β ELISAs

TNF-α and IL-6 ELISAs: purified anti-human TNF-α (#50282), biotinylated anti-human TNF-α (#502904), purified anti-human IL-6 (#501102) and biotinylated anti-human IL-6 (#501202) matching antibody pairs were all purchased from Biolegend. Immunosorbent plates (#442404, NUNC-IMMUNO Plate F96 Immunosorp) were coated overnight at 4 °C by agitation with capture antibody solutions (anti-TNF-α, 2 µg/mL; or anti-IL-6, 1 µg/mL) in a pH 9.4 Na_2CO_3/$NaHCO_3$ buffer. The next day, plates were aspirated and washed four times with PBS/0.05% Tween®20 (#P5927, Sigma-Aldrich) using a Molecular Devices Skan Washer 400, then blocked with 300 µL assay diluent [PBS/0.05% Tween®20/2% bovine serum albumin (#A7906, Sigma-Aldrich)] for one hour at room temperature. Plates were aspirated and washed again, then 50 µL of assay supernatant or 50 µL of standard solution in assay diluent (TNF-α standard: #25-45-97B, Insightbio; IL-6 standard: #39-8069, eBioscience) were added and plates sealed and incubated for a further two hours at room temperature. Standard curves were performed as ten serial halving dilutions from

4000 pg/mL, with assay diluents as the 0 pg/mL control. Plates were washed/aspirated again, then detection antibodies added (both at 0.5 μg/mL), and plates sealed and incubated at room temperature for one hour. After another wash/aspirate step, 100 μL/well of a horse radish peroxidise conjugated streptavadin solution (#016-030-084, Jackson ImmunoResearch Laboratories) in assay diluent was added, and plates sealed and incubated at room temperature for one hour. Following a final wash/aspirate, 100 μL/well of 2,2′-Azino-bis(3-ethylbenzothiazoline-6-sulfonic acid) (2,2-ABS) liquid substrate (#A3219, Sigma-Aldrich) was added, and the plates analysed at 405 nm every five minutes on a Anthos Lucy 1 luminometer.

IL-1β ELISAs: Human IL-1β Ready-SET-Go! ELISA kits (#88-7010) were purchased from eBioscience and used according to the manufacturer's instructions. Additional reagents needed but not supplied in the kits were the same as those detailed above.

6.4.5 Luminex assays

Mo-DCs from three donors were produced as described in Section 6.2.1, then incubated overnight in flat-bottomed 96-well plates with two/three particle sizes for each of the three main LDH compositions at 500 μg/mL (MgAl-CO_3, 40, 190 and 2560 nm; LiAl-CO_3, 10 and 810 nm; MgFe-CO_3, 20 and 100 nm). LPS (10 ng/mL) was used as a positive control and untreated cells as a negative control. After overnight incubation, supernatants were harvested. These were then analysed using two Milliplex® Map kits (#HCYTOMAG-60K-09, Merck Millipore) covering the range of cytokines/chemokines described in Chapter Three, according to the manufacturer's instructions. Plates were washed using a Tecan Hydroflex plate washer. Samples were analysed on a Luminex200® instrument (Merck Millipore) using Xponent software. Thanks are given to Dr. Janet Digby, (Division of Cardiovascular Medicine, University of Oxford, West Wing, John Radcliffe Hospital) for her assistance with running the assays.

6.4.6 General data processing

Much of the data in Chapter Three was collected for multiple donors. Therefore, to normalise data between donors, linear mixed effects models [lme() function in the nlme library in [R]][2,3] was fitted by the restricted maximum likelihood approach (REML) on the logged raw data, with donor as a random effect and the conditions as fixed effects. This produced estimates and 95% confidence intervals which, for graphing purposes, may be converted back into experimental units by calculating the corresponding exponential values. Visual checks for

normality in the logged data were performed by looking at density plots. Additionally, significance data (p-values) were calculated in the lmerTest package in [R], using similar models to those outlined above (i.e. donor as a random effect, conditions as fixed effects).[4]

6.4.7 Statistical modelling

Statistical modelling was conducted in [R][3] by Dr George Nicholson, Department of Statistics, University of Oxford.

6.4.7.1 Data pre-processing

Values above or below the detectable range for the DC cytokine responses were limited to the upper or lower values for the limits of detection. To obtain estimated mean differences between the DC response for each condition and the unstimulated control condition across technical replicates and donors, a robust linear model [rlm() function in [R]][5] with donor and condition as fixed effects was fitted. The LDH property data was analysed for correlation between properties. When high correlation was found between a pair of properties (correlation coefficient, $|r| > 0.95$), only one property in the pair was used in the analysis. The standard reduction potential of $M^{1+/2+}$ correlated strongly with the electronegativity of $M^{1+/2+}$ ($r = 0.99$), and *a*-parameter ($r = -0.95$), so only the standard reduction potential of $M^{1+/2+}$ was retained in the analysis. Particle size was log-transformed and standardised to zero mean and unit variance.

6.4.7.2 Model fitting

After normalisation, linear models [lm() function in [R]] were fitted to the estimates of DC response for each of the various permutations of three or four LDH properties using linear regression. The function of size [*f*(size)] takes the form of a natural cubic spline [ns() function in [R]].[6] Up to four basis functions, (Equation 6.1) referred to in Chapter Three as degrees of freedom (DOFs), were used to model each response, giving a maximum of three knots, interpolated in such as a way as to maintain continuous first and second derivatives throughout the spline. The Bayesian Information Criterion (BIC) was used to select models (Equation 6.2).[7]

$$y = a + bx + cx^2 + dx^3$$

Equation 6.1: Basis function for natural cubic spline. *a*, *b*, *c* and *d* are constants.

$$BIC = -2\ell + Klog(n)$$

Equation 6.2: The Bayesian Information Criterion. ℓ is the maximum likelihood, K is the number of parameters in the model and n is the sample size.

6.4.7.3 Model evaluation

The predictive ability of a model was assessed by excluding all sizes of a given LDH composition from the data, then using the remaining data and the physicochemical properties specified to predict the excluded values. Comparisons between the predicted and observed values could then be made, to assess how well the model predicts the responses to the excluded LDH composition. The four measures used to assess the predictive ability of 'leave-one-composition-out' cross-validation are supplied in Equations 6.3 to 6.6.

$$RMSE = \sqrt{\frac{1}{n}\sum_{i=1}^{n}\left(y_i^{pred} - y_i\right)^2}$$

Equation 6.3: Root mean square error. $\boldsymbol{y_i^{pred}}$ and $\boldsymbol{y_i}$ are the predicted and observed values respectively for a given LDH size and composition.

$$LS = \sum_{i=1}^{n} logN\left(y_i | y_i^{pred}, SE(y_i^{pred})\right)$$

Equation 6.4: Logarithmic score of a Gaussian probabilistic prediction. SE = standard error. N is the density function of a normal distribution with mean μ and standard deviation σ.[8]

$$r = \frac{E\left[\left(y_i - \mu_y\right)\left(y_i^{pred} - \mu_{y^{pred}}\right)\right]}{\sigma_y \sigma_{y^{pred}}}$$

Equation 6.5: Pearson's correlation coefficient. E denotes the expectation value (or mean), $\boldsymbol{\mu_y}$ and $\boldsymbol{\mu_{y^{pred}}}$ are the observed and predicted means respectively, and $\boldsymbol{\sigma_y}$ and $\boldsymbol{\sigma_{y^{pred}}}$ are the standard deviations of the means of all observed and predicted values respectively.

$$Q^2 = 1 - \frac{RMSE^2}{\frac{1}{n}\sum_{i=1}^{n}\left(y_i - \mu_y\right)}$$

Equation 6.6: Equation for Q^2. RMSE is the root mean square error as determined in Equation 6.3.

6.5 Experimental procedures for Chapter Four

6.5.1 LiAl-CO_3 LDH synthesis from gibbsite

LiAl-Cl LDH was synthesised by treating a suspension of gibbsite with a four-fold molar excess of LiCl at 90 °C for 24 hours. The product was isolated by vacuum filtration and washed repeatedly with water and acetone. To form the carbonate intercalated product, 1 g of the LiAl-Cl LDH was added to 200 mL of a 0.1 M Na_2CO_3 solution and stirred at 80 °C for three hours. The product was isolated using centrifugation as outlined in Section 6.3.

6.5.2 Naïve and memory T cell isolation

PBMCs were isolated as described in the Mo-DC preparation in Section 6.2.1. To isolate naïve/memory T cells, Stemcell Easysep™ human naïve/memory $CD4^+$ (naïve: #19155/memory: #19157) and $CD8^+$ (naïve: #19158/memory: #19159) enrichment kits were used according to the manufacturer's instructions. Small samples of cells were frozen for later purity analysis. Whole T cells were isolated using the Easysep™ human T cell enrichment kit (#19051).

6.5.3 Mixed leukocyte reaction set-up

Freshly isolated $CD4^+$ and $CD8^+$ naïve/memory T cells (or whole T cells in the prelimnary timecourse experiment) were washed once with HBS, then re-suspended in 2 mL of a 10 μM solution of carboxyfluoroscein succinimidyl ester (CFSE, eBiocience #65-0850-85) in RPMI medium (without FCS, antibiotics etc.) and incubated for 10 minutes at 37 °C in a waterbath. The reaction was quenched by adding 10 mL of complete RPMI. Cells were then centrifuged (1200 RPM, 10 minutes) and re-suspended in fresh medium at a concentration of 1×10^6 T cells/mL in a 1:1 $CD4^+$:$CD8^+$ ratio. 100 μL/well of T cells were seeded in 96-well tissue culture plates, then the total volume per well was made up to 200 μL by adding 100 μL of a 1×10^5 cells/mL suspension of fresh allogeneic Mo-DCs (cultured as detailed in Section 6.2.1), to give final concentrations of 5×10^5 T cells/mL and 5×10^4 Mo-DCs/mL (1:10 ratio). For T cell only wells, 100 μL of complete RPMI was added instead of DCs. Stimuli were then added: positive controls (LPS), negative controls (sterile PBS), commercial adjuvants and LDH suspensions were used as detailed in Section 6.4.1. For the initial time course, each condition was tested in duplicate. For the main naïve/memory T cell experiments, all conditions were set up in triplicate. Due to the length of incubation time, only wells in the middle of the plate were used, and the outer wells were filled with 200 μL PBS to

reduce evaporation. Plates were subsequently incubated for the lengths of time specified in Chapter Four at 37 °C in a humidified 5% CO_2 atmosphere.

6.5.4 Generation of positive controls for intracellular cytokine staining

All antibody controls were generated from stocks of frozen human PBMCs/T cells, treated as described in Section 6.2.3.

6.5.4.1 IFN-γ (T_h1) positive cells

PBMCs and T cells were each diluted to 1 x 10^6 cells/mL in complete RPMI and mixed in a 1:1 ratio. The cell mix was placed in a 6-well plate, 5 mL of cells per well and incubated at 37 °C in a humidified 5% CO_2 atmosphere for two days. On day two, LPS was added at a final concentration of 25 ng/mL and cells incubated for a further three days. On day five, cells were frozen at 1 x 10^6 cells/vial, as described in Section 6.2.3. Analysis by flow cytometry of the live cells in the lymphocyte gate showed approximately 20% were IFN-γ positive.

6.5.4.2 IL-4 (T_h2) positive cells

A 1:1 mix of T cells with allogeneic PBMCs was prepared as outlined for the IFN-γ positive cells. Monophosphoryl lipid A (MPLA, InvivoGen, #tlrl-mpl) was added at 1μg/mL, cells were placed in flat-bottomed 96-well plates (200 μL/well) and incubated for seven days. On day seven, cells were pooled, and frozen at 1 x 10^6 cells/vial, as described in Section 6.2.3.

6.5.4.3 IL-17 (T_h17) positive cells

PBMCs were thawed and diluted to 5 x10^5 cells/mL in complete RPMI. Peptidoglycan (InvivoGen, #tlrl-pgnsa) was added at 5 μg/mL and plates incubated overnight. The next day, PBMCs were centrifuged and re-suspended at 1 x 10^6 cells/mL, then mixed in a 1:1 ratio with allogeneic T cells and placed in flat-bottomed 96-well plates. The cell mix was incubated for a further five days before being frozen at 1 x 10^6 cells/vial, using the protocol described in Section 6.2.3.

6.5.5 Intracellular cytokine staining

On the day of analysis, positive control cells for each of the three conditions were thawed, then diluted to approximately 5 x 10^5 cells/mL in complete RPMI for analysis alongside the main experiments, to ensure effective cytokine staining had been performed. 10 μg/mL brefeldin A (#B5936), 1 μM Ionomycin (#I0634) and 20 ng/mL phorbol 12-myristate 13-acetate (PMA, #P8139, all from Sigma-Aldrich) were added directly to the wells to block protein transport and promote cytokine production. Plates were then incubated for five hours.

After incubation, supernatants were harvested and frozen for later ELISA analysis. Cells were then stained for CD4, CD8 and CD209 (DC sign, to exclude DCs from the analysis) for 30 minutes on ice using the antibodies described in Table 6.2. Cells were washed with PBS, then stained using fixable viability dye-efluor® 660 (equivalent fluorophore to APC, #65-0864-14, eBioscience) for 30 minutes in the fridge. Cells were then fixed and permeabilised using the eBioscience fixation/permeabilisation concentrate and diluents (#00-5123-43/#00-5223-56).

Table 6.2: Antibody details for surface molecule and intracellular cytokine staining in MLR experiments.

Surface molecule	Antibody and fluorophore	Manufacturer	Catalogue number	Isotype	Catalogue number
Surface staining mix					
CD4	anti-CD4 APC-eFluor® 780	eBioscience	#47-0048	mouse IgG1κ	#47-4714
CD8	anti-CD8a PE-Cy7	eBioscience	#25-0088	mouse IgG1κ	#25-2714
CD209	anti-CD209 APC	eBioscience	#17-2099	mouse IgG1κ	#17-4714
Cytokine staining mix					
IFN-γ	anti-IFN-γ PerCP Cy5.5	eBioscience	#45-7319	mouse IgG1κ	#45-4714
IL-4	anti-IL4 Brilliant Violet™ 421	Biolegend	#500826	rat IgG1	#400430
IL-17	anti-IL-17A PE	eBioscience	#12-7178	mouse IgG1κ	#12-4714

All subsequent washing and staining was performed in a 1 x solution of permeabilisation buffer (eBioscience, #00-8333-56). Cells were washed twice, then re-suspended in cytokine staining mix (Table 6.2) supplemented with 2% mouse serum (#M5905, Sigma-Aldrich) and incubated for 30 minutes at room temperature. Pooled isotype controls for every condition were included to determine gate positions in analysis of the data. Cells were then washed twice with permeabilisation buffer, re-suspended in PBS with 1% PFA and kept in the fridge (~4 °C) until flow cytometric analysis. All plates were analysed within 48 hours.

6.5.6 IL-2 ELISAs

Supernatants from the MLR assays were analysed for IL-2 using eBioscience human IL-2 Ready-SET-Go! ELISA kits (#88-7025) according to the maufacturer's instructions.

6.5.7 Tritiated thymidine incorporation assays

MLRs were set up as described in Section 6.5.3, with four replicates for each condition. On the days specified, cells were pulsed for 18 hours overnight with 0.74 MBq tritiated thymidine/well [(methyl-^{3}H)-thymidine, specific activity: 2 Ci (74.0 GBq)/mM, #NET027A005MC, Perkin Elmer]. At this point, plates were frozen until the final day of the timecourse, when all plate contents were thawed and harvested onto filter cards using a Micro96 Harvester (Skatron Instruments). Once the filter cards were dry, they were

thermosealed into plastic pouches with 10 mL of Betaplate Scint fluid (#1205-440, Perkin Elmer) and analysed on a 1205 Betaplate (Wallac) Liquid Scintiallation Coutner.

6.5.8 T cell purity assessment

Naïve/memory T cell samples were thawed and re-suspended in complete RPMI at approximately 5×10^5 cells/mL. T cells were plated in round-bottomed 96–well plates and stained for CD3, CD4, CD8, CD45RA and CD45RO (antibodies/fluorophores in Table 6.3), then analysed immediately using flow cytometry.

Table 6.3: Details of antibodies and isotype controls used for T cell purity assessment.

Surface molecule	Antibody and fluorophore	Manufacturer	Catalogue number	Isotype	Catalogue number
CD3	anti-CD3 eFluor® 450	eBioscience	#48-0037	mouse IgG2aκ	#48-4724
CD4	anti-CD4 APC-eFluor® 780	eBioscience	#47-0048	mouse IgG1κ	#47-4714
CD8	anti-CD8a PE-Cy7	eBioscience	#25-0088	mouse IgG1κ	#25-2714
CD45RA	anti-CD45RA APC	eBioscience	#17-0458	mouse IgG2bκ	#17-4732
CD45RO	anti-CD45RO PE	eBioscience	#12-0457	mouse IgG2aκ	#12-4732

6.5.9 Data processing

For the preliminary timecourse experiment, significance data between all conditions for each day was calculated in [R] using a linear model [lm() function] regressed on the conditions imposed on the T cells.[3] For the main naïve/memory T cell MLR experiments, processing of CFSE dilution, IL-2 secretion, tritiated thmidine incorporation and cytokine expression data was similar to that described in Section 6.4.6. Normalisation, taking into account variability between donor pairs was performed on logged raw data using a linear mixed effects model [lme() function, nlme library in [R]][2,3] with donor as a random effect, and the conditions as fixed effects. This produced estimates and confidence intervals which were converted back into experimental units by calculating the corresponding exponential values. Additionally, significance data was produced using the lmerTest package relative to a reference level fixed effect (untreated cells, LPS, commercial adjuvants etc).[4]

6.6 Experimental procedures for Chapter Five

6.6.1 Synthesis of FITC-labelled LDHs

6.6.1.1 FITC-labelled MgAl-CO_3 LDHs

All unlabelled MgAl-CO_3 LDHs were produced using similar procedures to those outlined in Section 6.3.2. The 14 nm MgAl-CO_3 LDH was synthesised using the same high pH technique as that described for the 20 nm MgAl-CO_3 LDH. The 60 nm MgAl-CO_3 LDH was synthesised by co-precipitation in the same way as the 60 nm MgAl-CO_3 LDH. The 140 and 350 nm MgAl-CO_3 LDHs were synthesised using the hydrothermal method, for 160 and 180 °C overnight, respectively. The 920 and 1610 nm MgAl-CO_3 LDHs were synthesised using the ARR method with HMT (0.24 and 0.22 M respectively).

Fluoroscein isothiocyanate (FITC) labelling was performed on dried samples by re-dispersing approximately 0.8 g of LDH in 50 mL DI water using sonication then adding this to 50 mL of a 700 μM solution of Na_2FITC, formed from reaction of FITC Isomer 1 (#F2502, Sigmal-Aldrich,) with NaOH. The mixture was heated at 60 °C for 30 minutes, then the labelled products washed using centrigfugation as previously described.

6.6.1.2 Other FITC-labelled LDHs

The LiAl-CO_3 LDH used for FITC labelling was a sample of the 100 nm LiAl-CO_3 LDH detailed in Section 6.3.3. The MgFe-CO_3 LDH was a sample of the 70 nm MgFe-CO_3 LDH detailed in Section 6.3.4. All other FITC-labelled LDHs (MgAl-NO_3, MgAl-Cl, MgFe-NO_3, CaAl-NO_3, and CaAl-Cl LDH) were synthesised in the same way as those described in Section 6.3. All LDH samples were labelled with FITC as described in the preceding Section.

6.6.2 Temperature dependence assays

FITC-labelled LDHs were prepared by placing a weighed amount in a 1.5 mL eppendorf tube, then repeatedly washing with PBS, pelleting samples by centrifuging for a few seconds at 7000 RPM using a microcentrifuge between washes. Once supernatants appeared colourless, the particles were re-suspended in a volume of PBS to give a concentration of approximately 10 mg/mL, assuming little LDH was lost during the washing process. These were then sonicated for 30 minutes to ensure an even suspension.

Mo-DCs were seeded in round-bottomed 96-well plates at 5 x 10^5 cells/mL, 200 μL cells/well. 10 μL of LDH suspension was added to the cells, either on ice or at room temperature. The

two room temperature plates were transferred to incubators at 37 °C. Plates were incubated for either 15 minutes or two hours, then transferred onto ice and cells labelled with anti-human CD209-APC, and analysed immediately by flow cytometry. For the fluorescence microscopy studies, after incubation for the specified time/temperature, cells were fixed and mounted as described in Section 6.6.4. In these studies all LDHs were used at a working concentration of 100 μg/mL.

6.6.3 Lucifer yellow assays

Lucifer yellow experiments were performed on THP-1 cells. Cells were made up to 5×10^5 per mL in complete RPMI and seeded at 200 μL/well in round-bottomed 96-well plates. Lucifer Yellow (lithium salt, #L-453, Life Technologies) was added at a final concentration of 20 μg/mL. The LDHs specified in Section 5.2.3 were prepared and added as specified in Section 6.4.1 (500 μg/mL). Polystyrene beads (#79166, Fluka Analytical) were diluted 1 in 100 in PBS, and 10 μL added to the positive control wells. 10 μL of PBS was added to the negative control wells. Cells were incubated for 2 hours at 37 °C, 5% CO_2 in a humidified atmosphere. After incubation, cells were washed once with PBS/FCS, then re-suspended in PBS/FCS and analysed immediately using flow cytometry.

For the confocal studies, following experimental set-up as detailed above, cells were washed once with PBS, then mounted onto slides for confocal microscopy as described in Section 6.6.5.

6.6.4 Fluorescence microscopy

Fluorescence microscopy was conducted on a Leica DM2000 fluorescence microscope. Cells in round-bottomed 96-well plates were fixed with 4% paraformaldehyde (PFA, #28906, Thermoscientific) in PBS at room temperature for 15 minutes. After this, cells were pelleted (1500 RPM, two minutes, 4 °C), washed once with 200 μL PBS and stained with 3 μM of the nuclear dye 4',6-diamidino-2-phenylindole (DAPI, #D21490, Invitrogen) in PBS for 15 minutes at room temperature. Cells were then re-suspended in PBS and mounted onto glass slides using a Cytospin 2 (Shandon) at 800 RPM for 3 minutes. Coverslips were mounted with Vectashield hard-set mounting medium (#H-1400), sealed with clear nail polish, and left to dry in the dark prior to analysis.

6.6.5 Laser scanning confocal microscopy

Mo-DC were plated and treated with FITC-labelled LDH prepared as detailed in Section 6.6.2 at a concentration of 100 μg/mL for two hours at 37 °C, in a humidified 5% CO_2 atmosphere.

After one hour, Lysotracker Red (Life Technologies, #L-7528) was added directly to wells at a final concentration of 100 nM, and then plates were returned to the incubator for the final hour. Slides were prepared as described in Section 6.6.4. Confocal microscopy was performed on a Zeiss 780 Inverted Microscope using a Plan Apochromat 63x/1.4 oil objective at the Weatherall Institute of Molecular Medicine, University of Oxford. Images were collected using Zen 2011 LSM software, and analysed using Image J with the LOCI bioformats package.[1,9]

6.6.6 Uptake inhibition assays

THP-1 cells were seeded in complete RPMI at 5×10^5 cells/mL, 200 μL cells/well in round-bottomed 96-well plates, then the uptake inhibitors added at the concentrations detailed in Table 6.4 and plates incubated overnight at 37 °C in a humidified 5% CO_2 atmosphere.

The following morning, FITC-labelled LDHs (60, 300 and 1610 nm FITC-labelled MgAl-CO_3 LDH) were prepared as described in Section 6.6.2, and added to the cells at 500 μg/mL. FITC-labelled beads (#17147, Polysciences) were diluted 1 in 100 in PBS and added to the control wells. After this, plates were incubated for a further two hours at 37 °C, then cells washed twice with PBS/FCS, re-suspended in PBS with 2% PFA, then analysed by flow cytometry.

Table 6.4: Inhibitors used in uptake inhibition experiments.

Inhibitor	Working concentration	Manufacturer	Catalogue number
Latrunculin A	250 nM	Sigma-Aldrich	#L5163
Chlorpromazine	10 μg/mL	Sigma-Aldrich	#C1838
Amiloride	1 mM	Sigma-Aldrich	#A7410
Chloroquine	50 μM	InvivoGen	#tlrl-chq
Fillipin III	2.5 μg/mL	Sigma-Aldrich	#F4767

6.6.7 Trypsin assays

Cells (either PBMCs, Mo-DCs or THP-1 cells, as specified in Chapter Five) were seeded in round-bottomed 96-well plates in complete RPMI at 5×10^5 cells/mL, 200 μL cells/well. In specified experiments, prior to LDH addition, cells were fixed for 15 minutes at room temperature with 4% PFA in PBS, pelleted, then re-suspended in a 30 mM glycine (#G8898, Sigma-Aldrich) solution in PBS for 5 minutes to quench the activity of PFA. All cells were washed once in PBS, then re-suspended in 200 μL complete RPMI. FITC-labelled MgAl-CO_3 LDHs were prepared (Section 6.6.2) and added at 500 μg/mL. Control wells containing LDH particles without cells were also included to check that trypsin did not alter the FITC

fluorescence of the particles directly, and that all effects observed could be solely attributed to binding to cells.

Plates were either incubated at 37 °C, or kept on ice as specified in Chapter Five. Following incubation, cells were washed twice with PBS then treated for 10 minutes at 37 °C with 100 µL of either a 1 x or a 10 x working concentration of trypsin (0.25 or 2.5% weight/volume, #T4549, Sigma-Aldrich,) in PBS/EDTA, or PBS as a control. After 10 minutes, 100 µL of PBS/FCS was added directly to the wells, cells were washed twice with PBS then analysed by flow cytometry. For the cells which were trypsinised before LDH addition, similar procedures were followed, except cells were fixed and trypsinised before incubation for 30 minutes with FITC-labelled LDHs. Cells were then washed once with PBS and analysed by flow cytometry

For the control experiment establishing the influence of trypsinisation on surface molecules, thawed Mo-DCs were seeded in flat-bottomed 96-well plates in complete RPMI (5×10^5 cells/mL, 200 µL cells/well), and treated with LPS (10 ng/mL) overnight. The next day, cells were transferred to round-bottomed 96-well plates, and trypsinised as detailed above. After two washes with PBS/FCS, aliquots from identically-treated wells were pooled for isotype controls and cells were stained for the surface molecules given in Table 6.5.

Table 6.5: Details of antibodies and isotype controls used to test the effect of trypsin on Mo-DC surface molecules.

Surface molecule	Antibody and fluorophore	Manufacturer	Catalogue number	Isotype	Catalogue number
CD1a	anti-CD1a FITC	BD bioscience	#555806	mouse IgG1κ	#555748
CD14	anti-CD14 PE	eBioscience	#12-0149	mouse IgG1κ	#17-4714
CD209	anti-human CD209 APC	eBioscience	#17-2099	mouse IgG1κ	#17-4714
CD274 (B7-H1)	anti-B7-H1 PE-Cy7	eBioscience	#25-5983	mouse IgG1κ	#25-2714
MHC class II (HLA-DR)	anti-HLA-DR APCefluor®780	eBioscience	#47-9956	mouse IgG2bκ	#47-4732
CD40	anti-CD40 APC	eBioscience	#17-0409	mouse IgG1κ	#17-4714
CD86	anti-CD86 PE	eBioscience	#12-0869	mouse IgG2bκ	#12-4732
CD275 (B7-H2)	anti-CD275 PE	eBioscience	#12-5889	mouse IgG1κ	#17-4714
CD283 (TLR3)	anti-CD283 PE	eBioscience	#12-9039	mouse IgG1κ	#12-4714

6.6.8 Pepsin assays

THP-1 cells were seeded in round-bottomed 96-well plates in complete RPMI (5×10^5 cells/mL, 200 µL cells/well). Cells were then fixed (as outlined in Section 6.6.7), washed once with PBS, then treated with either a 0.4 or 0.04% (weight/volume) solution of pepsin (#P7000, Sigma-Aldrich) dissolved in 10 mM HCl supplemented with NaCl

(0.138 M), and KCl (0.0027 M), for one hour at 37 °C. Negative controls used the same solution but without added pepsin. After one hour, cells were washed once with a pH 9.7 $Na_2CO_3/NaHCO_3$ buffer to inactivate the pepsin and neutralise the acidity. Cells were then re-suspended in 200 µL complete RPMI and FITC-labelled LDHs prepared as described in Section 6.6.2 were added at 500 µg/mL. After incubating at 37 °C for one hour, cells were washed once with PBS and re-suspended in PBS for analysis by flow cytometry.

6.6.9 Papain assays

THP-1 cells were seeded in round-bottomed 96-well plates in complete RPMI (5×10^5 cells/mL, 200 µL cells/well), fixed as described in Section 6.6.2, washed once with PBS, then re-suspended in 200 µL 0.05 or 0.5 mg/mL papain solution (from papaya latex, #P3125, Sigma-Aldrich) in PBS/EDTA supplemented with 0.5% L-cysteine (#W326305, Sigma-Aldrich). Negative control wells were treated with PBS/EDTA/0.5% L-cysteine without papain. Plates were incubated for one hour at 37 °C, then the activitiy of papain quenched by addition of 20 µL of 0.3 M iodoacetamide solution (#I1149, Sigma-Aldrich). Cells were washed once with PBS/FCS, re-suspended in complete RPMI and FITC-labelled LDH added as described previously. Cells and LDH were incubated for 30 minutes at 37 °C, then washed once with PBS and re-suspended in PBS for analysis by flow cytometry. For specified experiments, LDHs were incubated with fixed cells for an hour before papain treatment.

To evaluate the effect of papain treatment on surface molecules, THP-1 cells were treated overnight with LPS as described for Mo-DC in Section 6.6.7, then treated with papain and stained for the surface molecules detailed in Table 6.6.

Table 6.6: Details of antibodies and isotype controls used to test the effect of papain on THP-1 cell surface molecules.

Surface molecule	Antibody and fluorophore	Manufacturer	Catalogue number	Isotype	Catalogue number
CD1a	anti-CD1a FITC	BD bioscience	#555806	mouse IgG1κ	#555748
CD14	anti-CD14 PE	eBioscience	#12-0149	mouse IgG1κ	#17-4714
CD209	anti-human CD209 APC	eBioscience	#17-2099	mouse IgG1κ	#17-4714
CD274 (B7-H1)	anti-B7-H1 PE-Cy7	eBioscience	#25-5983	mouse IgG1κ	#25-2714
CD40	anti-CD40 APC	eBioscience	#17-0409	mouse IgG1κ	#17-4714
CD86	anti-CD86 PE	eBioscience	#12-0869	mouse IgG2bκ	#12-4732
CD275 (B7-H25)	anti-B7-H2 APC	eBioscience	#17-5889	mouse IgG1κ	#17-4714
CD283 (TLR3)	anti-CD283 PE	eBioscience	#12-9039	mouse IgG1κ	#12-4714
MHC class I (HLA-A,B,C)	anti-HLA-ABC PE-Cy7	eBioscience	#25-9983	mouse IgG2aκ	#25-4724

6.6.10 pH dependence assays

A series of bufferes from pH 3 to 10 were made according to Table 6.7. All buffers were made up in a stock solution of NaCl (0.138 M) and KCl (0.0027 M) to prevent osmotic lysis of cells. The pH of the buffers was measured using a Hanna instruments 8424 microcomputer pH meter.

Table 6.7: Buffers prepared for investigating the pH dependence of cell-LDH particle interactions.

pH	Buffer	Solution 1	Solution 2	Mixing ratio (solution 1:solution 2)
3.5	AcOH/NaOAc	0.2 M AcOH	0.2 M NaOAc	9:1
3.9	AcOH/NaOAc	0.2 M AcOH	0.2 M NaOAc	4:1
4.5	AcOH/NaOAc	0.2 M AcOH	0.2 M NaOAc	1:1
5.1	AcOH/NaOAc	0.2 M AcOH	0.2 M NaOAc	1:4
5.5	AcOH/NaOAc	0.2 M AcOH	0.2 M NaOAc	1:9
5.7	Na_2HPO_4/NaH_2PO_4	0.2 M Na_2HPO_4	0.2 M NaH_2PO_4	9:1
6.1	Na_2HPO_4/NaH_2PO_4	0.2 M Na_2HPO_4	0.2 M NaH_2PO_4	4:1
6.7	Na_2HPO_4/NaH_2PO_4	0.2 M Na_2HPO_4	0.2 M NaH_2PO_4	1:1
7.3	Na_2HPO_4/NaH_2PO_4	0.2 M Na_2HPO_4	0.2 M NaH_2PO_4	1:4
7.7	Na_2HPO_4/NaH_2PO_4	0.2 M Na_2HPO_4	0.2 M NaH_2PO_4	1:9
8.0	Na_2HPO_4/NaH_2PO_4	0.2 M Na_2HPO_4	0.2 M NaH_2PO_4	19:1
8.7	$Na_2CO_3/NaHCO_3$	0.1 M Na_2CO_3	0.1 M $NaHCO_3$	1:39
8.8	$Na_2CO_3/NaHCO_3$	0.1 M Na_2CO_3	0.1 M $NaHCO_3$	1:19
9.1	$Na_2CO_3/NaHCO_3$	0.1 M Na_2CO_3	0.1 M $NaHCO_3$	1:9
9.4	$Na_2CO_3/NaHCO_3$	0.1 M Na_2CO_3	0.1 M $NaHCO_3$	1:4
9.7	$Na_2CO_3/NaHCO_3$	0.1 M Na_2CO_3	0.1 M $NaHCO_3$	1:1
9.9	$Na_2CO_3/NaHCO_3$	0.1 M Na_2CO_3	0.1 M $NaHCO_3$	4:1
10.0	$Na_2CO_3/NaHCO_3$	0.1 M Na_2CO_3	0.1 M $NaHCO_3$	9:1

Thawed Mo-DCs were plated at 5×10^5 cells/mL, 200 µL cells/well in round-bottomed 96-well plates, fixed and washed once with PBS. Fixed cells were then re-suspended in 200 µL of buffer, then the 300 nm FITC-labelled MgAl-CO_3 LDH (prepared as detailed in Section 6.6.2) was added at a working concentration of 500 µg/mL. Cells were left for approximately 30 minutes for LDH adhesion to occur, then analysed by flow cytometry.

For zeta potential measurements, fixed Mo-DC (1×10^5 cells/mL) and LDH (500 µg/mL) were measured separately in the above buffers on a Malvern Zetasizer (Nano series) in a folded capillary cell. For background FITC fluorescence measurements, the 300 nm FITC-labelled MgAl-CO_3 LDH was dispersed in the various buffers in flexible flat-bottomed plates (BD Falcon), 200 µL suspension per well. These were then analysed at 525 cm^{-1} on a Fluostar Omega microplate reader (BMG Labtech) in the Department of Zoology, University of Oxford.

6.6.11 Data analysis in Chapter Five

All significance data for Chapter Five were calculated using a one-way analysis of variance between conditions with a Bonferroni test for pair-wise mean comparisons, using OriginPro 8.5.1 software. Generally, data sets were much smaller, and from single donor experiments, so extensive linear/linear mixed effects modelling was not conducted.

6.7 References

(1) Rasband, W. ImageJ v1.48, National Institutes of Health, USA, http://imagej.
(2) Pinheiro, J.; Bates, D.; DebRoy, S.; Sarkar, D.; R core devlopment team. nlme: Linear and Nonlinear Mixed Effects Models., 2011.
(3) R Development Core Team; R Foundation for Statistical Computing. R: A language and environment for statistical computing, 2011.
(4) Kuznetsova, A.; Brockhoff, P. B.; Christensen, R. H. B. Package "lmerTest," 2014.
(5) Venables, W. N.; Ripley, B. D. *Modern Applied Statistics with S*; 4th ed.; Springer New York, 2002.
(6) Ruppert, D.; Wand, M. P.; Carroll, R. J. *Semiparametric Regression*; Cambridge University Press: Cambridge, 2003.
(7) Schwarz, G. *Ann. Stat.* **1978**, *6*, 461.
(8) Gneiting, T.; Katzfuss, M. *Annu. Rev. Stat. its Appl.* **2014**, *1*, 125.
(9) Linkert, M.; Rueden, C. T.; Allan, C.; Burel, J.-M.; Moore, W.; Patterson, A.; Loranger, B.; Moore, J.; Neves, C.; Macdonald, D.; Tarkowska, A.; Sticco, C.; Hill, E.; Rossner, M.; Eliceiri, K. W.; Swedlow, J. R. *J. Cell Biol.* **2010**, *189*, 777.

Appendix A – Appendices to Chapter Two

A.1 Elemental analysis results

Calculated LDH formulae were derived from combining the energy dispersive X-ray diffraction (EDX), elemental analysis (EA, for C, H and N using the quantitative combustion technique) and thermogravimetric analysis (TGA) data. The percentage H_2O was defined as the first mass-loss event in the TGA data.

A.1.1 MgAl-CO_3 LDHs

Table A.1: EDX, EA and TGA data used to calculate approximate formulae for MgAl-CO_3 LDHs.

MgAl-CO_3 LDH approx size (nm)	EDX Mg:Al atomic ratio	EA (weight %) C	H	N	TGA % H_2O by mass
20	3.13	2.6	3.7	<0.1	17.3
40	2.57	2.6	3.7	<0.1	15.5
60	1.73	2.6	3.5	<0.1	14.1
70	2.84	2.6	3.6	<0.1	14.7
190	2.98	2.5	3.6	<0.1	13.8
210	2.92	2.5	3.8	<0.1	13
400	2.87	2.5	3.8	<0.1	12
1070	2.15	2.8	3.9	<0.1	12.7
2160	2.16	2.7	3.7	<0.1	12.7
2560	2.14	3.6	3.7	<0.1	12
9900	2.18	2.7	3.8	<0.1	12.4

A.1.2 LiAl-CO_3 LDHs

Table A.2: EDX, EA and TGA data used to calculate approximate formulae for LiAl-CO_3 LDHs. ** indicates Li:Al assumed to be 1:2, as Li is too light for detection using EDX.

LiAl-CO_3 LDH approx size (nm)	EDX** Mg:Al atomic ratio	EA (weight %) C	H	N	TGA % H_2O by mass
10	0.5	2.8	3.8	<0.1	11.9
30	0.5	2.4	3.7	<0.1	11
100	0.5	4.7	3.5	<0.1	21
350	0.5	3.2	3.7	<0.1	10.9
810	0.5	3.2	4.0	<0.1	12.6
1240	0.5	2.8	3.9	<0.1	13.3

A.1.3 MgFe-CO_3 LDHs

Table A.3: EDX, EA and TGA data used to calculate approximate formulae for MgFe-CO_3 LDHs.

MgFe-CO_3 LDH approx size (nm)	EDX Mg:Al atomic ratio	EA (weight %) C	H	N	TGA % H_2O by mass
20	3.08	2.4	3.17	<0.1	15.5
60	3.26	2.3	3.2	<0.1	14.2
70	4.16	2.1	3.25	<0.1	13.7
100	3.92	2.3	3.14	<0.1	13.3
180	3.92	2.2	3.225	<0.1	13.9

A.2 Powder X-ray diffraction pattern indexing

A.2.1 MgAl-CO_3 LDHs

Initial parameters: hexagonal, $a = b = 3.046$ Å, $c = 22.77$ Å, space group $R\bar{3}m$.[1]

Table A.4. Indexed reflections for the 20 nm MgAl-CO_3 LDH [$a = b = 3.058(2)$ Å, $c = 23.31(4)$ Å].

h	*k*	*l*	2d(obs)/Å	2d(calc)/Å	Residual
0	0	3	7.695863	7.77104	-0.07518
0	0	6	3.882542	3.885538	-0.003
0	0	9	2.588942	2.590355	-0.00141
1	0	7	2.077154	2.072855	0.004299
1	1	0	1.527645	1.529012	-0.00137
1	1	3	1.49774	1.500248	-0.00251
1	1	6	1.42477	1.422812	0.001958

Table A.5: Indexed reflections for the 40 nm MgAl-CO_3 LDH [$a = b = 3.054(3)$ Å, $c = 23.21(8)$ Å].

h	*k*	*l*	2d(obs)/Å	2d(calc)/Å	Residual
0	0	3	7.673913	7.739133	-0.06522
0	0	6	3.836773	3.869558	-0.03279
0	1	2	2.578915	2.578828	8.62E-05
0	1	5	2.31524	2.298243	0.016997
1	0	7	2.080106	2.067915	0.012192
0	1	8	1.953785	1.954874	-0.00109
1	1	0	1.526118	1.527045	-0.00093
1	1	3	1.496804	1.498158	-0.00135
1	1	6	1.41793	1.420439	-0.00251

Table A.6: Indexed reflections for the 60 nm MgAl-CO_3 LDH [$a = b = 3.048(7)$ Å, $c = 22.78(1)$ Å].

h	*k*	*l*	2d(obs)/Å	2d(calc)/Å	Residual
0	0	3	7.669936	7.59391	0.076026
0	0	6	3.803604	3.79696	0.006644
0	1	2	2.596061	2.572051	0.02401
0	0	9	2.525362	2.531302	-0.00594
1	1	0	1.524641	1.524341	0.0003
1	1	3	1.494937	1.494528	0.00041
1	1	6	1.41492	1.414598	0.000321
2	0	2	1.31103	1.31134	-0.00031

Table A.7: Indexed reflections for the 70 nm MgAl-CO_3 LDH [$a = b = 3.056(8)$ Å, $c = 23.50(0)$ Å].

h	*k*	*l*	2d(obs)/Å	2d(calc)/Å	Residual
0	0	3	7.733403	7.832957	-0.09955
0	0	6	3.86755	3.916475	-0.04893
0	1	2	2.587422	2.58239	0.005032
0	1	5	2.33726	2.30643	0.03083
1	0	7	2.08325	2.078615	0.004635
0	1	8	1.970457	1.966421	0.004036
1	1	0	1.528763	1.528313	0.00045
1	1	3	1.499833	1.500028	-0.00019
1	1	6	1.421686	1.42375	-0.00206

Table A.8: Indexed reflections for the 190 nm MgAl-CO_3 LDH [$a = b = 3.059(0)$ Å, $c = 23.51(3)$ Å].

h	*k*	*k*	2d(obs)/Å	2d(calc)/Å	Residual
0	0	3	7.794511	7.837314	-0.0428
0	0	6	3.877031	3.918638	-0.04161
0	1	2	2.584026	2.584207	-0.00018
1	0	7	2.083753	2.07997	0.003783
1	1	0	1.529861	1.529401	0.00046
1	1	3	1.500511	1.501086	-0.00058
1	1	6	1.422301	1.424735	-0.00243
2	0	2	1.31617	1.316173	-0.000003
1	0	16	1.286432	1.285014	0.001418

Table A.9: Indexed reflections for the 210 nm MgAl-CO_3 LDH [*a* = *b* = 3.195(4) Å, *c* = 22.56(5) Å].

h	*k*	*l*	2d(obs)/Å	2d(calc)/Å	Residual
0	0	3	7.75502	7.521867	0.233152
0	0	6	3.790659	3.760942	0.029717
1	0	1	2.75333	2.746723	0.006607
0	0	9	2.527357	2.507288	0.020069
0	1	5	2.337785	2.359127	-0.02134
1	0	7	2.110982	2.099752	0.011229
1	0	7	2.083981	2.099752	-0.01577
0	0	15	1.499964	1.504373	-0.00441

Table A.10: Indexed reflections for the 400 nm MgAl-CO_3 LDH [*a* = *b* = 3.047(8) Å, *c* = 22.51(4) Å].

h	*k*	*l*	2d(obs)/Å	2d(calc)/Å	Residual
0	0	3	7.737447	7.504198	0.233249
0	0	6	3.853498	3.752109	0.101389
1	0	1	2.60454	2.61443	-0.00989
0	0	9	2.507484	2.501404	0.00608
1	0	10	1.702955	1.710874	-0.00792
1	1	0	1.528443	1.519726	0.008717
0	0	15	1.499026	1.500843	-0.00182
1	0	13	1.443538	1.446725	-0.00319

Table A.11: Indexed reflections for the 1070 nm MgAl-CO_3 LDH [*a* = *b* = 3.047(6) Å, *c* = 22.72(1) Å].

h	*k*	*l*	2d(obs)/Å	2d(calc)/Å	Residual
0	0	3	7.591897	7.573314	0.018583
0	0	6	3.789385	3.78665	0.002735
1	0	1	2.624355	2.621534	0.002821
0	1	2	2.572608	2.570694	0.001914
0	0	9	2.525087	2.524434	0.000653
0	1	5	2.282663	2.282158	0.000505
0	1	8	1.933335	1.933273	6.21E-05
1	0	10	1.722375	1.721844	0.000531
0	1	11	1.6262	1.626546	-0.00035
1	1	0	1.524074	1.52372	0.000354
1	1	3	1.493011	1.493785	-0.00077
1	0	13	1.456642	1.457152	-0.00051
1	1	6	1.413269	1.413568	-0.0003
0	1	14	1.38246	1.382406	5.39E-05

Table A.12: Indexed reflections for the 2160 nm MgAl-CO_3 LDH [*a* = *b* = 3.047(2) Å, *c* = 22.72(0) Å].

h	*k*	*l*	2d(obs)/Å	2d(calc)/Å	Residual
0	0	3	7.593845	7.572797	0.021047
0	0	6	3.789544	3.786411	0.003133
1	0	1	2.623461	2.62114	0.002321
0	1	2	2.572323	2.570323	0.001999
0	0	9	2.524674	2.524276	0.000398
0	1	5	2.282996	2.281864	0.001132
0	1	8	1.933296	1.933059	0.000237
0	0	12	1.892659	1.893207	-0.00055
1	0	10	1.721415	1.72167	-0.00025
0	1	11	1.626095	1.626388	-0.00029
1	1	0	1.523212	1.523489	-0.00028
1	1	3	1.493249	1.493565	-0.00032

Table A.13: Indexed reflections for the 2560 nm MgAl-CO_3 LDH [*a* = *b* = 3.042(3) Å, *c* = 22.62(7) Å].

h	*k*	*l*	2d(obs)/Å	2d(calc)/Å	Residual
0	0	3	7.576351	7.542182	0.034169
0	0	6	3.779702	3.771078	0.008624
1	0	1	2.621154	2.616843	0.004311
0	1	2	2.56961	2.565865	0.003745
0	0	9	2.516799	2.514051	0.002748
0	1	5	2.279282	2.276789	0.002493
0	1	8	1.928845	1.927757	0.001088
1	0	10	1.71675	1.716485	0.000265
0	1	11	1.621498	1.621307	0.000191
1	1	0	1.521041	1.521041	0.000000
1	1	3	1.491048	1.491022	0.000003
1	0	13	1.450075	1.452201	-0.00213

Table A.14: Indexed reflections for the 9900 nm MgAl-CO_3 LDH [a = b = 3.046(1) Å, c = 22.71(5) Å].

h	*k*	*l*	2d(obs)/Å	2d(calc)/Å	Residual
0	0	3	7.549299094	7.571312	-0.02201
1	0	1	2.618184588	2.620218	-0.00203
0	1	5	2.280278324	2.281148	-0.00087
0	1	8	1.93387826	1.932513	0.001366
0	1	11	1.626464125	1.625971	0.000493
1	1	0	1.522238902	1.52295	-0.00071
1	1	3	1.493097719	1.493044	5.4E-05
1	0	13	1.45625518	1.456663	-0.00041
1	1	6	1.413098052	1.412903	0.000195
0	1	14	1.381921348	1.381954	-3.2E-05
2	0	2	1.310494755	1.310108	0.000387

A.2.2 LiAl-CO_3 LDHs

Reflections for LiAl-CO_3 LDHs were indexed using a monoclinic unit cell, space group C2/m, a = 5.090(1) Å, b = 8.801(1) Å, c = 7.730(1) Å, β = 103.08(1)°.[2,3]

Table A.15: Indexed reflections for the 10 nm LiAl-CO_3 LDH [a = 5.123(9) Å, b = 8.671(6) Å, c = 7.701(8) Å, β = 101.0(7)°].

h	*k*	*l*	2d(obs)/Å	2d(calc)/Å	Residual
0	0	1	7.528818	7.558423	-0.02961
1	1	0	4.393778	4.350055	0.043723
-1	1	1	4.16264	4.074156	0.088484
0	0	2	3.771961	3.779227	-0.00727
0	2	2	2.817548	2.848912	-0.03136
1	1	2	2.628685	2.643784	-0.0151
-2	0	0	2.514821	2.514262	0.000559
-1	3	1	2.432635	2.449738	-0.0171
2	0	1	2.265207	2.259335	0.005872
0	4	1	2.082703	2.083885	-0.00118
2	0	2	1.923994	1.929428	-0.00543
-2	2	3	1.814332	1.801019	0.013313
0	2	4	1.741346	1.732252	0.009094
2	4	1	1.565764	1.564265	0.001498
1	5	2	1.47164	1.470856	0.000785
2	4	2	1.441865	1.441281	0.000584
-3	1	4	1.369746	1.376158	-0.00641

Table A.16: Indexed reflections for the 30 nm LiAl-CO_3 LDH [a = 5.078(7) Å, b = 8.781(7) Å, c = 7.588(9) Å, β = 100.5(5)°].

h	*k*	*l*	2d(obs)/Å	2d(calc)/Å	Residual
0	0	1	7.394056	7.466408	-0.07235
1	1	0	4.318519	4.343782	-0.02526
0	0	2	3.745818	3.733209	0.012609
0	0	3	2.486805	2.488803	-0.002
2	0	1	2.2511	2.248592	0.002509
2	0	2	1.919094	1.920152	-0.00106
-3	3	1	1.46611	1.465719	0.000391
1	3	4	1.439424	1.439113	0.000311

Table A.17: Indexed reflections for the 100 nm LiAl-CO_3 LDH [a = 5.082(2) Å, b = 8.910(9) Å, c = 7.824(2) Å, β = 100.3(7)°].

h	*k*	*l*	2d(obs)/Å	2d(calc)/Å	Residual
0	0	1	7.64352	7.69633	-0.05281
1	1	0	4.37024	4.359881	0.01036
-1	1	1	4.1467	4.078071	0.068633
0	0	2	3.83107	3.848169	-0.0171
0	2	2	2.9159	2.912294	0.003606
1	1	2	2.68191	2.683583	-0.00167
-2	0	1	2.51366	2.514031	-0.00037
-2	0	0	2.49784	2.499552	-0.00171
2	0	1	2.25829	2.260732	-0.00244
1	1	3	2.08024	2.073329	0.006914
0	4	2	1.93012	1.927969	0.002151
-2	2	3	1.80838	1.807131	0.001251
-3	3	1	1.46897	1.470789	-0.00182
-1	5	3	1.4442	1.445308	-0.00111
-1	3	5	1.37431	1.375405	-0.00109

Table A.18: Indexed reflections for the 350 nm LiAl-CO_3 LDH [*a* = 4.998(2) Å, *b* = 9.012(3) Å, *c* = 7.740(0) Å, *β* = 102.1(6)°].

h	*k*	*l*	2d(obs)/Å	2d(calc)/Å	Residual
0	0	1	7.525628	7.565958	-0.04033
1	1	0	4.402185	4.295134	0.107052
-1	1	1	4.160328	4.072975	0.087353
0	2	1	3.928411	3.871336	0.057075
0	0	2	3.768338	3.782967	-0.01463
0	2	2	2.920083	2.897265	0.022819
1	1	2	2.626891	2.609332	0.017559
-1	3	1	2.512778	2.509517	0.003261
-2	0	0	2.430858	2.442872	-0.01201
-2	0	2	2.275415	2.282963	-0.00755
0	4	2	1.928343	1.93567	-0.00733
0	6	1	1.472184	1.473211	-0.00103
1	3	4	1.445216	1.446691	-0.00148
2	4	2	1.440693	1.443311	-0.00262
-3	1	4	1.370133	1.370871	-0.00074

Table A.19: Indexed reflections for the 810 nm LiAl-CO_3 LDH [*a* = 5.137(0) Å, *b* = 8.992(0) Å, *c* = 7.724(1) Å, *β* = 101.5(7)°].

h	*k*	*l*	2d(obs)/Å	2d(calc)/Å	Residual
0	0	1	7.552509	7.566796	-0.01429
1	1	0	4.411276	4.391349	0.019927
-1	1	1	4.167465	4.124241	0.043224
0	2	1	3.941129	3.865013	0.076117
0	0	2	3.774327	3.783395	-0.00907
0	2	2	2.926616	2.894739	0.031877
1	1	2	2.63093	2.646473	-0.01554
-1	3	1	2.515707	2.517803	-0.0021
2	0	1	2.256071	2.256033	0.000004
-2	2	2	2.078288	2.06212	0.016168
0	4	2	1.928228	1.932501	-0.00427
0	6	1	1.472916	1.470022	0.002894
-1	5	3	1.444436	1.452001	-0.00757
-3	3	3	1.370889	1.374746	-0.00386

Table A.20: Indexed reflections for the 1240 nm LiAl-CO_3 LDH [*a* = 5.129(9) Å, *b* = 8.845(5) Å, *c* = 7.790(0) Å, *β* = 103.6(9)°].

h	*k*	*l*	2d(obs)/Å	2d(calc)/Å	Residual
0	0	1	7.549941	7.56815	-0.01821
0	2	0	4.408241	4.422474	-0.01423
0	2	1	3.950463	3.818336	0.132127
0	0	2	3.773223	3.784077	-0.01085
1	1	2	2.598394	2.599519	-0.00112
1	3	0	2.534263	2.537529	-0.00327
0	0	3	2.514412	2.522718	-0.00831
-2	0	0	2.487337	2.491881	-0.00454
1	3	1	2.319138	2.322986	-0.00385
2	0	1	2.221816	2.216171	0.005645
-2	2	2	2.081518	2.077027	0.004491
1	3	2	1.997678	1.999029	-0.00135
2	2	1	1.975812	1.981317	-0.00551
0	0	4	1.893734	1.892037	0.001697
1	3	3	1.692028	1.690092	0.001936
-2	2	4	1.598268	1.599025	-0.00076
0	6	0	1.472037	1.474156	-0.00212
-1	5	3	1.443139	1.444436	-0.0013
3	3	1	1.371047	1.37037	0.000677

A.2.3 MgFe-CO_3 LDHs

Reflections for MgFe-CO_3 LDHs were indexed to a hexagonal unit cell, $a = b = 3.107(8)$ Å, $c = 23.07(9)$ Å, space group $R\bar{3}m$.[4]

Table A.21: Indexed reflections for the 20 nm MgFe-CO_3 LDH [$a = b = 3.102(9)$ Å, $c = 23.54(2)$ Å].

h	*k*	*l*	2d(obs)/Å	2d(calc)/Å	Residual
0	0	3	7.733403	7.846944	-0.11354
0	0	6	3.859932	3.923467	-0.06353
0	1	2	2.628236	2.619617	0.00862
0	1	5	2.356992	2.333699	0.023293
0	1	8	1.998262	1.98422	0.014042
1	1	0	1.551353	1.551346	7.09E-06
1	1	3	1.520545	1.521888	-0.00134
1	1	6	1.440256	1.442665	-0.00241
1	1	9	1.334197	1.334311	-0.00011
2	0	5	1.293075	1.291935	0.00114

Table A.22: Indexed reflections for the 60 nm MgFe-CO_3 LDH [$a = b = 3.108(0)$ Å, $c = 23.07(9)$ Å].

h	*k*	*l*	2d(obs)/Å	2d(calc)/Å	Residual
0	0	3	7.7584	7.69246	0.065945
0	0	6	3.8887	3.84625	0.042491
0	1	2	2.612	2.62107	-0.00909
0	1	5	2.321	2.325	-0.00402
1	0	7	2.0758	2.08489	-0.00909
0	1	8	1.962	1.9679	-0.0059
1	1	0	1.5525	1.55389	-0.00138
1	1	3	1.5225	1.52313	-0.0006
2	0	2	1.3362	1.33665	-0.00044
2	0	5	1.2939	1.29192	0.002008

Table A.23: Indexed reflections for the 70 nm MgFe-CO_3 LDH [$a = b = 3.101(7)$ Å, $c = 23.15(7)$ Å].

h	*k*	*l*	2d(obs)/Å	2d(calc)/Å	Residual
0	0	3	7.728017	7.719148	0.008869
0	0	6	3.852839	3.859585	-0.00675
0	1	2	2.624653	2.616636	0.008017
0	1	5	2.332251	2.323614	0.008636
1	0	7	2.076972	2.085293	-0.00832
0	1	8	1.971833	1.968985	0.002847
1	1	0	1.552655	1.550836	0.001819
1	1	3	1.522443	1.520454	0.001988
1	1	6	1.440217	1.439014	0.001203
2	0	2	1.333655	1.334118	-0.00046

Table A.24: Indexed reflections for the 100 nm MgFe-CO_3 LDH [$a = b = 3.102(7)$ Å, $c = 23.24(2)$ Å].

h	k	l	2d(obs)/Å	2d(calc)/Å	Residual
0	0	3	7.738121	7.746967	-0.00885
0	0	6	3.853827	3.873466	-0.01964
0	1	2	2.627862	2.617755	0.010108
0	0	9	2.570466	2.582318	-0.01185
0	1	5	2.332657	2.326154	0.006503
0	1	8	1.986577	1.972526	0.014051
0	0	12	1.936678	1.936737	-5.8E-05
1	1	0	1.552513	1.551233	0.00128
1	1	3	1.522646	1.521039	0.001607
1	1	6	1.440633	1.440046	0.000587
2	0	2	1.335234	1.334518	0.000716
2	0	5	1.288958	1.290586	-0.00163

Table A.25: Indexed reflections for the 180 nm MgFe-CO_3 LDH [a = b = 3.102(9) Å, c = 23.20(9) Å].

h	*k*	*l*	2d(obs)/Å	2d(calc)/Å	Residual
0	0	3	7.679887	7.735963	-0.05608
0	0	6	3.861751	3.867981	-0.00623
0	1	2	2.613965	2.617717	-0.00375
0	0	9	2.574039	2.578656	-0.00462
0	1	5	2.332192	2.325438	0.006755
1	0	7	2.076338	2.087495	-0.01116
0	1	8	1.9912	1.971302	0.019897
0	0	12	1.936133	1.933991	0.002142
1	1	0	1.551306	1.55133	-0.000002
1	1	3	1.520658	1.521046	-0.00039
1	1	6	1.437624	1.439842	-0.00222
2	0	2	1.336802	1.334576	0.002226
0	0	18	1.288416	1.289328	-0.00091

A.3 Characterising data for other LDHs

A.3.1 Elemental analysis

Table A.26: EDX, EA (C, H, N) and TGA data used to calculate approximate formulae for other LDH compositions.

LDH	EDX	EA (weight %)			TGA
	Mg:Al atomic ratio	C	H	N	% H_2O by mass
MgAl-NO_3 (70 nm)	1.64	0	3.075	4.06	6.4
MgAl-NO_3 (160 nm)	1.64	0	3.03	5.325	7.6
MgAl-Cl	2.35	<0.1	4.525	<0.1	15.6
MgFe-NO_3	1.77	0	2.335	3.59	8.8
CaAl-NO_3	1.66	0.49	2.945	3.845	6.6
CaAl-Cl	1.69	<0.1	3.44	<0.1	10.1

A.3.2 Powder X-ray diffraction

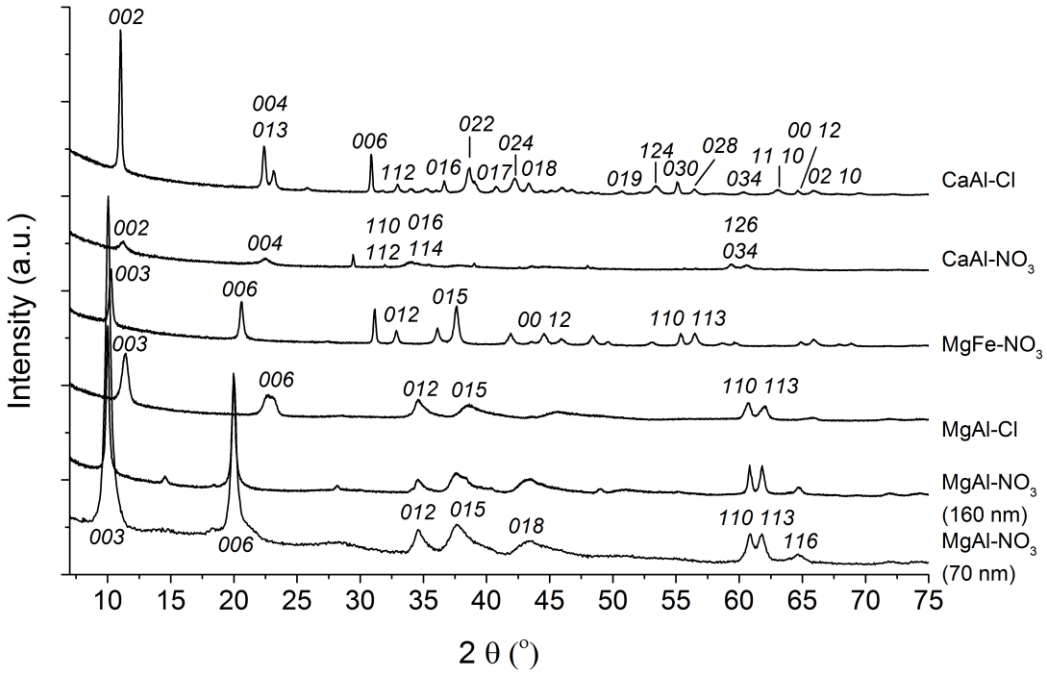

Figure A.1: Indexed powder XRD data for other LDH compositions.

A.3.3 Powder X-ray diffraction pattern indexing

MgAl-NO_3 LDHs were indexed to a similar unit cell to MgAl-CO_3 LDHs, but with a larger *c* parameter, since NO_3^- is larger than CO_3^{2-}, i.e. hexagonal unit cell, $a = b = 3.05$ Å, $c = 26.4$ Å, space group $R\bar{3}m$.[1]

Table A.27: Indexed reflections for the 70 nm MgAl-NO_3 LDH [$a = b = 3.046(4)$ Å, $c = 26.90(8)$ Å].

h	*k*	*l*	2d(obs)/Å	2d(calc)/Å	Residual
0	0	3	8.842263	8.968997	-0.12673
0	0	6	4.445861	4.484498	-0.03864
0	1	2	2.593913	2.588797	0.005116
0	1	5	2.384456	2.368779	0.015677
0	1	8	2.083059	2.075753	0.007305
1	1	0	1.524049	1.523108	0.000941
1	1	3	1.501259	1.501609	-0.00035
1	1	6	1.440296	1.442197	-0.0019

Table A.28: Indexed reflections for the 160 nm MgAl-NO_3 LDH [$a = b = 3.037(6)$ Å, $c = 26.74(8)$ Å].

h	*k*	*l*	2d(obs)/Å	2d(calc)/Å	Residual
0	0	3	8.84244	8.915699	-0.07326
0	0	6	4.446258	4.45786	-0.0116
0	1	2	2.595915	2.581029	0.014886
0	1	5	2.39409	2.360533	0.033556
0	1	8	2.087688	2.06734	0.020348
1	0	10	1.857329	1.875478	-0.01815
0	1	11	1.785926	1.785561	0.000365
1	1	0	1.523144	1.518711	0.004433
1	1	3	1.500467	1.497146	0.003321
1	1	6	1.439048	1.437575	0.001473
0	2	1	1.311581	1.313653	-0.00207
2	0	5	1.276631	1.277205	-0.00057

The MgAl-Cl LDH was indexed to an analogous unit cell to MgAl-CO_3 LDHs i.e. hexagonal unit cell, $a = b = 3.046(0)$ Å, $c = 22.77(2)$ Å, space group $R\bar{3}m$.[1]

Table A.29: Indexed reflections for the MgAl-Cl LDH [$a = b = 3.047(5)$ Å, $c = 23.73(5)$ Å].

h	k	l	2d(obs)/Å	2d(calc)/Å	Residual
0	0	3	7.750957	7.911216	-0.16026
0	0	6	3.907456	3.955599	-0.04814
0	1	2	2.590319	2.576101	0.014217
0	1	5	2.334636	2.306526	0.028109
0	0	12	1.98255	1.977804	0.004747
1	1	0	1.524074	1.52365	0.000424
1	1	6	1.41835	1.421818	-0.00347
2	0	2	1.312432	1.311436	0.000996

The MgFe-NO_3 LDH was indexed using a similar unit cell to MgFe-CO_3: hexagonal, $a = b = 3.107(8)$ Å, $c = 24.07(9)$ Å, space group $R\bar{3}m$ (increased *c*-parameter as NO_3 larger).[4]

Table A.30: Indexed reflections for the MgFe-NO_3 LDH [$a = b = 3.109(7)$ Å, $c = 24.48(8)$ Å].

h	*k*	*l*	2d(obs)/Å	2d(calc)/Å	Residual
0	0	3	7.882411	8.162688	-0.28028
0	0	6	3.952197	4.081346	-0.12915
0	1	2	2.634456	2.630174	0.004282
0	1	5	2.38473	2.359818	0.024912
0	0	12	2.058648	2.04067	0.017978
1	1	0	1.555789	1.554826	0.000963
1	0	13	1.541823	1.543569	-0.00175
1	1	3	1.525141	1.527366	-0.00223

CaAl-NO_3 LDH, initial parameters indexed to: hexagonal unit cell, $a = b = 5.744(5)$ Å, $c = 17.23(5)$ Å, space group $P\bar{3}c1$.[5,6]

Table A.31: Indexed reflections for the CaAl-NO_3 LDH [$a = b = 5.742(8)$ Å, $c = 17.24(5)$ Å].

h	*k*	*l*	2d(obs)/Å	2d(calc)/Å	Residual
0	0	2	8.624871	8.622188	0.002683
0	0	4	4.312918	4.311095	0.001822
1	1	0	2.87222	2.871213	0.001007
1	1	2	2.725291	2.724147	0.001145
0	1	6	2.48767	2.488397	-0.00073
1	1	4	2.391819	2.389724	0.002095
0	0	8	2.157223	2.155552	0.001671
1	1	6	2.031376	2.031263	0.000112
0	1	8	1.974064	1.977759	-0.00369
1	2	0	1.87994	1.879652	0.000288
1	2	2	1.834825	1.836518	-0.00169
0	0	10	1.725384	1.724441	0.000943
0	3	0	1.658468	1.657696	0.000771
0	3	2	1.627889	1.627884	5.28E-06
1	2	6	1.571684	1.573098	-0.00141
0	3	4	1.548263	1.547255	0.001009
0	3	6	1.436125	1.435964	0.000162
2	2	2	1.415947	1.416112	-0.00017

CaAl-Cl LDH, initial parameters indexed to: hexagonal unit cell, $a = b = 5.702(9)$ Å, $c = 17.31(9)$ Å, space group $P\bar{3}c1$.[5,6]

Table A.32: Indexed reflections for the CaAl-Cl LDH [$a = b = 5.706(9)$ Å, $c = 17.32(0)$ Å].

h	*k*	*l*	2d(obs)/Å	2d(calc)/Å	Residual
0	0	2	8.027853	8.659735	-0.63188
0	1	3	3.841022	3.754309	0.086713
0	0	6	2.896358	2.886589	0.009769
1	1	2	2.718375	2.709955	0.008419
0	1	6	2.547984	2.492549	0.055435
0	1	6	2.493212	2.492549	0.000662
0	2	1	2.451791	2.446229	0.005561
0	2	2	2.333181	2.376161	-0.04298
0	1	7	2.21388	2.21243	0.00145
0	2	4	2.139569	2.146117	-0.00655
0	1	8	1.973293	1.98301	-0.00972
0	1	9	1.798928	1.793235	0.005693
1	2	4	1.715946	1.715112	0.000833
0	3	0	1.665949	1.647334	0.018616
0	2	8	1.630377	1.628365	0.002012
0	3	3	1.584872	1.584107	0.000765
0	3	4	1.53374	1.539666	-0.00593
1	1	10	1.474739	1.480542	-0.0058
0	0	12	1.442323	1.443295	-0.00097
0	2	10	1.417815	1.418264	-0.00045
0	1	12	1.382837	1.38542	-0.00258
1	3	2	1.351835	1.353811	-0.00198
0	3	8	1.309835	1.310968	-0.00113

A.3.4 Fourier transform infrared spectroscopy

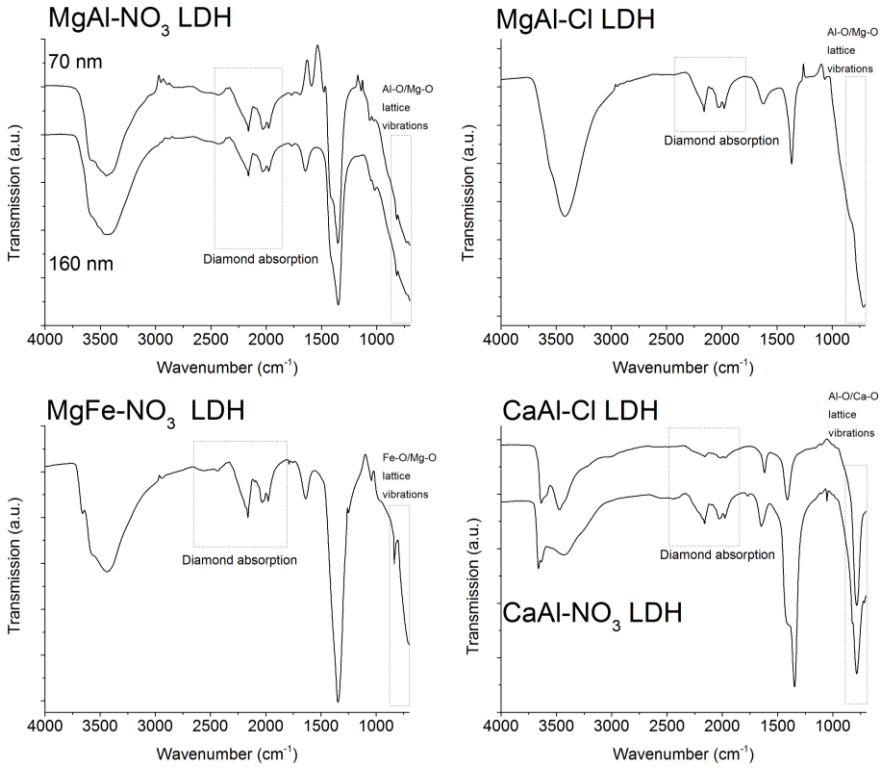

Figure A.2: IR spectra for all other LDH compositions. The strong absorption at 1635 cm^{-1} is attributable to the NO_3^- ion, and appears with a shoulder due to overlap between the symmetric and antisymmetric stretches.

A.3.5 Transmission electron microscopy

Table A.33: LDH particle diameters from TEM images, means obtained from measurement of > 100 particles. 'σ' = standard deviation, 'σ^2' = variance.

LDH	Mean size (nm)	σ	σ^2
$MgAl\text{-}NO_3$ (70 nm)	68.6	17	289
$MgAl\text{-}NO_3$ (160 nm)	157	45.4	2060
MgAl-Cl	48	12	144
$MgFe\text{-}NO_3$	46.7	12.6	159
$CaAl\text{-}NO_3$	537	267	71300
CaAl-Cl	554	218	47500

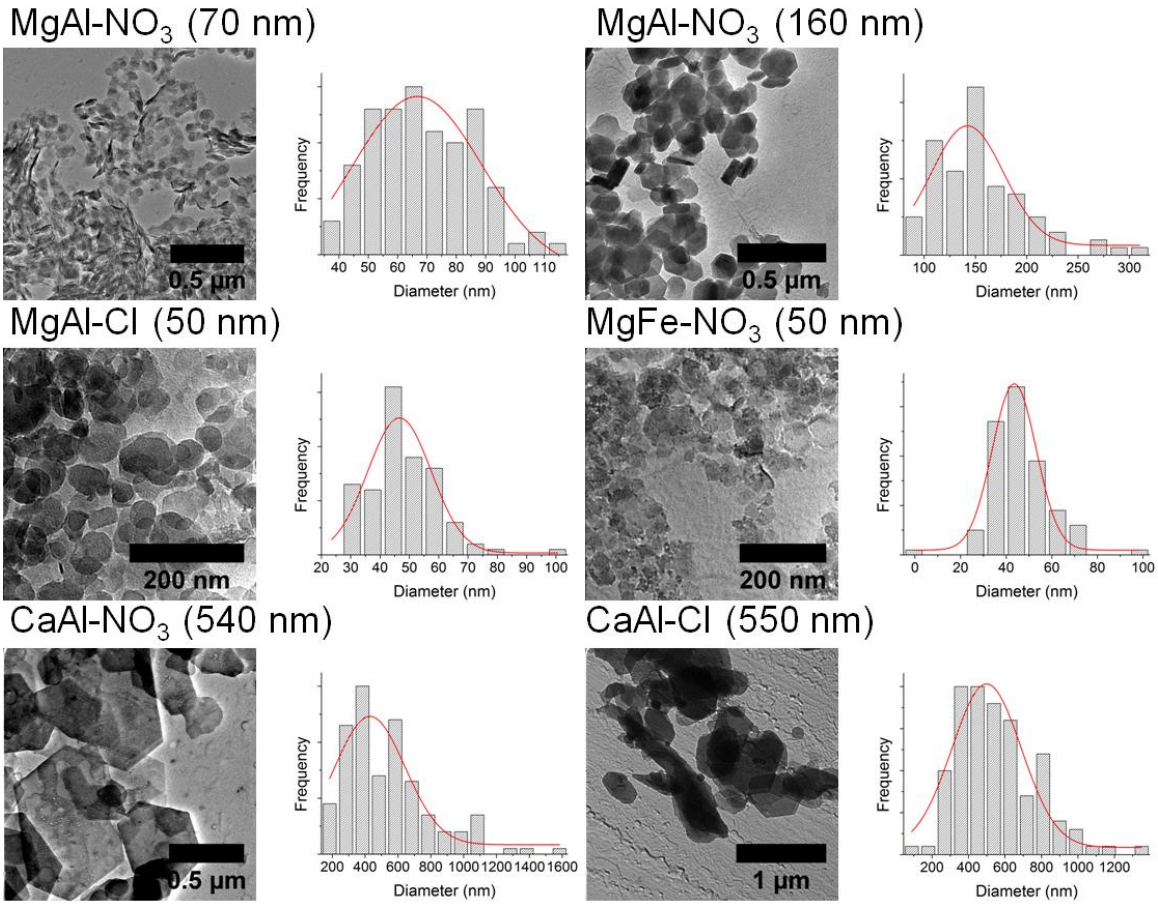

Figure A.3: Illustrative TEM images and size distribution plots for the other LDH compositions. Red lines indicate the best fit of a Gaussian curve, showing approximately normal distribution.

A.3.6 Zeta potential measurements

Table A.34: Zeta potential and pH measurements for other LDH compositions at 10 mg/mL in PBS. 'σ' = standard deviation, all measurements performed at 25 °C.

LDH	Zeta potential (mV)	σ	pH (meter)	pH (paper)
MgAl-NO_3 (70 nm)	4.5	2.48	7.43	7
MgAl-NO_3 (160 nm)	-19.5	7.53	7.55	7
MgAl-Cl	-17.2	4.42	7.97	7.5
MgFe-NO_3	-5.0	3.64	9.29	8
CaAl-NO_3	42.2	3.70	10.8	11
CaAl-Cl	-37.0	8.75	10.25	11

A.3.7 Dynamic light scattering measurements

Table A.35: Data for the most intense peak from DLS studies of other LDH comopsitions. 'σ' = standard deviation.

LDH	Diameter (nm)	σ	Peak area (%)	σ
MgAl-NO_3 (70 nm)	497	219	64.7	17.9
MgAl-NO_3 (160 nm)	257	1781	66.2	15.6
MgAl-Cl	951	516	74.4	10.9
MgFe-NO_3	1860	1030	82.1	16.8
CaAl-NO_3	1113	103	78.7	9.9
CaAl-Cl	760	78	92.0	1.1

Appendix B – Appendices to Chapter Three

B.1 Significance data for LDH titration

B.1.1 Viability

Table B.1: Significance data for percentages of dead Mo-DC (7-AAD positive cells) in preliminary LDH titration experiment, for each condition compared to the four controls (unstimulated, LPS, Imject and Alhydrogel). p-values greater than 0.05 taken as significant. NS = no stimulus, Imj = Imject, Alhyd = Alhydrogel. Two particle sizes of MgAl-CO_3 LDH, 60 and 2160 nm, were used. Significance data were calculated using the lmerTest package in [R].[7,8]

	Dead (% 7-AAD positive)			
Conditions	**NS**	**LPS**	**Imj**	**Alhyd**
NS	NA	0.64	**0.00**	**0.00**
LPS	0.64	NA	**0.00**	**0.00**
Imj	**0.00**	**0.00**	NA	0.83
Alhyd	**0.00**	**0.00**	0.83	NA
60 nm 50µg/mL	0.06	**0.02**	**0.00**	**0.00**
60 nm 250µg/mL	**0.00**	**0.00**	**0.00**	**0.00**
60 nm 500µg/mL	**0.00**	**0.00**	**0.03**	**0.02**
60 nm 1250µg/mL	**0.00**	**0.00**	0.10	0.06
60 nm 2500µg/mL	**0.00**	**0.00**	0.56	0.72
2160 nm 50µg/mL	0.06	**0.02**	**0.00**	**0.00**
2160 nm 250µg/mL	**0.00**	**0.00**	**0.01**	**0.01**
2160 nm 500µg/mL	**0.00**	**0.00**	0.17	0.11
2160 nm 1250µg/mL	**0.00**	**0.00**	0.26	0.36
2160 nm 2500µg/mL	**0.00**	**0.00**	0.76	0.93

B.1.2 Surface molecule expression

Table B.2: Significance data for surface molecule expression by viable Mo-DC (CD86, CD274, CD40 and MHC class II) in preliminary LDH titration experiment for each condition, compared to the four controls (unstimulated, LPS, Imject and Alhydrogel). p-values greater than 0.05 taken as significant. NS = no stimulus, Imj = Imject, Alhyd = Alhydrogel. Two particle sizes of MgAl-CO_3 LDH, 60 and 2160 nm, were used. Significance data were calculated using the lmerTest package in [R].[7,8]

	CD86				CD274 (B7-H1)			
Conditions	**NS**	**LPS**	**Imj**	**Alhyd**	**NS**	**LPS**	**Imj**	**Alhyd**
NS	NA	**0.00**	**0.00**	**0.00**	NA	NA	NA	NA
LPS	**0.00**	NA	**0.00**	**0.00**	NA	NA	**0.00**	**0.00**
Imj	**0.00**	**0.00**	NA	0.63	NA	**0.00**	NA	0.13
Alhyd	**0.00**	**0.00**	0.63	NA	NA	**0.00**	0.13	NA
60 nm 50µg/mL	0.71	**0.00**	**0.00**	**0.00**	NA	**0.00**	**0.00**	0.09
60 nm 250µg/mL	0.06	**0.00**	**0.00**	**0.00**	NA	**0.00**	0.15	0.72
60 nm 500µg/mL	**0.00**	**0.00**	**0.00**	**0.01**	NA	**0.00**	0.48	0.38
60 nm 1250µg/mL	**0.00**	**0.00**	0.72	0.40	NA	**0.00**	0.84	0.10
60 nm 2500µg/mL	**0.00**	0.07	0.14	0.05	NA	**0.00**	0.85	0.10
2160 nm 50µg/mL	**0.01**	**0.00**	**0.00**	**0.00**	NA	**0.00**	0.57	0.30
2160 nm 250µg/mL	**0.00**	0.44	**0.01**	**0.00**	NA	**0.02**	**0.01**	**0.00**
2160 nm 500µg/mL	**0.00**	0.92	**0.00**	**0.00**	NA	0.08	**0.00**	**0.00**
2160 nm 1250µg/mL	**0.00**	**0.00**	0.56	0.92	NA	**0.00**	0.57	0.05
2160 nm 2500µg/mL	0.53	**0.00**	**0.00**	**0.00**	NA	**0.00**	**0.00**	**0.01**

	CD40				MHC class II			
Conditions	**NS**	**LPS**	**Imj**	**Alhyd**	**NS**	**LPS**	**Imj**	**Alhyd**
NS	NA	**0.02**	**0.03**	0.76	NA	0.08	**0.00**	0.20
LPS	**0.02**	NA	**0.00**	**0.04**	0.08	NA	**0.00**	**0.00**
Imj	**0.03**	**0.00**	NA	**0.02**	**0.00**	**0.00**	NA	0.05
Alhyd	0.76	**0.04**	**0.02**	NA	0.20	**0.00**	0.05	NA
60 nm 50µg/mL	0.73	**0.04**	**0.01**	0.97	0.53	0.25	**0.00**	0.06
60 nm 250µg/mL	0.24	0.22	**0.00**	0.39	0.71	0.16	**0.00**	0.10
60 nm 500µg/mL	0.18	0.28	**0.00**	0.31	0.81	0.13	**0.00**	0.13
60 nm 1250µg/mL	0.77	**0.04**	**0.02**	0.98	0.90	0.06	**0.00**	0.25
60 nm 2500µg/mL	**0.00**	**0.00**	0.25	**0.00**	0.57	**0.02**	**0.01**	0.48
2160 nm 50µg/mL	0.14	0.36	**0.00**	0.24	0.94	0.09	**0.00**	0.18
2160 nm 250µg/mL	**0.04**	0.85	**0.00**	0.06	0.57	0.23	**0.00**	0.07
2160 nm 500µg/mL	0.06	0.97	**0.00**	0.10	0.52	0.26	**0.00**	0.06
2160 nm 1250µg/mL	0.51	0.14	**0.01**	0.70	0.06	**0.00**	0.19	0.53
2160 nm 2500µg/mL	**0.00**	**0.00**	**0.01**	**0.00**	**0.00**	**0.00**	**0.00**	**0.00**

B.2 Significance data for cell viability assessments

Table B.3: Significance data for viability assessment of Mo-DC in response to every LDH, compared to the four controls (unstimulated, LPS, Imject and Alhydrogel). Significance data performed on data from flow cytometry (percentage of necrotic/apoptotic cells from 7-AAD/Annexin V staining) and from the resazurin assays (percentage viable cells). p-values greater than 0.05 taken as significant. NS = no stimulus, Imj = Imject, Alhyd = Alhydrogel. Significance data were calculated using the lmerTest package in [R].[7,8]

Conditions		Necrotic (7-AAD positive)				Apoptotic (Annexin V positive)				% cells viable (resazurin assays)		
		NS	**LPS**	**Imj**	**Alhyd**	**NS**	**LPS**	**Imj**	**Alhyd**	**NS**	**Imj**	**Alhyd**
	NS	NA	**0.00**	**0.00**	**0.00**	NA	0.67	**0.00**	0.06	NA	0.38	**0.01**
	LPS	**0.00**	NA	**0.00**	**0.00**	0.67	NA	**0.00**	**0.02**	NA	NA	NA
	Imject	**0.00**	**0.00**	NA	0.91	**0.00**	**0.00**	NA	0.25	0.38	NA	0.08
	Alhyd	**0.00**	**0.00**	0.91	NA	0.06	**0.02**	0.25	NA	**0.01**	0.08	NA
$MgAl\text{-}CO_3$	**20 nm**	**0.01**	0.95	**0.00**	**0.00**	0.44	0.71	**0.00**	**0.01**	0.47	0.88	0.06
	40 nm	**0.00**	**0.00**	**0.00**	**0.00**	0.52	0.30	**0.03**	0.28	0.65	0.67	**0.03**
	60 nm	**0.00**	**0.00**	**0.00**	**0.00**	**0.02**	**0.01**	0.63	0.55	0.25	0.79	0.14
	70 nm	**0.00**	**0.00**	**0.02**	**0.04**	0.79	0.51	**0.01**	0.15	0.21	0.71	0.17
	190 nm	**0.00**	**0.00**	0.17	0.18	**0.01**	**0.00**	0.78	0.43	**0.00**	**0.00**	**0.00**
	210 nm	**0.00**	**0.00**	**0.00**	**0.00**	**0.00**	**0.00**	0.59	0.11	**0.00**	**0.00**	**0.00**
	400 nm	**0.00**	**0.00**	0.05	0.06	0.14	0.06	0.19	0.80	**0.00**	**0.00**	0.22
	1070 nm	**0.00**	**0.00**	0.84	0.77	**0.01**	**0.00**	0.97	0.27	**0.00**	**0.00**	0.25
	2160 nm	**0.00**	**0.00**	**0.05**	0.09	0.97	0.73	**0.01**	0.08	**0.00**	**0.00**	0.14
	2560 nm	**0.00**	**0.00**	**0.05**	0.09	0.79	0.90	**0.00**	**0.05**	**0.00**	**0.00**	**0.00**
	9900 nm	**0.00**	**0.00**	**0.00**	**0.00**	0.45	0.72	**0.00**	**0.01**	**0.01**	0.07	0.92
$LiAl\text{-}CO_3$	**10 nm**	**0.00**	**0.00**	0.18	0.25	0.12	**0.05**	0.14	0.76	0.90	0.45	**0.01**
	30 nm	**0.00**	0.09	**0.00**	**0.00**	0.77	0.53	**0.03**	0.22	0.83	0.51	**0.02**
	100 nm	**0.00**	**0.00**	**0.00**	**0.01**	0.24	0.11	0.07	0.49	0.15	0.58	0.23
	350 nm	**0.00**	**0.00**	**0.00**	**0.00**	**0.00**	**0.00**	0.98	0.23	**0.01**	0.11	0.89
	810 nm	**0.00**	**0.00**	**0.00**	**0.00**	**0.04**	**0.01**	0.37	0.81	0.07	0.35	0.42
	1240 nm	**0.00**	**0.00**	**0.03**	**0.05**	0.25	0.12	0.06	0.46	**0.01**	0.06	0.90
$MgFe\text{-}CO_3$	**20 nm**	**0.00**	**0.00**	**0.00**	**0.01**	0.55	0.30	**0.02**	0.20	**0.00**	**0.01**	0.40
	60 nm	**0.00**	**0.00**	**0.00**	**0.00**	0.71	0.96	**0.00**	**0.03**	**0.00**	**0.00**	**0.01**
	70 nm	**0.00**	**0.00**	0.14	0.20	0.60	0.88	**0.00**	**0.03**	**0.00**	**0.00**	0.13
	100 nm	**0.00**	**0.00**	0.29	0.27	0.84	0.53	**0.01**	0.10	**0.00**	**0.00**	**0.01**
	180 nm	**0.00**	**0.00**	0.13	0.13	0.20	0.09	0.08	0.55	**0.00**	**0.04**	0.72
Other LDHs	**$MgAl\text{-}NO_3$ (70 nm)**	**0.00**	**0.00**	0.25	0.33	**0.05**	**0.02**	0.43	0.78	0.14	0.54	0.26
	$MgAl\text{-}NO_3$ (160 nm)	**0.00**	**0.00**	**0.00**	**0.00**	0.81	0.92	**0.01**	0.08	0.12	0.49	0.29
	MgAl-Cl	**0.00**	**0.00**	**0.01**	**0.02**	0.33	0.19	0.14	0.59	**0.01**	**0.05**	0.62
	$MgAl\text{-}NO_3$	**0.00**	**0.00**	**0.04**	0.07	**0.00**	**0.00**	**0.00**	**0.00**	0.79	0.62	**0.05**
	CaAl-NO	**0.00**	**0.00**	**0.00**	**0.00**	0.27	0.14	0.09	0.53	0.48	0.86	0.06
	CaAl-Cl	**0.00**	**0.00**	**0.00**	**0.00**	0.21	0.10	0.15	0.68	0.33	0.92	0.10

B.3 Significance data for forward scatter/side scatter measurements

Table B.4: Significance data from measurements of forward scatter (FSC) and side scatter (SSC) for viable Mo-DC in response to every LDH, compared to the four controls (unstimulated, LPS, Imject and Alhydrogel). p-values greater than 0.05 taken as significant. NS = no stimulus, Imj = Imject, Alhyd = Alhydrogel. Significance data were calculated using the lmerTest package in [R].[7,8]

		FSC				SSC			
	Conditions	**NS**	**LPS**	**Imj**	**Alhyd**	**NS**	**LPS**	**Imj**	**Alhyd**
	NS	NA	**0.00**	0.55	**0.00**	NA	0.59	**0.00**	**0.00**
	LPS	**0.00**	NA	**0.00**	**0.05**	0.59	NA	**0.00**	**0.00**
	Imject	0.55	**0.00**	NA	**0.00**	**0.00**	**0.00**	NA	0.08
	Alhyd	**0.00**	**0.05**	**0.00**	NA	**0.00**	**0.00**	0.08	NA
MgAl-CO_3	**20 nm**	**0.00**	0.16	**0.00**	**0.00**	**0.00**	**0.00**	**0.00**	0.20
	40 nm	**0.00**	0.49	**0.00**	0.20	**0.00**	**0.00**	0.47	0.30
	60 nm	**0.00**	0.23	**0.00**	0.40	**0.00**	**0.00**	**0.00**	**0.00**
	70 nm	**0.00**	**0.02**	**0.00**	0.81	**0.00**	**0.00**	0.21	**0.01**
	190 nm	**0.00**	0.63	**0.00**	**0.02**	**0.00**	**0.00**	**0.00**	**0.00**
	210 nm	0.24	**0.00**	0.08	**0.00**	**0.00**	**0.00**	**0.00**	**0.00**
	400 nm	0.13	**0.00**	**0.04**	**0.00**	**0.00**	**0.00**	**0.00**	**0.00**
	1070 nm	**0.00**	**0.04**	**0.00**	**0.00**	**0.00**	**0.00**	**0.00**	**0.00**
	2160 nm	**0.00**	0.12	**0.00**	**0.00**	**0.00**	**0.00**	**0.00**	**0.00**
	2560 nm	0.71	**0.00**	0.34	**0.00**	**0.00**	**0.00**	**0.00**	**0.00**
	9900 nm	**0.00**	0.65	**0.00**	0.13	**0.00**	**0.00**	0.91	0.11
LiAl-CO_3	**10 nm**	**0.00**	**0.02**	**0.00**	0.68	**0.00**	**0.00**	**0.00**	**0.00**
	30 nm	0.25	**0.00**	0.11	**0.00**	**0.00**	**0.00**	0.80	0.22
	100 nm	**0.00**	0.16	**0.00**	0.60	**0.00**	**0.00**	**0.00**	**0.00**
	350 nm	0.25	**0.00**	0.10	**0.00**	**0.00**	**0.00**	**0.00**	**0.00**
	810 nm	0.06	**0.00**	0.18	**0.00**	**0.00**	**0.00**	**0.00**	**0.00**
	1240 nm	0.44	**0.00**	0.81	**0.00**	**0.00**	**0.00**	**0.00**	**0.00**
MgFe-CO_3	**20 nm**	**0.05**	**0.01**	**0.01**	**0.00**	**0.00**	**0.00**	**0.05**	0.83
	60 nm	**0.00**	0.05	**0.00**	**0.00**	**0.00**	**0.00**	0.47	0.31
	70 nm	**0.00**	0.60	**0.00**	0.25	**0.00**	**0.00**	**0.00**	**0.00**
	100 nm	**0.00**	0.79	**0.00**	**0.04**	**0.00**	**0.00**	**0.00**	**0.00**
	180 nm	**0.02**	**0.02**	**0.00**	**0.00**	**0.00**	**0.00**	**0.00**	**0.00**
Other LDHs	**MgAl-NO_3 (70 nm)**	**0.00**	0.26	**0.00**	0.51	**0.00**	**0.00**	0.55	**0.04**
	MgAl-NO_3 (160 nm)	**0.00**	0.16	**0.00**	0.76	**0.00**	**0.00**	**0.00**	**0.00**
	MgAl-Cl	**0.00**	0.41	**0.00**	**0.02**	**0.00**	**0.00**	0.55	0.37
	MgAl-NO_3	0.31	**0.00**	0.15	**0.00**	**0.00**	**0.00**	0.20	0.87
	CaAl-NO_3	**0.01**	0.06	**0.00**	**0.00**	**0.00**	**0.00**	0.05	**0.00**
	CaAl-Cl	**0.01**	0.08	**0.00**	**0.00**	**0.00**	**0.00**	**0.00**	**0.00**

B.4 Significance data for surface molecule expression

Table B.5: Significance data from measurements of surface molecule expression [CD86, CD83, CD274 (B7-H1), CD275 (B7-H2), MHC class I, MHC class II and CD40] for viable Mo-DC in response to every LDH, compared to the four controls (unstimulated, LPS, Imject and Alhydrogel). p-values greater than 0.05 taken as significant. NS = no stimulus, Imj = Imject, Alhyd = Alhydrogel. Significance data were calculated using the lmerTest package in [R].[7,8]

Conditions		CD86				CD83				CD274 (B7-H1)				CD275 (B7-H2)			
		NS	LPS	Imj	Alhyd	NS	LPS	Imj	Alhyd	NS	LPS	Imj	Alhyd	NS	LPS	Imj	Alhyd
	NS	NA	**0.00**	**0.00**	**0.00**	NA	**0.00**	**0.00**	**0.00**	NA	**0.00**	**0.00**	0.11	NA	**0.00**	**0.00**	**0.00**
	LPS	**0.00**	NA	**0.00**	**0.00**	**0.00**	NA	**0.00**	**0.00**	**0.00**	NA	**0.00**	**0.00**	**0.00**	NA	0.57	0.63
	Imject	**0.00**	**0.00**	NA	**0.00**	**0.00**	**0.00**	NA	**0.00**	**0.00**	**0.00**	NA	**0.00**	**0.00**	0.57	NA	0.29
	Alhyd	**0.00**	**0.00**	**0.00**	NA	**0.00**	**0.00**	**0.00**	NA	0.11	**0.00**	**0.00**	NA	**0.00**	0.63	0.29	NA
MgAl-CO_3	**20 nm**	**0.00**	**0.00**	**0.00**	**0.00**	**0.00**	**0.00**	**0.00**	**0.01**	**0.00**	**0.00**	0.09	0.11	0.65	**0.00**	**0.00**	**0.00**
	40 nm	**0.00**	**0.00**	**0.00**	**0.00**	**0.00**	**0.00**	**0.00**	0.11	**0.00**	**0.00**	**0.02**	0.23	0.88	**0.00**	**0.00**	**0.00**
	60 nm	**0.00**	**0.00**	**0.00**	**0.00**	**0.00**	**0.00**	**0.00**	0.35	**0.00**	**0.00**	**0.01**	0.37	0.26	**0.01**	**0.00**	**0.03**
	70 nm	**0.00**	**0.00**	**0.02**	**0.04**	**0.00**	**0.00**	**0.02**	**0.00**	**0.00**	**0.00**	0.17	**0.00**	**0.00**	0.24	0.53	0.09
	190 nm	**0.00**	**0.00**	**0.00**	**0.00**	**0.00**	**0.02**	0.43	**0.00**	**0.00**	**0.00**	**0.00**	**0.00**	**0.00**	**0.00**	**0.00**	**0.00**
	210 nm	**0.00**	**0.00**	**0.02**	**0.00**	**0.00**	**0.02**	0.33	**0.00**	**0.00**	**0.00**	**0.03**	**0.00**	**0.00**	**0.00**	**0.00**	**0.00**
	400 nm	**0.00**	0.07	**0.00**	**0.00**	**0.00**	0.17	0.06	**0.00**	**0.00**	**0.00**	**0.00**	**0.00**	**0.00**	**0.00**	**0.00**	**0.00**
	1070 nm	**0.00**	**0.00**	0.49	**0.00**	**0.00**	**0.03**	0.29	**0.00**	**0.00**	**0.00**	**0.00**	**0.00**	**0.00**	**0.00**	**0.00**	**0.00**
	2160 nm	**0.00**	**0.00**	0.94	**0.00**	**0.00**	**0.00**	0.87	**0.00**	**0.00**	**0.00**	**0.00**	**0.00**	**0.00**	0.21	0.48	0.08
	2560 nm	**0.00**	0.08	**0.00**	**0.00**	**0.00**	0.58	**0.01**	**0.00**	**0.00**	**0.00**	**0.00**	**0.00**	**0.00**	**0.00**	**0.00**	**0.00**
	9900 nm	**0.00**	**0.00**	**0.00**	0.96	**0.00**	**0.00**	**0.00**	**0.03**	**0.00**	**0.00**	0.54	**0.00**	**0.01**	0.29	0.10	0.56
LiAl-CO_3	**10 nm**	**0.00**	**0.00**	**0.00**	**0.00**	**0.02**	**0.00**	**0.00**	**0.00**	**0.00**	**0.00**	0.21	0.19	0.99	**0.00**	**0.00**	**0.00**
	30 nm	0.56	**0.00**	**0.00**	**0.00**	**0.01**	**0.00**	**0.00**	**0.01**	0.58	**0.00**	**0.00**	0.52	0.38	**0.01**	**0.00**	**0.02**
	100 nm	**0.00**	**0.00**	0.10	**0.00**	**0.00**	**0.00**	0.75	**0.00**	**0.00**	**0.00**	**0.02**	**0.00**	**0.00**	0.97	0.54	0.65
	350 nm	**0.00**	**0.00**	**0.04**	**0.00**	**0.00**	**0.00**	0.75	**0.00**	**0.00**	**0.00**	0.62	**0.02**	**0.00**	**0.00**	**0.00**	**0.00**
	810 nm	**0.00**	**0.00**	0.24	**0.00**	**0.00**	**0.00**	0.86	**0.00**	**0.00**	**0.00**	0.05	0.26	**0.00**	**0.00**	**0.00**	**0.00**
	1240 nm	**0.00**	**0.00**	**0.00**	0.17	**0.00**	**0.00**	**0.01**	**0.00**	0.08	**0.00**	**0.00**	0.93	**0.00**	0.13	0.33	**0.04**
MgFe-CO_3	**20 nm**	**0.00**	**0.00**	**0.00**	**0.00**	0.16	**0.00**	**0.00**	**0.00**	0.14	**0.00**	**0.00**	0.84	0.99	**0.00**	**0.00**	**0.00**
	60 nm	**0.00**	**0.00**	**0.00**	**0.00**	**0.00**	**0.00**	**0.00**	**0.02**	**0.03**	**0.00**	**0.01**	0.59	**0.00**	0.16	0.38	0.05
	70 nm	**0.00**	**0.00**	**0.00**	**0.00**	**0.00**	**0.00**	**0.00**	0.24	**0.00**	**0.00**	0.47	0.08	**0.00**	**0.00**	**0.01**	**0.00**
	100 nm	**0.00**	**0.03**	**0.00**	**0.00**	**0.00**	**0.01**	0.71	**0.00**	**0.00**	**0.00**	**0.00**	**0.00**	**0.00**	**0.00**	**0.00**	**0.00**
	180 nm	**0.00**	0.10	**0.00**	**0.00**	**0.00**	**0.00**	0.72	**0.00**	**0.00**	**0.00**	**0.00**	**0.00**	**0.00**	**0.00**	**0.00**	**0.00**
Other LDHs	**MgAl-NO_3 (70 nm)**	**0.00**	**0.00**	**0.00**	**0.00**	**0.00**	**0.00**	**0.00**	0.33	**0.00**	**0.00**	0.36	0.11	**0.02**	0.15	**0.04**	0.32
	MgAl-NO_3 (160 nm)	**0.00**	**0.00**	**0.00**	0.19	**0.00**	**0.00**	**0.00**	**0.01**	**0.02**	**0.00**	0.24	0.29	**0.00**	0.66	0.31	0.97
	MgAl-Cl	**0.00**	**0.00**	**0.00**	**0.00**	**0.00**	**0.00**	**0.00**	0.35	0.45	**0.00**	**0.00**	0.65	0.18	**0.02**	**0.00**	0.05
	MgAl-NO_3	**0.00**	**0.00**	**0.00**	**0.00**	0.24	**0.00**	**0.00**	**0.00**	0.61	**0.00**	**0.00**	0.49	0.34	**0.00**	**0.00**	**0.00**
	CaAl-NO_3	**0.00**	**0.00**	**0.00**	**0.00**	**0.02**	**0.00**	**0.00**	**0.00**	0.88	**0.00**	**0.00**	0.15	0.25	**0.01**	**0.00**	**0.03**
	CaAl-Cl	**0.00**	**0.00**	**0.00**	**0.00**	**0.00**	**0.00**	**0.00**	0.37	0.83	**0.00**	**0.00**	0.15	0.50	**0.00**	**0.00**	**0.01**

Conditions		MHC class I				MHC class II				CD40			
		NS	LPS	Imj	Alhyd	NS	LPS	Imj	Alhyd	NS	LPS	Imj	Alhyd
	NS	NA	**0.00**	**0.00**	**0.00**	NA	**0.00**	0.25	0.13	NA	**0.00**	0.13	**0.00**
	LPS	**0.00**	NA	**0.00**	**0.00**	**0.00**	NA	**0.00**	**0.00**	**0.00**	NA	**0.00**	**0.00**
	Imject	**0.00**	**0.00**	NA	**0.01**	0.25	**0.00**	NA	0.63	0.13	**0.00**	NA	**0.01**
	Alhyd	**0.00**	**0.00**	**0.01**	NA	0.13	**0.00**	0.63	NA	**0.00**	**0.00**	**0.01**	NA
MgAl-CO_3	**20 nm**	0.96	**0.00**	**0.00**	**0.00**	0.63	**0.00**	0.12	0.06	**0.00**	**0.00**	0.10	0.27
	40 nm	0.89	**0.00**	**0.00**	**0.00**	0.18	**0.00**	0.81	0.80	**0.00**	**0.00**	**0.01**	0.75
	60 nm	**0.03**	**0.00**	**0.00**	0.39	0.77	**0.00**	0.40	0.23	**0.00**	**0.00**	**0.00**	0.87
	70 nm	0.99	**0.00**	**0.00**	**0.00**	0.28	**0.00**	0.97	0.62	**0.00**	**0.01**	**0.00**	**0.01**
	190 nm	**0.02**	**0.00**	**0.00**	0.41	0.63	**0.00**	0.11	0.06	**0.00**	**0.00**	**0.00**	0.17
	210 nm	**0.03**	**0.00**	**0.00**	0.40	0.99	**0.00**	0.26	0.14	**0.00**	**0.00**	**0.00**	0.88
	400 nm	0.09	**0.00**	**0.00**	0.17	**0.04**	**0.00**	**0.00**	**0.00**	**0.00**	**0.00**	**0.00**	0.39
	1070 nm	**0.00**	**0.00**	0.06	0.39	**0.00**	**0.02**	**0.00**	**0.00**	**0.00**	**0.00**	**0.00**	0.27
	2160 nm	**0.00**	**0.00**	0.08	0.33	**0.00**	0.06	**0.00**	**0.00**	**0.00**	**0.00**	**0.00**	0.13
	2560 nm	0.21	**0.00**	**0.00**	0.07	**0.00**	0.48	**0.00**	**0.00**	**0.00**	**0.00**	**0.00**	0.47
	9900 nm	**0.00**	**0.00**	0.72	**0.02**	**0.02**	**0.00**	**0.00**	**0.00**	**0.00**	**0.00**	**0.00**	0.53
LiAl-CO_3	**10 nm**	0.36	**0.00**	**0.00**	**0.03**	0.44	**0.00**	0.08	**0.04**	0.22	**0.00**	1.00	**0.02**
	30 nm	0.61	**0.00**	**0.00**	**0.01**	0.29	**0.00**	0.87	0.81	0.42	**0.00**	0.95	0.07
	100 nm	**0.00**	**0.00**	**0.03**	0.57	**0.01**	**0.01**	**0.00**	**0.00**	**0.00**	**0.00**	**0.03**	0.76
	350 nm	**0.00**	**0.00**	0.20	0.16	0.20	**0.00**	0.79	0.85	**0.02**	**0.00**	0.25	0.26
	810 nm	**0.00**	**0.00**	0.20	0.15	**0.02**	**0.00**	0.18	0.44	0.19	**0.00**	0.86	**0.05**
	1240 nm	**0.00**	**0.00**	0.48	**0.00**	0.07	**0.00**	0.45	0.79	**0.01**	**0.00**	0.20	0.24
MgFe-CO_3	**20 nm**	0.10	**0.00**	**0.00**	0.15	0.86	**0.00**	0.40	0.23	**0.00**	**0.00**	**0.00**	0.56
	60 nm	0.96	**0.00**	**0.00**	**0.00**	0.36	**0.00**	0.06	**0.03**	**0.00**	**0.00**	**0.00**	0.13
	70 nm	0.39	**0.00**	**0.00**	**0.03**	**0.03**	**0.00**	0.23	0.48	**0.00**	0.15	**0.00**	**0.01**
	100 nm	0.36	**0.00**	**0.00**	**0.03**	0.10	**0.00**	**0.01**	**0.00**	**0.00**	**0.00**	**0.00**	0.42
	180 nm	**0.00**	**0.00**	**0.02**	0.71	0.39	**0.00**	0.06	**0.03**	**0.00**	**0.00**	**0.00**	0.45
Other LDHs	**MgAl-NO_3 (70 nm)**	**0.01**	**0.00**	**0.00**	0.58	0.20	**0.00**	**0.03**	**0.01**	**0.00**	**0.00**	**0.00**	0.24
	MgAl-NO_3 (160 nm)	**0.01**	**0.00**	**0.00**	0.68	0.06	**0.01**	**0.01**	**0.00**	**0.00**	**0.00**	**0.03**	0.76
	MgAl-Cl	0.09	**0.00**	**0.00**	0.16	0.79	**0.00**	0.25	0.14	**0.00**	**0.00**	**0.04**	0.86
	MgAl-NO_3	0.33	**0.00**	**0.00**	**0.03**	0.72	**0.00**	0.22	0.12	**0.00**	**0.00**	**0.03**	0.74
	CaAl-NO_3	0.62	**0.00**	**0.00**	**0.01**	0.30	**0.00**	0.05	**0.03**	0.19	**0.00**	0.77	0.09
	CaAl-Cl	0.21	**0.00**	**0.00**	0.07	**0.03**	**0.01**	**0.00**	**0.00**	0.05	**0.00**	0.33	0.31

B.5 Significance data for cytokine secretion

Table B.6: Significance data from measurements of cytokine concentration (TNF-α, IL-6, IL-1β) by Mo-DC in response to every LDH compared to the four controls (unstimulated, LPS, Imject and Alhydrogel). p-values greater than 0.05 taken as significant. NS = no stimulus, Imj = Imject, Alhyd = Alhydrogel. IL-1β readings for the unstiumalted cells negative control were below the limit of detection, therefore comparisons to it could not be made. Significance data were calculated using the lmerTest package in [R].[7,8]

	Conditions	TNF-α				IL-6				IL-1β			
		NS	**LPS**	**Imj**	**Alhyd**	**NS**	**LPS**	**Imj**	**Alhyd**	**NS**	**LPS**	**Imj**	**Alhyd**
	NS	NA	**0.00**	**0.00**	0.12	NA	0.05	**0.00**	0.18	NA	NA	NA	NA
	LPS	**0.00**	NA	**0.00**	**0.00**	0.05	NA	0.63	0.23	NA	NA	NA	NA
	Imject	**0.00**	**0.00**	NA	0.84	**0.00**	0.63	NA	0.13	NA	0.10	NA	NA
	Alhyd	0.12	**0.00**	0.84	NA	0.18	0.23	0.13	NA	NA	NA	NA	NA
$MgAl\text{-}CO_3$	**20 nm**	**0.00**	**0.00**	0.29	0.78	**0.00**	0.77	0.70	0.08	NA	**0.02**	0.17	NA
	40 nm	0.29	**0.00**	0.09	0.32	0.06	0.27	0.17	0.77	NA	NA	NA	NA
	60 nm	**0.00**	**0.00**	0.90	0.88	**0.02**	0.36	0.34	0.50	NA	**0.04**	0.28	NA
	70 nm	**0.00**	**0.00**	0.24	0.76	**0.00**	0.17	**0.00**	**0.00**	NA	NA	NA	NA
	190 nm	**0.00**	**0.00**	**0.00**	0.26	**0.00**	0.11	**0.00**	**0.00**	NA	**0.04**	0.70	NA
	210 nm	**0.00**	**0.00**	0.45	0.91	**0.03**	0.31	0.24	0.63	NA	0.13	0.88	NA
	400 nm	**0.00**	**0.00**	0.13	0.69	**0.00**	0.71	0.06	**0.00**	NA	0.71	0.12	NA
	1070 nm	**0.00**	**0.00**	**0.00**	**0.05**	**0.00**	**0.00**	**0.00**	**0.00**	NA	**0.02**	0.47	NA
	2160 nm	**0.00**	**0.00**	**0.00**	0.07	**0.00**	**0.02**	**0.00**	**0.00**	NA	**0.00**	**0.00**	NA
	2560 nm	**0.00**	**0.00**	**0.00**	**0.01**	**0.00**	**0.03**	**0.00**	**0.00**	NA	**0.00**	**0.01**	NA
	9900 nm	**0.00**	**0.00**	**0.00**	0.30	**0.00**	0.50	**0.01**	**0.00**	NA	**0.00**	**0.00**	NA
$LiAl\text{-}CO_3$	**10 nm**	0.10	**0.00**	0.70	0.67	0.53	0.13	**0.04**	0.57	NA	0.14	0.77	NA
	30 nm	0.58	**0.00**	0.12	0.16	**0.03**	**0.00**	**0.00**	**0.01**	NA	0.06	0.39	NA
	100 nm	**0.01**	**0.00**	0.92	0.89	**0.00**	0.82	0.17	**0.01**	NA	**0.03**	0.61	NA
	350 nm	**0.00**	**0.00**	**0.04**	0.42	**0.00**	0.56	**0.04**	**0.00**	NA	**0.04**	0.71	NA
	810 nm	**0.00**	**0.00**	0.44	0.79	**0.00**	0.90	0.51	**0.05**	NA	**0.01**	0.27	NA
	1240 nm	0.60	**0.00**	0.14	0.27	**0.04**	0.39	0.41	0.52	NA	**0.01**	0.32	NA
$MgFe\text{-}CO_3$	**20 nm**	0.34	**0.00**	0.70	0.65	0.92	0.06	**0.01**	0.22	NA	0.45	0.23	NA
	60 nm	**0.00**	**0.00**	**0.00**	0.11	**0.01**	0.65	0.99	0.20	NA	0.79	0.06	NA
	70 nm	**0.04**	**0.00**	0.66	0.89	0.44	0.21	0.16	0.82	NA	0.70	0.12	NA
	100 nm	**0.00**	**0.00**	**0.01**	0.17	0.20	0.24	0.16	0.98	NA	0.24	**0.00**	NA
	180 nm	**0.00**	**0.00**	0.19	0.61	0.70	**0.04**	**0.00**	0.14	NA	0.25	0.43	NA
Other LDHs	**$MgAl\text{-}NO_3$ (70 nm)**	**0.01**	**0.00**	0.19	0.41	0.17	0.33	0.35	0.79	NA	0.09	**0.00**	NA
	$MgAl\text{-}NO_3$ (160 nm)	0.29	**0.00**	0.75	0.70	0.68	0.20	0.19	0.72	NA	0.11	0.83	NA
	MgAl-Cl	0.34	**0.00**	0.95	0.86	0.29	0.40	0.51	0.81	NA	0.06	**0.00**	NA
	$MgAl\text{-}NO_3$	0.29	**0.00**	0.74	0.69	0.51	0.27	0.29	0.90	NA	0.65	0.14	NA
	$CaAl\text{-}NO_3$	0.58	**0.00**	0.12	0.16	0.82	0.12	0.07	0.50	NA	0.11	**0.00**	NA
	CaAl-Cl	0.15	**0.00**	0.96	0.91	0.80	0.07	**0.02**	0.26	NA	0.84	0.06	NA

B.6 Significance data for Luminex experiment

Table B.7: Significance data from measurements of cytokine/chemokine secretion by Mo-DC in response to selected LDHs, using the Luminex system. p-values greater than 0.05 taken as significant. NS = no stimulus. Significance data were calculated using the lmerTest package in [R].[7,8]

		Controls		$MgAl\text{-}CO_3$			$LiAl\text{-}CO_3$		$MgFe\text{-}CO_3$	
		NS	LPS	40 nm	190 nm	2160 nm	10 nm	810 nm	20 nm	100 nm
G-CSF	NS	NA	**0.00**	0.12	0.14	**0.03**	**0.00**	**0.00**	0.13	**0.00**
	LPS	**0.00**	NA	**0.00**	**0.00**	**0.00**	**0.00**	**0.00**	**0.00**	**0.00**
	40 nm	0.12	**0.00**	NA	**0.01**	**0.00**	**0.00**	**0.00**	**0.00**	**0.00**
	190 nm	0.14	**0.00**	**0.01**	NA	0.61	**0.00**	0.11	0.90	0.26
	2160 nm	**0.03**	**0.00**	**0.00**	0.61	NA	**0.00**	0.23	0.48	0.49
	10 nm	**0.00**	**0.00**	**0.00**	**0.00**	**0.00**	NA	**0.00**	**0.00**	**0.00**
	810 nm	**0.00**	**0.00**	**0.00**	0.11	0.23	**0.00**	NA	0.06	0.60
	20 nm	0.13	**0.00**	**0.00**	0.90	0.48	**0.00**	0.06	NA	0.17
	100 nm	**0.00**	**0.00**	**0.00**	0.26	0.49	**0.00**	0.60	0.17	NA
IFNα	NS	NA	0.21	0.07	0.32	0.49	**0.01**	0.08	0.76	0.37
	LPS	0.21	NA	**0.00**	0.89	0.56	**0.00**	0.62	0.33	0.71
	40 nm	0.07	**0.00**	NA	**0.01**	**0.01**	0.49	**0.00**	**0.04**	**0.01**
	190 nm	0.32	0.89	**0.01**	NA	0.70	**0.00**	0.56	0.47	0.85
	2160 nm	0.49	0.56	**0.01**	0.70	NA	**0.00**	0.28	0.70	0.83
	10 nm	**0.01**	**0.00**	0.49	**0.00**	**0.00**	NA	**0.00**	**0.01**	**0.00**
	810 nm	0.08	0.62	**0.00**	0.56	0.28	**0.00**	NA	0.15	0.39
	20 nm	0.76	0.33	**0.04**	0.47	0.70	**0.01**	0.15	NA	0.55
	100 nm	0.37	0.71	**0.01**	0.85	0.83	**0.00**	0.39	0.55	NA
IFNγ	NS	NA	**0.00**	0.95	0.13	0.92	1.00	**0.03**	0.49	0.55
	LPS	**0.00**	NA	**0.00**	**0.00**	**0.00**	**0.00**	**0.00**	**0.00**	**0.00**
	40 nm	0.95	**0.00**	NA	0.12	0.97	0.95	**0.02**	0.45	0.51
	190 nm	0.13	**0.00**	0.12	NA	0.11	0.13	0.63	0.37	0.33
	2160 nm	0.92	**0.00**	0.97	0.11	NA	0.92	**0.02**	0.43	0.49
	10 nm	1.00	**0.00**	0.95	0.13	0.92	NA	**0.03**	0.49	0.55
	810 nm	**0.03**	**0.00**	**0.02**	0.63	**0.02**	**0.03**	NA	0.13	0.11
	20 nm	0.49	**0.00**	0.45	0.37	0.43	0.49	0.13	NA	0.92
	100 nm	0.55	**0.00**	0.51	0.33	0.49	0.55	0.11	0.92	NA
IL-1β	NS	NA	**0.00**	0.13	**0.00**	**0.00**	0.06	**0.00**	**0.00**	**0.00**
	LPS	**0.00**	NA	**0.00**	**0.00**	0.08	**0.00**	0.17	**0.00**	**0.00**
	40 nm	0.13	**0.00**	NA	**0.00**	**0.00**	0.68	**0.00**	**0.00**	**0.00**
	190 nm	**0.00**	**0.00**	**0.00**	NA	0.11	**0.00**	0.05	0.36	0.64
	2160 nm	**0.00**	0.08	**0.00**	0.11	NA	**0.00**	0.68	**0.01**	0.21
	10 nm	0.06	**0.00**	0.68	**0.00**	**0.00**	NA	**0.00**	**0.00**	**0.00**
	810 nm	**0.00**	0.17	**0.00**	0.05	0.68	**0.00**	NA	**0.00**	0.10
	20 nm	**0.00**	**0.00**	**0.00**	0.36	**0.01**	**0.00**	**0.00**	NA	0.13
	100 nm	**0.00**	**0.00**	**0.00**	0.64	0.21	**0.00**	0.10	0.13	NA
IL-5	NS	NA	**0.00**	0.90	**0.02**	0.31	0.98	**0.00**	0.89	0.09
	LPS	**0.00**	NA	**0.00**	**0.00**	**0.00**	**0.00**	**0.00**	**0.00**	**0.00**
	40 nm	0.90	**0.00**	NA	**0.02**	0.37	0.89	**0.01**	0.79	0.11
	190 nm	**0.02**	**0.00**	**0.02**	NA	0.12	**0.01**	0.85	**0.01**	0.35
	2160 nm	0.31	**0.00**	0.37	0.12	NA	0.30	0.05	0.25	0.48
	10 nm	0.98	**0.00**	0.89	**0.01**	0.30	NA	**0.00**	0.90	0.08
	810 nm	**0.00**	**0.00**	**0.01**	0.85	0.05	**0.00**	NA	**0.00**	0.21
	20 nm	0.89	**0.00**	0.79	**0.01**	0.25	0.90	**0.00**	NA	0.06
	100 nm	0.09	**0.00**	0.11	0.35	0.48	0.08	0.21	0.06	NA
TNF-α	NS	NA	**0.00**	0.45	**0.00**	**0.00**	**0.02**	**0.00**	0.24	**0.00**
	LPS	**0.00**	NA	**0.00**	**0.00**	**0.00**	**0.00**	**0.00**	**0.00**	**0.00**
	40 nm	0.45	**0.00**	NA	**0.00**	**0.00**	0.09	**0.00**	0.66	**0.00**
	190 nm	**0.00**	**0.00**	**0.00**	NA	0.62	**0.02**	0.06	**0.00**	0.70
	2160 nm	**0.00**	**0.00**	**0.00**	0.62	NA	**0.00**	0.11	**0.00**	0.90
	10 nm	**0.02**	**0.00**	0.09	**0.02**	**0.00**	NA	**0.00**	0.20	**0.00**
	810 nm	**0.00**	**0.00**	**0.00**	0.06	0.11	**0.00**	NA	**0.00**	0.09
	20 nm	0.24	**0.00**	0.66	**0.00**	**0.00**	0.20	**0.00**	NA	**0.00**
	100 nm	**0.00**	**0.00**	**0.00**	0.70	0.90	**0.00**	0.09	**0.00**	NA
IL-8	NS	NA	**0.00**	0.24	**0.00**	**0.00**	0.16	**0.00**	**0.00**	**0.00**
	LPS	**0.00**	NA	**0.00**	**0.00**	**0.00**	**0.00**	**0.00**	**0.00**	**0.00**
	40 nm	0.24	**0.00**	NA	**0.00**	**0.00**	0.83	**0.00**	**0.01**	**0.00**
	190 nm	**0.00**	**0.00**	**0.00**	NA	0.47	**0.00**	0.15	**0.00**	0.61
	2160 nm	**0.00**	**0.00**	**0.00**	0.47	NA	**0.00**	0.42	**0.00**	0.81
	10 nm	0.16	**0.00**	0.83	**0.00**	**0.00**	NA	**0.00**	**0.02**	**0.00**
	810 nm	**0.00**	**0.00**	**0.00**	0.15	0.42	**0.00**	NA	**0.00**	0.30
	20 nm	**0.00**	**0.00**	**0.01**	**0.00**	**0.00**	**0.02**	**0.00**	NA	**0.00**
	100 nm	**0.00**	**0.00**	**0.00**	0.61	0.81	**0.00**	0.30	**0.00**	NA

		Controls		$MgAl\text{-}CO_3$			$LiAl\text{-}CO_3$		$MgFe\text{-}CO_3$	
		NS	LPS	40 nm	190 nm	2160 nm	10 nm	810 nm	20 nm	100 nm
IL-10	NS	NA	**0.00**	0.53	**0.00**	**0.03**	0.19	**0.01**	0.08	**0.00**
	LPS	**0.00**	NA	**0.00**	**0.00**	**0.00**	**0.00**	**0.00**	**0.00**	**0.00**
	40 nm	0.53	**0.00**	NA	**0.00**	0.12	0.06	0.06	0.25	**0.00**
	190 nm	**0.00**	**0.00**	**0.00**	NA	**0.04**	**0.00**	0.07	**0.02**	0.73
	2160 nm	**0.03**	**0.00**	0.12	**0.04**	NA	**0.00**	0.75	0.68	0.05
	10 nm	0.19	**0.00**	0.06	**0.00**	**0.00**	NA	**0.00**	**0.00**	**0.00**
	810 nm	**0.01**	**0.00**	0.06	0.07	0.75	**0.00**	NA	0.47	0.11
	20 nm	0.08	**0.00**	0.25	**0.02**	0.68	**0.00**	0.47	NA	**0.02**
	100 nm	**0.00**	**0.00**	**0.00**	0.73	0.05	**0.00**	0.11	**0.02**	NA
IL-12p70	NS	NA	**0.00**	0.71	0.06	0.43	1.00	0.86	1.00	0.23
	LPS	**0.00**	NA	**0.00**	**0.00**	**0.00**	**0.00**	**0.00**	**0.00**	**0.00**
	40 nm	0.71	**0.00**	NA	**0.03**	0.67	0.71	0.59	0.71	0.41
	190 nm	0.06	**0.00**	**0.03**	NA	**0.01**	0.06	0.09	0.06	**0.00**
	2160 nm	0.43	**0.00**	0.67	**0.01**	NA	0.42	0.33	0.43	0.69
	10 nm	1.00	**0.00**	0.71	0.06	0.42	NA	0.87	1.00	0.23
	810 nm	0.86	**0.00**	0.59	0.09	0.33	0.87	NA	0.86	0.17
	20 nm	1.00	**0.00**	0.71	0.06	0.43	1.00	0.86	NA	0.23
	100 nm	0.23	**0.00**	0.41	**0.00**	0.69	0.23	0.17	0.23	NA
IL-15	NS	NA	**0.00**	0.11	**0.01**	0.12	0.34	0.31	0.21	0.09
	LPS	**0.00**	NA	**0.00**	**0.00**	**0.00**	**0.00**	**0.00**	**0.00**	**0.00**
	40 nm	0.11	**0.00**	NA	**0.00**	**0.00**	**0.01**	**0.01**	0.73	**0.00**
	190 nm	**0.01**	**0.00**	**0.00**	NA	0.23	0.09	0.09	**0.00**	0.30
	2160 nm	0.12	**0.00**	**0.00**	0.23	NA	0.55	0.59	**0.01**	0.85
	10 nm	0.34	**0.00**	**0.01**	0.09	0.55	NA	0.96	**0.03**	0.44
	810 nm	0.31	**0.00**	**0.01**	0.09	0.59	0.96	NA	**0.03**	0.47
	20 nm	0.21	**0.00**	0.73	**0.00**	**0.01**	**0.03**	**0.03**	NA	**0.00**
	100 nm	0.09	**0.00**	**0.00**	0.30	0.85	0.44	0.47	**0.00**	NA
IP10	NS	NA	**0.00**	0.24	**0.00**	**0.00**	0.53	**0.00**	0.59	**0.04**
	LPS	**0.00**	NA	**0.00**	**0.00**	**0.00**	**0.00**	**0.00**	**0.00**	**0.00**
	40 nm	0.24	**0.00**	NA	**0.00**	**0.00**	0.08	**0.00**	0.09	**0.00**
	190 nm	**0.00**	**0.00**	**0.00**	NA	0.94	**0.02**	0.16	**0.01**	0.25
	2160 nm	**0.00**	**0.00**	**0.00**	0.94	NA	**0.01**	0.10	**0.01**	0.23
	10 nm	0.53	**0.00**	0.08	**0.02**	**0.01**	NA	**0.00**	0.93	0.14
	810 nm	**0.00**	**0.00**	**0.00**	0.16	0.10	**0.00**	NA	**0.00**	**0.01**
	20 nm	0.59	**0.00**	0.09	**0.01**	**0.01**	0.93	**0.00**	NA	0.12
	100 nm	**0.04**	**0.00**	**0.00**	0.25	0.23	0.14	**0.01**	0.12	NA
MCP1	NS	NA	**0.00**	0.56	0.48	0.06	**0.00**	**0.00**	0.84	**0.03**
	LPS	**0.00**	NA	**0.00**	**0.00**	**0.00**	**0.00**	**0.00**	**0.00**	**0.00**
	40 nm	0.56	**0.00**	NA	0.86	0.20	**0.00**	**0.01**	0.43	0.12
	190 nm	0.48	**0.00**	0.86	NA	0.33	**0.01**	**0.03**	0.37	0.23
	2160 nm	0.06	**0.00**	0.20	0.33	NA	**0.04**	0.17	**0.04**	0.79
	10 nm	**0.00**	**0.00**	**0.00**	**0.01**	**0.04**	NA	0.52	**0.00**	0.08
	810 nm	**0.00**	**0.00**	**0.01**	**0.03**	0.17	0.52	NA	**0.00**	0.26
	20 nm	0.84	**0.00**	0.43	0.37	**0.04**	**0.00**	**0.00**	NA	**0.02**
	100 nm	**0.03**	**0.00**	0.12	0.23	0.79	0.08	0.26	**0.02**	NA
MIP1β	NS	NA	**0.00**	0.65	**0.00**	**0.00**	0.12	**0.00**	0.36	**0.00**
	LPS	**0.00**	NA	**0.00**	**0.00**	**0.00**	**0.00**	**0.00**	**0.00**	**0.00**
	40 nm	0.65	**0.00**	NA	**0.00**	**0.00**	0.26	**0.00**	0.64	**0.00**
	190 nm	**0.00**	**0.00**	**0.00**	NA	0.40	**0.00**	0.31	**0.00**	0.85
	2160 nm	**0.00**	**0.00**	**0.00**	0.40	NA	**0.00**	0.85	**0.00**	0.25
	10 nm	0.12	**0.00**	0.26	**0.00**	**0.00**	NA	**0.00**	0.51	**0.00**
	810 nm	**0.00**	**0.00**	**0.00**	0.31	0.85	**0.00**	NA	**0.00**	0.18
	20 nm	0.36	**0.00**	0.64	**0.00**	**0.00**	0.51	**0.00**	NA	**0.00**
	100 nm	**0.00**	**0.00**	**0.00**	0.85	0.25	**0.00**	0.18	**0.00**	NA

B.7 Statistical analysis

B.7.1 LDH physicochemical properties used in modelling

Table B.8: LDH physicochemical properties used as explanatory variables in building linear mixed effects models of Mo-DC response. Certain properties ($M^{1+/2+}$ and M^{3+} radii; $M^{1+/2+}$ and M^{3+} Pauling electronegativities; $M^{1+/2+}$ and M^{3+} standard reduction potentials) are fundamental to each LDH composition, others are from the characterisating data supplied in Chapter Two (size, zeta potential, *a*- and *c*-parameters, pHs, atomic ratio M^{+}/M^{2+}:M^{3+} and percent carbon by mass). Size = particle diameter from TEM measurements in nm; Size stdev = standard deviation of the size measurements; Zeta = zeta potential; M^{+}/M^{2+} and M^{3+} = ionic radii of M^{+}/M^{2+} or M^{3+} respectively; SRP M^{+}/M^{2+} or SRP M^{3+} = standard reduction potential of M^{+}/M^{2+} or M^{3+} respectively; *a*/*c*-para = *a*/*c*-parameter in Å; pH.a = approximate pH of a 10 mg/mL LDH suspension in PBS measured using pH paper, pH.b = approximate pH of a 10 mg/mL LDH suspension in PBS measured using Hanna Instruments pH meter; Atomic ratio M^{+}/M^{2+}:M^{3+} = atomic ratio of M^{+}/M^{2+} to M^{3+} measured by EDX spectroscopy.

	Approx size (nm)	Size	Size stdev	Zeta	M^{+}/M^{2+}	M^{3+}	EN M^{+}/M^{2+}	EN M^{3+}	SRP M^{+}/M^{2+}	SRP M^{3+}	*a*-para	*c*-para	pH.a	pH.b	Atomic ratio M^{+}/M^{2+}:M^{3+}	%C by mass
MgAl-CO_3	**20**	19.6	5.2	-12.6	0.72	0.54	1.31	1.61	-2.37	-1.66	3.06	23.3	9.25	9.2	3.13	2.6
	40	42.4	13	-15.2	0.72	0.54	1.31	1.61	-2.37	-1.66	3.05	23.2	8.5	8.97	2.57	2.6
	60	64	14	-26.7	0.72	0.54	1.31	1.61	-2.37	-1.66	3.05	22.8	9	9.16	1.73	2.6
	70	71.56	21.2	-14.8	0.72	0.54	1.31	1.61	-2.37	-1.66	3.06	23.5	8	8.57	2.84	2.6
	190	187.7	70.4	-18.6	0.72	0.54	1.31	1.61	-2.37	-1.66	3.06	23.5	8	8.17	2.98	2.5
	210	205.1	74.7	-11.5	0.72	0.54	1.31	1.61	-2.37	-1.66	3.2	22.6	8	8.16	2.92	2.5
	400	400.2	141.6	-14.6	0.72	0.54	1.31	1.61	-2.37	-1.66	3.04	22.5	8	7.4	2.87	2.5
	1070	1071	300	13.6	0.72	0.54	1.31	1.61	-2.37	-1.66	3.05	22.7	8	7.82	2.15	2.8
	2160	2158	790	2.7	0.72	0.54	1.31	1.61	-2.37	-1.66	3.05	22.7	8	7.94	2.16	2.7
	2560	2560	485	1.7	0.72	0.54	1.31	1.61	-2.37	-1.66	3.04	22.6	8.25	8.7	2.14	3.6
	9900	9897	1379	-0.6	0.72	0.54	1.31	1.61	-2.37	-1.66	3.05	22.6	8	7.86	2.18	2.7
LiAl-CO_3	**10**	10.1	2.3	-35.9	0.76	0.54	0.98	1.61	-3.04	-1.66	5.08	7.82	10	9.56	0.5	2.8
	30	29.2	7.67	-40.6	0.76	0.54	0.98	1.61	-3.04	-1.66	5.08	7.6	8.5	9.12	0.5	2.4
	100	98.5	33.69	-42.1	0.76	0.54	0.98	1.61	-3.04	-1.66	5.12	7.7	10	10.12	0.5	4.7
	350	350.6	153.3	13.5	0.76	0.54	0.98	1.61	-3.04	-1.66	5	7.74	10	9.57	0.5	3.2
	810	810	230.8	2.7	0.76	0.54	0.98	1.61	-3.04	-1.66	5.14	7.72	9	9.52	0.5	3.2
	1240	1236	416	3.1	0.76	0.54	0.98	1.61	-3.04	-1.66	5.13	7.8	8	7.88	0.5	2.8
MgFe-CO_3	**20**	19.7	4.3	-23.0	0.72	0.645	1.31	1.83	-2.37	0.771	3.1	23.5	9	9.34	3.08	2.4
	60	57.1	18.8	-14.1	0.72	0.645	1.31	1.83	-2.37	0.771	3.11	23.1	8.5	9.15	3.26	2.3
	70	66.66	19.7093	-19.3	0.72	0.645	1.31	1.83	-2.37	0.771	3.1	23.2	8.5	9.06	3.92	2.2
	100	97.1	36.6	-22.8	0.72	0.645	1.31	1.83	-2.37	0.771	3.1	23.2	8	8.7	4.16	2.1
	180	183.7	58.9	-19.0	0.72	0.645	1.31	1.83	-2.37	0.771	3.1	23.2	8	8.32	3.92	2.3
Other LDHs	**MgAl-NO_3 (70 nm)**	68.6	17	4.5	0.72	0.54	1.31	1.61	-2.37	-1.66	3.05	26.9	7	7.43	1.64	0.0
	MgAl-NO_3 (160 nm)	156.5	45.4	-19.5	0.72	0.54	1.31	1.61	-2.37	-1.66	3.04	26.7	7	7.55	1.64	0.0
	MgAl-Cl	48	12	-17.2	0.72	0.54	1.31	1.61	-2.37	-1.66	3.05	23.7	7.5	7.97	2.35	0.0
	MgFe-NO_3	46.7	12.6	-5.0	0.72	0.645	1.31	1.83	-2.37	0.771	3.11	24.5	8	9.29	1.77	0.0
	CaAl-NO_3	537	267	42.2	1	0.54	1	1.61	-2.87	-1.66	5.74	17.2	11	10.8	1.66	0.5
	CaAl-Cl	554	218	-37.0	1	0.54	1	1.61	-2.87	-1.66	5.71	17.3	11	10.25	1.69	0.0

B.7.2 Model coefficients

Table B.9: Table of coefficients used in linear models for each LDH physicochemical property. Value in brackets after each entry indicates the standard error for that coefficient. SRP M^+/M^{2+} or SRP M^{3+} = standard reduction potential of M^+/M^{2+} or M^{3+} respectively; pH.a = approximate pH of a 10 mg/mL LDH suspension in PBS measured using pH paper, pH.b = approximate pH of a 10 mg/mL LDH suspension in PBS measured using Hanna Instruments pH meter; Atomic ratio M^+/M^{2+}:M^{3+} = atomic ratio of M^+/M^{2+} to M^{3+} measured by EDX spectroscopy.

		LDH property								
	Response	Zeta Potential	Radius M^+/M^{2+}	Radius M^{3+}	SRP M^+/M^{2+}	*c*-parameter	pH.a	pH.b	Atomic ratio M^+/M^{2+}:M^{3+}	% C by mass
Original	CD86	0.32 (0.23)	-0.26 (0.24)			-0.13 (0.24)				
	CD274 (B7-H1)	0.09 (0.11)	-0.25 (0.12)			-0.00 (0.11)				
	CD40	0.01 (0.04)	-0.09 (0.04)			0.11 (0.04)				
	MHC class II	-0.01 (0.04)	0.05 (0.04)			0.08 (0.04)				
	TNF-α	0.43 (0.20)	-0.46 (0.21)			-0.10 (0.21)				
	IL-6	0.44 (0.18)	-0.46 (0.18)			-0.07 (0.18)				
	MHC class I	-0.09 (0.04)	0.07 (0.04)			0.09 (0.04)				
	CD275 (B7-H2)	-0.09 (0.08)	0.13 (0.08)			0.04 (0.08)				
	CD83	0.24 (0.18)	-0.35 (0.19)			-0.08 (0.19)				
	IL-1β	0.41 (0.15)	-0.33 (0.16)			-0.28 (0.16)				
Original with size	CD86	-0.06 (0.12)	-0.48 (0.11)			-0.05 (0.11)				
	CD274 (B7-H1)	-0.07 (0.10)	-0.33 (0.09)			0.08 (0.09)				
	CD40	-0.04 (0.04)	-0.11 (0.04)			0.11 (0.04)				
	MHC class II	-0.01 (0.04)	0.05 (0.04)			0.08 (0.04)				
	TNF-α	-0.03 (0.19)	-0.64 (0.17)			0.15 (0.18)				
	IL-6	0.18 (0.18)	-0.49 (0.17)			-0.02 (0.16)				
	MHC class I	-0.01 (0.03)	0.08 (0.03)			0.08 (0.03)				
	CD275 (B7-H2)	0.02 (0.06)	0.22 (0.05)			0.02 (0.05)				
	CD83	-0.14 (0.10)	-0.53 (0.08)			-0.04 (0.09)				
	IL-1β	-0.06 (0.12)	-0.51 (0.11)			-0.09 (0.11)				
New without size	CD86	0.28 (0.19)						-0.45 (0.19)		0.50 (0.19)
	CD274 (B7-H1)	0.06 (0.08)						-0.26 (0.08)		0.36 (0.08)
	CD40	-0.01 (0.04)						-0.14 (0.04)		0.02 (0.04)
	MHC class II	-0.00 (0.04)						-0.02 (0.04)		-0.00 (0.04)
	TNF-α	0.39 (0.15)						-0.40 (0.15)		0.71 (0.15)
	IL-6	0.39 (0.13)						-0.37 (0.13)		0.61 (0.13)
	MHC class I	-0.07 (0.04)						0.08 (0.04)		-0.07 (0.04)
	CD275 (B7-H2)	-0.07 (0.07)						0.16 (0.07)		-0.18 (0.07)
	CD83	0.19 (0.14)						-0.45 (0.14)		0.50 (0.14)
	IL-1β	0.37 (0.13)						-0.22 (0.13)		0.48 (0.13)
New with size	CD86		-0.32 (0.12)			-0.00 (0.19)			0.11 (0.15)	0.26 (0.13)
	CD274 (B7-H1)		-0.13 (0.09)			0.22 (0.14)			0.02 (0.11)	0.33 (0.10)
	CD40		-0.11 (0.05)			0.03 (0.08)			0.09 (0.07)	-0.01 (0.06)
	MHC class II		0.10 (0.04)			0.23 (0.07)			-0.11 (0.06)	0.12 (0.05)
	TNF-α		-0.24 (0.18)			0.65 (0.29)			-0.18 (0.23)	0.68 (0.20)
	IL-6		-0.05 (0.18)			0.72 (0.30)			-0.37 (0.24)	0.73 (0.21)
	MHC class I		0.11 (0.04)			0.10 (0.06)			0.02 (0.05)	0.06 (0.04)
	CD275 (B7-H2)		0.22 (0.04)			0.22 (0.07)			-0.27 (0.05)	0.01 (0.05)
	CD83		-0.37 (0.09)			0.03 (0.14)			0.08 (0.12)	0.28 (0.10)
	IL-1β		-0.34 (0.13)			0.28 (0.20)			-0.28 (0.17)	0.32 (0.14)
Non-shared without size	CD86		0.68 (0.26)					-0.92 (0.24)		0.75 (0.21)
	CD274 (B7-H1)		0.25 (0.12)			0.24 (0.10)		-0.33 (0.10)		0.54 (0.10)
	CD40						-0.12 (0.04)		0.10 (0.04)	
	MHC class II					0.06 (0.04)				
	TNF-α	0.39 (0.15)						-0.40 (0.15)		0.71 (0.15)
	IL-6	0.35 (0.12)		-0.36 (0.13)	0.47 (0.13)					0.62 (0.12)
	MHC class I	-0.07 (0.03)				0.13 (0.03)		0.14 (0.03)		
	CD275 (B7-H2)	-0.11 (0.06)				0.40 (0.11)		0.22 (0.07)	-0.39 (0.10)	
	CD83		0.84 (0.28)				-1.08 (0.27)			0.90 (0.19)
	IL-1β	0.38 (0.13)								0.46 (0.13)
Non-shared with size	CD86		-0.35 (0.10)							0.25 (0.09)
	CD274 (B7-H1)				0.29 (0.07)					0.35 (0.06)
	CD40						-0.12 (0.04)		0.10 (0.04)	
	MHC class II					0.07 (0.03)				
	TNF-α		-1.13 (0.19)	-0.21 (0.12)	0.47 (0.15)		0.86 (0.20)			
	IL-6			-0.33 (0.13)	0.48 (0.13)					0.54 (0.12)
	MHC class I			-0.11 (0.04)			-0.15 (0.07)	0.23 (0.07)	0.15 (0.03)	
	CD275 (B7-H2)		0.21 (0.03)			0.21 (0.05)			-0.26 (0.05)	
	CD83		-0.40 (0.08)							0.25 (0.07)
	IL-1β		-0.73 (0.13)					0.33 (0.12)		

B.7.3 Correlation coefficients between cell death and response

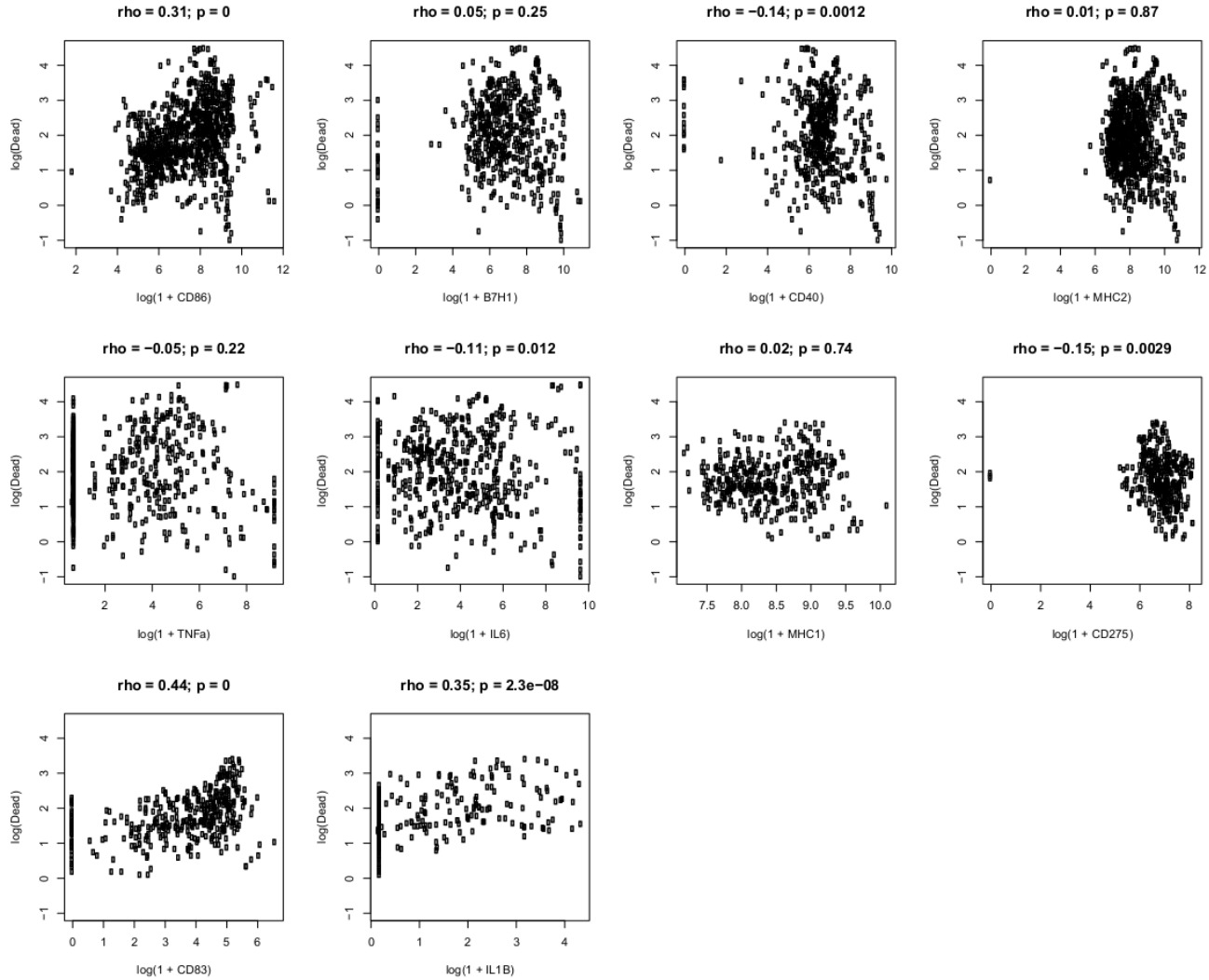

Figure B.1: Log-log scatter plots with correlation coefficients (rho = Spearman's rank correlation coefficient) for each Mo-DC response compared to the percentage dead cells (as determined by 7-AAD staining).

Appendix C – Appendices to Chapter Four

C.1 Characterising data for LiAl-CO_3 LDH synthesised from gibbsite

C.1.1 Elemental analysis

Table C.1: EDX, CHN and TGA data used to calculate approximate formulae for the LiAl-CO_3 LDH synthesised from gibbsite. ** indicates Li:Al assumed to be 1:2, as Li is too light for detection using EDX.

Approximate chemical formula	EDX	EA (weight %)			TGA
	Mg:Al atomic ratio	C	H	N	% H_2O by mass
$[LiAl_2(OH)_6](CO_3)_{0.5}\cdot 0.8H_2O$	0.5**	2.56	3.91	<0.1	12.0

C.1.2 Powder X-ray diffraction

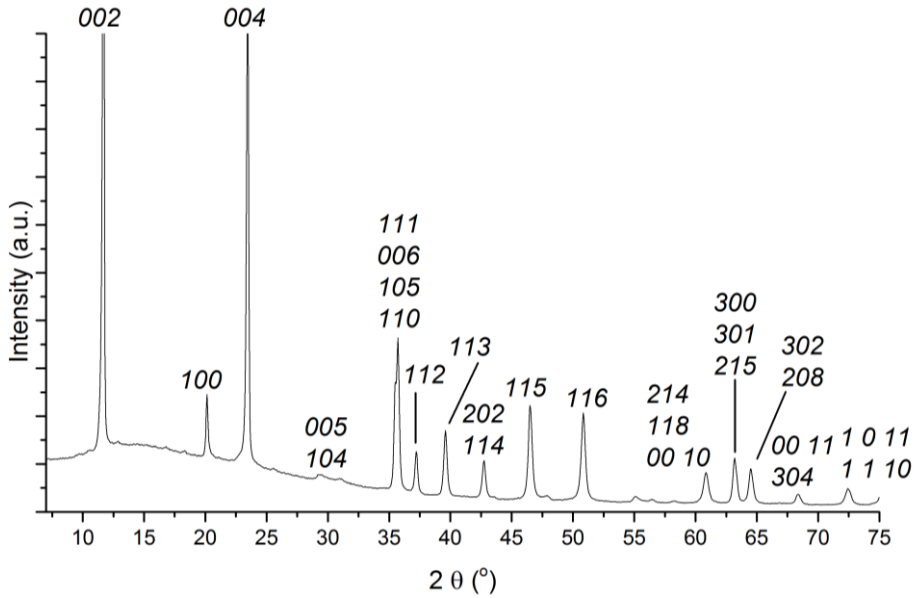

Figure C.1: Indexed powder XRD data for LiAl-CO_3 LDH synthesised from gibbsite. Reflections were indexed to a hexagonal unit cell, space group P63/m, a = b = 5.0979(4) Å, c = 15.1019(5) Å.[3]

C.1.3 Fourier transform infrared spectroscopy

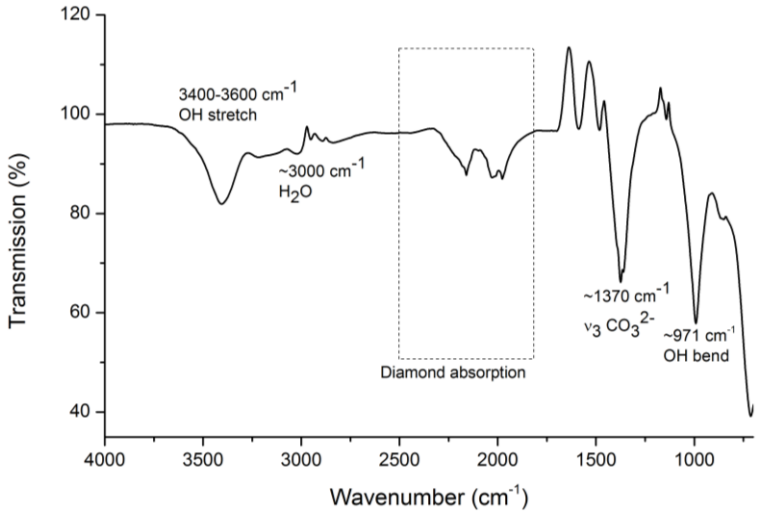

Figure C.2: FTIR spectra for LiAl-CO_3 LDH synthesised from gibbsite.

C.1.4 Transmission electron microscopy

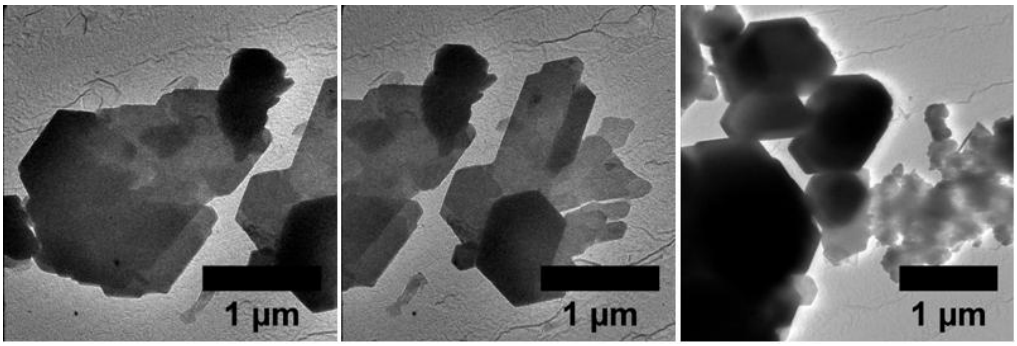

Figure C.3: Representative TEM images for LiAl-CO_3 LDH synthesised from gibbsite. Large (>1 µm) fragmented platelets were observed alongside smaller particles (left hand image).

C.2 Significance data for preliminary time course experiment

C.2.1 CFSE dilution

Table C.2: Significance data for cell division, as determined from CFSE dilution, in the preliminary timecourse experiment on whole T cells with allogeneic Mo-DC. p-values greater than 0.05 taken as significant. T cells only = control wells without allo-DC; NS (no stimulus), LPS, Imject and LDH treatments were all for T cells with allo-DC. Significance data were calculated using the lm() function in [R].[7] LDH = LiAl-CO_3 LDH synthesised from gibbsite.

		Divided $CD4^+$ T cell + allo-DCs					Divided $CD8^+$ T cell + allo-DCs				
		T cells only	**NS**	**LPS**	**Imject**	**LDH**	**T cells only**	**NS**	**LPS**	**Imject**	**LDH**
Day 3	**T cell only**	NA	0.89	1.00	**0.01**	0.98	NA	**0.03**	0.06	0.64	**0.04**
	NS	0.89	NA	0.89	**0.01**	0.84	**0.03**	NA	0.87	**0.03**	0.94
	LPS	1.00	0.89	NA	**0.01**	0.98	0.06	0.87	NA	0.06	0.92
	Imject	**0.01**	**0.01**	**0.01**	NA	**0.01**	0.64	**0.03**	0.06	NA	**0.03**
	LDH	0.98	0.84	0.98	**0.01**	NA	**0.04**	0.94	0.92	**0.03**	NA
Day 5	**T cell only**	NA	**0.01**	0.24	**0.00**	**0.00**	NA	0.06	**0.01**	0.23	**0.01**
	NS	**0.01**	NA	**0.03**	0.08	**0.04**	0.06	NA	**0.03**	**0.00**	0.09
	LPS	0.24	**0.03**	NA	**0.01**	**0.00**	**0.01**	**0.03**	NA	**0.00**	0.48
	Imject	**0.00**	0.08	**0.01**	NA	0.62	0.23	**0.00**	**0.00**	NA	**0.00**
	LDH	**0.00**	**0.04**	**0.00**	0.62	NA	**0.01**	0.09	0.48	**0.00**	NA
Day 7	**T cell only**	NA	**0.01**	**0.03**	**0.02**	**0.02**	NA	**0.00**	**0.00**	0.26	**0.01**
	NS	**0.01**	NA	0.27	0.43	0.46	**0.00**	NA	0.07	**0.01**	0.38
	LPS	**0.03**	0.27	NA	0.74	0.70	**0.00**	0.07	NA	**0.00**	**0.03**
	Imject	**0.02**	0.43	0.74	NA	0.96	0.26	**0.01**	**0.00**	NA	**0.02**
	LDH	**0.02**	0.46	0.70	0.96	NA	**0.01**	0.38	**0.03**	**0.02**	NA
Day 10	**T cell only**	NA	**0.00**	**0.00**	**0.00**	**0.00**	NA	**0.00**	**0.00**	**0.00**	**0.00**
	NS	**0.00**	NA	0.79	**0.00**	0.49	**0.00**	NA	0.15	**0.00**	0.30
	LPS	**0.00**	0.79	NA	**0.00**	0.39	**0.00**	0.15	NA	**0.00**	**0.05**
	Imject	**0.00**	**0.00**	**0.00**	NA	**0.00**	**0.00**	**0.00**	**0.00**	NA	**0.00**
	LDH	**0.00**	0.49	0.39	**0.00**	NA	**0.00**	0.30	**0.05**	**0.00**	NA

C.2.2 Cytokine secretion

Table C.3: Significance data for cytokine positive populations, determined using intracellular cytokine staining, in the preliminary timecourse experiment on whole T cells with allogeneic Mo-DC. p-values greater than 0.05 taken as significant. T cells only = control wells without allo-DC; NS (no stimulus), LPS, Imject and LDH treatments were all for T cells with allo-DC. Significance data were calculated using the lm() function in [R].[7] LDH = LiAl-CO_3 LDH synthesised from gibbsite.

		Day 3	T cells + allo-DCs				Day 5	T cells + allo-DC			
		Tcell only	NS	LPS	Imject	LDH	Tcell only	NS	LPS	Imject	LDH
IFN-γ	T cell only	NA	0.45	0.76	0.34	0.84	NA	**0.00**	**0.00**	**0.00**	**0.00**
	NS	0.45	NA	0.30	0.09	0.49	**0.00**	NA	0.09	**0.00**	0.37
	LPS	0.76	0.30	NA	0.52	0.58	**0.00**	0.09	NA	**0.00**	0.38
	Imject	0.34	0.09	0.52	NA	0.20	**0.00**	**0.00**	**0.00**	NA	**0.00**
	LDH	0.84	0.49	0.58	0.20	NA	**0.00**	0.37	0.38	**0.00**	NA
IL-4	T cell only	NA	**0.00**	0.12	**0.00**	**0.00**	NA	**0.00**	0.08	0.05	**0.00**
	NS	**0.00**	NA	**0.00**	**0.00**	**0.03**	**0.00**	NA	**0.02**	**0.00**	0.23
	LPS	0.12	**0.00**	NA	**0.00**	**0.00**	0.08	**0.02**	NA	**0.00**	**0.01**
	Imject	**0.00**	**0.00**	**0.00**	NA	**0.00**	0.05	**0.00**	**0.00**	NA	**0.00**
	LDH	**0.00**	**0.03**	**0.00**	**0.00**	NA	**0.00**	0.23	**0.01**	**0.00**	NA
IL-17	T cell only	NA	0.30	0.60	0.48	0.37	NA	0.38	**0.02**	0.24	0.18
	NS	0.30	NA	0.61	0.63	0.83	0.38	NA	**0.00**	**0.03**	0.42
	LPS	0.60	0.61	NA	0.91	0.73	**0.02**	**0.00**	NA	**0.04**	**0.00**
	Imject	0.48	0.63	0.91	NA	0.78	0.24	**0.03**	**0.04**	NA	**0.02**
	LDH	0.37	0.83	0.73	0.78	NA	0.18	0.42	**0.00**	**0.02**	NA
IFN-γIL-4	T cell only	NA	0.66	0.83	0.99	0.97	NA	**0.00**	**0.00**	0.43	**0.00**
	NS	0.66	NA	0.51	0.58	0.63	**0.00**	NA	0.28	**0.00**	0.14
	LPS	0.83	0.51	NA	0.82	0.78	**0.00**	0.28	NA	**0.00**	0.63
	Imject	0.99	0.58	0.82	NA	0.95	0.43	**0.00**	**0.00**	NA	**0.00**
	LDH	0.97	0.63	0.78	0.95	NA	**0.00**	0.14	0.63	**0.00**	NA
IFN-γIL-17	T cell only	NA	0.27	0.67	0.93	0.41	NA	**0.01**	**0.00**	0.92	**0.01**
	NS	0.27	NA	0.49	0.18	0.67	**0.01**	NA	0.08	**0.00**	0.32
	LPS	0.67	0.49	NA	0.57	0.71	**0.00**	0.08	NA	**0.00**	0.36
	Imject	0.93	0.18	0.57	NA	0.29	0.92	**0.00**	**0.00**	NA	**0.00**
	LDH	0.41	0.67	0.71	0.29	NA	**0.01**	0.32	0.36	**0.00**	NA
		Day 7	**T cells + allo-DCs**				**Day 10**	**T cells + allo-DCs**			
		Tcell only	**NS**	**LPS**	**Imject**	**LDH**	**Tcell only**	**NS**	**LPS**	**Imject**	**LDH**
IFN-γ	T cell only	NA	0.18	**0.01**	**0.00**	0.15	NA	**0.00**	**0.00**	0.06	**0.00**
	NS	0.18	NA	**0.02**	**0.00**	0.76	**0.00**	NA	**0.03**	**0.00**	**0.02**
	LPS	**0.01**	**0.02**	NA	**0.00**	**0.03**	**0.00**	**0.04**	NA	**0.00**	**0.00**
	Imject	**0.00**	**0.00**	**0.00**	NA	**0.00**	0.06	**0.00**	**0.00**	NA	**0.00**
	LDH	0.15	0.76	**0.03**	**0.00**	NA	**0.00**	**0.02**	**0.00**	**0.00**	NA
IL-4	T cell only	NA	**0.01**	**0.02**	0.15	**0.02**	NA	**0.00**	**0.01**	1.00	**0.00**
	NS	**0.01**	NA	0.86	**0.00**	0.95	**0.00**	NA	**0.02**	**0.00**	0.15
	LPS	**0.02**	0.86	NA	**0.00**	0.83	**0.01**	**0.02**	NA	**0.01**	0.24
	Imject	0.15	**0.00**	**0.00**	NA	**0.00**	1.00	**0.00**	**0.01**	NA	**0.00**
	LDH	**0.02**	0.95	0.83	**0.00**	NA	**0.00**	0.15	0.24	**0.00**	NA
IL-17	T cell only	NA	0.06	**0.03**	0.81	0.07	NA	0.29	1.00	1.00	**0.00**
	NS	0.06	NA	**0.00**	**0.04**	0.98	0.29	NA	0.19	0.19	**0.00**
	LPS	**0.03**	**0.00**	NA	**0.01**	**0.00**	1.00	0.19	NA	1.00	**0.00**
	Imject	0.81	**0.04**	**0.01**	NA	0.06	1.00	0.19	1.00	NA	**0.00**
	LDH	0.07	0.98	**0.00**	0.06	NA	**0.00**	**0.00**	**0.00**	**0.00**	NA
IFN-γIL-4	T cell only	NA	0.09	**0.03**	0.27	0.16	NA	**0.00**	**0.00**	0.52	**0.00**
	NS	0.09	NA	0.26	0.38	0.70	**0.00**	NA	0.45	**0.00**	**0.00**
	LPS	**0.03**	0.26	NA	0.10	0.18	**0.00**	0.45	NA	**0.00**	**0.00**
	Imject	0.27	0.38	0.10	NA	0.63	0.52	**0.00**	**0.00**	NA	**0.00**
	LDH	0.16	0.70	0.18	0.63	NA	**0.00**	**0.00**	**0.00**	**0.00**	NA
IFN-γIL-17	T cell only	NA	0.90	0.55	0.43	0.87	NA	0.09	0.09	0.88	0.06
	NS	0.90	NA	0.35	0.25	0.70	0.09	NA	0.86	**0.04**	0.60
	LPS	0.55	0.35	NA	0.82	0.59	0.09	0.86	NA	**0.04**	0.75
	Imject	0.43	0.25	0.82	NA	0.45	0.88	**0.04**	**0.04**	NA	**0.03**
	LDH	0.87	0.70	0.59	0.45	NA	0.06	0.60	0.75	**0.03**	NA

C.3 Significance data for naïve T cell MLR experiments

C.3.1 CFSE dilution

Table C.4: Significance data for cell division, as determined from CFSE dilution, in the naïve T cells with allogeneic Mo-DC MLR experiments. p-values greater than 0.05 taken as significant. T cells only = control wells without allo-DC; NS (no stimulus), LPS, Alhydrogel (Alhyd) and LDH treatments were all for T cells with allo-DC. Significance data were calculated using the lmerTest package in [R].[7,8]

		Divided CD4+								
		Tcells only	**NS**	**LPS**	**Alhyd**	**MgAl-CO_3**	**MgAl-NO_3**	**LiAl-CO_3**	**CaAl-NO_3**	**MgFe-CO_3**
Day 5	**Tcells only**	NA	**0.00**	**0.00**	**0.00**	**0.00**	**0.00**	**0.00**	**0.00**	**0.00**
	NS	**0.00**	NA	**0.01**	**0.00**	**0.00**	**0.00**	**0.00**	**0.00**	**0.01**
	LPS	**0.00**	**0.01**	NA	0.12	**0.00**	**0.00**	**0.01**	**0.00**	0.81
	Alhyd	**0.00**	**0.00**	0.12	NA	**0.00**	**0.00**	0.30	**0.03**	0.07
	MgAl-CO_3	**0.00**	**0.00**	**0.00**	**0.00**	NA	0.43	**0.00**	**0.02**	**0.00**
	MgAl-NO_3	**0.00**	**0.00**	**0.00**	**0.00**	0.43	NA	**0.00**	0.10	**0.00**
	LiAl-CO_3	**0.00**	**0.00**	**0.01**	0.30	**0.00**	**0.00**	NA	0.20	**0.00**
	CaAl-NO_3	**0.00**	**0.00**	**0.00**	**0.03**	**0.02**	0.10	0.20	NA	**0.00**
	MgFe-CO_3	**0.00**	**0.01**	0.81	0.07	**0.00**	**0.00**	**0.00**	**0.00**	NA
Day 10	**Tcells only**	NA	**0.00**	**0.00**	**0.00**	**0.00**	**0.00**	**0.00**	**0.00**	**0.00**
	NS	**0.00**	NA	0.57	**0.03**	0.45	0.52	0.80	0.24	**0.00**
	LPS	**0.00**	0.57	NA	**0.01**	0.20	0.24	0.75	0.10	**0.00**
	Alhyd	**0.00**	**0.03**	**0.01**	NA	0.14	0.11	**0.02**	0.28	**0.00**
	MgAl-CO_3	**0.00**	0.45	0.20	0.14	NA	0.90	0.31	0.67	**0.00**
	MgAl-NO_3	**0.00**	0.52	0.24	0.11	0.90	NA	0.37	0.59	**0.00**
	LiAl-CO_3	**0.00**	0.80	0.75	**0.02**	0.31	0.37	NA	0.15	**0.00**
	CaAl-NO_3	**0.00**	0.24	0.10	0.28	0.67	0.59	0.15	NA	**0.00**
	MgFe-CO_3	**0.00**	**0.00**	**0.00**	**0.00**	**0.00**	**0.00**	**0.00**	**0.00**	NA
		Divided CD8+								
		Tcells only	**NS**	**LPS**	**Alhyd**	**MgAl-CO_3**	**MgAl-NO_3**	**LiAl-CO_3**	**CaAl-NO_3**	**MgFe-CO_3**
Day 5	**Tcells only**	NA	0.14	**0.00**	**0.01**	**0.00**	**0.00**	**0.00**	**0.00**	**0.01**
	NS	0.14	NA	**0.00**	0.25	0.06	**0.04**	**0.00**	**0.01**	0.20
	LPS	**0.00**	**0.00**	NA	**0.00**	**0.00**	**0.00**	**0.00**	**0.00**	**0.00**
	Alhyd	**0.01**	0.25	**0.00**	NA	0.48	0.39	0.08	0.20	0.92
	MgAl-CO_3	**0.00**	0.06	**0.00**	0.48	NA	0.88	0.27	0.55	0.53
	MgAl-NO_3	**0.00**	**0.04**	**0.00**	0.39	0.88	NA	0.33	0.65	0.44
	LiAl-CO_3	**0.00**	**0.00**	**0.00**	0.08	0.27	0.33	NA	0.61	0.08
	CaAl-NO_3	**0.00**	**0.01**	**0.00**	0.20	0.55	0.65	0.61	NA	0.22
	MgFe-CO_3	**0.01**	0.20	**0.00**	0.92	0.53	0.44	0.08	0.22	NA
Day 10	**Tcells only**	NA	**0.00**	**0.00**	**0.00**	**0.00**	**0.00**	**0.00**	**0.00**	**0.00**
	NS	**0.00**	NA	0.15	**0.00**	**0.05**	0.47	0.58	0.09	**0.00**
	LPS	**0.00**	0.15	NA	**0.00**	**0.00**	**0.04**	0.35	**0.00**	**0.00**
	Alhyd	**0.00**	**0.00**	**0.00**	NA	**0.03**	**0.00**	**0.00**	**0.02**	**0.00**
	MgAl-CO_3	**0.00**	**0.05**	**0.00**	**0.03**	NA	0.19	**0.01**	0.76	**0.00**
	MgAl-NO_3	**0.00**	0.47	**0.04**	**0.00**	0.19	NA	0.21	0.31	**0.00**
	LiAl-CO_3	**0.00**	0.58	0.35	**0.00**	**0.01**	0.21	NA	**0.03**	**0.00**
	CaAl-NO_3	**0.00**	0.09	**0.00**	**0.02**	0.76	0.31	**0.03**	NA	**0.00**
	MgFe-CO_3	**0.00**	**0.00**	**0.00**	**0.00**	**0.00**	**0.00**	**0.00**	**0.00**	NA

C.3.2 IL-2 secretion

Table C.5: Significance data for IL-2 secretion in the naïve T cells with allogeneic Mo-DC MLR experiments. p-values greater than 0.05 taken as significant. T cells only = control wells without allo-DC; NS (no stimulus), LPS, Alhydrogel (Alhyd) and LDH treatments were all for T cells with allo-DC. Significance data were calculated using the lmerTest package in [R].[7,8]

		IL-2								
		Tcells only	**NS**	**LPS**	**Alhyd**	**MgAl-CO_3**	**MgAl-NO_3**	**LiAl-CO_3**	**CaAl-NO_3**	**MgFe-CO_3**
Day 5	**Tcells only**	NA	**0.00**	**0.00**	**0.00**	**0.00**	**0.00**	**0.00**	**0.00**	**0.00**
	NS	**0.00**	NA	**0.00**	0.18	0.17	0.97	0.17	0.41	0.62
	LPS	**0.00**	**0.00**	NA	**0.00**	**0.00**	**0.00**	**0.00**	**0.00**	**0.00**
	Alhyd	**0.00**	0.18	**0.00**	NA	0.99	0.19	**0.01**	0.58	0.38
	MgAl-CO_3	**0.00**	0.17	**0.00**	0.99	NA	0.19	**0.01**	0.58	0.38
	MgAl-NO_3	**0.00**	0.97	**0.00**	0.19	0.19	NA	0.15	0.44	0.65
	LiAl-CO_3	**0.00**	0.17	**0.00**	**0.01**	**0.01**	0.15	NA	**0.03**	0.06
	CaAl-NO_3	**0.00**	0.41	**0.00**	0.58	0.58	0.44	**0.03**	NA	0.74
	MgFe-CO_3	**0.00**	0.62	**0.00**	0.38	0.38	0.65	0.06	0.74	NA
Day 10	**Tcells only**	NA	**0.00**	**0.00**	**0.00**	**0.00**	**0.00**	**0.00**	**0.00**	**0.00**
	NS	**0.00**	NA	0.40	0.09	0.25	0.67	0.33	0.35	0.12
	LPS	**0.00**	0.40	NA	0.44	0.05	0.21	0.08	0.09	0.52
	Alhyd	**0.00**	0.09	0.44	NA	**0.01**	**0.04**	**0.01**	**0.01**	0.89
	MgAl-CO_3	**0.00**	0.25	0.05	**0.01**	NA	0.46	0.85	0.81	**0.01**
	MgAl-NO_3	**0.00**	0.67	0.21	**0.04**	0.46	NA	0.58	0.61	0.05
	LiAl-CO_3	**0.00**	0.33	0.08	**0.01**	0.85	0.58	NA	0.97	**0.01**
	CaAl-NO_3	**0.00**	0.35	0.09	**0.01**	0.81	0.61	0.97	NA	**0.02**
	MgFe-CO_3	**0.00**	0.12	0.52	0.89	**0.01**	0.05	**0.01**	**0.02**	NA

C.3.3 Tritiated thymidine incorporation

Table C.6: Significance data for tritiated thymidine incorporation in the naïve T cells with allogeneic Mo-DC MLR experiments. p-values greater than 0.05 taken as significant. T cells only = control wells without allo-DC; NS (no stimulus), LPS, Imject, (Imj), Alhydrogel (Alhyd) and LDH treatments were all for T cells with allo-DC. Significance data were calculated using the lmerTest package in [R].[7,8]

	Conditions	**Tcells only**	**NS**	**LPS**	**Imj**	**Alhyd**	**MgAl-CO_3**	**MgAl-NO_3**	**LiAl-CO_3**	**CaAl-NO_3**	**MgFe-CO_3**
Day 2	**Tcells only**	NA	**0.00**	**0.00**	**0.00**	**0.00**	**0.00**	**0.00**	**0.00**	**0.00**	**0.00**
	NS	**0.00**	NA	0.81	0.96	**0.00**	0.40	0.21	0.49	**0.00**	**0.00**
	LPS	**0.00**	0.81	NA	0.85	**0.00**	0.28	0.14	0.66	**0.00**	**0.00**
	Imj	**0.00**	0.96	0.85	NA	**0.00**	0.37	0.19	0.53	**0.00**	**0.00**
	Alhyd	**0.00**	**0.00**	**0.00**	**0.00**	NA	**0.00**	**0.00**	**0.00**	**0.00**	**0.00**
	MgAl-CO_3	**0.00**	0.40	0.28	0.37	**0.00**	NA	0.67	0.13	**0.03**	**0.00**
	MgAl-NO_3	**0.00**	0.21	0.14	0.19	**0.00**	0.67	NA	0.05	0.07	**0.00**
	LiAl-CO_3	**0.00**	0.49	0.66	0.53	**0.00**	0.13	0.05	NA	**0.00**	**0.00**
	CaAl-NO_3	**0.00**	**0.00**	**0.00**	**0.00**	**0.00**	**0.03**	0.07	**0.00**	NA	0.09
	MgFe-CO_3	**0.00**	**0.00**	**0.00**	**0.00**	**0.00**	**0.00**	**0.00**	**0.00**	0.09	NA
Day 3	**Tcells only**	NA	**0.00**	**0.00**	**0.00**	**0.00**	**0.00**	**0.00**	**0.00**	**0.00**	**0.00**
	NS	**0.00**	NA	0.14	0.85	**0.00**	**0.01**	**0.00**	0.48	**0.00**	**0.00**
	LPS	**0.00**	0.14	NA	0.19	**0.00**	**0.00**	**0.00**	0.43	**0.00**	**0.00**
	Imj	**0.00**	0.85	0.19	NA	**0.00**	**0.00**	**0.00**	0.61	**0.00**	**0.00**
	Alhyd	**0.00**	**0.00**	**0.00**	**0.00**	NA	**0.00**	**0.00**	**0.00**	**0.00**	**0.00**
	MgAl-CO_3	**0.00**	**0.01**	**0.00**	**0.00**	**0.00**	NA	0.36	**0.00**	0.10	0.23
	MgAl-NO_3	**0.00**	**0.00**	**0.00**	**0.00**	**0.00**	0.36	NA	**0.00**	0.49	0.80
	LiAl-CO_3	**0.00**	0.48	0.43	0.61	**0.00**	**0.00**	**0.00**	NA	**0.00**	**0.00**
	CaAl-NO_3	**0.00**	**0.00**	**0.00**	**0.00**	**0.00**	0.10	0.49	**0.00**	NA	0.65
	MgFe-CO_3	**0.00**	**0.00**	**0.00**	**0.00**	**0.00**	0.23	0.80	**0.00**	0.65	NA
Day 4	**Tcells only**	NA	**0.00**	**0.00**	**0.00**	**0.00**	**0.00**	**0.00**	**0.00**	**0.00**	**0.00**
	NS	**0.00**	NA	0.27	0.12	**0.00**	**0.00**	**0.00**	0.92	**0.00**	**0.00**
	LPS	**0.00**	0.27	NA	**0.01**	**0.00**	**0.00**	**0.00**	0.23	**0.00**	**0.00**
	Imj	**0.00**	0.12	**0.01**	NA	**0.00**	**0.00**	**0.01**	0.15	**0.00**	**0.00**
	Alhyd	**0.00**	**0.00**	**0.00**	**0.00**	NA	**0.00**	**0.00**	**0.00**	**0.00**	**0.00**
	MgAl-CO_3	**0.00**	**0.00**	**0.00**	**0.00**	**0.00**	NA	0.37	**0.00**	0.05	0.24
	MgAl-NO_3	**0.00**	**0.00**	**0.00**	**0.01**	**0.00**	0.37	NA	**0.00**	**0.01**	**0.04**
	LiAl-CO_3	**0.00**	0.92	0.23	0.15	**0.00**	**0.00**	**0.00**	NA	**0.00**	**0.00**
	CaAl-NO_3	**0.00**	**0.00**	**0.00**	**0.00**	**0.00**	0.05	**0.01**	**0.00**	NA	0.45
	MgFe-CO_3	**0.00**	**0.00**	**0.00**	**0.00**	**0.00**	0.24	**0.04**	**0.00**	0.45	NA

C.3.4 Cytokine secretion

Table C.7: Significance data for cytokine positive populations, determined using intracellular cytokine staining, in the naïve T cells with allogeneic Mo-DC MLR experiments. p-values greater than 0.05 taken as significant. T cells only = control wells without allo-DC; NS (no stimulus), LPS, Alhydrogel (Alhyd) and LDH treatments were all for T cells with allo-DC. Significance data were calculated using the lmerTest package in [R]. (Day 10 on next page)

	Day 5	Tcells only	NS	LPS	Alhyd	$MgAl\text{-}CO_3$	$MgAl\text{-}NO_3$	$LiAl\text{-}CO_3$	$CaAl\text{-}NO_3$	$MgFe\text{-}CO_3$
IFN-γ	**Tcells only**	NA	**0.03**	0.14	0.15	0.87	**0.01**	0.07	**0.04**	0.47
	NS	**0.03**	NA	**0.00**	0.50	**0.02**	0.66	**0.00**	**0.00**	0.13
	LPS	0.14	**0.00**	NA	**0.00**	0.16	**0.00**	0.71	0.50	**0.02**
	Alhyd	0.15	0.50	**0.00**	NA	0.09	0.27	**0.00**	**0.00**	0.42
	$MgAl\text{-}CO_3$	0.87	**0.02**	0.16	0.09	NA	**0.01**	0.08	**0.04**	0.35
	$MgAl\text{-}NO_3$	**0.01**	0.66	**0.00**	0.27	**0.01**	NA	**0.00**	**0.00**	0.05
	$LiAl\text{-}CO_3$	0.07	**0.00**	0.71	**0.00**	0.08	**0.00**	NA	0.76	**0.01**
	$CaAl\text{-}NO_3$	**0.04**	**0.00**	0.50	**0.00**	**0.04**	**0.00**	0.76	NA	**0.00**
	$MgFe\text{-}CO_3$	0.47	0.13	**0.02**	0.42	0.35	0.05	**0.01**	**0.00**	NA
IL-4	**Tcells only**	NA	**0.01**	0.06	0.15	**0.03**	**0.02**	**0.00**	0.92	0.78
	NS	**0.01**	NA	0.49	**0.00**	**0.00**	**0.00**	0.69	**0.01**	**0.00**
	LPS	0.06	0.49	NA	**0.00**	**0.00**	**0.00**	0.28	0.06	**0.02**
	Alhyd	0.15	**0.00**	**0.00**	NA	0.42	0.32	**0.00**	0.10	0.21
	$MgAl\text{-}CO_3$	**0.03**	**0.00**	**0.00**	0.42	NA	0.84	**0.00**	**0.01**	**0.04**
	$MgAl\text{-}NO_3$	**0.02**	**0.00**	**0.00**	0.32	0.84	NA	**0.00**	**0.01**	**0.02**
	$LiAl\text{-}CO_3$	**0.00**	0.69	0.28	**0.00**	**0.00**	**0.00**	NA	**0.00**	**0.00**
	$CaAl\text{-}NO_3$	0.92	**0.01**	0.06	0.10	**0.01**	**0.01**	**0.00**	NA	0.68
	$MgFe\text{-}CO_3$	0.78	**0.00**	**0.02**	0.21	**0.04**	**0.02**	**0.00**	0.68	NA
IL-17	**Tcells only**	NA	0.64	0.85	0.36	0.94	0.36	0.72	0.60	0.14
	NS	0.64	NA	0.48	0.63	0.68	0.63	0.90	0.95	0.29
	LPS	0.85	0.48	NA	0.25	0.78	0.24	0.56	0.45	0.08
	Alhyd	0.36	0.63	0.25	NA	0.38	0.99	0.55	0.67	0.57
	$MgAl\text{-}CO_3$	0.94	0.68	0.78	0.38	NA	0.37	0.77	0.63	0.14
	$MgAl\text{-}NO_3$	0.36	0.63	0.24	0.99	0.37	NA	0.55	0.68	0.55
	$LiAl\text{-}CO_3$	0.72	0.90	0.56	0.55	0.77	0.55	NA	0.85	0.23
	$CaAl\text{-}NO_3$	0.60	0.95	0.45	0.67	0.63	0.68	0.85	NA	0.31
	$MgFe\text{-}CO_3$	0.14	0.29	0.08	0.57	0.14	0.55	0.23	0.31	NA
IFN-γIL-4	**Tcells only**	NA	0.52	0.07	**0.00**	**0.01**	0.29	0.88	0.10	**0.04**
	NS	0.52	NA	0.22	**0.00**	**0.00**	0.07	0.40	**0.02**	**0.01**
	LPS	0.07	0.22	NA	**0.00**	**0.00**	**0.00**	**0.04**	**0.00**	**0.00**
	Alhyd	**0.00**	**0.00**	**0.00**	NA	0.52	**0.03**	**0.00**	0.13	0.26
	$MgAl\text{-}CO_3$	**0.01**	**0.00**	**0.00**	0.52	NA	0.12	**0.01**	0.36	0.61
	$MgAl\text{-}NO_3$	0.29	0.07	**0.00**	**0.03**	0.12	NA	0.33	0.52	0.29
	$LiAl\text{-}CO_3$	0.88	0.40	**0.04**	**0.00**	**0.01**	0.33	NA	0.11	**0.05**
	$CaAl\text{-}NO_3$	0.10	**0.02**	**0.00**	0.13	0.36	0.52	0.11	NA	0.68
	$MgFe\text{-}CO_3$	**0.04**	**0.01**	**0.00**	0.26	0.61	0.29	**0.05**	0.68	NA
IFN-γIL-17	**Tcells only**	NA	0.56	0.07	0.41	0.35	0.65	0.58	0.80	0.35
	NS	0.56	NA	**0.01**	0.79	0.70	0.26	0.22	0.37	0.71
	LPS	0.07	**0.01**	NA	**0.01**	**0.00**	0.15	0.18	0.09	**0.00**
	Alhyd	0.41	0.79	**0.01**	NA	0.92	0.18	0.15	0.26	0.93
	$MgAl\text{-}CO_3$	0.35	0.70	**0.00**	0.92	NA	0.14	0.11	0.20	0.99
	$MgAl\text{-}NO_3$	0.65	0.26	0.15	0.18	0.14	NA	0.92	0.83	0.14
	$LiAl\text{-}CO_3$	0.58	0.22	0.18	0.15	0.11	0.92	NA	0.75	0.11
	$CaAl\text{-}NO_3$	0.80	0.37	0.09	0.26	0.20	0.83	0.75	NA	0.21
	$MgFe\text{-}CO_3$	0.35	0.71	**0.00**	0.93	0.99	0.14	0.11	0.21	NA

Table C.7 continued.

	Day 10	Tcells only	NS	LPS	Alhyd	$MgAl-CO_3$	$MgAl-NO_3$	$LiAl-CO_3$	$CaAl-NO_3$	$MgFe-CO_3$
IFN-γ	Tcells only	NA	**0.00**	**0.00**	**0.00**	**0.00**	**0.00**	**0.00**	**0.00**	0.72
	NS	**0.00**	NA	**0.00**	0.14	0.29	**0.01**	0.69	0.35	**0.00**
	LPS	**0.00**	**0.00**	NA	**0.00**	**0.00**	**0.00**	**0.00**	**0.00**	**0.00**
	Alhyd	**0.00**	0.14	**0.00**	NA	0.65	0.23	0.27	0.56	**0.00**
	$MgAl-CO_3$	**0.00**	0.29	**0.00**	0.65	NA	0.10	0.51	0.90	**0.00**
	$MgAl-NO_3$	**0.00**	**0.01**	**0.00**	0.23	0.10	NA	**0.03**	0.08	**0.00**
	$LiAl-CO_3$	**0.00**	0.69	**0.00**	0.27	0.51	**0.03**	NA	0.59	**0.00**
	$CaAl-NO_3$	**0.00**	0.35	**0.00**	0.56	0.90	0.08	0.59	NA	**0.00**
	$MgFe-CO_3$	0.72	**0.00**	**0.00**	**0.00**	**0.00**	**0.00**	**0.00**	**0.00**	NA
IL-4	Tcells only	NA	0.21	0.28	0.85	**0.00**	0.51	0.06	0.11	0.91
	NS	0.21	NA	0.90	0.26	**0.00**	0.52	0.51	0.72	0.15
	LPS	0.28	0.90	NA	0.34	**0.00**	0.63	0.45	0.63	0.21
	Alhyd	0.85	0.26	0.34	NA	**0.00**	0.63	0.08	0.14	0.75
	$MgAl-CO_3$	**0.00**	**0.00**	**0.00**	**0.00**	NA	**0.00**	**0.00**	**0.00**	**0.00**
	$MgAl-NO_3$	0.51	0.52	0.63	0.63	**0.00**	NA	0.20	0.32	0.42
	$LiAl-CO_3$	0.06	0.51	0.45	0.08	**0.00**	0.20	NA	0.77	**0.04**
	$CaAl-NO_3$	0.11	0.72	0.63	0.14	**0.00**	0.32	0.77	NA	0.07
	$MgFe-CO_3$	0.91	0.15	0.21	0.75	**0.00**	0.42	**0.04**	0.07	NA
IL-17	Tcells only	NA	0.78	1.00	0.95	0.82	0.05	0.72	0.12	0.84
	NS	0.78	NA	0.78	0.71	0.95	**0.02**	0.94	0.18	0.93
	LPS	1.00	0.78	NA	0.95	0.82	0.05	0.72	0.12	0.84
	Alhyd	0.95	0.71	0.95	NA	0.76	0.05	0.66	0.09	0.77
	$MgAl-CO_3$	0.82	0.95	0.82	0.76	NA	**0.02**	0.89	0.16	0.99
	$MgAl-NO_3$	0.05	**0.02**	0.05	0.05	**0.02**	NA	**0.02**	**0.00**	**0.02**
	$LiAl-CO_3$	0.72	0.94	0.72	0.66	0.89	**0.02**	NA	0.20	0.88
	$CaAl-NO_3$	0.12	0.18	0.12	0.09	0.16	**0.00**	0.20	NA	0.16
	$MgFe-CO_3$	0.84	0.93	0.84	0.77	0.99	**0.02**	0.88	0.16	NA
IFN-γIL-4	Tcells only	NA	**0.00**	**0.00**	**0.00**	**0.00**	**0.02**	**0.01**	**0.00**	0.73
	NS	**0.00**	NA	**0.00**	0.95	0.63	0.23	0.55	0.97	**0.00**
	LPS	**0.00**	**0.00**	NA	**0.00**	**0.00**	**0.00**	**0.00**	**0.00**	**0.00**
	Alhyd	**0.00**	0.95	**0.00**	NA	0.59	0.21	0.51	0.93	**0.00**
	$MgAl-CO_3$	**0.00**	0.63	**0.00**	0.59	NA	0.46	0.90	0.65	**0.00**
	$MgAl-NO_3$	**0.02**	0.23	**0.00**	0.21	0.46	NA	0.54	0.24	**0.01**
	$LiAl-CO_3$	**0.01**	0.55	**0.00**	0.51	0.90	0.54	NA	0.57	**0.00**
	$CaAl-NO_3$	**0.00**	0.97	**0.00**	0.93	0.65	0.24	0.57	NA	**0.00**
	$MgFe-CO_3$	0.73	**0.00**	**0.00**	**0.00**	**0.00**	**0.01**	**0.00**	**0.00**	NA
IFN-γIL-17	Tcells only	NA	0.95	0.50	0.94	**0.03**	**0.01**	0.61	0.25	0.22
	NS	0.95	NA	0.44	1.00	**0.02**	**0.01**	0.64	0.20	0.22
	LPS	0.50	0.44	NA	0.44	**0.00**	**0.00**	0.23	0.65	0.06
	Alhyd	0.94	1.00	0.44	NA	**0.02**	**0.01**	0.64	0.20	0.23
	$MgAl-CO_3$	**0.03**	**0.02**	**0.00**	**0.02**	NA	0.72	0.07	**0.00**	0.27
	$MgAl-NO_3$	**0.01**	**0.01**	**0.00**	**0.01**	0.72	NA	**0.03**	**0.00**	0.14
	$LiAl-CO_3$	0.61	0.64	0.23	0.64	0.07	**0.03**	NA	0.09	0.45
	$CaAl-NO_3$	0.25	0.20	0.65	0.20	**0.00**	**0.00**	0.09	NA	**0.02**
	$MgFe-CO_3$	0.22	0.22	0.06	0.23	0.27	0.14	0.45	**0.02**	NA

C.4 Significance data for memory T cell experiments

C.4.1 CFSE dilution

Table C.8: Significance data for cell division, as measured using CFSE dilution, in the memory T cells with allogeneic Mo-DC MLR experiments. p-values greater than 0.05 taken as significant. T cells only = control wells without allo-DC; NS (no stimulus), LPS, Imject (Imj) and Alhydrogel (Alhyd) and LDH treatments were all for T cells with allo-DC. Significance data were calculated using the lmerTest package in [R].[7,8]

		Divided CD4+									
		Tcells only	**NS**	**LPS**	**Imj**	**Alhyd**	**MgAl-CO_3**	**MgAl-NO_3**	**LiAl-CO_3**	**CaAl-NO_3**	**MgFe-CO_3**
Day 2	**Tcells only**	NA	0.81	0.97	0.46	**0.05**	0.07	**0.01**	0.56	0.58	0.15
	NS	0.81	NA	0.83	0.62	**0.03**	**0.04**	**0.00**	0.74	0.76	0.09
	LPS	0.97	0.83	NA	0.48	**0.04**	0.06	**0.01**	0.58	0.61	0.14
	Imj	0.46	0.62	0.48	NA	**0.01**	**0.01**	**0.00**	0.87	0.85	**0.03**
	Alhyd	**0.05**	**0.03**	**0.04**	**0.01**	NA	0.85	0.41	**0.01**	**0.01**	0.56
	MgAl-CO_3	0.07	**0.04**	0.06	**0.01**	0.85	NA	0.31	**0.02**	**0.02**	0.70
	MgAl-NO_3	**0.01**	**0.00**	**0.01**	**0.00**	0.41	0.31	NA	**0.00**	**0.00**	0.16
	LiAl-CO_3	0.56	0.74	0.58	0.87	**0.01**	**0.02**	**0.00**	NA	0.97	**0.04**
	CaAl-NO_3	0.58	0.76	0.61	0.85	**0.01**	**0.02**	**0.00**	0.97	NA	**0.05**
	MgFe-CO_3	0.15	0.09	0.14	**0.03**	0.56	0.70	0.16	**0.04**	**0.05**	NA
Day 5	**Tcells only**	NA	**0.00**	**0.00**	**0.00**	**0.03**	0.49	0.77	**0.00**	**0.00**	0.17
	NS	**0.00**	NA	0.45	0.32	**0.00**	**0.00**	**0.00**	0.08	0.33	**0.00**
	LPS	**0.00**	0.45	NA	0.82	**0.00**	**0.00**	**0.00**	**0.01**	0.83	**0.00**
	Imj	**0.00**	0.32	0.82	NA	**0.00**	**0.00**	**0.00**	**0.01**	0.99	**0.00**
	Alhyd	**0.03**	**0.00**	**0.00**	**0.00**	NA	0.11	**0.05**	**0.00**	**0.00**	0.41
	MgAl-CO_3	0.49	**0.00**	**0.00**	**0.00**	0.11	NA	0.68	**0.00**	**0.00**	0.46
	MgAl-NO_3	0.77	**0.00**	**0.00**	**0.00**	**0.05**	0.68	NA	**0.00**	**0.00**	0.26
	LiAl-CO_3	**0.00**	0.08	**0.01**	**0.01**	**0.00**	**0.00**	**0.00**	NA	**0.01**	**0.00**
	CaAl-NO_3	**0.00**	0.33	0.83	0.99	**0.00**	**0.00**	**0.00**	**0.01**	NA	**0.00**
	MgFe-CO_3	0.17	**0.00**	**0.00**	**0.00**	0.41	0.46	0.26	**0.00**	**0.00**	NA
Day 7	**Tcells only**	NA	**0.00**	**0.00**	**0.00**	**0.00**	**0.00**	**0.00**	**0.00**	**0.00**	**0.00**
	NS	**0.00**	NA	0.34	0.72	0.54	0.49	0.20	0.13	0.42	**0.03**
	LPS	**0.00**	0.34	NA	0.19	0.12	0.10	**0.03**	0.56	0.88	**0.00**
	Imj	**0.00**	0.72	0.19	NA	0.80	0.73	0.35	0.06	0.24	0.06
	Alhyd	**0.00**	0.54	0.12	0.80	NA	0.93	0.49	**0.04**	0.16	0.10
	MgAl-CO_3	**0.00**	0.49	0.10	0.73	0.93	NA	0.55	**0.03**	0.14	0.12
	MgAl-NO_3	**0.00**	0.20	**0.03**	0.35	0.49	0.55	NA	**0.01**	**0.04**	0.33
	LiAl-CO_3	**0.00**	0.13	0.56	0.06	**0.04**	**0.03**	**0.01**	NA	0.47	**0.00**
	CaAl-NO_3	**0.00**	0.42	0.88	0.24	0.16	0.14	**0.04**	0.47	NA	**0.00**
	MgFe-CO_3	**0.00**	**0.03**	**0.00**	0.06	0.10	0.12	0.33	**0.00**	**0.00**	NA
		Divided CD8+									
		Tcells only	**NS**	**LPS**	**Imj**	**Alhyd**	**MgAl-CO_3**	**MgAl-NO_3**	**LiAl-CO_3**	**CaAl-NO_3**	**MgFe-CO_3**
Day 2	**Tcells only**	NA	0.06	0.19	0.50	0.60	0.69	0.41	0.45	0.25	0.28
	NS	0.06	NA	0.57	**0.01**	0.17	0.14	0.29	0.26	0.46	0.41
	LPS	0.19	0.57	NA	0.05	0.43	0.35	0.62	0.57	0.87	0.81
	Imj	0.50	**0.01**	0.05	NA	0.23	0.28	0.14	0.15	0.07	0.08
	Alhyd	0.60	0.17	0.43	0.23	NA	0.89	0.77	0.82	0.53	0.58
	MgAl-CO_3	0.69	0.14	0.35	0.28	0.89	NA	0.67	0.72	0.45	0.49
	MgAl-NO_3	0.41	0.29	0.62	0.14	0.77	0.67	NA	0.95	0.74	0.80
	LiAl-CO_3	0.45	0.26	0.57	0.15	0.82	0.72	0.95	NA	0.69	0.75
	CaAl-NO_3	0.25	0.46	0.87	0.07	0.53	0.45	0.74	0.69	NA	0.94
	MgFe-CO_3	0.28	0.41	0.81	0.08	0.58	0.49	0.80	0.75	0.94	NA
Day 5	**Tcells only**	NA	**0.02**	**0.01**	0.21	**0.04**	**0.04**	**0.03**	**0.00**	**0.03**	0.73
	NS	**0.02**	NA	0.64	0.25	**0.00**	**0.00**	**0.00**	**0.03**	0.85	**0.05**
	LPS	**0.01**	0.64	NA	0.11	**0.00**	**0.00**	**0.00**	0.08	0.51	**0.02**
	Imj	0.21	0.25	0.11	NA	**0.00**	**0.00**	**0.00**	**0.00**	0.33	0.37
	Alhyd	**0.04**	**0.00**	**0.00**	**0.00**	NA	0.99	0.87	**0.00**	**0.00**	**0.02**
	MgAl-CO_3	**0.04**	**0.00**	**0.00**	**0.00**	0.99	NA	0.86	**0.00**	**0.00**	**0.02**
	MgAl-NO_3	**0.03**	**0.00**	**0.00**	**0.00**	0.87	0.86	NA	**0.00**	**0.00**	**0.01**
	LiAl-CO_3	**0.00**	**0.03**	0.08	**0.00**	**0.00**	**0.00**	**0.00**	NA	**0.02**	**0.00**
	CaAl-NO_3	**0.03**	0.85	0.51	0.33	**0.00**	**0.00**	**0.00**	**0.02**	NA	0.07
	MgFe-CO_3	0.73	**0.05**	**0.02**	0.37	**0.02**	**0.02**	**0.01**	**0.00**	0.07	NA
Day 7	**Tcells only**	NA	**0.00**	**0.00**	**0.00**	**0.00**	**0.00**	**0.00**	**0.00**	**0.00**	**0.00**
	NS	**0.00**	NA	**0.01**	0.57	0.73	**0.00**	**0.04**	**0.00**	**0.00**	0.56
	LPS	**0.00**	**0.01**	NA	**0.00**	**0.03**	0.17	0.63	0.18	0.34	**0.00**
	Imj	**0.00**	0.57	**0.00**	NA	0.37	**0.00**	**0.01**	**0.00**	**0.00**	0.99
	Alhyd	**0.00**	0.73	**0.03**	0.37	NA	**0.00**	0.08	**0.00**	**0.00**	0.36
	MgAl-CO_3	**0.00**	**0.00**	0.17	**0.00**	**0.00**	NA	0.07	0.96	0.67	**0.00**
	MgAl-NO_3	**0.00**	**0.04**	0.63	**0.01**	0.08	0.07	NA	0.07	0.15	**0.01**
	LiAl-CO_3	**0.00**	**0.00**	0.18	**0.00**	**0.00**	0.96	0.07	NA	0.70	**0.00**
	CaAl-NO_3	**0.00**	**0.00**	0.34	**0.00**	**0.00**	0.67	0.15	0.70	NA	**0.00**
	MgFe-CO_3	**0.00**	0.56	**0.00**	0.99	**0.00**	**0.00**	**0.01**	**0.00**	**0.00**	NA

C.4.2 IL-2 secretion

Table C.9: Significance data for IL-2 secretion in the memory T cells with allogeneic Mo-DC MLR experiments. p-values greater than 0.05 taken as significant. T cells only = control wells without allo-DC; NS (no stimulus), LPS, Imject (Imj) and Alhydrogel (Alhyd) and LDH treatments were all for T cells with allo-DC. Significance data were calculated using the lmerTest package in [R].[7,8]

	IL-2	Tcells only	NS	LPS	Imj	Alhyd	$MgAl\text{-}CO_3$	$MgAl\text{-}NO_3$	$LiAl\text{-}CO_3$	$CaAl\text{-}NO_3$	$MgFe\text{-}CO_3$
Day 2	**Tcells only**	NA	**0.00**	**0.00**	**0.00**	**0.00**	**0.00**	**0.00**	**0.00**	**0.00**	**0.00**
	NS	**0.00**	NA	0.76	**0.01**	0.06	0.56	0.20	0.83	0.08	**0.00**
	LPS	**0.00**	0.76	NA	**0.00**	**0.03**	0.37	0.11	0.60	**0.04**	**0.00**
	Imj	**0.00**	**0.01**	**0.00**	NA	0.50	**0.05**	0.19	**0.02**	0.41	0.71
	Alhyd	**0.00**	0.06	**0.03**	0.50	NA	0.19	0.53	0.09	0.89	0.29
	$MgAl\text{-}CO_3$	**0.00**	0.56	0.37	**0.05**	0.19	NA	0.48	0.71	0.24	**0.02**
	$MgAl\text{-}NO_3$	**0.00**	0.20	0.11	0.19	0.53	0.48	NA	0.28	0.62	0.09
	$LiAl\text{-}CO_3$	**0.00**	0.83	0.60	**0.02**	0.09	0.71	0.28	NA	0.12	**0.01**
	$CaAl\text{-}NO_3$	**0.00**	0.08	**0.04**	0.41	0.89	0.24	0.62	0.12	NA	0.23
	$MgFe\text{-}CO_3$	**0.00**	**0.00**	**0.00**	0.71	0.29	**0.02**	0.09	**0.01**	0.23	NA
Day 5	**Tcells only**	NA	**0.00**	**0.00**	**0.00**	**0.00**	**0.00**	**0.00**	**0.00**	**0.00**	**0.00**
	NS	**0.00**	NA	0.12	**0.00**	**0.00**	**0.01**	**0.00**	**0.00**	**0.00**	**0.03**
	LPS	**0.00**	0.12	NA	**0.04**	0.12	0.20	0.09	**0.01**	0.06	0.52
	Imj	**0.00**	**0.00**	**0.04**	NA	0.62	0.44	0.73	0.41	0.90	0.18
	Alhyd	**0.00**	**0.00**	0.12	0.62	NA	0.79	0.88	0.19	0.71	0.39
	$MgAl\text{-}CO_3$	**0.00**	**0.01**	0.20	0.44	0.79	NA	0.67	0.11	0.52	0.55
	$MgAl\text{-}NO_3$	**0.00**	**0.00**	0.09	0.73	0.88	0.67	NA	0.25	0.83	0.31
	$LiAl\text{-}CO_3$	**0.00**	**0.00**	**0.01**	0.41	0.19	0.11	0.25	NA	0.35	**0.04**
	$CaAl\text{-}NO_3$	**0.00**	**0.00**	0.06	0.90	0.71	0.52	0.83	0.35	NA	0.22
	$MgFe\text{-}CO_3$	**0.00**	**0.03**	0.52	0.18	0.39	0.55	0.31	**0.04**	0.22	NA
Day 7	**Tcells only**	NA	**0.00**	**0.00**	**0.00**	**0.00**	**0.00**	**0.00**	**0.00**	**0.00**	**0.00**
	NS	**0.00**	NA	**0.02**	0.38	0.39	0.95	0.25	**0.02**	0.67	0.66
	LPS	**0.00**	**0.02**	NA	**0.00**	**0.00**	**0.02**	0.25	0.94	0.06	**0.01**
	Imj	**0.00**	0.38	**0.00**	NA	0.98	0.41	**0.04**	**0.00**	0.19	0.66
	Alhyd	**0.00**	0.39	**0.00**	0.98	NA	0.43	**0.05**	**0.00**	0.20	0.67
	$MgAl\text{-}CO_3$	**0.00**	0.95	**0.02**	0.41	0.43	NA	0.22	**0.02**	0.62	0.71
	$MgAl\text{-}NO_3$	**0.00**	0.25	0.25	**0.04**	**0.05**	0.22	NA	0.22	0.46	0.11
	$LiAl\text{-}CO_3$	**0.00**	**0.02**	0.94	**0.00**	**0.00**	**0.02**	0.22	NA	0.05	**0.01**
	$CaAl\text{-}NO_3$	**0.00**	0.67	0.06	0.19	0.20	0.62	0.46	0.05	NA	0.39
	$MgFe\text{-}CO_3$	**0.00**	0.66	**0.01**	0.66	0.67	0.71	0.11	**0.01**	0.39	NA

C.4.3 Cytokine secretion

Table C.10: Significance data for cytokine positive populations, determined using intracellular cytokine staining, in the naïve T cells with allogeneic Mo-DC MLR experiments. p-values greater than 0.05 taken as significant. T cells only = control wells without allo-DC; NS (no stimulus), LPS, Imject (Imj) and Alhydrogel (Alhyd) and LDH treatments were all for T cells with allo-DC. Significance data were calculated using the lmerTest package in [R].[7,8] (Days five and seven on following pages)

	Day 2	Tcells only	NS	LPS	Imj	Alhyd	$MgAl\text{-}CO_3$	$MgAl\text{-}NO_3$	$LiAl\text{-}CO_3$	$CaAl\text{-}NO_3$	$MgFe\text{-}CO_3$
IFN-γ	**Tcells only**	NA	0.14	0.96	0.11	**0.00**	0.60	**0.04**	0.66	0.35	0.40
	NS	0.14	NA	0.13	0.89	**0.00**	0.34	0.55	0.30	**0.02**	0.52
	LPS	0.96	0.13	NA	0.10	**0.00**	0.57	**0.04**	0.62	0.37	0.37
	Imj	0.11	0.89	0.10	NA	**0.00**	0.27	0.65	0.24	**0.01**	0.43
	Alhyd	**0.00**	**0.00**	**0.00**	**0.00**	NA	**0.00**	**0.00**	**0.00**	**0.00**	**0.00**
	$MgAl\text{-}CO_3$	0.60	0.34	0.57	0.27	**0.00**	NA	0.12	0.94	0.14	0.75
	$MgAl\text{-}NO_3$	**0.04**	0.55	**0.04**	0.65	**0.00**	0.12	NA	0.10	**0.00**	0.22
	$LiAl\text{-}CO_3$	0.66	0.30	0.62	0.24	**0.00**	0.94	0.10	NA	0.17	0.69
	$CaAl\text{-}NO_3$	0.35	**0.02**	0.37	**0.01**	**0.00**	0.14	**0.00**	0.17	NA	0.08
	$MgFe\text{-}CO_3$	0.40	0.52	0.37	0.43	**0.00**	0.75	0.22	0.69	0.08	NA
IL-4	**Tcells only**	NA	**0.04**	**0.00**	**0.00**	**0.00**	**0.00**	**0.00**	0.38	**0.00**	**0.04**
	NS	**0.04**	NA	0.22	**0.00**	**0.00**	**0.00**	**0.00**	0.23	**0.00**	**0.00**
	LPS	**0.00**	0.22	NA	**0.00**	**0.00**	**0.00**	**0.00**	**0.02**	**0.00**	**0.00**
	Imj	**0.00**	**0.00**	**0.00**	NA	**0.00**	**0.00**	**0.00**	**0.00**	**0.00**	**0.00**
	Alhyd	**0.00**	**0.00**	**0.00**	**0.00**	NA	**0.03**	**0.03**	**0.00**	0.09	**0.00**
	$MgAl\text{-}CO_3$	**0.00**	**0.00**	**0.00**	**0.00**	**0.03**	NA	**0.00**	**0.00**	0.62	0.08
	$MgAl\text{-}NO_3$	**0.00**	**0.00**	**0.00**	**0.00**	**0.03**	**0.00**	NA	**0.00**	**0.00**	**0.00**
	$LiAl\text{-}CO_3$	0.38	0.23	**0.02**	**0.00**	**0.00**	**0.00**	**0.00**	NA	**0.00**	**0.00**
	$CaAl\text{-}NO_3$	**0.00**	**0.00**	**0.00**	**0.00**	0.09	0.62	**0.00**	**0.00**	NA	**0.03**
	$MgFe\text{-}CO_3$	**0.04**	**0.00**	**0.00**	**0.00**	**0.00**	0.08	**0.00**	**0.00**	**0.03**	NA
IL-17	**Tcells only**	NA	0.10	0.13	**0.00**	**0.00**	0.09	**0.03**	0.61	0.75	**0.00**
	NS	0.10	NA	0.91	**0.00**	**0.02**	0.93	0.60	**0.03**	0.19	0.18
	LPS	0.13	0.91	NA	**0.00**	**0.01**	0.84	0.52	**0.05**	0.23	0.15
	Imj	**0.00**	**0.00**	**0.00**	NA	**0.00**	**0.00**	**0.00**	**0.00**	**0.00**	**0.00**
	Alhyd	**0.00**	**0.02**	**0.01**	**0.00**	NA	**0.02**	0.06	**0.00**	**0.00**	0.27
	$MgAl\text{-}CO_3$	0.09	0.93	0.84	**0.00**	**0.02**	NA	0.66	**0.03**	0.16	0.21
	$MgAl\text{-}NO_3$	**0.03**	0.60	0.52	**0.00**	0.06	0.66	NA	**0.01**	0.07	0.41
	$LiAl\text{-}CO_3$	0.61	**0.03**	**0.05**	**0.00**	**0.00**	**0.03**	**0.01**	NA	0.41	**0.00**
	$CaAl\text{-}NO_3$	0.75	0.19	0.23	**0.00**	**0.00**	0.16	0.07	0.41	NA	**0.01**
	$MgFe\text{-}CO_3$	**0.00**	0.18	0.15	**0.00**	0.27	0.21	0.41	**0.00**	**0.01**	NA
IFN-γIL-4	**Tcells only**	NA	0.22	**0.03**	**0.00**	**0.01**	0.75	**0.00**	0.28	0.35	0.88
	NS	0.22	NA	0.31	**0.00**	**0.00**	0.12	**0.00**	0.89	**0.03**	0.28
	LPS	**0.03**	0.31	NA	**0.00**	**0.00**	**0.01**	**0.00**	0.25	**0.00**	**0.04**
	Imj	**0.00**	**0.00**	**0.00**	NA	**0.00**	**0.00**	0.06	**0.00**	**0.00**	**0.00**
	Alhyd	**0.01**	**0.00**	**0.00**	**0.00**	NA	**0.03**	**0.03**	**0.00**	0.10	**0.01**
	$MgAl\text{-}CO_3$	0.75	0.12	**0.01**	**0.00**	**0.03**	NA	**0.00**	0.16	0.54	0.64
	$MgAl\text{-}NO_3$	**0.00**	**0.00**	**0.00**	0.06	**0.03**	**0.00**	NA	**0.00**	**0.00**	**0.00**
	$LiAl\text{-}CO_3$	0.28	0.89	0.25	**0.00**	**0.00**	0.16	**0.00**	NA	**0.05**	0.35
	$CaAl\text{-}NO_3$	0.35	**0.03**	**0.00**	**0.00**	0.10	0.54	**0.00**	**0.05**	NA	0.28
	$MgFe\text{-}CO_3$	0.88	0.28	**0.04**	**0.00**	**0.01**	0.64	**0.00**	0.35	0.28	NA
IFN-γIL-17	**Tcells only**	NA	0.89	0.56	**0.00**	**0.00**	0.43	**0.00**	**0.00**	0.14	**0.04**
	NS	0.89	NA	0.47	**0.00**	**0.00**	0.36	**0.00**	**0.00**	0.10	0.05
	LPS	0.56	0.47	NA	**0.00**	**0.00**	0.84	**0.00**	**0.01**	0.36	**0.01**
	Imj	**0.00**	**0.00**	**0.00**	NA	**0.05**	**0.00**	**0.00**	**0.00**	**0.00**	**0.00**
	Alhyd	**0.00**	**0.00**	**0.00**	**0.05**	NA	**0.00**	**0.02**	**0.00**	**0.00**	**0.00**
	$MgAl\text{-}CO_3$	0.43	0.36	0.84	**0.00**	**0.00**	NA	**0.00**	**0.02**	0.47	**0.01**
	$MgAl\text{-}NO_3$	**0.00**	**0.00**	**0.00**	**0.00**	**0.02**	**0.00**	NA	**0.00**	**0.00**	0.29
	$LiAl\text{-}CO_3$	**0.00**	**0.00**	**0.01**	**0.00**	**0.00**	**0.02**	**0.00**	NA	0.08	**0.00**
	$CaAl\text{-}NO_3$	0.14	0.10	0.36	**0.00**	**0.00**	0.47	**0.00**	0.08	NA	**0.00**
	$MgFe\text{-}CO_3$	**0.04**	0.05	**0.01**	**0.00**	**0.00**	**0.01**	0.29	**0.00**	**0.00**	NA

Table C.10 continued.

	Day 5	Tcells only	NS	LPS	Imj	Alhyd	MgAl-CO_3	MgAl-NO_3	LiAl-CO_3	CaAl-NO_3	MgFe-CO_3
IFN-γ	**Tcells only**	NA	0.43	0.74	**0.00**	**0.02**	0.35	0.70	**0.00**	0.08	**0.03**
	NS	0.43	NA	0.64	**0.00**	**0.00**	0.88	0.23	**0.01**	0.30	**0.00**
	LPS	0.74	0.64	NA	**0.00**	**0.01**	0.53	0.46	**0.00**	0.14	**0.01**
	Imj	**0.00**	**0.00**	**0.00**	NA	0.08	**0.00**	**0.00**	**0.00**	**0.00**	0.08
	Alhyd	**0.02**	**0.00**	**0.01**	0.08	NA	**0.00**	**0.05**	**0.00**	**0.00**	0.96
	MgAl-CO_3	0.35	0.88	0.53	**0.00**	**0.00**	NA	0.18	**0.01**	0.38	**0.00**
	MgAl-NO_3	0.70	0.23	0.46	**0.00**	**0.05**	0.18	NA	**0.00**	**0.03**	0.06
	LiAl-CO_3	**0.00**	**0.01**	**0.00**	**0.00**	**0.00**	**0.01**	**0.00**	NA	0.09	**0.00**
	CaAl-NO_3	0.08	0.30	0.14	**0.00**	**0.00**	0.38	**0.03**	0.09	NA	**0.00**
	MgFe-CO_3	**0.03**	**0.00**	**0.01**	0.08	0.96	**0.00**	0.06	**0.00**	**0.00**	NA
IL-4	**Tcells only**	NA	0.05	**0.02**	**0.00**	0.36	0.08	**0.00**	0.10	**0.00**	0.32
	NS	0.05	NA	0.73	**0.00**	**0.00**	**0.00**	**0.00**	0.74	**0.00**	0.34
	LPS	**0.02**	0.73	NA	**0.00**	**0.00**	**0.00**	**0.00**	0.50	**0.00**	0.20
	Imj	**0.00**	**0.00**	**0.00**	NA	**0.00**	**0.00**	**0.00**	**0.00**	**0.00**	**0.00**
	Alhyd	0.36	**0.00**	**0.00**	**0.00**	NA	0.39	**0.04**	**0.01**	**0.00**	0.06
	MgAl-CO_3	0.08	**0.00**	**0.00**	**0.00**	0.39	NA	0.21	**0.00**	**0.04**	**0.01**
	MgAl-NO_3	**0.00**	**0.00**	**0.00**	**0.00**	**0.04**	0.21	NA	**0.00**	0.41	**0.00**
	LiAl-CO_3	0.10	0.74	0.50	**0.00**	**0.01**	**0.00**	**0.00**	NA	**0.00**	0.53
	CaAl-NO_3	**0.00**	**0.00**	**0.00**	**0.00**	**0.00**	**0.04**	0.41	**0.00**	NA	**0.00**
	MgFe-CO_3	0.32	0.34	0.20	**0.00**	0.06	**0.01**	**0.00**	0.53	**0.00**	NA
IL-17	**Tcells only**	NA	0.10	0.48	**0.00**	0.35	0.23	0.94	**0.00**	**0.05**	0.87
	NS	0.10	NA	0.33	**0.00**	0.47	0.65	0.11	0.18	0.69	0.07
	LPS	0.48	0.33	NA	**0.00**	0.80	0.60	0.52	**0.02**	0.17	0.39
	Imj	**0.00**	**0.00**	**0.00**	NA	**0.00**	**0.00**	**0.00**	**0.00**	**0.00**	**0.00**
	Alhyd	0.35	0.47	0.80	**0.00**	NA	0.78	0.37	**0.04**	0.26	0.27
	MgAl-CO_3	0.23	0.65	0.60	**0.00**	0.78	NA	0.25	0.07	0.40	0.17
	MgAl-NO_3	0.94	0.11	0.52	**0.00**	0.37	0.25	NA	**0.00**	**0.05**	0.80
	LiAl-CO_3	**0.00**	0.18	**0.02**	**0.00**	**0.04**	0.07	**0.00**	NA	0.34	**0.00**
	CaAl-NO_3	**0.05**	0.69	0.17	**0.00**	0.26	0.40	**0.05**	0.34	NA	**0.03**
	MgFe-CO_3	0.87	0.07	0.39	**0.00**	0.27	0.17	0.80	**0.00**	**0.03**	NA
IFN-γIL-4	**Tcells only**	NA	0.09	**0.02**	**0.00**	0.83	0.60	0.24	**0.04**	0.15	0.96
	NS	0.09	NA	0.46	**0.00**	0.13	**0.02**	**0.00**	0.69	**0.00**	0.08
	LPS	**0.02**	0.46	NA	**0.00**	**0.03**	**0.00**	**0.00**	0.73	**0.00**	**0.02**
	Imj	**0.00**	**0.00**	**0.00**	NA	**0.00**	**0.00**	**0.01**	**0.00**	**0.02**	**0.00**
	Alhyd	0.83	0.13	**0.03**	**0.00**	NA	0.45	0.15	0.06	0.09	0.79
	MgAl-CO_3	0.60	**0.02**	**0.00**	**0.00**	0.45	NA	0.49	**0.01**	0.34	0.64
	MgAl-NO_3	0.24	**0.00**	**0.00**	**0.01**	0.15	0.49	NA	**0.00**	0.79	0.26
	LiAl-CO_3	**0.04**	0.69	0.73	**0.00**	0.06	**0.01**	**0.00**	NA	**0.00**	**0.03**
	CaAl-NO_3	0.15	**0.00**	**0.00**	**0.02**	0.09	0.34	0.79	**0.00**	NA	0.17
	MgFe-CO_3	0.96	0.08	**0.02**	**0.00**	0.79	0.64	0.26	**0.03**	0.17	NA
IFN-γIL-17	**Tcells only**	NA	**0.00**	**0.02**	**0.00**	0.44	0.05	0.56	**0.00**	**0.02**	**0.04**
	NS	**0.00**	NA	0.39	**0.00**	**0.01**	0.20	**0.01**	**0.01**	0.39	**0.00**
	LPS	**0.02**	0.39	NA	**0.00**	0.11	0.68	0.07	**0.00**	1.00	**0.00**
	Imj	**0.00**	**0.00**	**0.00**	NA	**0.00**	**0.00**	**0.00**	**0.00**	**0.00**	0.35
	Alhyd	0.44	**0.01**	0.11	**0.00**	NA	0.22	0.85	**0.00**	0.11	**0.01**
	MgAl-CO_3	0.05	0.20	0.68	**0.00**	0.22	NA	0.16	**0.00**	0.68	**0.00**
	MgAl-NO_3	0.56	**0.01**	0.07	**0.00**	0.85	0.16	NA	**0.00**	0.07	**0.01**
	LiAl-CO_3	**0.00**	**0.01**	**0.00**	**0.00**	**0.00**	**0.00**	**0.00**	NA	**0.00**	**0.00**
	CaAl-NO_3	**0.02**	0.39	1.00	**0.00**	0.11	0.68	0.07	**0.00**	NA	**0.00**
	MgFe-CO_3	**0.04**	**0.00**	**0.00**	0.35	**0.01**	**0.00**	**0.01**	**0.00**	**0.00**	NA

Table C.10 continued.

	Day 7	Tcells only	NS	LPS	Imj	Alhyd	MgAl-CO_3	MgAl-NO_3	LiAl-CO_3	CaAl-NO_3	MgFe-CO_3
IFN-γ	**Tcells only**	NA	**0.00**	**0.00**	**0.00**	0.60	0.37	0.30	**0.00**	**0.00**	0.98
	NS	**0.00**	NA	0.74	**0.00**	**0.00**	**0.02**	**0.00**	0.76	0.72	**0.00**
	LPS	**0.00**	0.74	NA	**0.00**	**0.00**	**0.01**	**0.00**	0.98	0.49	**0.00**
	Imj	**0.00**	**0.00**	**0.00**	NA	**0.00**	**0.00**	**0.00**	**0.00**	**0.00**	**0.00**
	Alhyd	0.60	**0.00**	**0.00**	**0.00**	NA	0.16	0.60	**0.00**	**0.00**	0.58
	MgAl-CO_3	0.37	**0.02**	**0.01**	**0.00**	0.16	NA	0.06	**0.01**	**0.04**	0.38
	MgAl-NO_3	0.30	**0.00**	**0.00**	**0.00**	0.60	0.06	NA	**0.00**	**0.00**	0.29
	LiAl-CO_3	**0.00**	0.76	0.98	**0.00**	**0.00**	**0.01**	**0.00**	NA	0.51	**0.00**
	CaAl-NO_3	**0.00**	0.72	0.49	**0.00**	**0.00**	**0.04**	**0.00**	0.51	NA	**0.00**
	MgFe-CO_3	0.98	**0.00**	**0.00**	**0.00**	0.58	0.38	0.29	**0.00**	**0.00**	NA
IL-4	**Tcells only**	NA	**0.03**	0.48	**0.00**	**0.02**	0.26	0.06	0.06	**0.00**	0.35
	NS	**0.03**	NA	0.14	**0.00**	**0.00**	**0.00**	**0.00**	0.75	**0.00**	**0.00**
	LPS	0.48	0.14	NA	**0.00**	**0.00**	0.07	**0.01**	0.24	**0.00**	0.11
	Imj	**0.00**	**0.00**	**0.00**	NA	**0.00**	**0.00**	**0.00**	**0.00**	**0.00**	**0.00**
	Alhyd	**0.02**	**0.00**	**0.00**	**0.00**	NA	0.17	0.54	**0.00**	0.21	0.12
	MgAl-CO_3	0.26	**0.00**	0.07	**0.00**	0.17	NA	0.44	**0.00**	**0.01**	0.84
	MgAl-NO_3	0.06	**0.00**	**0.01**	**0.00**	0.54	0.44	NA	**0.00**	0.06	0.34
	LiAl-CO_3	0.06	0.75	0.24	**0.00**	**0.00**	**0.00**	**0.00**	NA	**0.00**	**0.01**
	CaAl-NO_3	**0.00**	**0.00**	**0.00**	**0.00**	0.21	**0.01**	0.06	**0.00**	NA	**0.01**
	MgFe-CO_3	0.35	**0.00**	0.11	**0.00**	0.12	0.84	0.34	**0.01**	**0.01**	NA
IL-17	**Tcells only**	NA	0.23	0.64	**0.00**	0.80	0.95	0.62	0.68	0.38	0.81
	NS	0.23	NA	0.10	**0.00**	0.33	0.25	0.09	0.42	0.73	0.15
	LPS	0.64	0.10	NA	**0.00**	0.47	0.60	0.98	0.38	0.18	0.82
	Imj	**0.00**	**0.00**	**0.00**	NA	**0.00**	**0.00**	**0.00**	**0.00**	**0.00**	**0.00**
	Alhyd	0.80	0.33	0.47	**0.00**	NA	0.85	0.46	0.87	0.53	0.63
	MgAl-CO_3	0.95	0.25	0.60	**0.00**	0.85	NA	0.58	0.72	0.42	0.76
	MgAl-NO_3	0.62	0.09	0.98	**0.00**	0.46	0.58	NA	0.36	0.17	0.80
	LiAl-CO_3	0.68	0.42	0.38	**0.00**	0.87	0.72	0.36	NA	0.65	0.51
	CaAl-NO_3	0.38	0.73	0.18	**0.00**	0.53	0.42	0.17	0.65	NA	0.27
	MgFe-CO_3	0.81	0.15	0.82	**0.00**	0.63	0.76	0.80	0.51	0.27	NA
IFN-γIL-4	**Tcells only**	NA	**0.00**	**0.00**	0.45	0.40	0.07	0.86	**0.00**	0.13	0.22
	NS	**0.00**	NA	0.88	**0.00**	**0.00**	0.06	**0.00**	0.78	**0.03**	**0.02**
	LPS	**0.00**	0.88	NA	**0.00**	**0.00**	0.08	**0.00**	0.91	**0.04**	**0.02**
	Imj	0.45	**0.00**	**0.00**	NA	0.93	**0.01**	0.35	**0.00**	**0.03**	**0.05**
	Alhyd	0.40	**0.00**	**0.00**	0.93	NA	**0.01**	0.31	**0.00**	**0.02**	**0.04**
	MgAl-CO_3	0.07	0.06	0.08	**0.01**	**0.01**	NA	0.11	0.10	0.78	0.57
	MgAl-NO_3	0.86	**0.00**	**0.00**	0.35	0.31	0.11	NA	**0.00**	0.18	0.29
	LiAl-CO_3	**0.00**	0.78	0.91	**0.00**	**0.00**	0.10	**0.00**	NA	0.06	**0.03**
	CaAl-NO_3	0.13	**0.03**	**0.04**	**0.03**	**0.02**	0.78	0.18	0.06	NA	0.78
	MgFe-CO_3	0.22	**0.02**	**0.02**	**0.05**	**0.04**	0.57	0.29	**0.03**	0.78	NA
IFN-γIL-17	**Tcells only**	NA	**0.00**	**0.00**	0.29	0.46	**0.03**	0.83	**0.00**	**0.01**	0.19
	NS	**0.00**	NA	0.88	**0.00**	**0.00**	0.31	**0.00**	0.88	0.57	0.05
	LPS	**0.00**	0.88	NA	**0.00**	**0.00**	0.38	**0.01**	0.76	0.68	0.07
	Imj	0.29	**0.00**	**0.00**	NA	0.75	**0.00**	0.20	**0.00**	**0.00**	**0.02**
	Alhyd	0.46	**0.00**	**0.00**	0.75	NA	**0.00**	0.34	**0.00**	**0.00**	**0.04**
	MgAl-CO_3	**0.03**	0.31	0.38	**0.00**	**0.00**	NA	**0.04**	0.24	0.64	0.34
	MgAl-NO_3	0.83	**0.00**	**0.01**	0.20	0.34	**0.04**	NA	**0.00**	**0.01**	0.28
	LiAl-CO_3	**0.00**	0.88	0.76	**0.00**	**0.00**	0.24	**0.00**	NA	0.47	**0.04**
	CaAl-NO_3	**0.01**	0.57	0.68	**0.00**	**0.00**	0.64	**0.01**	0.47	NA	0.16
	MgFe-CO_3	0.19	0.05	0.07	**0.02**	**0.04**	0.34	0.28	**0.04**	0.16	NA

Appendix D – Appendices to Chapter Five

D.1 Characterising data for FITC-labelled LDHs

D.1.1 FITC-labelled MgAl-CO_3 LDHs

D.1.1.1 Elemental analysis

Table D.1: EDX, EA and TGA data used to calculate approximate formulae for FITC-labelled MgAl-CO_3 LDHs.

FITC-labelled MgAl-CO_3 LDH approx size (nm)	EDX	EA (weight %)			TGA
	Mg:Al atomic ratio	C	H	N	% H_2O by mass
14	1.81	2.5	4.0	0	13.1
60	2.67	4.2	2.9	0	12.5
140	2.83	3.0	3.1	0	14.2
300	2.04	2.9	3.0	0	13.1
920	2.06	2.9	3.0	0	12.7
1640	3.22	2.9	3.0	0	16.2

D.1.1.2 Powder X-ray diffraction

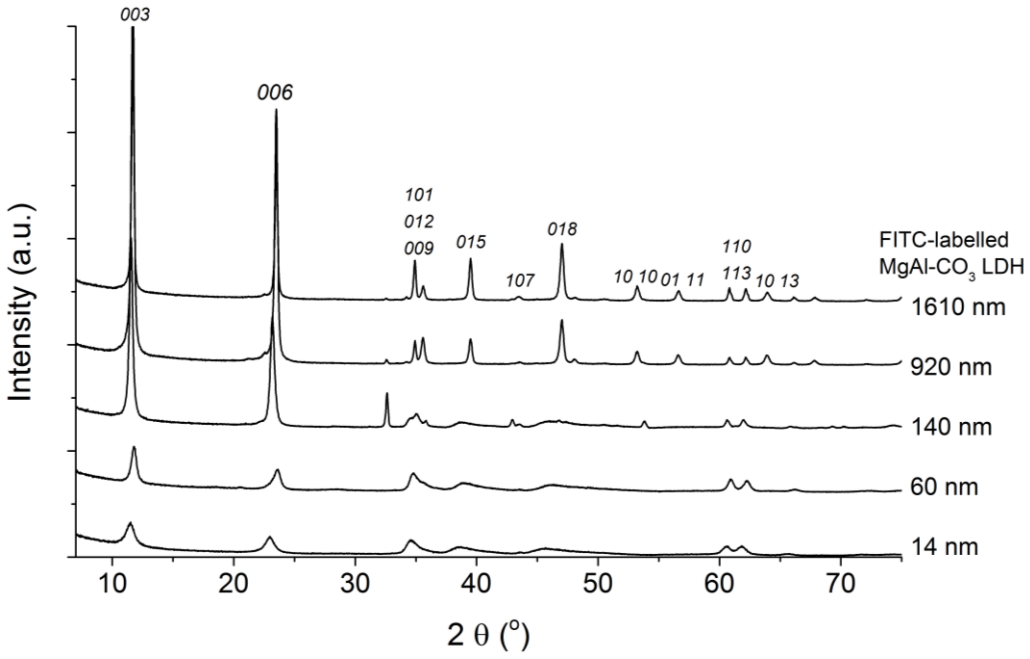

Figure D.1: Indexed powder XRD data for FITC-labelled MgAl-CO_3 LDHs. All XRD patterns show LDH structure consistent with analogous unlabelled MgAl-CO_3 LDHs. *00l* reflections are at similar positions to those for unlabelled LDHs, showing minimal FITC intercalation. Data indexed to a hexagonal unit cell, $a = b = 3.046$ Å, $c = 22.77$ Å, space group $R\bar{3}m$.[1]

D.1.1.3 Fourier transform infrared spectroscopy

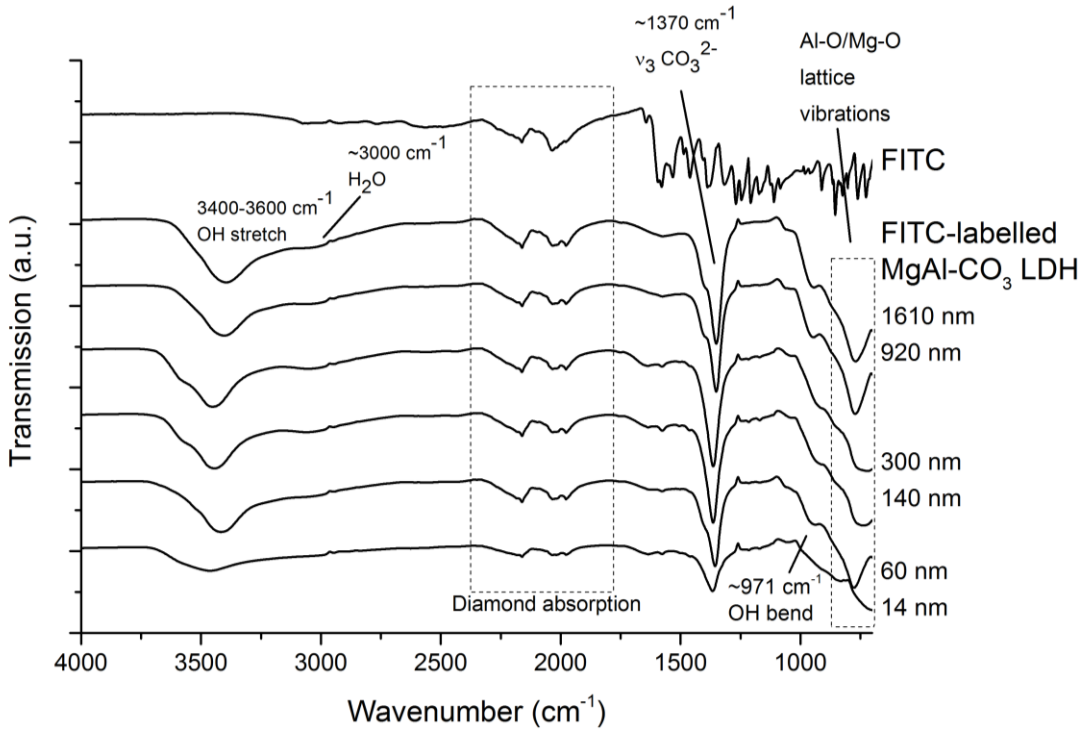

Figure D.2: FTIR spectra for FITC-labelled MgAl-CO_3 LDHs. All FTIR spectra are similar to those for unlabelled LDH analogues, some small absoprtions may indicate FITC molecules adsorbed on the LDH surface.

D.1.1.4 Transmission electron microscopy

Table D.2: FITC-labelled MgAl-CO_3 LDH particle diameters from TEM images, means obtained from measurement of > 100 particles. 'σ' = standard deviation, 'σ^2' = variance.

FITC-labelled MgAl-CO_3 LDH (approx size/nm)	Mean size (nm)	σ	σ^2
14	14	4.8	22.6
60	59.6	14.6	213
140	144	52.4	2750
300	301.8	123.9	15400
320	923	323	104000
1610	1607	603	364000

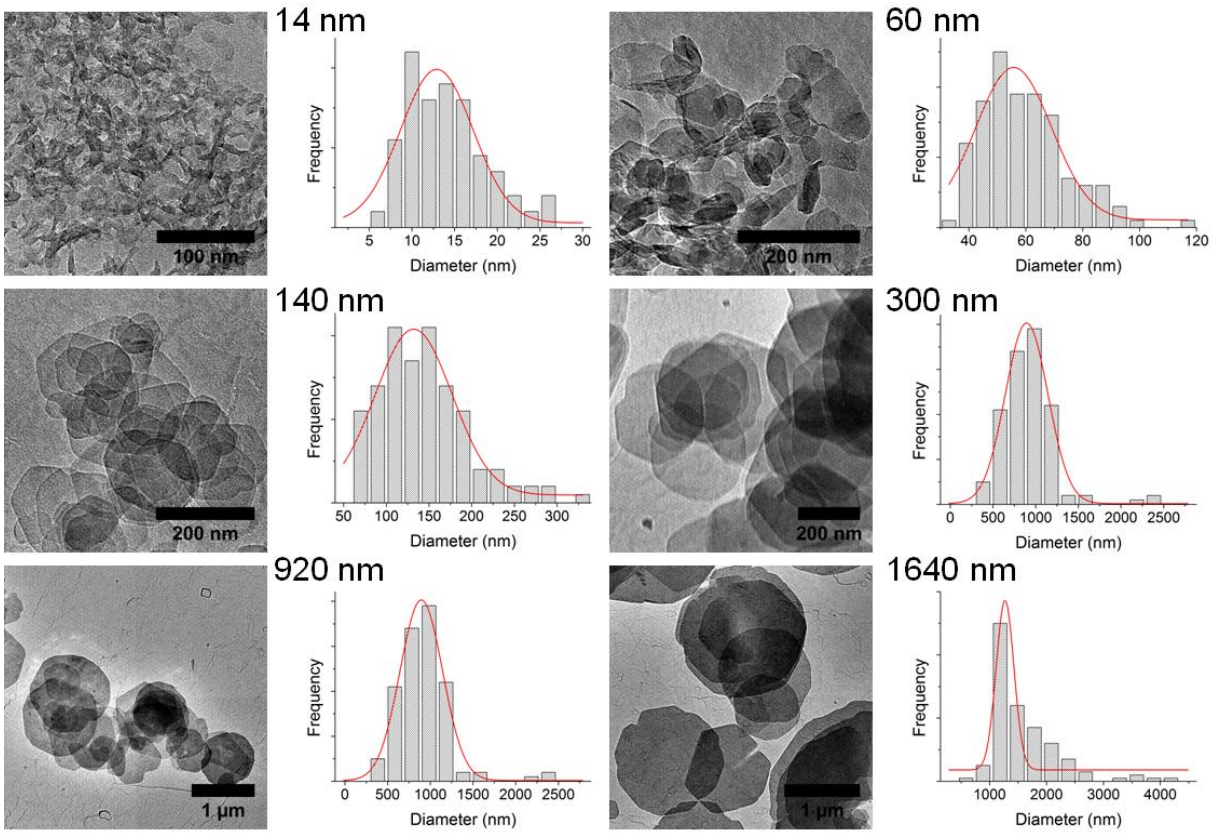

Figure D.3: Illustrative TEM images and size distribution plots for the FITC-labelled MgAl-CO_3 LDHs. Red lines indicate the best fit of a Gaussian curve, showing approximately normal distribution.

D.1.2 Other FITC-labelled LDHs

D.1.2.1 Elemental analysis

Table D.3: EDX, EA and TGA data used to calculate approximate formulae for other FITC-labelled LDHs.

	EDX	EA (weight %)			TGA
FITC-labelled LDH	**Mg:Al atomic ratio**	**C**	**H**	**N**	**% H_2O by mass**
MgAl-NO_3	1.63	2.5	3.2	2.5	10.9
MgAl-Cl	1.70	0.2	4.1	0.0	13.5
LiAl-CO_3	0.50	2.8	3.2	0.0	27.1
MgFe-CO_3	2.84	2.6	2.6	0.0	14.4
MgFe-NO_3	2.20	2.2	3.6	0.0	12.1
CaAl-NO_3	2.72	2.4	2.0	3.8	7.7
CaAl-Cl	1.12	0.4	3.4	0.0	9.0

D.1.2.2 Powder X-ray diffraction

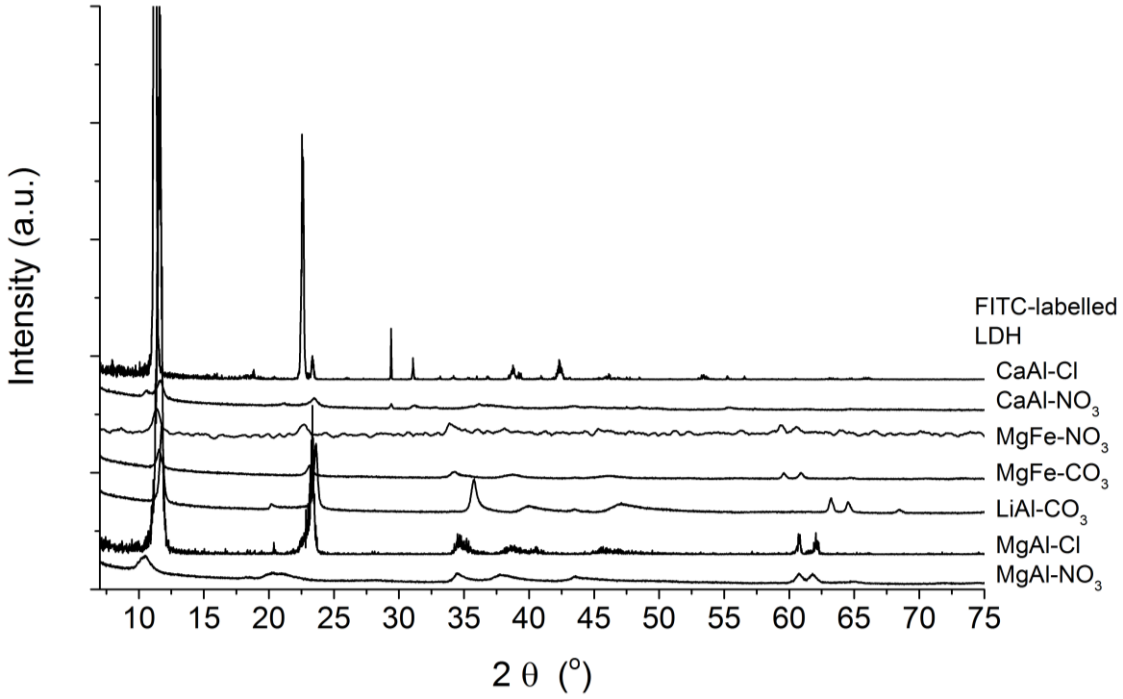

Figure D.4: Powder XRD data for other FITC-labelled LDHs. All XRD patterns show LDH structure consistent with analogous unlabelled LDHs. *00l* reflections are at similar positions to those for unlabelled LDHs, showing minimal FITC intercalation.

D.1.2.3 Fourier transform infrared spectroscopy

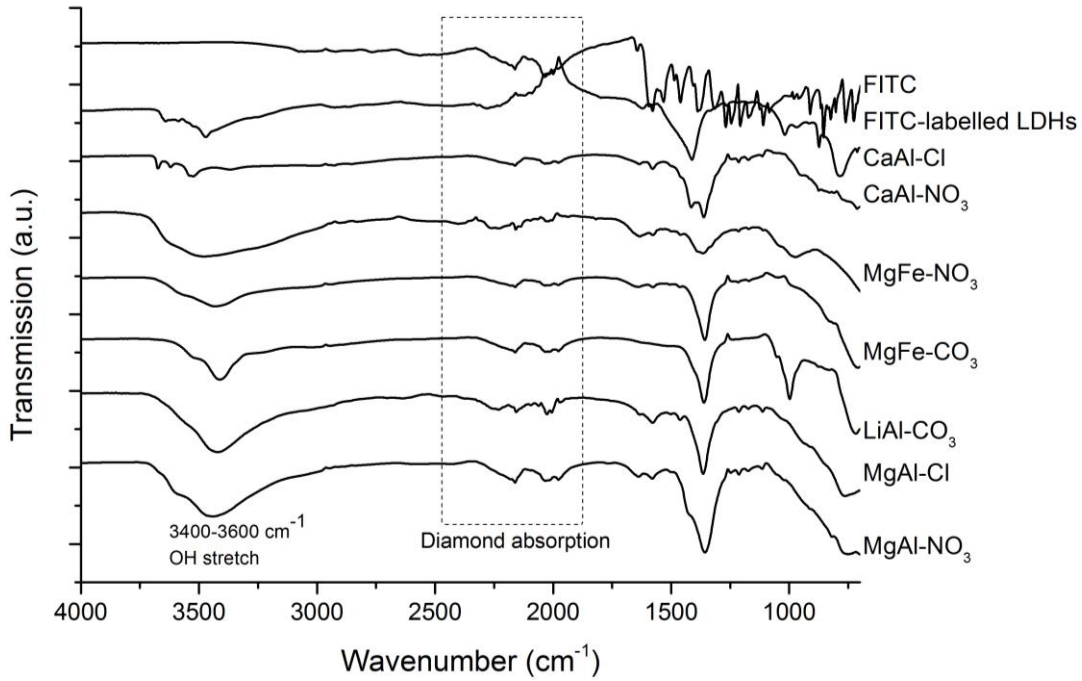

Figure D.5: FTIR spectra for other FITC-labelled LDHs. All FTIR spectra are similar to those for unlabelled LDH analogues, some small absoprtions may indicate FITC molecules adsorbed on the LDH surface.

D.1.2.4 Transmission electron microscopy

Table D.4: FITC-labelled LDH particle diameters from TEM images, means obtained from measurement of > 100 particles. 'σ' = standard deviation, 'σ^2' = variance. '**' indicates the presence of both smaller (<100 nm) and larger particles (>200 nm).

FITC-labelled LDH	Mean size (nm)	σ	σ^2
MgAl-NO_3	54.3	16.0	255
MgAl-Cl	40.4	13.2	174
LiAl-CO_3	83.1	26.7	714
MgFe-CO_3	56.6	18.3	333
MgFe-NO_3	26.3	7.8	60.2
CaAl-NO_3	**		
CaAl-Cl	**		

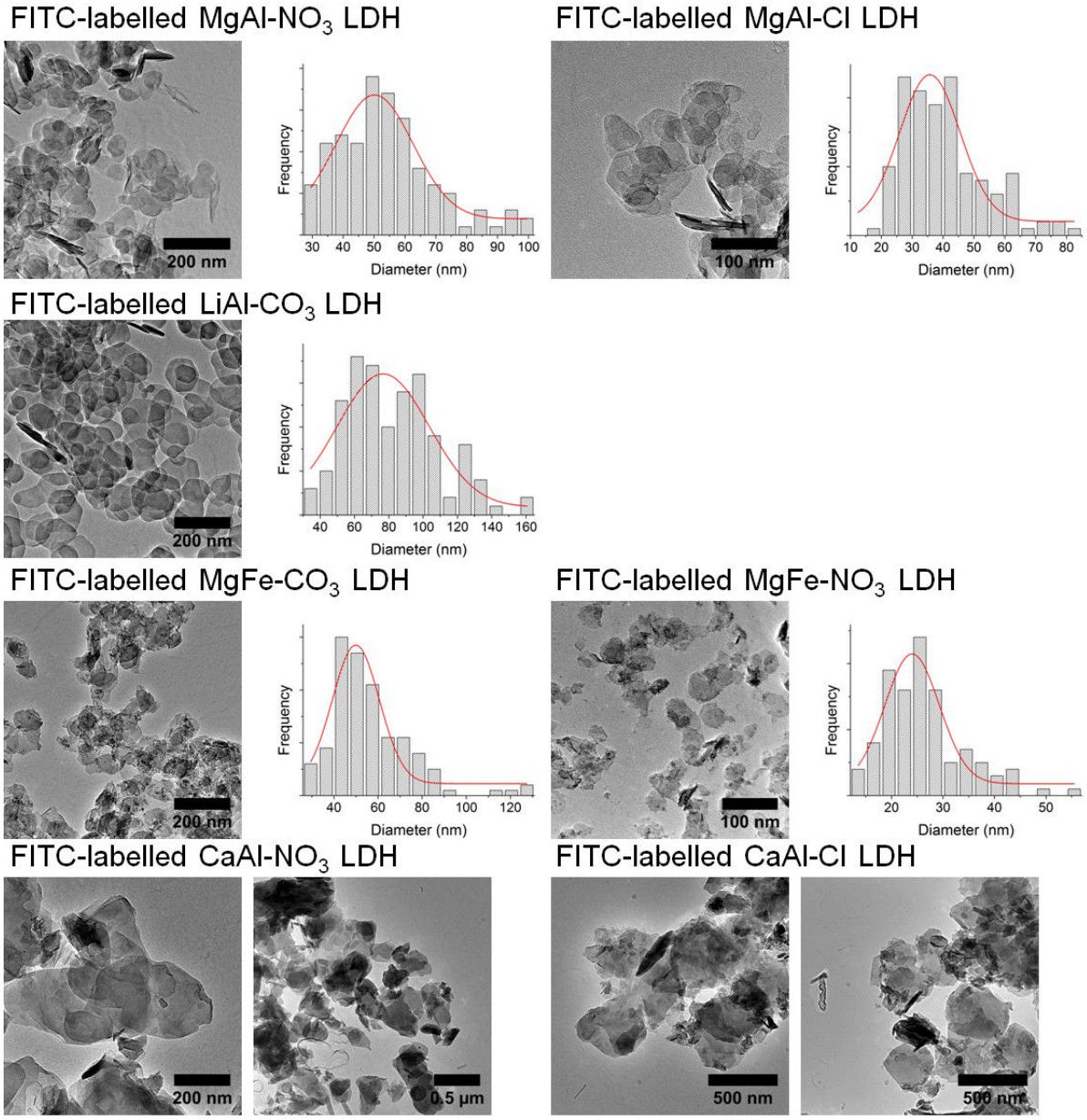

Figure D.6: Illustrative TEM images and size distribution plots for the other FITC-labelled LDHs. Red lines indicate the best fit of a Gaussian curve, showing approximately normal distribution. Images for CaAl-NO_3 and CaAl-Cl show both smaller (<100 nm) and larger particles (>200 nm).

D.2 Z-stacked images for other FITC-labelled MgAl-CO_3 LDHs

D.2.1 14 nm FITC-labelled MgAl-CO_3 LDH

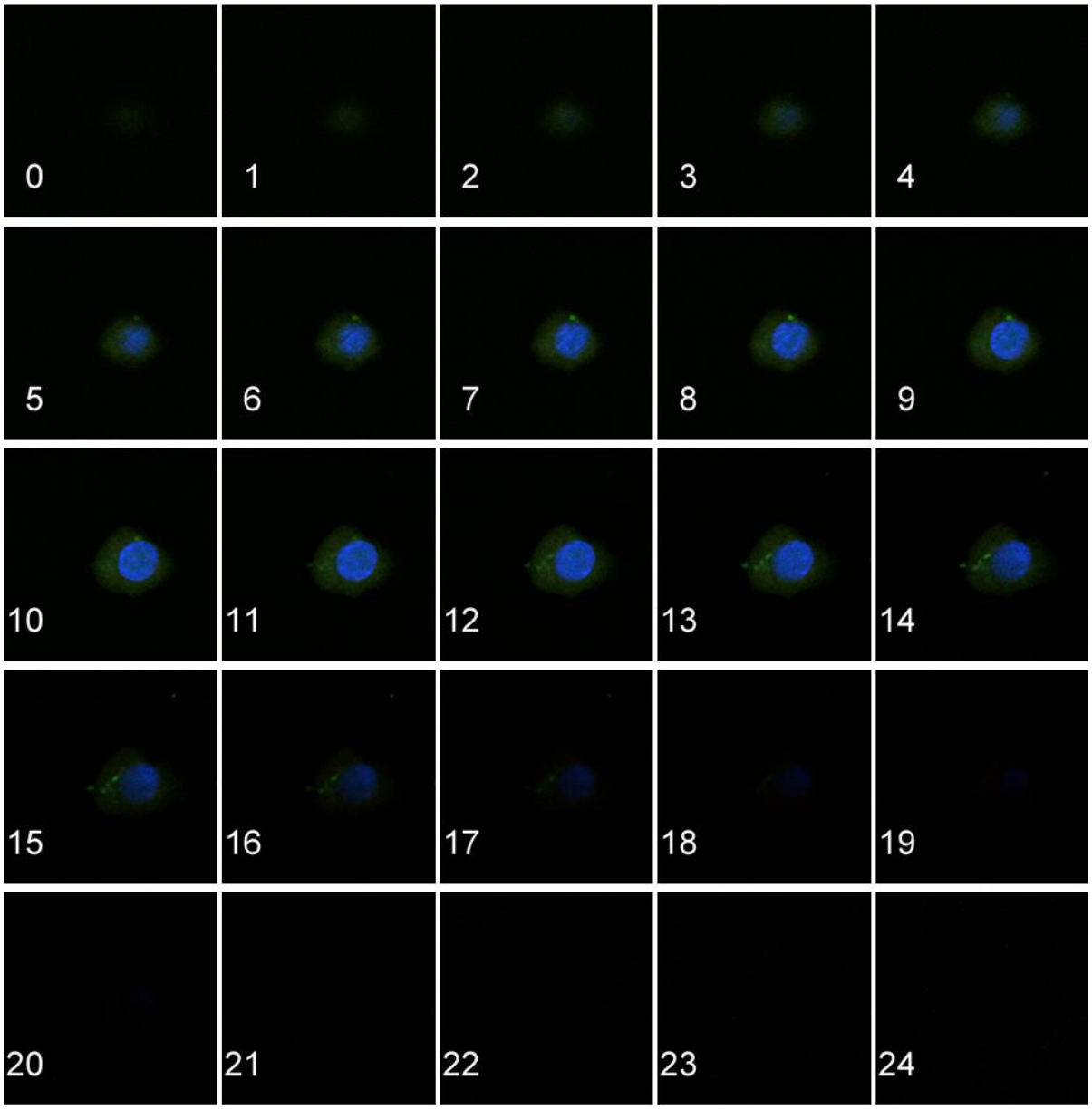

Figure D.7: *Z*-stacked images of Mo-DC incubated with 14 nm FITC-labelled MgAl-CO_3 LDH particles. *Z*-stacked images for Mo-DC treated with 140 nm FITC labelled MgAl-CO_3 LDH. Mo-DC were incubated for two hours with LDH particles. Cells were then fixed with PFA, the nuclei stained with DAPI and cells mounted onto slides for analysis using laser scanning confocal microscopy. Images display merged fluorescence for two channels (DAPI (blue) = nucleus, FITC (green) = LDH particles) taken at 0.5 μm intervals through the sample.

D.2.2 60 nm FITC-labelled MgAl-CO_3 LDH

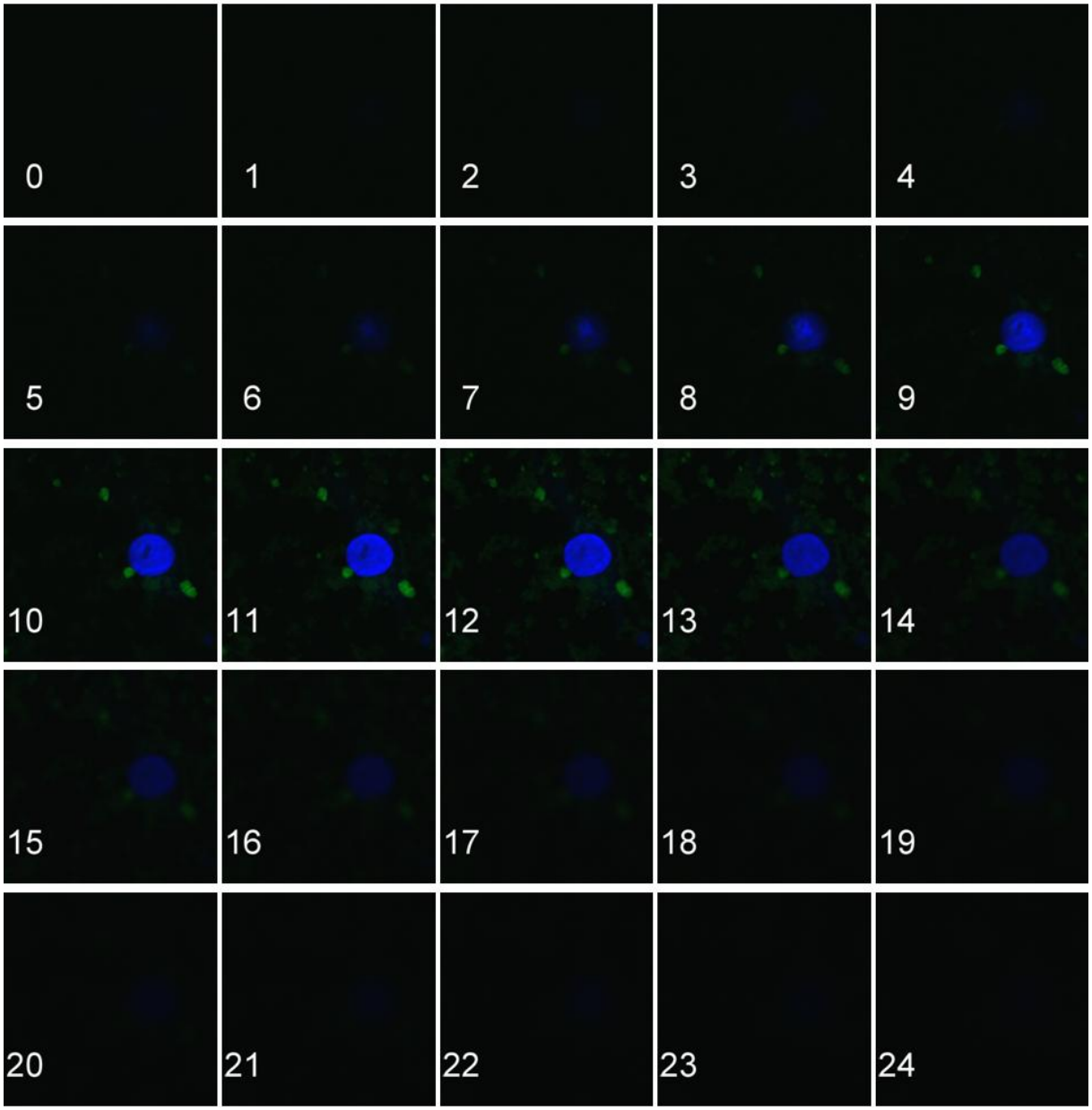

Figure D.8: *Z*-stacked images of Mo-DC incubated with 60 nm FITC-labelled MgAl-CO_3 LDH particles. *Z*-stacked images for Mo-DC treated with 140 nm FITC labelled MgAl-CO_3 LDH. Mo-DC were incubated for two hours with LDH particles. Cells were then fixed with PFA, the nuclei stained with DAPI and cells mounted onto slides for analysis using laser scanning confocal microscopy. Images display merged fluorescence for two channels (DAPI (blue) = nucleus, FITC (green) = LDH particles) taken at 0.5 μm intervals through the sample.

D.2.3 300 nm FITC-labelled MgAl-CO_3 LDH

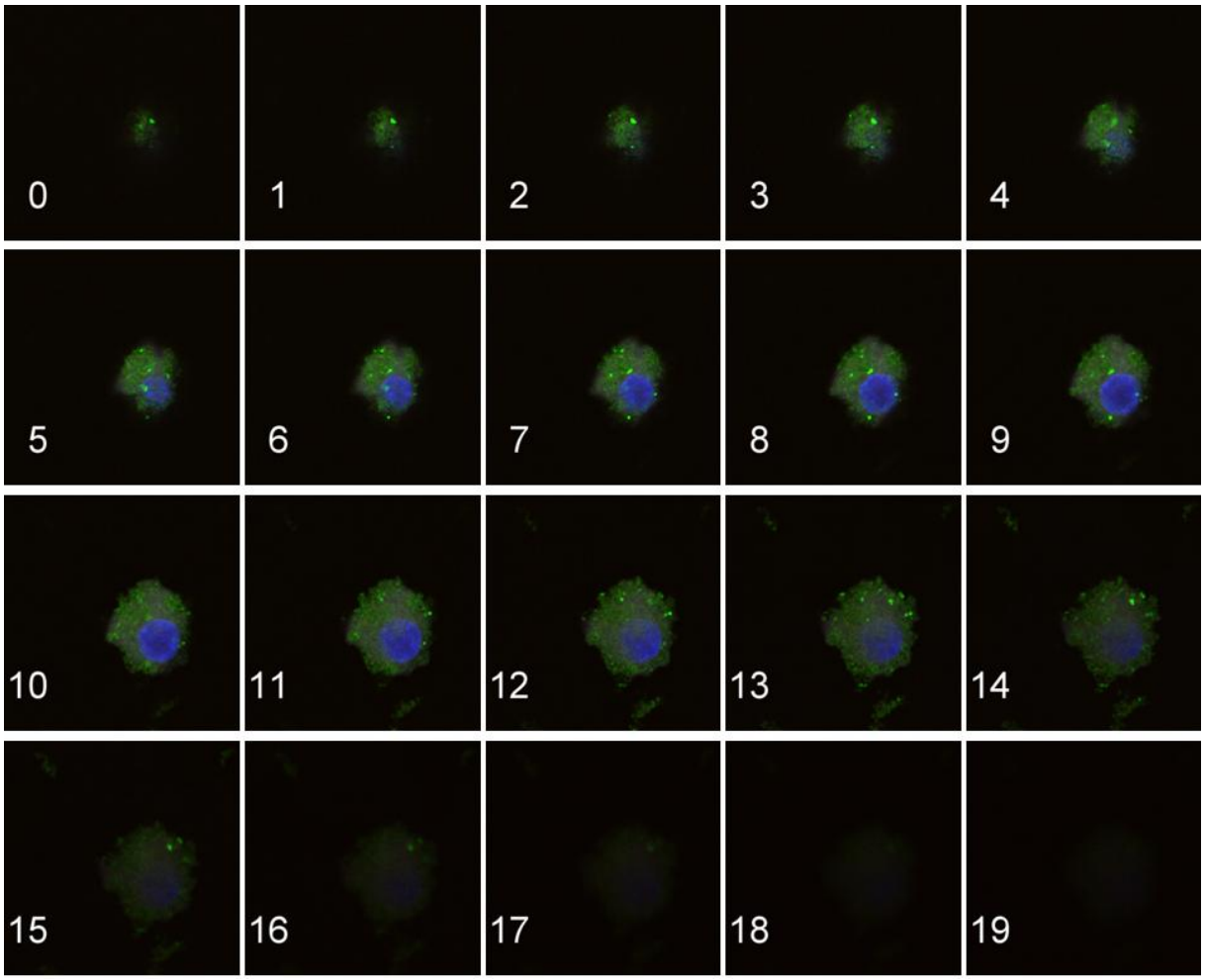

Figure D.9: *Z*-stacked images of Mo-DC incubated with 300 nm FITC-labelled MgAl-CO_3 LDH particles. *Z*-stacked images for Mo-DC treated with 140 nm FITC labelled MgAl-CO_3 LDH. Mo-DC were incubated for two hours with LDH particles. Cells were then fixed with PFA, the nuclei stained with DAPI and cells mounted onto slides for analysis using laser scanning confocal microscopy. Images display merged fluorescence for two channels (DAPI (blue) = nucleus, FITC (green) = LDH particles) taken at 0.5 μm intervals through the sample.

D.2.4 920 nm FITC-labelled MgAl-CO_3 LDH

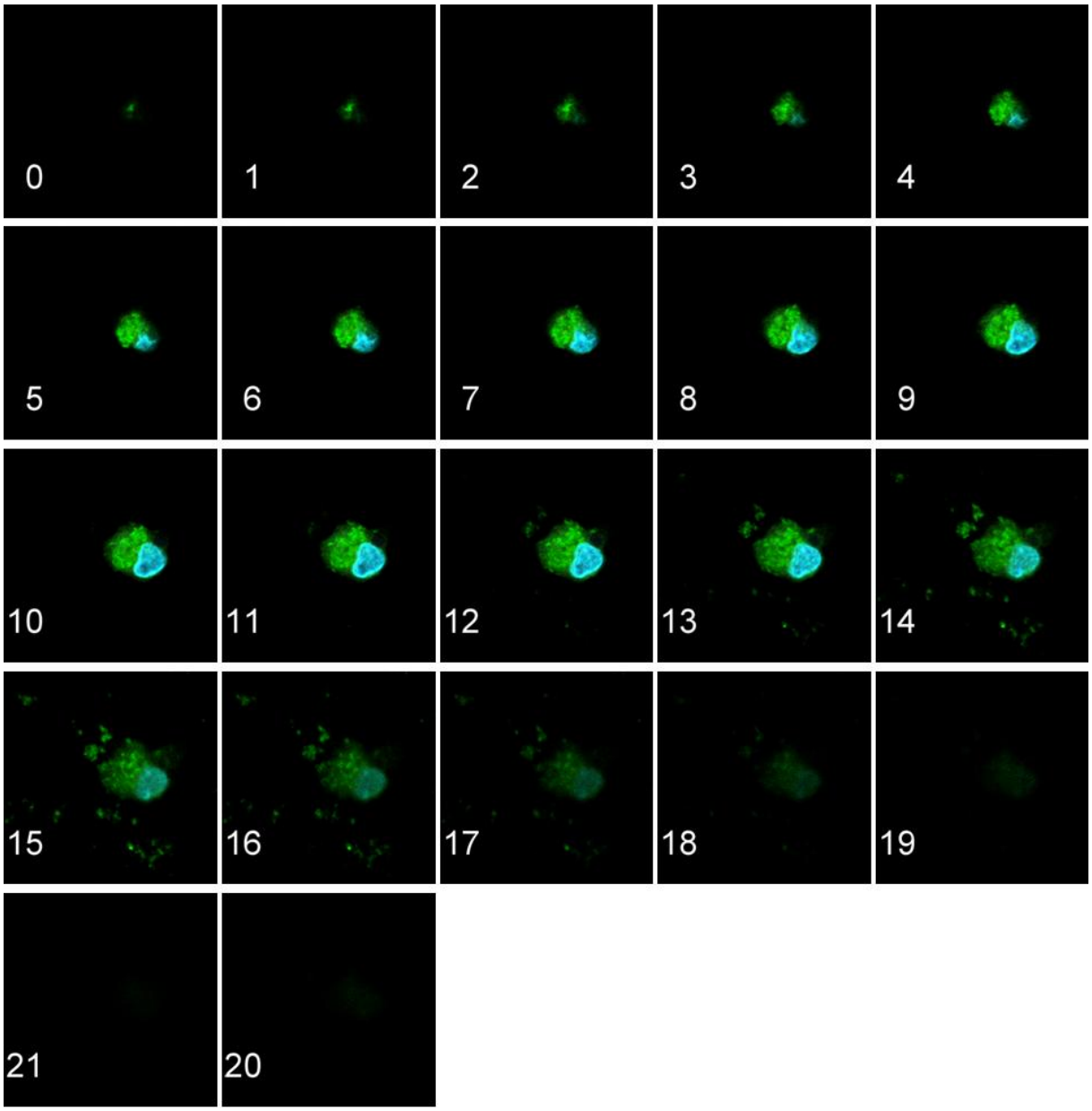

Figure D.10: *Z*-stacked images of Mo-DC incubated with 920 nm FITC-labelled MgAl-CO_3 LDH particles. *Z*-stacked images for Mo-DC treated with 140 nm FITC labelled MgAl-CO_3 LDH. Mo-DC were incubated for two hours with LDH particles. Cells were then fixed with PFA, the nuclei stained with DAPI and cells mounted onto slides for analysis using laser scanning confocal microscopy. Images display merged fluorescence for two channels (DAPI (blue) = nucleus, FITC (green) = LDH particles) taken at 0.5 μm intervals through the sample.

D.2.5 1610 nm FITC-labelled MgAl-CO_3 LDH

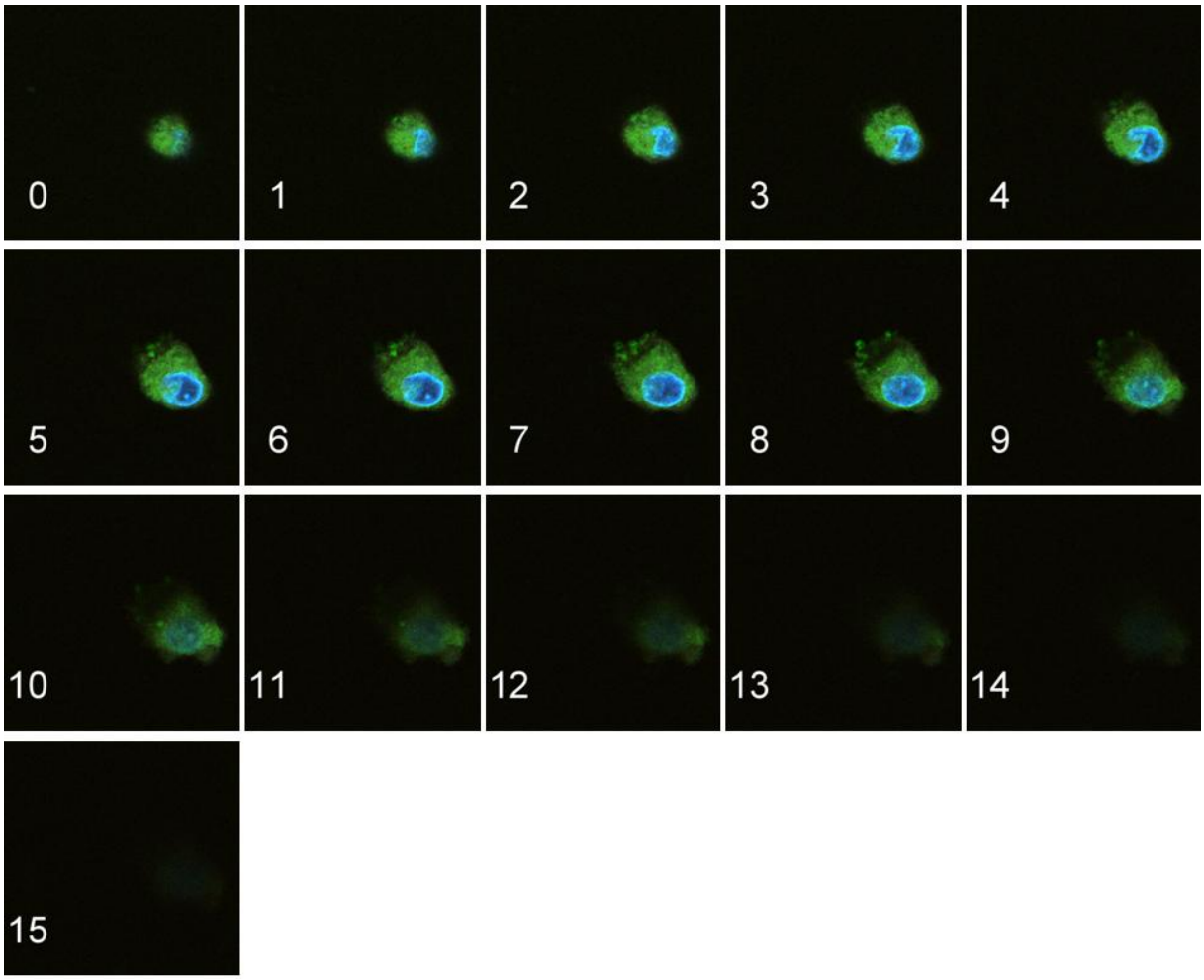

Figure D.11: *Z*-stacked images of Mo-DC incubated with 1610 nm FITC-labelled MgAl-CO_3 LDH particles. *Z*-stacked images for Mo-DC treated with 140 nm FITC labelled MgAl-CO_3 LDH. Mo-DC were incubated for two hours with LDH particles. Cells were then fixed with PFA, the nuclei stained with DAPI and cells mounted onto slides for analysis using laser scanning confocal microscopy. Images display merged fluorescence for two channels (DAPI (blue) = nucleus, FITC (green) = LDH particles) taken at 0.5 µm intervals through the sample.

D.3 Surface molecule assessment of trypsin-treated Mo-DC

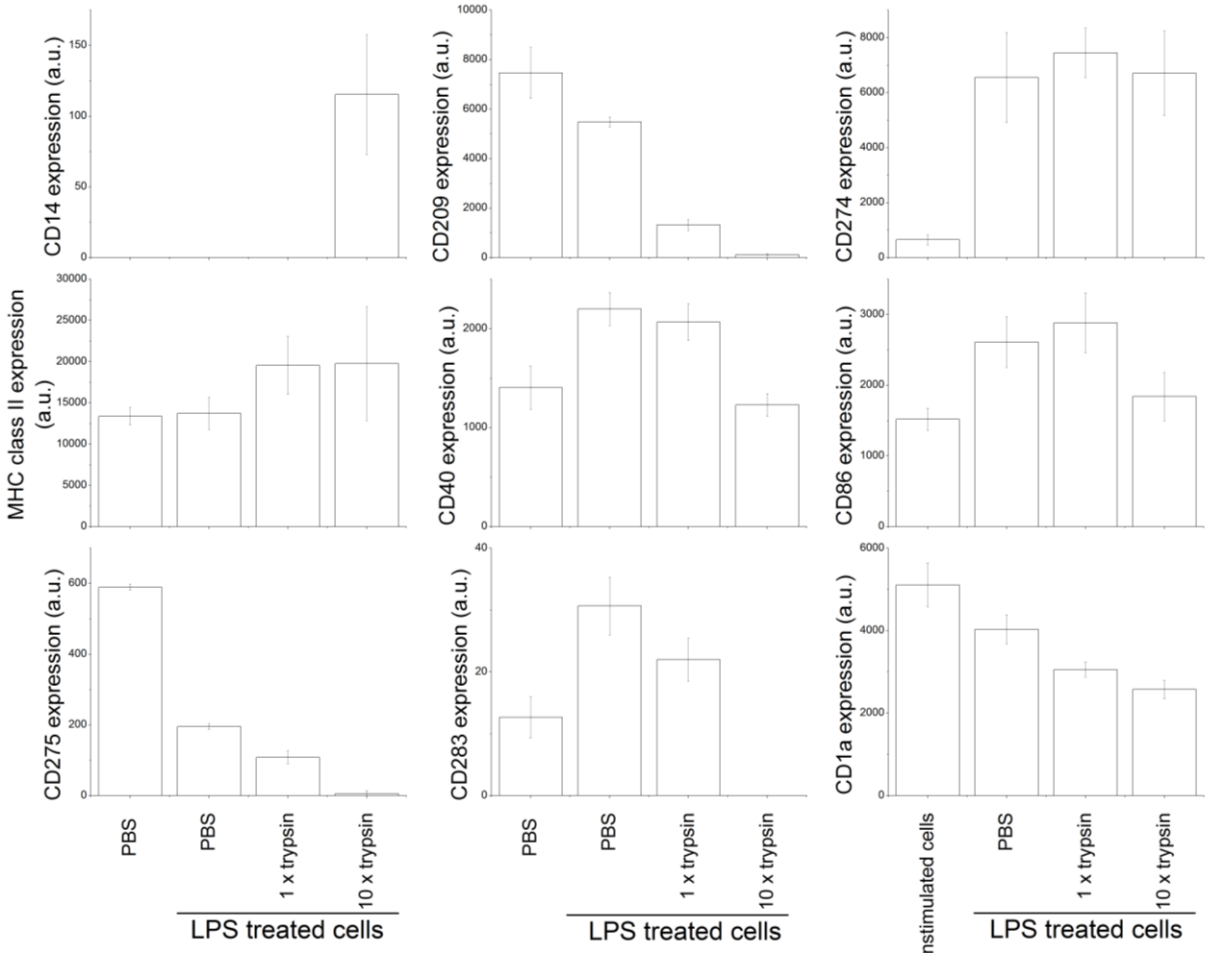

Figure D.12: Effect of trypsin on Mo-DC surface molecules. Mo-DC were incubated overnight with LPS, then treated with either PBS or 1 x or 10 x trypsin concentrations. Cells were immediately stained for the surface molecules indicated and analysed by flow cytometry. Unstimulated cells washed with PBS only were included as a control.

Table D.5: Significance data comparing between conditions from experiment assessing surface molecules on Mo-DC after trypsinisation. $p<0.05$ were taken as significant.

Condition 1	Condition 2	CD1a	CD14	CD209	CD274	MHC class II	CD40	CD86	CD275	CD283
Unstimulated cells/PBS	**LPS/PBS**	**0.02**	0.25	**0.00**	**0.00**	1.00	**0.00**	**0.01**	**0.00**	1.00
Unstimulated cells/PBS	**LPS/1x trypsin**	**0.00**	0.06	**0.00**	**0.00**	0.37	**0.00**	**0.00**	**0.00**	1.00
Unstimulated cells/PBS	**LPS/10x trypsin**	**0.00**	**0.03**	**0.00**	**0.00**	0.33	1.00	1.00	**0.00**	1.00
LPS/PBS	**LPS/1x trypsin**	**0.03**	1.00	**0.00**	1.00	0.45	1.00	1.00	**0.00**	1.00
LPS/PBS	**LPS/10x trypsin**	**0.00**	1.00	**0.00**	1.00	0.40	**0.00**	0.07	**0.00**	0.46
LPS+1/trypsin	**LPS/10x trypsin**	0.54	1.00	0.08	1.00	1.00	**0.00**	**0.01**	**0.00**	0.77

D.4 Surface molecule assessment of papain-treated THP-1 cells

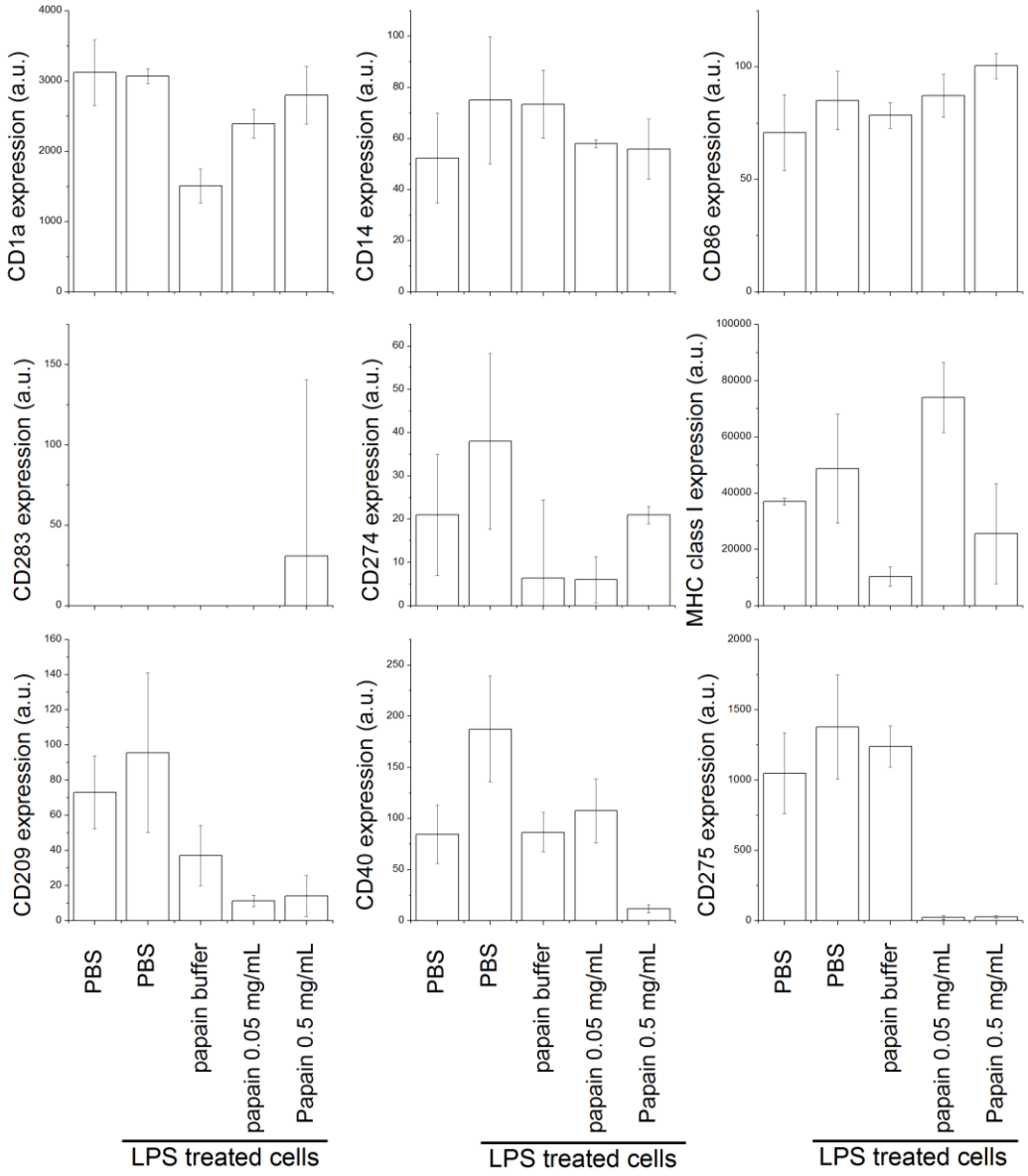

Figure D.13: Effect of papain on THP-1 cell surface molecules. THP-1 cells were incubated overnight with LPS, then treated with either PBS or papain buffer with/without papain (0.05 mg/mL or 0.5 mg/mL). Cells were immediately stained for the surface molecules indicated and analysed by flow cytometry.

Table D.6: Significance data comparing between conditions from experiment assessing surface molecules on THP-1 cells after treatment with papain. $p<0.05$ were taken as significant.

Condition 1	Condition 2	CD1a	CD14	CD86	CD283	CD274	MHC class I	CD209	CD40	CD275
Unstimulated cells/PBS	**LPS/PBS**	1.00	0.06	0.10	1.00	0.14	0.54	0.46	**0.00**	**0.04**
Unstimulated cells/PBS	**LPS/papain buffer**	**0.00**	0.08	1.00	0.22	0.27	**0.01**	**0.04**	1.00	0.58
Unstimulated cells/PBS	**LPS/papain 0.05 mg/mL**	**0.00**	1.00	**0.04**	1.00	0.25	**0.00**	**0.00**	1.00	**0.00**
Unstimulated cells/PBS	**LPS/papain 0.5 mg/mL**	0.31	1.00	**0.00**	1.00	1.00	0.58	**0.00**	**0.00**	**0.00**
LPS/PBS	**LPS/papain buffer**	**0.00**	1.00	1.00	1.00	**0.00**	**0.00**	**0.00**	**0.00**	1.00
LPS/PBS	**LPS/papain 0.05 mg/mL**	**0.00**	0.25	1.00	0.86	**0.00**	**0.01**	**0.00**	**0.00**	**0.00**
LPS/PBS	**LPS/papain 0.5 mg/mL**	0.60	0.14	0.06	0.08	0.14	**0.02**	**0.00**	**0.00**	**0.00**
LPS/papain buffer	**LPS/papain 0.05 mg/mL**	**0.00**	0.38	0.82	0.14	1.00	**0.00**	0.26	1.00	**0.00**
LPS/papain buffer	**LPS/papain 0.5 mg/mL**	**0.00**	0.21	**0.01**	**0.01**	0.27	0.17	0.41	**0.00**	**0.00**
LPS/papain 0.05 mg/mL	**LPS/papain 0.5 mg/mL**	0.10	1.00	0.14	1.00	0.25	**0.00**	1.00	**0.00**	1.00

References

(1) Bellotto, M.; Rebours, B.; Clause, O.; Lynch, J.; Cedex, R. M.; Bazin, D.; Elkaı, E. *J. Phys. Chem.* **1996**, *100*, 8527.
(2) Kang, H.; Leoni, M.; He, H.; Huang, G.; Yang, X. *Eur. J. Inorg. Chem.* **2012**, *2012*, 3859.
(3) Britto, S.; Kamath, P. V. *Inorg. Chem.* **2011**, *50*, 5619.
(4) Manohara, G. V; Prasanna, S. V; Kamath, P. V. *Eur. J. Inorg. Chem.* **2011**, 2624.
(5) Renaudin, G.; Francois, M. *Acta Crystallogr. C* **1999**, *55*, 835.
(6) Renaudin, G.; Humbert, B. *Cem. Concr. Res.* **2000**, *30*, 307.
(7) R Development Core Team; R Foundation for Statistical Computing. R: A language and environment for statistical computing, 2011.
(8) Kuznetsova, A.; Brockhoff, P. B.; Christensen, R. H. B. Package "lmerTest," 2014.